

# **Metal Complexes in Fossil Fuels**



A C S   S Y M P O S I U M   S E R I E S   **344**

# **Metal Complexes in Fossil Fuels**

## **Geochemistry, Characterization, and Processing**

**Royston H. Filby, EDITOR**  
*Washington State University*

**Jan F. Branthaver, EDITOR**  
*Western Research Institute*

Developed from a symposium sponsored  
by the Divisions of Geochemistry and Petroleum Chemistry, Inc.  
at the 191st Meeting  
of the American Chemical Society,  
New York, New York,  
April 13-18, 1986



American Chemical Society, Washington, DC 1987



### Library of Congress Cataloging-in-Publication Data

Metal complexes in fossil fuels.

(ACS symposium series, ISSN 0097-6156; 344)

“Developed from a symposium sponsored by the Divisions of Geochemistry and Petroleum Chemistry at the 191st Meeting of the American Chemical Society, New York, New York, April 13-18, 1986.”

Includes bibliographies and indexes.

1. Petroleum—Analysis—Congresses. 2. Complex compounds—Congresses.

I. Filby, Royston H. II. Branthaver, Jan F., 1936- . III. American Chemical Society. Division of Geochemistry. IV. American Chemical Society. Division of Petroleum Chemistry. V. American Chemical Society. Meeting (191st: 1986: New York, N.Y.) VI. Series.

TP691.M436 1987 553.2 87-14418  
ISBN 0-8412-1404-2

Copyright © 1987

American Chemical Society

All Rights Reserved. The appearance of the code at the bottom of the first page of each chapter in this volume indicates the copyright owner's consent that reprographic copies of the chapter may be made for personal or internal use or for the personal or internal use of specific clients. This consent is given on the condition, however, that the copier pay the stated per copy fee through the Copyright Clearance Center, Inc., 27 Congress Street, Salem, MA 01970, for copying beyond that permitted by Sections 107 or 108 of the U.S. Copyright Law. This consent does not extend to copying or transmission by any means—graphic or electronic—for any other purpose, such as for general distribution, for advertising or promotional purposes, for creating a new collective work, for resale, or for information storage and retrieval systems. The copying fee for each chapter is indicated in the code at the bottom of the first page of the chapter.

The citation of trade names and/or names of manufacturers in this publication is not to be construed as an endorsement or as approval by ACS of the commercial products or services referenced herein; nor should the mere reference herein to any drawing, specification, chemical process, or other data be regarded as a license or as a conveyance of any right or permission, to the holder, reader, or any other person or corporation, to manufacture, reproduce, use, or sell any patented invention or copyrighted work that may in any way be related thereto. Registered names, trademarks, etc., used in this publication, even without specific indication thereof, are not to be considered unprotected by law.

PRINTED IN THE UNITED STATES OF AMERICA

American Chemical Society  
Library  
1155 16th St., N.W.  
Washington, D.C. 20036

# ACS Symposium Series

**M. Joan Comstock, *Series Editor***

## *1987 Advisory Board*

Harvey W. Blanch  
University of California—Berkeley

Alan Elzerman  
Clemson University

John W. Finley  
Nabisco Brands, Inc.

Marye Anne Fox  
The University of Texas—Austin

Martin L. Gorbaty  
Exxon Research and Engineering Co.

Roland F. Hirsch  
U.S. Department of Energy

G. Wayne Ivie  
USDA, Agricultural Research Service

Rudolph J. Marcus  
Consultant, Computers &  
Chemistry Research

Vincent D. McGinniss  
Battelle Columbus Laboratories

W. H. Norton  
J. T. Baker Chemical Company

James C. Randall  
Exxon Chemical Company

E. Reichmanis  
AT&T Bell Laboratories

C. M. Roland  
U.S. Naval Research Laboratory

W. D. Shults  
Oak Ridge National Laboratory

Geoffrey K. Smith  
Rohm & Haas Co.

Douglas B. Walters  
National Institute of  
Environmental Health

## Foreword

The ACS SYMPOSIUM SERIES was founded in 1974 to provide a medium for publishing symposia quickly in book form. The format of the Series parallels that of the continuing ADVANCES IN CHEMISTRY SERIES except that, in order to save time, the papers are not typeset but are reproduced as they are submitted by the authors in camera-ready form. Papers are reviewed under the supervision of the Editors with the assistance of the Series Advisory Board and are selected to maintain the integrity of the symposia; however, verbatim reproductions of previously published papers are not accepted. Both reviews and reports of research are acceptable, because symposia may embrace both types of presentation.

# Preface

THE EXISTENCE OF METAL COMPLEXES IN FOSSIL FUELS was established by Alfred Treibs in the 1930s. It is claimed by some that this work laid the foundation for the modern science of organic geochemistry. Out of it was derived the concept of the biomarker as well as definitive evidence that organic matter in fossil fuels is largely of biological origin.

Since the 1930s, much work has been published on the geochemistry of porphyrins and other metal complexes in geological materials. The emphasis of most of this work is on metalloporphyrins and chlorins because these compounds possess spectral characteristics that permit detection in small concentrations and chemical properties that sometimes allow substantial purification from background materials. Investigations of geoporphyrins have featured structure determinations, the results of which have shown that a great variety and number of compounds are derived apparently from a few biological precursors as a consequence of geochemical processes. The nature of these geochemical processes has been inferred from the observed transformations. These processes are of particular interest to those who search for fossil fuels, particularly petroleum.

While the geochemistry of metal complexes was being studied, it was found that metal complexes in fossil fuels cause serious problems in processing. Thus, while geochemists attempted to discover how metal complexes occur in fossil fuels, chemical engineers were trying to find ways to get them out or otherwise deal with their deleterious effects. Interaction between the two groups of researchers has been somewhat limited.

This volume covers to some degree topics in the geochemistry, analytical chemistry, and processing chemistry of metal complexes in fossil fuels, principally petroleum. To the best of our knowledge, this is one of the first attempts to cover this wide array of subjects in one volume. As a result, we hope that a clearer picture of the role of these interesting compounds in the generation and use of fossil fuels emerges. We may thus learn about processing considerations through our study of geochemistry.

As nonpetroleum resources are used to obtain products now derived from crude oil, metal complexes in those resources doubtless will behave chemically much as they do in petroleum. In addition, more metal complexes may be generated by reactions of organic material with intimately associated mineral matter during processing.

Most of the chapters in this book come from the symposium on which this book is based. To complete the coverage of this topic, however, some

chapters were updated from an earlier symposium on hydrodemetallization catalysts organized by A. W. Aldag and J. Smith. A few chapters were written expressly for the book also. The wide variety of topics reflects the diversity of research in the field.

We thank many people for their parts in making this book possible. We especially thank the many secretaries who typed the manuscripts and the reviewers who provided helpful and conscientious reviews. We thank the staff of the ACS Books Department, who performed the mechanics of putting the volume together. We also thank our employers, Washington State University and Western Research Institute, for the help and services we received when we prepared this volume. Jan F. Branthaver thanks the U.S. Department of Energy, Bartlesville Project Office, for its support of this project under contract number DE-FC21-83FE-60177.

**ROYSTON H. FILBY**  
Washington State University  
Department of Chemistry  
Pullman, WA 99164

**JAN F. BRANTHAVER**  
Western Research Institute  
University Station  
Laramie, WY 82070

March 2, 1987

## Chapter 1

# Geochemistry of Metal Complexes in Petroleum, Source Rocks, and Coals: An Overview

Royston H. Filby and Gary J. Van Berkel

Department of Chemistry and Nuclear Radiation Center, Washington State University,  
Pullman, WA 99164-1300

The geochemistry of metal complexes in fossil fuels and their precursors is almost entirely that of the metalloporphyrins. The evolution of the metalloporphyrins during early-late stage diagenesis and catagenesis of sediments involves primarily the progressive defunctionalization and reduction of chlorophylls -a, -b, -c<sub>1</sub>, -c<sub>2</sub> and bacteriochlorophylls -a, -b, -d followed by metallation of the free-base porphyrins in maturing sediments. The role of the mineral matrix and sedimentary kerogens in porphyrin evolution is discussed. The geochemical processes involved in petroleum generation (migration, maturation, alteration), their effects on Ni(II) and VO(II) porphyrin evolution and implications for exploration are also discussed. The geochemistry of the Fe(III), Ga(III), and Mn(III) porphyrins in coals reflects the different, more oxidic, depositional conditions of coal formation compared to those of petroleum source beds.

The purpose of this overview is to survey the geochemistry of the metalloporphyrins and other metal complexes in fossil fuels. Emphasis is given to the metalloporphyrins in petroleum and source rocks because these have been the major focus of recent research. This review covers the origin and evolution of the geoporphyrins from the biological source material to their incorporation into crude oils and coals. It is not intended to be an exhaustive review of the literature and previous reviews of porphyrin geochemistry (1-9), particularly the excellent reviews by Baker and co-workers (4, 5, 7), should be consulted.

The geochemistry of metal complexes in petroleum and sediments that are potential petroleum source rocks is primarily that of the Ni(II) and VO(II) porphyrins, although Cu(II) porphyrins may be found in the early stages of sediment diagenesis. Although there is evidence for the existence of non-porphyrin complexes of nickel and vanadium in crude oils, oil-sand bitumens and asphalts, no discrete complexes have been unequivocally identified and there is some evidence that non-porphyrin species are, in fact, porphyrinic.

In the case of coals, the specific metal complexes that have been identified are the Ga(III), Fe(III) and Mn(III) porphyrins (9).

0097-6156/87/0344-0002\$10.50/0  
© 1987 American Chemical Society

However, the geochemistry of metal-organic species in low rank coals, at least, may involve humate complexes of many metals.

## I. The Geoporphyrins

The metalloporphyrins were the first compounds of conclusive biological origin (10-12) identified in petroleum, but their geochemical evolution is still incompletely understood. In part, this is due to the analytical difficulty encountered in the isolation and separation of small amounts of complex mixtures of Ni(II) or VO(II) homologues of each porphyrin type (desoxyphylloerythroetioporphyrin, DPEP; etioporphyrin, etio; etc.) and the identification of individual molecular species. However, advances in the identification and quantitation of porphyrins and their precursors by mass spectrometry (MS) and HPLC have stimulated recent developments in porphyrin geochemistry. Nuclear Overhauser effect (nOe) NMR, X-ray diffraction, and MS/MS have been used with great success to determine the actual structures of many individual, geochemically significant, metalloporphyrins. These analytical advances are discussed by Quirke in this volume (13).

Treibs (14) proposed a sequence of reactions to account for the transformation of plant chlorophylls into the geoporphyrins. The Treibs scheme was based on incomplete knowledge of porphyrin structures and has since undergone significant modification. Despite these modifications, the conversion of chlorophyll-a to C<sub>32</sub>DPEP-metalloporphyrins has essentially been confirmed by the determination of the structure of the VO(II) and Ni(II) C<sub>32</sub>DPEP complexes (15-17) and by the typing of intermediates (5,7). The scheme proposed by Treibs (14) is outlined in Figure 1 with the thermal scission of the isocyclic ring of the DPEP-porphyrin proposed by Corwin (1) shown to account for the etio-porphyrins without requiring a separate heme-containing source (e.g., cytochrome c). Figure 2 outlines schematically the broad evolutionary scheme of the geoporphyrins from source material to petroleum. In addition to the Treibs scheme, the most important alternate pathways and mechanisms that have been proposed, and which are discussed in this review, are shown in Figure 2.

Despite the progress made in recent years, there are many aspects of the geochemical evolution of the metalloporphyrins which are still not well understood, for example:

- i) The origin of metalloporphyrins for which no biological precursor is known.
- ii) The influence of the sedimentary environment (e.g., pH, E<sub>h</sub>, etc.) on metallation of the free-base porphyrins or precursors.
- iii) The role of the mineral matrix in the diagenetic and catagenetic reactions of porphyrins and their precursors.
- iv) The role of kerogen and the effects of kerogen catagenesis on the evolution of the metalloporphyrins in source rocks.
- v) The DPEP-etio porphyrin relationship and the mechanism of etio-porphyrin formation in petroleum source rocks and coals.
- vi) The mechanism of formation of high carbon number (>C<sub>33</sub>) porphyrins.
- vii) The effects of migration and petroleum alteration processes (maturation, biodegradation, deasphalting, water washing, etc.) on metalloporphyrin distributions in crude oils.

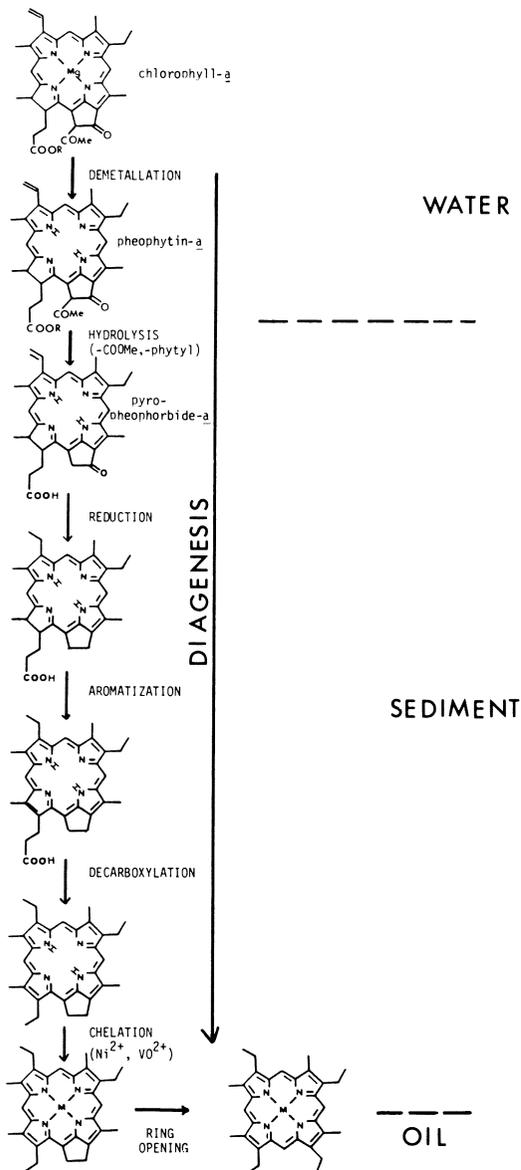


Figure 1. Treibs-Corwin Scheme for geochemical conversion of chlorophyll-a to C<sub>32</sub> metalloporphyrins (from 1, 14, cf, 4, 5, 7). R = phytyl (C<sub>20</sub>H<sub>39</sub>).

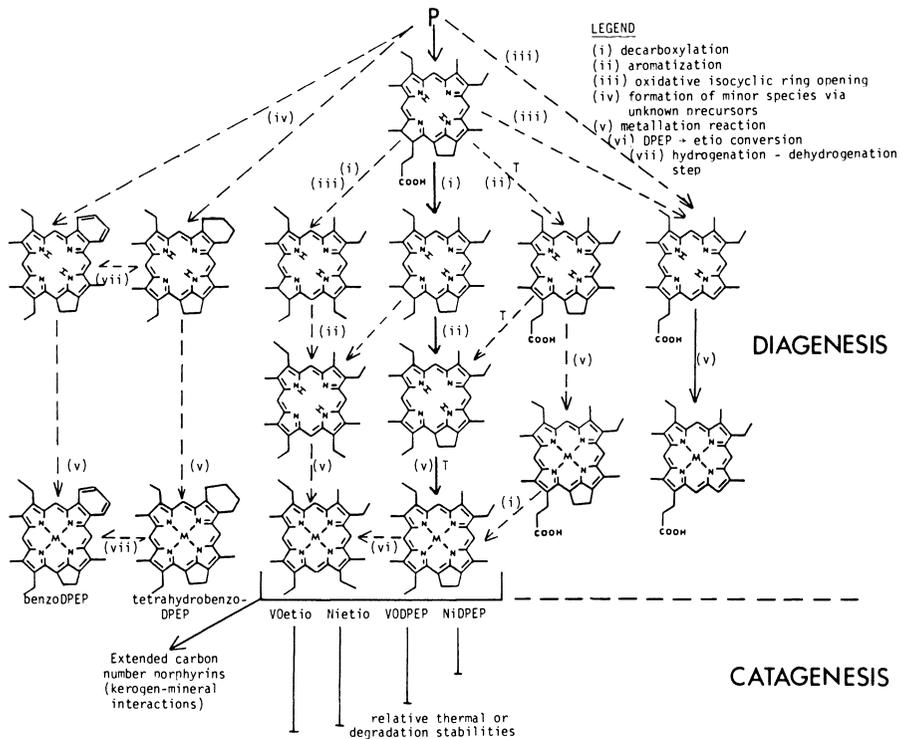


Figure 2. Diagenetic pathways proposed for evolution of the geoporphyrins. Major pathways are shown with solid arrows and proposed, but unconfirmed, pathways shown with broken arrows. Treibs Scheme steps labeled (T). Not shown are exocyclic species. P = porphyrin precursors (unidentified: includes reduction of vinyl group in major chlorophylls).

viii) The mechanism of association of porphyrins with petroleum components (e.g., asphaltenes, resins).

In this discussion, the geochemistry of the porphyrins is treated in the following sequence:

- i) Source material and biological precursors.
- ii) Depositional environment.
- iii) Early diagenesis.
- iv) Late diagenesis and catagenesis.
- v) Porphyrins in petroleum migration.
- vi) Petroleum alteration processes.

Source Materials and Biological Precursors. Fossil fuels represent a "leak" in the global carbon cycle. Although the inorganic origin of petroleum still has proponents (18), it is widely held by geochemists that most petroleum deposits have originated from organic material preserved in sediments deposited in primarily lacustrine or marine coastal environments (19,20). This source material is derived mostly from phytoplankton in the oxic surface waters with contributions from photosynthetic bacteria (autochthonous material), terrestrially derived organic debris transported into the sedimentary basin (allochthonous material), and microorganisms acting on surficially-derived organic remains within the sediment. The deposited organic matter undergoes a complex series of reactions (early to middiagenesis) involving microbial and chemical degradation of biopolymeric source material, redox reactions, and repolymerization of products to less ordered "geopolymers" which under increasing thermal stress form sedimentary kerogens (predominantly type I and II kerogens under marine-lacustrine conditions, 19). Essential to the preservation of the organic material in the sediment are anoxic depositional conditions that prevent aerobic microbial respiration of the organic matter to carbon dioxide. Late diagenesis, or catagenesis, includes the breakdown of the kerogen under increasing thermal stress to give, in part, the hydrocarbons of source rock bitumens which, under suitable geologic conditions, may migrate from the source rock to form petroleum deposits in a trap or reservoir.

Unlike petroleum, coals have formed primarily from plant debris in terrestrial environments under conditions of high organic productivity and under less reducing, or more oxic, conditions than those found in petroleum producing environments. Under these conditions, type-III kerogens are dominant (19,21).

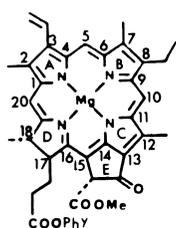
Geoporphyrins are found in high abundances (i.e., >10 µg/g) only in petroleum, asphalts, oil shales, and associated source rocks in which they occur as the Ni(II) and VO(II) metal complexes. Free-base porphyrins and minor amounts of allochthonous Cu(II) etio-porphyrins are found in sediments in the early stages of diagenesis (7,22). Minor amounts of geoporphyrins are found in coals (9,12, 23-26), but primarily as Fe(III), Ga(III) or Mn(III) complexes. The presence of trivalent iron and manganese porphyrins reflects the less reducing depositional environment of coals compared to petroleum and the different source materials of petroleum and coals.

The structural characterization of the geoporphyrins has been motivated, in part, by the need to identify their biological precursors so that they can be used as biomarkers. The Treibs scheme (14), as originally postulated, assumes that the precursor to VO(II)

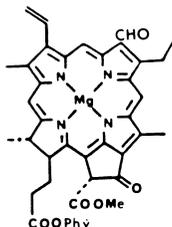
C<sub>32</sub>DPEP is chlorophyll-a, the most abundant of the plant pigments. As several authors have pointed out (5,7,8), chlorophyll-a is not the only precursor to C<sub>32</sub>DPEP and diagenetic pathways similar to that of Treibs (14) can be proposed starting from chlorophylls-b, -c, bacteriochlorophyll-a, and other chlorophylls, except for the Chlorobium chlorophylls (e.g., bacteriochlorophylls-d). There is now strong evidence from the determination of structures of specific geoporphyrins that chlorophylls-b, -c<sub>1</sub>, -c<sub>2</sub> (8,27-29) and bacteriochlorophylls-d (27-29) also may be precursors in certain depositional environments. Examples of confirmed porphyrin structures and most likely porphyrin-precursor pairs are discussed in this volume by Chicarelli et al. (8). Chlorophyll structures are shown in Figure 3 and porphyrin structures are shown in detail in Chicarelli et al. (8).

The observation that the petroleum porphyrins (both DPEP and etio) occur as complex homologous series with carbon numbers extending considerably beyond C<sub>33</sub> (30-32) was initially regarded as evidence for Chlorobium-type chlorophyll precursors as these are the only natural bacteriochlorophylls that occur as homologous series (33). However, it has been established that the alkylation patterns expected from bacteriochlorophylls-d are not consistent with those observed for the high molecular weight DPEP-porphyrins in crude oils and carbon numbers would extend only to C<sub>37</sub> (see Figure 3). Analyses of maleimides from high molecular weight geoporphyrins has shown that the isobutyl substituent on the pyrrole ring at C-8 expected for bacteriochlorophyll-d products is not found (4,34,35). Thus, Quirke et al. (34) found alkyl substituents on maleimides of up to eleven carbons which could not have arisen from a bacteriochlorophyll-d precursor. Several mechanisms have been proposed to account for high carbon number (>C<sub>33</sub>) porphyrins from chlorophyll-a (and other abundant chlorophylls), via transalkylation (30,36), alkylation-dealkylation (5,7,37), and kerogen binding (7,38-40), and it is indeed unnecessary to propose a Chlorobium chlorophyll origin. Although it appears that Chlorobium chlorophylls are not major contributors to the porphyrins found in petroleum, Ocampo et al. (27-29) have shown that bacteriochlorophylls-d are specific precursors to three Ni(II) DPEP carboxylic acids isolated from the Messel oil shale. Thus, it appears that bacteriochlorophylls-d contribute to the source material in certain depositional environments but that they are not the precursors to the majority of high carbon-number geoporphyrins found in mature sediments or petroleum.

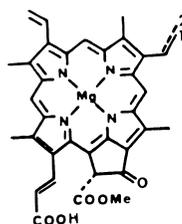
Although most of the thirty-five porphyrins for which structures have been confirmed can be related to specific or selected chlorophyll precursors, several porphyrins have been identified in sediments and crude oils for which no obvious precursors are known (8). Principal among this class are those porphyrins with 6, 7, and non-DPEP-type 5 membered cycloalkano rings (15,17 cycloalkano, 41-44), the benzo-DPEP- and benzo-etio-porphyrins, previously referred to as rhodo-porphyrins (31,35,45,46), and the tetrahydrobenzo-DPEP porphyrins (THBD, previously referred to as diDPEP) (47). Diagenetic reactions involving acid-catalyzed rearrangements or condensations of chlorophyll derivatives have been suggested for the exocyclic ring DPEP-6 and DPEP-7 porphyrins found in the Messel (29,43) and Serpiano (8,41,42) shales. A bacterial origin has been suggested for the precursor to the VO(II) benzo-DPEP-porphyrins from the Boscan oil (45). The structure of the



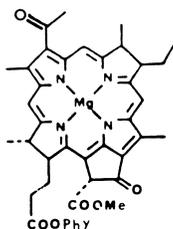
Chlorophyll-a  
(Phy = phytol)



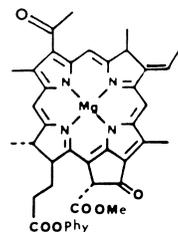
Chlorophyll-b



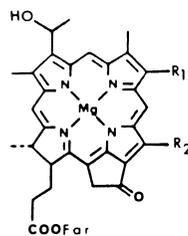
Chlorophyll-c<sub>1</sub> and-c<sub>2</sub>



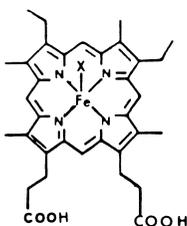
Bacteriochlorophyll-a



Bacteriochlorophyll-b



Bacteriochlorophylls-d  
Far = farnesyl  
R<sub>1</sub> = ethyl, n-prop, i-but  
R<sub>2</sub> = methyl, ethyl



Meso-heme from hemeprotein

Figure 3. Structures of geoporphyrin precursors (chlorophylls, bacteriochlorophylls and mesoteme from cytochromes).

benzo-DPEP-porphyrins has been confirmed by Kaur *et al.* (45) to contain the aromatic ring at the C-7 and C-8 positions (B-ring) on the macrocycle rather than the C-17 and C-18 positions (on the D-ring) which had been proposed previously by Barwise and Roberts (47). It would appear logical that the benzo-porphyrins are dehydrogenation products of the THBD species; however, this would require re-examination of the structure of the C<sub>33</sub>THBD species proposed by Barwise and Roberts (47) in which the exocyclic ring is attached to the C-17 and C-18 positions, or consideration that the THBD isolated from the El Lajun shale (47) is the precursor to a different benzo-DPEP structure than the one reported from the Boscan oil (45). The THBD- and benzo-porphyrin species and their possible inter-relationships are shown in Figure 2 without identification of precursors. In Figure 2, the 6-membered ring is shown at the C-7 and C-8 positions. Until recently the benzo- and THBD-porphyrins had been identified only as the metal complexes (31,35,45,47), but Baker and Louda (46) and Quirke *et al.* (48) have shown that the free-base forms are present in immature black Cretaceous and Jurassic shales and in an immature Tunisian shale, respectively, indicating that the benzo and THBD species may be formed early in the diagenetic sequence and have, as yet, unidentified precursors, as suggested by Kaur *et al.* (45). These porphyrins thus represent an interesting class that may have considerable utility in correlation or depositional-environment reconstruction studies (49).

The etio-porphyrins in petroleum and sedimentary systems were originally interpreted by Treibs to be Fe(III) complexes (10-12) derived from heme proteins. Glebovskaya and Volkenstein (50) later suggested these to be Ni(II) etio-complexes. Although there is still uncertainty about the mechanisms of formation of etio-porphyrins (1,5,7,47,50-52) it is now well established that the vast majority of etio-porphyrins in lacustrine/marine sedimentary sequences and in petroleum have been derived from chlorophylls or bacteriochlorophylls via oxidative opening of the isocyclic ring on the DPEP-porphyrin precursors (47,52) rather than thermal scission of the ring and conversion of DPEP- to etio-porphyrins as originally proposed by Corwin (1) and later by Didyk *et al.* (51). Thus a diagenetic scheme for the etio-porphyrins with a chlorin precursor parallel to that for the DPEP-porphyrins (*i.e.*, Treibs scheme) is shown diagrammatically in Figure 2. Chicarelli *et al.* (8) have pointed out, however, that etioporphyrin-III complexes in sediments could have been derived from decarboxylation of mesoporphyrin-IX, a dicarboxylic acid, which has been isolated as the Fe(III) complex in coals (53), and which probably originated from the heme of cytochromes present in the coal-forming environment. Fookes (54), however, concluded that the Ni(II) etio-porphyrins (including Ni(II) etioporphyrin-III) in Julia Creek oil shale were derived from chlorophylls and not from cytochrome degradation products, as may be the case for coals (53) formed in a more oxic environment than that of the Julia Creek sediments.

Less is known about the precursors to the Ga(III), Mn(III) and Fe(III) porphyrins (predominantly etio-type) found in coals, because of the difficulty of obtaining absolute structures. This is due largely to the analytical difficulties associated with the much lower porphyrin contents of coals and lignites compared to petroleum and associated sediments (generally <10 µg/g *vs* >100 µg/g for petroleum). Bonnett *et al.* (9) have reviewed the geochemistry of porphy-

rins in coals and concluded that, despite the much more oxic nature of the terrestrial coal depositional environment compared to anoxic marine sediments, and the subsequent degradation of much of the autochthonous plant and bacterial chlorophylls, the etio-porphyrins are predominantly chlorophyll degradation products. However, they point out that heme-based cytochrome pigments also may be important contributors. Palmer *et al.* (25) also concluded that the etio-porphyrins found in coals (and their precursors in peats) are derived from chlorophylls and that opening of the isocyclic ring occurred early in the diagenetic sequence under the more oxic conditions of the depositional environment.

In summary, the major chlorophylls (-a, -b, -c) and bacteriochlorophylls (-a, -b) appear to be the primary source materials of the geoporphyrins found in sedimentary systems. However, contributions of bacteriochlorophylls-d may have been important in specific depositional environments (e.g., the Messel shale) and the cytochromes may be minor precursors to the M(III) etio-porphyrins found in coals. In Figure 2, specific precursors of the petroleum porphyrins are thus not identified.

Early Diagenesis of Chlorophylls and Products. In the original Treibs scheme, the diagenetic conversion of chlorophyll-a to VO(II) C<sub>32</sub>DPEP involved demetallation, hydrolysis of the phytyl and carbomethoxy groups, reduction, aromatization and decarboxylation to give C<sub>32</sub>DPEP which is metallated by VO<sup>2+</sup> (Figure 1). These reactions were considered to occur under increasing thermal stress as a result of sediment compaction and burial. It is now evident that these diagenetic stages overlap and that the sequence is complicated by competing reactions or alternate pathways (e.g., early scission of the isocyclic ring (29,47), etc.) that are not part of the original Treibs scheme (see Figure 2). Much of the available information on chlorophyll diagenesis has been obtained by Baker and his group from the study of Deep Sea Drilling Project (DSDP) marine sediments. These studies have been comprehensively reviewed by Baker and Louda (5,7) who consider the geochemical evolution of the porphyrins to begin with the phorbides. Thus, the initial stages of chlorophyll-a decomposition to pheophorbide-a (precursor to pyropheophorbide-a; Figure 1) are chemically or biologically mediated in the water column or in the upper sedimentary layer. The initial stages of pheophorbide-a diagenesis in the newly formed sediment involve defunctionalization, which may be chemically or microbially mediated, to give dihydroporphyrins. Baker and Louda (5,7) regard the preservation of minor amounts of chlorins (and hence etio-porphyrins) to occur only under oxic conditions and high chlorophyll input, e.g., bottom waters and surface sediments oxygenated by currents. The relatively abundant Ni(II) etio-porphyrins and etio-porphyrin carboxylic acids found in the thermally immature Messel oil shale (27,28) and in Japanese Pliocene mudstones (55) and the free-base etio-porphyrins in the Gafsa Basin chert (48) supports the idea of isocyclic ring opening during early diagenetic stages (5,7,47). This conclusion is supported by the presence, in the Messel oil shale, of Ni(II) etio-porphyrin carboxylic acids (propionic group on C-17) which implies that ring scission has occurred before decarboxylation of the pheophorbide species (29). Baker and Louda (5,7) also have shown that in most sediments, the phorbide and porphyrin species in

the bitumen are decarboxylated and have proposed that decarboxylation occurs in two modes. In the majority of cases, low temperature (8–20°C) microbial decarboxylation may predominate. Strictly thermal decarboxylation of metalloporphyrin carboxylic acids is probably complete at 50°–60°C under geological conditions. Thus, in Figure 2 the major pathway is shown as decarboxylation of phorbide species with the Treibs pathway as a minor one.

Baker and Louda (5,7) have demonstrated complete dehydroporphyrin to porphyrin transitions in two sedimentary sequences (Black Sea and Guayamas Basin, Gulf of California). In both sequences the profiles are similar and the aromatization step to give the free-base porphyrins begins at depths corresponding to sediment temperatures between 20° and 30°C and is essentially complete between 50° and 60°C.

Mass spectrometric examination of the free-base porphyrins found in sediment cores from many regions (5,7) indicates that extractable free-base porphyrins are a limited number of homologues (C<sub>28</sub>–C<sub>32</sub>) of DPEP. Thus, at this diagenetic stage (50°–60°C) neither the extended carbon number range and high MW (>C<sub>33</sub>) DPEP porphyrins, nor the etio-porphyrins typical of petroleum metalloporphyrins (or of mature source rocks) are observed. Baker and Louda (5,7) observed minor amounts of free-base etio species, however, in two specific locations (San Miguel Gap, California borderlands and the Guayamas Basin, Southern rift). These etio-porphyrins were characterized by being highly dealkylated (C<sub>23</sub>–C<sub>30</sub>) and to have probably arisen from allochthonous terrestrial input of dealkylated Cu(II) etio-porphyrins from coal weathering (7) followed by *in-situ* demetallation, possibly on clay surfaces. A similar origin has been proposed (22) for the highly dealkylated Cu(II) and Ni(II) etio-porphyrins observed in immature sediments (*i.e.*, demetallation of Cu(II) etio-porphyrin followed by Ni(II) chelation). This contrasts with the findings of Quirke *et al.* (48), who have shown abundant high molecular-weight free-base (C<sub>29</sub>–C<sub>32</sub>) etio-porphyrins in the Gafsa Basin chert, which appear to have arisen by early diagenetic isocyclic-ring opening.

Recently Quirke *et al.* (48) have shown that the predominantly free-base porphyrins of the Gafsa Basin immature chert contain C<sub>32</sub> and C<sub>33</sub> benzo-DPEP-porphyrins. Similar observations have been made by Baker and Louda (46), who identified these free-base porphyrins in Jurassic-Cretaceous black shales of the Falkland Plateau. These porphyrins, which have been previously detected in oil shales and petroleum as Ni(II) or VO(II) complexes, have not been previously reported as free-base species. Although these species may be derived from bacteriochlorophylls-*d* by reactions yet unidentified (45,48), early diagenetic formation from chlorophyll-*b* by an external cyclization reaction may be possible (48). However, neither their precursor chlorophylls nor their diagenetic pathways can be established at this time.

Although it may be concluded that, in general, metal chelation occurs during late diagenesis, predominantly by the fully aromatized porphyrin species (largely with DPEP, but also with etio species), there is evidence that chelation of phorbides may occur under certain conditions, and that sediment mineralogy is probably a determining factor. Shiobara and Taguchi (55) have shown the presence of metallated phorbides in immature Japanese sediments. The abundances of the carboxylated metal species decreased rapidly with increasing

sediment depth. Zellmer and Man (56,57) have shown that the rates of Cu(II) chelation of the model compounds deoxomesopyropheophorbide-a methyl ester (DOMPP) and the porphyrin deoxophylloerythrin methyl ester (DPE) depend on solvent conditions. Under polar protic solvent conditions, Cu(DOMPP) aromatizes to Cu(DPE) faster than Cu(DOMPP) forms. Thus, although no Cu(II) phorbides or porphyrins, other than the highly dealkylated "allochthonous" etio-porphyrins (22), have been shown to occur in sediments, it is possible that Cu(II) tetrapyrroles enter the diagenetic process as clay-mineral associated species and which are not isolated as such.

Late Diagenesis and Catagenesis. Late diagenesis is the stage in the evolution of the geoporphyrins during which metal chelation, primarily by the fully aromatized porphyrin species, takes place. During catagenesis, which is the principal stage of oil generation from kerogen, the distribution and types of metalloporphyrins in the source rock undergo changes due primarily, but not solely, to thermal effects (5,7,38). In these stages of porphyrin diagenesis and thermal maturation, the roles of the mineral matrix and the kerogen may be important, but are not well understood.

The Sedimentary Environment and Metalloporphyrin Formation. Metallation results in greater stability of the porphyrin macrocycle and results in its preservation throughout the geological record. Although other metalloporphyrins such as Cu(II), Ga(III) (as  $\text{GaOH}^{2+}$ ), Mn(III), and Fe(III) are found in sediments (22,58) and coals (9,23-26), Ni(II) and V(IV) (as  $\text{VO}^{2+}$ ) are the predominant porphyrins found in sediments, shales, and crude oils (2-5).

Baker and Louda (5,7) have reviewed the evidence for metallation of free-base porphyrins during late diagenesis. These authors concluded that metallation is predominantly by  $\text{Ni}^{2+}$  in the maturing sediment. Thus, data for a sediment profile from the Tarfaya Basin show a smooth transition from 85% free-base porphyrin to 100% Ni(II) porphyrins with increasing depth. From these data and from a corresponding profile (100% free-base to 100% metalloporphyrin) from the San Miguel Gap, it was concluded that  $\text{Ni}^{2+}$  chelation was essentially complete at depths corresponding to a temperature of approximately 60°C. Although Cu(II) and Ni(II) etio-porphyrins were present in the San Miguel Gap sediments, many of these were attributed to allochthonous input of highly dealkylated Cu(II) and Ni(II) porphyrins from terrestrial sources (22). The virtual absence of VO(II) porphyrins from sediments at this diagenetic stage was attributed by Baker and Louda (5,7) to a different chelation pathway for VO(II) porphyrins in sediments (i.e., "bound" to kerogen). However, Baker and Louda (46) have recently described VO(II) DPEP-porphyrins, predominantly C<sub>31</sub> and C<sub>32</sub>, from Falkland Plateau Jurassic-Cretaceous shales that contain Ni(II) DPEP of similar carbon numbers and which also contain free-base porphyrins. These sediments also contain free-base, Ni(II), and VO(II) THBD and benzo-DPEP porphyrins. Baker and Louda (46) concluded that the presence of VO(II) DPEP porphyrins in this suite of sediments which show incomplete tetrapyrrole metallation, indicates early release from their "bound" state in the kerogen. However, as they state, the presence of VO(II) DPEP porphyrins in these shales, co-existent with Ni(II) and free-base species, indicates that metallation of the "free" porphyrin species

by  $\text{VO}^{2+}$  may occur in certain depositional environments. Thus, the dominance of one metal ion ( $\text{Ni}^{2+}$  or  $\text{VO}^{2+}$ ) in porphyrins of pre-catagenetic sediments may be related more to the depositional environment than to selective binding of  $\text{VO}(\text{II})$  porphyrins to evolving kerogens, or other different pathways for the two metal species.

The predominance of  $\text{Ni}(\text{II})$  and  $\text{VO}(\text{II})$  species among the geoporphyrins has been interpreted as evidence for a biological origin of the nickel and vanadium in the complexes (59). Lewan and Maynard (60), however, have concluded that the enrichment of nickel and vanadium in sedimentary bitumens relative to typical marine-biota sources show that, except for rare exceptions, the source of nickel and vanadium cannot be endemic and that the water column overlaying the sediment was the likely source of the metals for chelation. Thus, effective metallation would require an "open" sediment, *i.e.*, diffusion of metal ions from the overlying water column. This "open" system proposed by Lewan and Maynard (60) may not be a necessary constraint because clay-mineral surfaces in more compacted, deeper sediments may be the metal-ion source for metallation, a process which most likely involves a mineral surface given the insolubility of the free-base and the metalloporphyrins in water.

The formation of  $\text{Ni}(\text{II})$  and  $\text{VO}(\text{II})$  porphyrins in the maturing sediment thus results from a combination of factors, including the abundance and speciation of the metals in the sedimentary environment and the thermodynamic and kinetic stability of the metalloporphyrins over geological time (60,61). A few elements, because of their low abundances in sediments, may not form significant amounts of metalloporphyrins, even though these metalloporphyrins are relatively stable (61). Chemical speciation of the element is extremely important since an efficient metal-ion carrier (60-62) is necessary for porphyrin metallation. If the appropriate oxidation state of the metal is not present at a suitable concentration, metallation may not occur relative to other competing diagenetic reactions (*e.g.*, degradation of the porphyrins). Lewan and Maynard (60) calculated the Eh-pH stability fields of the first transition series divalent cations and found that under the reducing conditions of petroleum formation  $\text{Cu}^{2+}$ ,  $\text{Cr}^{2+}$ , and  $\text{Ti}^{2+}$  would not be available for metallation, but the other cations would be. They concluded that the abundance of  $\text{Ni}(\text{II})$  and  $\text{VO}(\text{II})$  porphyrins relative to other metalloporphyrins of the first transition series must be due to the high thermodynamic and kinetic stability of the  $\text{Ni}^{2+}$  and  $\text{VO}^{2+}$  porphyrin macrocycle in the sedimentary environment.

Baker and Louda (5,7) have noted that there is a weak correlation between high-sulphur high-asphaltene crude oils and their source rock extracts, and higher  $\text{VO}(\text{II})$  relative to  $\text{Ni}(\text{II})$  porphyrin content compared to samples with lower sulfur and asphaltene contents. They suggested that a sulfur species (not specified) may act as a catalyst for formation of the  $\text{VO}(\text{II})$  porphyrins. However, it is more likely that the sedimentary environment which resulted in the high sulfur contents of the organic matter (anoxic, production of biogenic  $\text{H}_2\text{S}$ ) limited the formation of  $\text{Ni}(\text{II})$  porphyrins by lowering the concentration of  $\text{Ni}^{2+}$  by precipitation of  $\text{NiS}$ . Under these conditions at  $\text{pH} < 7$ ,  $\text{VOS}(\text{s})$  would not form and  $\text{VO}^{2+}$  would not be removed as an insoluble sulfide species. Thus,  $\text{VO}^{2+}$  would be available for complexation whereas  $\text{Ni}^{2+}$  would not. The relationship

between the depositional environment and Ni(II) versus VO(II) complexation of porphyrins has been discussed by Lewan (62) who showed that source rocks deposited under highly reducing, H<sub>2</sub>S-rich regimes are associated with oils of higher V/Ni ratios than those generated from source rocks of more oxic environments. Therefore, the relative abundances of the two metalloporphyrins in a particular bitumen, oil, or source rock is probably related to the availability of the metal ion for complexation under the sedimentary conditions (60-62). The importance of the depositional environment has been confirmed by Moldowan et al. (63) who studied a Lower Toarcian shale sequence that was of constant, relatively low maturity (i.e., pre-"oil-window"). The shallower Middle Lias shales contained essentially only VO(II) porphyrins (Ni(II)P/[Ni(II)P + VO(II)P] < 0.2) and were deposited under highly reducing conditions whereas the deeper Lower Lias shales were deposited under sub-oxic conditions and contain essentially 100% Ni(II) porphyrins. A transition zone between these depositional environments contained both Ni(II) and VO(II) porphyrins and the Ni(II)P/[Ni(II)P + VO(II)P] ratio changed from 0.1 to 1.0 in this zone.

In addition to the availability and speciation of the metal ions in the sedimentary environment, the question of metalloporphyrin thermodynamic and kinetic stability also needs to be considered. Lewan (60) showed that the ligand field stabilization energies of Ni<sup>2+</sup> and VO<sup>2+</sup> in square planar and octahedral coordination systems (i.e., Ni(II) and VO(II) porphyrins) were the highest among the bivalent cations of the first transition series because Ni<sup>2+</sup> and VO<sup>2+</sup> have the smallest ionic radii, thus allowing a better "fit" into porphyrin macrocycle in which the axial distance between nitrogens is on the order of 3.6-4.0 Å (64). However, it should be stressed that the thermodynamic stabilities of the metalloporphyrins under geological conditions must be compared for competing degradation reactions (e.g., thermal destruction, dealkylation, demetallation, etc.) and these data are not currently available. In addition to thermodynamic considerations, the preservation of Ni(II) and VO(II) porphyrins may be also a function of their kinetics of metallation, demetallation, transmetallation, and tetrapyrrole destruction relative to the other metalloporphyrins. Buchler (65) classified metalloporphyrins into five stability classes based on the ability of acids of various strengths to demetallate the complexes. Quirke (61) noted that there is good correlation between the stability class of the metalloporphyrin and macrocycle meso-position reactivity. In general, metalloporphyrins formed from metal species of low electronegativity have low stability and will activate the meso positions on the porphyrin macrocycle towards electrophilic attack. The opposite is true for metalloporphyrins formed from metal species with higher electronegativities. Thus, Ni(II) and VO(II) porphyrins are among the most stable with respect to demetallation, transmetallation, or destruction of the tetrapyrrole ring (i.e., destruction by reaction at the meso positions). However, since Ni<sup>2+</sup> is less electronegative than VO<sup>2+</sup>, the Ni(II) porphyrins may be more likely to be destroyed by attack at the meso positions than the VO(II) porphyrins.

The role of the mineral matrix in metalloporphyrin formation in the sedimentary environment may also be important. The importance

of catalytic effects of the mineral matrix in promoting the formation of petroleum (66,67) and in kerogen formation and decomposition (68,69) is well recognized, but the effects on metalloporphyrin stability have been largely overlooked. Bergaya and Van Damme (70) showed that clay minerals could contribute to the accumulation of Ni(II) and VO(II) porphyrins in sediments and bitumens by acting as selective demetallation catalysts. They found that in mixed solutions of various metalloporphyrins in which montmorillonites were present that Mg(II) porphyrins were readily demetallated, Cu(II) porphyrins were also extensively demetallated, but the Ni(II) and VO(II) porphyrins were essentially unaffected. Similar results were found for kaolinite, although this clay was less effective in demetallating porphyrins than the swelling class. Bergaya and Van Damme (70) found that the surface acidity of the mineral was an important factor in the adsorption and demetallation of the porphyrins; *i.e.*, the nature of the clay minerals in the sediment is important. Therefore, the clays may play a role in accelerating the transformation of chlorophylls to pheophytins (*i.e.*, loss of magnesium), and limit the accumulation of Cu(II) porphyrins which are otherwise relatively stable. The demetallation kinetics of Cu(II) porphyrins on clay surfaces may explain the relatively rapid disappearance of allochthonous Cu(II) etio-porphyrins in maturing sediments observed by Baker and Louda (5,7,22). Also, by selectively demetallating other metalloporphyrins, clay minerals may favor the accumulation of Ni(II) and VO(II) porphyrins in the maturing sediment. The possible roles of mineral surfaces in diagenetic reactions among metalloporphyrins (MP), the free-base species ( $H_2P$ ) and the porphyrin dication ( $H_4P^{+}$ ) are shown schematically in Figure 4.

The Role of Kerogen in Porphyrin Evolution. Changes in the relative abundances of Ni(II) and VO(II) porphyrins, in the DPEP/etio ratio, and in the carbon number ranges of pseudo homologies occur during catagenesis. The mechanisms of these changes are not well understood and are based to a great extent on indirect evidence. Although thermal and thermocatalytic reactions may be largely responsible for the observed changes in metalloporphyrin distributions, the source-rock kerogen and the mineral matrix may play a significant role.

The chemical composition and structure of kerogen and the relative abundances and composition of its thermal maturation products, gas, bitumen, and solid residues is a function of the depositional environment and thermal history of the sediment (21). Bitumen formation is highly dependent on the mineral matrix with which the kerogen is associated because the catalytic and adsorptive properties of the minerals influence the rate of kerogen breakdown and also the nature of the extractable products through catalysis of specific reactions and/or preferential adsorption of bitumen components on the mineral surface (68,69,71-75). The formation of bitumen from the kerogen has been related to the geochemical evolution of metalloporphyrins because of the possible association of tetrapyrrole complexes with the kerogen and their subsequent release during kerogen catagenesis (5,7,38). Most of the evidence for a porphyrin-kerogen association is indirect and based on the analysis of porphyrins from bitumens in sedimentary profiles (5,7,22,38). Recently, however, Van Berkel and Filby (40) were able to provide experimental confirma-

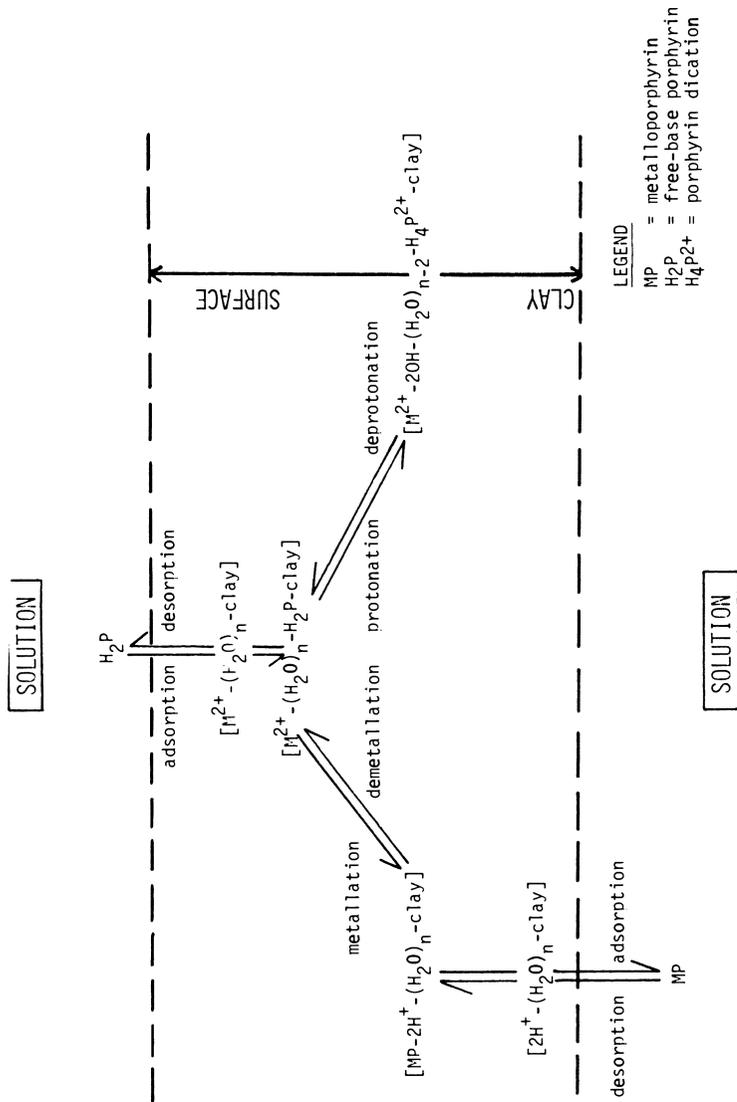


Figure 4. Schematic diagram of clay mineral-porphyrin reactions in sediments (modified from 70).

tion of this association by generating metalloporphyrins by pyrolysis of kerogens from Mississippian-Devonian oil shales.

Laboratory experiments have also shown that minerals may play a role in structural alteration of porphyrins and porphyrin precursors during catagenesis (36,51,76-78).

The most significant changes in the content, types and distribution of porphyrins in a sediment that occur as catagenesis proceeds include: i) a decrease in the DPEP/etio ratio (5,7,38,47,51); (ii) a decrease in the Ni(II) porphyrin to VO(II) porphyrin ratio (5,7,38); (iii) alkylation (31) and dealkylation (51) of the porphyrins; and (iv) the appearance of alternate porphyrin series (e.g., benzo and THBD) and very high molecular weight porphyrins (7,8,22,38).

(i) DPEP/etio Ratio. The DPEP/etio ratio has been used as a sensitive indicator of the thermal maturity of a sediment (79). With increasing thermal stress the ratio decreases as the etio-type porphyrins become relatively more abundant than the DPEP-type (7,38,47,51). It was originally proposed by Corwin (1) and later by Didyk et al. (51) that cleavage of the DPEP isocyclic ring as a result of thermal stress accounted for this change, but in laboratory heating experiments Burkova et al. (52) found that thermal conversion of VO(II) DPEP- to etio-type porphyrins occurred only to a limited extent (ca., 5%). Barwise (80) proposed three additional mechanisms that would lower the DPEP/etio ratio, all of which may contribute in varying degrees to the overall change. These mechanisms are: 1) oxidative cleavage of the DPEP isocyclic ring during early diagenesis forming etio-porphyrins; 2) preferential thermal destruction of DPEP-type porphyrins; and 3) preferential generation of etio-porphyrins from kerogen during catagenesis, which will dilute the DPEP-rich bitumen present in the sediment prior to kerogen catagenesis. Of the mechanisms proposed by Barwise, only the second would cause changes in the DPEP/etio ratio of porphyrins in maturing oils.

Oxidative cleavage of the isocyclic ring during early diagenesis has been suggested for the predominance of the etio-porphyrins in coal (7,9,25). Early-stage cleavage of the isocyclic ring in a reducing environment is also implied by the presence of Ni(II) etio-porphyrin carboxylic acids in the Messel oil shale (27-29; i.e., cleavage has occurred prior to decarboxylation).

If it is assumed that no thermal DPEP- to etio-porphyrin conversion occurs, then a rapid change in DPEP/etio ratio could be accounted for by only small differences in the thermal stability of these two porphyrin types as suggested by Barwise (80). The observations of Mackenzie et al. (38) and others (7,52) indicate that the DPEP-porphyrins of both Ni(II) and VO(II) are thermally less stable than the etio-species with Ni(II) DPEP being the least stable of all. Interestingly, Rosscup and Bowman (81) showed in a laboratory study that Ni(II) alkyl-porphyrins are thermally more stable than their VO(II) counterparts. Unfortunately, no information on the DPEP/etio ratio of either metal species was given in this study. Baker et al. (82) found that only Ni(II) etio-porphyrins survived in sediments under the thermal stress imposed by close proximity to a diabase sill, indicating a higher thermal stability of Ni(II) etio-porphyrins than all the other porphyrin types. However, Mackenzie et al. (38) found that the Ni(II) DPEP/etio ratio decreased more rapidly with

depth in maturing sediments than did the corresponding ratio for VO(II) porphyrins. They also found with increasing thermal stress (i.e., depth) that the Ni(II) porphyrins disappeared faster than the VO(II) species. Therefore, the relative thermal stabilities of the geoporphyrins appears to be:



Barwise (80) examined a suite of samples from a Gulf of Suez formation and found that the concentration of VO(II) DPEP-porphyrins decreased and etio-porphyrins increased coincident with the onset of petroleum generation, and the maximum concentration of etio-porphyrins reached a level greater than the initial DPEP concentration. Therefore, even if total conversion of DPEP- to etio-porphyrins occurred, another source of porphyrins in these sediments would be needed to explain these observations. Barwise (80) interpreted this to be due to preferential generation of substantial quantities of etio-type porphyrins from kerogen. Van Berkel and Filby (40) showed that both VO(II) and Ni(II) DPEP- and etio-porphyrins could be generated from kerogen by pyrolysis, although the DPEP/etio ratio of the VO(II) porphyrins measured by HPLC decreased as pyrolysis temperature increased. Mass spectrometric analysis (83) indicated the same trend for Ni(II) as for VO(II) porphyrins, but the DPEP/etio ratio decreased more rapidly with temperature for the Ni(II) porphyrins. Thus, the relative abundances of Ni(II) and VO(II) porphyrins generated from the kerogen will influence the final DPEP/etio ratio of the bitumen. In fact, Van Berkel and Filby (40) showed that the Ni/V ratio, Ni(II) porphyrin/VO(II) porphyrin ratio, and the DPEP/etio ratio of the bitumen accumulating in a source rock may increase, decrease, or remain constant depending on the kerogen composition and temperature regime. These changes in an accumulating bitumen may be substantial because the kerogens in this study were found to liberate a far greater amount of nickel and vanadium complexes during pyrolysis than the corresponding amount of the metal complexes in the bitumen isolated from the shale.

Kerogen thus can generate DPEP- and etio-porphyrins of both Ni(II) and VO(II). What has not been considered is the combined effect of the generation of porphyrins from the kerogen and thermal maturation of the porphyrins in both the inherited and the catagenetic bitumen. The apparent generation of large amounts of etio-porphyrins during catagenesis observed by Barwise (80) may be due to the relative thermal stabilities of the porphyrins. If the rate of DPEP destruction is greater, and etio destruction smaller, than the rate of porphyrin generation from the kerogen, the net effect would be the generation of predominantly etio-porphyrins.

(ii) Nickel to Vanadyl Porphyrin Ratio. Baker et al. (5,7,82, 84) and Mackenzie et al. (38) have noted a decrease in the Ni(II) porphyrin to VO(II) porphyrin ratio with increasing maturation in suites of sediments which have undergone increasing levels of thermal stress. As discussed in the previous section, based on thermal stabilities alone, one would predict an increase in the VO(II) to Ni(II) porphyrin ratio with increasing thermal stress. However, other factors are probably involved in determining the Ni(II) to VO(II) porphyrin ratio.

Reduction in the Ni(II)/VO(II) porphyrin ratio may be due to clay-mineral catalyzed demetallation resulting in the kinetically controlled accumulation of VO(II) porphyrins relative to Ni(II) porphyrins. Bergaya and Van Damme (70) found no measurable difference in the demetallation rates of Ni(II) and VO(II) tetraphenylporphyrin (TPP) on clay minerals. However, if demetallation of the Ni(II) porphyrins is favored, even slightly, in the sedimentary environment over geologic time, a decrease in the Ni(II) to VO(II) porphyrin ratio with increasing maturation (temperature-time) would be noted. Furthermore, it has been demonstrated in laboratory experiments that VO(II) porphyrins are more stable to demetallation in an acid environment (85) and Ni(II) octethylporphyrin (OEP) can be converted to VO(II) OEP, whereas VO(II) OEP cannot be converted to Ni(II) OEP (38), thus indicating demetallation/remetallation as a possible mechanism for this observed change. However, natural sequences of metallo-(Ni<sup>2+</sup> vs VO<sup>2+</sup>) porphyrin homologies do not support this (5,7,38).

Generation of VO(II) porphyrins from the kerogen during catagenesis has also been proposed by Baker and Louda (5,7) to account for these observations. Nickel porphyrins are considered to form as "free" or solvent extractable species from free-base porphyrins of limited homology, whereas the VO(II) porphyrins form in a "bound" or nonextractable state linked to kerogen. When thermal stress breaks the kerogen-porphyrin linkage, the VO(II) porphyrins are released to the bitumen with extended carbon number ranges. This proposal is based on evidence that Ni(II) DPEP-porphyrins of limited homology are found in all but the most immature sediments, whereas VO(II) porphyrins are more commonly isolated from sediments which have undergone a moderate degree of thermal stress. This concept is supported by indirect evidence from a number of studies (38,47,80,84).

At the present time, there is no satisfactory explanation for the apparent kerogen-enhanced bonding of primarily VO(II) porphyrins, and evidence presented by Van Berkel and Filby (40) indicates this concept needs to be revised. There is also no firm evidence that chemical bonding via C-C bonds occurs. Recent analyses have shown some kerogens to contain significant quantities of both organically bound nickel and vanadium (39,40,86,87). Spiro *et al.* (87) found that the Ni/V ratio of the kerogen in some Israeli oil shales and the Ni(II) to VO(II) porphyrin ratio of the associated bitumen were similar, indicating that there may be a correlation between the porphyrin contents of the bitumen and the nickel and vanadium contents of the kerogen. Van Berkel and Filby (40) measured mineral-free concentrations of nickel and vanadium of 2130 and 700 µg/g, respectively, in New Albany oil-shale kerogen and 350 and 3260 µg/g, respectively, in the Woodford oil shale. Also, Van Berkel (83) demonstrated that there is a correlation between the Ni/V ratios of the kerogen, bitumen, and asphaltenes of certain oil shales. Formation of a porphyrin-kerogen association (e.g., chemisorption) via interaction of metalloporphyrins in the sediment with the kerogen is highly probable given the polar nature of the porphyrins, and is supported by the work of Nguyen and Filby (88). They demonstrated that asphaltenes and both Ni(II) octaethylporphyrin (OEP) and Ni(II) mesoporphyrin IX dimethyl ester (DME) formed strong associations ( $\pi$ - $\pi$  bonding or functional group association), with

Ni(II) DME having greater affinity for the asphaltenes than Ni(II) OEP. The fact that kerogen and asphaltenes are probably structurally related (89,90) suggests that porphyrins may associate with kerogen in a similar manner. Thus, Ni(II) and VO(II) porphyrins may physisorb and/or chemisorb strongly to the kerogen with the VO(II) more strongly associated than the Ni(II) species based on the greater polarity of the former. Philp and Gilbert (90) have also demonstrated that other biomarkers (e.g., gammacerane) are present in kerogens and are not bonded to the kerogen but probably "associate." This process might explain the differences in apparent kerogen affinity of the Ni(II) and VO(II) porphyrin species in sediments.

In the study by Van Berkel and Filby (40), it was shown that a decrease in the Ni(II) porphyrin to VO(II) porphyrin ratio in the bitumen can occur as a result of the generation of metalloporphyrins from kerogen during pyrolysis, but the change in this ratio depends on the composition (i.e., nickel and vanadium contents) of the kerogen.

(iii) Alkylation/Dealkylation. During late diagenesis and catagenesis the sedimentary porphyrins are found to exist as homologous series (4,31,34) with carbon numbers well below and above the expected C<sub>32</sub> predicted by the Treibs scheme (Figure 1). Among the first explanations for the extended carbon numbers were transalkylation (31) and evolution of porphyrins from bacteriochlorophylls (e.g., Chlorobium) that exist as homologous series (31,33). It has been shown in laboratory experiments (37,51,76,77) that the molecular weights of the geoporphyrins decrease as thermal stress is increased as a result of alkyl cleavage from the porphyrin macrocycle and, concurrently, higher carbon number porphyrins are produced in the sample via a transalkylation process. Quirke et al. (34) showed that the substitution pattern on the maleimides from Boscan oil showed a predominant methyl, n-alkyl pattern indicating a specific process was involved in extending alkylation. Transalkylation would be expected to produce a random alkylation pattern on the porphyrins. As mentioned earlier, the Chlorobium chlorophylls do not have an alkylation pattern consistent with the extended porphyrin homologues for which structures have been determined.

Thermal cracking of porphyrins chemically bound to the kerogen matrix has been suggested (7,34) to account for the higher homologues. Oehler et al. (91) have shown that tetrapyrrole complexes can become "grafted" onto cellular macromolecules. These complexes may then be incorporated into the proto-kerogen matrix during kerogen formation. Assimilation of porphyrin precursors or immature metalloporphyrins into kerogen during diagenesis could take place through alkyl (e.g., anti-Markovnikov addition to the kerogen to the vinyl group on the porphyrin precursor, 34) or carbonyl substituents (i.e., ester and ether linkages, 5,7,61), for example. Breakdown of kerogen during catagenesis might release these complexes in discrete form or bound to fragments of kerogen (i.e., asphaltenes). However, preliminary data from the pyrolysis of kerogen (40) shows no indication that the porphyrins generated during kerogen catagenesis are chemically bound to the matrix via C-C bonds. This is based on the observation that porphyrin homologs generated from the kerogen extend to carbon numbers no higher than those porphyrins present in the bitumen (83). Comparison of the alkyl substitution patterns on the two sets of

porphyrins would be a better indication of a bonding mechanism since these should differ for the porphyrins which were bound to the kerogen compared to those present in a free state in the bitumen or associated with the kerogen by a mechanism other than direct chemical bonding.

In summary, the mode of association of the porphyrins with the kerogen has not been determined; some possible mechanisms are:

(a) Physisorption/chemisorption of discrete porphyrins.

(b) Chemical bonding of porphyrins or their precursors to the kerogen matrix through alkyl, ester linkages, etc., or through axial bonding to the metal ion.

(c) Molecular sieve trapping of discrete porphyrins or their precursors in the relatively open kerogen polymeric structure.

(iv) Very High Molecular Weight Porphyrins and Alternate Porphyrin Series. Several workers have reported high molecular weight Ni(II) and VO(II) porphyrin-type complexes in size exclusion chromatographic (SEC) fractions of asphaltic material (92,93). Blumer and Rudrum (93) isolated tetrapyrrole complexes of high molecular weight (>1000 daltons) as dimers, and a homologous series of complexes with MW>20,000 was isolated from a Triassic oil shale (92). However, it is debatable whether these latter species are discrete high molecular-weight porphyrins. Nguyen and Filby (88) have shown that Ni(II) DME adsorbed (or chemisorbed) onto asphaltenes from a chloroform solution is distributed throughout the asphaltene molecular-weight ranges (from >8000 to <1000) during SEC separation. Hence, SEC separations do not separate porphyrin species from high molecular-weight bitumen components with which they are chemically associated.

The THBD and benzo-porphyrins (usually minor components) have been identified in several studies as the Ni(II) or VO(II) complexes. Baker and Louda (7) proposed initially that these complex porphyrins were originally bound to the kerogen matrix. For example, the benzo-porphyrins could arise from a Diels-Alder type addition with a quinone type structure in the bitumen or kerogen (4), or by condensation of side chains on the porphyrin precursor during diagenesis (7,47). The formation of both the THBD and benzo-DPEP species can be rationalized by a diagenetic scheme in which the tetrahydrobenzo-porphyrin is formed from a functionalized chlorophyll precursor via external cyclization. Subsequent aromatization of the newly-formed six-membered ring with increased thermal maturation produces the benzo-porphyrin. However, it is not clear which species originates first, and if, in fact, interconversion via hydrogenation/dehydrogenation actually takes place. The placement of the exocyclic ring of the THBD (47) and benzo-DPEP (45) species on different positions of the porphyrin macrocycle argues against this hypothesis (46,48). The presence of these porphyrins in immature sediments as free-base forms indicates that the exocyclic ring formation mechanism does not necessarily involve kerogen binding but does point to the importance of mineral surfaces in promoting such reactions. Catalytic addition and rearrangement of porphyrin precursors and porphyrins on mineral surfaces as a source for these alternate series is an area of porphyrin geochemistry which should be given more attention. A schematic diagram of the possible porphyrin pathways in kerogen is shown in Figure 5. Not included in this diagram are possible reactions of metalloporphyrins involving the kerogen-mineral interface.

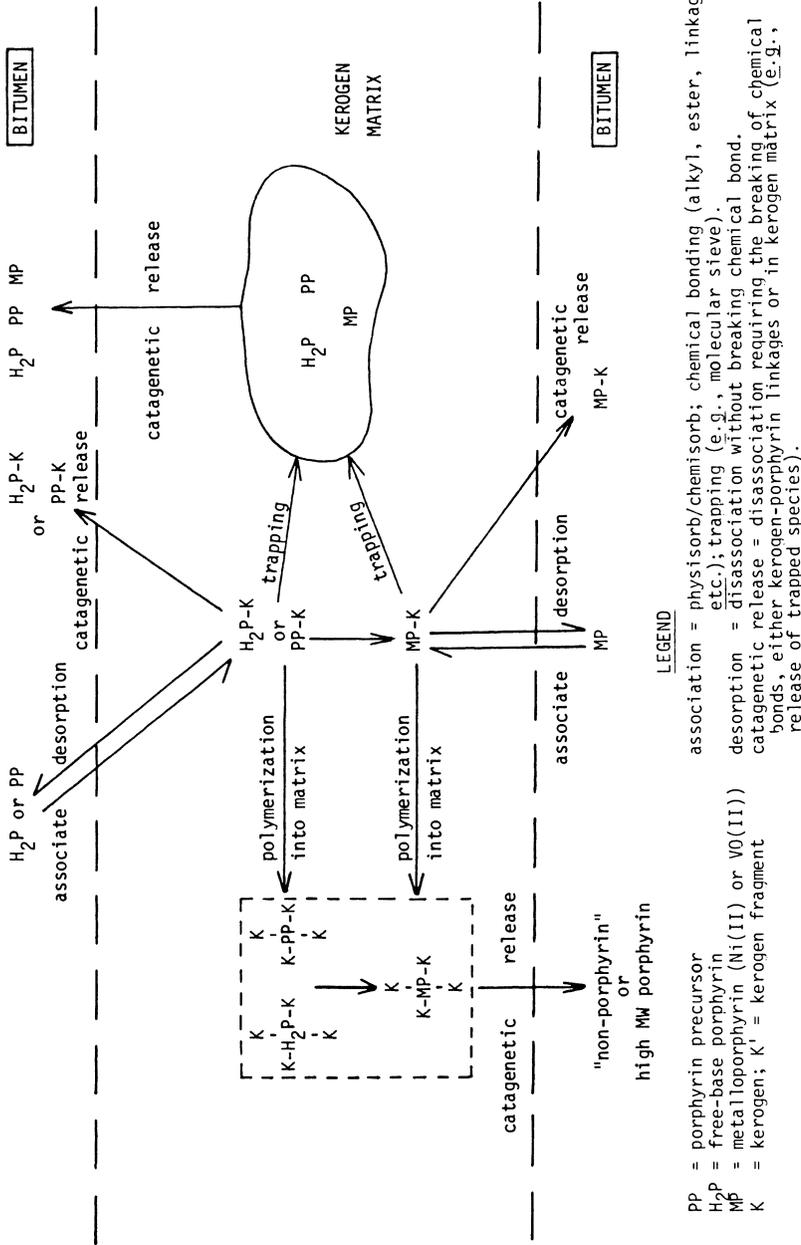


Figure 5. Suggested kerogen-porphyrin association mechanisms.

The Effect of Petroleum Migration on Metalloporphyrin Distributions.

The mechanism of mobilization of bitumen in a source-rock and migration of a crude oil to a trap or reservoir has not been adequately explained and is still controversial (19,94,95). Two major stages are involved; these may be defined as: (i) primary migration in which dispersed bitumen migrates within the source rock to form discrete oil globules, ultimately leading to expulsion of oil from the source rock into more porous pathways; and (ii) secondary migration of this oil into traps or reservoirs (94). Neither process is well understood and the behavior of metalloporphyrins in the source rock bitumen during migration is essentially unknown.

Durand (94) and Leythaeser *et al.* (95) have concluded that the primary migration stage involves a number of chromatographic effects that act on bitumen components. Leythaeser *et al.* (95) have shown that the main stage of primary migration is probably preceded by an early stage of oil expulsion in which strong chromatographic effects result from a complex hydrocarbon-water-mineral phase interaction. Thus, the early migrating fluid front is enriched in light, less polar, hydrocarbons and the residue remaining in the source rock is composed of more polar higher molecular-weight species. Although the metalloporphyrins were not studied in this investigation, fractionation would be expected to occur based on porphyrin polarity and relative affinity for mineral surfaces. The overall effect on a short time scale (*i.e.*, equivalent to that observed in a chromatographic column) is to produce an oil which contains lower proportions of polar compounds (*e.g.*, asphaltenes and more polar porphyrins) than does the associated source-rock bitumen. However, migration on a geological time scale, or over large distances, in which a barrier may be eventually reached, will eliminate such chromatographic effects (*i.e.*, equivalent to complete elution from a column into a reservoir). Chakhmachkev *et al.* (96) have attempted to simulate geologic migration of porphyrins in the laboratory by passing an oil with a high VO(II) porphyrin content through clay-sand columns. These authors found that polar VO(II) porphyrins were retained on the column relative to non-polar VO(II) porphyrins (not defined) and that the DPEP/etio ratio in the initial effluents were lower than the crude oil ratio, as expected from polarity considerations. However, no systematic variation was noted in later effluents. Although no explanation was given, the variation in the DPEP/etio may have resulted from a combination of increased polarity of DPEP versus etio for a given carbon number and the increase in polarity for a given series with decreasing alkyl substitution. The authors attributed the changes in the DPEP/etio ratio of the VO(II) porphyrins in the W. Surgut oils studied by Burkova *et al.* (97) to lateral migration effects within the W. Surgut dome. Burkova *et al.* (97) also concluded that chromatographic effects during migration resulted in the least migrated Pravda oil containing virtually no non-polar VO(II) porphyrins while the genetically related most migrated W. Surgut oils are depleted in polar VO(II) porphyrins. Further work on the mechanism of porphyrin-substrate interactions during oil migration is obviously needed.

Although chromatographic effects change the original metalloporphyrin distribution of a bitumen during migration, it may be possible to "reconstruct" the porphyrin distributions of the source-rock bitumen by examination of the porphyrin contents of the source-

rock bitumen and crude oil asphaltenes. Several authors have shown that biomarkers can be transported by asphaltenes in a crude oil and protected from biodegradation after emplacement in a reservoir and that these biomarkers can be liberated by pyrolysis (98,99). Porphyrins retained within the asphaltene micelles of migrating oils may be similarly protected from chromatographic effects and may not have been subjected to fractionation as may have the "free" porphyrins present in the hydrocarbon (maltenes) fraction. The application of metalloporphyrin distributions to migration problems is discussed further by Branthaver and Filby (100) in this volume.

Metalloporphyrins in Crude Oils. As products of kerogen maturation within the "oil window," crude oils contain metalloporphyrins that reflect the catagenetic stage of porphyrin evolution. Although there is a recent report of a Fe(II) DPEP porphyrin in a Fe-rich Venezuelan oil (101), the porphyrins in crude oils are almost entirely the defunctionalized Ni(II) and VO(II) etio-, DPEP-, and minor-series (THBD, benzo-etio, benzo-DPEP). The Fe(II) porphyrin reported by Franceskin *et al.* (101) was separated from Jobo (Venezuela) crude oil and was characterized by Mossbauer, UV, and mass spectrometry. The data presented, however, cannot be interpreted as conclusive identification because the Mössbauer chemical shift and quadropole-splitting parameters are consistent with Fe(III) inorganic salts and the UV data are similar to those for Ni(II) porphyrins. Also, the MS data are consistent with Ni(II) THBD. Mass spectra are not shown, hence isotopic clusters which are different for Ni or Fe porphyrins cannot be compared. Thus, the only porphyrins that have been identified in crude oils are those that have been identified in sedimentary sequences. Free-base porphyrins are generally of very low abundance (5,7) and although metalloporphyrin carboxylic acids have been reported in younger (Pliocene, Miocene, Cretaceous) crude oils (102,103), it is not clear whether they are of primary origin. Baker and Louda (5,7) have shown that thermal decarboxylation of porphyrin species in sediments should occur below 60°C, *i.e.*, below the "oil window" (50-150°C approximation) where catagenesis takes place. The presence of carboxylated metalloporphyrins may thus be secondary and result from incorporation into the migrating petroleum from less mature sedimentary sequences in the migration pathway.

The presence of very high molecular-weight porphyrins (*i.e.*, >1000 daltons) in crude oils and oil shales has been reported by several authors (92,93,104,105). Blumer and Snyder (92) reported porphyrin-type UV spectra in components of a Triassic oil shale with MW up to 20,000 daltons and dimeric species of metalloporphyrins have been identified (93). There is also evidence that very high molecular-weight porphyrins in crude oils are alkyl porphyrins, similar to those species found in crude oils, and that these associate with high molecular-weight polar species (*i.e.*, asphaltenes) in crude oils, as discussed previously.

Although Treibs (11,12,14) reported the presence of VO(II) porphyrins in 66 crude oils, there have been no systematic studies reported of the abundances of metalloporphyrins in crude oils as a function of the depositional environment of the source material, age of source rocks, locality, or crude oil composition. Table I summarizes some representative Ni(II) and VO(II) porphyrin contents

Table I. Ni, V, Ni(II) Porphyrin (NiP), VO(II) Porphyrin (VOP), and Total Porphyrin Contents (MP) of Crude Oils

Sample Locality	Age	NiP		VOP		MP (ppm) <sup>c</sup>	Reference
		Ni (µg/g) <sup>a</sup>	Ni (µg/g) <sup>b</sup>	V (µg/g) <sup>a</sup>	V (µg/g) <sup>b</sup>		
Morinville, Canada	Devonian	2.8	0.4	2.2	0.4	80	102
Duhame1, Canada	Devonian	3.9	0.9	2.9	1	18	102
Lac St. Anne, Canada	Devonian	27	1.6	84	17	190	102
Daly, Canada	Mississippian	5.3	0.1	7.0	1.3	15	102
Roselea, Canada	Mississippian	2.9	0.1	4.3	0.7	8	102
Coleville, Canada	Mississippian	5.0	2.7	13.3	20	235	102
Wapella, Canada	Jurassic	17.0	3.3	29.8	10.4	140	102
Centaur, Canada	Jurassic	52.3	4.4	135	16	205	102
Eastend, Canada	Jurassic	33.0	7.4	83.5	27	355	102
Pravda, USSR	Cretaceous	-	-	-	9.2	9.9	97
W. Surgut, USSR	Cretaceous	-	-	-	24	264	97
W. Surgut, USSR	Cretaceous	-	-	-	6.6	72	97
Pembina, Canada	Cretaceous	0.8	trace	0.4	trace	-	102
Lloydminster, Canada	Cretaceous	48	2	105	21	240	102
Athabasca, Canada	Cretaceous	71	2.5	184	55	500	106
Athabasca, Canada	Cretaceous	75	<10	196	93	980	49
Boscan, Venezuela	Cretaceous	110	-	1200	320	3500	31
Mara, Venezuela	Cretaceous	-	-	-	-	300	31
Belridge, Calif.	Cretaceous	-	-	-	-	3100	31
La Paz, Venezuela	Cretaceous	-	1.0	-	58	628	107
Yabase, Japan	Tertiary	5.0	7.0	1.0	2.2	88	102
Ishinazaha, Japan	Tertiary	15.0	5	11.0	5.1	108	102
Chokaizen, Japan	Tertiary	50.0	5.2	170	1.6	64	102

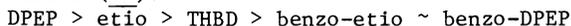
<sup>a</sup>Expressed as µg metal per g oil (*viz.* elemental, total).

<sup>b</sup>Expressed as µg metal as porphyrin per g oil.

<sup>c</sup>Expressed as µg metalloporphyrin per g oil.

in crude oils. These data show the metalloporphyrin contents of oils range from those with only trace quantities (e.g., Roselea, Pravda) to those with very large porphyrin contents (e.g., Boscan). It should be pointed out that many of the porphyrin contents reported in Table I are only approximate. Quantitative determination of metalloporphyrin concentrations in crude oils is difficult, particularly when determined by UV-visible spectroscopy, and the results depend on the extraction or separation methods used. Metalloporphyrins associate with asphaltenes (49,88) in petroleum and the effective molar absorptivity ( $\epsilon$ ) of a metal complex associated with an asphaltene micelle is much lower than that of an associated porphyrin (49,108). Demetallation procedures followed by determination of free-base porphyrins may also give incomplete conversion of those porphyrins associated with the asphaltene matrix because of the inability of methanesulfonic acid, for example, to diffuse completely into the asphaltene structure. It should also be noted that the percentage of total metal as metalloporphyrin varies greatly from oil to oil and is different for nickel and vanadium. From the data in Table I it can be calculated that the percentage nickel as Ni(II) porphyrin varies from 2 to 54%; the corresponding values for vanadium as VO(II) porphyrin are 1 to 47%. Baker and Louda (7) present nickel and vanadium data on nineteen oils from the Big Horn Basin, Wyoming and the Monterey Formation, California. These oils covered a wide range of maturities. The mean percentages of nickel and vanadium present in porphyrin forms were 7.2% and 12.4%, respectively. These data show that, in general terms, the readily extractable porphyrins account for a small fraction of the total metal content of the oil.

The Boscan oil, a heavily biodegraded, high sulfur Cretaceous oil from Venezuela, has been the most studied (31,34,109-114) because of its very high VO(II) porphyrin content (approximately 3500  $\mu\text{g V/g oil}$ ). The VO(II) porphyrins in this oil occur in the abundance series (31):



This oil contains both DPEP and etio-porphyrins which are present in wide carbon number ranges (25 to greater than 40 carbons) typical of porphyrins extracted from mature sediments. Quirke *et al.* (115) have recently shown (by MS/MS) that Boscan oil contains complex non-polar porphyrins with up to 48 carbons and that these unusual porphyrins are benzo-porphyrins with no pyrrole-ring alkyl substituent greater than  $\text{C}_1$ . Whether these contain more than one benzo-ring or are substituted on the monobenzo-ring is not clear, but they represent a minor species in Boscan that cannot be directly related to specific chlorophyll precursors and, to date, have not been identified in sedimentary sequences. The abundances of the minor porphyrin series in crude oils have been determined only in oils with relatively high porphyrin contents, e.g., Boscan and Athabasca oil sand (31,49), but they probably occur in many crudes.

The genetic relationships among the DPEP and etio-porphyrins and the relationship between the Ni(II) and VO(II) species discussed in the section on the evolution of porphyrins in maturing sediments is reflected in the nature of the porphyrins in crude oils, although no systematic studies of the interrelationships among the porphyrin types in crude oils or comparisons with sedimentary porphyrins have been reported. It is apparent from the crude oil data shown in

Table I that a generalization cannot be made as to the Ni(II) to VO(II) porphyrin ratio as a function of source-rock or reservoir age, as has been made by Mackenzie et al. (38) for sedimentary sequences. Several authors (116-118) have attempted to correlate Ni/V ratios in oils with age, but the results are conflicting (104,119). The decrease in the Ni(II) to VO(II) porphyrin ratio with increasing maturation in sediments (22) has not been confirmed for crude oils; Hodgson (116) concluded the opposite from studies of oils from the W. Canada Basin. As Mackenzie et al. (38) have pointed out for sedimentary sequences, the Ni(II) to VO(II) porphyrin variation with age depends on a) the relative thermal stabilities of Ni(II) and VO(II) porphyrins, and b) the acid-catalyzed demetallation stabilities of the porphyrins. For crude oils, these relative effects will be different compared to the sedimentary environment because mineral-catalyzed reactions may be less significant. In addition, another important factor may be demetallation caused by H<sub>2</sub>S released during oil maturation in the reservoir.

There is also no obvious correlation of the DPEP/etio ratio of crude oil porphyrins with reservoir age, as shown in Table II. However, Yen and Silverman (120) have concluded that the DPEP/etio ratio for a number of unrelated crude oils does show a decrease with depth. Barwise and Park (79), on the other hand, have presented qualitative data on four oils generated from the same source rock but reservoirized at different depths (no locations or age cited). The HPLC chromatograms of the demetallated porphyrins show a decrease in the DPEP/etio ratio with depth, but the authors point out that the shallower oils have been extremely biodegraded. If thermal conversion of DPEP- to etio-porphyrins does not occur, the change in the DPEP/etio ratio of oils maturing in reservoirs must be the result of preferential degradation of DPEP-porphyrins (thermal decomposition, demetallation, etc.) relative to the etio species. It is clear that further work needs to be done on the effect of maturation of crude oils on the metalloporphyrin distributions in order that comparisons can be made with the diagenetic-catagenetic pathways that are better documented in sediments.

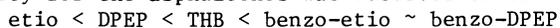
Metalloporphyrins in Crude Oil Components. The distribution of Ni(II) and VO(II) porphyrins among the components of a crude oil or bitumen is of direct significance to oil-oil and oil-source correlations and, in particular, to metalloporphyrin behavior during migration and petroleum alteration processes. Metalloporphyrins distribute among petroleum components during such fractionation processes as asphaltene precipitation (31,111), distillation (103), and chromatographic separation (13) based either on functionality or molecular weight. A major problem in the quantitative determination or isolation of porphyrins in crude oils is the difficulty of separating the porphyrins from other petroleum components, particularly from the asphaltenes with which strong chemical associations are formed (121-123). Baker and Palmer (4) have shown that the DPEP/etio ratio of Boscan porphyrins is different for the porphyrins in the maltenes and for the porphyrins when demetallated and extracted from the total crude oil. Although this comparison is between VO(II) porphyrins and total porphyrins, the comparison is valid because the VO(II) porphyrins are of much greater abundance than the Ni(II) porphyrins in

Table II. DPEP to Etio Ratios of Some Crude Oils of Different Ages

Oil	Geologic Age	DPEP/etio	Reference	Oil	Geologic Age	DPEP/etio	Reference
Alberta	Devonian	2.0	(5)	Boscan <sup>a</sup>	Cretaceous	1.2	(5)
Grosmont <sup>a</sup>	Devonian	2.9	(137)	Burgan	Cretaceous	0.7	(5)
Tensleep	Pennsylvanian	1.3	(5)	Athabasca <sup>a</sup>	Cretaceous	1.8	(49)
Boundary Lake	Triassic	0.22	(49)	Cold Lake <sup>a</sup>	Cretaceous	1.4	(49)
Regusa	Triassic	3.1	(5)	Peace River <sup>a</sup>	Cretaceous	1.6	(49)
Gela	Jurassic	2.4	(5)	La Paz <sup>a</sup>	Cretaceous	0.56	(107)
Pravda <sup>a</sup>	Jurassic	0.2	(97)	W. Surgut <sup>a</sup>	Cretaceous	0.49	(97)

<sup>a</sup>DPEP/etio measured for V0(II) porphyrins; others from total demetallated porphyrins.

Boscan oil (Table I). Didyk *et al.* (107) also reported that the DPEP/etio ratio of demetallated porphyrins (predominantly VO(II)) from the asphaltenes of the La Paz Cretaceous oil (Table II) is approximately twice that of the crude oil (0.96 vs 0.56) and that the carbon number range was smaller. Didyk *et al.* (107) interpreted these results to indicate a distribution based on porphyrin polarity. Strong and Filby (49) have investigated the distribution of VO(II) porphyrins (DPEP, etio, THBD, benzo) in Athabasca oil sand bitumen and components. They observed that the distributions of the porphyrin types in the porphyrin aggregate (extraction of oil with toluene-methanol), the maltenes, an *n*-pentane extract of the asphaltenes (resins), and a methanol-acetone extract of the asphaltenes were different and could be explained on the basis of VO(II) porphyrin affinity for the asphaltenes, equating approximately to porphyrin polarity, which is dependent upon a) presence or absence of an isocyclic ring, b) carbon number (*viz.* degree of alkylation), and c) the number of unsubstituted  $\beta$  positions (34,61). The approximate order of affinity for the asphaltenes was observed to be:



The metalloporphyrins distribute in a crude oil or bitumen between the low polarity, low molecular weight hydrocarbon bulk phase and the asphaltene micelles in the oil which contain both high molecular weight non-polar and low molecular-weight polar species. The DPEP/etio ratio changes in the transition from a very polar asphaltene core (highest DPEP/etio) through the intermediate polarity outer region of the micelle to the bulk low polarity hydrocarbon phase (lowest DPEP/etio ratio). The association of the porphyrins with the asphaltenes appears to be based on polarity, and probably is an expression of  $\pi$ - $\pi$  interactions and/or functional group bonding to the metal ion as suggested by Yen (104) and by Nguyen and Filby (88). The latter authors showed that Ni(II) mesoporphyrin IX dimethyl ester (labeled with  $^{63}\text{Ni}$ ) and Ni(II)OEP added to a toluene solution of Athabasca oil sand bitumen distributed between the asphaltenes and the maltenes with the Ni(II)DME adsorption greater than that of Ni(II)OEP. Separation of the asphaltenes into molecular weight fractions by GPC showed that Ni(II)DME was distributed among all molecular weight fractions in a similar pattern to that observed for the inherent Ni content (porphyrin and non-porphyrin) of the asphaltenes. Thus, the observation of porphyrin UV spectra in high molecular weight asphaltene fractions (92,93,106) does not necessarily imply metalloporphyrins of unusual structure (104).

Effects of Biodegradation on Porphyrins in Oils. The effects of biodegradation and associated water washing on porphyrin distributions have also not been fully investigated. Barwise and Park (79) concluded that biodegraded oils from a maturation sequence had total demetallated porphyrin distributions (*e.g.*, DPEP/etio ratios) similar to those of related non-degraded oils of similar maturity, although no quantitative data were presented. Palmer (124) studied the VO(II) porphyrins from a series of genetically related highly degraded seep oils, reservoir biodegraded, and non-degraded oils from Colombia. She found that the DPEP/etio ratios, the series maxima ( $C_{31}$  for DPEP,  $C_{29}$  for etio) and the carbon number ranges were very similar for the three related oils. She did notice, however, that in the most degraded seep oil the VO(II) porphyrins were enriched relative to

Ni(II) porphyrins compared with non-degraded oils. It is not clear, however, whether this enrichment is a result of selective biological processes (selective degradation of Ni(II) porphyrins), of selective dissolution by associated water washing, or of selective oxidation of Ni(II) porphyrins relative to the VO(II) species. Strong and Filby (49) have also concluded that biodegradation had little effect on VO(II) porphyrin distributions in the highly degraded Alberta oil sands.

Metalloporphyrins in Coals. Three major differences are exhibited by the porphyrins in coals compared to those found in petroleum and petroleum source rocks:

i) The coal metalloporphyrins appear to be chelates only of trivalent Fe(III), Ga(III), and Mn(III), compared to the divalent ions Ni(II) and VO(II) of petroleum metalloporphyrins (9,23,24,26).

ii) The abundances of the metalloporphyrins in coals are very much lower than for most crude oils--typically less than 10 µg metalloporphyrin/g-coal (9,23-26).

iii) The coal porphyrins are almost entirely etio-species, with the exception of traces of DPEP in some low-rank bituminous coals (9,25) and lignites (125,126).

Because of their low abundances, the coal porphyrins have received much less attention than have their petroleum counterparts. The presence of trivalent metal ions in the coal porphyrins is evidence of metallation conditions considerably more oxidic than found in marine sedimentary environments in which the divalent Ni(II) and VO(II) porphyrins predominate. This observation, plus the very low metalloporphyrin abundances in coals, is evidence that in the terrestrial environment in which coals form, most of the chlorophylls are degraded. Although Palmer *et al.* (25) have concluded that the etio-porphyrins found in coals have been derived from chlorophylls via early oxidative cleavage of the isocyclic ring, Bonnett *et al.* (126) have presented convincing evidence that cytochromes may be important precursors to the Fe(III) porphyrins in coals. They identified Ga(III), Mn(III), and Fe(III) porphyrins in a Turkish lignite (e.g., 30 µg total porphyrins/g-coal), with the Fe(III) species accounting for 95% of the porphyrins. Small amounts of free-base porphyrins and chlorins were identified. The Fe(III) species were shown to contain a mono- and a di-carboxylic acid and the latter was suggested to be the Fe(III) complex of mesoporphyrin-IX (based on comparison of the methyl ester with synthetic Fe(III) mesoporphyrin-IX dimethyl ester). The probable diagenetic pathways for the coal porphyrins are shown in Figure 6, based largely on the work of Bonnett *et al.* (126).

Bonnett *et al.* (9) and Palmer *et al.* (25) have shown that, in general, the abundances of porphyrins in coals decrease with coal rank and are virtually absent from anthracites. Thus, as coalification proceeds from peats through sub-bituminous coals, to bituminous coals, the abundance of the carboxylated porphyrins decrease rapidly, the Fe(III)/Ga(III) porphyrin ratio decreases, and the weighted mean of the molecular masses decreases. The origin of the metal ion in coal porphyrins is, at present, obscure. Bonnett *et al.* (9) have suggested that, because Ga(III) porphyrins are found in coals and not in biological systems, the Ga<sup>3+</sup> ion (as GaOH<sup>2+</sup>) is secondary and thus the Fe<sup>3+</sup> ion found in the Fe(III) etio-porphyrins in coal may not be the biological Fe<sup>3+</sup> ion present in the heme precursor.

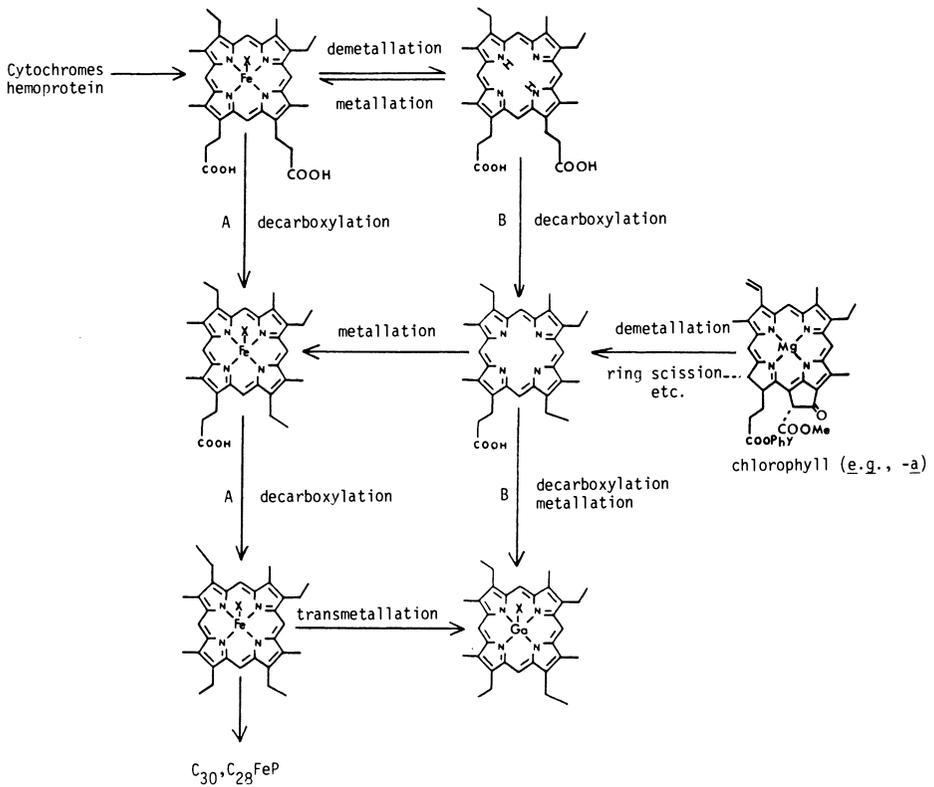


Figure 6. Possible diagenetic pathways of geoporphyrins in coals (modified from 126, 25). Pathway A: biochemical  $\text{Fe}^{3+}$  retained. Pathway B: precursor demetallation;  $\text{Fe}^{3+}$  inserted geochemically.

In Figure 6, the two pathways are shown as A (biochemical  $\text{Fe}^{3+}$  retained) and B (demetallation followed by re-insertion of  $\text{Fe}^{3+}$ ). However, the fact that the  $\text{Fe(III)/Ga(III)}$  porphyrin ratio decreases with coalification may also indicate a transmetallation process, or the greater stability of  $\text{Ga(III)}$  porphyrins. Gallium is thought to occur in coals associated in the clay mineral fraction (127) and the mineral surface may act as the source of  $\text{Ga(III)}$  for the metallation or transmetallation of a precursor to form the  $\text{Ga(III)}$  porphyrin.

Bonnett *et al.* (126) have proposed that a "Porphyrin Index of Coalification" be used as a measure of coal rank. This index is calculated from the weighted mean of the porphyrin molecular masses determined by mass spectrometry (*cf.*, 25).

#### Non-Porphyrin Metal Complexes: Geochemical Significance

The previous discussion has focused on  $\text{Ni(II)}$ ,  $\text{VO(II)}$ ,  $\text{Fe(III)}$ ,  $\text{Ga(III)}$  and  $\text{Mn(III)}$  porphyrins in crude oils, coals, and in sedimentary sequences containing maturing organic matter. However, many other trace elements are present in crude oils (104,105) and although trace element distributions have been used for geochemical correlations, as discussed elsewhere in this volume (100), the chemical nature of the metal species is not known. Some of the trace element content of most crudes may be present in associated mineral matter, entrained formation waters or present as salts of organic acids. Most of the trace element content of crude oils is apparently associated with the asphaltic component (105) and the possibility of complexation of metal ions into the asphaltenes structure has been proposed (104-106).

During the initial stages of sedimentation, organic substances undoubtedly play an important role in metal ion transport and speciation (128,129) and a large number of simple organic compounds (*e.g.*, amino acids, quinones, *etc.*) have been shown to form metal complexes in sediments (130). However, probably more important in metal speciation are the humic substances that have large capacities for metal complexation (131) and which may be precursors to kerogen. This aspect of metal-organic geochemistry is beyond the scope of this article and has been reviewed by Saxby (130).

Of considerable geochemical interest are the methyl- and phenyl-arsonic acids identified by Fish and Brinckman (132) in methanol extracts of Green River oil shale. These compounds are the only examples of true organometallic compounds (*i.e.*, containing carbon-metal bonds) identified in fossil fuels. These compounds may not, however, be of primary origin (*i.e.*, formed in the early diagenesis stage) and may have formed by kerogen catagenesis products reacting with the mineral skutterudite ( $\text{Co,Fe,Ni}$ ) $\text{As}_4$  present in the shale (133). Jaganathan *et al.* (133) suggested an organic-matter-skutterudite reaction to account for the formation of organoarsenicals during oil-shale retorting.

The recognition that most crude oils contain nickel and vanadium in porphyrin and non-porphyrin forms (associated predominantly with the asphaltenes) has led to efforts to identify the non-porphyrin species. As stated previously, the extractable metalloporphyrins normally account for a small fraction of the total nickel and vanadium contents of crude oils. Branthaver (119) in this volume has reviewed much of the evidence for true non-porphyrin nickel and vanadium

species, as opposed to the concept of the non-porphyrin species being porphyrins strongly associated with asphaltenes and which do not exhibit typical spectroscopic properties or yield free-base porphyrins with typical demetallation procedures. The existence of non-porphyrin species has not been conclusively established because no non-porphyrin nickel or vanadium complexes have been unequivocally identified in petroleum constituents. Erdman and Harju (134) and Nguyen and Filby (88) have shown that petroleum asphaltenes are capable of complexing large amounts of VO(II), Cu(II) and Ni(II), but the nature of the complexing ligands in the asphaltenes has not been determined. It seems unlikely, however, that these ligands are free-base porphyrins. Asphaltenes contain a number of heteroatom functionalities (e.g., phenolic-OH, ring-N, etc.) that are good ligands for the formation of complexes of transition metal ions.

Because no non-porphyrin complexes of nickel and vanadium have been identified in crude oils or source-rock bitumens, the origin and geochemical significance of the non-porphyrin nickel and vanadium in crude oils cannot be assessed. The fact that the most abundant organically combined non-porphyrin metals in crude oil asphaltenes are normally nickel and vanadium suggests a genetic relationship between the porphyrin and non-porphyrin species. Yen (104) has suggested that the non-porphyrin complexes may in fact be metallo-porphyrin degradation products that remain associated with the asphaltene structure. Although non-porphyrin nickel and vanadium species may occur in crude oils, asphalts, etc., their presence in the bitumens of maturing sediments has not been established. There may, in fact, be a genetic relationship between non-porphyrin nickel and vanadium species in kerogens from maturing sediments and those present in source rock bitumens and crude oils as has been demonstrated for the metalloporphyrins (40).

### Conclusions

The geochemical evolution of the DPEP-porphyrins is consistent with the scheme proposed by Treibs in 1936. Subsequent modifications to the scheme include the identification of other chlorophyll (-b, -c) and bacteriochlorophyll (-a, -b, -d) precursors and the recognition of similar pathways for etio-porphyrins in which isocyclic ring opening of a DPEP precursor occurs early in diagenesis. The latter concept is more strongly supported by the available evidence than the DPEP to etio-porphyrin conversion originally proposed by Corwin. Chlorophylls appear to be the major precursors for the M(III) metallo-porphyrins in coals, although cytochromes may contribute to the precursors to Fe(III) porphyrins.

Despite much recent progress in porphyrin geochemistry, there are several aspects that require further investigation.

1) The origin of the etio-porphyrins has not been conclusively determined. The major pathway of etio-porphyrin evolution in sediments appears to be oxidative isocyclic-ring opening on DPEP precursors during early diagenesis rather than thermal conversion of DPEP to etio-porphyrins. The decrease in the DPEP/etio ratio with increasing thermal stress in sediments or crude oils appears to result from the preferential degradation of DPEP relative to etio-porphyrins. This effect is greater for Ni(II) porphyrins than for VO(II) porphyrins. Further research on the DPEP-etio-porphyrin

relationship is warranted by the use of DPEP/etio ratios in correlation, maturity, and sedimentary environment reconstruction studies.

ii) The relationship between the chemistry of the depositional environment and metal speciation of the geoporphyrins needs to be better substantiated. Evidence indicates that highly reducing, H<sub>2</sub>S-rich, environments favor the formation of VO(II) porphyrins by inhibiting Ni(II) porphyrin formation through precipitation of NiS. The major factors that control metal speciation, however, have not been determined. In particular, research on the effects of mineral components and organic matter on porphyrin metallation is needed.

iii) The factors that determine porphyrin stability in the geological record are not well known. The mechanisms of thermal degradation, demetallation (either acid catalyzed or H<sub>2</sub>S induced), transmetallation, and dealkylation need to be determined both for porphyrins in sediments as well as in oils. Thermodynamic data on individual porphyrins are largely lacking.

iv) Kerogen appears to play an important role in the sequestering of metallo- or free-base porphyrins (or precursors) and in the subsequent release of metalloporphyrins in catagenesis. Both Ni(II) and VO(II) porphyrins are released from kerogens, as are DPEP and etio species. The stage of kerogen evolution at which porphyrins or their precursors become incorporated needs to be determined. The relative affinities of different kerogen types for the metalloporphyrin classes also need to be measured.

v) Mineral-porphyrin interactions have received little attention. Evidence exists that the highly acidic nature of swelling clay surfaces plays a significant role in porphyrin metallation-demetallation reactions and that such reactions may determine the relative survivals of different metal complexes. Recent work on the mechanisms of mineral-organic matter reactions in petroleum formation should be extended to porphyrin-mineral assemblages.

vi) The origin and the geochemical pathways of the THBD and benzo-porphyrins in sedimentary sequences are, as yet, undetermined. Identification of their precursors and determination of their pathways is of value because of their potential for use in correlation studies.

vii) Despite many published studies, the nature of "non-porphyrin" complexes of Ni(II) and VO(II) in crude oils is virtually unknown. Identification of these species in both oils and source-rock bitumens should provide information on the geochemical pathways of non-porphyrin complexes, if they exist.

viii) The very low concentrations of M(III) metalloporphyrins in coals indicates a depositional environment in which most of the chlorophyll input has been degraded. However, the strong association of Ni(II) and VO(II) porphyrins with oil shale kerogens implies that metalloporphyrins may be present in coals in abundances much higher than reported but, because of their association with coal macerals, cannot be extracted with conventional solvents.

#### Literature Cited

1. Corwin, A.H. Proc. 5th World Petroleum Congress 1960, paper V-10, Section V, 119-29, New York.
2. Dunning, H.N. Intern. Series of Monographs on Earth Sciences 1963, 16 (I.A. Breger, cf), 367-430.

3. Hodgson, G.W.; Baker, B.L.; Peake, E. In "Fundamental Aspects of Petroleum Geochemistry"; Nagy, B. and Colombo, U., Eds.; Elsevier: Amsterdam, 1967; pp. 197-260.
4. Baker, E.W.; Palmer, S.E. In "The Porphyrins"; Dolphin, D., Ed.; Vol. IA; Academic Press: New York, 1978; pp. 486-552.
5. Baker, E.W.; Louda, J.W. In "Advances in Organic Geochemistry, 1981"; Bjorøy, M., Ed.; John Wiley: London, 1983; pp. 401-21.
6. Maxwell, J.R.; Quirke, J.M.E.; Eglinton, G. In "Internationales Alfred Treibs Symposium, 1979"; Prashnowsky, A.A., Ed.; Universitat Wurzburg: Munich, 1980; pp. 37-55.
7. Baker, E.W.; Louda, J.W. In "Biological Markers in the Sedimentary Record"; John, R.B., Ed.; Elsevier: Amsterdam, 1986; pp. 125-225.
8. Chicarelli, I.M.; Kaur, S.; Maxwell, J.R. (this volume).
9. Bonnet, R.; Burke, P.J.; Czechowski, F. (this volume).
10. Treibs, A. Ann. Chem. 1934, 509, 103-14.
11. Treibs, A. Ann. Chem. 1934, 510, 42-62.
12. Treibs, A. Ann. Chem. 1935, 517, 172-96.
13. Quirke, J.M.E. (this volume).
14. Treibs, A. Angew. Chemie 1936, 49, 682-86.
15. Quirke, J.M.E.; Maxwell, J.R.; Eglinton, G.; Sanders, J.K.M. Tetrahedron Lett. 1980, 21, 2987-90.
16. Fookes, C.J.R. J. Chem. Soc., Chem. Commun. 1983, 1472-73.
17. Ekstrom, A.; Fookes, C.J.R.; Hambley, T.; Loeh, H.J.; Miller, S.A.; Taylor, J.C. Nature 1983, 206, 173-74.
18. Gold, T.; Gordon, B.E.; Streett, W.; Bilson, E.; Patnaile, P. Geochim. Cosmochim. Acta 1986, 50, 2411-18.
19. Tissot, B.P.; Welte, D.H. "Petroleum Formation and Occurrence," 2nd Ed.; Springer Verlag: Berlin, 1984.
20. Tissot, B.P. Bull. Am. Ass. Petrol. Geol. 1984, 68, 545-63.
21. Durand, B. In "Kerogen"; Durand, B., Ed.; Editions Technip.: Paris, 1980; pp. 13-34.
22. Baker, E.W.; Louda, J.W. Org. Geochem. 1984, 6, 183-92.
23. Bonnett, R.; Czechowski, F. Nature 1980, 283, 465-67.
24. Bonnett, R.; Czechowski, F. Phil. Trans. Roy. Soc. London Ser. A. 1981, 300, 51-63.
25. Palmer, S.E.; Baker, E.W.; Charney, L.S.; Louda, J.W. Geochim. Cosmochim. Acta 1982, 46, 1233-41.
26. Bonnett, R.; Burke, P.J. Geochim. Cosmochim. Acta 1985, 49, 1487-89.
27. Ocampo, R.; Callot, H.J.; Albrecht, P. J. Chem. Soc., Chem. Commun. 1985, 198-200.
28. Ocampo, R.; Callot, H.J.; Albrecht, P. J. Chem. Soc., Chem. Commun. 1985, 200-201.
29. Ocampo, R.; Callot, H.J.; Albrecht, P. (this volume).
30. Baker, E.W. J. Am. Chem. Soc. 1966, 88, 2311-15.
31. Baker, E.W.; Yen, T.F.; Dickie, J.P.; Rhodes, R.E.; Clark, L.F. J. Am. Chem. Soc. 1967, 89, 3631-39.
32. Thomas, D.W.; Blumer, M. Geochim. Cosmochim. Acta 1964, 28, 1147-54.
33. Holt, A.S.; Purdie, J.W.; Wasley, J.W.F. Can. J. Chem. 1966, 44, 88-93.
34. Quirke, J.M.E.; Shaw, G.J.; Soper, P.D.; Maxwell, J.R. Tetrahedron 1980, 35, 3261-67.

35. Barwise, A.J.G.; Whitehead, E.V. In "Advances in Organic Geochemistry, 1979"; Maxwell, J.R.; Douglas, A.G., Eds.; Pergamon Press: Oxford, 1980; pp. 181-92.
36. Bonnett, R.; Brewer, P.; Noro, K.; Noro, T. J. Chem. Soc., Chem. Commun. 1972, 562-63.
37. Bonnett, R.; Brewer, P.; Noro, K.; Noro, T. Tetrahedron 1978, 34, 379-85.
38. Mackenzie, A.S.; Quirke, J.M.E.; Maxwell, J.R. In "Advances in Organic Geochemistry, 1979"; Maxwell, J.R.; Douglas, A.G., Eds.; Pergamon Press: Oxford, 1980; pp. 239-48.
39. Van Berkel, G.J.; Filby, R.H. In "Geochemical Biomarkers"; Yen, T.F.; Moldowan, J.M., Eds.; Gordon and Breach Publishers: London (in press).
40. Van Berkel, G.J.; Filby, R.H. (this volume).
41. Wolff, G.A.; Murray, M.; Maxwell, J.R.; Hunter, B.K.; Sanders, J.K.M. J. Chem. Soc., Chem. Commun. 1983, 922-24.
42. Chicarelli, M.I.; Wolff, G.A.; Murray, M.; Maxwell, J.R. Tetrahedron 1984, 40, 4033-39.
43. Ocampo, R.; Callot, H.J.; Albrecht, P.; Kintzinger, J.P. Tetrahedron Lett. 1984, 25, 2589-92.
44. Fookes, C.J.R. J. Chem. Soc., Chem. Commun. 1983, 474-76.
45. Kaur, S.; Chicarelli, M.I.; Maxwell, J.R. J. Am. Chem. Soc. 1986, 108, 1347-48.
46. Baker, E.W.; Louda, J.W. Org. Geochem. 1986, 10, 904-14.
47. Barwise, A.J.G.; Roberts, I. Org. Geochem. 1984, 6, 167-76.
48. Quirke, J.M.E.; Yost, R.A.; Britton, E.D.; Trichet, J. In "Geochemical Biomarkers"; Yen, T.F.; Moldowan, J.M., Eds.; Gordon and Breach Publishers: London (in press).
49. Strong, D.; Filby, R.H. (this volume).
50. Glebovskaya, E.A.; Volkenstein, M.V. J. Gen. Chem. (USSR) 1948, 18, 1440-51.
51. Didyk, B.M.; Alturki, Y.I.A.; Pillinger, C.T.; Eglinton, G. Nature 1975, 256, 563-65.
52. Burkova, U.N.; Ryadova, O.V.; Serebrennikova, O.V.; Titov, V.I. Geokimiya 1980, 9, 1417-21.
53. Bonnett, R.; Burke, P.J.; Rezka, A. J. Chem. Soc., Chem. Commun. 1983, 1085-87.
54. Fookes, C.J.R. J. Chem. Soc., Chem. Commun. 1985, 706-8.
55. Shiobara, M.; Taguchi, K. In "Advances in Organic Geochemistry, 1975"; Campos, R.; Coni, J., Eds.; ENADISMA: Madrid, 1977; pp. 237-51.
56. Zellmer, P.P.; Man, E.H. Org. Geochem. 1983, 5, 43-49.
57. Zellmer, P.P.; Man, E.H. Org. Geochem. 1984, 7, 223-29.
58. Palmer, S.E.; Baker, E.W. Science 1978, 201, 49-51.
59. Manskaya, S.M.; Drozdova, T.V. "Geochemistry of Organic Substances"; Pergamon Press: Oxford, 1968.
60. Lewan, M.D.; Maynard, J.B. Geochim. Cosmochim. Acta 1982, 46, 2547-60.
61. Quirke, J.M.E. (this volume).
62. Lewan, M.D. Geochim. Cosmochim. Acta 1984, 48, 2231-38.
63. Moldowan, J.M.; Sundararaman, P.; Schoell, M. Org. Geochem. 1986, 10, 915-26.
64. Robertson, J.M. J. Chem. Soc. 1936, 1195-1209.
65. Buchler, J.W. In "Porphyrins and Metalloporphyrins"; Smith, K.M., Ed.; Elsevier: Amsterdam, 1975; pp. 157-237.

66. Johns, W.D. Ann. Rev. Earth Planet Sci. 1979, 7, 183-98.
67. Whitacher, A.H.; Dyson, P. Oil and Gas J. 1980, 156-66.
68. Tannenbaum, E.; Kaplan, I.R. Geochim. Cosmochim. Acta 1985, 49, 2589-2604.
69. Tannenbaum, E.; Kaplan, I.R. Bull. Am. Ass. Petrol. Geol. 1986, 70, 1156-65.
70. Bergaya, F.; Van Damme, H. Geochim. Cosmochim. Acta 1982, 46, 349-60.
71. Horsefield, B.; Douglas, A.G. Geochim. Cosmochim. Acta 1980, 44, 1119-31.
72. Espitalie, J.; Madec, M.; Tissot, B. Bull. Amer. Ass. Petrol. Geol. 1980, 64, 59-66.
73. Espitalie, J.; Senga Makadi, K.; Trichet, J. In "Advances in Organic Geochemistry, 1983"; Schenk, P.A.; De Loeuw, J.W.; Lijmbach, G.W.M., Eds.; Pergamon Press: Oxford, 1984; pp. 365-82.
74. Spiro, B. Org. Geochem. 1984, 6, 543-59.
75. Jeong, K.M.; Koblynoki, T.P. Prepr. Div. Petrol. Chem. ACS 1983, 28, 209-19.
76. Casagrande, D.J.; Hodgson, G.W. Nature 1971, 233, 123-24.
77. Casagrande, D.J.; Hodgson, G.W. Geochim. Cosmochim. Acta 1974, 38, 1745-58.
78. Ikan, R.; Aizenshtat, Z.; Baedeker, M.J.; Kaplan, I.R. Geochim. Cosmochim. Acta 1975, 39, 173-85.
79. Barwise, A.J.G.; Park, P.J.P. In "Advances in Organic Geochemistry, 1981"; Bjorøy, M., Ed.; John Wiley: London, 1983; pp. 668-74.
80. Barwise, A.J.G. (this volume).
81. Rosscup, R.J.; Bowman, D.N. Prepr. Div. Petrol. Chem. ACS 1967, 12, 77-81.
82. Baker, E.W.; Palmer, S.E.; Huang, W.Y. In "Initial Reports of the Deep Sea Drilling Project-XLI"; Vol. 41; Lancelot, Y.; Siebold, W., Eds.; U.S. Govt. Printing Office: Washington, 1977; pp. 825-37.
83. Van Berkel, G.J. Ph.D. Dissertation; Department of Chemistry; Washington State University, 1987.
84. Baker, E.W.; Palmer, S.E.; Huang, W.Y.; Rankin, J.G. In "Analytical Chemistry of Liquid Fuel Sources"; Uden, P.C.; Siggia, S.S.; Jensen, H.B. Advances in Chemistry Series No. 170; American Chemical Society: Washington, 1978; pp. 159-80.
85. Erdman, J.G.; Walter, J.N.; Wanson, W.E. Div. Petrol. Chem. ACS 1957, 2, 259-67.
86. Riley, K.W.; Saxby, J.D. Chem. Geol. 1982, 37, 265-75.
87. Spiro, B.; Dinur, D.; Aizenshtat, Z. Chem. Geol. 1983, 39, 184-214.
88. Nguyen, S.N.; Filby, R.H. (this volume).
89. Bandurski, E. Energy Sources 1982, 6, 47-66.
90. Philp, R.P.; Gilbert, T.D. Geochim. Cosmochim. Acta 1985, 49, 1421-32.
91. Oehler, J.H.; Aizenshtat, Z.; Schopp, W.J. Bull. Amer. Ass. Petrol. Geol. 1974, 58, 124-32.
92. Blumer, M.; Snyder, W.D. Chem. Geol. 1967, 2, 35-45.
93. Blumer, M.; Rudrum, M. J. Inst. Petrol. 1970, 56, 99-106.
94. Durand, B. In "Advances in Organic Geochemistry, 1981"; Bjorøy, M., Ed.; John Wiley: London, 1983; pp. 117-128.

95. Leythaeuser, D.; Mackenzie, A.; Schaefer, R.G.; Bjorøy, M. Bull. Amer. Ass. Petrol. Geol. 1984, 68, 196-219.
96. Chakhmachkev, V.A.; Burkova, V.N.; Zharkov, N.I.; Punanova, S.A.; Serebrennikova, O.V.; Titov, V.I. Geokhimiya 1985, 381-86.
97. Burkova, V.N.; Serebrennikova, O.V.; Titov, V.I. Geokhimiya 1978, 945-50.
98. Rubinstein, I.; Spyckerelle, C.; Strausz, O.P. Geochim. Cosmochim. Acta 1979, 43, 1-6.
99. Rubinstein, I.; Strausz, O.P. Geochim. Cosmochim. Acta 1979, 43, 1887-94.
100. Branthaver, J.F.; Filby, R.H. (this volume).
101. Franceskin, P.J.; Gonzalez-Jimenez, F.; La Rosa, M.G.; Abrams, O.; Katan, L. Hyperfine Interact. 1986, 28, 825-8.
102. Hodgson, G.W.; Peake, E.; Baker, B.L. In "Athabasca Oil Sands: K.A. Clark Volume"; Carrigy, M.A., Ed.; Information Series 45; Research Council of Alberta: Edmonton, 1963; pp. 75-100.
103. Dunning, H.N.; Moore, J.W.; Bieber, N.; Williams, R.B. J. Chem. Eng. Data 1960, 5, 546-9.
104. Yen, T.F. In "Role of Trace Metals in Petroleum"; Yen, T.F., Ed.; Ann Arbor Science: Ann Arbor, 1975; pp. 1-30.
105. Filby, R.H. In "Role of Trace Metals in Petroleum"; Yen, T.F., Ed.; Ann Arbor Science: Ann Arbor, 1975; pp. 31-58.
106. Jacobs, F.S. Ph.D. Dissertation; Department of Chemistry; Washington State University, 1982.
107. Didyk, B.; Alturki, Y.I.A.; Pillinger, C.T.; Eglinton, G. Chem. Geol. 1975, 15, 193-208.
108. Goulon, J.; Retournard, A.; Frient, P.; Goulon-Ginet, C.; Berthe, C.; Muller, J.F.; Poncet, J.L.; Guillard, R.; Escalier, J.C.; Neff, B. J. Chem. Soc. Dalton Trans. 1984, 1095-1103.
109. Rosscup, R.J.; Pohlmann, H.P. Preprints Div. Petrol Chem. ACS 1967, 12, A103-109.
110. Branthaver, J.F.; Wu, G.Y.; Sugihara, J.M. Preprints Div. Petrol. Chem. ACS 1967, 12, A73-75.
111. Sugihara, J.M.; Branthaver, J.F.; Wu, G.Y.; Weatherbee, C. Preprints Div. Petrol. Chem. ACS 1970, 15, C5-12.
112. Gransch, J.A.; Eisma, E. In "Advances in Organic Geochemistry, 1966"; Hobson, G.D.; Speers, G.C., Eds.; Pergamon: Oxford, 1970; pp. 69-86.
113. Hajibrahim, S.K.; Quirke, J.M.E.; Eglinton, G. Chem. Geol. 1981, 32, 173-88.
114. Johnson, J.V.; Britton, E.D.; Yost, R.A.; Quirke, J.M.E.; Cuesta, L.L. Anal. Chem. 1986, 58, 1325-29.
115. Quirke, J.M.E.; Perez, M.; Britton, E.D.; Yost, R.A. In "Geochemical Biomarkers"; Yen, T.F.; Moldowan, J.M., Eds.; Gordon and Breach: London (in press).
116. Hodgson, G.W. Bull. Amer. Ass. Petrol. Geol. 1954, 38, 2537-54.
117. Al-Shahristani, H.; Al-Atiya, M.J. Geochim. Cosmochim. Acta 1972, 36, 929-37.
118. Saban, M.; Vitorovic, O.; Vitorovic, D. In "Symposium on Characterization of Heavy Crude Oils and Petroleum Residues"; Editions Technip.: Paris, 1984; pp. 122-27.
119. Branthaver, J.F. (this volume).
120. Yen, T.F.; Silverman, S.R. Preprints Div. Petrol. Chem. ACS 1969, 14, E32-39.
121. Tynan, E.C.; Yen, T.F. Fuel 1969, 43, 191-208.

122. Yen, T.F.; Boucher, L.J.; Dickie, J.P.; Tynan, E.C.; Vaughan, G.B. J. Inst. Petrol. Geol. 1969, 55, 87-99.
123. Vaughan, G.B.; Tynan, E.C.; Yen, T.F. Chem. Geol. 1970, 6, 203-19.
124. Palmer, S.E. Abstract, 186th Amer. Chem. Soc. Meeting; Washington, DC, 1983.
125. Bonnett, R.; Czechowski, F. Phil. Trans. Roy. Soc. Lond. A 1981, 300, 51-63.
126. Bonnett, R.; Burke, P.J.; Czechowski, F.; Rezka, A. Org. Geochem. 1984, 6, 177-82.
127. Dalton, I.M.; Pringle, W.J.E. Fuel 1962, 42, 41-48.
128. Krauskopf, K.B. Geochim. Cosmochim. Acta 1956, 9, 1-32.
129. Hallbero, R.O.; Bubela, B.; Ferguson, J. Geomicrobiol. J. 1980, 2, 99-113.
130. Saxby, J.D. Rev. Pure. Appl. Chem. 1969, 19, 131-50.
131. Choudhry, G.G. Toxicol. Envir. Chem. 1983, 6, 127-71.
132. Fish, R.H.; Brinckman, F.E. Preprints Div. Petrol. Chem. ACS 1983, 28, 177-80.
133. Jaganathan, J.; Mohan, M.S.; Zingaro, R.A. Fuel 1986, 65, 266-69.
134. Erdman, J.G.; Harju, P.H. Preprints Div. Petrol. Chem. ACS 1962, 7, 43-56.
135. Tissot, B.P. Bull. Amer. Ass. Petrol. Geol. 1984, 68, 545-63.
136. Yang, Z.; Li, Y.; Cheng, Z.; Zhang, D. In "Geochemical Biomarkers"; Yen, T.F.; Moldowan, J.M., Eds.; Gordon and Breach: London (in press).
137. Hoffman, C.F.; Strausz, O.P. Bull. Amer. Ass. Petrol. Geol. 1986, 70, 1113-28.
138. Shi, J.Y.; Mackenzie, A.S.; Alexander, R.; Eglinton, G.; Gowar, A.P.; Wolff, G.A.; Maxwell, J.R. Chem. Geol. 1982, 35, 1-31.

RECEIVED March 30, 1987

## Chapter 2

# Sedimentary Porphyrins: Unexpected Structures, Occurrence, and Possible Origins

M. Inès Chicarelli, Surinder Kaur, and James R. Maxwell

Organic Geochemistry Unit, University of Bristol, School of Chemistry, Cantock's Close,  
Bristol BS8 1TS, United Kingdom

The occurrences of sedimentary porphyrins whose structures have been fully or partially established are reviewed. The compounds range from components with carbon skeletons providing clear evidence of specific precursor chlorophylls to those which are not obviously related to known biological pigments. Three examples from the latter category are reported: a  $C_{34}$  component from Serpiano oil shale (Triassic, Monte San Giorgio, Switzerland), containing a fused ring system, and two components ( $C_{32}$ ,  $C_{33}$ ) from Gilsonite bitumen (Eocene, Utah, U.S.A.), containing a methyl-substituted, five membered exocyclic alkanone ring. In addition, evidence is presented that Boscan crude oil contains extended (>  $C_{33}$ ) monobenzoporphyrins.

In molecular organic geochemistry, assignment of the structures of selected members of any class of biological markers is essential before the distributions of the class in question can be used in an applied sense. Such assignments involve either synthesis of suspected compounds and coinjection (e.g. using combined gas chromatography-mass spectrometry) with a sedimentary fraction containing them, or isolation of individual components and direct structure analysis (e.g. using nuclear magnetic resonance spectroscopy or X-ray crystallography). A knowledge of the detailed structures of the compounds then provides a basis for: (i) understanding the origins and diagenetic pathways involved in their formation, (ii) using their

distributions for correlation and maturation studies, and in providing information about depositional environment.

To date, most of the developments in, and applications of, biological marker geochemistry have been associated with steroids and triterpenoids; this results from a fairly detailed knowledge of their origins and geological fate (1). Despite the fact that the occurrence of sedimentary alkyl porphyrins was recognised in the early 1930's, these compounds have not been very extensively used in applied geochemical studies. They occur widely and mainly as nickel-II and/or vanadyl complexes (2), although generally smaller amounts and more restricted occurrences of other metal chelates have been reported, for example manganese-II, iron-III (3,4) and gallium-III (5,6) complexes in coals and copper-II complexes in immature oceanic sediments (7,8). Free base species have also been detected in oceanic sediments (9-11) and shales (12,13). In recent years, the availability of efficient HPLC and  $^1\text{H}$  NMR techniques has contributed effectively to the structure elucidation of individual components of these complex mixtures. HPLC, used on an analytical scale (14), allows the distribution to be obtained efficiently and routinely, and the isolation of mg amounts of individual components in high purity when used on a preparative scale under normal (15) or reversed phase (16,17) conditions.  $^1\text{H}$  NMR, in conjunction with n.o.e. difference studies, has now become the most important and widely used method of structure assignment.

Since the first full assignments, after demetallation, of two aetio porphyrins, a  $\text{C}_{29}$  (1) and a  $\text{C}_{32}$  (2) component (18,19), and the partial determination (20) of a demetallated  $\text{C}_{32}$  component (8) with an exocyclic alkanol ring, the structures of a number of compounds from a variety of geological samples have been elucidated. These studies have been concerned mainly with components having an exocyclic alkanol ring, which exhibit a wide variety of structural types, and more recently with functionalised components. Indeed, the structures of more than thirty five sedimentary porphyrins have now been fully or partly established (Tables I, II and references therein). In relation to origins in terms of precursor biological pigments, these can be divided into four categories: (a) compounds whose carbon skeletons can be related to selected types of precursors, (b) compounds whose carbon skeletons can be related to specific precursors, (c) compounds which can only be related to non-specific precursors, and (d) compounds whose carbon skeletons are not at present obviously related to known precursors. In addition, it is probably useful to define another category (e), comprising compounds of a type whereby the structure which occurs naturally may have been

Table 1. Reported Occurrences of Individual Alkyl Porphyrins\* in Sedimentary Organic Matter

Occurrence <sup>+</sup> (Structure)	Reference	Porphyrin Structural Type (Structure)	
a(1-4,8,9,12 <sup>§</sup> ,13 <sup>§</sup> )	<u>18-21</u>		
b(5,8,9,11,14)	<u>22-24</u>		
c(2,8)	<u>25</u>		
d(2,4,6,8-10)	<u>26-28</u>		
e(7,8 <sup>**</sup> ,10 <sup>**</sup> )	<u>29</u>		
f(9)	<u>30</u>		
g(2 <sup>**</sup> )	<u>4</u>		
b(15,16,18,19)	<u>23,31,32</u>		
d(15-17)	<u>33</u>		
e(15 <sup>**</sup> ,20,21)	<u>29,34</u>		
b(25 <sup>§</sup> )	<u>23,42</u>		
h(22)	<u>35</u>		
i(23,24)	<u>36</u>		

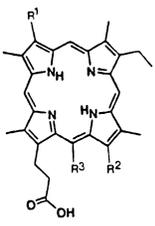
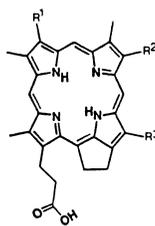
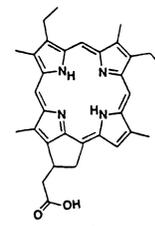
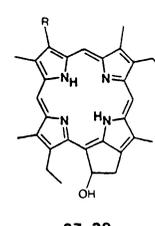
\* Present as Ni(II) and/or V=O complexes (unless stated otherwise); metal not reported for simplicity.

+ Occurrence: a) Gilsonite bitumen: Eocene, Uinta Basin, Utah, USA; b) Serpiano oil shale: Mid-Triassic, Monte San Giorgio, Switzerland; c) Marl Slate: Permian shale, N.E. England; d) Julia Creek oil shale: Cretaceous, Toolebuc formation, Queensland, Australia; e) Messel oil shale: Eocene, near Darmstadt, W. Germany; f) Abelsonite: Parachute Creek, Green River formation, Uinta Basin, Utah, USA; g) several lignites and coals, see 4 (and ref. therein). In this case, 2 characterised as Fe(III) complex; h) El Lajjun shale: Upper-Cretaceous, Jordan; i) Boscan crude oil: Cretaceous, Maracaibo Basin, Venezuela.

§ Structural studies presented in this paper.

\*\* Assignment by comparison with literature <sup>1</sup>H NMR spectrum.

Table 11. Reported Occurrences of Individual Functionalised Porphyrins\* in Sedimentary Organic Matter

Occurrence <sup>+</sup> (Structure)	Reference	Porphyrin Structural Type (Structure)
e (26-29,31-35)	<u>16, 17, 37</u>	 26-30
g (30)	<u>38</u>	 31-35
e (36)	<u>16</u>	 36
c (37,38)	<u>39</u>	 37,38

\* Reported as Ni(II) complexes only, with the exception of 30 which has been characterised as Fe(III) and Ga(III) complexes (38 and ref. therein).

+ Occurrence: c, e and g, see Table I

chemically modified in some way as a result of the isolation or purification procedures. Careful attention has to be paid to compounds which may be candidates for this category (artefacts) in order to avoid confusion between a diagenetic reaction occurring naturally in the sediment and a laboratory reaction. Examples of compounds within each category are given as follows. Although all of the components occur as Ni(II) and/or V=O complexes (unless stated otherwise), they are listed as the free base for convenience.

#### Compounds related to selected precursor types (Tables I,II)

This category includes deoxophylloerythroetioporphyrin (8) itself and its C<sub>31</sub> counterpart (9), which appear to occur almost ubiquitously in sedimentary alkyl porphyrin mixtures and are probably [as the Ni(II) and V=O complexes] the two most abundant porphyrins in the geosphere, the quantities probably far outweighing any biological pigment. They have been proposed as arising from defunctionalisation of chlorophyll a on the basis of its high relative abundance in the biosphere. It should be noted, however, that other chlorophylls (e.g. 41,42) could be additional precursors and could undergo analogous degradative pathways. Similar compounds in the category include the C<sub>30</sub> analogue (10) of 8 and 9 and the carboxylic acids 26-29,31,32. Other alkyl porphyrin examples are represented by a widely occurring C<sub>30</sub> mono βH aetioporphyrin (5), the C<sub>32</sub>, C<sub>31</sub> and C<sub>30</sub> 15,17-butanoporphyrins (15-17), and the C<sub>32</sub> and C<sub>31</sub> (15<sup>1</sup>-methyl)-15,17-propanoporphyrins (18,19). In the case of 15-19, it has been proposed that the exocyclic alkanone ring has formed by way of a condensation reaction of a functionalised intermediate on the degradative pathway (23,31-33).

#### Compounds related to specific precursors (Table I, II)

The carbon skeleton of a C<sub>31</sub> mono βH-13,15-ethanoporphyrin (11), present in Serpiano oil shale mainly as the vanadyl complex, has been suggested (24) as arising from degradation of chlorophyll b (40). The occurrence in Messel shale of components with a methyl-substituted five membered exocyclic ring (20,21) and related acid (36) led to the suggestion (16,34) of a diagenetic acid catalysed rearrangement of an intermediate from chlorophyll c (41), which occurs only in certain types of algae. Further evidence of a microbial input to this immature shale by way of photosynthetic bacteria came from the discovery of the higher (C<sub>34</sub> to C<sub>36</sub>) porphyrin acids (33-35; 17). In this case, there is clear evidence that the sedimentary products have arisen from bacteriochlorophylls d (43).

### Compounds related to non-specific precursors (Tables I,II)

Compounds of this type are perhaps best represented by certain of the aetioporphyryns. Aetioporphyryn III (2) has been suggested (19) as arising from chlorophyll a (39), or other chlorophylls, by way of opening at some stage in the degradative pathway of the five membered exocyclic ring in the precursor or a degradative product. It is equally apparent, however, that it could have arisen from decarboxylation of mesoporphyrin IX [30, iron(III) complex]. A di-acid whose <sup>1</sup>H NMR spectrum and chromatographic properties were indistinguishable from the latter has been isolated as the Fe(III) complex from coals, and it was proposed that the di-acid could be a diagenetic product of cytochromes, since most organisms (including many micro-organisms) contain cytochromes with substituted mesohaem prosthetic groups (4).

### Compounds not obviously related to known precursors (Table I)

Two recent examples exemplify the problem. Despite the fact that the so-called rhodoporphyryns have been known for many years to occur widely in sediments and petroleum, only recently has it been shown that the two major rhodoporphyryns in Boscan oil are monobenzo[g]-porphyryns (23,24). These components contain the five membered exocyclic ring found in all chlorophylls; it is difficult to envisage, however, how the benzene ring could arise from a known chlorophyll, although the suggestion of a bacterial origin has been made (36).

### Components possibly of artefact origin (Table II)

The isolation of two porphyryn alcohols (37,38), component 37 being the hydroxylated counterpart of the most abundant alkyl porphyryn in the geosphere, raises the possibility that they might be artefacts of the isolation procedure used to obtain them from Marl slate. This possibility comes from the reported hydroxylation, at the same exocyclic ring position of a synthesised (13<sup>1</sup>-methyl)-13,15-ethano porphyryn when chromatographed on silica (40).

### Present Study

Apart from reviewing the occurrences of individual sedimentary porphyryns reported to our knowledge, we report here structural

studies of three sedimentary alkyl porphyrins which appear to belong to category (d) as a result of their unusual structures, although the possibility of their being artifacts is also considered. The three components are: (i) a  $C_{34}$  (13<sup>1</sup>-methyl)-13,15-ethano-13<sup>2</sup>,17-prop-13<sup>2</sup>(15<sup>2</sup>)-enoporphyrin from Serpiano oil shale (cf. Table I). (ii) a  $C_{32}$  and a  $C_{33}$  (13<sup>1</sup>-methyl)-13,15-ethano-porphyrin from Gilsonite bitumen (cf. Table I). In addition, preliminary evidence is presented that the Boscan oil shown recently to contain monobenzoporphyrins (cf. Table I) contains higher molecular weight components of this type, adding further complexity to understanding the origin of these other category (d) compounds.

## Experimental

### 1. Methods:

Low resolution mass spectra were obtained, using the direct insertion probe, on a Finnigan 4000 spectrometer coupled to an INCOS 2300 data system. Conditions: emission current 350 $\mu$ A; ionisation voltage 40eV, source 250<sup>o</sup>C and probe programmed from 90<sup>o</sup> to 300<sup>o</sup>C. High resolution spectra were recorded on a VGMS9 spectrometer coupled to a VG data system. Conditions: ionisation voltage 70eV, source 200<sup>o</sup>C and probe programmed from 50<sup>o</sup> to 250<sup>o</sup>C; resolution 10,000; perfluorokerosene as internal reference.

<sup>1</sup>H NMR spectral data for the individual porphyrins, as zinc(II) chelates, were obtained on a JEOL FX200 FT instrument and/or on a Bruker WH 400 instrument. Samples were examined in (CD<sub>3</sub>)<sub>2</sub>CO/5% C<sub>5</sub>D<sub>5</sub>N or C<sub>6</sub>D<sub>6</sub>/5% C<sub>5</sub>D<sub>5</sub>N. Concentrations were typically 2-4mg ml<sup>-1</sup>. Details of decoupling experiments and n.o.e. studies have been described previously (22-24).

High performance liquid chromatography (HPLC) analyses were performed using a Spectra Physics SP8700 ternary solvent delivery system and Rheodyne 7125 injector. Detection (400 nm) was obtained using an LDC 1202 Spectromonitor II variable wavelength detector. Analytical runs were performed using three columns (Spherisorb S3W; each 150 x 4.6 mm) connected in series, using a combination of solvents as described in 14. The preparative-scale conditions were similar, except that there were minor changes in the solvent programme (15), and the analyses were performed on Spherisorb S5W column (250 x 10 mm). The components obtained were demonstrated to be >95% pure by analytical HPLC.

## 2. Isolation:

The isolation of rhodoporphyrins from Boscan crude oil has been described previously (36). The total metalloporphyrins were extracted from Serpiano oil shale and Gilsonite bitumen as described previously (22,23;18). The individual compounds obtained by preparative-scale HPLC were converted to their zinc(II) chelates and purified by TLC (SiO<sub>2</sub> gel G, 5% acetone/toluene). Volatile impurities were removed under high-vacuum (generally 100°C; 10<sup>-6</sup> Torr; ca. 5h) prior to <sup>1</sup>H NMR analyses. General spectroscopic properties of 25, 12, 13 are summarised as follows:

- a) (13<sup>1</sup>-methyl)-13,15-ethano-3,8-diethyl-2,7,12,18-tetramethyl-13<sup>2</sup>,17-prop-13<sup>2</sup>(15<sup>2</sup>)-enoporphyrin (25): HRMS: found 500.2952, C<sub>34</sub>H<sub>36</sub>N<sub>4</sub> requires 500.2944; EIMS(40eV) significant ions: 500 (100%), 485 (19), 250 (20); uv/vis (CH<sub>2</sub>Cl<sub>2</sub>): λ<sub>max</sub> = 512, 548, 582, 639nm; rel. int. 100:17:33:13, Soret 416nm; <sup>1</sup>H NMR, see text.
- b) (13<sup>1</sup>-methyl)-13,15-ethano-8,17-diethyl-2,3,7,12,18-pentamethylporphyrin (12): HRMS: found 476.2946, C<sub>32</sub>H<sub>36</sub>N<sub>4</sub> requires 476.2940; EIMS (40eV) significant ions: 476 (100%), 461 (35), 448 (15), 238 (40); uv/vis (CH<sub>2</sub>Cl<sub>2</sub>): λ<sub>max</sub> = 500, 533, 564, 618nm (IV>II>I>III), Soret 400nm; <sup>1</sup>H NMR, see text.
- c) (13<sup>1</sup>-methyl)-13,15-ethano-3,8,17-triethyl-2,7,12,18-tetramethylporphyrin (13): EIMS (40eV) significant ions: 490 (100%), 475 (25), 245 (40); uv/vis (CH<sub>2</sub>Cl<sub>2</sub>): λ<sub>max</sub> = 500, 532, 565, 618nm (IV>II>I>III), Soret 400nm; <sup>1</sup>H NMR, see text.

Structural Studies

1. (13<sup>1</sup>-methyl)-13,15-ethano-3,8-diethyl-2,7,12,18-tetramethyl-13<sup>2</sup>,17-prop-13<sup>2</sup>(15<sup>2</sup>)-enoporphyrin (25):

This C<sub>34</sub>H<sub>36</sub>N<sub>4</sub> species was isolated, after demetallation (present mainly as the V=O complex), from Serpiano oil shale using high performance liquid chromatography. Although the molecular weight corresponds formally to a rhodo-type component, the electronic spectrum is markedly different from that expected for such a species (41). The <sup>1</sup>H NMR spectrum of the Zn(II) complex (Figure 1; Table III) indicated the presence of 4 β-methyls, 2 β-ethyls, 1 CH<sub>3</sub>CH-moiety, 3 meso-H's, 1 olefinic-H and 2 more -CH<sub>2</sub>- signals (see 42 for preliminary report). Based on the results of the selective decoupling experiments, the exocyclic ring moiety below could be proposed:

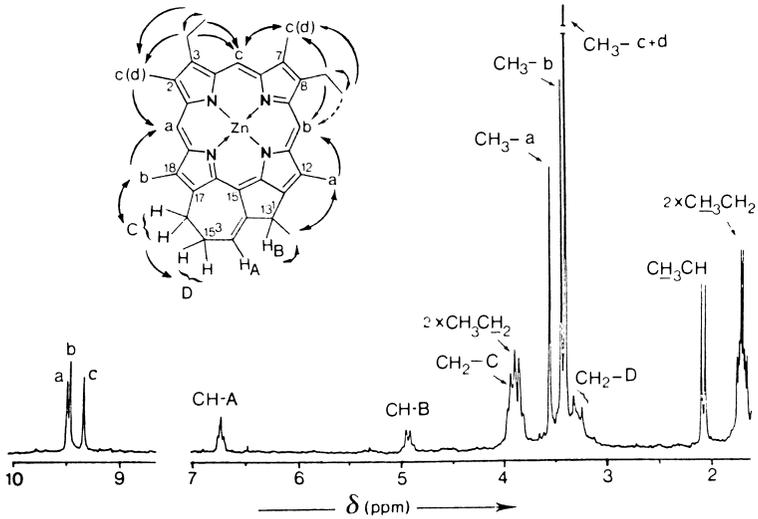
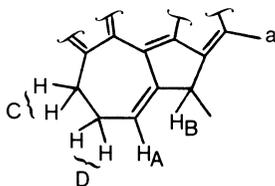


**Figure 1.** 200 MHz  $^1\text{H}$  NMR spectrum of (13<sup>1</sup>-methyl)-13,15-ethano-3,8-diethyl-2,7,12,18-tetramethyl-13<sup>2</sup>,17-prop-13<sup>2</sup>(15<sup>2</sup>)-enoporphyrin (25, as zinc complex) in  $\text{CDCl}_3$ . Arrows indicate n.o.e. enhancements observed; dotted arrow indicates weak n.o.e. observed.

Table III. 200 MHz  $^1\text{H}$  NMR data for component 25 (as zinc complex) in  $\text{CDCl}_3$ 

$\delta$ (ppm)	Multiplicity	n.o.e.*	Code <sup>+</sup>	Assignment
9.46	s	n.d.	meso-Ha	H-20
9.43	s	n.d.	meso-Hb	H-10
9.31	s	3.39	meso-Hc	H-5
6.73	dd	no n.o.e. observed	CH-A	CH-15 <sup>2</sup>
4.93	bq	2.06**	CH-B	CH-13 <sup>1</sup>
3.96 <sup>§</sup>	m	{ 9.43, 9.31, 3.43 3.39, 3.27, 1.70, 1.68	CH <sub>2</sub> -C	CH <sub>2</sub> -15 <sup>4</sup>
3.90 <sup>§</sup>	m		CH <sub>3</sub> CH <sub>2</sub> (x2)	CH <sub>3</sub> CH <sub>2</sub> -8,3
3.54	d	9.43, 2.06	CH <sub>3</sub> -a	CH <sub>3</sub> -12
3.43	s	n.d.	CH <sub>3</sub> -b	CH <sub>3</sub> -18
3.39 <sup>§</sup>	s	9.46, 9.31, <u>ca.</u> 3.94	CH <sub>3</sub> -c and d	CH <sub>3</sub> -2,7
3.27 <sup>§</sup>	m	n.d.	CH <sub>2</sub> -D	CH <sub>2</sub> -15 <sup>3</sup>
2.06	d	4.93, 3.54	CH <sub>3</sub> CH-B	CH <sub>3</sub> CH-13 <sup>1</sup>
1.70 <sup>++</sup>	t	{ 9.43, 9.31, 3.90, 3.39	CH <sub>3</sub> CH <sub>2</sub>	CH <sub>3</sub> CH <sub>2</sub> -8
1.68 <sup>++</sup>	t		CH <sub>3</sub> CH <sub>2</sub>	CH <sub>3</sub> CH <sub>2</sub> -3

\* Chemical shifts where enhancements seen when  $\delta$  signal irradiated. + Codes used in Figure 1 and 2. <sup>§</sup> Partially overlapping signals. \*\* Weak n.o.e., although CH<sub>3</sub>CH-B confirmed by decoupling. ++ Simultaneous irradiation (Figure 2d). n.d. = not determined. s = singlet, d = doublet, t = triplet, q = quartet, m = multiplet, b = broad.



The n.o.e experiments listed in Table III were performed under low power irradiation to allow good frequency selectivity. Some of them are discussed as follows (see also Figure 2): (i) irradiation of  $\text{CH}_3\text{-a}$  at 3.54 ppm caused an enhancement in meso- $\text{H}_b$  at 9.43 ppm and in the  $\text{CH}_3$  doublet (2.06 ppm), thus providing extra ring evidence for the position of  $\text{CH}_3\text{-a}$  in relation to the exocyclic ring moiety (Figure 2a); (ii) irradiation of the two overlapping triplets ( $\text{CH}_3\text{CH}_2$ 's) at ca. 1.69 ppm enhanced the signals of the  $\text{CH}_3\text{CH}_2$ 's, as well as of the overlapping  $\text{CH}_3\text{-c}$  and  $\text{CH}_3\text{-d}$  (both were enhanced, as indicated by the intensity of the n.o.e.) and the meso-H's at 9.31 ( $\text{H}_c$ ) and 9.43 ( $\text{H}_b$ ) ppm (Figure 2d); similar connections have been observed before (17,27,33); (iii) irradiation at ca. 3.94 ppm (i.e. simultaneous irradiation of the partially overlapping  $\text{CH}_3\text{CH}_2$  (x2) and  $\text{CH}_2\text{-C}$  signals) resulted in enhancements of the signals from meso protons  $\text{H}_c$  and  $\text{H}_b$  (9.31 and 9.43 ppm),  $\text{CH}_3\text{-b}$  (3.43 ppm),  $\text{CH}_3$ 's c and d (both at 3.39 ppm),  $\text{CH}_2\text{-D}$  (3.27 ppm) and of the two partially overlapping triplets ( $\text{CH}_3\text{CH}_2$ 's) at ca. 1.69 ppm (Figure 2c). Bearing in mind experiment (ii), the enhancements of the two methyls (c + d), the two meso-H's and the two triplets were attributed to connections with the two methylenes at 3.90 ppm, while the enhancements of the  $\text{CH}_3\text{-b}$  and  $\text{CH}_2\text{-D}$  were attributed to irradiation of  $\text{CH}_2\text{-C}$ . These results eliminate possibilities of structures with two ethyl groups flanking the same meso-H, or with two ethyls attached to the same pyrrole ring; (iv) irradiation of meso- $\text{H}_c$  at 9.31 ppm confirmed the spacial connections with  $\text{CH}_3\text{-c}$  (or d) and a  $\text{CH}_3\text{CH}_2$  group.

Thus, structure 25 could be assigned. The component was also examined by mass spectrometry under chemical ionisation, using  $\text{H}_2$  as reagent gas; the spectrum is compatible with the proposed structure (23).

- (13<sup>1</sup>-methyl)-13,15-ethano-8,17-diethyl-2,3,7,12,18-pentamethylporphyrin (12) and  $\text{C}_{33}$  counterpart (13):

These components, isolated as the free bases from Gilsonite bitumen, in which they occur as the Ni(II) complexes, were examined by  $^1\text{H}$  NMR

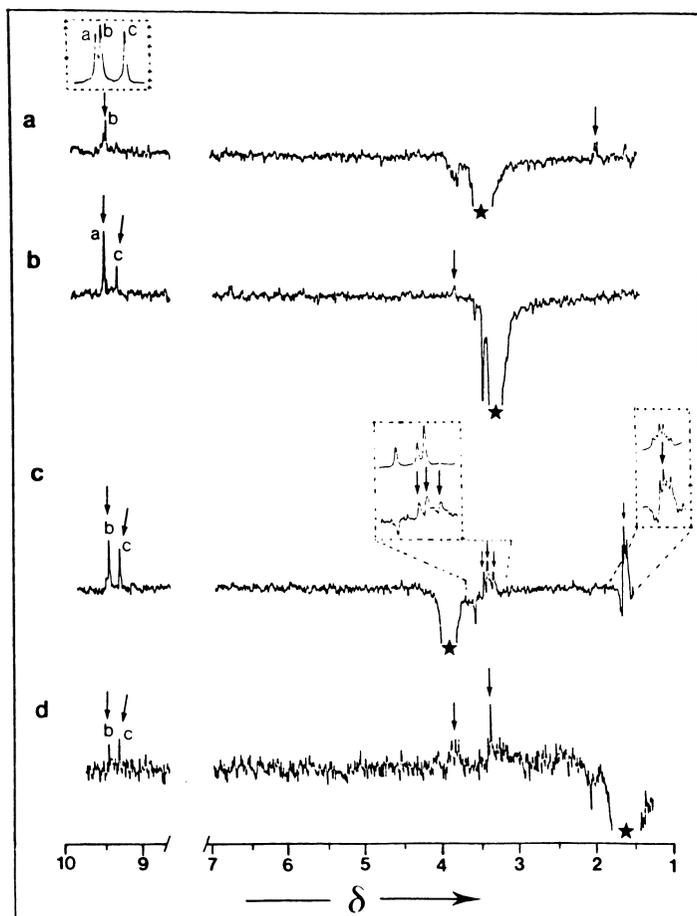


Figure 2. Examples of n.O.e. experiments performed on component 25 (as zinc complex) in  $\text{CDCl}_3$ . The insert in (a) shows the expanded meso-H region of the normal spectrum; in (c) they show expanded regions of the normal spectrum (top) and of the n.O.e. difference spectrum (bottom). Arrows indicate n.O.e. enhancements observed. Asterisk indicates point of irradiation.

at 200 and 400 MHz in two different solvents [ $(\text{CD}_3)_2\text{CO}/5\% \text{C}_5\text{D}_5\text{N}$  and  $\text{C}_6\text{D}_6/5\% \text{C}_5\text{D}_5\text{N}$ ]. The spectra of 12 (e.g. Figure 3) showed the presence of 5  $\beta$ -methyls, 2  $\beta$ -ethyls and 3 meso-H's. The  $-\text{CH}_2\text{CHCH}_3-$  moiety in the exocyclic ring was determined by decoupling experiments (Table IV). The appropriate n.o.e. studies were performed and the resulting connections between  $\beta$ -substituents and meso-protons were established.

The  $^1\text{H}$  NMR spectra of 13 [as zinc(II) complex; not shown] were very similar to those of the  $\text{C}_{32}$  counterpart 12, except for the absence of the resonance at ca. 3.56 ppm ( $\text{CH}_3-3$ ) which was replaced by resonances at ca. 4.12 and 1.94 ppm ( $\text{CH}_3\text{CH}_2-3$ ). In summary, the connections between the 4  $\beta$ -methyls, 3  $\beta$ -ethyls, 3 meso-H's and the  $-\text{CH}_2\text{CHCH}_3-$  moiety were obtained in the same way as for 12, establishing the compound as (13<sup>1</sup>-methyl)-13,15-ethano-2,8,17-triethyl-2,7,12,18-tetramethylporphyrin.

It is noteworthy that the  $\text{C}_{32}$  compound (12) was isolated previously from Gilsonite bitumen and the structure given as 44 (43). Unfortunately, that sample was isolated for  $^1\text{H}$  NMR studies in lower purity and quantity; also, the  $\text{CH}_3$  at C-13<sup>1</sup> is masked in  $(\text{CD}_3)_2\text{CO}$  by a residual proton resonance [viz. of  $(\text{CH}_3)_2\text{CO}$  impurity] and led to assignment of the methyl substituted, five membered exocyclic ring as a six membered ring. This emphasises the importance of using more than one solvent for  $^1\text{H}$  NMR analyses of the small quantities of fossil porphyrins which can be isolated conveniently.

### 3. High molecular weight benzoporphyrins from Boscan crude oil:

A sequence of procedures involving flash chromatography on silica, demetallation and HPLC using normal and reversed phase conditions allowed isolation of a variety of fractions enriched in porphyrins showing rhodo-type characteristics (36; see also references therein). Reversed phase HPLC then afforded the two major components of this type, which were assigned in the usual way as monobenzo[g]porphyrins, having structures 23 and 24 (36). In addition, a fraction with a rhodo-type uv/visible spectrum was obtained (Figure 4a). Electron impact mass spectrometry showed the fraction to be concentrated in higher molecular weight components ( $> \text{C}_{33}$ ), extending to at least  $\text{C}_{38}$ , with molecular ions corresponding formally to monobenzoporphyrins with an exocyclic alkanone ring (Figure 4b).  $^1\text{H}$  NMR studies of individual components isolated from this fraction are in progress but it is already clear that the  $\text{C}_{34}$  component contains a benzene ring, suggesting indirectly that the components extending beyond  $\text{C}_{34}$  are also monobenzoporphyrins (44).

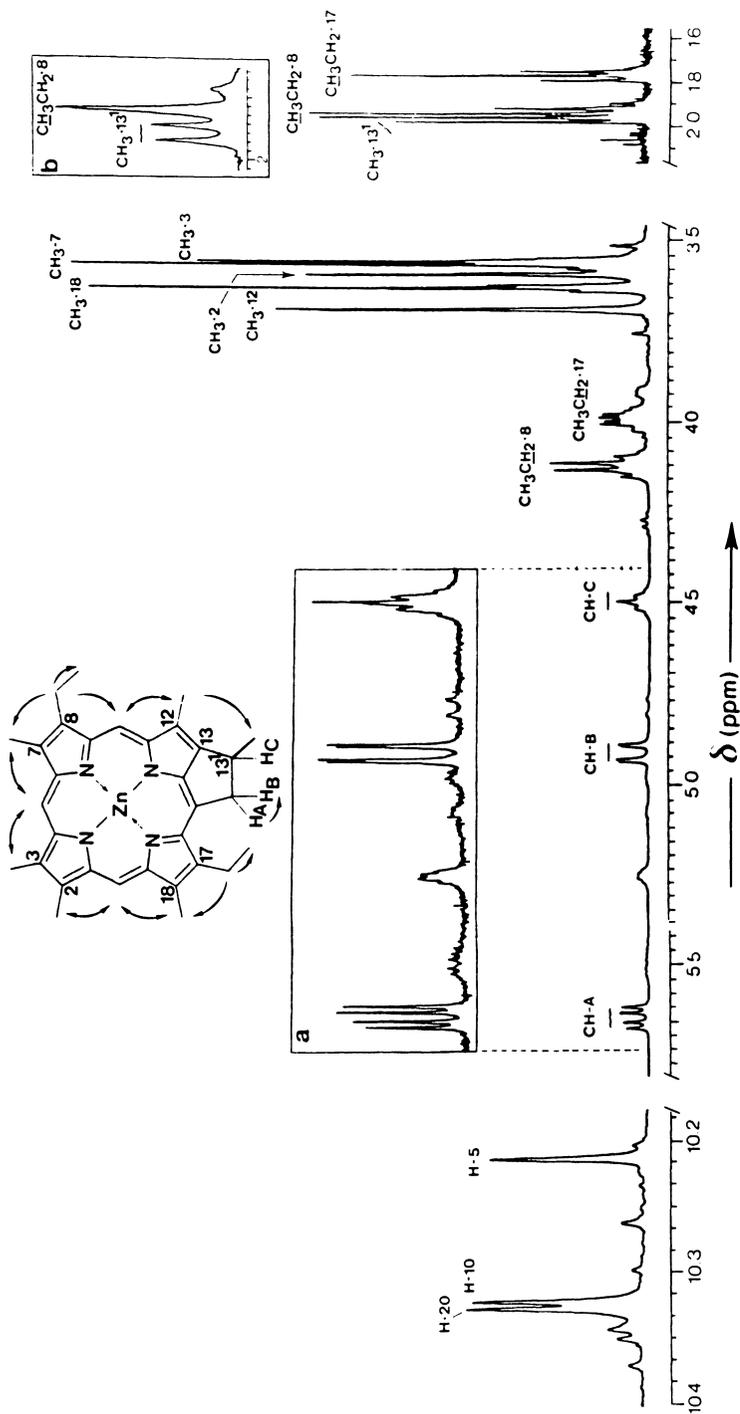


Figure 3. 400 MHz  $^1\text{H}$  NMR spectrum of (13-methyl)-13,15-ethano-8,17-diethyl-2,3,7,12,18-pentamethylporphyrin (12), as zinc complex) in  $\text{C}_6\text{D}_6/5\% \text{C}_5\text{D}_5\text{N}$ ; arrows indicate n.O.E. enhancements observed. Inserts: (a) expansion of the exocyclic ring protons; (b) after irradiation of  $\text{CH}_3\text{CH}_2$  at 4.118 ppm to decouple the  $\text{CH}_2\text{CH}_3$  at 1.937 ppm.

Table IV. 400 MHz  $^1\text{H}$  NMR data for component 12 (as zinc complex) in  $\text{C}_6\text{D}_6/5\% \text{C}_5\text{D}_5\text{N}$

$\delta$ (ppm)	Multiplicity*	n.o.e.+	Assignment
10.329	s	(3.687) <sup>§</sup> , 3.628, 3.590	<u>meso</u> H-20
10.323	s	3.687, (3.628, 3.590) <sup>§</sup>	<u>meso</u> H-10
10.215	s	3.564, 3.556	<u>meso</u> H-5
5.653	dd( $J_{\text{AB}}$ 16.6, 4.919 $J_{\text{AC}}$ 6.4, 4.502)	4.919	$\text{CH}_2(\text{A})-13^2$
4.919	dd( $J_{\text{BC}}$ 16.6, 5.653 $J_{\text{BC}}$ 2.2, 4.502)	n.d.	$\text{CH}_2(\text{B})-13^2$
4.502	m	n.d.	$\text{CH}_3\text{CH}(\text{C})-13^1$
4.118	q(7.7, 1.937)	10.323, 3.564, 1.937	$\text{CH}_2\text{CH}_3-8$
3.986	q(7.7, 1.778)	3.628, 1.778	$\text{CH}_2\text{CH}_3-17$
3.687	d(1.0, 4.502)	10.323, 1.963	$\text{CH}_3-12$
3.628	s	10.329	$\text{CH}_3-18$
3.590	s	10.329	$\text{CH}_3-2$
3.564	s	10.215	$\text{CH}_3-7$
3.556	s	10.215	$\text{CH}_3-3$
1.963**	d(7.1, 4.502)	n.d.	$\text{CH}_3\text{CH}-13^1$
1.937**	t(7.7, 4.118)	n.d.	$\text{CH}_3\text{CH}_2-8$
1.778	t(7.7, 3.986)	n.d.	$\text{CH}_3\text{CH}_2-17$

\* J Hz,  $\delta$  coupled nuclei. + Chemical shifts where enhancements seen when  $\delta$  signal irradiated. § Weak enhancement also observed due to partial saturation of close meso-H. \*\* Partially overlapping signals.

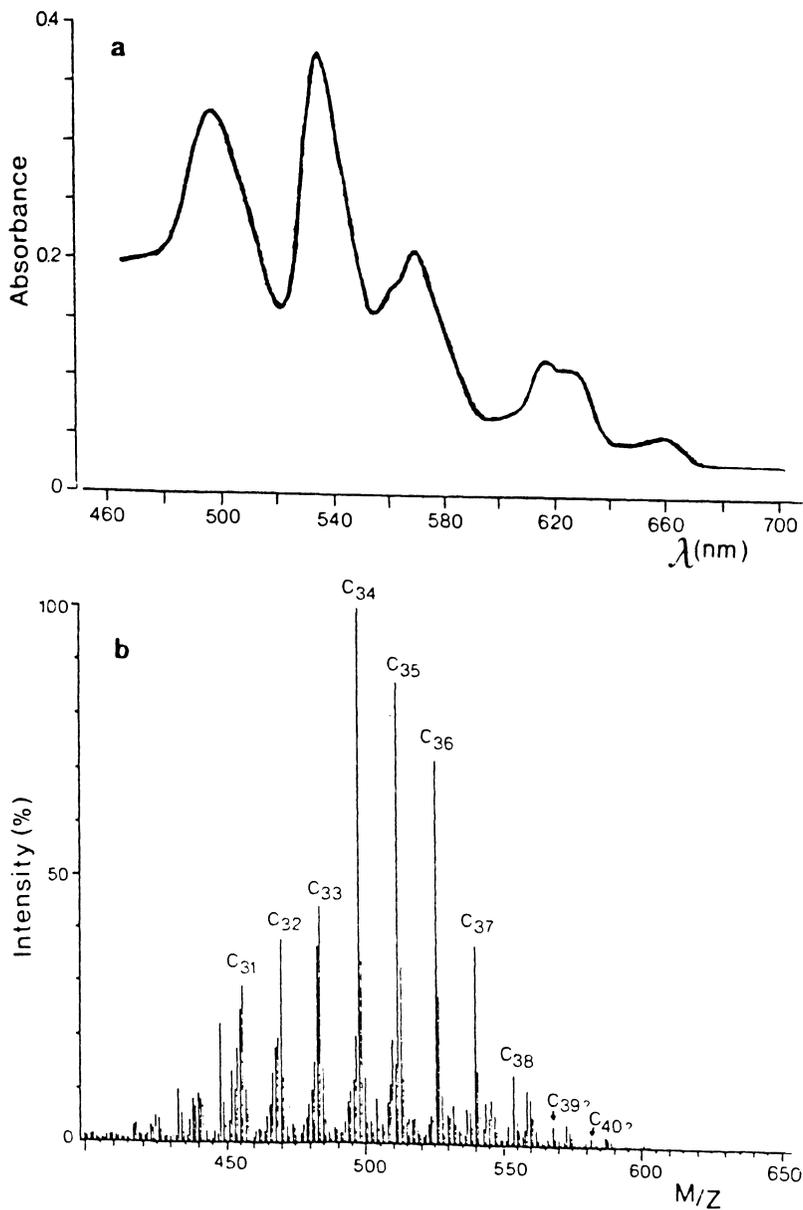


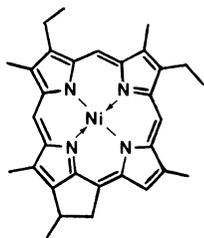
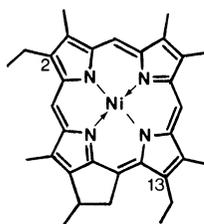
Figure 4. UV/visible (a) and EI probe mass (b) spectral data for a demetallated chromatographic fraction isolated from Boscan crude oil, and enriched in high molecular weight benzoporphyrins.

### Origin Considerations

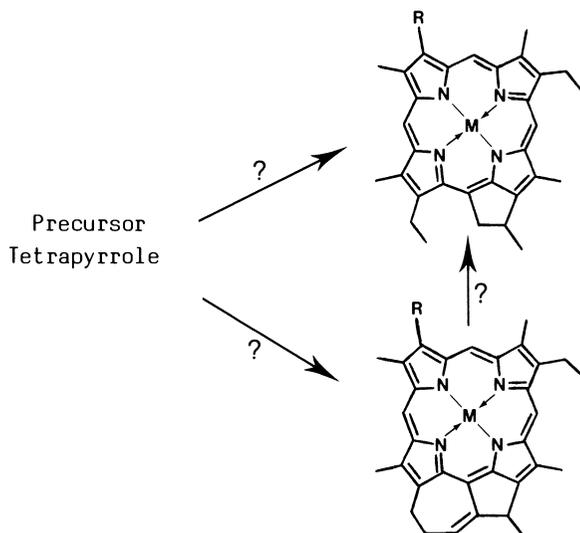
It is difficult to rationalise an origin for the Serpiano component having the unusual feature of a fused exocyclic ring moiety (25), since no known chlorophyll contains such a feature. On the other hand, a recent study showed the occurrence in a sponge of a chlorin with this feature, its presence being attributed to metabolism of dietary chlorophyll (45). It is possible, therefore, that the presence of 25 in Serpiano oil shale also reflects metabolic transformation of precursor pigments in the fossil water column, although the presence of the C-13<sup>1</sup> methyl substituent is a complicating factor.

The possibility of this C<sub>34</sub> porphyrin being an artefact can also be considered, for instance, by way of an unexpected internal condensation of a compound such as 45, during the treatment with methanesulphonic acid, after the Friedel-Crafts acetylation procedure employed for separation of components with a βH substituent from co-occurring fully alkylated species (24,32). Treatment of 45 [as the copper(II) complex] with methanesulphonic acid afforded solely the deacetylated counterpart as the free base 15 (23). The failure to detect this compound after treatment of the monoacetylated C<sub>32</sub> component with the seven membered ring does not prove that the C<sub>34</sub> compound is not an artefact formed from an unknown porphyrin in the total porphyrins (after demetallation). This possibility could be easily excluded by searching for the vanadyl C<sub>34</sub> complex in the total Serpiano metalloporphyrins. Such a search would be facilitated by using an HPLC procedure similar to that developed recently for the separation of sedimentary vanadyl porphyrins (46), and would eliminate any problems which might be associated with the demetallation procedure.

The two demetallated Gilsonite porphyrins (12,13) share with the demetallated fused ring Serpiano component the structural feature of a methyl substituent at C-13<sup>1</sup>. As indicated above, this feature has not been reported in any biological tetrapyrrole pigment which could be a precursor for the sedimentary compounds. The discovery in the Messel oil shale of the nickel(II) complex of a C<sub>31</sub> component with a five membered exocyclic ring containing a methyl substituent at C-15<sup>2</sup> led to the suggestion of an acid-catalysed rearrangement of a diagenetic product of chlorophyll c for the origin of the exocyclic ring (34). Bearing this in mind, one could perhaps envisage the Gilsonite porphyrins being formed in an analogous way to give structures such as the Gilsonite C<sub>32</sub> compound which can be represented as follows:

Messel C<sub>31</sub> componentGilsonite C<sub>32</sub> component

The Gilsonite component represented in this way has, however, a  $\beta$ -ethyl substituent in a position (i.e. at C-2) not known to have an ethyl or vinyl substituent in any biological tetrapyrrole; also, the condensation reaction proposed (34) to account for the exocyclic ring in the Messel component would not leave a C<sub>2</sub> substituent at C-13. In the absence of any other information, it appears that the Serpiano component and the two Gilsonite components may be related in some way because of the methyl substituent at C-13<sup>1</sup>. Indeed, the two structural types could even have a common precursor:



As indicated earlier, it is difficult to propose a rearrangement of a known chlorophyll which could give rise to the monobenzo[g]-porphyrins 23 and 24, although the possibility of a

bacterial origin for their precursor has been suggested (36). A further complexity is added by the preliminary evidence that there is a pseudo-homologous series of such components extending up to at least C<sub>38</sub>, i.e. components with several additional carbon atoms. Structural studies of the components > C<sub>33</sub> should reveal the sites of additional alkylation. This may provide further information either about the origin of the monobenzo[g]porphyrins or about the degradative pathways giving rise to them.

### Wider Geochemical Considerations

Although it is difficult at present to envisage plausible origins for some of the sedimentary porphyrin structures now known, a knowledge of the structures of as many of the sedimentary components as possible still provides a more reliable foundation for comparative studies of the overall distributions in different samples. For example, it is well known from the distributions obtained by HPLC that the abundance of components with an exocyclic alkanol ring relative to their aetioporphyrin counterparts decreases with increasing extent of maturation (47-50). This concept is readily illustrated in Figure 5, which shows the HPLC distributions of the demetallated porphyrins reported previously for four unrelated samples (21,23,50,51). Two of the samples have been used extensively to provide individual sedimentary porphyrins for structural studies (Tables I, II): (a) Gilsonite bitumen of Eocene age from the Uinta Basin (USA); the depositional environment of the source rock of this sample is thought to have been lacustrine and strongly saline (52). (b) Serpiano oil shale, Triassic, from Monte San Giorgio, Switzerland, with an enclosed marine depositional environment. The other two samples are: (c) Guang-33 oil, an immature oil shale of Eocene age from Jiangnan salt lake basin (central-eastern China, Hubei Province; 53). (d) An immature sample of Kimmeridge clay of Jurassic age from mainland U.K., from a shallow marine depositional environment (50).

The porphyrin distribution in Gilsonite bitumen is more mature than the other three samples in having a higher abundance of aetioporphyrins, which elute with retention times less than 32 minutes. Interestingly, the second most abundant component in Gilsonite, the C<sub>32</sub> component with the methyl substituted five membered exocyclic ring (12) has been characterised in Guang33 oil by comparison of spectral data, and co-chromatography with the component isolated from Gilsonite (51), although the structure of the component was previously given incorrectly as 44 (43). It is noteworthy that it

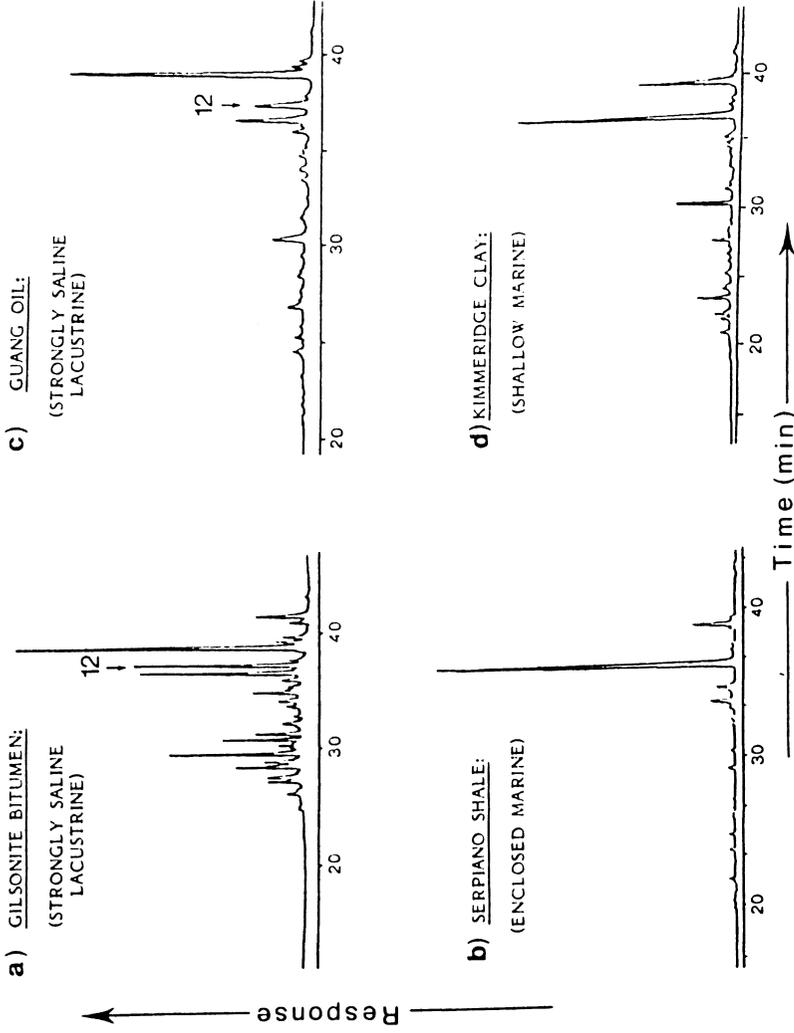
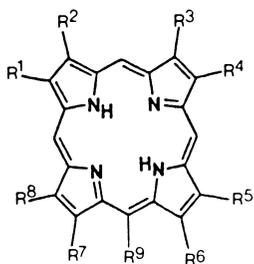
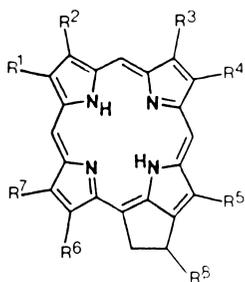


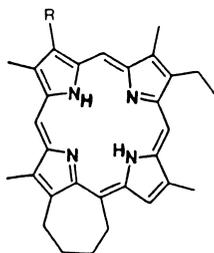
Figure 5. High-performance liquid chromatograms of the total porphyrins (after demetallation) from four unrelated geological samples.



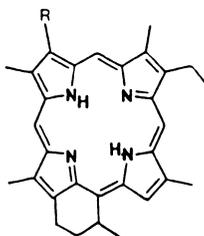
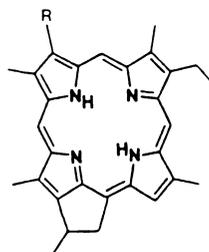
- 1: R<sup>2-8</sup> = CH<sub>3</sub>, R<sup>1</sup> = CH<sub>2</sub>CH<sub>3</sub>, R<sup>9</sup> = H  
 2: R<sup>1,3,5,8</sup> = CH<sub>3</sub>, R<sup>2,4,6,7</sup> = CH<sub>2</sub>CH<sub>3</sub>, R<sup>9</sup> = H  
 3a: R<sup>2,4,5,7,8</sup> = CH<sub>3</sub>, R<sup>1,3,6</sup> = CH<sub>2</sub>CH<sub>3</sub>, R<sup>9</sup> = H or  
 3b: R<sup>2,4,6-8</sup> = CH<sub>3</sub>, R<sup>1,3,5</sup> = CH<sub>2</sub>CH<sub>3</sub>, R<sup>9</sup> = H or  
 3c: R<sup>2-5,8</sup> = CH<sub>3</sub>, R<sup>1,6,7</sup> = CH<sub>2</sub>CH<sub>3</sub>, R<sup>9</sup> = H or  
 3d: R<sup>1,3-5,8</sup> = CH<sub>3</sub>, R<sup>2,6,7</sup> = CH<sub>2</sub>CH<sub>3</sub>, R<sup>9</sup> = H  
 4a: R<sup>1-3,5-7</sup> = CH<sub>3</sub>, R<sup>4,8</sup> = CH<sub>2</sub>CH<sub>3</sub>, R<sup>9</sup> = H or  
 4b: R<sup>1-3,5,6,8</sup> = CH<sub>3</sub>, R<sup>4,7</sup> = CH<sub>2</sub>CH<sub>3</sub>, R<sup>9</sup> = H  
 5: R<sup>1,3,5,8</sup> = CH<sub>3</sub>, R<sup>2,4,7</sup> = CH<sub>2</sub>CH<sub>3</sub>, R<sup>6,9</sup> = H  
 6: R<sup>1,3,5,8</sup> = CH<sub>3</sub>, R<sup>4,7</sup> = CH<sub>2</sub>CH<sub>3</sub>, R<sup>2,6,9</sup> = H  
 7: R<sup>1,3,5,8,9</sup> = CH<sub>3</sub>, R<sup>4,7</sup> = CH<sub>2</sub>CH<sub>3</sub>, R<sup>2,6</sup> = H



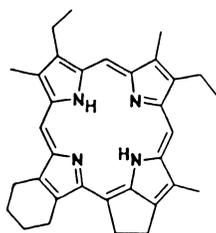
- 8: R<sup>1,3,5,7</sup> = CH<sub>3</sub>, R<sup>2,4,6</sup> = CH<sub>2</sub>CH<sub>3</sub>, R<sup>8</sup> = H  
 9: R<sup>1-3,5,7</sup> = CH<sub>3</sub>, R<sup>4,6</sup> = CH<sub>2</sub>CH<sub>3</sub>, R<sup>8</sup> = H  
 10: R<sup>1,3,5,7</sup> = CH<sub>3</sub>, R<sup>4,6</sup> = CH<sub>2</sub>CH<sub>3</sub>, R<sup>2,8</sup> = H  
 11: R<sup>1,5,7</sup> = CH<sub>3</sub>, R<sup>2,4,6</sup> = CH<sub>2</sub>CH<sub>3</sub>, R<sup>3,8</sup> = H  
 12: R<sup>1-3,5,7,8</sup> = CH<sub>3</sub>, R<sup>4,6</sup> = CH<sub>2</sub>CH<sub>3</sub>  
 13: R<sup>1,3,5,7,8</sup> = CH<sub>3</sub>, R<sup>2,4,6</sup> = CH<sub>2</sub>CH<sub>3</sub>  
 14a: R<sup>1,3,5,7</sup> = CH<sub>3</sub>, R<sup>2,4</sup> = CH<sub>2</sub>CH<sub>3</sub>, R<sup>6,8</sup> = H or  
 14b: R<sup>1,2,5,7</sup> = CH<sub>3</sub>, R<sup>3,4</sup> = CH<sub>2</sub>CH<sub>3</sub>, R<sup>6,8</sup> = H or  
 14c: R<sup>1,2,4,7</sup> = CH<sub>3</sub>, R<sup>3,5</sup> = CH<sub>2</sub>CH<sub>3</sub>, R<sup>6,8</sup> = H or  
 14d: R<sup>1,3,4,7</sup> = CH<sub>3</sub>, R<sup>2,5</sup> = CH<sub>2</sub>CH<sub>3</sub>, R<sup>6,8</sup> = H

15: R = CH<sub>2</sub>CH<sub>3</sub>16: R = CH<sub>3</sub>

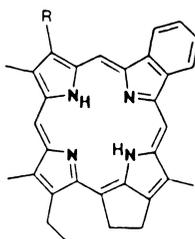
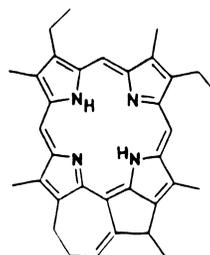
17: R = H

18: R = CH<sub>2</sub>CH<sub>3</sub>19: R = CH<sub>3</sub>20: R = CH<sub>2</sub>CH<sub>3</sub>

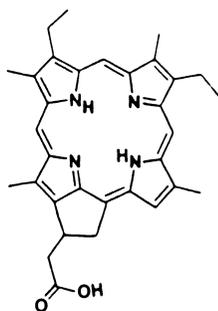
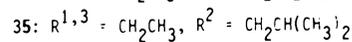
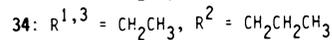
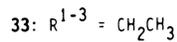
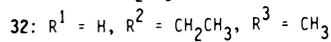
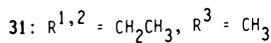
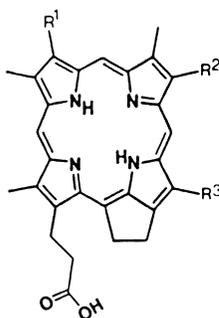
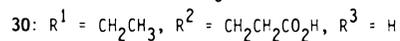
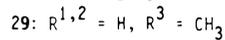
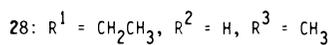
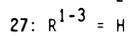
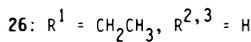
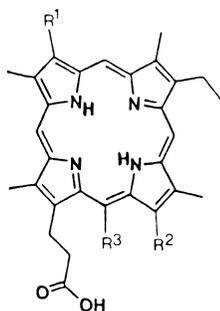
21: R = H



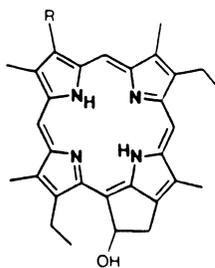
22

23: R = CH<sub>2</sub>CH<sub>3</sub>24: R = CH<sub>3</sub>

25

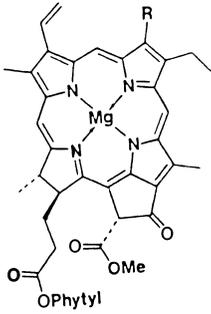


36



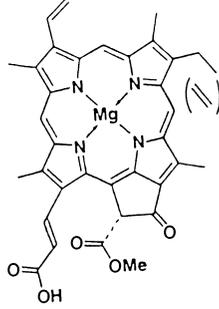
37:  $R = \text{CH}_2\text{CH}_3$

38:  $R = \text{H}$

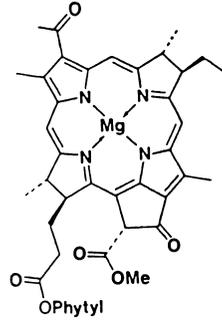


39: R = CH<sub>3</sub>

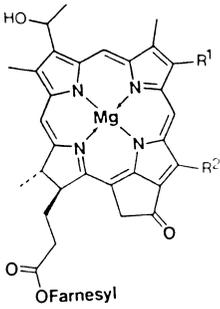
40: R = CHO



41

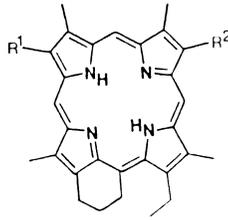


42



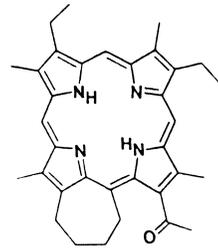
43: R<sup>1</sup> = CH<sub>2</sub>CH<sub>3</sub>, CH<sub>2</sub>CH<sub>2</sub>CH<sub>3</sub>,  
CH<sub>2</sub>CH(CH<sub>3</sub>)<sub>2</sub>, CH<sub>2</sub>C(CH<sub>3</sub>)<sub>3</sub>

R<sup>2</sup> = CH<sub>3</sub>, CH<sub>2</sub>CH<sub>3</sub>



44a: R<sup>1</sup> = CH<sub>3</sub>, R<sup>2</sup> = CH<sub>2</sub>CH<sub>3</sub>

44b: R<sup>2</sup> = CH<sub>3</sub>, R<sup>1</sup> = CH<sub>2</sub>CH<sub>3</sub>



45

does not occur in either of the two marine samples; its presence in two samples from lacustrine, strongly saline depositional environments suggests that it might be associated with such a type of environment. Further studies of the porphyrin distributions from a wide variety of samples are necessary to show whether these distributions can, indeed, provide information about depositional environments.

### Conclusions

1. The number of sedimentary porphyrin structures now elucidated emphasises the remarkable complexity of the mixtures which can occur in sediments and petroleums. This complexity arises from the variations which can occur in the diagenetic reactions which alter a variety of precursors, mainly chlorophylls. In addition, the structures of several of the compounds cannot at present be easily related to known biological pigments.

2. The determination of three novel structures is described, correcting a previous misassignment for one of them. This component has only been found to date in high relative abundance in samples from lacustrine, strongly saline, depositional environments.

3. Although possible origins of many of the compounds are not yet clear, a knowledge of their structures provides more effective comparison of the distributions obtained by HPLC from different sediments and petroleums.

4. In order to understand the origins of the more unusual sedimentary components and the degradative pathways leading to them, structural elucidation work similar to that described and reviewed herein should be applied to components isolated from contemporary sedimentary samples and from older samples with a milder thermal history than those examined to date (Table I, II).

### Acknowledgments

We are grateful to the British Petroleum plc and the Natural Environment Research Council (GR3/2951 and GR3/3758) for providing HPLC and MS facilities, respectively. Two of us thank the Brazilian National Research Council, CNPq (M.I.C.) and the Natural Environment Research Council (S.K.) respectively for Research Studentships. Drs. M. Murray (University of Bristol), O. Howarth and E. Curzon (University of Warwick) are gratefully acknowledged for running NMR spectra and Dr. I. Peakman for valuable discussions. Dr. K.A.G.

MacNeil (University of Bristol) is thanked for HRMS analyses, and R. Pitt for assistance with the isolation of the two Gilsonite porphyrins.

### Literature Cited

1. For example: Ourisson, G.; Albrecht, P.; Rohmer, M. Pure and Appl. Chem. 1979, 51,709-29; Mackenzie, A.S.; Brassell, S.C.; Eglinton, G.; Maxwell, J.R. Science 1982, 217, 491-504; Brassell, S.C.; Eglinton, G.; Maxwell, J.R. Biochem. Soc. Trans. 1984, 575-86; and references therein.
2. For example: Maxwell, J.R.; Quirke, J.M.E.; Eglinton, G. In "Internationales Alfred-Treibs-Symposium 1979"; Prashnowsky, A.A., Ed.; Universität Würzburg, Munich, 1980; pp. 37-55; and references therein.
3. Bonnett, R.; Czechowski, F. Phil. Trans. R. Soc. Lond. Ser. A, 1981, 300, 51-63
4. Bonnett, R.; Burke, P.J.; Reszka, A. J. Chem. Soc., Chem. Commun. 1983, 1085-87
5. Bonnett, R.; Czechowski, F. Nature 1980, 283, 465-67
6. Bonnett, R.; Czechowski, F. J. Chem. Soc., Perkin Trans. I, 1984, 125-31
7. Palmer, S.E.; Baker, E.W. Science 1978, 201, 49-51
8. Louda, J.W.; Baker, E.W. In "Initial Reports of the Deep Sea Drilling Project"; Yeats, R.S.; Haq, B.U. and the Shipboard Party, Ed.; U.S. Government Printing Office: Washington, 1981; vol. 63, pp. 785-818
9. Palmer, S.E.; Huang, W.Y.; Baker, E.W. In "Initial Reports of the Deep Sea Drilling Project-XLIIL"; Tucholke, B.E.; Vogt, P.R. and the Shipboard Party, Ed.; U.S. Government Printing Office: Washington, 1979; vol. 43, pp. 657-61
10. Baker, E.W.; Louda, J.W. In "Advances in Organic Geochemistry 1981"; Bjorøy, M. et al., Ed.; J. Wiley & Sons, Chichester 1983, pp. 401-21
11. Baker, E.W.; Louda, J.W. In "Advances in Organic Geochemistry 1985", Julich, in press
12. Treibs, A. Angew. Chem. 1936, 49, 682-86
13. Regtop, R.; Crisp, P.T.; Ellis, J. Proc. 1st. Australian Workshop on Oil Shale 1983,73-5
14. Barwise, A.J.G.; Evershed, R.P.; Wolff, G.A.; Eglinton, G.; Maxwell, J.R. J. Chromatogr. 1986, 368, 1-9; and references therein.
15. Chicarelli, M.I.; Wolff, G.A.; Maxwell, J.R. J. Chromatogr. 1986, 368, 11-19; and references therein.

16. Ocampo, R.; Callot, H.J.; Albrecht, P. J. Chem. Soc., Chem. Commun. 1985, 189-200
17. Ocampo, R.; Callot, H.J.; Albrecht, P. J. Chem. Soc., Chem. Commun. 1985, 200-01; and references therein.
18. Quirke, J.M.E.; Eglinton, G.; Maxwell, J.R. J. Am. Chem. Soc. 1979, 101, 7693-97
19. Quirke, J.M.E.; Maxwell, J.R. Tetrahedron 1980, 36, 3453-56
20. Quirke, J.M.E.; Maxwell, J.R.; Eglinton, G.; Sanders, J.K.M. Tetrahedron Lett. 1980, 21, 2987-90
21. Wolff, G.A. Ph. D. Thesis, University of Bristol, Bristol, 1983
22. Chicarelli, M.I.; Wolff, G.A.; Maxwell, J.R. J. Chem. Soc., Chem. Commun. 1985, 723-24
23. Chicarelli, M.I. Ph. D. Thesis, University of Bristol, Bristol, 1985
24. Chicarelli, M.I.; Maxwell, J.R. Tetrahedron Lett. 1984, 25, 4701-04
25. Krane, J.; Skjetne, T.; Telnaes, N.; Bjorøy, M.; Solli, H. Tetrahedron 1983, 39, 4109-19
26. Fookes, C.J.R. J. Chem. Soc., Chem. Commun. 1985, 706-08
27. Fookes, C.J.R. J. Chem. Soc., Chem. Commun. 1983, 1472-73
28. Ekstrom, A.; Fookes, C.J.R.; Hambley, T.; Loeh, H.J.; Miller, S.A.; Taylor, J.C. Nature 1983, 206, 173-174
29. Ocampo, R. Thesis Docteur ès Sciences, Université Louis Pasteur de Strasbourg, Strasbourg, 1985
30. Storm, C.B.; Krane, J.; Skjetne, T.; Telnaes, N.; Branthaver, J.F.; Baker, E.W. Science 1984, 233, 1075-76
31. Wolff, G.A.; Murray, M.; Maxwell, J.R.; Hunter, B.K.; Sanders, J.K.M. J. Chem. Soc., Chem. Commun. 1983, 922-24
32. Chicarelli, M.I.; Wolff, G.A.; Murray, M.; Maxwell, J.R. Tetrahedron 1984, 40, 4033-39
33. Fookes, C.J.R. J. Chem. Soc., Chem. Commun. 1983, 1474-76
34. Ocampo, R.; Callot, H.J.; Albrecht, P.; Kintzinger, J.P. Tetrahedron Lett. 1984, 25, 2589-92
35. Barwise, A.J.G.; Roberts, I. Org. Geochem. 1984, 6, 167-76
36. Kaur, S.; Chicarelli, M.I.; Maxwell, J.R. J. Am. Chem. Soc. 1986, 108, 1347-48
37. Habermehl, G.G.; Springer, G.; Frank, M.H. Naturwissenschaften 1984, 71, 261-63
38. Bonnett, R.; Burke, J.P. In this volume; and references therein
39. Krane, J.; Skjetne, T.; Telnaes, N.; Bjorøy, M.; Schou, L.; Solli, H. Org. Geochem. 1984, 6, 193-201

40. Ponomarev, G.V.; Shul'ga, A.M. Khim. Geterotsikl. Soedin. 1984, 19, 485-89; Chem. Abstr. 1984, 101, 110796a
41. Baker, E.W.; Palmer, S.E. In "The Porphyrins"; Dolphin, D., Ed.; Academic Press, New York, 1978; vol. IA, pp. 485-551
42. Chicarelli, M.I.; Maxwell, J.R. Tetrahedron Lett. 1986, 27, 4653-54
43. Wolff, G.A.; Chicarelli, M.I.; Shaw, G.J.; Evershed, R.P.; Quirke, J.M.E.; Maxwell, J.R. Tetrahedron 1984, 40, 3777-86
44. Kaur, S., unpublished data
45. Karuso, P.; Bergquist, P.R.; Buckleton, J.S.; Cambie, R.C.; Clark, G.R.; Rickard, C.E.F. Tetrahedron Lett. 1986, 27, 2177-78
46. Sundararaman, P. Anal. Chem. 1985, 57, 2204-06
47. Mackenzie, A.S.; Quirke, J.M.E.; Maxwell, J.R. In "Advances in Organic Geochemistry 1979"; Douglas, A.G.; Maxwell, J.R., Eds.; Pergamon Press, Oxford, 1980; pp. 239-48
48. Barwise, A.J.G.; Park, P.J.D. In "Advances in Organic Geochemistry 1981"; Bjorøy, M. et al.; J. Wiley & Sons, Chichester, 1983, pp. 668-74
49. Shi, Ji-Yang; Mackenzie, A.S.; Alexander, R.; Eglinton, G.; Gowar, A.P.; Wolff, G.A.; Maxwell, J.R. Chem. Geol. 1982, 35, 1-31
50. Farrimond, P.; Comet, P.; Eglinton, G.; Evershed, R.P.; Hall, M.A.; Park, D.W.; Wardroper, A.M.K. Mar. Pet. Geol. 1984, 1, 340-54
51. Xu Fenfang; Sheng Guoying; Fu Jia Mo; Evershed, R.P.; Jiang Jigang Geochimica 1985, 358-62; Chem. Abstr. 1986, 104, 71337s
52. Sugihara, J.M.; McGee, L.R. J. Org. Chem. 1957, 22, 795-98
53. Fu Jia Mo; Sheng Guoying; Peng Pingan; Brassell, S.C.; Eglinton, G.; Jiang Jigang In "Advances in Organic Geochemistry 1985"; Julich, in press

RECEIVED November 10, 1986

## Chapter 3

# Evidence for Porphyrins of Bacterial and Algal Origin in Oil Shale

R. Ocampo, H. J. Callot, and P. Albrecht

Département de Chimie, UA 31, Université Louis Pasteur, 1, rue Blaise Pascal,  
67008 Strasbourg, France

The petroporphyrins from the immature Messel oil shale consist almost exclusively of alkylporphyrins and monocarboxylic acids, complexed with nickel. Sixteen structures of pure isolated products (including ten carboxylic acids) were determined. Two groups of pigments could be specifically correlated with algal (chlorophylls  $\underline{c}$  +  $\underline{c}'$ ) and bacterial (bacteriochlorophylls  $\underline{d}$ ) precursors, while the remaining structures confirm a non specific chlorophyllic origin. The survival of a major monocarboxylic acid fraction with concomittant skeletal modifications both confirm the immaturity of the shale and underline the complexity of the diagenetic routes.

The transformation of chlorophyll into petroporphyrins was first suggested in 1934-36 when Treibs proposed what is now known as "Treibs scheme" (1) (Figure 1).

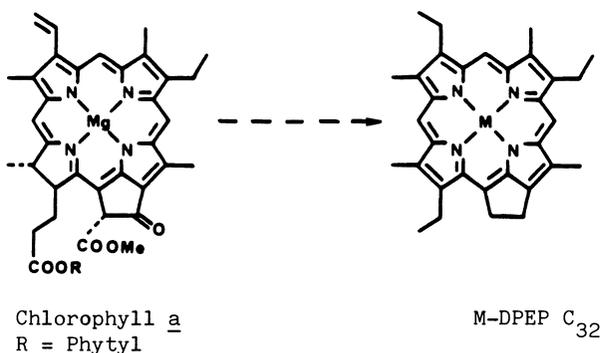


**Figure 1.** The Treibs' scheme leads from Chlorophyll to DPEP petroporphyrins by a sequence of geochemical transformations.

Although petroporphyrins were later detected in a variety of sediments the knowledge of their precise structure "regressed" as mass spectrometry revealed very complex mixtures (2-5). In recent years the development of very efficient chromatographic (e.g. HPLC) and spectroscopic techniques (FT NMR and NOE) has allowed several groups (6-23) to overcome the problems of separation and to assign the structures of a limited number of petroporphyrins. Crystal structures by X-ray diffraction confirmed the assignments for two products (20-21). All structures described from oil shales are compatible with chlorophyllic precursors as indicated by the presence, in many compounds, of an isocyclic five-membered ring, by specific modifications at position C-3, etc. In one instance a specific precursor, chlorophyll b, was suggested by the loss of the C-7 substituent (22).

However, several fundamental questions concerning the origin and the transformations of the petroporphyrins remained almost unanswered

a. with the exception cited above no specific chlorophyll precursor could be attributed to the petroporphyrins ; in consequence the role of porphyrins as biomarkers of sediments and petroleum remained limited ;

b. although intermediates in the "Treibs' scheme", especially carboxylic acids, could be valuable maturation indicators, they were unknown, again with only one exception (21) ;

c. conflicting hypotheses (24-26) concerning the petroporphyrins with C-number higher than that expected from chlorophyll a (> 32 in the alkyl series) could not be discussed until such compounds were purified and their structures clearly assigned : do they arise from bacterial homologated "Chlorobium chlorophylls" (Figure 3) or from transalkylation (alkylation - dealkylation) of pigments derived from "normal" chlorophylls ?

We chose to study the Messel oil shale for several reasons. The sediment was deposited at the bottom of a lake filling a narrow rift within the Odenwald plateau (near Darmstadt, West Germany). It is dated from Eocene (45-49 Myr ; contemporary to the sinking of the Rhine valley) and was never buried under more than a few meters of sand and gravel. It is thus rather immature as shown by earlier geochemical studies which identified a large number of lipids from the shale (27-28). Paleontological and geological studies (29) indicated that the lake waters were calm, partly anaerobic and in a warm tropical environment. All these data suggested that the petroporphyrins should be well preserved and indeed extraction of the shale, followed by separation and structural determination (30-33) led us to identify sixteen nickel complexes (Figure 2) which accounted for more than 90% of the extractible petroporphyrins.

Carboxylic acids (60-70% of the total porphyrin fraction, characterized as their methyl esters) outweigh the alkylpetroporphyrins and this confirms the immaturity of the Messel oil shale. The distribution of the acids does not reflect that of the alkylpetroporphyrins, in particular, compound 7 is a minor component of the acid fraction while its decarboxylated counterpart 6 dominates the acid fraction. The fact that some of these acids (8, 9, 10 and 11, phyllo- and pyrroporphyrin series) show a degraded isocyclic ring indicates that a linear "Treibs' scheme" should be replaced by several diagenetic routes in which the decarboxylation of the propionic side-chain

may occur before or after major skeletal modifications. This suggests that some compounds called etioporphyrins in the literature only on the basis of their composition and often correlated to the products of thermal ring opening of DPEP'S may in fact originate in an early degradation of the 5-membered ring of the chlorophylls.

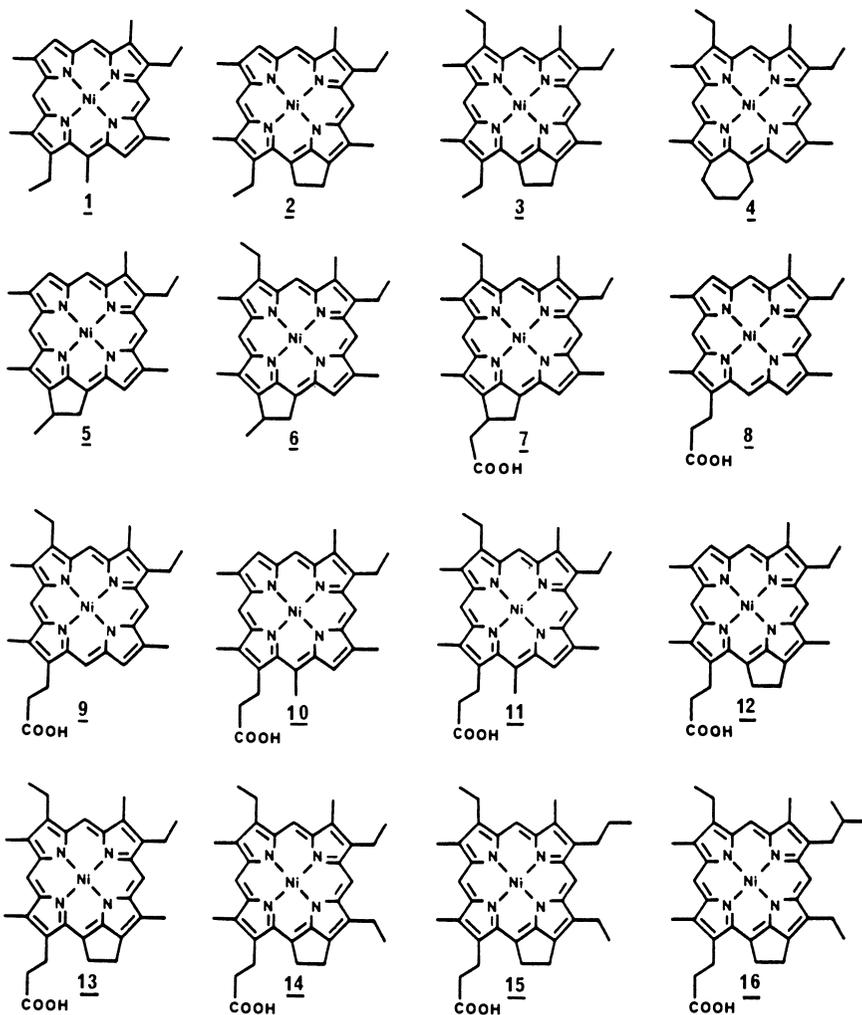


Figure 2. Petroporphyrins identified after their isolation from the Messel oil shale.

Of more fundamental importance is the structure of two groups of petroporphyrins viz 14-16 and 5-7. The first group of compounds possesses a carbon framework which is only compatible with bacteriochlorophylls d, positions 8 and 12 being specifically homologated (34-35) (Figure 3). The structures of the components of the second group of petroporphyrins 5 - 7 are typical of rearrangement products of chlorophyll c (or c') (36-37) since only these chlorophylls (Figure 3), which bear an acrylic instead of a propionic side-chain, are able to undergo such a rearrangement.

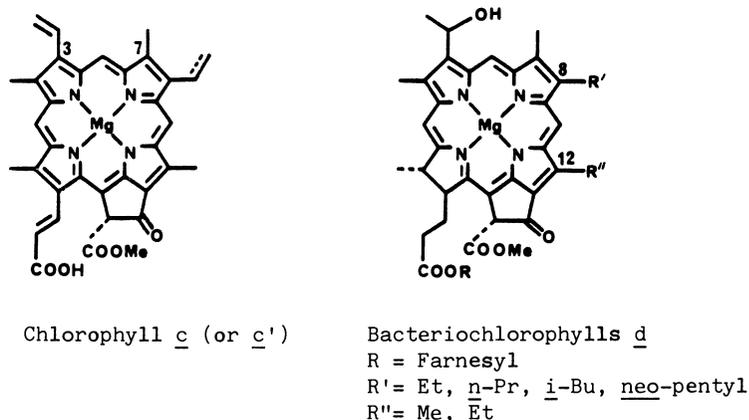


Figure 3. Specific precursors of the Messel oil shale's porphyrins.

The identification of specific precursors for six of the petroporphyrins from Messel oil shale demonstrates the bacterial and algal input in the organic matter since bacteriochlorophylls d are specific for Chlorobium group photosynthetic bacteria, and chlorophylls c and c' for algae. The importance of the algal contribution is illustrated by the fact that 6 is the major product of the alkylpetroporphyrin fraction. This is in agreement with the abundance in the shale of steroids and terpenoids whose origin is attributed to microalgae and bacteria (27-28).

Although it is not possible, from simple structural considerations, to attribute a specific precursor for the remaining compounds, all structures may be interpreted starting from chlorophyllic precursors (chlorophylls a, b, c and c'; bacteriochlorophylls a and b; lowest homolog of bacteriochlorophylls d). The absence of true etioporphyrins (alkyls on pyrroles exclusively) may be correlated again with the immaturity of the shale.

Comparison of the above results with the problem evoked in the introduction shows that, at least in the case of the Messel oil shale, we can find several answers :

a. specific precursors of petroporphyrins can be found and confirm the existing geological and geochemical data : under oxygenated waters containing algae, photosynthetic bacteria of the Chlorobium group (not exclusive) flourished in the anaerobic layers ;

b. carboxylic acids, key-intermediates in the "Treibs' scheme", can be major constituents of the porphyrin fraction, under favorable conditions, and a reinterpretation of the diagenetic scheme in terms of multiple routes is necessary ;

c. at least in the case of the Messel shale, the only "high molecular weight" extractable petroporphyrins are interpretable in terms of bacterial input ; no evidence was found for any contribution of transalkylation reactions (nor was any for a DPEP → etioporphyrins transformation).

Although these results concern one rather peculiar environment, these novel structural data give a new insight into the origin, diagenesis and significance of petroporphyrins in sediments. In particular, the identification of specific precursors for several petroporphyrins will favor their rational use as biological markers of sediments and petroleum.

Acknowledgments : We thank Dr. J.P. Kintzinger and Mrs E. Krempf for their assistance in the NMR studies, the C.N.R.S., Université Louis Pasteur and CONACYT (Mexico) for financial support and the Management of the Messel Mine for shale samples. We further thank Dr. von Koenigswald, Hessisches Landesmuseum, Darmstadt, FRG, for helpful discussions and help in the sample collection.

#### Literature Cited

1. Treibs, A. Angew. Chem. 1936, 49, 682-6.
2. Dean, R. A.; Whitehead, E. V. 6th World Petroleum Congr., Sect. V, 1963, p. 261.
3. Thomas, D. W.; Blumer, M. Geochim. Cosmochim. Acta 1964, 28, 1147-54.
4. Baker, E. W. J. Am. Chem. Soc. 1966, 88, 2311-5.
5. Baker, E. W.; Yen, T. F.; Dickie, J. P.; Rhodes, R. E.; Clark, L. F. J. Am. Chem. Soc. 1967, 89, 3631-9.
6. Quirke, J. M. E.; Eglinton, G.; Maxwell, J. R. J. Am. Chem. Soc. 1979, 101, 7693-7.
7. Quirke, J. M. E.; Maxwell, J. R.; Eglinton, G.; Sanders, J. K. M. Tetrahedron Lett. 1980, 21, 2987-90.
8. Quirke, J. M. E.; Maxwell, J. R. Tetrahedron 1980, 36, 3453-6.
9. Fookes, C. J. R. J. Chem. Soc., Chem. Commun. 1983, 1472-3.
10. Fookes, C. J. R. J. Chem. Soc., Chem. Commun. 1983, 1474-6.
11. Wolff, G. A.; Murray, M.; Maxwell, J. R.; Hunter, B. K.; Sanders, J. K. M. J. Chem. Soc., Chem. Commun. 1983, 922-4.
12. Wolff, G. A.; Chicarelli, M. I.; Shaw, G. J.; Evershed, R. P.; Quirke, J. M. E.; Maxwell, J. R. Tetrahedron 1984, 40, 3777-86.
13. Krane, J.; Skjetne, T.; Telnaes, N.; Bjoroy, M.; Solli, H. Tetrahedron 1983, 39, 4109-19.
14. Storm, C. B.; Krane, J.; Skjetne, T.; Telnaes, N.; Branthaver, J. F.; Baker, E. W. Science 1984, 223, 1075-6.
15. Chicarelli, M. I.; Wolff, G. A.; Maxwell, J. R. J. Chem. Soc., Chem. Commun. 1985, 723-4.
16. Chicarelli, M. I.; Wolff, G. A.; Murray, M.; Maxwell, J. R. Tetrahedron 1984, 40, 4033-9.
17. Fookes, C. J. R. J. Chem. Soc., Chem. Commun. 1985, 706-8.

18. Chicarelli, M. I.; Maxwell, J. R. Tetrahedron Lett. 1986, 27, 4653-4.
19. Verne-Mismer, J.; Ocampo, R.; Callot, H. J.; Albrecht, P. Tetrahedron Lett., in press.
20. Ekstrom, A.; Fookes, C. J. R.; Hambley, T.; Loeh, H. J.; Miller, S. A.; Taylor, J. C. Nature 1983, 306, 173-4.
21. Habermehl, G. G.; Springer, G.; Frank, M. H. Naturwissenschaften 1984, 71, 261-3.
22. Chicarelli, M. I.; Maxwell, J. R. Tetrahedron Lett. 1984, 25, 4701-4.
23. Kaur, S.; Chicarelli, M. I.; Maxwell, J. R. J. Am. Chem. Soc. 1986, 108, 1347-8.
24. Mackenzie, A. S.; Quirke, J. M. E.; Maxwell, J. R. In "Advances in Organic Geochemistry 1979"; Douglas, A. C.; Maxwell, J. R.; Eds.; Pergamon Press, Oxford, 1980; pp. 239-48.
25. Quirke, J. M. E.; Shaw, G. J.; Soper, P. D.; Maxwell, J. R. Tetrahedron 1980, 36, 3261-7.
26. Baker, E. W.; Louda, J. W. In "Advances in Organic Geochemistry 1981"; Bjoroy, M.; Albrecht, P.; Cornford, C.; De Groot, K.; Eglinton, G.; Galimov, E.; Leythaeuser, D.; Pelet, R.; Rullkotter, J.; Speers, G.; Eds.; Wiley, London, 1983; pp. 401-21.
27. Michaelis, W.; Albrecht, P. Naturwissenschaften 1979, 66, 420-1.
28. Robinson, N. Ph.D. Thesis, University of Bristol, U.K., 1985.
29. Von Koenigswald, W. Geol. Jb. Hessen 1980, 108, 23-38.
30. Ocampo, R.; Callot, H. J.; Albrecht, P.; Kintzinger, J. P. Tetrahedron Lett. 1984, 25, 2589-92.
31. Ocampo, R.; Callot, H. J.; Albrecht, P. J. Chem. Soc., Chem. Commun. 1985, 198-200.
32. Ocampo, R.; Callot, H. J.; Albrecht, P. J. Chem. Soc., Chem. Commun. 1985, 200-1.
33. Ocampo, R. Ph.D. Thesis, Université Louis Pasteur de Strasbourg, France, 1985.
34. Smith, K. M.; Goff, D. A.; Fajer, J.; Barkigia, K. M. J. Am. Chem. Soc., 1982, 104, 3747-9.
35. Smith, K. M.; Goff, D. A.; Fajer, J.; Barkigia, K. M. J. Am. Chem. Soc. 1983, 105, 1674-6.
36. Jackson, A. H. In "Chemistry and biochemistry of plant pigments"; Goodwin, T., Ed.; 2nd ed., vol. 1; Academic Press, New York, 1976; pp. 1-63.
37. Dougherty, R. C.; Strain, H. H.; Svec, W. W.; Uphaus, R. A.; Katz, J. J. J. Am. Chem. Soc. 1970, 92, 2826-33.

RECEIVED November 10, 1986

## Chapter 4

# Rationalization for the Predominance of Nickel and Vanadium Porphyrins in the Geosphere

J. M. E. Quirke

Department of Chemistry, Florida International University, Tamiami Trail,  
Miami, FL 33199

The predominance of nickel and vanadium porphyrins, over other metalloporphyrins in the geosphere may be explained by taking into account four factors: the abundances of the metals, and their environment within the sediments and/or the water column, the stability of the nitrogen-metal bonds, and the lability of the bridge positions of the metal porphyrin complexes.

Since the original isolation of porphyrins from a variety of sedimentary environments, two types of metal complex -the nickel(II) and vanadyl (V=O)- have dominated geoporphyrin chemistry.(1,2) The reason for the selection of these two metals is not immediately obvious in view of the array of potential metal candidates, some of which, e.g. chromium (III), can form more stable complexes than either nickel or vanadium.(Fig. 1, 3,4) The problem is further complicated because the timing of the metal insertion in the degradative pathway from the chlorophylls to the geoporphyrins is not well understood. Thus it is unclear whether metal insertion occurs in the water column, or in the water column-sediment boundary, or within the sediments.

One possible explanation is based on the probability that the metals in organic rich sediments occur as their sulphides because such sediments have high concentrations of hydrogen sulphide. For metal sulphides with low solubility products e.g. copper (II) sulphide the metal ion would be present in very low concentrations, and therefore would be less likely to chelate with the porphyrins than those sulphides with higher solubility products. This argument is not necessarily sound. The metal ions in solution, albeit in very low concentration, could chelate with porphyrins and chlorins, forcing more metal ion into solution until the porphyrins were

Li	Be																	B	
Na	Mg																	Al	Si
K	Ca	Sc	Ti	V	Cr	Mn	Fe	Co	Ni	Cu	Zn	Ga	Ge	As					
Rb	Sr	Y	Zr	Nb	Mo		Ru	Rh	Pd	Ag	Cd	In	Sn	Sb					
Cs	Ba	*La	Hf	Ta	W	Re	Os	Ir	Pt	Au	Hg	Tl	Pb	Bi					
		*Lanthanides																	
		Ce	Pr	Nd		Sm	Eu	Gd	Tb	Dy	Ho	Er	Tm	Yb	Lu				

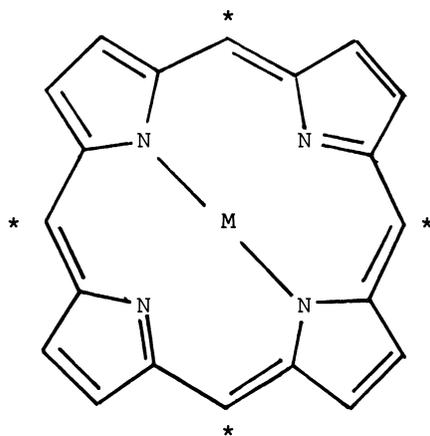
Fig. 1 Elements known to Form Chelates with Porphyrins.

completely chelated. In addition, the solubility product argument cannot readily account for the possibility that the porphyrins undergo chelation on the mineral surface.

A different approach to rationalising the selectivity of the chelation of the geoporphyrins will be presented. The hypothesis encompasses both the nature of the metal prior to chelation and the stability of the metalloporphyrins after chelation. It is assumed that the different skeletal types of porphyrin (1) will behave similarly in the chelation process, although the absolute rates of chelation may differ for each skeletal type of geoporphyrin. The factors which influence chelation are as follows:

- a) The availability of efficient metal ion carriers.
- b) The abundance of the elements.
- c) The stability of the metal-nitrogen bond in the porphyrin complex.
- d) The stability of the metal-nitrogen bond in porphyrins in the geological environment.
- e) The lability of the porphyrin meso (bridge) positions.

This hypothesis has the virtue of being sufficiently flexible so that it can be used to examine the possibility of metal insertion either at the water column-sediment interface or deeper down in the sediment. The hypothesis may be further refined by as more data are obtained on the nature of the porphyrins bound on mineral matrices.



\* = Meso-Position

(1)

## Results and Discussion

Each of the five parameters in the model will be discussed in turn. The post-chelation parameters are interrelated, and therefore these factors are discussed together.

The Importance of the Ion Carrier. The nature of the ion carrier in the sedimentary environment is of primary importance in determining the possibility of chelation because the first stage in the metal insertion is the deconvolution of the metal ion from the ion carrier. Very stable ion carriers are very inefficient reagents for the metallation of the porphyrins. In the laboratory, highly charged metal ions are more difficult to insert than lower valence species because the negatively charged anions, and/or the negatively polarised ligands are more tightly bound to the metal. This is particularly significant for the insertion of tetra- and penta-valent metals, many of which form stable metalloporphyrins. The laboratory syntheses of such compounds usually require vigorous conditions, and often use water sensitive metallating agents (e.g.  $\text{TiCl}_4$ ,  $\text{SiCl}_4$ ,  $\text{AlCl}_3$ ,  $\text{R}_2\text{AlH}$ ).<sup>(3)</sup> Thus, silicon porphyrins are among the most stable complexes known, but they are not found in nature because the silicon occurs in silicates, which are too stable to partake in the metallation procedure. Germanium, and aluminium are unlikely to chelate with porphyrins in the sediments because the ions will not be readily available for complexation in the sedimentary environment. Similarly, chromium (III) porphyrins are exceptionally stable; however, chromium (III) ion carriers are very unreactive.<sup>(3)</sup> Gold (III) porphyrins are also stable, but they are not prevalent in nature because gold occurs primarily as the native metal, which is quite inert.

For many transition elements, the nature of the ions in aqueous solution is complex. Consider the group IVB elements. Titanium would appear to be a good candidate for chelation in the geological environment. It is abundant, (Table I) and forms stable porphyrin complexes. However, the nature of the titanium in aqueous solution precludes chelation. There is no simple solvated  $\text{Ti}^{4+}$  ion, because of the high charge to radius ratio, nor is there evidence of simple  $\text{TiO}^{2+}$  ions.<sup>(5)</sup> The major mineral form of titanium is titanium oxide, a stable compound, which is a poor ion carrier. Similar problems are encountered with zirconium. There is no indication of  $\text{Zr}^{4+}$  or  $\text{ZrO}^{2+}$  in solution. Instead, polymeric forms of  $\text{ZrO}^{2+}$  seem dominant. Such species will further hinder the metallation process. Hafnium is likely to present the same difficulty in the light of the very great similarities in the chemistry of these two elements.<sup>(6)</sup>

In aqueous solution, molybdenum and tungsten can occur in a number of forms including the molybdate and tungstate anions. Such species will not lend themselves easily to chelation.<sup>(3)</sup> The cations of  $\text{Mo}^{4+}$  and  $\text{Mo}^{5+}$  are bimolecular.<sup>(7)</sup>

Vanadium is the easiest of the tetravalent elements to insert in the laboratory using a tetravalent chelating agent.<sup>(3,4)</sup> The metallation is effected rapidly in refluxing aqueous acetic acid using vanadyl sulphate as the chelating agent. In addition it is abundant both in the water column and in the sedimentary rocks

Table I. Average Abundances of Elements which Form Stable Metalloporphyrins in Seawater and Shale

Element	Seawater Concentration (ppm, <u>9</u> )	Shale Concentration (ppm, <u>10</u> )
Al	$1 \times 10^{-3}$	92,000
Si	2	238,000
Ti	$< 1 \times 10^{-6}$	4,500
V	$< 1 \times 10^{-3}$	130
Cr	$3.3 \times 10^{-4}$	100
Mn	$1 \times 10^{-5}$	850
Fe	$4 \times 10^{-5}$	47,000
Co	$2 \times 10^{-6}$	20
Ni	$4.8 \times 10^{-4}$	80
Cu	$1.2 \times 10^{-4}$	50
Ga	$1.5 \times 10^{-5}$	25
Ge	$5 \times 10^{-6}$	1.5
As	$2 \times 10^{-3}$	10
Y	$1.3 \times 10^{-5}$	35
Zr	$< 1 \times 10^{-3}$	180
Nb	$1 \times 10^{-6}$	15
Mo	$1.1 \times 10^{-2}$	2
Ru	$5 \times 10^{-7}$	$< 1 \times 10^{-3}$
Rh		$< 1 \times 10^{-3}$
Pd		$< 1 \times 10^{-3}$
Ag	$3 \times 10^{-6}$	0.1
In	$2 \times 10^{-7}$	0.06
Sn	$5 \times 10^{-7}$	6
Sb	$2 \times 10^{-4}$	0.6
La	$4 \times 10^{-6}$	40
Ce	$4 \times 10^{-6}$	70
Pr	$6 \times 10^{-7}$	9
Nd	$4 \times 10^{-6}$	30
Sm	$6 \times 10^{-7}$	7
Eu	$1 \times 10^{-7}$	1.4
Gd	$8 \times 10^{-7}$	6
Tb	$1 \times 10^{-7}$	1
Dy	$1 \times 10^{-6}$	5
Ho	$2 \times 10^{-7}$	1.5
Er	$9 \times 10^{-7}$	3.5
Tm	$2 \times 10^{-7}$	0.6
Yb	$9 \times 10^{-7}$	3.5
Lu	$2 \times 10^{-7}$	0.6
Hf	$< 8 \times 10^{-6}$	4
Ta	$< 2.5 \times 10^{-6}$	2
W	$1 \times 10^{-6}$	1.8
Re	$4 \times 10^{-6}$	$< 1 \times 10^{-3}$
Os		$< 1 \times 10^{-3}$
Ir		$< 1 \times 10^{-3}$
Pt		$< 1 \times 10^{-3}$
Au	$1.1 \times 10^{-5}$	$3 \times 10^{-3}$
Tl	$1.2 \times 10^{-5}$	1
Bi	$1 \times 10^{-5}$	0.2

(Table I); thus, it is no surprise that the vanadium porphyrins are abundant in the geosphere.

In addition to the problem of the deconvolution of the metal ion from the ion carrier, there is another factor to take into account. There are several metalloporphyrins including tin (IV) complexes, which are synthesised by inserting the metal in a low valence state, and subsequently allowing the metal to oxidise to the more stable, higher valence form. (3,4) In the sedimentary environment such auto-oxidation procedures will not always be feasible. Thus the route to many higher valence state metalloporphyrins e.g. tin (IV), arsenic (V) and antimony (V) may be blocked.

The Abundance of the Elements. A few elements may be discounted as major contributors to the geoporphyrin mixtures because of their rarity in the water column and in the sedimentary environment, or their irregular distribution in the geosphere. The platinum metals - ruthenium, osmium, rhodium, iridium, palladium and platinum - are all very rare elements (Table I) and for this reason, they may be discarded. (8) Similarly, rhenium is rare, and it displays little cation chemistry in aqueous solution. The insertion of the metal from anionic ion carriers is difficult. (3)

Postchelation Factors. Clearly the strength of the metal-nitrogen bond in the metalloporphyrins is a very important parameter to consider in the study of geoporphyrin stabilities; however, the reactivity of the metalloporphyrin meso positions (1) is also of major significance. This is the site of ring cleavage in either oxidising or reducing conditions. The reactivity of the meso positions is dependent on the chelated metal. (11) In addition the stability of the nitrogen-metal bonds in the porphyrins may be modified by the presence of the clay minerals (12).

The stability of the metal-nitrogen bonds may be estimated by determining the acid strength required for the demetallation of the metal complex. Porphyrins may be subdivided into five classes using this approach. (13)

Table II. Stability Classes of Metalloporphyrins

Stability Class	Demetallation Conditions (25°C, 2h)	
I	100% H <sub>2</sub> SO <sub>4</sub>	incomplete demetallation
II	100% H <sub>2</sub> SO <sub>4</sub>	complete demetallation
III	HCl/H <sub>2</sub> O-CH <sub>2</sub> Cl <sub>2</sub>	complete demetallation
IV	CH <sub>3</sub> CO <sub>2</sub> H	complete demetallation
V	H <sub>2</sub> O-CH <sub>2</sub> Cl <sub>2</sub>	complete demetallation

The reactivity of the porphyrin meso positions may be estimated by the using the stability index, S<sub>i</sub>, devised by Buchler (3):

$$S_i = 100 \cdot \text{En} \cdot Z / r_i$$

En = electronegativity of metal (Pauling Scale)  
 Z = charge  
 $r_i$  = effective ionic radius

There is good correlation between the value of the stability index, and meso reactivity. This is demonstrated by comparing the rates of meso deuteration- using the method of Kenner *et al.* (14)- of different metal complexes of octaethylporphyrin (OEP) with their stability indices as shown in Table III. Thus, metals of relatively low electronegativity on the Pauling scale, particularly in the monovalent or divalent state, have low stability indices, and will activate the meso positions towards electrophilic attack. More electronegative metals, in high valence states will stabilise the meso positions. (Table III)

Table III. Deuteration of Metal Complexes of OEP

OEP Metal Complex	SC	$S_i$	%Deuteration (Hexapyridyl Magnesium iodide- $\text{CH}_3\text{OD}$ , 24h) <sup>a</sup>
Mg	IV	3.78	100 <sup>b</sup>
Zn	III	4.46	100 <sup>b</sup>
Cu	II	6.12	28
Ni	II	6.37	28
VO	I	11.05	0

<sup>a</sup> Estimated by mass spectrometry, taking into account the isotopic contributions both from the metals and that of  $^{13}\text{C}$  and  $^{15}\text{N}$ .

Accuracy  $\pm$  5% (15)

<sup>b</sup> Reaction complete within 12 hr.

SC = Stability Class;  $S_i$  = Stability Index

Usually, porphyrins with low stability index, also have unstable metal-nitrogen bonds. If such compounds were formed under geological conditions they would undergo decomposition either by demetallation, or by destruction of the porphyrin ring, or by transmetallation in the presence of the appropriate metal ion carriers to yield more stable metal complexes. On the basis of their low stability indices (<6.0) and/or low stability in acid (Classes III, IV, V; Table II) the following elements would form unstable geoporphyrin complexes: the alkali metals, the alkaline earth metals, the group IIIB transition metals and the group IIB metals, the lanthanides, indium, niobium and tantalum. In addition, the low valence states of several elements- chromium (II), manganese (II), iron (II), cobalt (II), tin (II), thallium (I), lead(II) and bismuth (III) would be insufficiently stable to survive in the geological environment. Arsenic (III) and antimony (III) porphyrins are both thermally unstable, and decompose at  $>60^\circ\text{C}$ . (3)

Several metalloporphyrins which have a high stability index, when the metal is in a high valence state, are readily reduced to less stable, lower valence species. Thus iron (III), manganese (III) and cobalt (III) porphyrins will be reduced to their divalent

complexes in the reducing conditions in most organic rich sediments. Similarly, silver (II), and thallium (III) would be reduced to unstable complexes in the reducing sedimentary environment.

On consideration of the above factors, there are four metalloporphyrin complexes which might be expected to be widespread in the sedimentary geological environment: the vanadium (IV), nickel (II), gallium (III) and copper (II) porphyrins.

#### The role of Minerals in the Distribution of Metalloporphyrins.

Clearly, the stability of the porphyrins in the geosphere will be heavily dependent on the nature of their interactions with minerals. There is still little known about such interactions. In early studies, Hodgson and Peake showed that copper porphyrins undergo transmetallation to the nickel or vanadyl porphyrins in the presence of clays. (16) Similarly, it has been shown that nickel and vanadyl porphyrins are stable on dispersion on clays, in contrast to the copper complexes, which are extensively demetallated. (12) Copper porphyrins may also be transmetallated to the nickel or vanadyl complexes in the presence of sulphide. (17) In the light of these experimental data, it is unsurprising that the copper geoporphyrins are not found in anoxic sediments. (18)

It is clear that the geological environment has a major role in determining the nickel to vanadyl ratios in metalloporphyrin distributions. Lewan has postulated that the variation in distributions may be attributed to the Eh-PH conditions. (19) At high pH (8-9) with Eh - 0.0-0.2 volts, nickel porphyrin formation is favoured over vanadyl, because of the dominance of  $V_2O_4^-$  ion conversely at lower pH and more reducing conditions the nickel is predominantly present as the sulphide, a poor ion carrier, and vanadyl porphyrins are favoured.

Gallium porphyrins have been detected in coals from a variety of regions including Great Britain and the U.S.A. (20,21) It is unclear why gallium porphyrins are not more widespread as their stability index is high, 8.76, and they are a class II porphyrin (Table II). It is possible that the presence of gallium porphyrins will prove to be a depositional environment indicator. Until more is known of the gallium ion carrier, it is impossible to speculate further.

In addition to the four metalloporphyrins mentioned previously, iron (III) porphyrins and manganese (III) porphyrins have been detected in coal. (20) These observations fully support the present hypothesis. Coals are formed under much less strongly reducing conditions, than crude oils and oil shales. The iron (III) and manganese (III) porphyrins, both of which have high stability indices (8.58 and 7.15 respectively), will not undergo reduction to the unstable divalent metalloporphyrins in this environment. It is interesting that the Bonnett group has not reported either nickel or vanadyl porphyrins in the coal samples analysed. It is possible that nickel porphyrins are absent because the more stable iron (III) and gallium (III) porphyrins may be formed in the less reducing environments encountered in coal-formation; however, there have been insufficient samples analysed to determine whether this speculation is sound.

## CONCLUSIONS

The hypothesis that the presence of metalloporphyrins in sediments requires good ion carriers which can complex with the cyclic tetrapyrroles to form metal complexes with high stability indices, and stable metal-nitrogen bonds explains the predominance of nickel and vanadyl porphyrins in the geosphere. It also accounts for the occurrence of gallium, iron and manganese porphyrins in coals, and provides valid reasons why other metalloporphyrin complexes are not usually found in organic rich sediments. If the proposal is correct, it is possible than other metal geoporphyrins could occur provided that the appropriate ion carriers, were present, and the mineralogy and Eh of the sediments were favourable for chelation. Clearly, further studies on the stability of the different skeletal types of geoporphyrins as well as the role of the clays in porphyrin stability in the sedimentary environment are necessary to develop the hypothesis further.

Acknowledgments Acknowledgement is made to the Donors of the Petroleum Research Foundation for the support of this research PRF# 17024-B1. I am also indebted to Professor R. Filby, and Mr. G.J. van Berkel (Washington State University) for valuable discussions.

## References

1. Baker, E.W.; Palmer, S.E. In "The Porphyrins"; Dolphin, D., Ed.; Academic: New York, 1978; Vol. I, p. 485.
2. Treibs, A. Ann. Chem. 1934, 510, 42-62.
3. Buchler, J.W. In "Porphyrins and Metalloporphyrins"; Smith, K.M., Ed.; Elsevier; Amstrerdam, 1975; p.157.
4. Treibs, A. Ann. Chem. 1969, 728, 115-148.
5. van de Velde, G.M.H.; Harkema, S.; Gellings, P.J. Inorg. Nucl. Chem. Lett. 1973, 9, 1169-1173.
6. Cotton, F.A.; Wilkinson, G. "Advanced Inorganic Chemistry"; Wiley: New York, 1980; p.824.
7. Ardon, M.; Bino, A.; Yahav, G. J. J. Am. Chem. Soc. 1976, 98, 2338-2339.
8. Cotton, F.A.; Wilkinson, G. "Advanced Inorganic Chemistry"; Wiley: New York, 1980; p.900.
9. Quinby-Hunt, M.S. and Turekian, K.K. Trans. Amer. Geophys. Union, 1983, 64, 130.
10. Krauskopf, K.B. "Introduction to Geochemistry"; (Second Edition) McGraw Hill: New York, 1979; p. 544.
11. Fuhrhop, J.-H. In "The Porphyrins"; Dolphin, D., Ed.; Academic: New York, 1978; Vol. II, p.131.
12. Bergaya, F. and van Damme, H. Geochim. Cosmochim. Acta 1982, 46, 349-360.
13. Phillips, J.N. Rev. Pure Appl. Chem. 1960, 310, 35-60.
14. Kenner, G.W.; Smith, K.M.; Sutton, M.J. Tetrahedron Lett. 1973, 1303-1306.
15. Quirke, J.M.E., unpublished data.
16. Hodgson, G.W.; Baker, B.L. and Peake, E. In "Fundamental Aspects of Petroleum Geochemistry"; Nagy, B.; Colombo, V. Eds., Elsevier: Amsterdam, 1967; p. 170.

17. Schneider, W. In "The Nature of Seawater"; Goldberg, E.D., Ed.; Dahlem Konferenzen: Berlin, 1975; p. 375.
18. Palmer, S.E. and Baker, E.W. *Science* 1978, 201, 49-51.
19. Lewan, W.D. *Geochim. Cosmochim. Acta* 1984, 2231-2238.
20. Bonnett, R.; Czechowski, F. *Phil. Trans. Roy. Soc. Lond., Ser. A* 1981, 300, 51-63.
21. Bonnett, R.; Czechowski, F. *J. Chem. Soc., Perkin Trans. I*, 1984, 125-131.

RECEIVED March 11, 1987

## Chapter 5

# Application of Metal Complexes in Petroleum to Exploration Geochemistry

Jan F. Branthaver<sup>1</sup> and Royston H. Filby<sup>2</sup>

<sup>1</sup>Western Research Institute, Box 3395, University Station, Laramie, WY 82070

<sup>2</sup>Department of Chemistry and Nuclear Radiation Center, Washington State University, Pullman, WA 99164-1300

Metal complexes are part of the organic constituents of fossil fuels and source rocks of fossil fuels. The most studied metal complexes associated with petroleum and its source rocks are nickel (II) and vanadyl VO(II) porphyrins of the desoxophylloerythroetioporphyrin (DPEP) and etioporphyrin (etio) types. The relative abundances of the Ni(II) and VO(II) species and the DPEP/etio ratios of metalloporphyrin suites have been used as indicators of source rock maturity and in oil-source rock and oil-oil correlations. The nature of the ligands complexed with metals other than nickel and vanadium in petroleum is not known. However, the total metal content of a crude oil can provide a distinctive "fingerprint" which has been used to correlate related oils and to correlate oils with source rocks. The effects of migration and maturation processes experienced by petroleum on metalloporphyrin and trace element distributions have received little attention.

Geochemists have long attempted to improve their understanding of the details of the origin and migration of petroleum. The study of element ratios, isotope ratios, and biomarkers in petroleum and source rocks has yielded much information about the transformation of organic matter into crude oil. The identification of metalloporphyrins in shales and petroleum (1-3) provided convincing evidence that petroleum is derived from plant-derived organic matter and is not abiogenic.

The correlation of crude oils with their presumed source rocks is an objective of geochemical studies and is of value in petroleum exploration. Geochemical data are useful in developing correlations among different crude oils within a producing area. These data can be helpful in elucidating the frequently complex stratigraphy of petroleum bearing formations, particularly those that are heavily faulted. It is reasonable to assume that the metalloporphyrins and the suite of trace metals of a source rock leaves an imprint on its derived crude oils which might not be too greatly altered during

0097-6156/87/0344-0084\$06.00/0

© 1987 American Chemical Society

migration. If so, it might prove possible to establish correlations among crude oils and source rocks based on relative amounts of metals and comparisons of metalloporphyrin types. If, however, the distribution of metals or porphyrin suites of a crude oil are significantly altered during migration or after emplacement in reservoirs in an unpredictable fashion, then they will not be useful in correlation studies. Other areas in which metalloporphyrin and metal distribution data should provide useful information are in the reconstruction of depositional environments of sediments and the estimation of the maturity of organic matter in potential source rocks.

#### Metalloporphyrins in Maturity and Correlation Studies

Crude oils and petroleum source rocks often contain measurable amounts of metalloporphyrins, principally of the etioporphyrin (etio), desoxophylloerythroetioporphyrin (DPEP), and benzoporphyrin (benzo) types. The structures of these compounds are illustrated in the paper by Chicarelli *et al.* (4) in this volume. Although metalloporphyrins were the first compounds of conclusive biological origin (1-3) identified in petroleum, the reported use of these compounds in oil-oil and oil-source rock correlation studies, maturation studies, and in depositional environment reconstruction has been very limited compared to the application of hydrocarbon biomarkers (e.g., steranes, triterpanes, etc.). A major reason for this limited use has been the analytical difficulty encountered in the isolation and separation of the complex mixtures of Ni(II) or VO(II) homologues of each of the geoporphyrin types prior to the development of routine mass spectrometric (MS) and high resolution HPLC methods. A more fundamental reason, however, for the limited application of metalloporphyrins as biomarkers has been the incomplete understanding of the porphyrin-biological precursor relationship and of the relationship between depositional environment and porphyrin evolution. Also, the diagenetic/catagenetic reactions of the metal complexes in source rocks and their subsequent incorporation into bitumens and petroleum is incompletely understood. The recent (post-1979) determinations of absolute porphyrin structures by nuclear Overhauser effect (nOe) NMR, X-ray diffraction, and MS/MS have made possible the identification of many geochemically significant metalloporphyrins (5-7) and their precursors. Although the first reaction scheme proposed to account for the transformation of chlorophylls into geoporphyrins, referred to as the Treibs scheme (8), has undergone significant modification since 1936, the conversion of chlorophyll-a to C<sub>32</sub>DPEP metalloporphyrins in maturing sediments has been confirmed by the determination of the structure of the VO(II) and Ni(II) C<sub>32</sub>DPEP complexes (5-7) and by the identification of intermediates (9). The geochemical evolution of the metalloporphyrins has been recently reviewed by Baker and Louda (9) and by Filby and Van Berkel in this volume (10).

Several studies confirm that porphyrin species are useful indicators of sediment maturity (11-15). However, routine application of porphyrin distribution data in maturity studies is hampered by the time-consuming and expensive nature of the mass spectroscopic analysis of metalloporphyrin types. Progress has been made in applying porphyrin distributions to maturity studies (and to correlation studies) by the development of rapid HPLC techniques which permit

determination of amounts of metalloporphyrins having specific carbon numbers without recourse to mass spectrometry and which, in certain cases, separate structural isomers (16-21). Other problems are not solely of an operational nature, such as an incomplete understanding of the effects of catagenetic processes involving kerogen and mineral components of sediments on porphyrin distributions, the limited knowledge of the influence of sedimentary and early diagenetic conditions (pH, Eh, metal speciation, etc.) on Ni(II) and VO(II) chelation of free-base porphyrins, and the relative stabilities of the metalloporphyrins. Solutions to these problems are being vigorously pursued in some oil company geochemistry programs.

The use of %DPEP (i.e., [DPEP/(DPEP + etio)] x 100) determined from HPLC chromatograms as a measure of source rock maturity has been suggested by Barwise and Park (13), who found a linear relationship between %DPEP and vitrinite reflectance (% R<sub>o</sub>) in several source rocks. They concluded that the %DPEP is a very sensitive measure of maturity. These authors, however, do not make it clear whether the porphyrin ratio was measured on the demetallated Ni(II) or VO(II) porphyrins or on the total porphyrin content of the samples. Because %DPEP may vary differently with maturity for Ni(II) and VO(II) porphyrins, the Ni(II) and VO(II) species should be separated prior to HPLC analysis of the demetallated species. Mackenzie et al. (12) also have utilized the relative abundances of the Ni(II) and VO(II) porphyrins and the DPEP/etio ratios of both metal series to determine maturity levels in the Toarcian shales of the Paris Basin.

The use of metalloporphyrin distributions in depositional environment reconstruction has been described by Moldowan et al. (15) who studied a Lower Toarcian shale sequence from the Paris Basin that was of constant, relatively low, maturity (i.e., pre-"oil-window"). The shallower Middle Lias shales contained essentially only VO(II) porphyrins and were deposited under highly reducing conditions, whereas the deeper Lower Lias shales were deposited under sub-oxic conditions and contain essentially 100% Ni(II) porphyrins. A transition zone between these depositional environments contained both Ni(II) and VO(II) porphyrins. Although Lewan (22) has discussed the general effects of pH, Eh, H<sub>2</sub>S production, etc. on porphyrin evolution in sediments, few quantitative data are available.

Compared to the application of hydrocarbon biomarkers to oil-oil or oil-source rock correlation, the number of reported porphyrin studies is limited. Table I lists the major published studies. The first systematic use of porphyrins in oil-source rock correlation was a comparison of Ni(II) and VO(II) porphyrin concentrations in Ozouri, Gabon, oils and source rocks by Van Eggelpoel (23) who was able to show that the oils are mixtures derived from several sources. A major fraction of each of the oils is believed to be derived from one particular argillaceous source rock. He also pointed out the difficulties involved in determining the metalloporphyrin contents of crude oils using UV-visible spectrometry of whole oils. Polar organic material (i.e., asphaltenes, resins) modifies VO(II) porphyrin spectra and changes the molar absorptivity of the metal complex (24,25).

A more detailed study using UV-visible spectrometry was made of the VO(II) porphyrins from the Maracaibo Basin oils and source rocks

by Gransch and Eisma (26). These authors correlated Cretaceous and Tertiary oils (Boscan, La Paz, etc.) with the organic-rich La Luna shale (Cretaceous) using the VO(II) porphyrin concentrations of the oils and rock extracts. The relatively abundant VO(II) porphyrins of the western Venezuelan oils and source rock extracts permits reliable analysis by UV-visible spectrometry. Few other detailed basin-wide studies using either MS or HPLC techniques have been published (see Table I).

Most of the correlation studies reported in Table I involve a comparison of Ni(II) and VO(II) porphyrins, or a comparison of DPEP/etio porphyrin ratios of the subject materials. Strong and Filby (24) determined the etio/DPEP ratios of VO(II) porphyrins in Athabasca, Peace River, and Cold Lake oil sand bitumens and showed that these bitumens have etio/DPEP characteristic of oils that have migrated from deeper source rocks prior to the biodegradation that subsequently occurred in their shallow reservoirs. They concluded on the basis of increasing etio/DPEP ratio that the original source rock or pre-migration depth sequence corresponds to their present reservoir depth sequence, *i.e.*,

Cold Lake > Peace River > Athabasca

Similar to the etio/DPEP variations, but more pronounced, were the variations in the ratios of etio to minor porphyrin series, such as tetrahydrobenzo (THBD), benzo-DPEP, and benzo-etio porphyrins. This raises the possibility that the minor series porphyrins (*e.g.*, THBD, benzo) may have value in correlation studies, particularly since these porphyrins have recently been detected in sediments as the free bases (27,28) with as yet-to-be determined precursors and diagenetic pathways. The similar patterns observed for all the etio/other porphyrin ratios with depth argues against formation of etio-porphyrins in these oils by a direct DPEP to etio conversion because there is no apparent genetic relationship between DPEP and the minor series porphyrins.

#### Non-Porphyrin Complexes and Geochemical Correlations

The geochemical significance and utility of non-porphyrin nickel and vanadium complexes in crude oils is difficult to assess because no discrete complexes have been identified and their origin is obscure. The fact that the most abundant organically combined non-porphyrin metals in crude oil asphaltenes are normally nickel and vanadium suggests, however, a genetic relationship between the porphyrin and non-porphyrin species. Yen (29) has suggested that the non-porphyrin complexes may in fact be metalloporphyrin degradation products that remain in asphaltene structures. Branthaver (30) has determined that Ni/V ratios are similar throughout several gel permeation chromatography (GPC) fractions of Boscan crude oil. Porphyrin contents vary greatly among these fractions. In one fraction, all metals are accountable as porphyrins, while in another most metals are apparently non-porphyrinic. Other fractions are intermediate. This would further support a genetic relationship between porphyrins and non-porphyrins if these findings were verified in other crudes.

Although non-porphyrin nickel and vanadium species may occur in crude oils, asphalts, etc., there is little information on their occurrence in the bitumens of source rocks with which oils could be correlated. There may, in fact, be a correlation between nickel and

Table I. Applications of Porphyrins in Oil-Oil and Oil-Source Rock Correlations

Correlation	Region-Occurrence	Comments	Reference
Oil-Source Rock	W. Venezuela Lake Basin (Lake Maracaibo)	Correlates Cretaceous and Tertiary crudes with La Luna source rock on basis of VOP contents	<u>26</u>
Oil-Source Rock	Ozouri oil, Gabon	Spectroscopic determination of NiP and VOP of oils and known source rock	<u>23</u>
Oil-Source Rock	Boscan oil, Venezuela (Maracaibo Basin)	Used HPLC demethylated porphyrin chromatograms to show correlation of Boscan oils to La Luna shale	<u>18</u>
Oil-Source Rock	Senli, and other continental oil fields, China	Application of DPEP/etio ratios for correlation with source rocks	<u>73</u>
Oil-Oil	W. Venezuela Lake Maracaibo	Attempts correlation of Cretaceous and Tertiary oils with reservoir depth based on VOP contents	<u>26</u>
Oil-Oil	Venezuela, Boscan oils Maracaibo Basin	HPLC fingerprints show similarities of Boscan oils	<u>18</u>
Oil-Oil	Suite of oils: no location	HPLC chromatograms used to correlate sequence of oils at different levels of maturity	<u>16</u>

Oil-Oil	W. Surgut Oil Field, USSR	Correlates migrated oils on proportions of polar/non-polar VOP and DPEP/etio ratios	<u>67</u>
Oil-Oil	East Caucasus Foothills, USSR (bitumoids and crude oils)	Used VOP contents and DPEP/etio ratios to distinguish between Jurassic and Cretaceous bitumoids	<u>43</u>
Oil-Oil	Shengli Oil Field, China	HPLC chromatograms used to determine maturity sequence of Shengli oils (approx. DPEP/etio ratios)	<u>74</u>
Oil-Oil	Colombia oils	DPEP/etio ratios used to correlate degraded oils	<u>72</u>
Oil-Oil	Grosmont Formation bitumen, Alberta, Canada	DPEP/etio ratios of VOP used to correlate bitumen in Devonian Grosmont Formation with Cretaceous Athabasca deposit	<u>75</u>
Oil-Oil	Alberta oil sand deposits	Correlation of Athabasca, Cold Lake, and Peace River oil sands on basis of DPEP, etio, THBD, and benzo porphyrin abundances	<u>24</u>

vanadium species in kerogens from maturing sediments and those present in crude oil asphaltenes. Recently, several authors (31-34) demonstrated that oil shale kerogen concentrates contain substantial quantities of organically combined nickel and vanadium. Van Berkel and Filby (32) measured mineral-free concentrations of nickel and vanadium of 2130 and 700  $\mu\text{g/g}$ , respectively, in New Albany oil-shale kerogen and 350 and 3260  $\mu\text{g/g}$ , respectively, in the Woodford oil-shale kerogen. Although they showed that both kerogens generated Ni(II) and VO(II) porphyrins on pyrolysis, only a small fraction of the total metal was released from the kerogen. It was not possible to determine what fraction of the nickel and vanadium in the kerogen was porphyrinic.

During kerogen catagenesis, molecules associated with petroleum asphaltenes are thought to form as intermediates in the conversion of kerogen to hydrocarbons (35), as shown in Figure 1. Thus, an asphaltene moiety formed from kerogen probably contains Ni(II) and VO(II) porphyrin suites similar to those present in the parent kerogen, and may also contain the non-porphyrin complexes that may be part of the kerogen structure. Recent work (32) indicates that the metalloporphyrins probably are not bonded by aliphatic linkages to the kerogen but may be strongly chemisorbed, or trapped in the polymeric structure. Kerogens may thus retain polar nickel and vanadium non-porphyrin species in a similar fashion and these may be part of asphaltene structures after formation from the maturing kerogen. Thus, the asphaltenes of source rock bitumens and resulting crude oils may contain non-porphyrin metal complexes that are characteristic of the source-rock kerogens and their geochemical history and thus of potential use in correlation studies. An alternative origin for the non-porphyrin complexes in asphaltenes may be that the asphaltenes evolving from kerogen in source rocks complex  $\text{Ni}^{2+}$ ,  $\text{VO}^{2+}$  and other ions from mineral surfaces. If this is the case, the non-porphyrin metals in crude oil asphaltenes may still reflect the source rock environment (but not necessarily the kerogen composition) and be of value in correlation studies. The geochemical relationship between non-porphyrin metal complexes and porphyrins in crude oils and kerogens and their potential for use in correlation studies should be further investigated.

#### Metal Distributions in Exploration Studies

There have been a number of attempts to classify petroleum and source rock kerogens by examining entire metal suites in these materials. In these studies, porphyrin contents are not determined. For the metals other than nickel and vanadium, it is not known that the chelating ligands are porphyrinic. These studies parallel many similar investigations of coals, from which it is usually impossible to extract significant amounts of metal chelates, but which often contain substantial quantities of metals that appear to be associated with organic matter (36).

Several early workers attempted to use V/Ni ratios as indicators of maturation (or age) of crude oils, but many of the conclusions are contradictory. Hodgson (37) measured nickel, vanadium and iron in some Western Canada oils and concluded that the V/Ni ratio decreased with increasing maturation from asphaltic Cretaceous to less asphaltic deeper Devonian oils. Hodgson (37) also concluded that nickel,

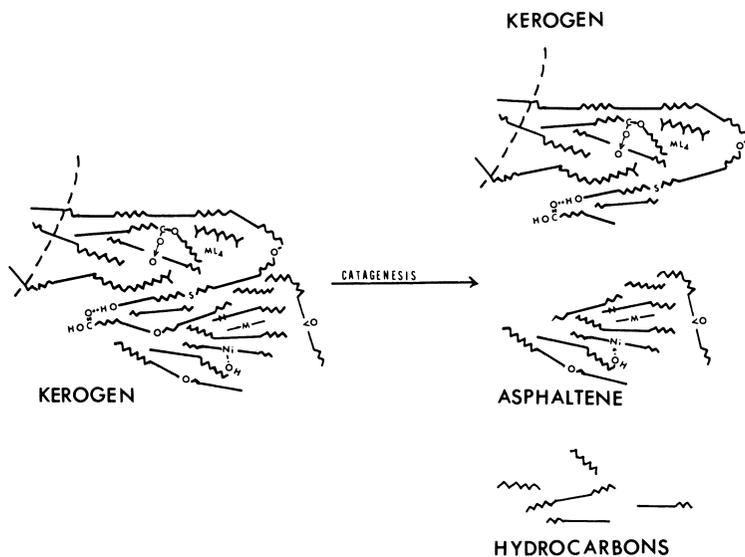


Figure 1. Schematic diagram of formation of asphaltene aggregate from kerogen showing Ni(II) and V(II) porphyrins and other metal complexes,  $ML_4$ ,  $-M-$ , in structure. Complexes are shown associated and bonded to the structure in different modes.

vanadium, and iron were derived from the original source material. Ball *et al.* (38) and Hyden (39), however, concluded that the V/Ni ratio increased with reservoir rock age. Much of this disagreement probably arises from the inability to distinguish between the porphyrin and non-porphyrin forms of the metals in these oils and the probable variation in the trace metal assemblages of the source rocks. Bonham (40) studied the metal contents of a number of American crude oils of various ages, with emphasis on Pennsylvanian crudes from the Andarko basin of Oklahoma. He found that the vanadium and nickel contents of the oils differed significantly from one basin to another. Bonham could not, on the basis of metal suites, correlate between oil pools in the same producing strata of individual basins or even differentiate between the same producing strata. Nevertheless, he claimed that the metal suites provided information about the paleogeography of the basins. Several attempts have been made to correlate trace metal distributions with the ages of reservoir rocks or other geochemical properties (41-45) of Russian oils. Thus, Kotova *et al.* (41) showed that nickel, vanadium, copper, gallium, and germanium varied systematically with age and depth of reservoir rocks. In most of these studies, little attention was paid to the nature of the metal species in the oils (e.g., mineral forms, entrained aqueous phase, etc.). The study by Chakhmachkev *et al.* (43) is significant because these authors attempt correlations between syngenetic and parautochthonous (*sic*) bitumens of Jurassic and Triassic source rocks and oils from producing strata of the same age. In this study, trace element distributions were used as parameters for oil-source rock and oil-oil correlations whereas VO(II) porphyrins were used to determine source rock maturity. The DPEP/etio ratios of VO(II) porphyrins in the bitumen decreased with depth. Trace element contents of oils and bitumens were similar for suites of the same age, indicating that the oils may be syngenetic with the Triassic and Jurassic host rocks, *i.e.*, that there are two hydrocarbon sources.

Mast *et al.* (46,47) determined the vanadium contents of a large number of Paleozoic crude oils from Illinois by neutron activation analysis. Like Bonham, these investigators found that vanadium distribution in the oils provided paleogeographic information. Relatively high vanadium concentrations were found in crudes accumulated in some deformationally high structural traps. These traps are believed to have formed at a time close to when the source rocks of the study crudes began generating oil. The authors contend that their data support the suggestion of Weeks (48) that heavy oils are formed from source rocks before light oils. It has been shown that the initial stages of kerogen decomposition involve a decrease in oxygen to carbon, nitrogen to carbon, and sulfur to carbon ratios (49); hence, carbon-heteroatom bonds of source rock kerogens break more readily under thermal stress than do carbon-carbon bonds. Thus, oils initially formed from source rocks will be relatively rich in sulfur, nitrogen, and oxygen. These oils would be less extensively cracked than those formed later in the oil generation process. These earlier formed, heavier oils would contain most of the metal complexes, which would accumulate in those traps existing at the onset of heavy oil generation. The paucity of information on the trace element contents of bitumens and kerogens, however, means a distinction between the inheritance of a trace element "fingerprint"

of the kerogen in the heavy bitumen and the complexation of metal ions from the mineral matrix by the evolving bitumen cannot be made at this time.

McIver (50) determined the nickel and vanadium contents of Wind River Basin, Wyoming, crudes of varying ages by X-ray fluorescence. He found that all of the Cretaceous oils had V/Ni ratios that were distinctly different from those of the Paleozoic oils that were studied. These differences were also reflected in other properties of the crudes. McIver interpreted these data to indicate differences in the environments of deposition of the source rocks of the two petroleum suites, which is reflected in the composition of the oils.

Hodgson *et al.* (51) used the vanadium and nickel contents of Alberta crudes to determine migration pathways. Their data indicate that within a given oil field, distance of migration is reflected in the metal contents of an oil pool. They suggest adsorption of metal chelates and other polar materials on rocks during migration as a major determinant of metal contents of a petroleum deposit. This chromatographic effect may be similar to that acting on the porphyrin species of migrating oils.

Radchenko (52) maintained that vanadium in crude oil and bitumens is of secondary origin. Radchenko invoked bacterial action in reservoirs to account for many of the unusual properties of heavy bitumens, including high vanadium contents. According to Radchenko, the vanadium content of a crude oil would thus not always be related to the trace element suite of the source rock of the crude, nor would migration effects necessarily be significant.

Al-Shahristani and Al-Atyia (53) measured the nickel and vanadium contents of crudes from three fields in Iraq. Their study was designed to resolve a controversy over the origin of the oils of northern Iraq. One school of thought (48) maintains that the source rocks from which the oils are derived are contemporaneous with the later Cretaceous and early Tertiary reservoirs in which they are found. Another school of thought (54) contends that the oils were derived from early Cretaceous rocks and initially accumulated in middle Cretaceous traps. Later, during extensive folding and fracturing during the Tertiary, much of the oil migrated (*i.e.*, secondary migration) vertically into Tertiary reservoirs. Al-Shahristani and Al-Atyia reasoned that if all the oils came from the same source rocks, but did not migrate far, nickel and vanadium contents and vanadium to nickel ratios should be similar, reflecting a common source. However, if extensive vertical migration of some of the oils had occurred, it was reasoned that these oils would have lower metals contents, but similar vanadium to nickel ratios, when compared with the oils remaining in the middle Cretaceous traps. The nickel and vanadium data obtained by Al-Shahristani and Al-Atyia were interpreted by them to confirm the theory of vertical migration from middle Cretaceous to late Cretaceous and early Tertiary traps. Abu-Elgheit *et al.* (55) concluded that three Gulf of Suez Miocene oils could be distinguished from five Western Desert Cretaceous oils on the basis of V/Ni contents and that the V/Ni ratio decreased with increasing age (not given). They also claimed that the V/Sb and Ni/Sb ratios could also be used to distinguish the two groups of oils. However, the small number of samples studied and the large variations in the V/Sb and Ni/Sb ratios in the groups makes the conclusions speculative.

Saban *et al.* (56) investigated trace element suites of oils of the Pannonian Basin and concluded that the V/Ni ratio is reliable for oil-oil correlations. They also express reservations about the use of V/Ni for determining absolute ages of oils, citing numerous conflicting studies in the literature.

Connor and Gerrild (57) studied trace element distributions and other properties of a number of crudes in the Elk Hills, California, field. They were among the first geochemists to analyze oil-oil correlation data by statistical techniques such as multiple-discriminant function analysis. They were able to classify the Elk Hills oils into three distinct types using these methods. Hitchon *et al.* (58) and Hitchon and Filby (59) measured 22 elements in Alberta Basin crude oils and applied Q- and R-mode factor analysis to the data. They concluded that the trace element distributions were controlled by oil maturation processes rather than by migration processes. They found that a major fraction of the cumulative variance could be assigned to sulfur, vanadium, selenium, and nickel. Hitchon and Filby (60) used multiple-discriminant function analysis to re-evaluate the Alberta oil trace element data, and were able to classify the Alberta crudes into three families. The elements found to be discriminating were sulfur, cobalt, vanadium, selenium and bromine. Statistical treatment of the trace element data yielded classifications of the crudes that were similar to those determined by the more expensive and time consuming methods of hydrocarbon and sulfur biomarker analysis used by Deroo *et al.* (61).

The advent of analytical techniques such as ICP spectrometry permits the convenient quantitative analysis of trace element suites of fossil fuels. Data need no longer be confined to those elements, such as vanadium and nickel, which are found in substantial concentrations. Curiale (62) has launched a comprehensive program to analyze a large number of heavy crude oils and solid bitumens for several trace elements. The objectives of the study are to determine whether or not trace metal data can be used to establish genetic relationships among bituminous substances and to discover internal relationships among elements in the metal suites. The ultimate purpose is to evaluate the utility of metal data in solving problems in fossil fuel geochemistry.

In more than a hundred heavy oils and solid bitumens studied, Curiale (62) found that a negative relationship exists between API gravity and concentrations of cadmium, chromium, molybdenum, nickel and vanadium, and that a positive correlation between the last four metals and asphaltene content exists. This suggests that these four metals are associated with heavy fractions of petroleum and bitumens. The same correlations were not observed for cobalt, copper, iron, manganese, and zinc. These metals may have different modes of coordination than the other metals. Using data from this study, Curiale was able to demonstrate a genetic relationship between crude oils and solid bitumens. The latter materials are derived from the former by a process that conserves metals. Solid bitumens do not have a mode of origin different from petroleum. In this manner, Curiale used metals data to provide a solution to a geochemical problem. Curiale (63) reports on further studies using trace element data in this volume.

Ellrich *et al.* (64) studied the concentrations of 12 trace elements in 45 crude oils from 17 oil fields in the Molasse Basin of

S. Germany. They found that they could classify the oils into three families on the basis of nickel, vanadium, and sulfur contents. They also showed that the iodine contents of the crudes could be correlated with the iodine contents of the formation waters. Hirner (65), in this volume, reports on a continuation of this study of the trace element distributions in German oils and also includes the metal contents of source rock kerogens in the correlation study.

#### Migration and Alteration Processes: Their Effects on the Distributions of Metal Complexes

The effects of crude oil migration on metalloporphyrin or trace metal abundances have not been fully investigated, although some of the early trace metal studies already cited have attempted to correlate V/Ni ratios with migration process (51-53). Chakhmachkev *et al.* (66) attempted to simulate geologic migration of porphyrins in the laboratory by passing an oil with high VO(II) porphyrin content through clay-sand columns. These authors found that polar VO(II) porphyrins were retained on the column relative to non-polar VO(II) porphyrins (not defined) and that the DPEP/etio ratio in the initial effluents were lower than the crude oil ratio, as expected from polarity considerations. Burkova *et al.* (22) used DPEP/etio ratios of VO(II) porphyrins from Cretaceous-Jurassic W. Surgut oils to correlate oils that had migrated to different degrees. Silverman (68) showed that porphyrin contents of some Venezuelan oils emplaced at various points along a migration path decreased with distance of migration. The effects of migration processes are discussed in more detail by Filby and Van Berkel (10) in this volume.

The trace metal abundances in source rock bitumens are undoubtedly affected when petroleum is generated from the rocks. Migration is believed to result in a decrease in asphaltene and resin content of a migrated oil. Thus the abundances of most metals which are concentrated in the asphaltenes should decrease with distance of migration, but their relative concentrations may be unaffected. This conclusion was reached by Lewan (9) who studied the effects of migration on the nickel and vanadium contents of crude oils compared with source rock bitumens.

However, if chromatographic effects do change the metalloporphyrin or trace metal distributions of migrated oils, it still may be possible to "reconstruct" the porphyrin or trace metal distributions characteristic of the bitumen in the source rock through analysis of the crude oil asphaltenes. Several authors have shown that biomarkers can be transported and protected from biodegradation as a consequence of being incorporated asphaltene structures in a crude oil and can be liberated by asphaltene pyrolysis (70,71). In a similar manner, porphyrins or other trace metal species retained within those asphaltene micelles which survive migration may not have been subjected to chromatographic fractionation during migration.

The effects of biodegradation (and associated water washing) on porphyrin and trace metal distributions also have not been fully investigated. As mentioned earlier, Barwise and Park (16) concluded that biodegraded oils from a maturation sequence had VO(II) porphyrin distributions (e.g., DPEP/etio ratios) similar to those of related non-degraded oils of similar maturity, although no quantitative data were presented. Palmer (72) studied the VO(II) porphyrins

from a series of genetically related oils from Colombia consisting of a highly degraded seep oil; a reservoir biodegraded oil; and non-degraded oils. She found that the DPEP/etio ratios, the series maxima ( $C_{31}$  for DPEP,  $C_{29}$  for etio), and the carbon number ranges were very similar for the oils. She did notice, however, that in the most degraded seep oil the VO(II) porphyrins were enriched relative in Ni(II) porphyrins compared to less degraded oils. It is not clear, however, whether this enrichment is a result of selective biological processes (selective degradation of Ni(II) porphyrins), of selective dissolution by associated water washing, or of selective oxidation of Ni(II) porphyrins relative to the VO(II) species. Strong and Filby (24) have also concluded that biodegradation had little effect on porphyrin distributions in the highly degraded Alberta oil sands.

If biodegradation has little effect on porphyrin or trace metal distributions, such distributions may be important correlation parameters when other biosensitive biomarkers (*i.e.*, most hydrocarbons) cannot be used.

### Summary

The study of porphyrin and trace metal suites in crude oils is a promising tool of geochemical analysis. In order to fulfill this promise, investigations in a number of areas would seem to be necessary. Relationships between organically associated metals in petroleum and those in source rocks need to be accurately determined. This requires investigation of the nature of minor porphyrin suites and any non-porphyrin complexes. Lack of appropriate analytical techniques and the intractability of these materials has caused research efforts to be focused on the more easily studied major porphyrins and those metals found in high concentrations.

If the etio/DPEP ratio is to be used as any kind of indicator, then the origin of etio-porphyrins and the mechanisms of etio and DPEP porphyrin degradation (*e.g.*, dealkylation, isocyclic ring scission; demetallation, *etc.*) must be understood. Are the etio porphyrins products of DPEP conversion, or are they better survivors in certain environments than DPEP-porphyrins? Or do they arise in some other manner?

Answers to the above problems will require application of analytical protocols for geoporphyrin analysis. As Quirke has shown in his overview article in this volume, separation techniques for geoporphyryns still lack standardization.

Improvements in our understanding of the geochemistry of metal chelates should result in a better understanding of petroleum migration, which in turn should assist in prospecting for petroleum. This activity is of considerably more than academic interest.

### Acknowledgments

J.F. Branthaver thanks the U.S. Department of Energy for support under Contract Number DE-FC21-83FE 60177.

Literature Cited

1. Treibs, A. Ann. Chem. 1934, 509, 103-14.
2. Treibs, A. Ann. Chem. 1934, 510, 42-62.
3. Treibs, A. Ann. Chem. 1934, 517, 172-96.
4. Chicarelli, I.M.; Kaur, S.; Maxwell, J.M. (this volume).
5. Quirke, J.M.E.; Maxwell, J.R.; Eglinton, G.; Sanders, J.K.M. Tetrahedron Lett. 1980, 21, 2987-90.
6. Fookes, C.J.R. J. Chem. Soc., Chem. Commun. 1983, 1472-73.
7. Ekstrom, A.; Fookes, C.J.R.; Hambley, T.; Loeh, H.J.; Miller, S.A.; Taylor, J.C. Nature 1983, 206, 173-74.
8. Treibs, A. Angew. Chemie 1936, 49, 682-786.
9. Baker, E.W.; Louda, J.W. In "Biological Markers in the Sedimentary Record"; Johns, R.B., Ed.; Elsevier: Amsterdam, 1986; pp. 125-225.
10. Filby, R.H. and Van Berkel, G.J. (this volume).
11. Baker, E.W.; Louda, J.W. In "Advances in Organic Geochemistry, 1981"; Bjorøy, M., Ed.; John Wiley: London, 1983; pp. 401-21.
12. Mackenzie, A.S.; Quirke, J.M.E.; Maxwell, J.R. In "Advances in Organic Geochemistry, 1979"; Maxwell, J.R.; Douglas, A.G., Eds.; Pergamon Press: Oxford, 1980; pp. 239-48.
13. Barwise, A.J.G.; Roberts, I. Org. Geochem. 1984, 6, 167-76.
14. Shiobara, M.; Taguchi, K. In "Advances in Organic Geochemistry, 1975"; Campos, R.; Goni, J., Eds.; ENADISMA: Madrid, 1977; pp. 237-51.
15. Moldowan, J.M.; Sundararaman, P.; Schoell, M. Org. Geochem. 1986, 10, 915-26.
16. Barwise, A.J.G.; Park, P.J.P. In "Advances in Organic Geochemistry, 1981"; Bjorøy, M., Ed.; John Wiley: London, 1983; pp. 668-74.
17. Barwise, A.J.G. (this volume).
18. Hajibrahim, S.K.; Quirke, J.M.E.; Eglinton, G. Chem. Geol. 1981, 32, 173-88.
19. Sundararaman, P. Anal. Chem. 1985, 57, 2204-06.
20. Barwise, A.J.G.; Evershed, R.P.; Wolff, G.A.; Eglinton, G.; Maxwell, J.M. J. Chromatography 1986, 368, 1-9.
21. Chicarelli, I.M.; Wolff, G.A.; Maxwell, J.M. J. Chromatography 1986, 368, 11-19.
22. Lewan, M.D. Geochim. Cosmochim. Acta 1984, 48, 2231-38.
23. Van Eggelpoel, A. In "Advances in Organic Geochemistry, 1964"; Hobson, G.D.; Louis, M.C., Eds.; Pergamon: Oxford, 1966; pp. 227-42.
24. Strong, D.; Filby, R.H. (this volume).
25. Goulon, J.; Retournard, A.; Frient, P.; Goulon-Ginet, C.; Berthe, C.; Muller, J.F.; Poncet, J.L.; Guilard, R.; Escalier, J.C.; Neff, B. J. Chem. Soc. Dalton Trans. 1984, 1095-1103.
26. Gransch, J.A.; Eisma, E. In "Advances in Organic Geochemistry, 1966"; Hobson, G.D.; Speers, G.C., Eds.; Pergamon: Oxford, 1970; pp. 69-86.
27. Baker, E.W.; Louda, J.W. Org. Geochem. 1984, 6, 183-92.
28. Quirke, J.M.E.; Yost, R.A.; Britton, E.D.; Trichet, J. In "Geochemical Biomarkers"; Yen, T.F.; Moldowan, J.M., Eds.; Gordon and Breach Publishers: London (in press).
29. Yen, T.F. In "Role of Trace Metals in Petroleum"; Yen, T.F., Ed.; Ann Arbor Science: Ann Arbor, 1975; pp. 1-30.

30. Branthaver, J.F. Ph.D. Thesis, North Dakota State University, Fargo, 1976.
31. Van Berkel, G.J.; Filby, R.H. In "Geochemical Biomarkers"; Yen, T.F.; Moldowan, J.M., Eds.; Gordon and Breach Publishers: London (in press).
32. Van Berkel, G.J.; Filby, R.H. (this volume).
33. Riley, K.W.; Saxby, J.D. Chem. Geol. 1982, 37, 265-75.
34. Spiro, B.; Dinur, D.; Aizenshtat, Z. Chem. Geol. 1983, 39, 184-214.
35. Tissot, B.P. Bull. Amer. Ass. Petrol. Geol. 1984, 68, 545-63.
36. Finkelman, R.B. Ph.D. Thesis, University of Maryland, 1980.
37. Hodgson, G.W. Bull. Am. Assoc. Petrol. Geol. 1954, 38, 2737-54.
38. Ball, J.S.; Wagner, W.J.; Hyden, H.J.; Horr, C.A.; Myers, A.T. J. Chem. Eng. Data 1960, 5, 553-57.
39. Hyden, H.J. U.S. Geol. Surv. Bull. 1100-B, 1961.
40. Bonham, L.C. Bull. Am. Assoc. Petrol. Geol. 1956, 40, 897-908.
41. Kotova, A.V.; Tokareva, L.N.; Berkovskii, V.G. Tr. Inst. Khim. Priir. Solei. Aked. Nauk. Kuz. SSR 1970, 21, 83.
42. Gilmanshin, A.F.; Gazinov, M.G.; Baturina, E.N. Tr. Tat. Neft. Nauk. Issled. Inst. 1971, No. 18, 113.
43. Chakhmachkev, V.A.; Lositskaya, I.F.; Punanova, S.A.; Semenova, R.A. Geokhimiya 1985, 703-09.
44. Katchenkov, S.M.; Flegentova, E.J. Vest. Akad. Nank. Belarus. SSR. Ser. Khim. Nauk. 1970, 95.
45. Mileshina, A.G.; Punanova, S.A.; Checkhovskitah, N.M. Geol. Neft. Gaza 1971, 15, 41.
46. Mast, R.F.; Ruch, R.R.; Atherton, E. Proc. Symposium on Future Petroleum Potential of NPC Region 9: Illinois Geol. Survey Illinois Petroleum 95 1971, 111, 126.
47. Mast, R.F.; Ruch, R.F.; Meents, W.F. Illinois Geol. Survey Circular 483 1973.
48. Weeks, L.G. In "Habitat of Oil"; Weeks, L.G., Ed.; Amer. Assoc. Petrol. Geol.: 1958; Tulsa; pp. 1-61.
49. Durand, G. and Monim, J.C. In "Kerogen"; Durand, B., Ed.; Edition Technip.: Paris, 1980; pp. 113-42.
50. McIver, R.D. In "Symposium on Early Cretaceous Rocks of Wyoming and Adjacent Areas"; Enyert, R.; Curry, W.H., Eds.; Wyoming Geol. Assoc., 17th Annual Field Conf. 1962, 248-51.
51. Hodgson, G.W.; Fiores, J.; Baker, B.L. Bull. Am. Assoc. Petrol. Geol. 1959, 43, 311-28.
52. Radchenko, O.A. "Geochemical Regularities in the Distribution of the Oil-Bearing Regions of the World"; Israel Program for Scientific Translations: Jerusalem; 1968; pp. 201-2.
53. Al-Shahristani, H.; Al-Atyia, M.J. Geochim. et Cosmochim. Acta 1972, 36, 929-37.
54. Dunnington, H.V. Inst. Petrol. J. 1967, 53, 129-61.
55. Abu-Elgehit, M.; Khalil, S.O.; Barakat, A.O. Prepr. Div. Petrol. Chem. ACS 1979, 24, 793-97.
56. Saban, M.; Vitorovic, O.; Vitorovic, D. In "Symposium on Characterization of Heavy Crude Oils and Petroleum Residues"; Editions Technip: Paris, 1984; pp. 122-27.
57. Connor, J.J.; Gerrild, P.M. Bull. Am. Assoc. Petrol. Geol. 1971, 55, 1802-13.

58. Hitchon, B.; Filby, R.H.; Shah, K.R. In "The Role of Trace Metals in Petroleum"; Yen, T.F., Ed.; Ann Arbor Science: Ann Arbor, 1975; pp. 111-22.
59. Hitchon, B.; Filby, R.H. Alberta Research Council Open File Report 1983-02, 144 p.
60. Hitchon, B.; Filby, R.H. Bull. Am. Assoc. Petrol. Geol. 1984, 68, 838-49.
61. Deroo, G.; Powell, T.G.; Tissot, B.; McCrossan, R.G. Bull. Geol. Soc. Canada 1977, 262, 136 p.
62. Curiale, J.A. In "Exploration for Heavy Oil and Bitumen"; Am. Assoc. Petrol. Geol. Research Conference, Santa Maria, Calif., Oct. 28-Nov. 2, 1984, Vol. 1, pp. 1-39.
63. Curiale, J.A. (this volume).
64. Ellrich, J.; Hirner, A.V.; Stark, H. Chem. Geol. 1985, 48, 313-23.
65. Hirner, A.V. (this volume).
66. Chakhmachkev, V.A.; Burkova, V.N.; Zharkov, N.I.; Punanova, S.A.; Serebrennikova, O.V.; Titov, V.I. Geokhimiya 1985, 381-86.
67. Burkova, V.N.; Serebrennikova, O.V.; Titov, V.I. Geokhimiya 1978, 945-50.
68. Silverman, S.R. In "Fluids in Subsurface Environments"; Young, A.; Galley, J.E., Eds.; Am. Assoc. Petrol. Geol., Memoir 4, Tulsa, 1965, 53-65.
69. Lewan, M.D. Ph.D. Thesis, University of Cincinnati, 1980.
70. Rubinstein, I.; Spyckerelle, C.; Strausz, O.P. Geochim. Cosmochim. Acta 1979, 43, 1-6.
71. Rubinstein, I.; Strausz, O.P. Geochim. Cosmochim. Acta 1979, 43, 1887-94.
72. Palmer, S.E. Abstract 186th ACS Meeting, Washington, DC, 1983.
73. Yang, Z.; Li, Y.; Cheng, Z.; Zhang, D. In "Geochemical Biomarkers"; Yen, T.F.; Moldowan, J.M., Eds.; Gordon and Breach: London (in press).
74. Shi, J.Y.; Mackenzie, A.S.; Alexander, R.; Eglinton, G.; Gowar, A.P.; Wolff, G.A.; Maxwell, J.R. Chem. Geol. 1982, 35, 1-31.
75. Hoffman, C.F.; Strausz, O.P. Bull. Amer. Ass. Petrol. Geol. 1986, 70, 1113-28.

RECEIVED March 30, 1987

## Chapter 6

# Mechanisms Involved in Altering Deoxophylloerythroetioporphyrin-Etioporphyrin Ratios in Sediments and Oils

A. J. G. Barwise<sup>1</sup>

Exploration and Production Division, BP Research Centre,  
Sunbury-on-Thames, England

The possible mechanisms which might be involved in causing alteration in DPEP/etio ratios in sediments and oils are discussed. Qualitative and quantitative data from a suite of source rock extracts show that several mechanisms may be involved. Data from related oils show that, whatever the mechanism, porphyrin ratios are extremely sensitive parameters for indicating the effects of thermal maturity.

Geochemists are interested in applying biomarker geochemistry to petroleum exploration problems, and many different biomarker reactions have been proposed as potential indicators of the thermal stress experienced by sediments or oils. One of the earliest parameters to be investigated as a potential maturity indicator (1) was the ratio of DPEP to etio type porphyrins (see Figure 1 for structures). With increasing thermal stress, the etio type becomes relatively more abundant compared with the DPEP type. The supposed mechanism for this reaction is an intramolecular scission of the isocyclic ring (1). However, with the advent of new analytical techniques such as high performance liquid chromatography (HPLC 2-4) and the structural elucidation of a number of porphyrin molecules from sediments (e.g. 5-8), there is a growing understanding of the diagenetic pathways leading to porphyrin molecules found in sediments and oils. This has led to doubts regarding the original simple explanation of the cause of changes in DPEP/etio ratios. (9)

In this paper, several alternative mechanisms are discussed and evidence is presented to show that a simple intramolecular scission is not the only mechanism which could explain the distribution of porphyrins observed in nature. In order to examine the effect of thermal maturity on porphyrin distributions, a suite of source rock

<sup>1</sup>Current address: Standard Oil Production Company, 8404 Esters Boulevard,  
Irving, TX 75063

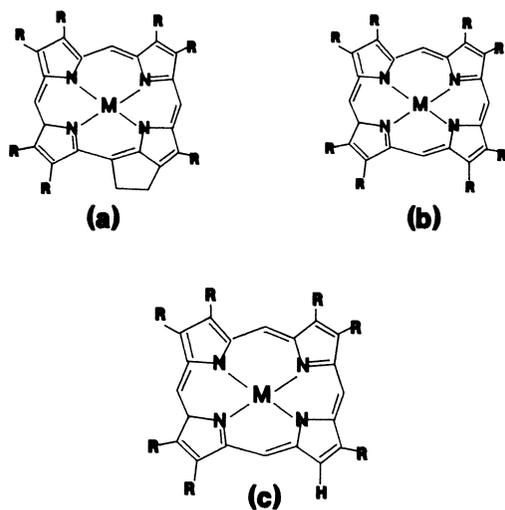


Figure 1: Generalised Porphyrin Structures. (a) DPEP type (b) Etio type (c) B-Unsubstituted type.

extracts from a Gulf of Suez Formation were examined. These rocks vary in maturity across the basin and present day depth reflects maximum maturity. There is little change in source facies, and thus the effects of maturity can be directly observed. The quantity of vanadyl porphyrins in each sediment was determined using visible absorption spectroscopy. Porphyrin distributions were determined by HPLC analysis. Integration of the HPLC distributions was used to determine DPEP/etio ratios. Oils thought to have been derived from this source rock were also examined. As for the sediments, the separated vanadyl fractions were demetallated and examined by HPLC.

### Experimental

Rock samples were ground and extracted with dichloromethane. Nickel and vanadyl fractions were separated and quantitated as described previously (10). The fractions were demetallated using hot methane sulphonic acid at 100°C. HPLC analysis of the demetallated fractions was performed as follows. The HPLC system consisted of a Rheodyne 7125 injection valve, three 25cm x 0.5cm i.d. 5µm Spherisorb silica HPLC columns linked in series, a Perkin-Elmer LC55 detector set at 400nm and an HP laboratory data system for integration of the peaks. The solvent program consisted of a gradient system as follows. Solvent A was 1% acetic acid in hexane. Solvent B was 4:1 dichloromethane:acetone. A linear gradient elution was used from 20%A:80%B to 80%A:20%B over 30 minutes with the final composition held for a further 15 minutes. Details of these and similar HPLC conditions have been published elsewhere (11). A parameter called the porphyrin index was devised from the HPLC measurements which reflects the overall DPEP/(DPEP+etio) ratio. This is based upon a summation of C32-C28 fully alkylated DPEP components and C32-C28 fully alkylated etioporphyrins. This avoids the inclusion of porphyrins which are not strictly DPEP molecules or B-unsubstituted etioporphyrins into the ratio.

### Results and Discussion

If the scission of the DPEP isocyclic ring is the main mechanism for the production of etioporphyrins then one would expect that meso-substituted porphyrins would be the most abundant etioporphyrin type to be found in sediment extracts and oils. However examination of many sediment extracts by this author has shown that this is not the case. As an example, Figure 2 shows a porphyrin HPLC distribution from Gilsonite, a natural bitumen. The major etioporphyrin types are a fully alkylated series and a B-unsubstituted series. Meso-substituted porphyrins, if present, are in low abundance in this sample and in all of the samples that this author has examined to date. Thus suspicion was raised as to the origin of etioporphyrins in sediments.

In order to test where the DPEP/etio ratios were changing in sediments, a series of rock extracts was examined. Figure 3 shows the DPEP/DPEP+etio ratio for the Suez sediments as a function of depth of burial. These were derived from the demetallated vanadyl fraction and show that a sudden decrease in value occurs at approximately 10,000 feet. At ca. 12,000 feet the value reaches

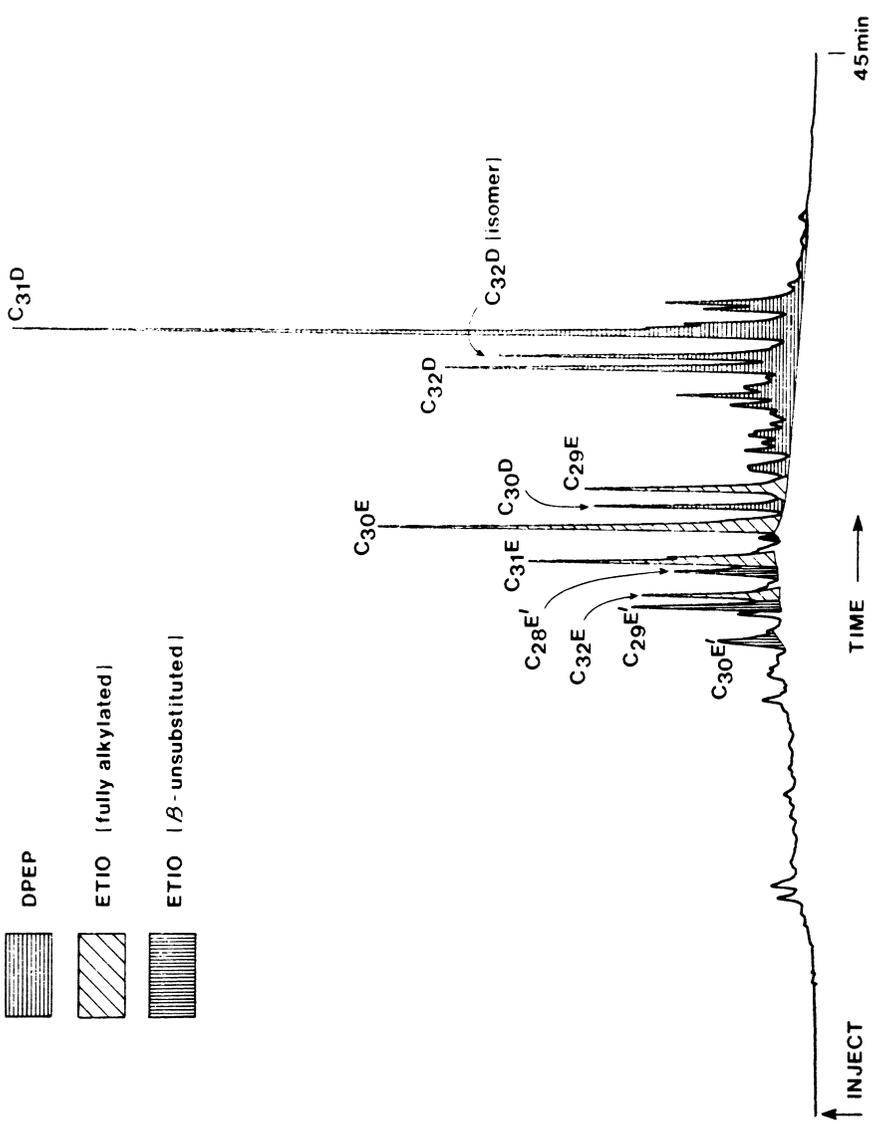


Figure 2. HPLC distribution of demetallated porphyrins from Gilsonite showing several major porphyrin types.

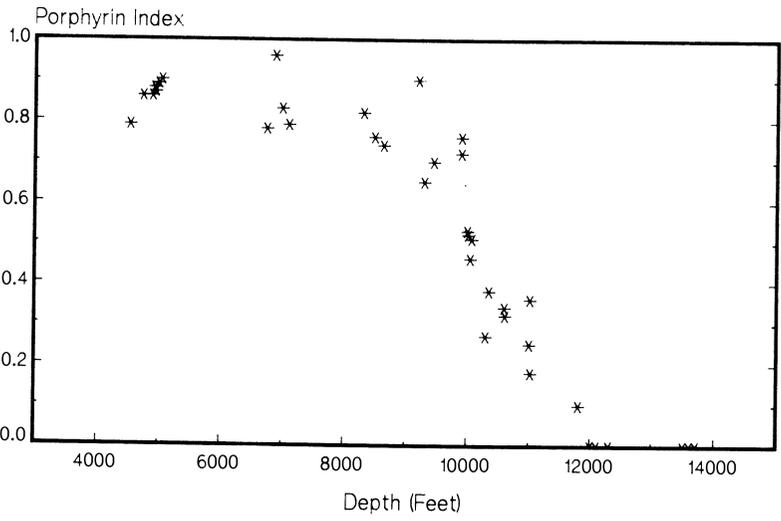


Figure 3: Porphyrin Index Versus Depth of Burial for Suez Sediments.

zero, i.e. no DPEP types could be detected. Thus DPEP/etio ratios do reflect a change in thermal maturity, but whether or not this change is due to an intramolecular reaction is unclear. In order to investigate this further, the concentration of vanadyl porphyrins in the sediments was determined and the concentration of etio and DPEP types estimated from HPLC. Figure 4 shows the results expressed as  $\mu\text{g}$  porphyrin per gram carbon in the sediment. There are several points of note in this plot. Firstly, etioporphyrins were detected in all sediments using the HPLC technique. Thus etioporphyrins must be derived from low temperature diagenetic processes. Secondly, a sudden increase in concentration of etioporphyrins is seen to be coincident with the onset of generation of oil from the source rock. This could imply that etioporphyrins are derived from the thermal decomposition of kerogen. Thirdly, at high maturities little or no porphyrin is observed implying that they are thermally destroyed. To complicate matters further, expulsion of oil from the source rock causes porphyrin concentrations to decrease with oil expelled in the first part of the window being relatively enriched in DPEP porphyrins. Thus in nature, there could be a combination of factors which alter DPEP/etio ratios in sediments and oils. These are discussed briefly below.

Oxidative Cleavage. Since etioporphyrins are present in sediments of low thermal maturity, another mechanism must be accountable, at least in part, for their formation. Oxidative cleavage of the isocyclic ring is well documented (12) and is a likely route by which etioporphyrins are generated. Alternate reduction or decarboxylation could produce both the fully alkylated and B-unsubstituted etioporphyrin series observed in geological samples, analogous to the formation of pristane and phytane. Oxidation produces highly functionalised intermediates which could chemically bind onto kerogen via a condensation reaction.

Generation From Kerogen. The results shown above suggest that large quantities of etioporphyrins are generated from kerogen under natural burial conditions. Laboratory studies using pyrolysis techniques (13) have also shown that significant quantities of etioporphyrins are released from kerogen during heating. This author now believes that this is the main mechanism by which DPEP/etio ratios change in sediments and oils. The oxidative mechanism probably gives rise to highly functionalised etioporphyrin precursors which could readily bond onto kerogen during early diagenesis. Tentative evidence so far suggests that more etioporphyrins are bound onto kerogen than are DPEP types. However, this is difficult to prove since it could be argued that the DPEP isocyclic ring is cleaved simultaneously during release from kerogen.

Thermal Destruction. At high subsurface temperatures, thermal destruction causes a rapid depletion of the concentration of porphyrins in a sediment or an oil. The ratio of DPEP/etio porphyrins may well alter simply because of a difference in thermal stability of the two types of molecule. It has been reported that etioporphyrins are thermally much more stable than DPEP types (14). A relatively small difference in thermal stabilities could easily

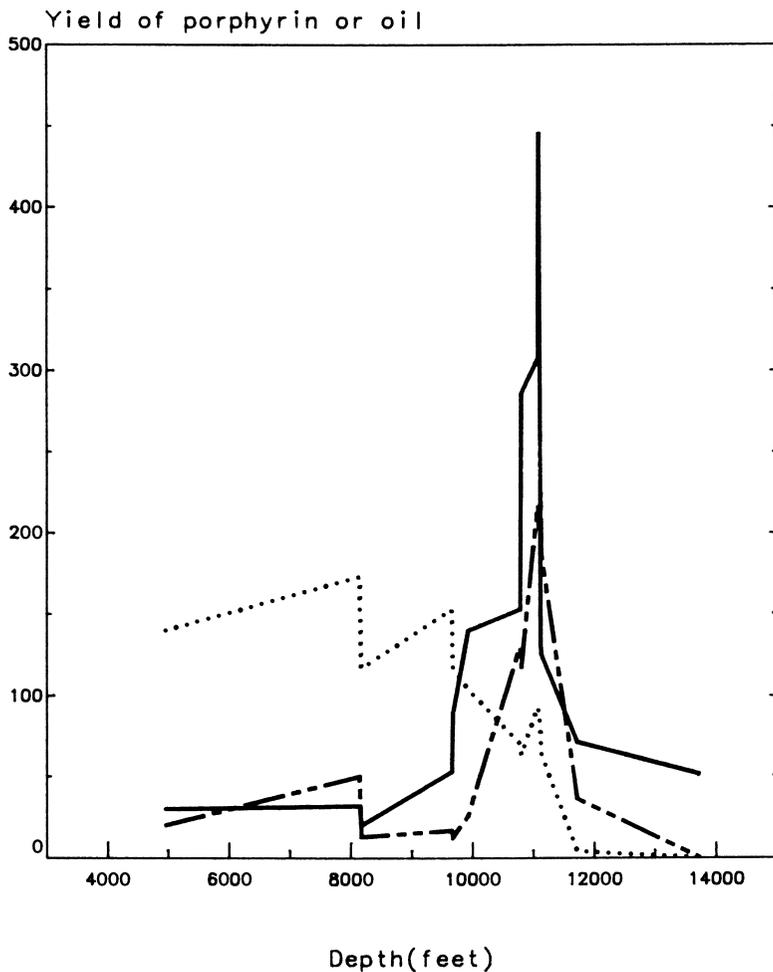


Figure 4: Data for the Suez sediments showing absolute concentrations of DPEP (.....) and etioporphyrins (---) versus depth and also the yield of soluble extract (—) versus depth. Porphyrin yields are expressed as ug porphyrin per g. rock. Extract yields are expressed as ppt. of rock (divided by 4 to fit scale).

account for a rapid change in DPEP/etio ratio during thermal destruction. This is illustrated in Figure 5 where a small difference in activation energies (ca. 10kJ/mol.) is assumed. This diagram shows a theoretical plot of DPEP/(etio+DPEP) ratios as a function of increasing temperature assuming burial under simulated geological conditions (continual burial at a rate of 1C/Myr). As can be seen, a molecular intraconversion reaction does not have to be invoked in order to explain changes in ratio. How important this mechanism is compared to the others remains to be seen. Detailed experimental work needs to be carried out to measure rates of destruction of both porphyrin types.

Expulsion. Since DPEP/etio ratios change over the oil generation window, the effect of expulsion should be considered. Over this window, material present in the indigenous bitumen (DPEP rich) is diluted with material generated from kerogen (etioporphyrin rich). Stepwise expulsion leads to the first products being enriched in DPEP porphyrins whilst later expulsion products contain relatively more etioporphyrins. Again, no molecular intraconversion reactions need to be invoked in order to explain changes in DPEP/etio ratios.

Overall, it appears that there are a number of different factors which affect DPEP/etio ratios in sediments and oils. No one single mechanism can be used to describe observed changes in nature. However the fact that porphyrin distributions are so sensitive to generation and expulsion effects makes them potentially very useful to geochemists. As an example, Table I shows properties of oils derived from the Suez source rock suite. These oils vary in property from low API gravity (14<sup>o</sup>) to moderately high API gravity (33<sup>o</sup>), high sulphur to low sulphur. Examination of their porphyrin distributions shows that these changes in bulk property are the effect of thermal maturity. There is a clear relationship between physical oil properties and DPEP/etio ratios and this is probably a reflection of the temperature at which the oils were expelled from the source rock. Comparison of the oil DPEP/etio ratios with the calibration plot for the sediments shows that the oils correspond to a temperature range of expulsion of ca. 100-140<sup>o</sup>C. Without knowing the source rock data it is possible to rank the oils in order of increasing maturity using porphyrin data alone. In many cases bulk properties and other biomarker parameters would not be able to readily rank the oils in maturity sequence.

### Conclusions

Data from the field study have shown that the mechanism for the change in DPEP/etio ratios with increasing thermal stress is more complex than was previously thought. Etioporphyrins appear to be produced via an oxidative mechanism during early diagenesis. The bulk of etioporphyrins appear to be generated from the decomposition of kerogen during oil and gas formation. Other mechanisms such as thermal destruction and expulsion effects may also have a role to play. Empirical observations suggest that porphyrin ratios are an extremely sensitive parameter for determining the maturity of an oil. There is little need to invoke an intramolecular bond scission to account for observed distributions in nature. Laboratory and field

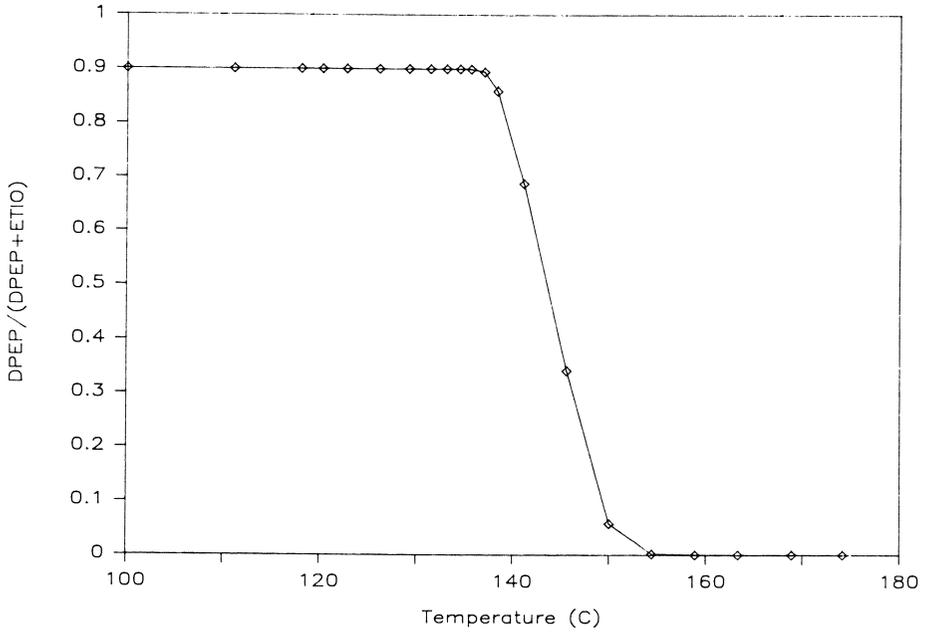


Figure 5: Theoretical plot of DPEP/(DPEP+etio) ratios for sediments heated over a geological timescale. It assumes a 10kJ/mol higher activation energy for destruction of etioporphyrin compared to DPEP ( $E(\text{DPEP}) = 200\text{kJ/mol}$   $E(\text{etio}) = 210\text{kJ/mol}$ ).

data need to be collected in order to investigate the possible involvement of the above mechanisms.

Table I.  
DATA FROM GULF OF SUEZ OILS

OIL	A	B	C	D	E	F	G	H	I
<sup>0</sup> API GRAVITY	13.7	17.8	21.6	25.2	28.6	29.1	30.5	31.1	32.7
SULPHUR (%)	5.2	3.8	3.3	2.2	1.9	1.6	1.7	1.2	1.0
NICKEL (ppm)	148	145	101	50	23	28	23	17	4
VANADIUM (ppm)	190	162	100	54	26	57	32	29	10
DPEP	0.80	0.66	0.63	0.34	0.54	0.52	0.26	0.28	0.11
DPEP + ETIO									

I would like to thank the management of British Petroleum for giving me permission to publish this paper and Alastair Mann for carrying out some of the analyses.

#### Literature Cited

1. Didyk, B.M.; Alturki, Y.I.A.; Pillinger, C.T.; and Eglinton, G. *Nature* 1975, 256, 563-565.
2. Hajibrahim, S.K.; Tibbetts, P.J.C.; Watts, C.D.; Maxwell, J.R.; Eglinton, G.; Colin, H.; and Guiochon, G. *Anal. Chem.* 1978, 50, 549-553.
3. Barwise, A.J.G. and Park, P.J.D. In "Advances in Organic Geochemistry" 1981 (eds. M. Bjoroy et al.) John Wiley and Sons Ltd. 1983; pp. 668-674.
4. Sundararaman, P. *Anal. Chem.* 1985, 57, 2204-2206.
5. Quirke, J.M.E.; Eglinton, G.; and Maxwell, J.R. *J. Amer. Chem. Soc.* 1979, 101, 763-769.
6. Ocampo, R.; Callot, H.J.; and Albrecht, P.J. *Chem. Soc., Chem. Commun.* 1985, 200-201.
7. Fookes, C.J.R. *ibid.* 1984, 1472-1473.
8. Chicarelli, M. and Maxwell, J.R. *Tetrahedron Lett.* 25, 1984, 4701-4704.
9. Barwise, A.J.G. and Roberts, I. 1985 In "Advances in Organic Geochemistry" 1983 (ed. P.A. Schenck et al.) Pergamon Press pp. 167-176.
10. Barwise, A.J.G. and Whitehead, E.V. 1981 In "Advances in Organic Geochemistry" 1979 (eds. A.G. Douglas and J.R. Maxwell) Pergamon Press 1980 pp. 181-192.
11. Barwise, A.J.G.; Evershed, R.P.; Wolff, G.A.; Maxwell, J.R.M.; and Eglinton, G., *J. Chromatogr.* 1986, 368, 1-9.
12. Baker, E.W. and Louda, J.W. 1983 In "Advances in Organic Geochemistry" 1981 (ed. M. Bjoroy et al.) Wiley, pp. 401-421.
13. Van Berkel, G. and Filby, R.H. 1986 A.C.S. Meeting. New York. April 13-18.
14. Burkova, U.N.; Ryadnova, O.V.; Serebrennikova, O.W.; and Titov, V.I. 1980, *Geokhimiya* 9 1417-1421.

RECEIVED January 29, 1987

## Chapter 7

# Generation of Nickel and Vanadyl Porphyrins from Kerogen During Simulated Catagenesis

Gary J. Van Berkel and Royston H. Filby

Department of Chemistry and Nuclear Radiation Center, Washington State University,  
Pullman, WA 99164-1300

The fate of the Ni and V complexes in Woodford and New Albany oil shale kerogens during simulated catagenesis was studied by laboratory pyrolysis at 100–450°C in toluene. Sequential pyrolysis of the same kerogen aliquot at increasing temperatures allowed a distinction to be made between metal complexes in the pyrolysate which were components of residual bitumen associated with the kerogen (low temperature pyrolysis) and those complexes generated from the kerogen matrix (high temperature pyrolysis). Both Ni(II) porphyrin (NiP) and VO(II) porphyrin (VOP) were generated from the kerogen matrix and in proportion to the amount of organically combined Ni and V in the kerogen. There is no indication that either type of porphyrin is chemically bound to the kerogen matrix, but the porphyrin compositions of the bitumen and pyrolysates are different. The pyrolysate VOP composition shifts to lower carbon number and increases in the amount of etio type porphyrins relative to DPEP type porphyrins as pyrolysis temperature increases. Results also indicate that release of Ni and V complexes from kerogen during catagenesis may substantially alter the Ni and V concentration, porphyrin content, and porphyrin composition of the bitumen accumulating in a source rock.

There is increasing evidence that kerogen plays a major role in the geochemistry of biomarker compounds, particularly the porphyrins, in source rocks. Several experimental studies have shown that kerogen liberates a variety of biomarkers upon heating (1–3), but no data on the porphyrins have been presented. Most of the evidence that indicates a kerogen-porphyrin association is indirect and is based on the analysis of porphyrins from sedimentary rocks, bitumens, and petroleums. For example, high molecular weight geoporphyrins ( $>C_{33}$ ) are hypothesized to originate during catagenesis as thermal cracking

of C-C bonds releases porphyrins chemically bound to the kerogen matrix (4,5). Studies of porphyrin distributions in bitumens from rocks at different degrees of thermal maturation in sedimentary basins (6,7) have been interpreted to indicate that substantial quantities of VOP are generated from kerogen during catagenesis. Also, Baker and Louda (8) have postulated that NiP and VOP form via different pathways in sediments. The NiP is considered to form primarily as free or solvent extractable species, whereas VOP forms in a bound, or non-extractable, state linked to kerogen and is only liberated when the thermal stress breaks the kerogen-VOP linkage.

At the present time, there is no satisfactory explanation for the apparent unique kerogen enhanced chelation and/or association of VOP. In fact, recent studies (9-11) have shown that some kerogens may contain significant quantities of both organically bound Ni and V. Moreover, Spiro *et al.* (11) found that the Ni/V ratio in the kerogen of some Israeli oil shales and the NiP/VOP ratio in the associated bitumen were proportional (but independent of the Ni and V contents of the mineral phase), indicating possible correlation between the porphyrin contents of the bitumen and the Ni and V concentrations in the kerogen. The chemical states of Ni and V in kerogen have not been determined, but a major fraction of both metals is probably present as stable tetrapyrrole complexes. Whether these complexes are chemically bound to the kerogen matrix (alkyl bonds, ester bonds, etc.), trapped in a molecular sieve type network, or strongly adsorbed is uncertain. The mechanism of incorporation of these metal ions and/or metal complexes into the kerogen is unknown, and the diagenetic stage during which incorporation takes place and the fate of these complexes during catagenesis has not been investigated.

In this paper, laboratory pyrolysis was used to study the release of Ni and V complexes from oil shale kerogens during simulated catagenesis. The objectives of this study were: (1) to determine the amount and type of Ni and V complexes released from a kerogen during simulated catagenesis, and (2) to determine the relationships among the Ni and V complexes in the kerogen, the complexes released from the kerogen during pyrolysis, and those complexes present in the associated oil shale bitumen. Sequential pyrolysis of the same kerogen aliquot at increasing temperatures was used to distinguish between metal complexes in the pyrolysate which were components of residual bitumen associated with the kerogen (or soluble organic matter (OM) originally present on the rock matrix but which associated with the kerogen after demineralization) and those complexes generated during thermal breakdown of the kerogen. The concentrations of Ni and V were determined by instrumental neutron activation analysis (INAA). The porphyrin contents of the bitumen and kerogen pyrolysates were determined by UV-visible spectrometry and high-performance liquid chromatography (HPLC).

## Experimental

Samples Selection and Preparation. Mississippian New Albany Shale (Henryville Bed Outcrop, Clark County, IN) and Mississippian-Devonian Woodford Shale (Springer Outcrop, Carter County, OK) were the sources of the kerogens used in this study. Detailed geological

information on these shales can be found elsewhere (12,13). The sample preparation scheme is outlined in Figure 1. Each shale was ground to 200 mesh and then bitumen-I was extracted by sonication with toluene/methanol (7:3 v/v; 2 mL solvent/g shale, 6 x 45 min) at 40°C. The extracts were combined and filtered (0.45 µm Fluoropore), and the solvent removed using a rotary evaporator.

Bitumen-I free shale (BF Shale) was dried in vacuo (80°C) and then demineralized using a procedure similar to that of Durand and Nicaise (14). After neutralization of residual HCl-HF on the kerogen with dilute NH<sub>3</sub> followed by several washings with double distilled H<sub>2</sub>O, the kerogen concentrate was dried in vacuo (80°C). The kerogen was then extracted with toluene/methanol (7:3 v/v; 2 mL solvent/g kerogen, 6 x 45 min) to remove bitumen (i.e., bitumen-II) liberated during the acid digestion, and again vacuum dried (80°C). Bitumen-II was isolated using the same procedure as for bitumen-I.

Kerogen Pyrolysis. The kerogens were pyrolysed at constant temperatures within the range of 100–450°C in a 1 L autoclave (Autoclave Engineers, Erie, PA) as shown in Figure 1. An aliquot of kerogen together with 350 mL of toluene was added to the autoclave and the system sealed. The system was purged with nitrogen for 5 min with constant stirring (1000 rpm), pressurized to 250 psi with nitrogen, then brought to the desired temperature. The temperature of the system was allowed to equilibrate (~1 h), maintained for 5 h, and then allowed to cool to below 80°C before opening the system. Pyrolysed kerogen was isolated from the pyrolysate by centrifugation and filtration (0.45 µm Fluoropore) and then further extracted by sonication with toluene (100 mL, 3 x 20 min) at 40°C (toluene/methanol (7:3 v/v) in the case of Woodford kerogen). The filtered extracts were combined and evaporated to dryness to yield the pyrolysate. The pyrolysate in this case is defined as the soluble organic material liberated from the kerogen which has a boiling point greater than that of toluene. The pyrolysed kerogen was vacuum dried (80°C), sampled, and transferred to the autoclave for subsequent pyrolysis at higher temperature. The pyrolysis procedure was then repeated.

Elemental Analysis. Elemental analysis (C,H,N,O) was carried out by Canadian Microanalytical, LTD (Vancouver, BC) using a Carlo Erba Model 1106 Elemental Analyzer.

X-Ray Diffraction (XRD). XRD patterns were obtained with a Norelco powder diffractometer using Cu-K<sub>α</sub> radiation.

Trace Element Analysis. Concentrations of Ni and V were determined by INAA. Sample aliquots and appropriate standards were weighed into clean 1.5 mL polyvials, re-encapsulated in 7.5 mL polyvials, both of which were heat sealed, and then irradiated in the Washington State University TRIGA III reactor. Gamma-ray spectra were recorded using the Nuclear Data ND 6700 Ge(Li) γ-ray spectrometer system. The nuclear reactions and methods used to reduce γ-ray spectra to metal concentrations were similar to those of Jacobs and Filby (15). Correction of the kerogen Ni or V content to a mineral-free basis was carried out in a manner similar to that of Van Berkel and Filby (9).

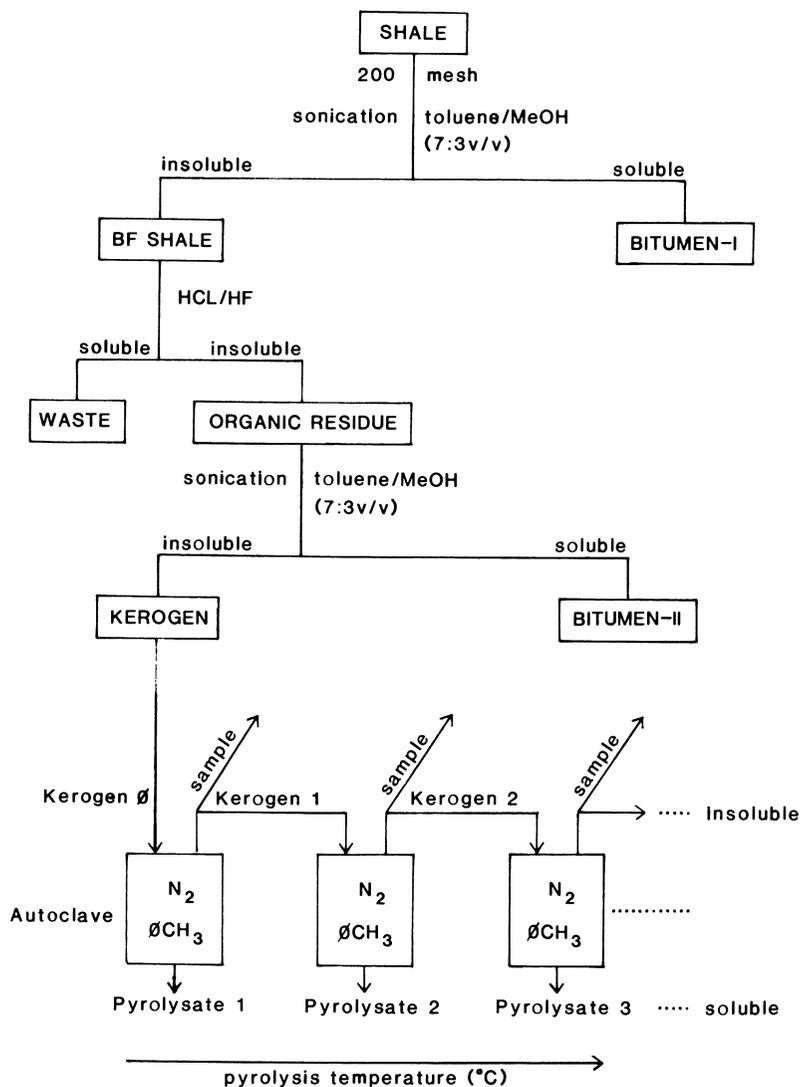


Figure 1. Sample preparation and sequential pyrolysis of a kerogen aliquot at increasing temperatures.

UV-Visible Spectrometry. UV-visible spectra were recorded on a Perkin-Elmer Model 320 UV-Visible Spectrometer. Samples were prepared as toluene dilutions of equal concentration (0.200 and 0.100 mg/mL for New Albany and Woodford samples, respectively). Metalloporphyrin Soret peak integrated absorbance was determined using the method of Filby (16).

High Performance Liquid Chromatography. HPLC analysis of the bitumen and kerogen pyrolysate VOP content was carried out at Chevron Oil Field Research Company (La Habra, CA) using a method similar to that of Sundararaman (17). Peak heights were used to measure the relative proportion of each porphyrin type present.

### Results

Kerogen Composition. The elemental composition and mineral impurities of the New Albany and Woodford kerogens are listed in Table I. The low H/C and O/C ratios of both samples indicate they are relatively mature type II kerogen which is consistent with the depositional environment and age of the oil shales (12,13).

Both kerogen samples were isolated relatively free from residual mineral matter, which was predominantly pyrite ( $\text{FeS}_2$ ) and the  $\text{FeS}_2$

Table I. Elemental Composition and Mineral Impurities of New Albany and Woodford Kerogen

	New Albany Shale Kerogen	Woodford Shale Kerogen
<b>Elemental Analysis</b>		
(wt%)		
C	67.90	68.22
H	5.74	6.71
N	2.67	2.24 <sup>a</sup>
O	6.87	4.83
H/C (atomic)	1.01	1.17
O/C (atomic)	0.08	0.05
<b>Mineral Impurities<sup>b</sup></b>	~17 wt%	~18 wt%
<b>and Relative</b>	pyrite > marcasite >	pyrite > marcasite >
<b>Abundances</b>	covellite ~ rutile	ammonium chloride

<sup>a</sup>Accuracy of organic nitrogen content is uncertain because of residual ammonium chloride ( $\text{NH}_4\text{Cl}$ ) in the kerogen matrix.

<sup>b</sup>Mineral impurity content uncorrected for organically bound metal contents. Organically combined Ni and V alone account for ~0.3 wt% of the apparent mineral component.

Table II. Nickel and Vanadium Content of New Albany and Woodford Kerogen

Element or Ratio <sup>a</sup>	Trace Element Content ( $\mu\text{g/g}$ )	
	New Albany Shale Kerogen	Woodford Shale Kerogen
$[\text{Ni}]_{\text{K}}$	$2500 \pm 34$	$505 \pm 19$
$[\text{V}]_{\text{K}}$	$730 \pm 16$	$3270 \pm 62$
$(\text{Ni}/\text{V})_{\text{K}}$	$3.42 \pm 0.09$	$0.154 \pm 0.007$
$[\text{Ni}]_{\text{MFK}}$	$2128 \pm 81$	$353 \pm 33$
$[\text{V}]_{\text{MFK}}$	$698 \pm 26$	$3262 \pm 97$
$(\text{Ni}/\text{V})_{\text{MFK}}$	$3.05 \pm 0.16$	$0.108 \pm 0.01$

<sup>a</sup> Concentrations ( $\mu\text{g/g}$ ) of Ni and V in the kerogen ( $[\text{X}]_{\text{K}}$ ) and mineral-free kerogen ( $[\text{X}]_{\text{MFK}}$ ). Mineral-free kerogen values were calculated in a manner similar to Van Berkel and Filby (9). Ni/V ratios are weight/weight ratios.

polymorph, marcasite. In addition to these minerals, New Albany kerogen also contained rutile ( $\text{TiO}_2$ ) and covellite ( $\text{CuS}$ ). Rutile was an expected impurity, but covellite, which is soluble in hot HCl, was unexpected. However, because of the high concentration of Cu in the shale (236 ppm, 13) and possible intergrowths of covellite and pyrite, the survival of the former in the rigorous acid digestion is probable.

In addition to pyrite and marcasite, the Woodford kerogen also contained ammonium chloride ( $\text{NH}_4\text{Cl}$ ), which formed on the kerogen by reaction of adsorbed HCl with dilute  $\text{NH}_3$ . The presence of  $\text{NH}_4\text{Cl}$  in the kerogen implies that the organic nitrogen content in this kerogen is overestimated.

The Ni and V contents of the kerogens are given in Table II. New Albany kerogen is enriched in Ni relative to V, whereas for Woodford kerogen the reverse is true. Correction of the kerogen Ni or V contents to a mineral-free basis is small (<15% of the total Ni or V in the kerogen is in mineral form) except for Ni in the Woodford sample. In this case, at least 30% of the total Ni in the kerogen is associated with the mineral phase. The large correction for mineral-bound Ni in the Woodford kerogen reduces the precision of the calculated mineral-free kerogen Ni content (i.e.,  $[\text{Ni}]_{\text{MFK}}$ ). In previous work with a purer fraction of Woodford kerogen, the  $[\text{Ni}]_{\text{MFK}}$  was found to be  $324.4 \pm 5.4$  ppm (18).

Pyrolysis Conditions and Pyrolysate Yields. The bitumen yields, pyrolysis conditions, and pyrolysate yields for both kerogens are shown in Table III. The sample preparation and pyrolysis scheme used allowed a distinction to be made between the readily extractable OM in the shale (bitumen-I), soluble OM associated with the kerogen after mineral dissolution (bitumen-II), and the soluble OM generated from the kerogen matrix during simulated catagenesis (pyrolysates).

Table III. Bitumen Yields, Pyrolysis Conditions, and Pyrolysate Yields

Sample	Pyrolysis			Kerogen Weight (g)	Pyrolysate Weight (g)	Yield <sup>a</sup> (g/g TOC)100
	Temperature (°C)	Pressure (PSI)	Time (h)			
New Albany						
Bitumen-I	-	-	-	-	-	5.435
Bitumen-II	-	-	-	-	-	1.488
Bitumen-I+II	-	-	-	-	-	6.923
Pyrolysate 1	110	290	5	36.0343	0.0596	0.244
Pyrolysate 2	210	440	5	34.3102	0.2386	1.013
Pyrolysate 3	300	680	5	30.9024	1.2070	5.550
Pyrolysate 4 <sup>b</sup>	350	640	5	26.7700	-	-
Pyrolysate 5	400	1130	5	9.8562	1.1808	16.605
Pyrolysate 6	450	1570	5	6.6461	1.2604	26.082
Woodford						
Bitumen-I	-	-	-	-	-	4.943
Bitumen-II	-	-	-	-	-	1.373
Bitumen-I+II	-	-	-	-	-	6.316
Pyrolysate 1	103	300	5	25.3984	0.0990	0.571
Pyrolysate 2	200	425	5	24.5138	0.2215	1.340
Pyrolysate 3	300	760	5	21.6964	0.8704	6.206
Pyrolysate 4	350	960	5	18.0952	0.8357	6.775
Pyrolysate 5	400	1240	5	15.0240	2.7991	26.722
Pyrolysate 6	450	1790	5	9.5252	3.3892	51.485

<sup>a</sup>Yields calculated per g shale TOC, g organic residue TOC, and g kerogen TOC for bitumen-I, bitumen-II, and the pyrolysates, respectively.

<sup>b</sup>Pressure leak during pyrolysis caused loss of volatile products.

Sequential pyrolysis of the raw shale does not permit this distinction to be made. Although the production of pyrolysate at each pyrolysis temperature is paralleled by the two kerogens, the overall pyrolysate yield is much greater for Woodford kerogen. This is not unexpected because Woodford kerogen has a higher H/C ratio, an indication of greater hydrocarbon generating potential, than New Albany kerogen.

Both shales yielded approximately the same amount of bitumen-I and bitumen-II, respectively. Considering bitumen-I plus bitumen-II as the true bitumen content of the shale significantly alters the bitumen content as normally defined (*i.e.*, bitumen-I versus bitumen I + II). Bitumen composition is also altered because of the different compositions of bitumen-I and bitumen-II (*e.g.*, the Ni and V concentrations are different).

Bitumen-II is soluble OM which strongly associates with the mineral matrix and is therefore difficult to extract before acid digestion. Jeong and Kobylinski (19) have shown that a substantial fraction of soluble OM in a shale forms a kerogen-mineral interfacial layer through chemical bonding or physisorption to carbonate and, more significantly, silicate minerals. Dissolution of the mineral matrix in acid solution results in interaction of these soluble polar organic species with the kerogen. Spiro (20) also showed that the soluble OM associated with the minerals was systematically different in composition from the bitumen. This difference was explained by the physical properties of the compounds, and by the catalysis (or inhibition) of certain reactions of these compounds by the associated mineral phases.

Pyrolysis at low temperature ( $\sim 100^{\circ}\text{C}$ ) results in further removal of soluble OM associated with the kerogen. This material is probably similar to bitumen-II. At this point, the kerogen is relatively free of any soluble OM or residual bitumen (pyrolysate 1 is  $\sim 3.5$  wt% and  $\sim 9.0$  wt% of the total soluble OM extracted from New Albany and Woodford shales, respectively). Pyrolysis at higher temperatures begins to depolymerize the kerogen matrix. The soluble OM produced is either cleaved from the kerogen matrix by bond rupture or is material so strongly adsorbed or associated with the kerogen matrix to be defined as part of it (in the conventional sense of solubility), and is only solubilized under these more drastic conditions. McKay (21) suggested that the kerogen of some shales is not an insoluble polymer, but material of similar composition to the bitumen, which can only be solubilized under conditions different than those required to extract the bitumen component.

Neither kerogen produces substantial quantities of pyrolysate below  $300^{\circ}\text{C}$ . Yields of pyrolysate become substantial at  $400^{\circ}\text{C}$  and  $450^{\circ}\text{C}$ ; however, the presence of toluene pyrolysis products increases the pyrolysate yield. Also, at  $450^{\circ}\text{C}$  the nature of the pyrolysate changes from a dark, viscous bitumen to an amber, non-viscous material. Other pyrolysis studies using toluene as the solvent have shown little evidence of thermal degradation of the pyrolysates produced at  $<350^{\circ}\text{C}$ , but at  $450^{\circ}\text{C}$  substantial pyrolytic effects are observed including reduction in molecular weight of the products, loss of heterocyclic and alkyl substituents, and the presence of toluene decomposition products (22,23). Therefore, the pyrolysates obtained in this study at temperatures  $>350^{\circ}\text{C}$  may not be entirely

representative of the organic constituents of which the kerogen is composed.

Effect of Pyrolysis on the Kerogen Composition. The change in the elemental composition of the kerogens after pyrolysis is presented in Table IV and shown graphically in Figure 2 by plotting the H/C versus O/C ratios of the kerogen and pyrolysed kerogens. For both New Albany and Woodford kerogens, the pyrolysis-induced maturation follows the typical pattern of decreasing H/C and O/C ratios as thermal maturation increases. The anomalous behavior of Woodford kerogen between 103°C and 200°C (O/C ratios greater than the original kerogen) may be the result of adsorbed methanol which was used with toluene to extract the pyrolysates from this kerogen. Pyrolysates from New Albany kerogen were extracted using only toluene.

Although the elemental composition of the kerogen changes at each pyrolysis temperature, the largest changes occur above 300°C which is the point at which the kerogens begin to generate substantial quantities of pyrolysate.

Effect of Pyrolysis on the Ni and V Contents of the Kerogen and Pyrolysates. The Ni and V contents of New Albany and Woodford kerogen and pyrolysed kerogens are shown in Table V. Below 450°C, the (Ni/V)<sub>MFK</sub> ratio is constant (within ± 3 s.d. of original kerogen value), but dramatically increases at 450°C in both shales.

Table IV. Elemental Composition of Kerogens and Pyrolysed Kerogens

Sample	Pyrolysis Temperature (°C)	%C	%H	%N	%O
New Albany					
Kerogen 0	-	67.90	5.74	2.67	6.87
Kerogen 1	110	68.62	5.82	2.73	6.79
Kerogen 2	210	70.37	5.71	2.72	5.98
Kerogen 3	300	70.98	5.47	2.71	5.64
Kerogen 4	350	72.15	5.29	2.75	5.57
Kerogen 5	400	72.71	4.51	2.93	5.34
Kerogen 6	450	73.85	3.32	3.01	4.45
Woodford					
Kerogen 0	-	68.22	6.71	2.24	4.83
Kerogen 1	103	67.42	6.59	2.04	5.08
Kerogen 2	200	64.64	6.12	1.97	5.16
Kerogen 3	300	68.17	6.13	2.02	4.46
Kerogen 4	351	69.72	6.00	2.12	4.09
Kerogen 5	400	69.11	5.07	2.34	3.92
Kerogen 6	450	70.87	3.15	2.81	3.07

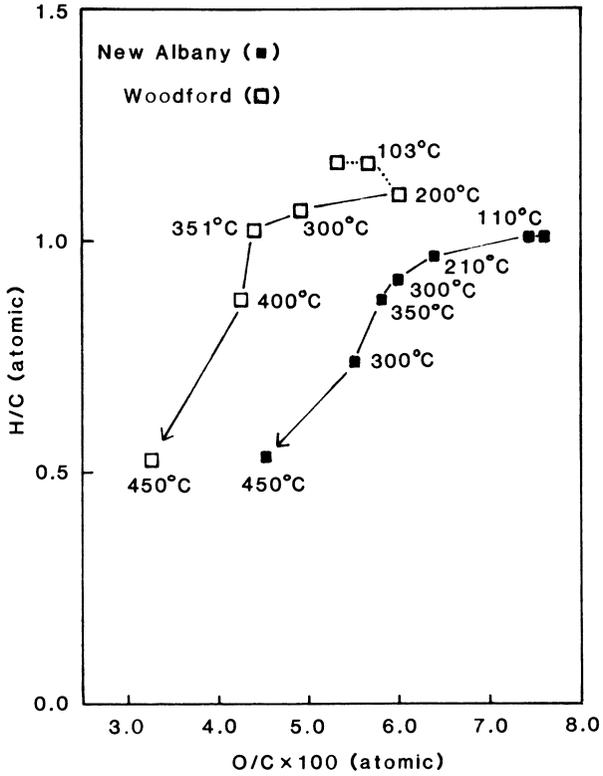


Figure 2. Variation of the elemental composition of the kerogens with sequential pyrolysis.

Table V. Nickel and Vanadium Concentrations and Ni/V Ratios for Kerogens and Pyrolysed Kerogens

Sample	Pyrolysis Temperature (°C)	Mineral-Free Kerogen Concentration (µg/g)		
		[Ni] <sub>MFK</sub>	[V] <sub>MFK</sub>	(Ni/V) <sub>MFK</sub>
New Albany				
Kerogen Ø	-	2128 ± 81	698 ± 26	3.05 ± 0.16
Kerogen 1	110	2187	669	3.27
Kerogen 2	210	2209	676	3.27
Kerogen 3	300	2289	730	3.14
Kerogen 4	350	2297	765	3.00
Kerogen 5	400	2729	830	3.29
Kerogen 6	450	3132	851	3.68
Woodford				
Kerogen Ø	-	353 ± 33	3262 ± 97	0.108 ± 0.01
Kerogen 1	103	385	3357	0.115
Kerogen 2	200	378	3663	0.103
Kerogen 3	300	362	3609	0.100
Kerogen 4	350	403	3513	0.115
Kerogen 5	400	543	4541	0.120
Kerogen 6	450	892	5479	0.163

<sup>a</sup>Concentrations (µg/g) of Ni and V in the mineral-free kerogen ([X]<sub>MFK</sub>). Mineral-free kerogen values were calculated in a manner similar to Van Berkel and Filby (9). Mineral-free Ni and V contents of the pyrolysed kerogens were calculated by multiplying the measured metal content by the percent of the total metal content which was organic. The organic fraction of the metal was estimated by adjusting the organic fraction of the metal in kerogen Ø to account for the amount of the element expelled (organic) with the pyrolysate at each temperature. Percent relative standard deviation (% RSD) of the pyrolysed kerogen values is ≥ the % RSD of the original kerogen values in each respective column.

After the kerogen starts to thermally break down ( $\sim 300^{\circ}\text{C}$ ), the concentration of both metals in the residue increases significantly above that in the original kerogen. This indicates that as catagenesis proceeds, the metals progressively concentrate in the insoluble kerogen fraction.

The percentage of the Ni and V organically bound in the kerogen which is expelled with the pyrolysates (*i.e.*, expulsion yield) is shown in Table VI. Expulsion yields for both elements are low at each temperature. The maximum expulsion yield for each kerogen was observed for the element in highest concentration in that kerogen (Ni for New Albany; V for Woodford). As seen in Figure 3, the expulsion yields of both elements show a parallel behavior. In fact, for New Albany kerogen the expulsion yields for Ni and V at each temperature are not statistically different ( $\pm 3$  s.d.). For Woodford kerogen, however, the expulsion yields are different with greater V expulsion than Ni at each temperature, except  $450^{\circ}\text{C}$ . However, as pyrolysis temperature increases, the Ni expulsion yield does increase relative to the V expulsion yield (New Albany kerogen appears to show a similar trend).

Since for both kerogens the expulsion rates of Ni and V ( $\mu\text{g}$  element/g TOC) at each temperature vary, the concentrations of the elements in the pyrolysates vary. For pyrolysis between  $200^{\circ}\text{C}$  and  $400^{\circ}\text{C}$ , the Ni/V ratios of the New Albany pyrolysates are equal to the corresponding kerogen (Ni/V)<sub>MFK</sub> ratios within the experimental error. However, the Ni/V ratios of the bitumen (I, II, or I + II) and the pyrolysates produced at these temperatures are not equal. In the case of Woodford, the Ni/V ratio of the pyrolysates produced in this temperature range is lower than the kerogen (Ni/V)<sub>MFK</sub> ratio, but equal to the Ni/V ratio of bitumen-I.

It is possible that the organic Ni/V ratio of the *in situ* kerogen is altered by HCl-HF demineralization of the shale. This effect may explain why there appears to be no systematic correlation among the Ni/V ratios of the bitumen, pyrolysates, and kerogen concentrate between the two samples. However, in the absence of a documented model for the association of metal species with the kerogen, it cannot be determined geochemically whether the Ni/V ratio of the bitumen, pyrolysates, and kerogen should be the same or different.

**Metalloporphyrins.** UV-visible spectral examination of the pyrolysates revealed the presence of NiP and VOP. Figure 4 shows the spectra of bitumen-I and the pyrolysates in toluene at the same concentrations. The New Albany samples contain significant quantities of both NiP and VOP, but the NiP/VOP ratio increases with increasing temperature from bitumen-I to the pyrolysates as indicated by the absorbance at the NiP and VOP Soret peaks (396 and 410 nm, respectively). This same trend is seen in the Ni/V ratio of the pyrolysates, which suggests that the NiP/VOP ratio and the Ni/V ratio of the pyrolysates are proportional. Further support for this contention is shown in Figure 5 where the combined NiP and VOP Soret peak integrated absorbance is plotted versus the combined concentration of Ni and V in the pyrolysates. The excellent correlation of Soret peak absorbance with metal content ( $r = 0.98$ ) indicates that the NiP/VOP ratio of the pyrolysates is proportional

Table VI. Expulsion Rates and Yields for Nickel and Vanadium in the Bitumens, Pyrolysates, and Respective Kerogens

Sample	Pyrolysis Temperature (°C)	Expulsion Rate <sup>a</sup> (ug X/g TOC)		Expulsion Yield <sup>b</sup> (ug X/ug X <sub>MFK</sub> )100		Ni/V (Ni/V) <sub>MFK</sub>
		Ni	V	Ni	V	
New Albany						
Bitumen-I	-	96.5	84.2	-	1.15±0.06	-
Bitumen-II	-	30.0	17.8	-	1.69±0.31	-
Bitumen-I+II	-	126.5	102.0	-	1.24±0.07	3.05±0.16
Pyrolysate 1	110	2.96	1.82	0.0946	0.1774	3.27
Pyrolysate 2	210	25.81	8.08	0.810	0.828	3.27
Pyrolysate 3	300	115.8	31.9	3.69	3.32	3.14
Pyrolysate 4	350	-	-	-	-	3.00
Pyrolysate 5	400	165.1	49.5	5.19	4.67	3.34±0.20
Pyrolysate 6	450	24.4	3.32	0.633	0.291	7.16±0.33
Woodford						
Bitumen-I	-	16.57	269	-	0.062±0.008	-
Bitumen-II	-	1.50	37.66	-	0.040±0.003	-
Bitumen-I+II	-	18.07	307	-	0.059±0.006	0.108±0.01
Pyrolysate 1	103	1.41	24.85	0.272	0.520	0.057±0.002
Pyrolysate 2	200	1.63	30.0	0.286	0.603	0.054±0.003
Pyrolysate 3	300	8.36	134.7	1.43	2.38	0.062±0.004
Pyrolysate 4	350	9.52	153.8	1.79	2.91	0.062±0.005
Pyrolysate 5	400	31.45	403.0	5.44	8.00	0.078±0.003
Pyrolysate 6	450	7.7	62.5	0.98	0.95	0.012±0.02

<sup>a</sup>Expulsion rate calculated per g shale TOC for the bitumens and per g kerogen TOC for the kerogen samples.

<sup>b</sup>Expulsion yield defined as weight percent of the organically combined Ni and V in the kerogen expelled with the pyrolysate.

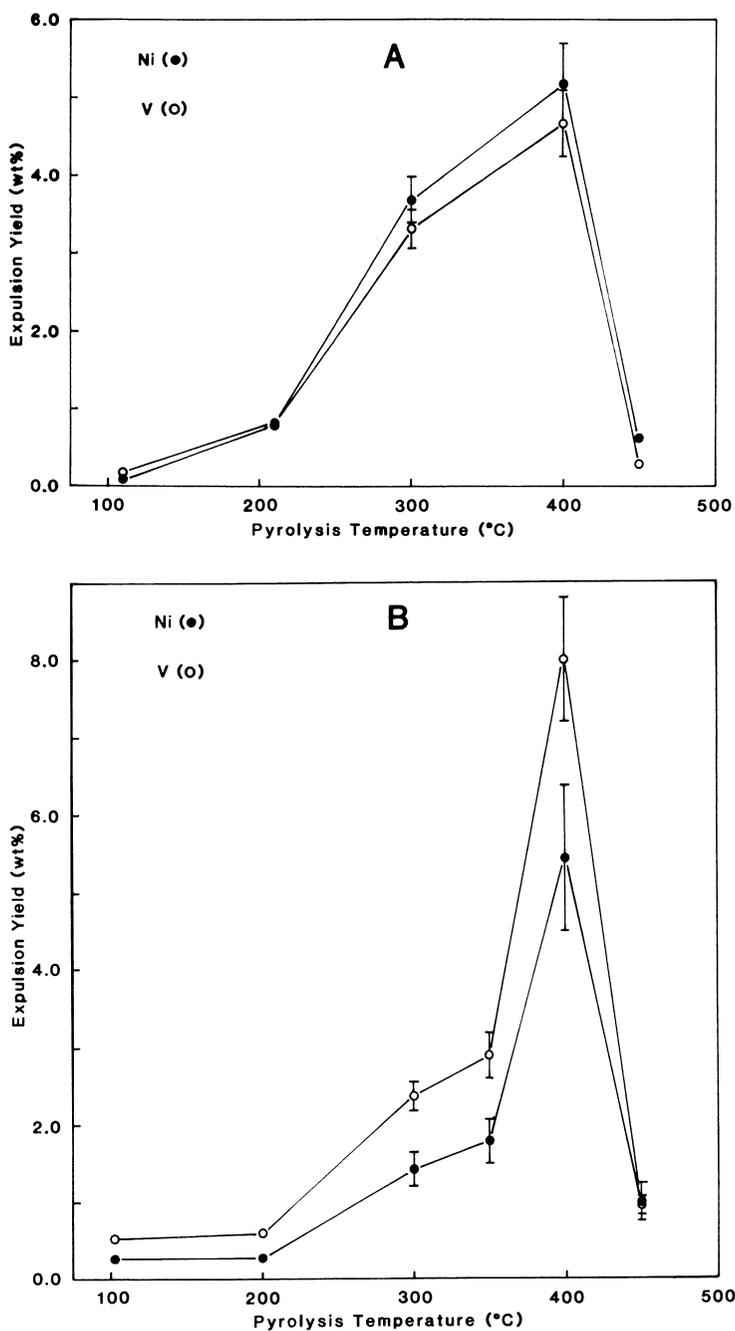


Figure 3. Weight percent of organic Ni and V in New Albany (A) and Woodford (B) kerogen expelled with the pyrolysate (Expulsion Yield) at each pyrolysis temperature (Error bars =  $\pm 1$  s.d.).

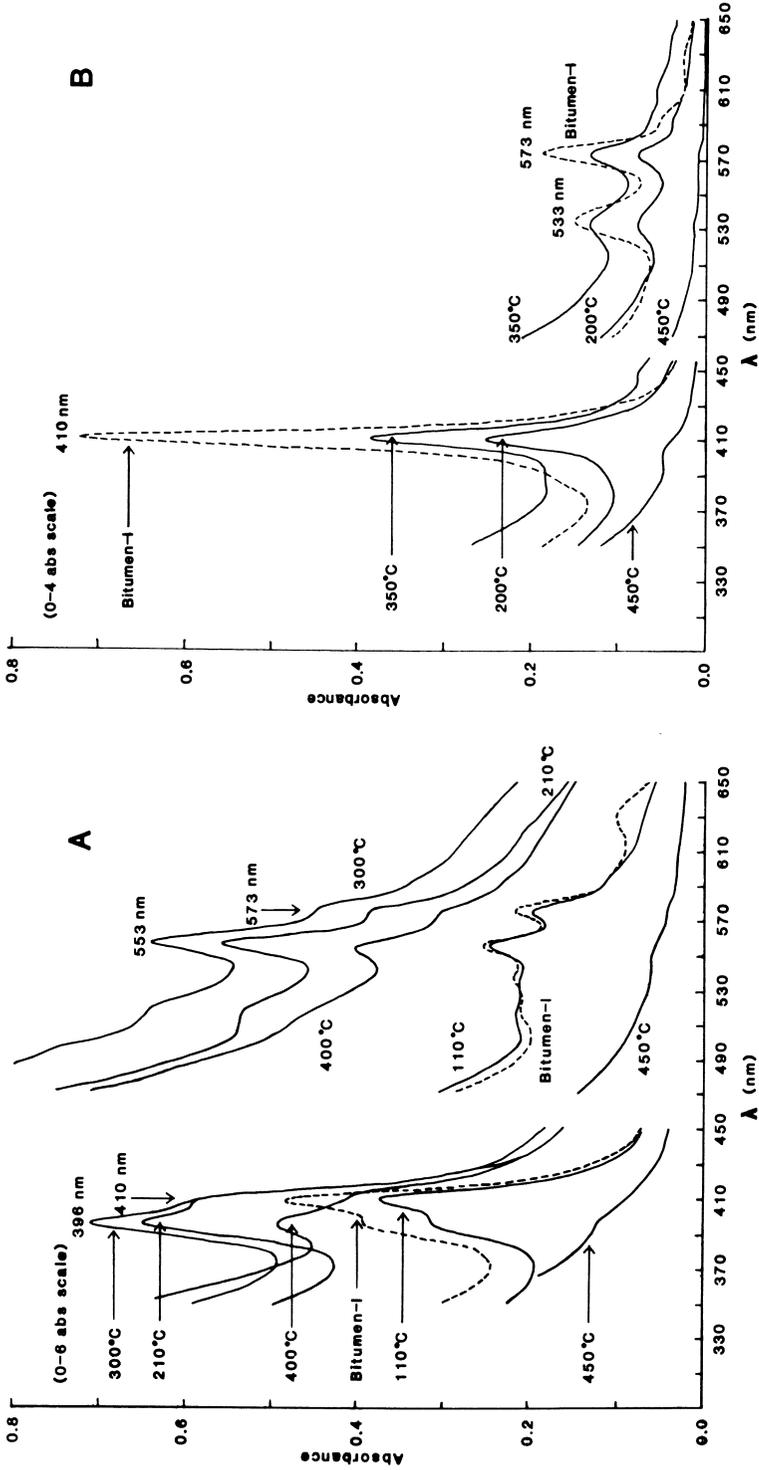


Figure 4. UV-visible spectra of New Albany (A) and Woodford (B) bitumen-I and kerogen pyrolysates.

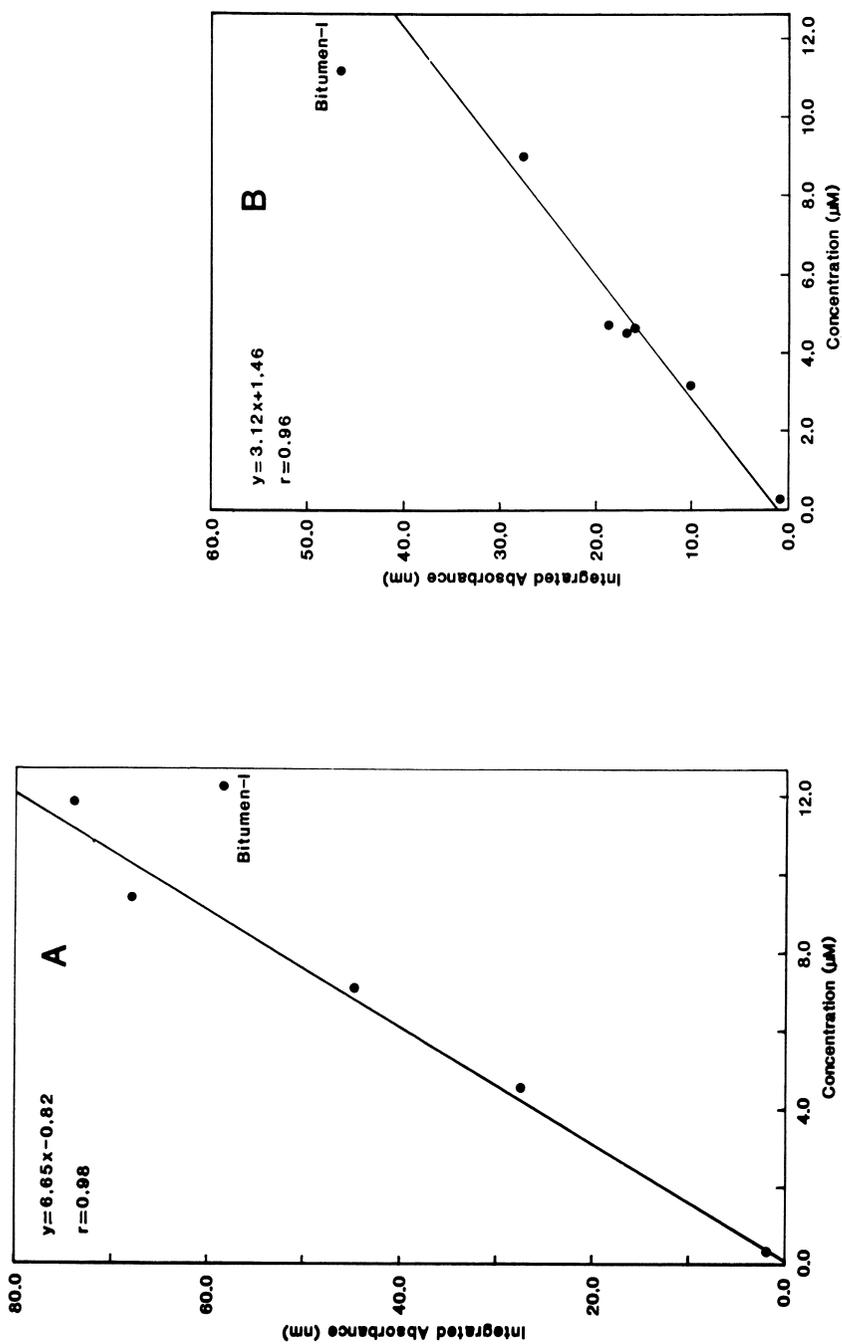


Figure 5. Combined NiP and VOP Soret peak integrated absorbance (nm) versus combined Ni and V concentrations ( $\mu\text{M}$ ) of New Albany (A) and Woodford (B) pyrolysates.

to the Ni/V ratio; however, the [Ni] and [V] need not be equal to the [NiP] and [VOP], respectively (i.e., "non-porphyrin" Ni and V may be present, but in the same relative proportions to NiP and VOP in each sample). The deviation of the bitumen-I point on this plot indicates that the fraction of Ni and V in the bitumen present as porphyrin complexes is less than that in the pyrolysates.

The UV-visible spectra of Woodford bitumen-I and pyrolysates show the presence of only VOP. However, column chromatography on SiO<sub>2</sub> allows separation of a NiP fraction from the samples. Because the NiP Soret peak is not detectable in the bulk samples, a visual correlation of NiP/VOP ratio with Ni/V ratio cannot be made. However, plotting Soret peak absorbance versus metal content of the pyrolysates, as for the New Albany samples, gives a straight line plot ( $r = 0.96$ ) indicating that the NiP/VOP ratio of the pyrolysates is proportional to the Ni/V ratio. In this case, the plot indicates that the fraction of Ni and V in the bitumen present as porphyrin complexes is greater than that in the pyrolysates.

For New Albany kerogen, the Ni/V ratio of the pyrolysates produced between 200°C and 400°C is approximately equal to the (Ni/V)<sub>MFK</sub> ratio. Since the Ni/V ratio and NiP/VOP ratio in this temperature range are proportional, the kerogen must be generating the NiP and VOP in the same ratio as their contents in the kerogen (i.e., (Ni/V)<sub>MFK</sub> ratio ~ NiP/VOP ratio of the kerogen). Interestingly, these ratios are over 2.5 times that of the bitumen-I Ni/V ratio. Over this temperature range, however, the Ni/V ratios of bitumen-I and the pyrolysates for Woodford are equal and proportional to the NiP/VOP ratio of the pyrolysates, but different from the (Ni/V)<sub>MFK</sub> ratio. The reason for the different behavior of the two kerogens is not obvious, but may reflect differences in the speciation and modes of association for the Ni and V in the New Albany and Woodford kerogens.

The porphyrin compositions of bitumen-I and the pyrolysates were investigated using HPLC (17). Relative abundances of four vanadyl porphyrins (C<sub>28</sub>etio, C<sub>29</sub>etio, C<sub>31</sub>DPEP, and C<sub>32</sub>DPEP) were measured in each sample (see Table VII). Porphyrin compositions of bitumen-I and the pyrolysates are different and change with pyrolysis temperature. The nature of the compositional change is similar for the New Albany and Woodford samples.

As pyrolysis temperature increases, two major changes in porphyrin distribution are noted: (1) the relative abundance of the lower carbon number porphyrin in both porphyrin series increases, and (2) the abundance of etio porphyrin increases relative to DPEP. Interpretation of these changes must take into account not only the possible generation of different porphyrins from the kerogen at different temperatures, but also thermal alteration of both the solvent soluble and kerogen-associated porphyrins.

### Discussion

The effect of HCl-HF demineralization of the shale on the trace element content of the isolated kerogen concentrate has not been assessed. However, both kerogen samples contain high concentrations of organically combined Ni and V. Variable amounts of mineral impurity in the kerogen samples will cause the calculated mineral-

Table VII. Relative Abundance of Four Vanadyl Porphyrins in Bitumen-I and the Pyrolysates<sup>a</sup>

Sample	Relative Abundance (%)			
	C <sub>28</sub> <sup>etio</sup>	C <sub>29</sub> <sup>etio</sup>	C <sub>31</sub> <sup>DPEP</sup>	C <sub>32</sub> <sup>DPEP</sup>
New Albany				
Bitumen-I	13.6	21.1	40.4	100
Pyrolysate 1 (110 <sup>o</sup> C)	25.0	23.7	62.9	100
Pyrolysate 2 (210 <sup>o</sup> C)	24.5	23.1	66.4	100
Pyrolysate 3 (300 <sup>o</sup> C)	40.2	43.3	82.0	100
Pyrolysate 4 (350 <sup>o</sup> C)	93.2	100	83.2	87.4
Pyrolysate 5 (400 <sup>o</sup> C)	100	68.2	50.9	34.7
Pyrolysate 6 (450 <sup>o</sup> C)	100	56.5	60.1	56.5
Woodford				
Bitumen-I	21.0	29.0	82.3	100
Pyrolysate 1 (103 <sup>o</sup> C)	26.4	24.4	100	91.4
Pyrolysate 2 (200 <sup>o</sup> C)	25.9	24.1	100	92.0
Pyrolysate 3 (300 <sup>o</sup> C)	24.2	32.3	96.8	100
Pyrolysate 4 (350 <sup>o</sup> C)	35.2	35.8	100	97.4
Pyrolysate 5 (400 <sup>o</sup> C)	100	64.2	90.2	57.5
Pyrolysate 6 (450 <sup>o</sup> C)	100	37.0	-	-

<sup>a</sup>DPEP = deoxophylloerythroetio porphyrin; etio = etio porphyrin.

free kerogen trace element contents to differ because as the mineral impurity content of the kerogen increases, the trace element content of the kerogen is diluted. This effect can be overcome by expressing concentrations per g of kerogen TOC instead of per g of kerogen. However, if kerogen trace element data are expressed as elemental ratios (e.g., Ni/V) the mineral dilution effect is of no consequence. The effect of various demineralization procedures on the trace element content of kerogen is currently under investigation in this laboratory.

During the simulated catagenesis NiP and VOP were generated from the kerogens implying that the concept of selective kerogen binding of VOP proposed by Baker and Louda (8) needs to be revised. Since both NiP and VOP are shown to associate with the kerogen, it would appear that the depositional environment of the sediment and the post-depositional evolution of the kerogen are more important factors in the kerogen-porphyrin association than any chemical property of either NiP or VOP favoring kerogen enhanced chelation or association. The data from this study suggest that both NiP and VOP associate with the kerogen in a similar manner. The most likely modes of association are:

- Physisorption of discrete porphyrins
- Chemisorption of discrete porphyrins
- Molecular sieve trapping of discrete porphyrins
- Chemical bonding of porphyrins to the kerogen through alkyl bonds, ester linkages, etc. or through axial bonding to the metal ion.

Any "non-porphyrin" Ni and V complexes generated from the kerogen are probably part of the asphaltene fraction of the pyrolysate and, therefore, would bear a close resemblance to the "non-porphyrin" complexes that have been described in asphaltenes (24). These asphaltene metal complexes have been considered to be either discrete complexes (adsorbed, chemisorbed, or actually bound chemically to the asphaltenes) or part of the asphaltene structure. However, they may be porphyrins in one of the association modes above (or yet another) which cannot be liberated from the kerogen or asphaltene as a discrete porphyrin species. Tooulakou and Filby (25) have shown that this is the case for at least 25% of the V in Athabasca oil sand asphaltenes.

A comparison of the VOP composition of bitumen-I and the pyrolysates reveals a general shift to lower carbon number for etio and DPEP type porphyrins, and an apparent increase in etio relative to DPEP type porphyrins as pyrolysis temperature increases. It is possible that kerogen generates porphyrins of lower carbon number as pyrolysis temperature increases. Lower carbon number for a given porphyrin type results in increased polarity. Thus, more polar porphyrins may be generated preferentially at higher pyrolysis temperatures because of a stronger association with kerogen than higher carbon number species. However, dealkylation of porphyrins during thermal maturation has been demonstrated in other laboratory studies (26-29) and is consistent with porphyrin data obtained from the analysis of bitumens from sample suites of increasing maturation (6,7,28). Therefore, the shift to lower carbon number porphyrins as pyrolysis temperature increases may be a secondary thermal effect which alters the porphyrins as they are generated from the kerogen.

The apparent increase in etio relative to DPEP type porphyrins with increasing pyrolysis temperature (maturation) must be interpreted with caution since this trend is based on analysis of only four members of the VOP series in the samples. The  $\Sigma$ DPEP/ $\Sigma$ etio ratio determined from the DPEP and etio mass spectral envelopes is a more reliable indicator of a compositional change and work is in progress to determine this ratio for both metalloporphyrins.

The apparent increase in etio relative to DPEP type porphyrins with increasing temperature has several possible explanations:

(1) Etio porphyrins are preferentially associated with kerogen. Therefore, the kerogen pyrolysate is enriched in etio type porphyrins relative to the bitumen. It has been suggested that oxidative cleavage of the DPEP isocyclic ring produces functionalized etio intermediates which could bind to the kerogen matrix (30).

(2) DPEP and etio type porphyrins are generated from the kerogen at the same rate at each temperature, but: (a) DPEP porphyrins are thermally converted to etio porphyrins after being generated, or (b) DPEP porphyrins are thermally degraded at a faster rate than etio porphyrins. Recent work (6,31) indicates that the thermal conversion of DPEP to etio is only a minor source of etio type porphyrins. Preferential thermal degradation of DPEP versus etio type porphyrins has been shown in the laboratory (31) and is the more plausible explanation of the two.

(3) The shift to lower carbon number (e.g., dealkylation) occurs more rapidly for the etio relative to the DPEP type porphyrins. However, if the entire homologous series envelope for both porphyrin types shifts to lower carbon number the  $\Sigma$ DPEP/ $\Sigma$ etio ratio will not change.

Of the explanations above, preferential degradation of kerogen generated DPEP type porphyrins relative to etio type porphyrins is probably the major mechanism producing the changes in composition. The data indicate that both types of porphyrin are present in the samples up to at least 400°C. Not until 200-300°C does the rapid change in relative abundance of the two porphyrin types appear. Burkova *et al.* (31) showed that substantial changes in DPEP/etio ratios take place with temperatures as low as 200-250°C due to preferential degradation. Another indication that this change is due to thermal degradation comes from the relative increase in Ni expulsion yield relative to V expulsion yield with increasing pyrolysis temperature. Rosscup and Bowman (32) showed that VOP was more thermally labile than NiP; hence, the decrease in V expulsion yield with increasing pyrolysis temperature may be due to preferential destruction of liberated VOP resulting in reassociation of the "inorganic" V with the kerogen.

The release of Ni and V from the kerogen during pyrolysis occurs at a rate such that the total amount generated per g of kerogen TOC is much larger than the amount of Ni and V in the bitumen isolated from an equivalent weight of kerogen in the shale. Therefore, the expulsion of the complexes from the kerogen could substantially alter (ignoring migration and *in situ* maturation) the Ni and V content, porphyrin content, and porphyrin composition of the bitumen accumulating in a source rock. Using the pyrolysate yields and metal expulsion rates at each temperature, and assuming: a) a closed system, b) a sample containing 1 g kerogen TOC, and c) no

in situ maturation, the Ni and V contents of the accumulating bitumens were estimated. The variation of the metal content of the accumulating bitumen is plotted versus pyrolysis temperature (maturation) in Figure 6, and the Ni/V ratio is plotted in Figure 7. The data at 450°C were not included because of pyrolytic effects which may have substantially altered the samples.

For Woodford, the expulsion rate of the metals is such that catagenesis reduces their concentrations in the accumulating bitumen. However, the Ni/V ratio remains constant up to 400°C, where it increases by ~12% over the original bitumen. The trend for New Albany, however, is different. The V concentration decreases as the bitumen accumulates, but the Ni concentration increases up to 300°C then decreases. Therefore, the Ni/V ratio of the accumulating bitumen shows a consistent increase.

The substantial quantities of porphyrin liberated from kerogen during maturation will alter the porphyrin content, and porphyrin composition, of the accumulating bitumen. Although kerogen is the source of the porphyrins, it is probably thermal effects which cause the compositional change in the liberated porphyrins rather than liberation of compositionally different porphyrins with increasing temperature. Nonetheless, as maturation (temperature) increases, the VOP series will shift to lower carbon number and etio type porphyrins will increase relative to DPEP type porphyrins. The behavior for NiP is expected to be similar, but differences have been noticed by others (7) in the relative of rates of NiP and VOP dealkylation during maturation, for example.

Changes in the porphyrin composition and content of the bitumens from sample suites of increasing maturity (e.g., 6,7) have been hypothesized to result, at least in part, from the release of porphyrins from the kerogen during catagenesis. This study provides experimental evidence of the generation of NiP and VOP from kerogen. However, the exact nature of the changes in the bitumen will depend on the kerogen and its thermal history and cannot be generalized to all sample suites.

### Conclusions

Several conclusions about the geochemistry of Ni and V complexes in kerogen can be drawn from this study.

- (1) The Woodford and New Albany oil shale kerogens contain substantial quantities of organically combined Ni and V.
- (2) Kerogen catagenesis simulated using laboratory pyrolysis is effective in liberating organic Ni and V complexes from kerogen, including substantial amounts of NiP and VOP. The respective amounts of NiP and VOP generated are directly proportional to the amount of organically combined Ni and V in the kerogen.
- (3) The composition of the VOP generated from the kerogen changes as a function of pyrolysis temperature. As pyrolysis temperature increases, the porphyrin series shift to lower carbon number and there is an increase in the abundance of the C<sub>28</sub> and C<sub>29</sub> etio porphyrins relative to C<sub>31</sub> and C<sub>32</sub> DPEP porphyrins. The apparent increase in generation of etio relative to DPEP type porphyrins with increasing pyrolysis temperature can only be confirmed by determining the carbon number distributions of each porphyrin type for both metalloporphyrins.

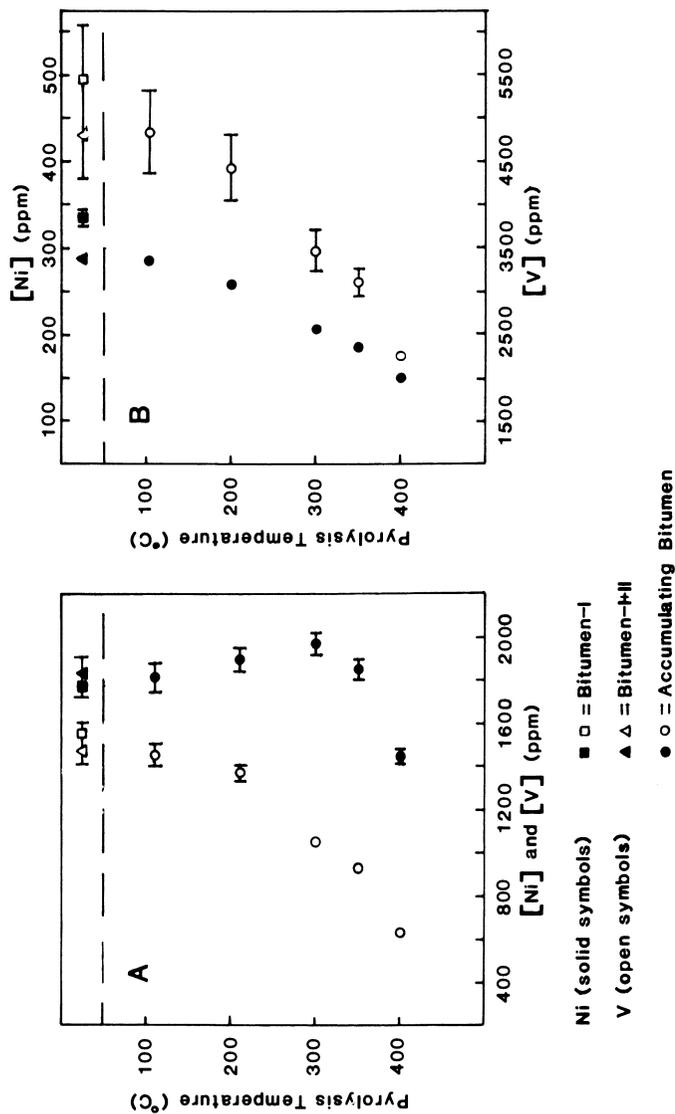


Figure 6. Calculated effect of kerogen maturation on the Ni and V concentration of New Albany (A) and Woodford (B) accumulating bitumen.

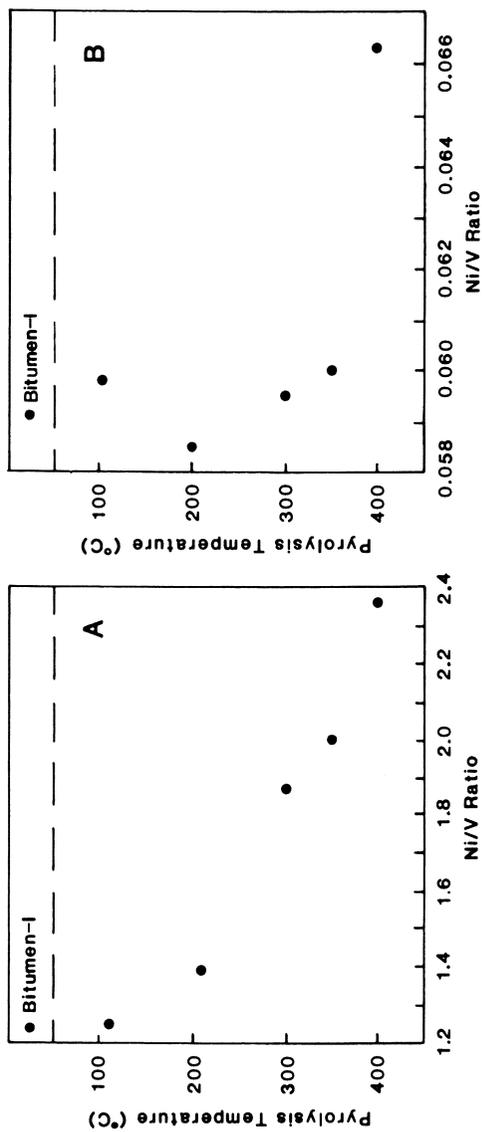


Figure 7. Calculated Ni/V ratio of New Albany (A) and Woodford (B) accumulating bitumen.

(4) Generation of Ni and V complexes from kerogen during catagenesis can substantially alter the Ni and V contents, porphyrin contents, and porphyrin composition of the bitumen accumulating in a source rock. The exact nature of the changes will be dependent on the particular kerogen and its post-depositional history.

#### Acknowledgments

The authors thank Dr. P. Sundararaman (Chevron Oil Field Research Co.) for the HPLC analyses and Dr. M.D. Lewan (Amoco Production Company, Research Center) and Dr. R.K. Leininger (Indiana Geological Survey) for the samples of Woodford and New Albany Shale, respectively. The assistance of Dr. F.F. Foit, Geology Department, Washington State University, in performing the X-ray diffraction work is acknowledged.

#### Literature Cited

1. Gallegos, E.J. Anal. Chem. 1975, 47, 1524-28.
2. Seifert, W.K. Geochim. Cosmochim. Acta 1978, 42, 473-84.
3. Burnham, A.K.; Clarkson, J.E.; Singleton, M.F.; Wong, C.M.; Crawford, R.W. Geochim. Cosmochim. Acta 1982, 46, 1243-51.
4. Quirke, J.M.E.; Shaw, G.J.; Soper, P.D.; Maxwell, J.R. Tetrahedron 1980, 36, 3261-7.
5. Blumer, M.; Rudrum, M. J. Inst. Petrol. 1970, 56, 99-106.
6. Barwise, A.J.G.; Roberts, I. Org. Geochem. 1984, 6, 167-76.
7. Mackenzie, A.S.; Quirke, J.M.E.; Maxwell, J.R. In "Advances in Organic Geochemistry 1979"; Douglas, A.G.; Maxwell, J.R., Eds.; Pergamon Press: Oxford, 1980; pp. 239-48.
8. Baker, E.W.; Louda, J.W. In "Advances in Organic Geochemistry 1981"; Bjorøy, M., Ed.; John Wiley: London, 1983; pp. 401-21.
9. Van Berkel, G.J.; Filby, R.H. In "Geochemical Biomarkers"; Yen, T.F.; Moldovan, J.M., Eds.; Gordon and Breach Publishers: London (in press).
10. Riley, K.W.; Saxby, J.D. Chem. Geol. 1982, 37, 265-75.
11. Spiro, B.; Dinur, D.; Aizenshtat, Z. Chem. Geol. 1983, 39, 189-214.
12. Ham, W.E.; Amsden, T.W.; Denison, R.E.; Derby, J.R.; Fay, R.O.; Graffham, A.A.; Rowland, T.L.; Squires, R.L.; Stitt, J.H.; Wiltse, E.W. "Regional Geology of the Arbuckle Mountains, Oklahoma"; Oklahoma Geological Survey Special Publication 73-3, 1973; 61 p.
13. Hasenmueller, N.R.; Woodward, G.S. "Studies of the New Albany Shale (Devonian and Mississippian) and equivalent strata in Indiana"; Indiana Geological Survey Contract Report to U.S. Department of Energy, Contract DE-AC-21-76MC05204, 1981; 100 p.
14. Durand, B.; Nicaise, G. In "Kerogen: Insoluble Organic Matter from Sedimentary Rocks"; Durand, B., Ed.; Editions Technip: Paris, 1980; pp. 35-53.
15. Jacobs, F.S.; Filby, R.H. Anal. Chem. 1982, 55, 74-7.
16. Filby, R.H. In "The Role of Trace Metals in Petroleum"; Yen, T.F., Ed.; Ann Arbor Science: Ann Arbor, 1975; pp. 31-58.
17. Sundararaman, P. Anal. Chem. 1985, 57, 2204-06.
18. Van Berkel, G.J., unpublished data.

19. Jeong, K.M.; Kobylnski, T.P. In "Geochemistry and Chemistry of Oil Shales"; Miknis, F.P.; Mckay, J.F., Eds.; ACS SYMPOSIUM SERIES NO. 230, American Chemical Society: Washington, D.C., 1983; pp. 493-512.
20. Spiro, B. Org. Geochem. 1984, 6, 543-59.
21. Mckay, J.F. Energy Sources 1984, 7, 257-70.
22. Compton, L.E. ACS Div. Fuel Chem. Preprints 1983, 28, 205-11.
23. Erdem-Senatalar, A.; Kadioglu, E.; Tolay, M.; Bartle, K.D.; Snape, C.E.; Taylor, N. Fuel 1985, 64, 1748-53.
24. Yen, T.F. In "The Role of Trace Metals in Petroleum"; Yen, T.F., Ed.; Ann Arbor Science: Ann Arbor, 1975; pp. 1-30.
25. Tooulakou, D.; Filby, R.H. In "Geochemical Biomarkers"; Yen, T.F.; Moldowan, J.M., Eds.; Gordon and Breach Publishers: London (in press).
26. Casagrande, D.J.; Hodgson, G.W. Nature 1971, 233, 123-24.
27. Casagrande, D.J.; Hodgson, G.W. Geochim. Cosmochim. Acta 1974, 38, 1745-58.
28. Didyk, B.M.; Alturki, Y.I.A.; Pillinger, C.T.; Eglington, G. Nature 1975, 256, 563-65.
29. Bonnett, R.; Brewer, P.; Noro, K.; Noro, T. Tetrahedron 1978, 34, 379-85.
30. Barwise, A.J.G. (this volume).
31. Burkova, V.N.; Ryadovaya, L.V.; Serebrennikova, O.V.; Titov, V.I. Geokhimiya 1980, 9, 1417-21.
32. Rosscup, R.J.; Bowman, D.H. Preprints Div. Pet. Chem. A.C.S. 1967, 12, 77-81.

RECEIVED March 11, 1987

## Chapter 8

# Distribution of Transition Metals in North Alaskan Oils

Joseph A. Curiale

Unocal Research, P.O. Box 76, Brea, CA 92621

Copper, iron, manganese, nickel and vanadium distributions have been studied for eleven oils derived from two genetically-distinct source rock sequences on the North Slope of Alaska. Both vanadium-nickel and nickel-API gravity correlations were observed. Each of these oils had been previously classified into a distinct oil family based on isotopic and biological marker data. Cluster analysis was successfully applied to classify the oils according to family, based solely on concentrations of these five transition metals. Canonical discriminant analysis was used to determine the linear combination of metal concentration values which gives (simultaneously) (a) the greatest intra-type similarity, and (b) the greatest inter-type dissimilarity. The derived canonical variable values clearly separate each oil into its respective family. The results of this study suggest that (a) ratios such as  $V/(V+Ni)$  and  $Fe/V$  are useful as oil type determinants for northern Alaskan oils, and (b) these oils can be successfully classified, using only transition metal concentrations and appropriate statistical methods, into source-defined oil families.

Knowledge of the occurrence and distribution of transition metals in crude oils is important to those engaged in exploring for, producing and refining petroleum. Because organometallic compounds are concentrated in the heavy ends of petroleum, transition element concentrations and ratios can serve as excellent oil-oil correlation parameters. An understanding of the occurrence of these metals is also helpful to refining chemists seeking to minimize catalyst poisoning during oil upgrading. Recognizing the importance of trace metal information, both organic geochemists and petroleum chemists have examined numerous oils worldwide in an effort to establish common transition element characteristics among them, and therefore

0097-6156/87/0344-0135\$06.00/0  
© 1987 American Chemical Society

better understand the reasons for metal concentration variations from oil to oil.

Metals in crude oils arise from several sources. Produced oil will contain metal contributions from original source rock organic matter, from minerals leached during migration and after emplacement in reservoirs, and from contamination during production and shipment. Nevertheless, studies of transition elements in oil usually presume that the distribution of these elements reflects their distribution in the source rock, ignoring both contamination and secondary gain or loss of metal during migration. Such complications are obviated to some degree by specifically studying organo-metallic compounds. However, such an approach introduces a procedural bias to the resulting data, insomuch as current organometallic isolation methods are not completely quantitative (1).

An alternative approach, in lieu of a complete understanding of the molecular association of transition elements in crude oils, is to study their concentration distributions in a selected suite of crude oils. This paper presents the results of such a study, involving a group of well-characterized oils from northern Alaska. The distributions of copper, iron, manganese, nickel and vanadium in two North Slope oil families are presented in an effort to assess the usefulness of trace metal data as a determinant of oil type.

### Background

The presence of transition elements in crude oil was initially established over fifty years ago (2). Several recent summaries on the subject are available (3-5). A review of studies on the first series metals, including those discussed in the present paper, is given elsewhere (Curiale, J. A., AAPG Studies in Geology No. 23, in press). The reader is referred to these papers for details.

Certain transition metal (vanadium and nickel) concentration data have recently been used as type determinants for crude oil families on the North Slope of Alaska (6). These oils are commonly grouped into two source-controlled groups based on biological marker distributions (Curiale, J. A., SEPM Special Publication, in press) and element concentrations and isotope ratios (7). This two-family concept for North Slope oils has wide support, as is suggested by recent summaries of a multi-group study of North Slope oil composition (8). Type A oils are characterized by oils from Prudhoe Bay and Kuparuk Fields, while type B oils, currently non-commercial, are characterized by oils from the Umiat and Simpson areas. Oils in the type A family, relative to those in the type B family, are higher in heteroatom concentrations, V/(V+Ni) ratios and tricyclic/pentacyclic terpane ratios, and have distinctive trisnorhopane distributions. While the type A oils are usually found in reservoirs in Cretaceous and older rocks, the type B oils are more often found in reservoirs in Cretaceous and younger rocks.

The distinction between oil types based on vanadium and nickel concentrations and ratios suggests that other transition elements may also serve as family determinants. In the present study, concentrations of five transition metals (copper, iron, manganese, nickel and vanadium) in eleven North Slope oils were examined; some data represent duplicate analyses of samples discussed in prior

publications (6). Eight of these oils have been classified by isotopic and biomarker data as type A oils; three are type B (Curiale, J. A., SEPM Special Publication, in press). The purpose of the present paper is to demonstrate the potential utility of transition metal concentrations and distributions as a parameter of distinction for oil types on the North Slope, and for worldwide source-related oil families in general.

### The Sample Suite

Eleven oils, ranging in API gravity from 13.6 to 27.8 degrees (at 60°F), were examined. Sample identifications and pre-assigned oil types (based largely on whole oil stable carbon isotope ratios and biological marker distributions) are given in Table I. The oils examined range in production depth from the surface to almost 13,000 ft, and cover an area of about 20,000 square miles. Sample locations are presented elsewhere (6). All samples were analyzed as aqueous solutions of ashes, by Inductively coupled plasma atomic emission spectrometry. Detection limits varied, depending upon sample size. Limited filtration experiments suggest that all metal-containing species in these oils will pass a five micron filter. Further details of the analytical procedures have been given previously (Appendix I of Curiale, J. A., AAPG Studies in Geology No. 23, in press).

Table I. North Slope Oil Sample Identification and Type Assignment

Sample ID	Description	Type
AA0085-1	Put River No. 1; 8720-9260 ft.	A
AA0085-3	Sag River State No. 1; 8540-9020 ft.	A
AB0097-11	Well 10, East of Prudhoe Field	A
AI7251-5	Simpson Core Test Oil; less than 400 ft.	B
AI7251-8	Oil from Simpson area shot hole; B19,SP53	B
AI7288	Well 20, West of Prudhoe Field	A
AI7291	Well 30, West of Prudhoe Field	A
AJ0031R	Well 40, East of Prudhoe Field	A
AJ0032	Well 50, East of Prudhoe Field	A
AJ6013-1	Well 60, East of Prudhoe Field	A
AK7467	Umiat No. 5	B

In the remainder of this paper, I will first present the metal concentrations and other relevant geochemical data, then discuss potential statistical separation of the oils into genetic types, using only transition element data. A final discussion will pursue potential application of trace metal data as an oil family determinant for other oils worldwide.

### Transition Metal Concentrations

Transition metal concentration data (in parts per million by weight) and API gravities are presented in Table II for each of the eleven

oils. An asterisk (\*) indicates that concentrations were below detection limits; concentrations less than 0.1 ppm are assigned values of 0.0. Total metal concentration (Cu + Fe + Mn + Ni + V) ranges from less than 1.0 ppm to over 180 ppm.

Table II. Element Concentrations (ppm) and Canonical Variables (CV)

Sample ID	Cu	Fe	Mn	Ni	V	Total	V/V+Ni	API	Type	CV
AA0085-1	0.3	1.1	3.0	9.6	19.0	33.0	0.66	27.8	A	3.48
AA0085-3	0.0	1.6	8.0	10.0	20.0	39.7	0.67	25.2	A	2.08
AB0097-11	7.4	13.0	*	16.0	30.0	66.4	0.65	22.3	A	----
AI7251-5	2.6	28.0	0.1	0.9	0.8	32.4	0.47	21.0	B	-6.25
AI7251-8	0.1	4.7	0.0	0.9	1.9	7.6	0.68	20.2	B	-5.49
AI7288	1.2	6.2	6.0	11.0	29.0	53.4	0.73	26.6	A	3.34
AI7291	0.7	1.2	*	23.0	66.0	90.9	0.74	21.3	A	----
AJ0031R	3.3	66.0	1.2	34.0	81.0	185.5	0.70	13.6	A	3.14
AJ0032	0.3	4.8	0.0	10.0	26.0	41.1	0.72	----	A	0.94
AJ6013-1	1.8	6.4	0.1	15.0	61.0	84.3	0.80	26.1	A	2.88
AK7467	0.1	0.4	0.0	0.2	0.0	0.7	0.17	36.8	B	-4.12

It is apparent from the data that (a) few internal correlations exist in the concentration data, (b) type A oils generally show higher total metal concentrations (predominantly vanadium and nickel) than type B oils, and (c) there appears to be a general relationship between API gravity and transition metal content. The only significant inter-metal correlation is present between concentrations of vanadium and nickel ( $r=0.95$ ; Figure 1). The data in this figure also show major concentration differences between type A and type B oils. Note particularly that, while type A oils show a large range of vanadium and nickel concentrations, the V/(V+Ni) ratio stays relatively constant, between 0.65 and 0.80. This ratio is often invoked as an oil-oil correlation parameter, because its value appears to remain relatively constant despite subsequent in-reservoir alteration of crude oil (9, and references cited therein). On this basis it would appear that the type A oils are derived from a single source rock suite, and that the differences in vanadium and nickel concentrations for these oils are caused by post-migration alteration. This is consistent with current thinking about this oil type (6).

It has been noted repeatedly that heavy oils contain unusually large amounts of transition metals (10-12). Thus it is plausible that the variation of vanadium and nickel concentrations within the type A oils shown in Figure 1 results from differences in API gravity (Curiale, J. A., SEPM Special Publication, in press). Figure 2 shows the relationship between API gravity and metal (vanadium and nickel) concentration of the type A oils. Both API gravity vs Ni and API gravity vs V show trends of increasing metal concentration with decreasing API gravity. Figure 2 shows the best fit line for Ni vs API gravity; the second line in the diagram is inferred for vanadium, based on an average V/(V+Ni) ratio for type A oils of 0.71 (see Table II). The difference in line fits for these

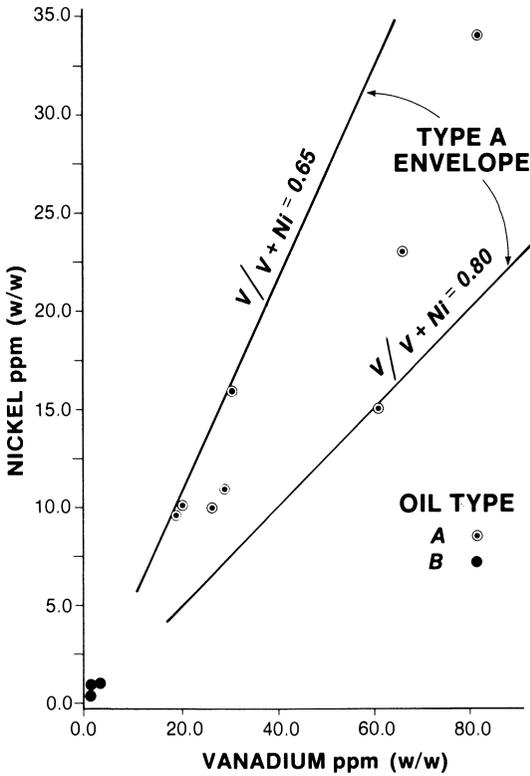


Figure 1. Concentration of nickel (ppm) vs vanadium (ppm) for types A and B North Slope oils. Type A oils fall within or very close to a  $V/(V+Ni)$  ratio envelope between 0.65 and 0.80.

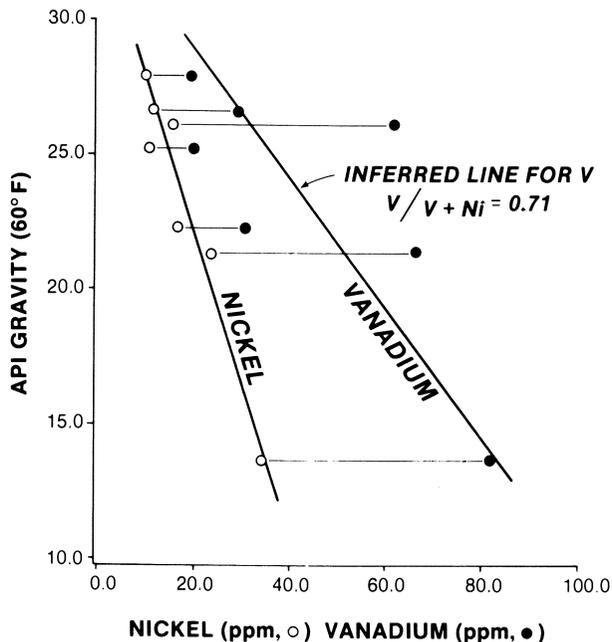


Figure 2. API gravity vs nickel and vanadium concentrations (ppm) in type A North Slope oils. Best-fit line for API gravity vs Ni is shown. The other line is inferred as an ideal fit for API gravity vs V, using an average  $V/(V+Ni)$  ratio of 0.71 for type A oils (Table II).

two metals may suggest that, in type A oils, the molecular species of nickel is different from that of vanadium. Alternatively, the differing source inputs to the type A oil family (6,13) may supply differing vanadium concentrations, but similar nickel concentrations.

### Statistical Discrimination Between Oil Types Using Metal Data

Efforts at oil-oil correlations using metal data from a group of oils comprising more than one source family are implicit attempts at either cluster or discriminant analysis. Such efforts commonly involve only two or three metals, usually presented as ratios (14-16). In the present study, concentrations of five transition metals have been determined (Table II), and both cluster and discriminant analysis techniques have been applied.

Figure 3 shows clustering results using a model with these five metals as variables; data were read in the order listed in Table II, and distances were calculated using Bray-Curtis (BC) indices (17). Note that clustering using only eleven oils is capable of distinguishing two groups at the 1.0 BC level, and that these groups correspond exactly to the A and B oil types of the North Slope. Nevertheless, considerable variety within the groups is evident. Note particularly that geographically proximate oils do not necessarily cluster at low BC values (e.g., A17288 and A17291).

Cluster analysis has its greatest utility when oil types have not yet been established by other methods. For the oils listed in Table I however, the typing specifications are clear. In such situations, discriminant analysis can provide greater utility as a type determinant for classification of future samples (18). In the present study, canonical discriminant analysis has been used to determine the linear combination of the five transition elements that provides the greatest intra-type correlation within each oil type, while simultaneously providing maximum discrimination between types (19). The analysis, subject to a data limitation of only eleven oils comprising two classes, provides a single canonical variable (CV) capable of separating the oils according to type based solely on concentrations of copper, iron, manganese, nickel and vanadium (note that the strong correlation between nickel and vanadium shown in Figure 1 makes the addition of vanadium partially superfluous). The raw coefficients derived by the analysis are: Cu = 3.486; Fe = -0.419; Mn = -0.117; Ni = 1.340; V = -0.266 (residual = -4.562). The canonical variables for nine of the eleven oils are listed in Table II. A strong discrimination has been established between oil types A (CV = -6.25 to -4.12) and B (CV = 0.94 to 3.48). Thus each of these nine oils are easily classified using this technique into the two pre-determined oil types, indicating that transition metal data are useful as oil typing parameters independently of other geochemical data.

Mahalanobis' distances provide a measure of the extent of class separation achieved by the canonical variable discriminant analysis, and allow an estimate of the contribution of parameter pairs to the total separation (19). In the present case, the Mahalanobis' distance using Cu, Fe, Mn, Ni and V is 7.93, of which Fe and Ni

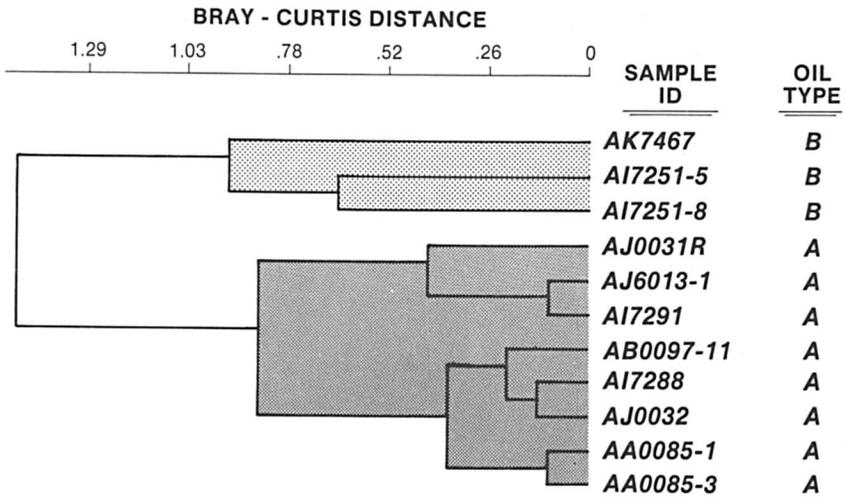


Figure 3. Results of cluster analysis using Bray-Curtis distance for type A and B North Slope oils. Concentrations of copper, iron, manganese, nickel and vanadium are used as clustering variables. Note the distinct separation between types A and B.

comprise 56.3% of the total separation. That is, the concentrations of iron and nickel in North Slope oils account for over half of the difference in the distribution of these five metals in the oils listed in Table I.

Although the intent of this study is to determine the capability of distinguishing North Slope oils based solely upon transition metal data, the addition of the API gravity (Table II) to the discriminant analysis provides an interesting result. The addition of this variable necessitates deleting three of the eleven samples (in addition to the two data gaps in Table II, sample AJ0032 drops out of the analysis, because API data are unavailable). The Mahalanobis distance resulting solely from the addition of API gravity increases from 7.93 to 23.58, suggesting that gravity differences between oil types are indeed significant. This was previously noted for non-biodegraded North Slope oils (7).

The unstandardized canonical coefficients noted above are useful in deriving unique ratios for defining North Slope oil types. For example, note that the CV's of type B oils (Table II) are significantly more negative than those for type A oils, while at the same time iron has the most negative canonical coefficient (as noted above). These two observations suggest that relative iron content may be a controlling factor in recognizing type B oils. Indeed, the Fe/V ratio is consistently greater than 1.0 for type B oils, and less than 1.0 for type A oils.

### Discussion

While metal concentration data have been used in the past to distinguish North Slope oil types, they have been limited to vanadium and nickel (Curiale, J. A., SEPM Special Publication, in press). The present study demonstrates that other first series transition elements, particularly iron, are also useful indicators of oil type. Further, the utility of cluster and discriminant analyses as determinants of oil type appears to transcend certain post-migration oil alteration effects, such as biodegradation and extreme thermal maturation. For example, sample AI7251-8, a heavily biodegraded type B oil, clusters consistently with AI7251-5, a relatively unaltered type B oil (Figure 3). Further, discriminant analysis separates these two oils by only one CV unit. In addition, sample AK7467, a very mature (API = 36.8) oil, also is clearly grouped by cluster analysis and force-grouped by discriminant analysis into type B oil, in agreement with other conclusions for Umiat oils (7). It can be concluded that transition metal data provide excellent supporting data for oil type classification on the North Slope.

Although transition metals successfully support a dual classification, it is unclear whether each oil type is necessarily source-distinctive. Published data appear to support multiple sourcing for type A (Prudhoe) oils (6,13), and the concept of a single source unit for type B oils is also subject to some question (Curiale, J. A., SEPM Special Publication, in press). Future efforts at establishing transition metal distributions in kerogens and bitumens of North Slope source units could potentially provide a distinctive classification for each oil listed in Table I. If successful, direct matching of a single oil to a series of source rocks will be

possible, allowing one to assign percentage contributions from each source to the mixed oil.

The successful application of transition metal data as an oil type indicator on the North Slope of Alaska suggests that these data could be applicable as oil family determinants elsewhere. Analytical developments over the past two decades have made it possible to determine a large number of transition elements rapidly, with constantly improving precision. In addition, improvements in filtration techniques allow efficient separation of mineral matter from the indigenous organic matter of crude oil, greatly increasing the accuracy of metals-in-oil determinations. Such advances now make the routine analysis of organically-associated trace metals in crude oils a reality; such data are no longer limited to determinations of vanadium and nickel concentration.

The future applications of trace metal geochemistry to oil typing and petroleum exploration in general appear to be extensive (3,4). As analytical methods for analysis of hydrocarbons in crude oils mature, research directions will begin to emphasize the heteroatom-containing molecules. Of these, organometallic compounds will undoubtedly provide a significant amount of information concerning the genesis and classification of oil.

#### Acknowledgments

Drs. G. H. Smith, J. R. Fox, S. R. Larter, R. E. Sweeney, R. J. Lukasiewicz and F. G. Dewalt, all of Unocal's Science & Technology Division, provided needed advice and expertise. S. A. Bharvani and M. Jacob assisted in the laboratory. Special thanks goes to Mary MacDonald for preparing the final manuscript. I also thank Unocal management for providing an environment where this type of work can continue, and for giving permission to publish the results.

#### Literature Cited

1. Fish, R. H.; Komlenic, J. J.; Wines, B. K. Anal. Chem. 1984, 56, 2452-2460.
2. Treibs, A. Annal. Chem. 1934, 510, 42-62.
3. Barwise, A. J. G.; Whitehead, E. V. In The Significance of Trace Elements in Solving Petrogenic Problems and Controversies; Augustithis, S. S., Ed.; Theophrastus: Athens, 1983; p. 599-643.
4. Jones, P. In Forum on Oil and Ore in Sediments; Imperial College of Science and Technology: London, 1977; p. 40-53.
5. Hitchon, B.; Filby, R. H. Bull. Amer. Assoc. Petr. Geol. 1984, 68, 838-849.
6. Curiale, J. A. In Oil/Rock Correlation Study on North Slope of Alaska; Magoon, L.B.; Claypool, G.E., Eds.; AAPG Studies in Geology Series No. 20; Amer. Assoc. Petr. Geol.: Tulsa, 1986; p. 203-232.
7. Magoon, L. B.; Claypool, G. E. Bull. Amer. Assoc. Petr. Geol. 1981, 65, 644-652.
8. Claypool, G. E.; Magoon, L. B. In Oil/Rock Correlation Study on North Slope of Alaska; Magoon, L. B.; Claypool, G. E., Eds.; AAPG Studies in Geology Series No. 20; Amer. Assoc. Petr. Geol.: Tulsa, 1986; p. 49-81.

9. Lewan, M. D. Geochim. Cosmochim. Acta 1984, 48, 2231-2238.
10. Skinner, D. A. Ind. Eng. Chem. 1952, 44, 1159-1165.
11. Erickson, R. L.; Myers, A. T.; Horr, C. A. Bull. Amer. Assoc. Petr. Geol. 1954, 38, 2211-2218.
12. Breger, I. A. In The Future of Heavy Crude Oils and Tar Sands; Barnea, J.; Bowman, C. W., Eds.; UNITAR: New York, 1977; p. 163-167.
13. Seifert, W. K.; Moldowan, J. M.; Jones, R. W. Proc. 10th World Petr. Cong., 1979, p. 425-440.
14. Bonham, L. C. Bull. Amer. Assoc. Petr. Geol. 1956, 40, 897-908.
15. Curiale, J. A. Ph.D. Thesis, University of Oklahoma, 1981.
16. Saban, M.; Vitorovic, O.; Vitorovic, D. In Characterization of Heavy Crude Oils and Petroleum Residues; Editions Technip: Paris, 1984; p. 122-127.
17. Seber, G. A. F. Multivariate Observations, John Wiley & Sons: New York, 1984.
18. O'Connor, J. T. In USGS Research on Energy Resources -- 1986 Program and Abstracts; Carter, L. M. H., Ed.; USGS Circular 974; USGS: Washington, D.C., 1984; p. 46.
19. Davis, J. C. Statistics and Data Analysis in Geology; John Wiley & Sons, Inc.: New York, 1973.

RECEIVED October 16, 1986

## Chapter 9

# Metals in Crude Oils, Asphaltenes, Bitumen, and Kerogen in Molasse Basin, Southern Germany

Alfred V. Hirner

Mineralogisch-Petrographisches Institut der Universität, Theresienstrasse 41,  
D-8000 München 2, Federal Republic of Germany

In the course of organic geochemical investigations in the Southern German Molasse Basin, the use of trace element studies on maltene, asphaltene and kerogen fractions of crude oils, bitumens and potential source rocks for oil-oil and oil-source rock correlations has been tested.

The Ni, V and Co contents of crude oil-maltenes and -asphaltenes enabled the differentiation of two oil families to be made in conjunction with other geochemical analyses. Elemental concentrations in the asphaltene fraction of bitumen and in the kerogen of potential source rocks are similar to those in the corresponding crudes. However, these correlations are not true for Zn and I.

It could be shown that Ni in kerogen is associated with the organic phase, whereas Ti is derived from the mineral matrix.

Organic substances play a dominant role in geochemical cycling, especially in the local concentration of trace metals (1-3). Metal-organic and organometallic species in sediments may originate from the biomass without major chemical changes, or they may be formed during sedimentation and/or diagenesis from organic molecules and metal ions derived from different biogenic (biomass) and abiogenic sources (weathering of minerals). Thus, in many of these geochemical cycles inorganic as well as organic associations of the metals are involved, and often they directly or indirectly interact with each other. Complex situations result, and correlations between metal concentrations and either inorganic or organic sediment fractions may not always be found. For example, in Australian oil shales nickel is associated with the organic as well as the inorganic fractions with no apparent preference (4).

In organic geochemical exploration however, only those metals are of significance, whose concentrations are closely associated with the organic matter. The coordination chemistry and abundance of these metals in crude oils provide useful information on the origin, migration, and maturation of petroleum (5).

In this study, former investigations (6) are extended to the maltene and asphaltene fractions of Southern German crude oils as well as the bitumen and kerogen fractions of potential source rocks of these crudes.

### Samples and Methods

Several geochemical investigations of crude oils have revealed the existence of only two oil families in the South German Molasse Basin (6-8). All crudes found at the stratigraphic base of the Tertiary belong to one group. The oils in Mesozoic reservoirs in the western part of the basin are supposed to be of a different origin.

Based on these results, representative samples from each oil family have been selected:

Mesozoic oils: Fronhofen 12, Pfullendorf 6, Ostrach 8

Tertiary base oils: Mönchsrot, Arlesried, Darching 1, Höhenrain 4.

Carbon isotopic studies gave some evidence for Sannoisian and Rupelian sediments as potential source rocks for the Tertiary base oils (9), although the samples investigated were still immature. Therefore, the bore core samples Teising 1 and Höhenrain 2 have been included in this study.

The concentrations of V, Cr, Fe, Co, Ni, Zn, Se, Br, Ag and I were determined by instrumental neutron activation analysis as already described (6); Ti in kerogen was determined by X-ray spectrometry. The asphaltenes were separated by precipitation with petroleum ether 40/60. Trace element concentrations of the maltenes (= deasphalted oils) were calculated by difference, using the analytical results of the total oil and the asphaltene fraction. The core samples were extracted with chloroform/methanol (2:1 v/v) for three days. The maltene and the asphaltene fractions of the extracts were analysed separately.

### Trace element concentrations

To indicate the concentration ranges of trace elements in Southern German oils and kerogens, previous data (6, 10) have been compiled as shown in Figure 1.

Trace element concentrations range over more than six orders of magnitude, i.e. from several parts per billion to several weight percent. With the exception of I, the elements are enriched in the asphaltene fraction by about one order of magnitude on the average, indicating an increase of the metal-binding capacity with increasing polarity and molecular weight of the organic molecule or, alternatively, an increase in metal-trapping capacity of asphaltenes. Se, Zn, Fe and Cr are enriched in the kerogen fraction compared to the asphaltenes. With respect to Ni, V and Co, however, these two fractions overlap, arguing for a common origin of these elements in both fractions. It must be considered, however, that the kerogen fraction can never be completely free of inorganic contributions.

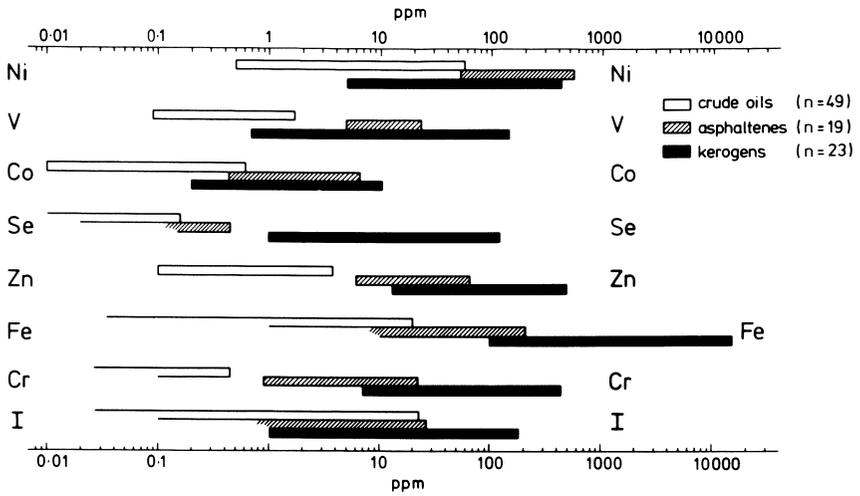


Figure 1. Ranges of trace element concentrations in crude oils, asphaltenes and kerogen from Southern Germany (6, 10).

### Results of correlation studies

Compared to the Tertiary-base oils, the Mesozoic crude oils show significantly lower contents of Ni, V and Co in the maltene as well as in the asphaltene fraction (Figure 2). This result is in accordance with the presumed association of these elements with the original source material (biomass). However, overlapping ranges are observed in the case of Zn and I, indicating an unknown association between compounds of these elements or just a contribution from inorganic matter (minerals). Other arguments for the latter hypothesis are the strong enrichment (7- to 15-fold) of Zn in the maltenes and asphaltenes of the extracted bitumen, whereas Ni and Co in the asphaltene fraction of the bitumen show similar abundances as in the crude oil asphaltenes. Because of the enrichment of the polar compounds in the non-migrated bitumen compared to the migrated crudes, and because Ni and Co are concentrated in the petroleum heavy ends, the observed enrichment (2- to 6-fold) of these elements in the bitumen maltenes compared to the oil maltenes is understandable.

In Figure 2, data for Co and Zn obtained from previous studies are included for comparison. This could not be done for Ni and V in the figures used because the usual low concentrations of these elements in Southern German crude oils precluded showing both data sets on the same graph.

Concerning Cr concentrations, all bitumen fractions (1.2 to 11.1 ppm) lie within the range of oil asphaltenes (0.9 to 22.7 ppm). Also, the Ag contents of bitumen maltenes are within the crude oil range (0.02 to 0.32 ppm). Whereas Fe in bitumen maltenes (35 to 38 ppm) is as abundant as in crudes, the bitumen asphaltenes (700 to 2100 ppm) are enriched compared to the oil asphaltenes (<10 to 208 ppm). Se in crudes is lower than 0.2 ppm and in oil asphaltenes lower than 0.5 ppm, but it is enriched in the bitumen (0.8 to 1.3 ppm). Br is strongly enriched in bitumen fractions: in bitumen maltenes (147 to 277 ppm) approximately 100-fold, in bitumen asphaltenes (1102 to 1157 ppm) approximately 500-fold compared to Molasse oils (0.3 to 6.3 ppm).

### Results of kerogen studies

The relatively high concentration of Ni in crude oils suggests the presence of organically-associated Ni in source rock kerogens. On the other hand, as Ti is very low in crudes (14), Ti in kerogen should be derived from the mineral matrix. To test this hypothesis, core samples with high source rock potential (Teising, Höhenrain) together with those of moderate (Gaisbeuren) and low potential (Dingelsdorf, Kastl) have been analysed for Ni and Ti.

In Figure 3 the elemental concentrations are compared to the H/C atomic ratio of the kerogens, and the silicate content of the bore core samples (15). It can clearly be seen in Figure 3, that the Ni content of the kerogen is proportional to its H/C ratio, and (with one exception) the Ti content of the kerogen is proportional to the silicate content of the whole rock. Thus, Ni and Ti stand in inverse proportionality to each other.

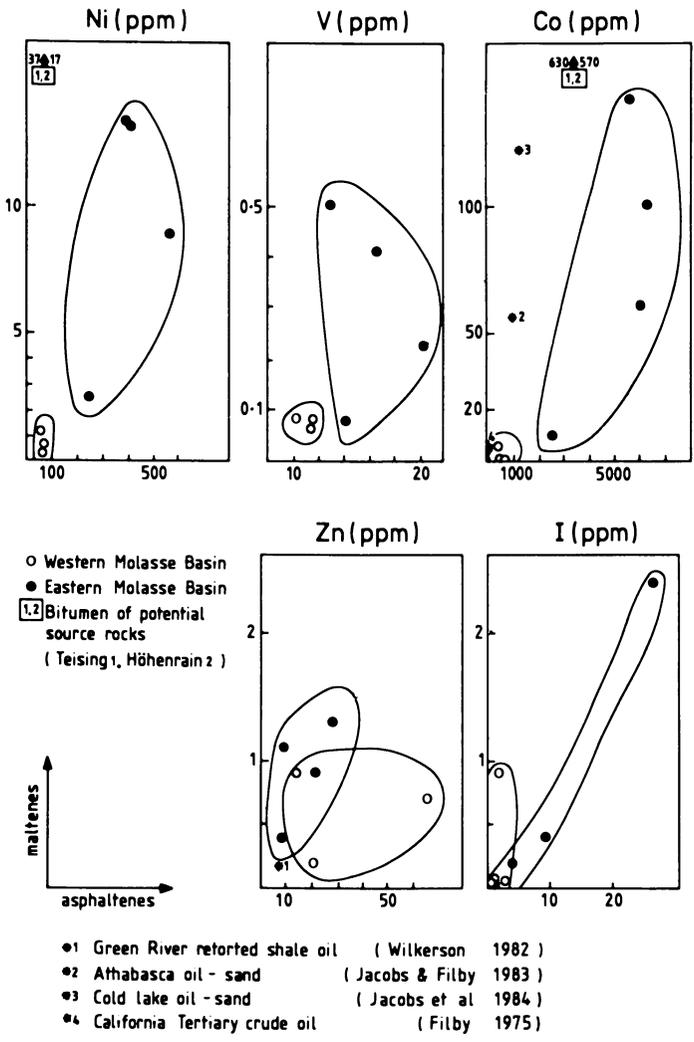


Figure 2. Ni, V, Co, Zn, and I in oil bitumen fractions.

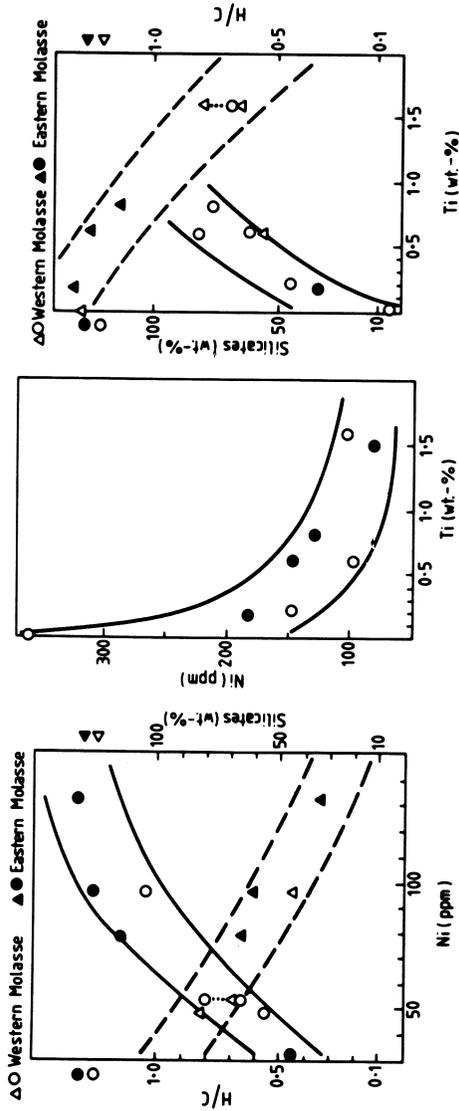


Figure 3. Relationship between the concentrations of Ni and Ti, and the H/C of the kerogen and the sillicate content of the whole rock.

### Conclusions

It is demonstrated for a carefully selected set of oil and kerogen samples, that the Ni, V and Co contents in maltenes and asphaltenes of Southern German crude oils enable a grouping into oil families in accordance with other geochemical parameters.

The close relationship of the Ni and Co contents in crude oils and the bitumen fractions as well as kerogens of potential source rocks suggest, that together with sophisticated statistical methods (16) the contents of biophile elements in maltenes, asphaltenes and kerogen may be successfully used in geochemical oil-oil and oil-source rock correlation studies.'

### Acknowledgments

The author is grateful to members of the Institute of Nuclear Sciences (DSIR, Lower Hutt) for assistance in preparing the manuscript, and to Dr H. Stärk (Technical University, Munich) for analytical help. This article has been written while the author was a Heisenberg-stipendiate of the Deutsche Forschungsgemeinschaft.

### Literature Cited

1. Saxby, J.D. Rev. Pure and Appl. Chem. 1969, 19, pp 131-150.
2. Saxby, J.D. In "Oil Shale", Yen, T.F.; Chilingarian, G.V., Eds.: DEVELOPMENT IN PETROLEUM SCIENCE, Vol. 5, Elsevier: Amsterdam, 1976; pp 155-174.
3. Stevenson, F.J. In "The Significance of Trace Elements in Solving Petrogenetic Problems and Controversies"; Augustithis, S.S., Ed.: Theophrastus Publications: Athens, 1983; pp 671-691.
4. Glikson, M.; Chappell, B.W.; Freeman, R.D.; Webber, E. Chem. Geol. 1985, 53, pp 155-174.
5. Filby, R.H. In "The Role of Trace Metals in Petroleum"; Yen, T.F., Ed.; Ann Arbor Science Publ. Inc.: Ann Arbor, 1975; pp 31-58.
6. Ellrich, J.; Hirner, A.V.; Stärk, H. Chem. Geol. 1985, 48, pp 313-323.
7. Hahn-Weinheimer, P.; Hirner, A.V. Org. Geochem. 1980, 2, pp 45-53.
8. Hirner, A.V.; Graf, W.; Treibs, R.; Melzer, A.N.; Hahn-Weinheimer, P. Geochim. Cosmochim. Acta 1984, 48, pp 2179-2186.
9. Hirner, A.V.; Graf, W.; Hahn-Weinheimer, P. J. Geochem. Explor. 1981, 15, pp 663-670.
10. Ellrich, J. Ph.D. Thesis, Technical University, Munich, 1982.
11. Wilkerson, C.L. Fuel 1982, 61, pp 63-70.
12. Jacobs, F.S.; Filby, R.H. Anal. Chem. 1983, 55, pp 74-77.
13. Jacobs, F.S.; Bachelor, F.W.; Filby, R.H. In "Characterization of Heavy Crude Oils and Petroleum Residues"; Editions Technip: Paris, 1984; pp 173-178.
14. Barwise, A.J.G.; Whitehead, E.V. In "The Significance of Trace Elements in Solving Petrogenetic Problems and Controversies"; Augustithis, S.S., Ed.: Theophrastus Publications: Athens, 1983; pp 599-643.

15. Graf, W.; Hirner, A.V.; Melzer, A.N.; Treibs, R. Bundesminister für Forschung und Technologie BMFT-FB-T 84-139: Bonn, 1984.
16. Hitchon, B.; Filby, R.H. Am. Assoc. Pet. Geol. Bull. 1984, 68, pp 838-849.

RECEIVED November 10, 1986

## Chapter 10

# Vanadyl Porphyrin Distribution in the Alberta Oil-Sand Bitumens

Despina Strong and Royston H. Filby

Department of Chemistry and Nuclear Radiation Center, Washington State University,  
Pullman, WA 99164-1300

The vanadyl etio, deoxophylloerythroetio (DPEP), tetrahydrobenzo-DPEP (THBD), benzo-etio, and benzo-DPEP porphyrins were determined by mass spectrometry in chromatographic fractions of Athabasca, Peace River, and Cold Lake oil sand bitumens. The vanadyl porphyrin distributions were determined in the total bitumen, the maltenes, a *n*-pentane extract of asphaltenes, and a methanol-acetone extract of the asphaltenes. The vanadyl porphyrins distribute among the bitumen components on the basis of polarity as exhibited by the trend in etio/other porphyrin ratios which increase in the order:

maltenes > *n*-pentane extract > methanol-acetone extract  
The oil-sand bitumens and components show a consistent increase in all etio/other porphyrin ratios in the sequence

Athabasca < Peace River < Cold Lake

This trend is consistent with the formation of conventional crude oils at depths in the same sequence with subsequent migration to existing reservoirs close to the surface. The etio/THBD and etio/benzo ratios show greater variation than the corresponding etio/DPEP ratios and may have potential use in correlation studies.

The geochemical evolution and history of an oil or source rock is reflected in the composition of the organic matter and its relationship to the original biological precursors. Several compound classes are known whose basic molecular skeletons can be related to biological precursor molecules. Most of these geochemical biomarkers are hydrocarbons, e.g., isoprenoids, diterpanes, tricyclic terpanes, pentacyclic triterpanes, and steranes (1), but other types including sulfur compounds (1) and the metalloporphyrins (2) have also been used in oil/oil and oil/source rock correlations, sediment maturity studies, and in reconstructing depositional environments.

Metalloporphyrins were the first biomarkers identified in oils (3), but the lack of simple analytical techniques for the separation and characterization of the geoporphyryns and the uncertainty about the geochemical origin and evolution of these compounds has resulted in their limited use as biomarkers.

Baker and co-workers (4,5) first documented the distribution of homologous members of the two major porphyrins types (DPEP, etio) found in crude oils and related materials. The relative abundances, expressed as DPEP/etio ratios, provided the first evidence of the difference in distributions between the two major types of porphyrins in different oil samples.

The distribution of DPEP relative to etio porphyrins in crude oils has been shown to be an excellent indicator of sediment maturity (2,6). The DPEP/etio ratio decreases with depth or increased thermal maturation, and it was proposed originally (6) that the decrease in the ratio resulted from conversion of DPEP to etio metalloporphyrins via thermal scission of the isocyclic ring. The change in the DPEP/etio ratio through thermal conversion of DPEP to etioporphyryns has been questioned, however, and alternative mechanisms have been proposed. The following mechanisms have been advanced to explain the DPEP/etio ratio change in sediments or crude oils:

- a) Thermal conversion of DPEP to etio metalloporphyrins (6).
- b) Conversion of DPEP precursors (e.g., phorbides) to etio precursors (e.g., chlorins) via low temperature oxidative opening of the 5-membered isocyclic ring during diagenesis (8).
- c) Catagenesis of kerogen in the "oil window" temperature region (9) which releases primarily etio porphyrins, thus decreasing the DPEP/etio ratio. This mechanism is not well understood and has not been confirmed experimentally. There is no obvious chemical reason why etio porphyrins should be preferentially associated with the kerogen compared to DPEP, and recent experimental work shows that, in fact, both types of vanadyl porphyrins are strongly associated with oil shale kerogens (10).
- d) Different rates of degradation (demetallation, macrocycle cleavage, etc.) of DPEP and etio porphyrins over a geological time frame. This has been proposed by Barwise (6) and could result from a slightly higher activation energy for the degradation of the etio porphyrins relative to DPEP.

It is important to recognize the differences in the four mechanisms and their influence on the use of the DPEP/etio ratio in oil-oil and oil-source rock correlations. Mechanisms b) and c) operate before and during the formation of the oil from the source rock kerogen, and would thus determine the DPEP/etio ratio in the source rock and bitumen. Thermal maturation that followed generation of the bitumen in the source rock or maturation of the crude oil in the reservoir would result in changes in the DPEP/etio ratio only via mechanisms a) and d). Significant changes in the DPEP/etio ratio due to maturation in a reservoir would limit the use of the ratio as a correlation parameter for oils or for oils and source rocks unless differences in maturation among the oils are known.

Little use has been made in correlation studies of the more complex metalloporphyrins (THBD, benzo) because of the uncertainty regarding their origin.

The effects of migration and of biodegradation/water washing in the reservoir on metalloporphyrin distributions must also be known in order to assess the usefulness of porphyrin distributions in correlation studies. The effect of oil migration is not well understood, although Chakhmachkev et al. (11) have shown that changes in the DPEP/etio ratios of vanadyl porphyrins occur when oils are passed through laboratory columns of sand and clay. There is evidence that

biodegradation does not affect the distributions of vanadyl porphyrins in degraded oils (2,12) by direct biological attack, although some enrichment of vanadyl relative to nickel porphyrins was observed in the most degraded oils of the suite studied by Palmer (12).

In this study, the vanadyl porphyrin distributions in the Athabasca (A), Peace River (PR), and Cold Lake (CL) bitumens (note: the term "bitumen" is used for the oil sands; it is not used in the same context as source rock bitumen) were investigated using the etio/DPEP ratio as well as the etio/THBD and etio/benzo porphyrin ratios. In this suite of highly biodegraded oils, the etio/other porphyrin ratios were used to correlate the three Alberta bitumens. The bitumens have been shown to be highly degraded conventional oils which probably migrated long distances from deeper source rocks within the basin and are emplaced in the shallow reservoirs (<300 m) in which biodegradation occurred (13-16).

The distributions of the different vanadyl porphyrin types among the bitumen components (maltenes, resins, asphaltenes) were investigated using the etio/DPEP, etio/benzo, and etio/THBD porphyrin ratios determined by EI-MS.

### Experimental Procedures

Bitumens were extracted from Athabasca, Peace River, and Cold Lake oil-sand samples by Soxhlet extraction of aliquots of the oil sand with toluene. The bitumen was then separated into maltenes and asphaltenes by precipitation with *n*-pentane (40:1 v/v, solvent/bitumen). The asphaltenes were Soxhlet extracted with *n*-pentane and then extracted with methanol-acetone (azeotrope mixture 12:88 v/v, b.p. 57°C) in ten refluxing steps as shown in Figure 1. The oil sands were also Soxhlet extracted directly with methanol-acetone (12:88 v/v) for the isolation of total bitumen porphyrins (referred to as porphyrin aggregate). Details of the separation steps can be found elsewhere (17).

The vanadyl porphyrins in the maltenes, *n*-pentane extract, methanol-acetone extract and porphyrin aggregate were separated from saturates, aromatics and resins using the chromatographic scheme (shown in Figure 2), modified from Spencer *et al.* (18). The samples were dissolved in THF, silica was added to form a slurry, and the solvent was evaporated under a stream of nitrogen. The coated silica was packed onto a prepared silica gel column (Bulk Silica, 60-200 mesh, Davison Chemicals, 1x40 cm glass column). Two separate fractions were eluted with hexanes. The first (predominantly saturates) exhibited no porphyrin UV absorbances. The second fraction contained small amounts of nickel porphyrins (Figure 3). The vanadyl porphyrins were eluted in fraction 4 (Figure 3) with 20% chloroform in hexanes. Fractions 3 and 5 preceding and following the main vanadyl porphyrin band exhibited weak vanadyl porphyrin absorbances but were quantitatively insignificant.

The vanadyl porphyrins were purified on a neutral alumina column. The alumina was coated with a methylene chloride solution of the sample and the solvent was evaporated under a stream of nitrogen before packing the coated alumina into the column. The vanadyl porphyrins were eluted with methylene chloride.

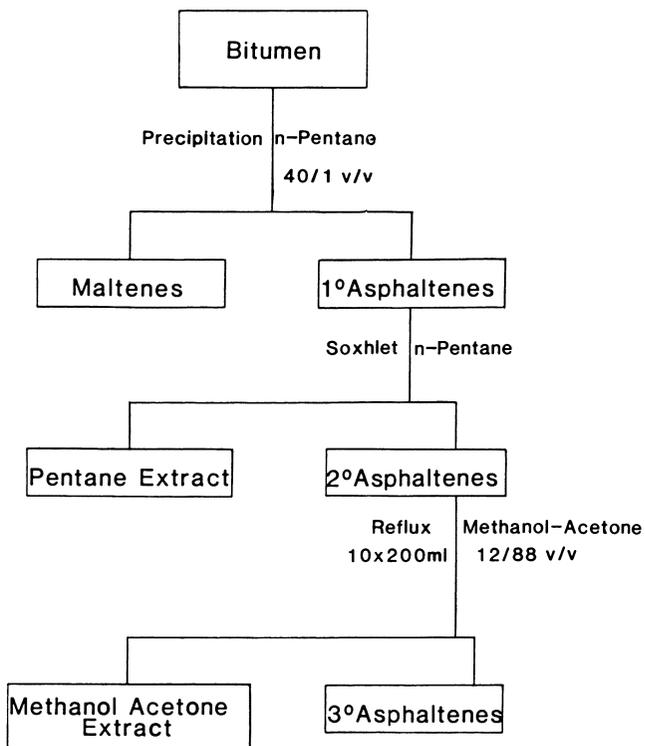


Figure 1. Separation scheme for bitumen components.

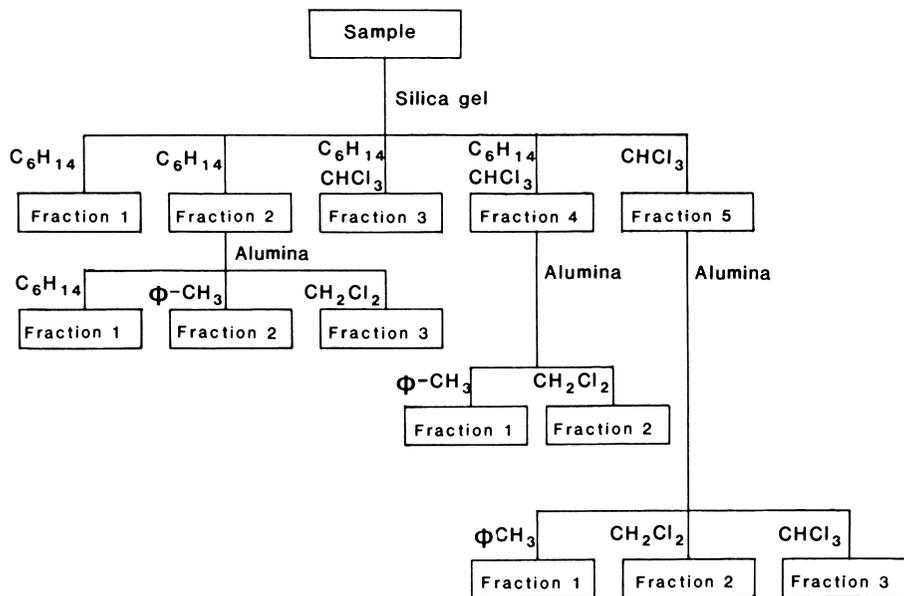


Figure 2. Scheme for chromatographic separation of vanadyl porphyrins from bitumen components. Main vanadyl porphyrin fractions are fraction 4 ( $SiO_2$ ) and fraction 2 ( $Al_2O_3$ ).



Figure 3. UV-visible absorption spectra of fractions 1-5 from silica column separation of Athabasca porphyrin aggregate. Fraction 4 diluted 1:1000 relative to other fractions.

A VG Analytical extended ion-path 7070E instrument was used for EI-MS of the vanadyl porphyrins. Instrument parameters were: accelerating voltage = 6keV; resolution = 1000 (10% valley definition); ionizing voltage = 70eV. The samples were analyzed using a solid probe with a modified sample cup (sample tube with a shallow cup) to enhance porphyrin volatilization. The source temperature was kept at 250°C and the probe was heated using a temperature program of 1°C/sec from 25-300°C and 10°C/sec from 300-400°C. Porphyrins were not subjected to temperatures over 350°C because of a temperature differential of approximately 50°C between the heating coils (400°C) and the sample cup. Under these experimental conditions, porphyrins were volatilized over a narrow range of spectral files. The spectra containing the porphyrins were averaged over the entire porphyrin range and background subtracted (usually 5 files preceding and/or following the porphyrin spectra). For presentation, the mass spectra were normalized (most intense peak = 100%), background subtracted and the mass spectra peak intensities of the etio series were corrected for isotopic contributions (<sup>13</sup>C) of the (M+2) DPEP series.

### Results

The mass spectra of the vanadyl porphyrins isolated from the maltenes, *n*-pentane extracts of asphaltenes, and methanol-acetone extracts of the Athabasca, Peace River, and Cold Lake oil sands are shown in Figures 4-7. For clarity, only the two major series (DPEP and etio) are shown; however, the spectral characteristics of the other three series were reported from the original average scan and were used in quantitative calculations. The relative abundances of the five porphyrin types (shown in Table I) in all samples was in the following order:

DPEP > etio > THBD > benzo-etio > benzo-DPEP

The carbon numbers of the vanadyl porphyrins in the Alberta oil-sand bitumens and their components extend from C<sub>27</sub> to C<sub>40</sub>, characteristic of most geoporphyrins isolated from mature sediments or from crude oils (19). The carbon number ranges of both etio and DPEP series decrease from the maltenes to the *n*-pentane extract of the asphaltenes and the range tends to be narrowest in the methanol-acetone extracts. In the maltenes, the homologous series (DPEP, etio) extend from C<sub>27</sub> to C<sub>40</sub> whereas a range as low as C<sub>27</sub> to C<sub>34</sub> is found for the etio porphyrins in the Athabasca methanol-acetone extract. As a result, the porphyrins with carbon number >34 represent a larger fraction of the total intensity in the spectrum of the maltenes than for the asphaltene. For the Athabasca maltenes, 74% of the total ion intensity in the etio series can be attributed to the homologues C<sub>28</sub>-C<sub>32</sub>. In contrast, in the methanol-acetone extract, the C<sub>28</sub>-C<sub>32</sub> homologues account for 90% of the total etio ion intensity. A similar trend is noted for the DPEP porphyrins. The carbon number distributions of porphyrins from Peace River and Cold Lake are similar to those observed for Athabasca.

### Vanadyl Porphyrin Distributions

A qualitative interpretation of the mass spectra is that fractionation is occurring between the etio and DPEP porphyrins in the oil-sand bitumen components. Table I shows the etio/DPEP, etio/THBD,

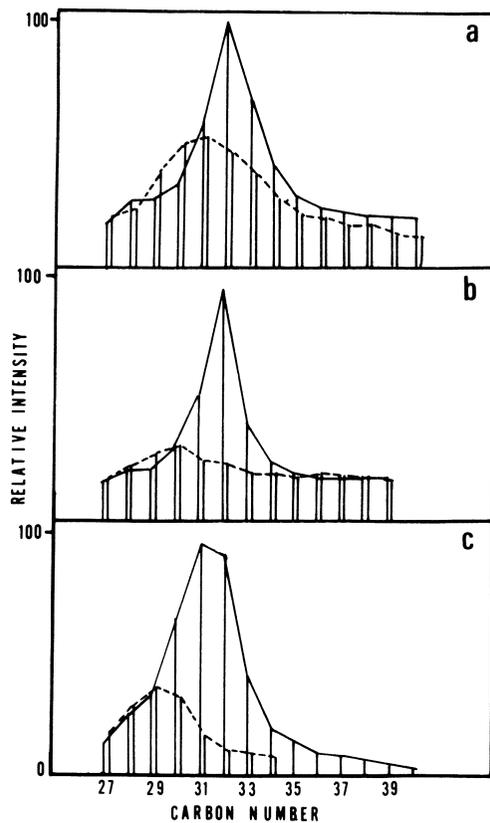


Figure 4. Molecular ion histograms of etio (....) and DPEP (—) vanadyl porphyrins isolated from Athabasca a) maltenes, b) *n*-pentane extract of asphaltenes, c) methanol-acetone extract of asphaltenes.

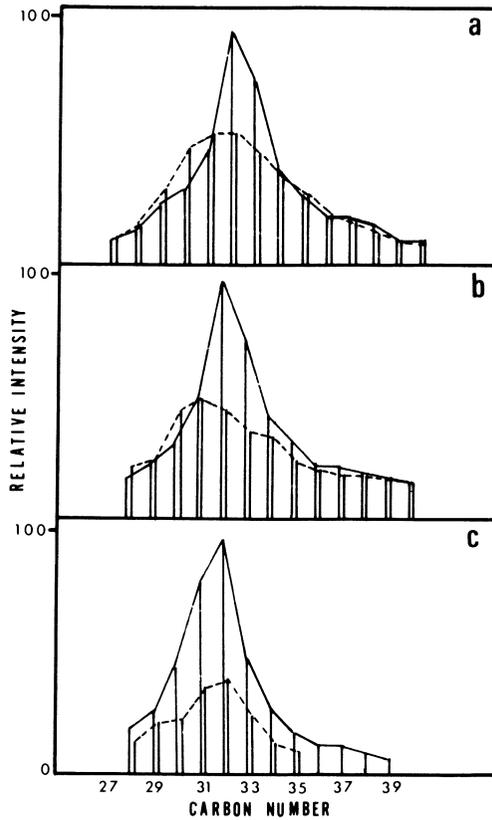


Figure 5. molecular ion histograms of etio (....) and DPEP (—) vanadyl porphyrins isolated from Peace River a) maltenes, b) *n*-pentane extract of asphaltenes, c) methanol-acetone extract of asphaltenes.

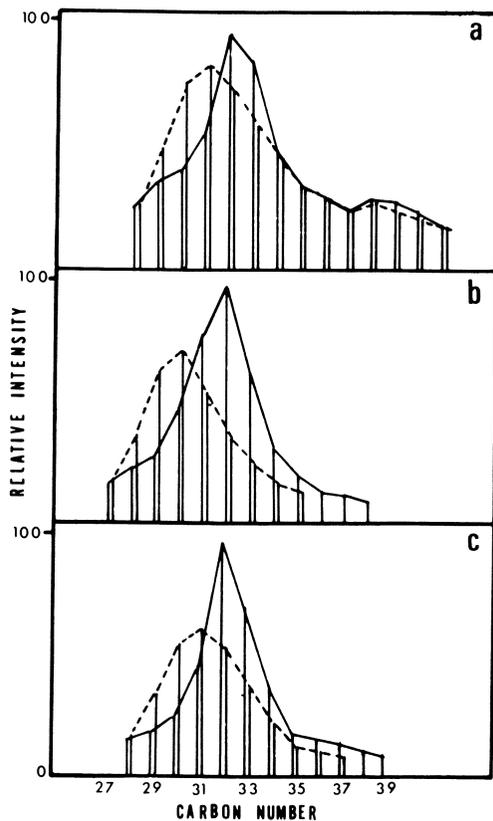


Figure 6. Molecular ion histograms of etio (...) and DPEP (—) vanadyl porphyrins isolated from Cold Lake a) maltenes, b) *n*-pentane extract of asphaltenes, c) methanol-acetone extract of asphaltenes.

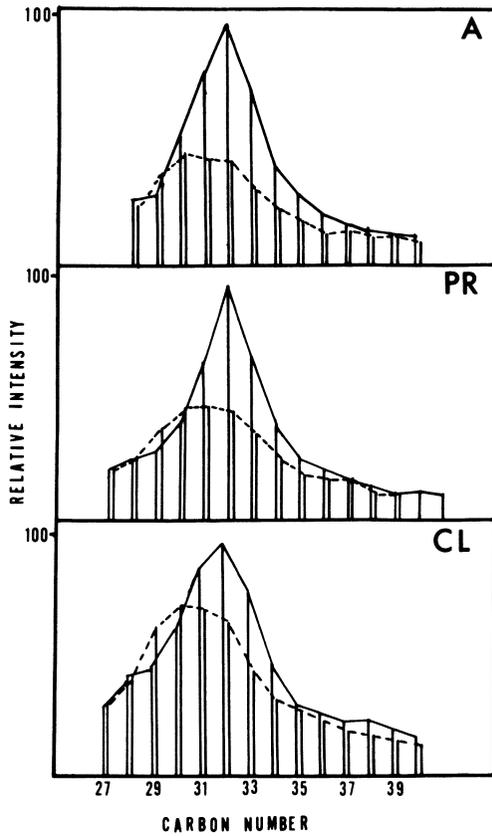


Figure 7. Molecular ion histograms of etio (....) and DPEP (—) vanadyl porphyrin aggregates isolated from the Athabasca, Peace River, and Cold Lake bitumens.

Table I. Etio/Other Ratios for Vanadyl Porphyrins<sup>a</sup> Determined from MS Parent Ion Intensities for Athabasca (A), Peace River (PR), and Cold Lake (CL) Oil Sands

Component	Etio/DPEP <sup>b</sup>		Etio/THBD		Etio/benzo-etio		Etio/benzo-DPEP		THBD/benzo-DPEP						
	A	PR	A	PR	A	PR	A	PR	A	PR					
Whole bitumen <sup>c</sup>	0.56	0.61	0.72	1.71	2.62	3.14	1.99	3.35	3.51	2.40	4.55	5.92	1.40	1.74	1.88
Maltenes	0.65	0.77	0.84	3.75	5.22	6.29	6.00	7.66	11.3	7.73	12.77	13.5	2.06	2.45	2.15
n-Pentane extract of asphaltenes	0.60	0.66	0.70	2.40	3.82	4.20	3.23	4.81	5.22	3.53	5.36	5.51	1.47	1.40	1.31
Methanol-acetone extract of asphaltenes	0.34	0.39	0.68	1.28	1.52	2.58	1.41	1.74	3.25	1.94	2.47	5.76	1.51	1.62	2.23

<sup>a</sup> Etio/other porphyrin ratios calculated from averaged MS scans and calculated over entire carbon number range of envelope.

<sup>b</sup> DPEP intensities include not only true DPEP species (i.e., cycloethano) but also identical mass species of possible alternate cycloalkano (CAP) porphyrins (9, 31-32).

<sup>c</sup> Whole bitumen porphyrins extracted in porphyrin aggregate.

etio/benzo-etio and etio/benzo-DPEP ratios expressed as the sum of ion intensities over the total carbon number range. Porphyrin abundances are expressed relative to etio, the least polar of the porphyrins studied. The etio/DPEP or etio/other ratios in individual components (maltenes, asphaltenes, etc.) of the Alberta oil-sand bitumens, or of other conventional crude oils, have not been reported, although Baker and Palmer (19) have shown that the DPEP/etio ratio of vanadyl porphyrins in Boscan maltenes is different to that of the demetallated porphyrins extracted from the whole oil. The data presented in Table I indicate that porphyrin analyses must be performed on the whole oil or bitumen, particularly if inter-sample comparisons are to be made.

For each oil sand, the etio/DPEP ratio of the vanadyl porphyrins decreases in the order:

maltenes > n-pentane extract > methanol-acetone extract  
This trend shows clearly that the vanadyl etio and DPEP porphyrins distribute differently between the less polar maltenes and the more polar fractions of the bitumen, i.e., the n-pentane and methanol-acetone extracts of the asphaltenes.

The factors which control the distribution of organic constituents in the micellar structure of the bitumen are not well understood, but probably the most important are polarity (determined largely by functionality) and molecular weight (1,20). The metalloporphyrins in an oil-sand bitumen will be distributed among components of the microstructure and thus the differences in the association between the DPEP and etio series in the maltenes and in the asphaltene extracts may be explained in terms of differences in porphyrin polarity. In general, the polarity of each vanadyl porphyrin class (DPEP, etio, benzo-etio, benzo-DPEP, THBD) is inversely proportional to carbon number as has been observed during chromatographic separation of porphyrin mixtures (21,22). Thus, the higher carbon number homologues of both the etio and the DPEP are relatively more abundant in the mass spectra of the less polar maltenes compared to the methanol-acetone extracts of the asphaltenes. In the Athabasca maltenes, the DPEP porphyrins with carbon number greater than 32 comprise 30% of the total intensity of the DPEP series, whereas in the methanol-acetone extract they account for only 12% of the total DPEP intensity. Porphyrins with isocyclic rings, in general, are also more polar than porphyrins without isocyclic rings of similar carbon number. Hence, the DPEP, the THBD, and the benzo porphyrins of the same carbon number are more polar than the corresponding etio porphyrins. Thus, the ratio of etio/DPEP which decreases from maltenes to methanol-acetone extract (Table I) is consistent with an association of the metalloporphyrins with the asphaltenes and other bitumen components based on polarity. The etio/THBD, etio/benzo-etio and etio/benzo-DPEP porphyrin ratios are highest in the maltenes of each oil sand bitumen, and also decrease in the order:

maltenes > n-pentane extract > methanol-acetone extract  
Thus this trend is also consistent with polarity differences among these porphyrins.

The distribution of the vanadyl porphyrins among bitumen components is in agreement with previous work (17) in which it was shown the porphyrins are actually distributed between the maltenes and the asphaltenes in the bitumen and do not fractionate during asphaltene

precipitation. Thus there is a decrease in the polar/less polar porphyrin ratios from the polar core of the asphaltene micelle through the intermediate polarity resins that "peptize" the micelles in the maltenes to the relatively non-polar maltenes in which the less polar porphyrins predominate. No evidence has been found for the unusually high molecular weight porphyrins in the asphaltenes, suggested by Blumer and Snyder (23), or for the very complex, aromatic type porphyrins (apart from THBD and benzo) as suggested by Yen (24) or Jacobs (25). However, such porphyrins may be strongly associated with the asphaltenes and are not extractable with methanol-acetone, and thus are classified with the "non-porphyrin" vanadium.

The methanol-acetone extract of the whole bitumen (similar to the porphyrin aggregate obtained from conventional oils) has values for etio/other porphyrin ratios that are intermediate between the maltenes and the methanol-acetone extract of the asphaltenes. It is clear, however, that the porphyrin abundances in the porphyrin aggregates of oils of similar origin and thermal history may be influenced by the amount and polarity of the asphaltenes (or polar components of the resins). Also, the degree of extraction is important because it is not known what fraction of the vanadium remaining in the tertiary asphaltenes (between 52.8-63.9% of total) (17) is vanadyl porphyrin, and what the nature of these vanadyl porphyrins might be. The UV spectrum of the extracted tertiary asphaltene still shows a Soret absorbance at 408 nm. Based on the extraction data, it would be expected that the vanadyl porphyrins remaining in the extracted asphaltenes would contain a higher proportion of THBD and benzo, and possibly other species.

#### Porphyrin Ratios as Geochemical Correlation Parameters

The strong association of the porphyrins with the asphaltenes in the oil-sand bitumens has implications regarding their fate during the migration of the original oil and subsequent alteration processes in the reservoir. Rubinstein et al. (26,27) have shown that geochemical biomarkers can be liberated from the asphaltenes during pyrolysis. This investigation shows that metalloporphyrins can also be isolated from the asphaltenes and that the distributions of porphyrin types associated with the asphaltenes are different from those in the maltenes. It has also been shown that it is not necessary to pyrolyze the asphaltenes to extract a substantial fraction of the vanadium as vanadyl porphyrins.

The etio/other porphyrin ratios of the three oil sands are shown graphically in Figure 8 and geochemical data are given in Table II. The etio/DPEP ratio increases in the order

Athabasca < Peace River < Cold Lake

This trend is seen in each of the bitumen components. The same trend is exhibited by the etio/THBD, and the etio/benzo porphyrin ratios in the bitumen components. The etio/DPEP ratios may be interpreted to represent a maturation sequence among the three bitumens, although the Athabasca, Peace River, and Cold Lake oil sand samples were all reservoirized at less than 300 m; thus, *in situ* maturation cannot explain the porphyrin distributions. The oil sands have been subjected also to extensive biodegradation/water washing (13,14), but

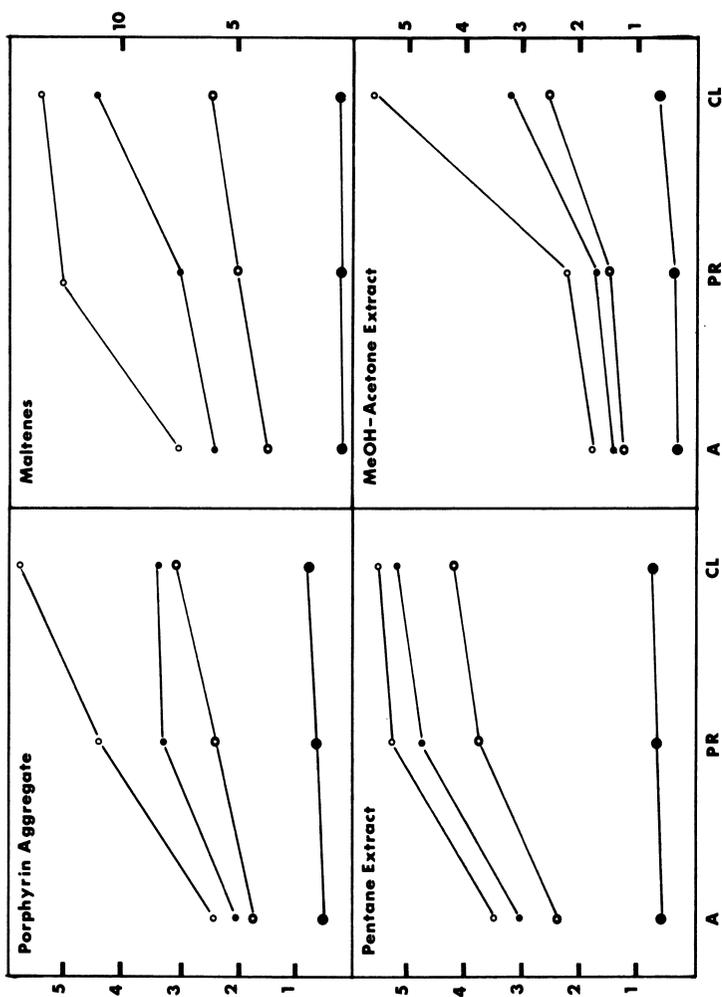


Figure 8. Etio/DPEP (●), etio/THBD (○), etio/benzo-etio (●) and etio/benzo-DPEP (●) ratios for bitumen components of Athabasca (A), Peace River (PR), and Cold Lake (CL) oil sands.

Table II. Geochemical, V, Ni and Vanadyl Porphyrin Data for the Athabasca, Peace River and Cold Lake Oil Sands

Property	Athabasca	Peace River	Cold Lake
Present depth of reservoir	0	169	444
Degree of biodegradation	Very high	Very high	High
V concentration ( $\mu\text{g/g}$ ) <sup>a</sup>	$196 \pm 3$	$180 \pm 3$	$191 \pm 3$
Ni concentration ( $\mu\text{g/g}$ ) <sup>a</sup>	$74.8 \pm 3$	$62.4 \pm 1$	$62.6 \pm 5$
V/Ni <sup>a</sup>	$2.6 \pm 0.1$	$2.9 \pm 0.1$	$3.1 \pm 0.2$
VOP ( $\mu\text{g V/g}$ ) <sup>b</sup>	92.5	92.0	76.8
Extractable VOP <sup>b,c</sup>	47.2%	51.1%	40.1%
DPEP/etio	1.80	1.64	1.39
DPEP/(DPEP + etio) <sup>d</sup>	0.64	0.62	0.58

<sup>a</sup>Taken from Strong (17); V/Ni ratio is demetal weight ratio.

<sup>b</sup>Vanadyl porphyrin contents estimated to have relative error  $\neq 10-15\%$ .

<sup>c</sup>Expressed as percent of total V in bitumen (17).

<sup>d</sup>When multiplied by 100, equivalent to %DPEP calculated by Barwise and Roberts (9).

previous work by Palmer (12) and Barwise (2) has shown that biodegradation has little effect on the vanadyl porphyrin distributions of heavy oils. The total vanadyl porphyrin contents of the oil-sand bitumens (A: 92.5  $\mu\text{g V/g}$ ; PR: 92.0  $\mu\text{g V/g}$ ; CL: 76.8  $\mu\text{g V/g}$ ) are high and not statistically different among the three samples, confirming the relatively little, if any, effect of biodegradation/water washing. The etio/DPEP and etio/other porphyrin ratios thus probably reflect the depth (temperature) of formation of the original crude oils prior to migration to the present reservoirs, because in-reservoir maturation has been small (assuming similar migration pathways). The origin of the bitumen in the oil sands has been debated, but most theories involve long-range migration of conventional oils from down-dip Lower Cretaceous source rocks (13,14,28), although recent research (16,29) indicates possible Devonian contributions. Thus if the theoretical DPEP/(DPEP + etio) versus expulsion temperature curve of Barwise (8) is used (assumes 10 KJ/mole differences in activation energy for etio and DPEP degradation), expulsion temperatures of 145-150°C are computed. Although these temperatures are probably too high, they do confirm the formation, or expulsion, of the original crude oils at depths greater than the present reservoirs and indicate a depth of original oil formation in the sequence Athabasca < Peace River < Cold Lake.

The effect of long range migration of crude oils on the vanadyl porphyrin distributions has not been assessed but may be of significance given the different polarities of different porphyrin types. Burkova *et al.* (30) examined the vanadyl porphyrins from the Surgut, W. Siberian oil field and concluded that the proportion of non-polar vanadyl porphyrins (defined by TLC  $R_f$  values) increased with increased migration distance. If the original oil migrated from deeper source rocks as a single phase, the different association of metalloporphyrins in the bulk hydrocarbon phase (maltenes) and in the asphaltenes may have affected the etio/DPEP, etio/THBD, and etio/benzo distributions during the migration from the source rock to reservoir. The "free" porphyrins which are present in the hydrocarbon or maltenes fraction of the oil may have been more subject to differential chromatographic retention of the rock matrix than the porphyrins present within the asphaltene micelles. These asphaltene-associated porphyrins were probably protected during migration much like biosensitive marker compounds are protected within the asphaltene during biodegradation (26,27). The etio/other porphyrin ratios for the methanol-acetone extract of the asphaltenes (Figure 8) show similar trends among the three oil sands, but there are qualitative differences in the methanol-acetone extracts compared to the ratios for the other bitumen components. These differences may reflect the effects of migration, which need to be further evaluated.

The etio/other porphyrin ratios for components of the three oil sand bitumens shown in Figure 8 show that the trends for the etio/THBD and etio/benzo porphyrin ratios are similar to that observed for the etio/DPEP ratio. However, differences among the etio/THBD and etio/benzo ratios for the three oil sands are greater than among the etio/DPEP ratios, particularly for the porphyrin aggregate and the methanol extract of the asphaltenes. If the differences among the etio/THBD and etio/benzo ratios are due to maturation effects, then these porphyrin ratios may be more sensitive indicators of

maturation effects. However, until the origin of these species has been determined and the effects of migration assessed, use of these ratios is unwarranted. The porphyrin fractionation data also indicate that the change in etio/DPEP ratio in the oil sand bitumens is not a result of a DPEP to etio conversion during bitumen maturation. There is no obvious genetic relationship among the etio and the THBD and benzo porphyrins, but the same trend in the etio/other porphyrin ratios as for the etio/DPEP ratios is observed.

Recently Kaur *et al.* (31) have shown that the benzo-DPEP porphyrins contain the aromatic ring on the C-7 and C-8 positions (B ring) rather than the C-17 and C-18 positions (D ring) proposed by Barwise and Roberts (9) who also proposed that the 6-membered ring in THBD was on the D ring. This would imply no genetic relationship between benzo-DPEP and THBD porphyrins unless the structure of THBD proposed by Barwise and Roberts (9) is incorrect. If, however, the 6-membered ring in THBD and benzo-DPEP porphyrins are both on the B ring, then the benzo-DPEP may arise by dehydrogenation of THBD during maturation. If this is the case, the THBD/benzo-DPEP ratio should decrease during maturation. The THBD/benzo-DPEP ratios shown in Table I show no obvious pattern; for the porphyrin aggregate, the reverse order is seen, *i.e.*,

THBD/benzo-DPEP: Athabasca < Peace River < Cold Lake  
Thus these limited data cannot be used to support a genetic relationship between THBD and benzo-DPEP, although a re-examination of the structure of THBD proposed by Barwise and Roberts (9) is warranted.

### Conclusions

The vanadyl etio, DPEP, THBD, benzo-etio and benzo-DPEP porphyrins distribute among the components of oil-sand bitumens on the basis of porphyrin polarity. This effect is demonstrated by the progression to a smaller carbon number range, and to a lower base-peak carbon number for etio and DPEP types from the less polar maltenes to the most polar methanol-acetone extract of the asphaltenes.

The Athabasca, Peace River, and Cold Lake oil-sand bitumens show a consistent increase in all etio/other porphyrin ratios in the sequence

Athabasca < Peace River < Cold Lake

This sequence is observed for the porphyrin aggregate as well as the maltenes, *n*-pentane extract, and methanol-acetone extract of the asphaltene.

The porphyrin distribution data can be interpreted to show that the oil-sand bitumens are degraded conventional crude oils that formed at depths greater than their current reservoirs and that the source rock depth sequence was probably

Athabasca < Peace River < Cold Lake

and/or post-generation maturation followed the same sequence.

The etio/THBD and etio/benzo porphyrin ratios appear to be more sensitive indices of thermal maturity than the etio/DPEP ratios. Alternatively, the benzo and THBD series may be selectively removed during migration. However, their use as thermal maturity indices is restricted by lack of information on the origin of the THBD and benzo porphyrins.

Acknowledgments

The authors would like to thank Mr. F. Doolittle, Department of Chemistry, for assistance in mass spectrometric analyses.

Literature Cited

1. Tissot, B.P.; Welte, D.H. "Petroleum Formation and Occurrence"; 2nd Ed.; Springer-Verlag: New York, 1984.
2. Barwise, A.J.G.; Park, P.S.D. In "Advances in Organic Geochemistry 1981"; Bjorøy, M. et al., Eds.; John Wiley: London, 1983; 668.
3. Treibs, A. Ann. Chem. 1934, 517, 103.
4. Baker, E.W. J. Amer. Chem. Soc. 1966, 88, 2311.
5. Baker, E.W.; Yen, T.F.; Dickie, J.P.; Rhodes, R.E.; Clark, L.F. J. Amer. Chem. Soc. 1967, 89, 3631.
6. Didyk, B.M.; Alturki, Y.I.A.; Pillinger, C.T.; Eglinton, G. Nature 1975, 256, 563-65.
7. Burkova, V.N.; Ryadovaya, L.V.; Serebrennikova, O.V.; Titov, V.I. Geokhimiya 1980, 1417-21.
8. Barwise, A.J.G. (this volume).
9. Barwise, A.J.G.; Roberts, I. Org. Geochem. 1984, 167-176.
10. Van Berkel, G.J.; Filby, R.H. (this volume).
11. Chakhmachkev, V.A.; Burkova, V.N.; Eharkov, N.I.; Punarova, S.A.; Serebrennikova, O.V.; Titov, V.I. Geokhimiya 1985, 381-386.
12. Palmer, S.E. Amer. Chem. Soc. Annual Meeting, Washington, DC, Abstract, August 28-September 2, 1983.
13. Vigrass, L.W. Bull. Amer. Ass. Petrol. Geol. 1968, 52, 1984-99.
14. Deroo, G.; Powell, T.G.; Tissot, B.; McCrossan, R.G. Geol. Survey Canada Bull. 262 1977, 136 p.
15. Moshier, S.O.; Waples, D.W. Bull. Amer. Ass. Petrol. Geol. 1985, 69, 161-72.
16. Hitchon, B.; Filby, R.H. Bull. Amer. Ass. Petrol. Geol. 1984, 68, 838-49.
17. Strong, D. Ph.D. Thesis, Department of Chemistry, Washington State University, Pullman, WA, 1986.
18. Spencer, W.A.; Galobardes, J.F.; Curtis, M.A.; Rogers, B.L. Separation Sci. Technol. 1982, 17, 797.
19. Baker, E.W.; Palmer, S.E. In "The Porphyrins"; Dolphin, D., Ed.; Academic Press: New York, 1978; pp. 486-552.
20. Speight, S.G.; Long, R.B. In "Atomic and Nuclear Methods in Fossil Energy Research"; Filby, R.H.; Carpenter, B.S.; Ragaini, R.C., Eds.; Plenum Press: New York; pp. 295-321.
21. Quirke, J.M.E.; Eglinton, G.; Maxwell, J.R. J. Amer. Chem. Soc. 1978, 101, 7693.
22. Hajibrahim, S.K.; Quirke, J.M.E.; Eglinton, G. Chem. Geol. 1982, 35, 69.
23. Blumer, M.; Snyder, W.D. Chem. Geol. 1967, 2, 35.
24. Yen, T.F. In "The Role of Trace Metals in Petroleum"; Yen, T.F., Ed.; Ann Arbor: Ann Arbor, 1975; pp. 1-30.
25. Jacobs, F.S. Ph.D. Thesis, Department of Chemistry, Washington State University, Pullman, WA, 1982.
26. Rubinstein, I.; Spyckerelle, C.; Strausz, O.P. Geochim. Cosmochim. Acta 1979, 43, 1.

27. Rubinstein, I.; Strausz, O.P. Geochim. Cosmochim. Acta 1979, 43, 1887.
28. Jones, R.W. Bull. Amer. Ass. Petrol. Geol. 1981, 65, 103-22.
29. Hoffman, C.F.; Strausz, O.P. Amer. Ass. Pet. Geol. 1986, 70(9), 1113.
30. Burkova, V.N.; Serebrennikova, O.V.; Titov, V.I. Geokhimiya 1978, 945-50.
31. Kaur, S.; Chicarelli, M.I.; Maxwell, J.R. J. Am. Chem. Soc. 1986, 108, 1347-48.
32. Ocampo, R.; Callot, H.J.; Albrecht, P. (this volume).
33. Chicarelli, I.M.; Kaur, S.; Maxwell, J.R. (this volume).

RECEIVED March 11, 1987

## Chapter 11

# Metalloporphyrins in Lignite, Coal, and Calcite

Raymond Bonnett, Philip J. Burke, and Franciszek Czechowski

Department of Chemistry, Queen Mary College, Mile End Road, London E1 4NS,  
United Kingdom

The present understanding of work on porphyrins and metalloporphyrins in coals and lignites is summarised. New results are described on the isolation of individual porphyrins from the heme fraction of Colorado coal, from which two crystalline porphyrins have been obtained, and on the examination of iron and gallium porphyrins in the lithotypes (vitrain, durain) from a Polish sub-bituminous coal (Janina). Gallium mesoporphyrin IX has been identified in a pink calcite from a hydrothermal region (Deutsch-Altenburg) in Austria.

The occurrence of metals, including some rather rare metals, in coals is well known (1). That some of these metals are present in part as tetrapyrrole complexes might, perhaps, have been inferred from early observations on pigmented leaf compressions in brown coal (Middle Eocene) (2), but it was Treibs, in his pioneering papers on organic geochemistry, who first reported iron and vanadyl porphyrins in coals (3, 4). In his studies on fossil fuels, Treibs concentrated on crude oil and its relatives, possibly because in certain of these materials the porphyrin content was larger and more amenable to extraction. Subsequent workers have followed Treibs in this predilection as is illustrated by the programme of the present meeting: of 14 or so scheduled papers on porphyrins in relation to the geosphere, this is the only one to have coal in the title.

The renaissance of the subject occurred in the late 1970's, with the discovery of gallium porphyrins in bituminous coals (5, 6). Subsequently iron porphyrins, manganese porphyrins (one example) and metal-free porphyrins were also detected (7). Vanadyl and nickel porphyrins, which are commonly encountered in crude oil and its relatives (8), have not as yet been found in lignite and coal. Using extraction procedures which cause demetallation, Palmer and coworkers (9) reported porphyrins in a number of US humic coals, and, more recently, Bonnett and Burke (10) demonstrated the occurrence of iron porphyrins in seven such samples, in some of which metal-free and gallium porphyrins were also detected (Table I).

Table I. Tetrapyrroles in Coals from the U.S.A.

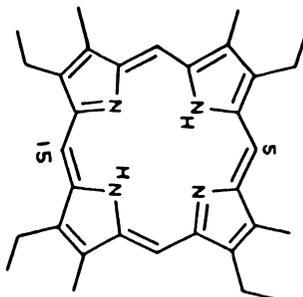
Coal Class (Rank)	Origin <sup>a</sup> (Code)	Age	Porphyrins $\mu\text{g/g}$ (duplicate)		
			2H	Fe	Ga
Bituminous (HVA)	W. Virginia (PSOC-1001)	Pennsylvanian	-	0.35 (0.34)	0.07 (0.09)
Bituminous (HVC)	Indiana (PSOC-677)	Pennsylvanian	-	0.38 (0.50)	0.22 (0.25)
Bituminous (HVC)	Colorado (PSOC-850)	Cretaceous	-	12.9 (13.1)	0.20 (0.18)
Sub-bituminous	Washington (PSOC-230A3)	Eocene	-	0.82 (0.89)	-
Lignite	Montana (PSOC-833)	Cretaceous	0.14 (0.15)	1.05 (1.03)	-

<sup>a</sup> Pennsylvania State University Collection

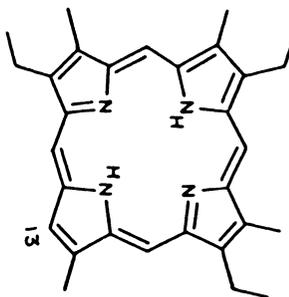
The coal porphyrin story is still at an early stage of development, but it is useful to summarise the main results so far.

1. Metalloporphyrins (Ga, Fe, Mn) and metal-free porphyrins and chlorins have been detected in lignites and bituminous coals in amounts from 0 to 20  $\mu\text{g/g}$ .
2. The major group of tetrapyrroles consists of a mixture of homologous polyalkylporphyrins in approximately the C<sub>26</sub>-C<sub>32</sub> range, the C<sub>30</sub> and C<sub>32</sub> members often being dominant (6, 7, 9, 11). The C<sub>32</sub> compound has not been distinguished from etio-porphyrin (type III isomer shown at 1). The <sup>1</sup>H spectrum of the mixed homologues shows the presence of unsubstituted  $\beta$ -positions, presumably occurring in lower homologues as a result of acid-catalysed dealkylation processes (7), or arising at C-13 (as in 2) from chlorophyll precursors.
3. Sub-bituminous coals and, especially, lignites often contain etio-porphyrin mono- and di-carboxylic acids (metallated and metal-free). Purification of the iron etio-porphyrin dicarboxylic acid (Fe C<sub>32</sub> diCOOH) fraction from an Australian lignite gives a component (as the diester) which is identical with mesoporphyrin IX (3, as the diester) on the basis of tlc and hplc comparisons with the authentic reference samples, and on the basis of nmr spectroscopy (11, 12).
4. The following generalisations appear to hold. As coal rank increases, less porphyrin can be extracted (anthracites yield only traces of tetrapyrrole: 6, 7); carboxylic acid derivatives decrease and vanish; the FeP/GaP ratio decreases (7); and the weighted mean of the porphyrin molecular masses moves to lower values (9, 12). It has been suggested that the latter parameter has some merit in providing an independent scientifically-based assessment of coal rank (Porphyrin Index of Coalification: 12).
5. The generation of lower homologues of a C<sub>32</sub>-porphyrin accords with the geochemical transformation of the chlorophylls: however, the observation of mesoporphyrin IX suggests that an additional pathway from microbial heme proteins may also be significant (11).

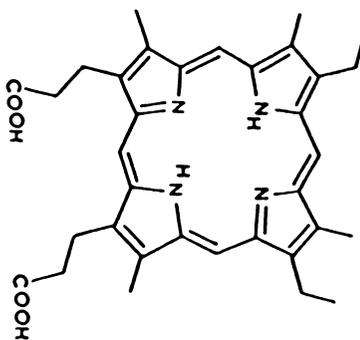
(1) Etiloporphyrin III



(2) 13-Desethyletiloporphyrin III



(3) Mesoporphyrin IX



Iron Porphyrins in Colorado Coal

It has recently been shown (10) that a Cretaceous coal from Colorado is particularly rich in iron porphyrins (ca. 12  $\mu\text{g/g}$ , Table I). This coal was kindly supplied from the Pennsylvania State University Collection through the courtesy of Professor P.H. Given, and some characteristics of the coal are provided in Table II. Petrographically the coal is of interest in being particularly rich in vitrinite.

Table II. Characteristics of Colorado Coal

<u>Age:</u> Cretaceous		<u>Rank:</u> HVC	
<u>Proximate analysis</u>		<u>Ultimate analysis</u> (daf)	
Ash (d) 6.19%		C	78.92%
Volatile matter (daf) 35.72%		H	5.49%
		N	1.72%
		S	0.43%
<u>Maceral composition</u> (dmmf, vol. %)			
<u>Vitrinite</u>	<u>Fusinite</u>	<u>Semi-fusinite</u>	<u>Micrinite</u>
91.5	2.3	4.0	1.4
<u>Source/Code</u> PSOC-850, Seam D			

Mass spectrometry has shown a range of lower homologues of etioheme (accurate molecular ion measurements for the iron complexes of C<sub>28</sub>, C<sub>29</sub>, C<sub>30</sub>, C<sub>31</sub> and C<sub>32</sub> porphyrins): no porphyrin carboxylic acids were detected (10).

The separation of the components of this homologous series is now in hand, the aim being to produce adequate quantities of crystalline single components for X-ray crystallography. The separation is a lengthy process, and is summarised in Figure 1. It has not yet proved possible to fractionate iron porphyrins by high pressure liquid chromatography (hplc) in a satisfactory manner, so the mixture is demetallated. Starting with 4 Kg of the powdered coal, and following the usual extraction (6, 11) with 7% H<sub>2</sub>SO<sub>4</sub>/MeOH and repeated separation by tlc, an iron porphyrin concentrate (36 mg) was obtained. Demetallation gave a mixture of porphyrins the components of which could be analysed by reverse phase hplc, as shown in Figure 2. This showed that the mixture was very complex, but, encouragingly, there were apparently only four principal components. For further separation, the mixture was metallated with zinc, and the product was subjected to further stages of separation using semi-preparative hplc to give four fractions, all four still being mixtures. These are labelled A-D in Figure 1, where A is the most polar, and D is the least so.

Repeated fractionation using the same procedure showed that A was obtained in only minor amount, B gave two components, B4B and B4C, which have not as yet been crystallised; C gave C3B as a major crystalline product (2.8 mg); while D gave D4C as a crystalline

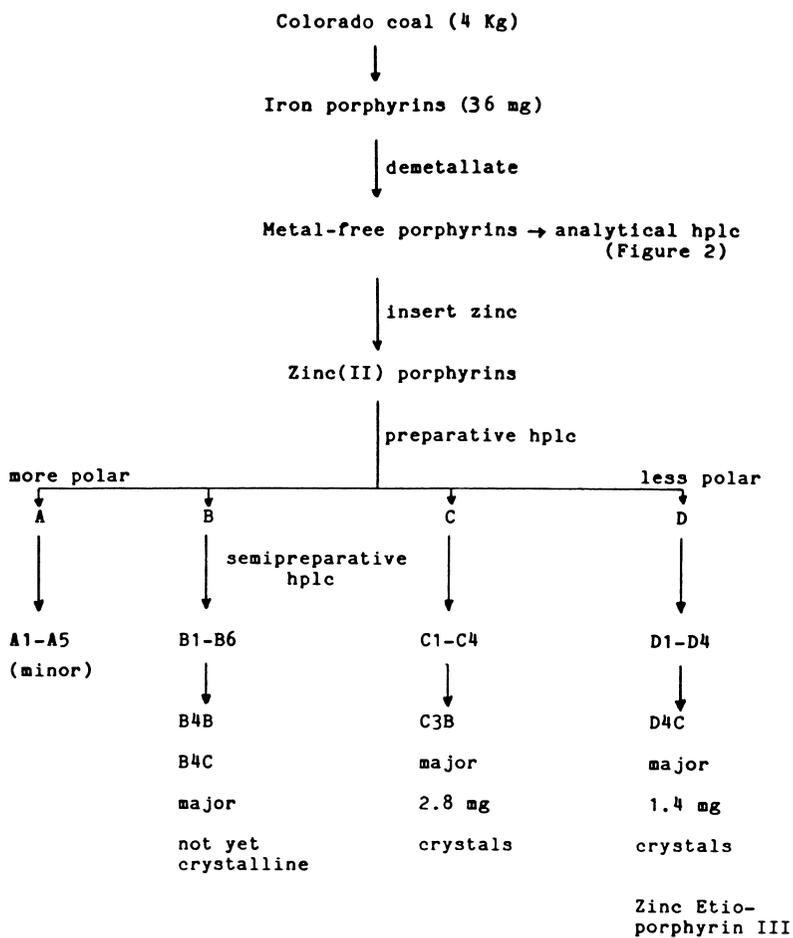


Figure 1. Isolation of metalloporphyrins from Colorado coal (PSOC-850). Note that the iron porphyrins are demetallated and then converted to zinc complexes to aid separation and identification.

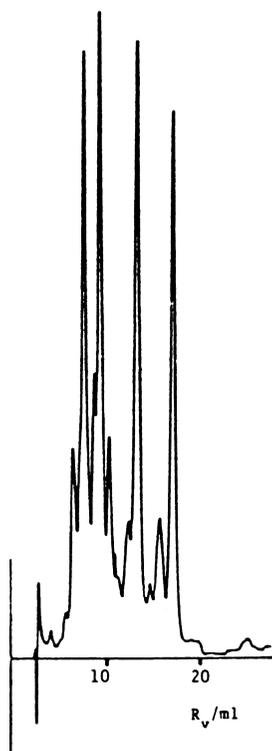


Figure 2. Analytical hplc of porphyrins obtained by demetallation of iron porphyrin fraction from Colorado coal (see Figure 1, Apex ODS, 3% MeOH/CH<sub>3</sub>CN).

product (1.4 mg). The latter compound is indistinguishable chromatographically from etioporphyrin III: but X-ray and nOe effect results on this sample, and on fraction C3B are awaited before secure conclusions can be drawn.

### Porphyrins in Relation to Petrographic Components

Up to the present time there has been no information on the variation of porphyrin content in relation to petrographic composition. An experiment has now been carried out to examine this question, a sub-bituminous coal from Janina Colliery (East High Silesian Coal Basin, Poland) being selected. The separation into petrographic constituent samples, vitrain and durain, and the petrographic analyses of these, was carried out with the help of Dr. H. Kidawa (Wroclaw): the results are shown in Table III. While the composition of the "durain" lithotype does not precisely fit the international definition for the durite microlithotype ( 95% inertinite + exinite, 5% vitrinite) (13) it does represent a considerable enrichment of inertinite and exinite over that of the raw coal (and a corresponding reduction in vitrinite).

Table III. Chemical and Petrographic Analyses of Janina Raw Coal and its Vitrain and Durain Lithotypes

	Raw Coal	Vitrain	Durain
<u>Chemical Analysis</u>			
Ash (d) %	5.76	3.30	7.69
Volatile matter (daf) %	40.6	36.5	38.0
C (daf) %	77.0	74.7	77.6
H (daf) %	4.9	4.6	4.5
N (daf) %	1.30	0.92	1.47
<u>Maceral Composition</u>			
Vitrinite	61.1	96.9	17.2
Exinite	14.7	0.9	28.1
Micrinite	1.7	0.2	9.8
Fusinite	21.5	1.8	44.6
Minerals	0.9	0.1	0.2
Pyrite	0.1	0.1	0.1

Janina coal contains appreciable amounts of both iron and gallium porphyrins: these were extracted and separated by tlc and estimated using the standard conventions which we have employed throughout (*viz.* a molecular weight of 600 is assumed, and the molar extinction of the Soret band is taken as 105,000 for iron porphyrins and as 400,000 for gallium porphyrins). The results are shown in Table IV.

Table IV. Metalloporphyrin Contents of Janina Coal and its Lithotypes ( $\mu\text{g/g}$ )

	FeP	GaP
Raw coal	5.83	0.67
Vitrain	1.03	0.96
Durain	0.24	0.27

The compositions of the six metalloporphyrins fractions were estimated by mass spectrometry, with the results shown in Figure 3. The porphyrin mixture comprises mainly polyalkylporphyrins in the C<sub>27</sub>-C<sub>32</sub> range, with a small amount of monocarboxylic acid (labelled C<sub>32</sub><sub>m</sub>) being detected in the heme spectra.

Three preliminary conclusions emerge from these results. Firstly, for these three samples there is a parallel between the vitrinite content and the amount of gallium porphyrin detected. Secondly, iron porphyrin seems to have been lost in preparing the lithotypes. This has led to the supposition that iron porphyrins are concentrated in boundary regions between maceral components, and we now have experimental evidence supporting this view. Thirdly, although the homologue compositions of the iron and gallium porphyrins (Figure 3) are not identical, they are rather similar. This suggests to us that they have similar origins. Since the gallium porphyrins are assumed to arise by metallation (since such complexes have not been detected in the biosphere) this implies that the iron porphyrins arise in the same way. In other words this evidence, although indirect, suggests that the iron present in the hemes obtained from coal is not the original iron present in possible biological heme precursors. However, we emphasise that these are the first results of this sort that have been obtained, and further examples are clearly needed before generalisations can be made.

Calcium carbonate is not infrequently associated with coal, and it is of interest in the context of coal microcomponents to draw attention to a rare pink calcite from a hydrothermal area in Austria (Deutsch-Altenburg) which was identified as containing a gallium porphyrin by Haberlandt (14) in 1944. We have obtained a small amount of this mineral which fluoresces red in ultraviolet light. The emission spectrum of the mineral is shown in Figure 4, and is typical of a metalloporphyrin where the metal has a filled (or completely empty) *d* shell. Extraction and chromatography reveal metal-free porphyrin and a metalloporphyrin, which is the major pigment component. The metalloporphyrin is not a single substance, but is predominantly gallium(III) mesoporphyrin IX (the axial ligand in the mineral is not known) as shown by metals analysis, tlc and hplc comparisons, and mass spectrometry. The comparison with authentic chlorogallium(III) mesoporphyrin IX by hplc - including coinjection - is shown in Figure 5. The origin of the mesoporphyrin is not known, but in our view a bacterial origin associated with the hydrothermal nature of the deposit deserves attention. The sequestration of gallium is also not understood, but study of this type of deposit may in the future throw some light on the occurrence of gallium porphyrins in coal and lignite.

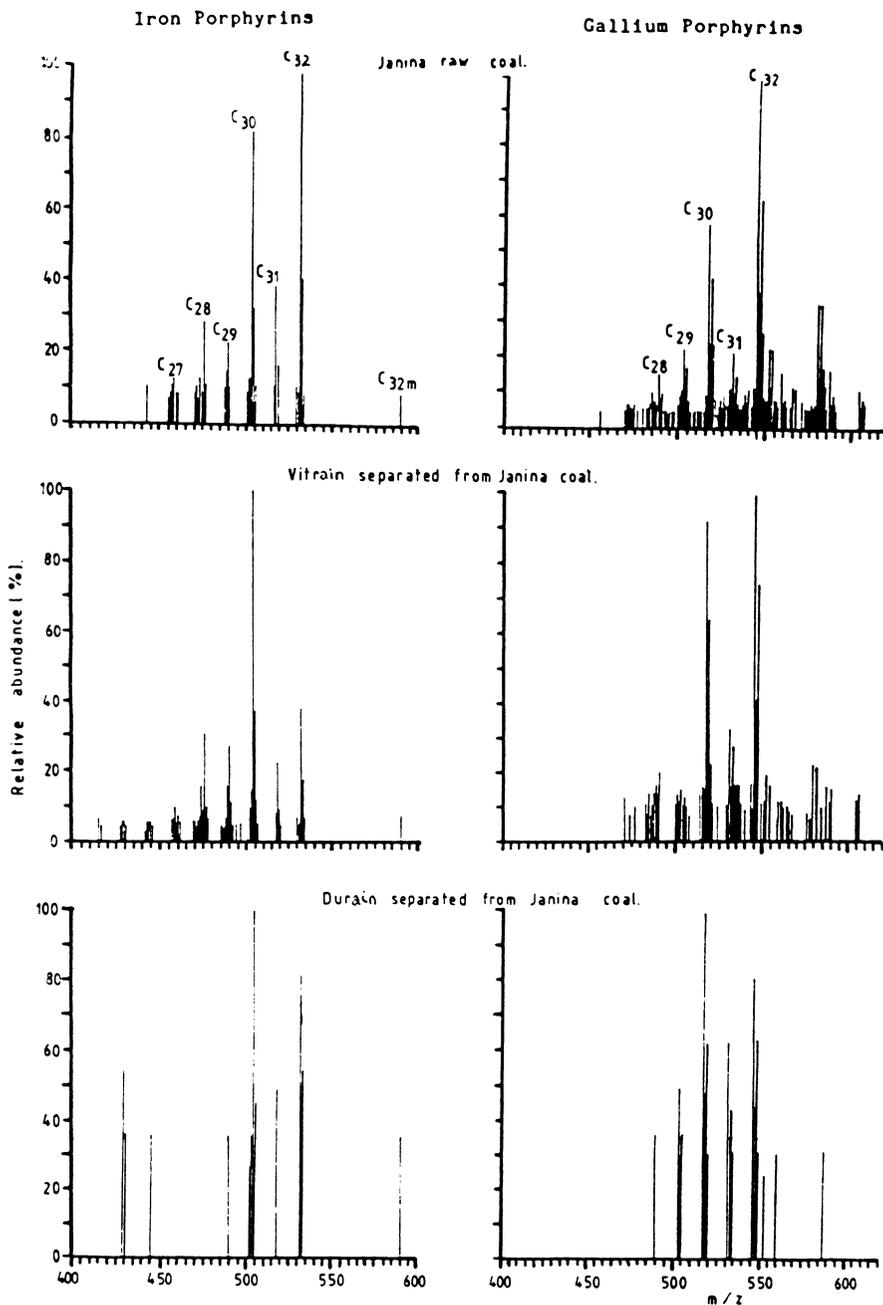


Figure 3. Mass spectra of metalloporphyrins from Janina coal and its vitrain and durain lithotypes (MS902, direct insertion, 300°C).

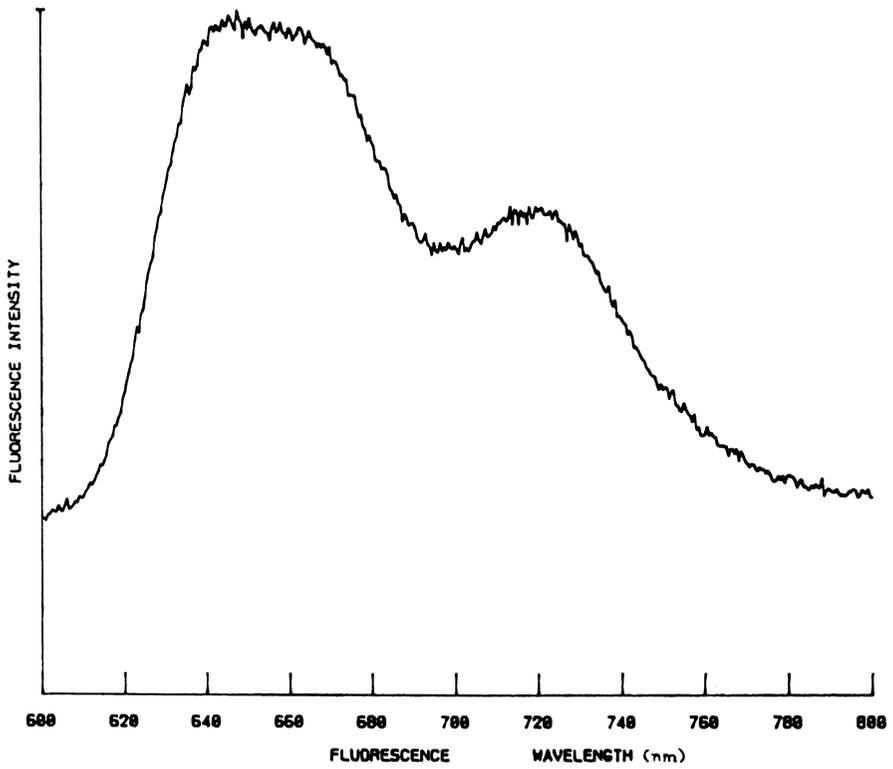


Figure 4. Emission spectrum from pink calcite from Deutsch-Altenburg (Excitation wavelength 415 nm).

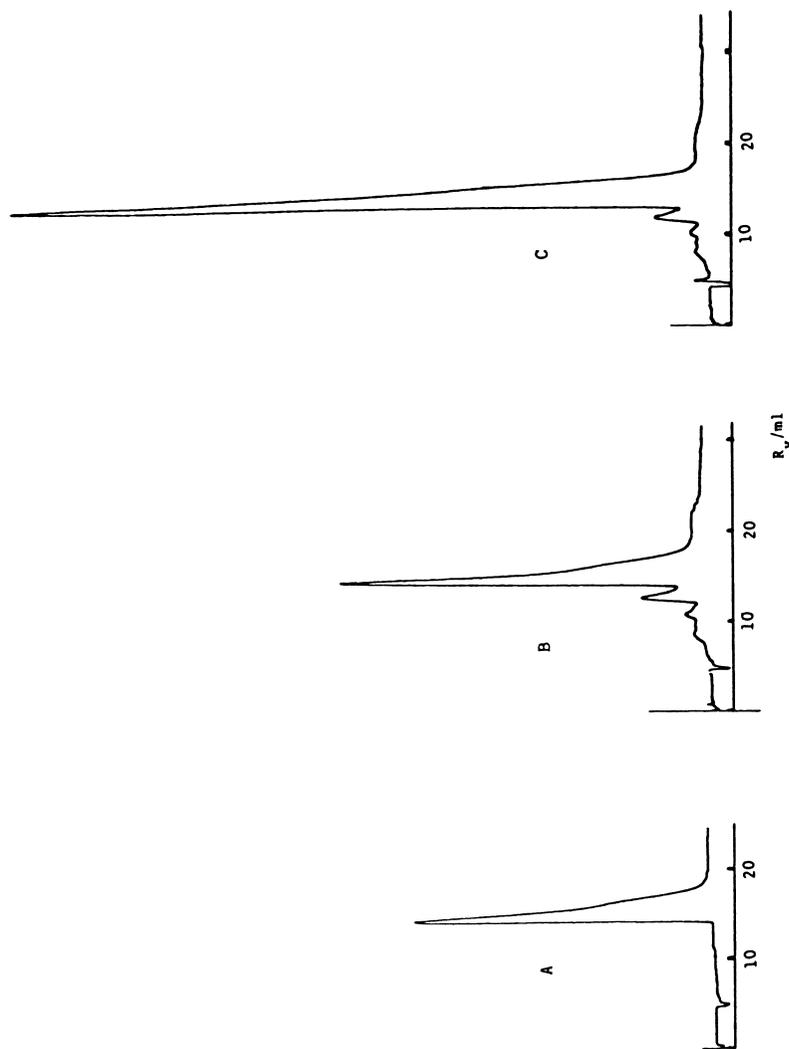


Figure 5. HPLC of gallium mesoporphyrin IX dimethyl ester. A: authentic sample, applied as ClGa(III) complex; B: material isolated from Deutsch-Altenburg calcite; and C: A+B coinjection (Techsil 5 C18, MeOH:H<sub>2</sub>O = 4:1).

### Prospect

The work on porphyrins in coal is at an exciting stage and has aroused our interest in the general area of coal chemistry. As far as the tetrapyrroles are concerned we see the area developing in two main directions in the immediate future.

First, there is a need for continued survey work, best carried out by LC/MS, which we have recently successfully demonstrated in the direct analysis of porphyrin concentrates from coal. We need to know what sort of porphyrins and metalloporphyrins are present in terms of carbon and carboxyl number, and how these vary with coal rank, and with maceral composition.

Second, there is a need to isolate and identify individual porphyrins. The work is made difficult by the low abundance of these compounds in coal, but the methods are now available and the aim - presently being exemplified by the continuing studies on Colorado coal - is to isolate crystalline individual porphyrins for X-ray and n.O.e. analysis. The results are expected to be important in allowing the origins of these biological markers to be identified securely, and in throwing light on the process of coalification.

### Acknowledgments

We are grateful to Professor P.H. Given (Pennsylvania State University), Mr. W.F. Wyss and Dr. D.F. Williams (National Coal Board), Professor A. Treibs (Munich), Dr. G. Niedermayr (Vienna), and Mr. R. Pekarsky (Pressbaum) for gifts of geological materials, and for discussions about them. The petrographic separations and analyses were carried out by Dr. H. Kidawa (Wroclaw) and the work on the lithotypes depended on materials which she prepared. The work has been supported by the Science and Engineering Research Council, the National Coal Board and the Royal Society. Dr. F. Czechowski was on leave from the Institute of Chemistry and Technology of Petroleum and Coal in Wroclaw, Poland, and his visit was supported by the British Council.

### Literature Cited

1. Goldschmidt, V.M. J. Chem. Soc. 1937, 655-673.
2. Weigelt, J.; Noack, K. Nova Acta Leopoldina 1932, 1, 87-96.
3. Treibs, A. Justus Liebig's Ann. Chem. 1935, 517, 172-196.
4. Treibs, A. Justus Liebig's Ann. Chem. 1935, 520, 144-150.
5. Bonnett, R.; Czechowski, F. Nature (London) 1980, 283, 465-467.
6. Bonnett, R.; Czechowski, F. J. Chem. Soc., Perkin Trans. 1 1984, 125-131.
7. Bonnett, R.; Czechowski, F. Philos. Trans. R. Soc. London Ser. A 1981, 300, 51-63.
8. Baker, E.W.; Palmer, S.E. In "The Porphyrins"; Dolphin, D., Ed.; Academic Press: New York, 1978; Vol. 1, pp. 486-552.
9. Palmer, S.E.; Baker, E.W.; Charney, L.S.; Louda, J.W. Geochim. Cosmochim. Acta 1982, 46, 1233-1241.
10. Bonnett, R.; Burke, P.J. Geochim. Cosmochim. Acta 1985, 49, 1487-1489.

11. Bonnett, R.; Burke, P.J.; Reszka, A. J. Chem. Soc., Chem. Commun. 1983, 1085-1087.
12. Bonnett, R.; Burke, P.J.; Czechowski, F.; Reszka, A. Org. Geochem. 1984, 6, 177-182.
13. International Committee for Coal Petrography, quoted by Berkowitz, N. "An Introduction to Coal Technology", Academic Press, New York, 1979, p. 25.
14. Haberlandt, H. Wien. Chem. Z. 1944, 47, 80-85.

RECEIVED December 5, 1986

## Chapter 12

# Influence of Metal Complexes in Fossil Fuels on Industrial Operations

Jan F. Branthaver

Western Research Institute, Box 3395, University Station, Laramie, WY 82070

Metal complexes are incorporated in the organic matter of most fossil fuels, sometimes in substantial concentration. These compounds significantly affect the processing of the materials in which they occur. Metal complexes decompose during hydrodesulfurization and catalytic cracking operations, resulting in metal deposition on catalysts. These metal deposits enhance undesirable side-reactions and cause reductions in catalyst activity and lifetime. As heavy crudes and other materials that usually are of high metal content replace conventional crudes as refinery feedstocks, it will be necessary to find ways to at least partially nullify the deleterious effects of metal complexes. Processes based on metals removal and passivation, hydrogen addition, carbon rejection, and improved catalyst design are actively under investigation.

While metal complexes in fossil fuels usually have adverse impacts on processing, product properties, and pose environmental problems, some fossil fuels may be sources of metals in the future.

As a consequence of their geochemical history, most crude oils, tar sands, coals, and oil shales contain measurable amounts of metal complexes. These complexes are not merely physically associated, as are dispersed mineral particles, but are part of the organic phases of fossil fuels. Concentrations of organically chelated metals in the above fossil fuels range from the ppm level to over 1000 ppm. Metals found as complexes in fossil fuels are transition metals, mostly those of the first long row of the periodic table. Among the best known metal complexes that occur in fossil fuels are metalloporphyrins, which are derived largely from the chlorins of the vegetable matter that was the source material for fossil fuels.

0097-6156/87/0344-0188\$06.00/0  
© 1987 American Chemical Society

### Metal Complexes in Petroleum

In the majority of crude oils, vanadium and nickel are the two metals which occur as chelates in greater than trace (>10 ppm) amounts (1). Some high-sulfur crudes have total vanadium and nickel contents exceeding 1000 ppm (2). Substantial amounts of iron have been detected in some crudes, but it is not certain to what extent iron compounds are native or become incorporated into crudes as a result of handling. Other metals occur in inorganic salts in brines associated with crude oils, but these salts are not true components of petroleum.

It is known that some fraction of the metal complexes found in petroleum are porphyrin complexes of such divalent ions as nickel and vanadyl. The structures of the porphyrins found in petroleum have been studied in some detail (3-4; Filby and Van Berkel, this volume). In most crudes, porphyrins consist of homologous series of desoxophylloerythroetio (DPEP), etio, and rhodo types (Figure 1). The nature of non-porphyrin metal chelates in petroleum is still a matter of some controversy. This is because no such compounds have been isolated and characterized with the rigor that has been the case with metalloporphyrins. Indeed, some investigators question whether non-porphyrin metal chelates are present in petroleum. Originally, the existence of non-porphyrin complexes in petroleum was inferred from the fact that metal contents of many crudes are observed to exceed porphyrin contents, as measured by UV-visible spectrometry. Because the heavier crudes which contain relatively large amounts of metals are colloidal systems involving dispersed molecular aggregations, it has been argued that UV-visible spectrometry understates the amounts of porphyrins in such systems (5), and that the existence of non-porphyrinic species is only apparent. Other investigators (6-12) have unearthed a variety of evidence to indicate that a substantial fraction of metals in petroleum are complexed with ligands that are not classical porphyrins. It has been suggested that the non-porphyrin coordination sites are part of large aromatic sheets (13). There is some evidence that non-porphyrin metal complexes of petroleum may not involve coordination with four nitrogen atoms (14-15; Fish, et al.; this volume). The nature of the ligands chelated with metals other than vanadium and nickel is not well known, although the existence of iron porphyrins in a heavy crude has been reported (16).

Metal complexes of vanadium and nickel are concentrated in asphaltene and resin fractions of petroleum. Asphaltenes and resins constitute the most polar and aromatic portion of a crude. Asphaltenes are precipitated as black solids by treating a crude with large volumes of an alkane solvent, usually n-pentane or n-heptane. Materials soluble in the alkane solvent are referred to as maltenes or petrolenes. The resin fraction is obtained by chromatographic treatment of maltenes. The most polar components of the maltenes become concentrated in the resins. Therefore residual fractions from distillation processes will contain almost all metals originally present in a crude. Metalloporphyrins are slightly volatile at higher temperatures, and therefore they may be present in higher distillation fractions.

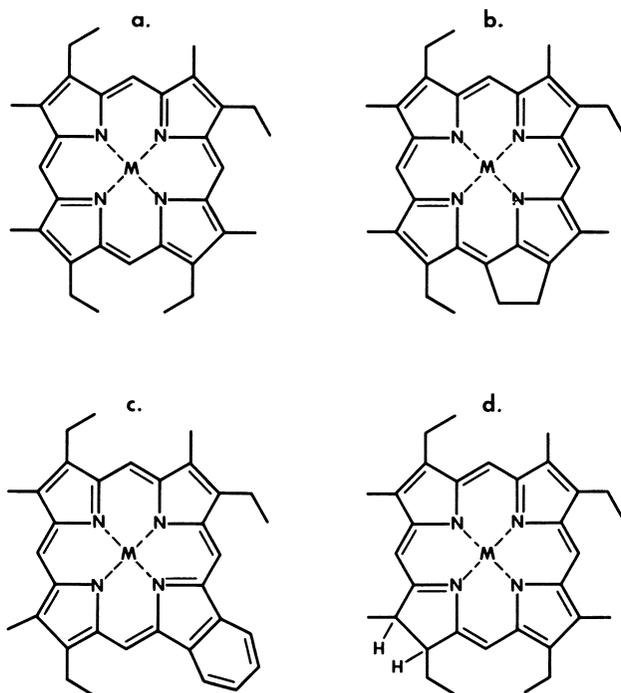


**Figure 1. Structures of Porphyrins and a Chlorin.**  
**M = Metal (Ni, V = O, etc.)**

- a. Metallated Etioporphyrin**
- b. Metallated Deoxophylloerythroetioporphyrin (DPEP)**
- c. Metallated Rhodoporphyrin**
- d. Metallated Chlorin**

### **Refining of Heavy Crudes**

The energy crises of the 1970's with the accompanying increases in the price of petroleum resulted in the processing of greater amounts of heavy crudes by refineries. Heavy crudes are characterized by low API gravity (<20), high asphaltene content, and relatively high concentrations of sulfur, nitrogen, and oxygen-containing compounds. Heavy crudes usually contain substantial concentrations of vanadium and nickel complexes (17). It has long been known that these metal complexes poison and foul catalysts used in refinery operations such as fluid catalytic cracking (FCC) and hydrodesulfurization (HDS) (18-20). The quality of some refinery products is adversely affected by the presence of even small amounts of metal complexes.

In modern refineries, crude oil is treated to remove detrital matter and brines, and is then subjected to atmospheric distillation. Products from atmospheric distillation are wet gas, unstabilized gasoline, kerosene, heavy gas oil, and topped crude. The topped crude is subjected to vacuum distillation to yield vacuum gas oil and reduced crude bottoms. Reduced crude bottoms are often subjected to a coking operation to yield wet gas, coker gasoline, coker gas oil, and coke. Most of the liquid products from the above operations are subjected to further treatments to yield commercial products.

### **Effect of Metal Complexes in Petroleum on Catalytic Cracking**

Catalytic cracking is one of the most important refinery operations. During catalytic cracking, alkanes of high carbon number are converted to alkanes and alkenes of lower carbon numbers. Yields of hydrocarbons having three or four carbon atoms are high. The produced alkenes are highly reactive and undergo carbon-carbon bond cleavage, isomerization, and aromatization. Naphthenic compounds react by carbon-carbon bond scission in rings and side-chains, and dehydrogenate to form aromatic molecules. Aromatic compounds undergo reduction in the size of or loss of side chains. The liquid products of catalytic cracking are fractionated and some fractions are further processed to improve quality. Aromatic compounds contribute greatly to octane number improvement in gasolines, so the generation of aromatics during catalytic cracking is economically desirable. Gas oil fractions from other refinery operations are prime feedstocks for catalytic cracking units. Some refineries mix residual fractions from atmospheric or vacuum distillation of heavy crudes with gas oils for catalytic cracker feedstocks (21). Whatever the composition, the feedstock is mixed with catalyst particles and the mixture is fed into a reactor, a vessel in which endothermic cracking reactions take place.

Several different types of materials have been used as catalysts in this process. Originally, natural clays and synthetic amorphous silica-alumina were the most widely used catalysts. Later, the more effective "molecular sieve" type catalysts were developed. These catalysts are small particles composed of porous, zeolite crystallites embedded in a matrix of silica-alumina (22).

Coke formation invariably accompanies cracking. Therefore the catalyst particles are transferred to a regenerator after volatile products of catalytic cracking are removed. Coke is burned off the catalyst particles in the regenerator vessel. The regenerated catalyst then is mixed with fresh feedstock, and this mixture is reintroduced into the reactor. Heavier feedstocks contain relatively large amounts of coke precursors. As more coke is laid down on a catalyst, higher regenerator temperatures result from burning the coke off. These higher temperatures adversely affect catalyst lifetimes.

Both vanadium and nickel seriously affect catalytic cracking catalysts, although in different ways. Both metals accumulate on catalyst particles over time (23-24). Nickel deposits cause excessive coke yield and hydrogen production from feedstocks, but do not lower overall catalyst activity, which is defined as the percentage of feed converted into coke, gas, and gasoline. Thus the deleterious effect of nickel lies in enhancement of undesirable reactions, not in decreasing the rate of processing feedstocks. Vanadium deposits cause alterations of catalyst structures, upon which activity and selectivity are dependent (24-25). Vanadium is particularly harmful to zeolite catalysts. This element deposits on the alumina-silica matrix and migrates to the zeolite particles, where crystallinity and activity are eventually destroyed. The migration of vanadium to zeolite particles is probably the result of vanadium pentoxide formation during catalyst regeneration. This oxide melts at a relatively low temperature (690°C) and is mobile at regenerator operating temperatures. Vanadium also attacks silica-alumina catalysts. It does not cause hydrogen production or excess coking to the same extent as nickel.

Of the two metals, nickel is the more harmful in catalytic cracking operations at lower concentrations. For amorphous catalysts, which were widely used when catalytic cracking was a relatively new process, a "contamination index" was developed based on the formula:

$$C.I. = (Cu + Fe + 4V + 14Ni)$$

In this formula, the metal content of catalysts is expressed in ppm. If the C.I. value exceeded 1000, a catalyst was considered to be badly contaminated (26). Catalysts in current use can tolerate much higher metal loadings, largely because of the activity of zeolites. This reduces contact times between feed molecules and catalyst particles, which does not allow time for extensive dehydrogenation and other unwanted side reactions. When concentrations of metals on zeolite catalysts exceed 1.0%, vanadium appears to be as harmful as nickel. Since most heavy crudes contain more vanadium than nickel, the overall negative effect of vanadium can be worse than that of nickel when feeds rich in metals are catalytically cracked.

Various means for alleviating the problems caused by metals in catalytic cracking operations have been studied. Two promising approaches are metals passivation and catalyst modification. An example of metals passivation is reported by Dale and McKay (27). They have shown that addition of certain antimony compounds to

catalytic cracker feedstocks results in a weakening of the deleterious effects of metals deposition. Antimony and nickel form an alloy that does not have the dehydrogenation activity characteristic of nickel. Gasoline selectivity and yield are improved by use of the antimony additive, and therefore larger amounts of heavy residual fractions, such as reduced crude bottoms, may be mixed with gas oils in making up feedstocks for catalytic cracking operations. Compounds of boron, and bismuth also are used as nickel passivators. Tin acts as a passivator for vanadium. Impregnation of catalysts with compounds such as zirconium oxide also confers greater metals tolerance to a catalyst. The development of passivators and additives that minimize the effects of metals on cracking catalysts is an area of active research in several energy companies.

Modification of catalysts to efficiently handle heavy feedstocks must take into account the differences in properties between heavy resids and the gas oils conventional cracking catalysts were designed to process.

Residual fractions contain on the average much larger molecules (or agglomerations of molecules) than gas oils, and most of the metal complexes of a crude oil become concentrated in residual fractions. These larger molecules do not enter the pores of most zeolite particles. They are cracked by the alumina-silica matrix of zeolite catalysts. If zeolite catalysts are used to crack feedstocks containing residual fractions at short contact times, some of the residual fractions will remain on the catalyst when the catalyst is transferred to the regenerator. This will cause high regenerator temperatures, which will exacerbate the destructive effects of vanadium.

Because the catalyst matrix is important in heavy feedstock cracking, there has been considerable interest in optimizing matrix properties. Ritter, et al. (21) claim that a large pore, low surface area matrix inhibits metal dispersion on catalyst particles and reduces gas and coke yields. Masselli and Peters (28) contend that a high surface area, catalytically active silica-alumina matrix will improve metals tolerance. The high surface area will cause vanadium to be more evenly distributed throughout a catalyst particle and will presumably spare zeolite structures from preferential attack. Nilsson, et al. (29) also emphasize that the catalyst matrix is critical to the cracking of large molecules in high boiling fractions and resids. They recommend that the matrix of a catalyst used to process these feedstocks have large pores, a high surface area, and a low zeolite content.

It also has been determined that "trapping" areas can be introduced into a catalyst matrix during manufacture. These "trapping" areas serve as sinks for vanadium and thus minimize the attack of that element on zeolite particles.

Another approach to the problem of metals deposition is catalyst cleanup. Advantage can be taken of specific chemical properties of nickel and vanadium, particularly the ability of nickel to form chelates with a variety of ligands (30-31). Catalyst cleanup of amorphous silica-alumina catalysts was in use commercially at one time.

If it proves difficult to manufacture catalysts which are specifically capable of cracking heavy feedstocks (and which will doubtless be expensive to manufacture) then either these feedstocks will have to be treated using cheaper, low-activity catalysts (21), or some procedure to remove metals must precede catalytic cracking in refining of heavy feeds.

The most obvious solution to the metals deposition problem is to use only materials having a low metals content as catalytic cracker feedstocks. This may be accomplished by processing only light crudes or demetallizing heavy crudes before cracking. The former option is hardly feasible for most refiners in an era of "energy crises". For the latter option, a number of processes are available for the production of low metal content feedstocks. Among these are various hydrotreatments, coking, solvent extraction, and deasphalting (17,32). All these processes involve costs, and their use will depend on the particular situation of a refinery. Thus it is desirable to be able to efficiently catalytically crack feedstocks that contain substantial amounts of metals.

Otterstedt et al. (24) discuss some unsolved problems in the catalytic cracking of heavy feeds. They recommend further characterization studies of heavy oils to identify "crackable" and "non-crackable" materials. They suggest that "crackability" of molecules be studied as a function of molecular weight. They point out that it may be necessary to remove the most intractable fractions from some heavy feeds before cracking, and that special separation procedures for these materials should be developed.

#### **Effect of Metal Complexes in Petroleum on Hydrodesulfurization**

Most heavy crudes are high in sulfur content, and high-sulfur crudes often contain large concentrations of vanadium. The removal of sulfur from crudes is an important refinery operation for economic and environmental reasons. Hydrodesulfurization (HDS) is one of the principal processes used to desulfurize petroleum. HDS is affected adversely by metal complexes, which poison and reduce the lifetimes of the catalysts employed in the process (33). This reduction in catalyst lifetime is caused by irreversible adsorption of metals on the catalyst, which blocks pores and prevents access to active sites (34). As metals deposits build up, higher HDS temperatures are necessary. In refineries which process large amounts of heavy crudes, hundreds of kilograms of metals can be deposited on HDS catalysts during each day of operation. The metals are deposited as sulfides (35). HDS catalysts thus cause demetallization of heavy crudes and their residual fractions, as well as desulfurization.

HDS treatments have been used with a variety of feedstocks, including light and middle distillates, high-boiling distillates, as well as heavy oils and residua. The more unsaturated the feedstock, the more hydrogen is consumed in the process, and the more heat is evolved during the exothermic HDS reaction. Catalysts commonly used in HDS are sulfided Co-Mo, Ni-Mo, or Ni-W supported on alumina. The catalyst bed is contained in a reactor into which feedstock and gas are introduced. The gas-feedstock mixture is preheated and pressurized. Because of the need for high partial

pressures of hydrogen, more hydrogen is present in the gas than is consumed in the HDS step. The nature and distribution of the products of HDS are a function of the reaction conditions. These products are transferred from the reactor to a separator, where excess hydrogen, hydrogen sulfide, ammonia, and light hydrocarbons are separated from higher-boiling materials. Most liquid products of HDS treatments are used in other refinery operations.

The mechanism of catalytic hydrodemetallization (HDM) of metal complexes in petroleum on HDS catalysts has been investigated by several research groups. Morales and Galiasso (36) studied the adsorption of porphyrins from Boscan crude on a Co-Mo HDS catalyst. The porphyrins were obtained by extracting Boscan asphaltenes with acetonitrile, followed by purification using alumina chromatography. It was demonstrated that vanadyl porphyrins bond to the catalyst through the vanadyl oxygen atom.

Silbernagel and Riley (37) provided evidence that the nature of metal chelation in a feed influences the metals deposition process on HDS catalysts. They studied the HDS of a heavy crude, its maltene fraction, and the hydrogen fluoride (HF)-treated heavy crude. These workers claim that HF removes most of the metals from crudes, particularly metals chelated with porphyrins. Each of the three substrates was introduced into one end of a reactor containing the catalyst bed. The maltene fraction, in which the metals are known to occur largely as porphyrin complexes, was relatively easily demetallized. Vanadyl species were found to be more easily removed than nickel species from the maltenes. The metals deposited on the catalyst during HDS of the maltenes were observed to be concentrated at the entrance to the catalyst bed. A more uniform metals deposition profile on the catalyst bed was observed when the parent crude and the HF-treated crude were subjected to HDS. These investigators assumed that, in the substrates they used, not all metals are complexed with porphyrins. A Co-Mo catalyst on alumina was used in this study.

Rankel and Rollman (35) showed that vanadium and nickel deposit on HDS catalysts as sulfides. They demonstrated that the deposited vanadium sulfide has some HDS activity. They also investigated the decomposition of synthetic vanadyl and nickel porphyrins under two different sets of conditions. In one series of experiments, hydrogen sulfide was observed to react non-catalytically with metalloporphyrins to effect porphyrin decomposition, vanadyl porphyrins being more labile than nickel porphyrins. In other experiments, metalloporphyrins were decomposed over a Co-Mo HDS catalyst in an atmosphere of hydrogen. Chlorins were detected as intermediates. Chlorins are hydrogenated porphyrins (Figure 1). No intermediates were identified in the reaction with hydrogen sulfide. Rankel and Rollman speculate that in the HDS process, when both hydrogen and hydrogen sulfide are present, porphyrins decompose primarily by hydrogenation, and what are believed to be non-porphyrin metal chelates may react preferentially with hydrogen sulfide. Further studies on petroporphyrins by Rankel are reported in this volume.

Agrawal and Wei (38) also investigated the decomposition of porphyrins during HDS. They studied model vanadyl and nickel etio-porphyrins on a Co-Mo HDS catalyst. It was found that these model

porphyrins lose metals by a two-step reaction sequence in nujol using HDS conditions. The first step is a reversible hydrogenation to a metallochlorin. The second step is hydrogenolysis of the chlorin, which fragments the ring system and results in demetallization.

The data of Agrawal and Wei suggest that if the hydrogenation and hydrogenolysis steps could be separated, metals deposition on HDS catalysts could be controlled. Both hydrogenation and hydrogenolysis are catalyzed by most catalysts, but to different degrees. Webster and Wei (39) experimented with a variety of transition metal catalysts to effect demetallization of nickel etioporphyrin I. They found that palladium and platinum catalyze hydrogenation rather than hydrogenolysis, and that rhodium and ruthenium have the reverse effect. Ware and Wei (40) showed that by doping a Co-Mo HDS catalyst with various reagents, the relative rates of the two reactions could be altered. Webster (41) found that the hydrogenolysis of a nickel porphyrin on a ruthenium catalyst is more affected by dilution of the ruthenium with copper than is hydrogenation. These phenomena may be explained if it is assumed that hydrogenation and hydrogenolysis do not take place on the same catalyst sites. Hydrogenation occurs on sites that are not composed of large arrays of atoms, whereas hydrogenolysis requires sites that are more extended and more structured. Dilution and doping would more greatly affect the sites having the extended arrays of atoms than sites composed only of a few atoms.

Galiasso, et al. (42) carried out a series of HDM experiments on maltene and asphaltene fractions of Jobo crude mixed with gas oils. The catalyst was presulfided Mo-Fe supported on alumina. This catalyst is more effective as a HDM catalyst than as a HDS catalyst. The vanadyl porphyrins in Jobo maltenes were found to be less reactive under the experimental conditions than all vanadyl complexes in the maltenes taken as a whole. It is claimed that Jobo maltenes contain substantial quantities of non-porphyrin vanadyl complexes. Nickel chelates in Jobo maltenes were found to be more reactive than vanadyl chelates. The metal complexes in the maltenes were more easily demetallized than those in the asphaltenes. The asphaltene fraction also exhibited greater reactivity of total vanadium compared with what the authors determined to be porphyrinic vanadium. These reactivity differences were determined by plotting vanadium loss vs. the ratio of total to porphyrinic vanadium at various reaction times. From these experiments, the authors contend that there is a large difference in reactivity in HDM between porphyrin and what are believed to be non-porphyrin metal complexes.

These workers also reported that a model vanadyl porphyrin, vanadyl etioporphyrin I, reacts much more rapidly than the petroporphyrins used in the study. They found that vanadyl etioporphyrin I is hydrogenated to a chlorin using the Mo-Fe catalyst at 300°C, but cautioned that this reaction may not be part of a predominant pathway of porphyrin decomposition at higher temperatures.

Galiasso, et al. (43) also examined the detailed course of deactivation of a Co-Mo catalyst by a heavy Orinoco oil. They found that for the HDM reaction, coke deposition in very small

pores is responsible for initial catalyst deactivation. After a time, vanadium deposits build up on the mouth of small-to-medium sized pores, which impedes diffusion of substrates into the pore system. Finally, vanadium deposits accumulate in such a number of sites in the catalyst that no large molecules can penetrate to the interior of the catalyst.

The breakup of asphaltene micelles in heavy feedstocks has been investigated by Asaoka, et al. (44) using a special catalyst designed to enhance asphaltene decomposition. In the procedure adopted by these investigators, there is only a small amount of hydrocracking, although asphaltene yields from products of this process are greatly reduced compared with asphaltene yields from feedstocks. Asphaltenes of the treated feeds also are lower in vanadium and sulfur content compared with feedstock asphaltenes. In designing their experiments, Asaoka, et al. (44) used as their model of asphaltene structure the model proposed by Tynan and Yen (45), in which fundamental asphaltene units are believed to be stacks of condensed aromatic rings. The data of Asaoka, et al. (44) indicate that vanadium and sulfur are critical to the stability of asphaltene aggregations, and therefore asphaltene cracking does not take place until compounds containing these elements begin to be removed from asphaltene aggregations, whatever their structure might be. A further study by Asaoka and co-workers is included in this volume.

Mitchell and Scott (46) studied the effect of synthetic porphyrins on the desulfurization of the model compound thiophene over a conventional Co-Mo catalyst. They found that unmetallated porphyrins are worse catalyst poisons than either vanadium or nickel porphyrins. They also found that small amounts of vanadyl porphyrins enhance hydrodesulfurization of thiophene. They conclude that demetallization of porphyrins occurs at molybdenum sites in their catalyst and proceeds through hydrogenation of a metalloporphyrin at meso-positions to a phlorin, which is a hydrogenated porphyrin isomeric with a chlorin. They emphasize that catalyst poisoning by porphyrins is a function of the whole molecule and does not merely involve metal atoms.

Metal distributions as a function of molecular size within crude oils and derived materials have been the subject of several recent publications by Biggs, et al. (7), Reynolds, et al. (8), and Reynolds and Biggs (47-49). In these studies, crude oils, resids, distillates, etc., were subjected to size-exclusion chromatography. Metal profiles of the chromatographic fractions were obtained by inductively coupled plasma (ICP) spectrometry. It was found that bimodal distributions were observed for both vanadium and nickel in a number of heavy crudes and resids. The peaks of this bimodal distribution correspond to substances having apparent molecular weights of several hundred and several thousand respectively. A large portion of the metal chelates in the lower molecular weight fractions are metalloporphyrins.

As part of this investigation, two atmospheric resids were thermally hydrotreated at 410°C and also were catalytically hydro-treated. After each treatment the products were fractionated by size-exclusion chromatography, and metal profiles were determined. One of the resids was subjected to short-path distillation. This

process provides a distillate in which all metals are accountable for as metalloporphyrins and a residual fraction. Both fractions were thermally hydrotreated.

The thermal treatment of the resids resulted in substantial metals removal and a large reduction in molecular size of remaining metal compounds. Thermal treatment readily decomposed the porphyrins that were distilled from one of the resids. Catalytic treatment of resids resulted in preferential decomposition of lower molecular weight metal chelates. These lower molecular weight species appear to be able to enter catalyst pores, which larger species cannot do.

An important result of this study is that the existence of non-porphyrin metal chelates is strongly supported. The hydrothermal treatment reduces the size of the metal-containing species in the resids. This shows that large structures resulting from asphaltene micelle aggregation are broken up. Using proven isolation techniques, only small amounts of metalloporphyrins could be obtained from these thermally treated resids. If the substances believed to be non-porphyrin chelates were really porphyrins that happen to be undetectable by UV-visible spectrometry by virtue of being part of asphaltene aggregations, then the breakup of such aggregations should result in the observation that most remaining low molecular weight metal chelates in the thermally treated resids are porphyrins. Further results in this study are reported in this volume in the paper by Reynolds, et al.

The above investigations have provided a great deal of information about the course of catalytic hydrodemetallization of heavy crudes and resids during hydrodesulfurization. From these studies it does appear that hydrogenation of porphyrins to chlorins and more reduced derivatives is an important step in porphyrin hydrodemetallization. Direct loss of a metal atom to form free porphyrins does not seem to be a significant pathway. This is not surprising in view of the fact that petroporphyrins are very stable molecules in which the metal ion is bonded tenaciously. Hydrogenation of porphyrin double bonds reduces aromaticity, upon which the stability of the porphyrin molecule largely depends. Hydrogenolysis of carbon-carbon bonds destroys almost all aromaticity. Reduced porphyrins do not complex with most metals as strongly as parent porphyrins.

While it is desirable to elucidate the fate of metalloporphyrins during HDS, it should be recalled that metals in HDS feeds are not entirely porphyrinic. These materials are subjected to thermal conditions during refinery distillation processes which cause porphyrin decomposition, yet the metals chelated with the porphyrins remain in the feeds. Also, a great deal of evidence indicates that some of the metal chelates associated with asphaltene micelle structures are in part not classical porphyrins. Granting that such compounds exist, then their ligand structures must differ from porphyrins, and demetallizing mechanisms might also be expected to differ.

It also may be that there are differences in HDM behavior among porphyrin types. For example, rhodo type porphyrins may not be as readily hydrogenated as DPEP and etio types. Porphyrins with extended alkyl substituents may require cracking before they can be

catalytically hydrogenated. Those associated with asphaltene micelle structures may require breakdown of these structures before hydrogenation can proceed to a significant extent. These structures are very stable and may persist even under processing conditions (50). If metal chelates are critical components of asphaltene micelle structures, then the HDM problem is somewhat of a dilemma.

Porphyrim suites, and presumably non-porphyrin metal chelate suites, of heavy crudes often differ markedly, as do the nature and amount of asphaltene micelle structures. Thus behavior of various heavy crudes during HDS might be expected to be quite different. This variance in processability is discussed by Dolbear, et al. in this volume. The diversity of heavy crude properties may account for some of the apparent confusion regarding relative reactivities of different metal chelates under varying reaction conditions. Hence it may be important to study a wide variety of heavy crudes to establish those chemical structural features which most influence processability not only for HDS but also for other operations. Part of such a program studying structure-property relationships will involve more detailed knowledge of the metal chelates in crude oils, both quantitatively and qualitatively.

### **Strategies for Processing Heavy Crudes**

It is evident that demetallization is critical to deep conversion of bottom-of-the-barrel fractions (51). Strategies to accomplish demetallization of heavy feeds without unacceptable catalyst loss have been suggested or are in use. These strategies may be classified under the categories of hydrogen addition, carbon rejection, and metal passivation or removal.

Carbon rejection processes utilize one of a number of coking processes (32). In many refineries reduced crude bottoms (vacuum residua) from vacuum distillation of topped crudes are fed into a coker. The coking process results in most of the metals in a feedstock being deposited along with the produced coke. The coke is reused in most coking processes, partly to provide process heat. Some of the coke (purge coke) must be removed to eliminate metals and ash. The distillates from coking operations may be subsequently hydrotreated or catalytically cracked. Other examples of carbon rejection processes are deasphaltening and solvent extraction. All of these processes require that there be some use for, or capability to dispose of, the poor quality products.

Hydrogen addition processes possess an inherent advantage over carbon rejection processes, which is that less crude is required to produce the same amount of product. For those hydrogen addition processes which are catalytic, proper design of catalysts is one approach to the problem of metals deactivation. The metal and sulfur distribution in a heavy crude will influence catalyst design (52). Large-pored catalysts probably will be required to fully hydroprocess metal-rich, high sulfur feedstocks. While HDS and HDM reactions may take place on the same catalyst, it does not appear feasible to have both reactions proceed efficiently on a given catalyst (53). Consequently a number of investigators have suggested the use of HDM guard beds to effect metal removal prior

to HDS operations. A similar approach was mentioned earlier, the use of catalysts which promote hydrogenation, but which do not cause porphyrin demetallization (39).

Thermal hydrocracking is also a viable process for demetallization of heavy feedstocks (51). This is because resin fractions of feeds react rapidly during catalytic treatments, which causes asphaltene flocculation. Under thermal hydrotreatment, resins and asphaltenes react at similar rates and the complications caused by asphaltene precipitation are not observed. Further details of non-catalytic hydrotreating processes are given by Dautzenberg and De Deken in this volume. This paper also discusses other HDM strategies and the criteria on which they are based.

Chemical and physical treatments of heavy crudes to remove metals have been proposed. Ishigaki (54) describes the combination of heavy crude processing with nickel ore smelting. A vacuum residue is heated with the ore to take advantage of the propensity of nickel to accelerate coking and cracking. Light products are generated, as well as nickel oxide coated with coke, and some heavy oil. The heavy oil is easily hydrodesulfurized, and coke is burned off the nickel oxide for process heat. The nickel is converted to a leachable form in this process.

Kukes and Aldag (55) have tested over 200 chemicals for the ability to demetallize heavy oils. Almost all of them cause degradation of the oil. However, they did find that some phosphorus compounds selectively react with vanadium complexes in crude oils. Further work in this area is reported in the paper by Kukes, et al. in this volume.

It would appear that, with the current state of knowledge, all of the above strategies have advantages and disadvantages. It is evident that each of the approaches is favored by one or more petroleum companies. The strategy used to process heavy crudes in the near future will be determined by the situation of individual refining operations. Considerations such as the nature of crudes processed, ability to modify operations, and environmental considerations, etc., must be evaluated in deciding which strategy to pursue until there exists a much better understanding of the chemistry of metal complexes in fossil fuels. Even then, it is not certain that any one process will be in standard use for metal removal.

### Other Economic Effects of Metal Chelates in Fossil Fuels

An important product of petroleum is asphalt, used mainly in roofing and the paving of highways. Asphalts from various sources differ in their tendencies to oxidize, and oxidation causes asphalt failure. Vanadyl porphyrins have been shown to catalyze asphalt oxidation (56), although complexes identified as non-porphyrin vanadyl chelates found in certain petroleum do not appear to do so (57). It is therefore necessary to exercise caution when using asphalts derived from crudes having high vanadyl porphyrin contents in asphalt blends.

Concerns about adverse effects upon the environment have strongly influenced fossil fuel operations for some years. Among the many concerns are acid rain from the burning of high-sulfur

fuels, marine pollution, and ground water contamination (58). The metals found in fossil fuels must be either utilized in industrial operations or safely disposed of. Vanadium and nickel, the principal metals found in petroleum, are toxic. As discussed at length above, they affect operations designed to remove sulfur and nitrogen, two primary air pollutants, from petroleum. When other fossil fuels such as shale oil and tar sand bitumens become commercially important, metal chelates found in them will doubtless present similar difficulties to those observed in petroleum. In this volume, Majid and Ripmeester report on metals associated with humic matter in tailings from Athabaska tar sands.

Thus far the adverse impact of metal chelates in fossil fuels has been emphasized. On the positive side, it has been suggested that certain metal-rich fossil fuels be exploited at least in part for residual metals. Etemad-Moghadan and Raisszadeh (59) report that one refinery processing heavy Venezuelan crudes recovered vanadium commercially up to 1972 from coke-fired boiler fly ash. Jack, et al. (60) have studied the acid extraction of vanadium, nickel, iron, and titanium from coke obtained from Athabasca tar sand bitumen. They found that vanadium and nickel in the coke can be treated so that they become readily susceptible to leaching.

Curiale and Harrison (61) point out that aberrant metal contents in crude oils may be indicators of nearby ore deposits. They also describe certain solid bitumens, impsonites and grahamites, which contain high concentrations of vanadium, as well as some gilsonites, which are rich in molybdenum. The economics of vanadium from fossil fuels has been studied by Fischer (62) and Shortsleeve (63).

### Summary

Metal chelates in fossil fuels have significant influence on the processing of petroleum. It is evident from the foregoing discussion and some of the other contributions to this volume that efficient utilization of heavy oils depends on an understanding of the chemistry of metal chelates in processing operations which requires detailed knowledge of the nature of metal chelate structures in petroleum. This same knowledge will be useful in geochemical studies. The information gained by the active research projects investigating metal chelates in heavy crudes will doubtless be of great use when such materials as tar sands, oil shales, and coal are exploited for liquid fuels, petrochemicals, or other uses which petroleum largely monopolizes today.

### Acknowledgment

The author thanks the U.S. Department of Energy for support under Contract Number DE-FC21-83FE60177.

### Literature Cited

1. Filby, R. H. In "The Role of Trace Metals in Petroleum"; Yen, T. F., Ed.; Ann Arbor Science Publishers: Ann Arbor, 1975; pp. 33-56.

2. Speight, J. G. "The Desulfurization of Heavy Crudes and Residua"; Marcel Dekker: New York, 1981; pp. 166-7.
3. Baker, E. W. In "Organic Geochemistry"; Eglinton, G., Murphy, M. T. J., Eds.; Springer-Verlag: New York, 1969; pp. 464-97.
4. Baker, E. W.; Palmer, S. E. In "The Porphyrins, Structure and Synthesis, Part A"; Dolphin, D., Ed.; Academic: New York, 1978, pp. 485-551.
5. Goulon, J.; Esselin, C.; Friant, P.; Berthe, C.; Muller, J. F.; Poncet, J. L.; Guilard, R.; Escalier, J. C.; Neff, B. In "Symposium on Characterization of Heavy Crude Oils and Petroleum Residues"; Editions Technip: Paris, 1984.
6. Branthaver, J. F. Ph.D. Thesis, North Dakota State University, Fargo, 1976.
7. Biggs, W. R.; Fetzer, J. C.; Brown, R. J.; Reynolds, J. G. Liq. Fuels Technol. 1985, 3, 397-422.
8. Reynolds, J. G.; Biggs, W. R.; Fetzer, J. C.; Liq. Fuels Technol. 1985, 3, 423-48.
9. Spencer, W. A.; Galobardes, J. F.; Curtis, M. A.; Rogers, L. B. Separation Sci. and Technol. 1982, 17, 797-819.
10. Crouch, F. W.; Sommer, C. S.; Galobardes, J. F.; Kraus, S.; Schmauch, E. H.; Galobardes, M.; Fatmi, A.; Pearsall, K.; Rogers, L. B. Separation Sci. and Technol. 1983, 18, 603-34.
11. Fish, R. H.; Komlenic, J. J.; Wines, B. K. Anal. Chem., 1984, 56, 2452-60.
12. Fish, R. H.; Komlenic, J. J. Anal. Chem. 1984, 56, 510-17.
13. Yen, T. F. Energy Sources, 1978, 3, 339-51.
14. Dickson, F. E.; Kunesh, C. J.; McGinnis, E. L.; Petrakis, L. Anal. Chem. 1972, 44, 978-81.
15. Dickson, F. E.; Petrakis, L. Anal. Chem. 1974, 46, 1129-30.
16. Franceskin, P. J.; Gonzalez-Jimenez, F.; La Rosa, M. G.; Abrams O.; Katan, L. Hyperfine Interactions 1986, 28, 825-8.
17. Schuetze, B.; Hofmann, H. Hydrocarbon Process. 1984, Feb., 75-82.
18. Farrar, G. L. Oil and Gas J. 1952, Apr. 7, 79.
19. Beach, L. K.; Shewmaker, J. E. Ind. and Eng. Chem. 1957, 49, 1156-64.
20. Bieber, H.; Hartzband, H. M.; Kruse, E. C. J. Chem. Eng. Data 1960, 5, 540-57.
21. Ritter, R. E.; Rheaume, L.; Welsh, W. A.; Magee, J. S. Oil and Gas J. 1981, July 6, 103-9.
22. Oblad, A. G. Oil and Gas J. 1972, Mar. 27, 84-106.
23. Venuto, P. B.; Habib, E. T. Catal. Rev. - Sci. Eng. 1978, 18, 1-150.
24. Otterstedt, J. E.; Gavert, S. B.; Jaras S. G.; Menon, P. G. Applied Catal. 1986, 22, 159-79.
25. Jaras, S. Applied Catal. 1982, 2, 207-18.
26. Gary, J. H.; Handwerk, G. E. "Petroleum Refining"; Marcel Dekker: New York, 1975; p. 98.
27. Dale, G. H.; McKay, D. H. Hydrocarbon Process. 1977, Sept, 97-102.
28. Masselli, J. M.; Peters, A. W. Catal. Rev.-Sci. Eng. 1984, 26, 525-554.
29. Nillson, P.; Massoth, F. E.; Otterstedt, J. E. Applied Catal. 1986, 26, 175-189.

30. Speight, J. G. "The Chemistry and Technology of Petroleum"; Marcel Dekker: New York, 1980, p. 325.
31. Edison, R. R.; Siemenson, J. O.; Masologites, G. P. Hydrocarbon Process. 1976, May, 133.
32. Busch, R. A.; Kociscin, J. J.; Schroeder, H. F.; Shah, G. N. Hydrocarbon Process 1979, Sept., 136-42.
33. Tamm, P. W.; Harnsberger, H. F.; Bridge, A. G. Ind. Eng. Chem. Process Des. Dev. 1981, 20, 262-73.
34. Speight, J. G. "The Desulfurization of Heavy Crudes and Residua"; Marcel Dekker: New York, 1981, p. 165.
35. Rankel, L. A.; Rollman, L. D. Fuel 1983, 62, 44-6.
36. Morales, A.; Galiasso, R. Fuel 1982, 61, 13-17.
37. Silbernagel, B. G.; Riley, K. L. In "Catalyst Deactivation"; Delmon, B.; Froment, G. F., Eds.; Elsevier: Amsterdam, 1980, pp. 313-21.
38. Agrawal, R.; Wei, J. Ind. Eng. Chem. Process Des. Dev. 1984, 23, 515-22.
39. Webster, I. A.; Wei, J. Preprints, Div. Petrol. Chem. ACS 1985, 30, 37-49.
40. Ware, R. A.; Wei, J. Preprints, Div. Petrol. Chem. ACS 1985, 30, 62-9.
41. Webster, I. A. Ph.D. Thesis, Massachusetts Institute of Technology, Cambridge, 1983.
42. Galiasso, R.; Garcia, J.; Caprioli, L.; Pazos, J. M.; Soto, A. Preprints, Div. Petrol. Chem. ACS 1985, 30, 50-61.
43. Galiasso, R.; Blanco, R.; Gonzales C.; Quinteros, N. Fuel 1983, 62, 817-22.
44. Asaoka, S.; Nakata, S.; Shioto Y.; Takeuchi, C. Ind. Eng. Chem. Process Des. Dev. 1983, 22, 242-8.
45. Tynan, E. C.; Yen, T. F. Fuel 1969, 43, 191-208.
46. Mitchell, P. C. H.; Scott, C. E. Polyhedron 1986, 5, 237-41.
47. Reynolds, J. G.; Biggs, W. R. Fuel Sci. Technol. Int. 1986, 4, 593-618.
48. Reynolds, J. G.; Biggs, W. R. Fuel Sci. Technol. Int. 1986, 4, 749-77.
49. Reynolds, J. G.; Biggs, W. R. Fuel Sci. Technol. Int. 1986, 4, 779-98.
50. Rao, B. L. M.; Serrano, J. E. Fuel Sci. Technol. Int. 1986, 4, 483-99.
51. Dautzenberg, F. M.; De DeKen, J. C. Preprints, Div. Petrol. Chem. ACS 1985, 30, 8-20.
52. Fischer, R. A.; Angevine, P. J. Applied Catal. 1986, 27, 275-83.
53. Toulhout, H.; Plumail, J. C.; Martino G.; Jacquin, Y. Preprints, Div. Petrol. Chem. ACS 1985, 30, 85-95.
54. Ishigaki, S. Chem. Econ. and Eng. Rev. 1985, 7, 7-13.
55. Kukes, S. G.; Aldag, A. W. Preprints, Div. Petrol. Chem. ACS 1985, 30, 119-29.
56. Branthaver, J. F.; Nazir, M.; Petersen, J. C.; Dorrence, S. M. Liq. Fuels Technol. 1983, 1, 355-69.
57. Branthaver, J. F.; Nazir, M.; Petersen, J. C.; Dorrence, S. M.; Ryan, M. J. Liq. Fuels Technol. 1984, 2, 67-89.
58. Vlakovic, V. "Trace Elements in Petroleum"; PPC Books: Tulsa, 1978, pp. 102-99.

59. Etemad-Moghadam, P.; Raisszadeh, M. A. The Iranian Petroleum Institute, Bulletin No. 50. 1973, 30-38.
60. Jack, T. R.; Sullivan, E. A.; Zajic, J. E. Fuel 1979, 58, 589-94.
61. Curiale, J. A.; Harrison, W. E. Bull. Am. Assoc. Petrol. Geol. 1981, 65, 2426-32.
62. Fischer, R. P. In "The Role of Trace Metals in Petroleum"; Yen, T. F., Ed.; Ann Arbor Science Publishers: Ann Arbor, 1975, pp. 201-5.
63. Shortsleeve, F. J. In "The Role of Trace Metals in Petroleum"; Yen, T. F., Ed.; Ann Arbor Science Publishers: Ann Arbor, 1975, pp. 290-14.

RECEIVED March 3, 1987

## Chapter 13

# Reaction Sequence of Metallopetroporphyrins During Heavy Residuum Upgrading

John G. Reynolds<sup>1</sup>, Wilton R. Biggs, and Susan A. Bezman

Chevron Research Company, Richmond, CA 94802

We analyzed the metallopetroporphyrins and the metallo-nonporphyrins during thermal and catalytic upgrading of heavy residua. Both types of processing remove metals. By size exclusion chromatography with element specific detection (SEC-ICP), we found thermal treatment reduces the size of the remaining metal-containing compounds, while for certain catalysts, fixed-bed treatment preferentially removes the metal-containing molecules in the size range of the catalyst pore.

In both processes, the metallopetroporphyrins are easily removed. UV-vis spectroscopic analysis of chromatographic fractions of products where V petroporphyrin removal is not complete indicates the presence of intermediates in the demetalation sequence for vanadyl petroporphyrins. Spectral properties of these potential intermediates are consistent with a pathway of initial porphyrin reduction to chlorins, then further reduction. The presence of chlorins as intermediates is in agreement with previously published work using metalloporphyrin model compounds. This work shows similar demetalation behavior of the V petroporphyrins in actual feeds under commercial processing conditions.

Heavy crudes and residua contain high metals levels, particularly Ni, V, and sometimes Fe. These impurities cause processing problems for traditional refining technology, and have stimulated research for new process options, for example, the development of large-pore, metals tolerant catalysts (1).

In order to better understand the mechanism of metals removal during residua processing, knowledge of the metal structures and their behavior during processing is essential. Research has been conducted examining both points.

<sup>1</sup>Current address: 722 Elm Street, El Cerrito, CA 94530

The Ni and the V in a crude or residuum can be divided into two chemical categories, the metallopetroporphyrins and the metallo-nonporphyrins (2). The metallopetroporphyrins are so far the only structurally characterized metal complexes, being first detected 50 years ago (3). The first two structures shown in Figure 1 are examples of porphyrin compounds which model the metallopetroporphyrins.

The metallo-nonporphyrins have not been unequivocally characterized, but some information exists about their possible structures. They are known to: (1) account for the majority of the metal-containing compounds in several crudes and residua (2), (2) span a much larger size range than the metallopetroporphyrins (2,4,5), (3) generally have more polar structures than metallopetroporphyrins (5), and (4) have average first coordination spheres about the metal center different from the four nitrogens of the porphyrin (6-8). Examples of model compounds having coordination spheres which possibly model the first coordination spheres of the metallo-nonporphyrins are also represented in Figure 1. Based on model compounds studies, metallo-nonporphyrin vanadium compounds appear to be vanadyl square planar complexes with idealized  $C_{4v}$  to distorted  $C_{2v}$  symmetry (9-12), with possible coordination in the axial position (13).

The behavior of both metallopetroporphyrins and metallo-nonporphyrin compounds during processing has also been studied to some extent. Model compound studies of etio and tetraphenyl porphyrins of both Ni and V processed under typical hydroprocessing conditions shows the porphyrins are hydrogenated before demetalation (14-21). Demetalation studies at hydroprocessing conditions (16) of metallopetroporphyrins extracted from Arabian Light vacuum residuum showed: (1) without a fixed-bed hydroprocessing catalyst, thermal reaction conditions must be reached (approximately 400°C) to significantly demetalate metallopetroporphyrins, (2) with a hydroprocessing catalyst, demetalation of metallopetroporphyrins starts around 200°C, (3) thermal treatment preferentially processes metallopetroporphyrins, (4) the extent of removal of metallopetroporphyrins is a function of process severity, and (5) hydrogen sulfide assists in metallopetroporphyrin demetalation.

The metallopetroporphyrin demetalation rate also has been shown to be different from the overall demetalation rate. This is due to either the environment around the metal center affecting the demetalation rate, or the metallo-nonporphyrins possessing a different intrinsic demetalation rate [which may be distinguished by the presence of hydrogen sulfide (22)]. The preference of metallopetroporphyrin demetalation to metallo-nonporphyrin demetalation has also been observed in the oxidative treatment of asphaltenes (23,24).

We have recently reported on the size profile changes of the V and Ni compounds of selected California residua during thermal and catalytic fixed-bed treatment (25). Under all the conditions examined, the metallopetroporphyrins appeared to be easy to process out. To discern the mechanisms by which demetalation occurs on the molecular level, we have examined the metallopetroporphyrin fractions from various reaction conditions by size-exclusion

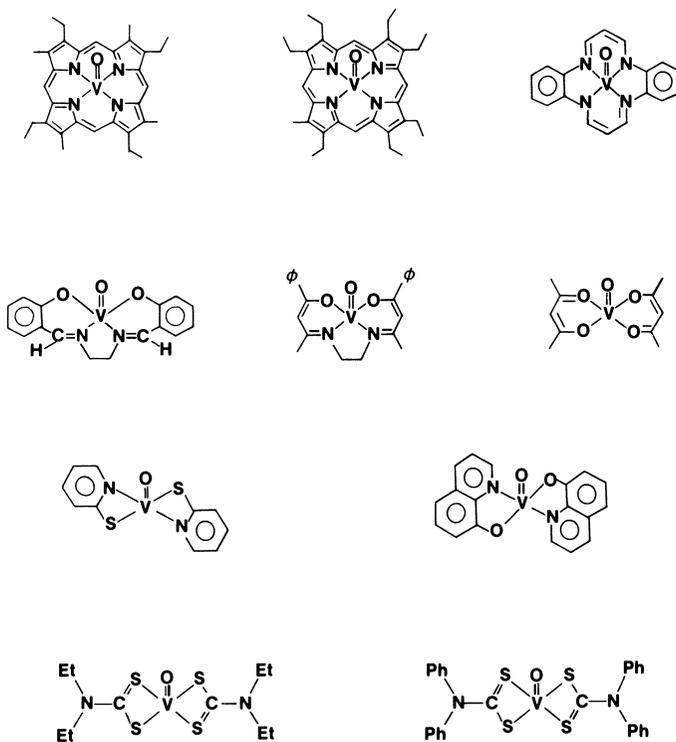


Figure 1. Vanadyl Porphyrin and Vanadyl Nonporphyrin Chemical Types Possibly in Crude Oils and Heavy Residua.

chromatography and UV-vis spectroscopy. This study reports qualitatively the demetalation behavior observed.

### Experimental

The size exclusion chromatography with inductively coupled plasma emission spectrometry (SEC-ICP) techniques applied here are discussed elsewhere (2). The output obtained from the technique, called the response profile, measures the selected elemental content as a function of elution time. Calibration with model compounds (4,5) and polystyrene standards changes the response profile from a time domain to a logarithmic size domain.

In general, the feeds examined exhibited a bimodal distribution, with maxima at MW 9000 and MW 800. (All molecular weights are defined as polystyrene equivalent). This low molecular weight maximum has been attributed to the metallopetroporphyrins by extraction techniques (2). The profiles shown below are in the time domain only, and with the size decreasing logarithmically from the left to the right.

The metallopetroporphyrin/metallo-nonporphyrin separation methods are also reported elsewhere (2). Routine determination of the metallopetroporphyrin and reduced porphyrin compound concentrations were performed by the following method: (1) ~0.5 g of residuum or product were loaded onto an alumina column (Basic or Neutral No. 2 and 3). Hydrocarbons were removed by elution with 90% *n*-hexane and 10% diethyl ether. The metallopetroporphyrins and reduced species were eluted with chloroform and methylene chloride. The column received a final wash with methanol. The methanol fraction exhibited ~0.5% of the metallopetroporphyrins in some cases (feeds only). All fractions were checked for petroporphyrin content by UV-vis spectroscopy on equipment described elsewhere (2).

The processing types and conditions are reported elsewhere (25).

The feeds processed were heavy residua California atmospheric residua (AR) No. 1, California AR No. 2, and California AR No. 3, which were obtained by single plate distillation of the corresponding crude to a 343°C (650°F) cut point. All AR are high in metals--each having over 500 ppm Ni plus V.

### Behavior of Metals During Thermal Processing

California AR No. 1 was thermally processed at different severities in a tubular flow reactor. The V SEC-ICP profiles for the feed and the processed products are shown in Figure 2. The profiles correspond to 78% and 38% V removal for the moderate and low severity conditions, respectively.

Three general features are evident for the profiles in Figure 2: (1) the larger size V-containing compounds are disappearing during thermal processing--they are either being removed or shifting in size, (2) the profile is shifted upon processing toward the smaller molecular size range, and (3) small molecular size materials, not apparent in the feed, are being formed.

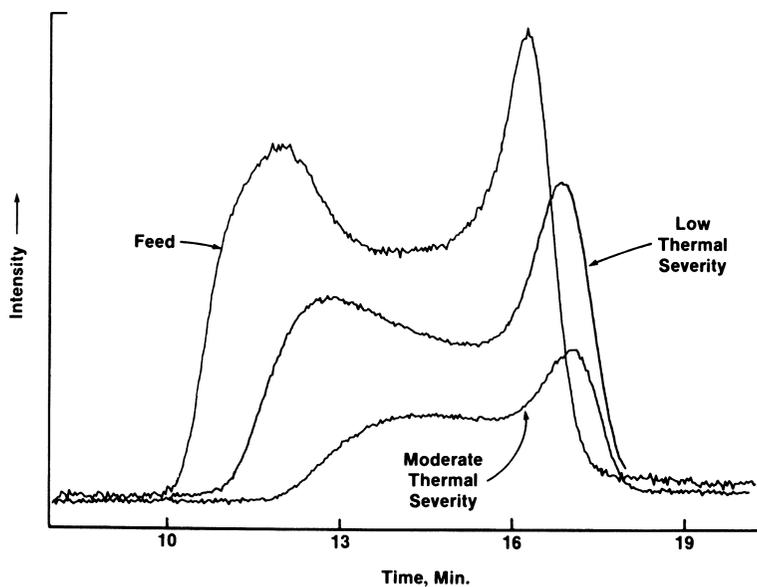


Figure 2. Changes in the Vanadium Distribution as Measured by SEC-ICP From the Thermal Treatment of California AR No. 1 at Different Temperatures. (Reproduced with permission from Reference 25. Copyright 1986 Marcel Dekker, Inc.)

Figure 3 shows the V SEC-ICP profiles for California AR No. 2 and thermal process products at constant temperature, but different reaction times. The changes in size distribution evident in the Figure 2 are also evident here. The different reaction times, however, do not appear to effect the size distribution in the profile.

From examination of several reaction conditions, we were able to make the following conclusions about thermal processing: (1) some metals are removed, (2) the net remaining metal-containing compounds are shifted to smaller size, (3) temperature affects the amount removed and the magnitude of size shift, and (4) reaction time, at a given temperature, affects the amount removed but has little effect on the size change.

#### Behavior of Metallopetroporphyrins During Thermal Processing

In Figure 2, the small molecular size maximum assigned as metallopetroporphyrins in the crude has shifted to even smaller size. This was originally thought to be related to the feed metallopetroporphyrins; but, in the moderate thermal severity case, direct metallopetroporphyrin determinations showed less than 2% of the petroporphyrins present in the feed were found in the product. In the lower severity case, the metallopetroporphyrin content was higher, 6%. These results prompted examination of the reactivity of the metallopetroporphyrins, independent of the metallo-nonporphyrins.

For California AR No. 1, the metallopetroporphyrins were separated from the metallo-nonporphyrins by short path distillation (25). At temperatures below 677°C (1275°F), metallopetroporphyrins have been found to distill (26). The distillation is efficient in that 98% of the feed metallopetroporphyrins are found in the volatile fraction. Ninety-two percent of the metals in this volatile fraction were accounted for as metallopetroporphyrins.

This metallopetroporphyrin fraction was diluted with vacuum gas oils to its original concentration in California AR No. 1 and was processed at moderate thermal severity. Figure 4 shows V SEC-ICP profiles for the feed and product. All the metallopetroporphyrins are processed out.

From these results, it is apparent that the metallopetroporphyrins are more susceptible to thermal processing than the metallo-nonporphyrins and are removed more readily than the metallo-nonporphyrins.

#### Behavior of Metals During Fixed-Bed Processing

California AR No. 1 was also processed under catalytic (fixed-bed) conditions. The V SEC-ICP profiles of the feed and process products at two different severities are shown in Figure 5. The long residence time product corresponds to 70% V removal, and the short residence time corresponds to 50% V removal.

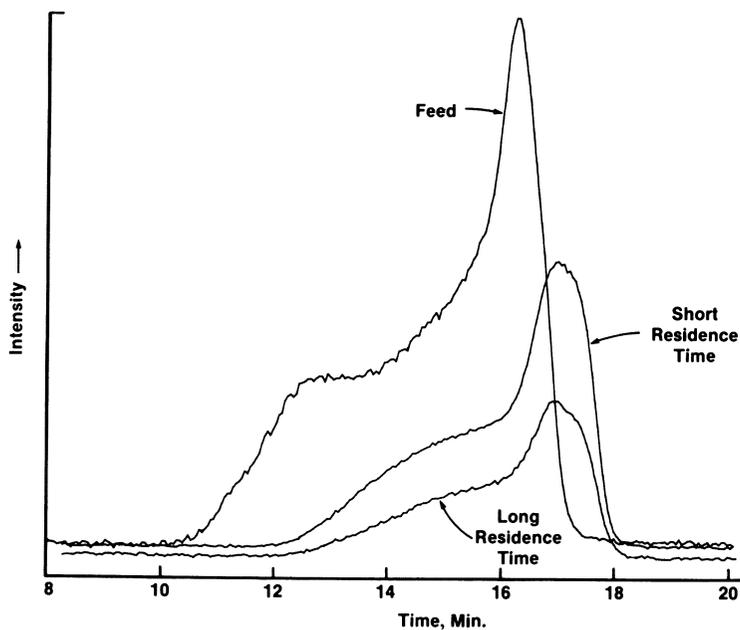


Figure 3. Changes in the Vanadium Distribution as Measured by SEC-ICP From the Thermal Treatment of California AR No. 2 at Different Reaction Times. (Reproduced with permission from Reference 25. Copyright 1986 Marcel Dekker, Inc.)

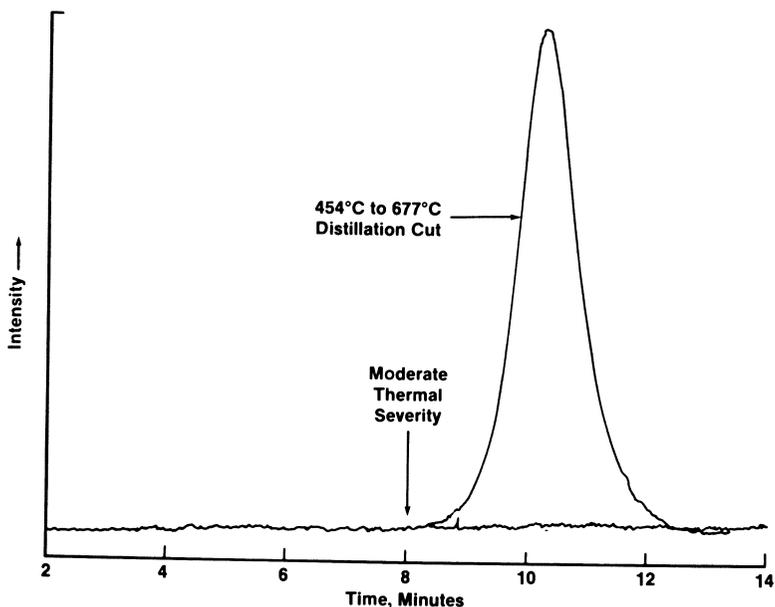


Figure 4. Changes in the Vanadium Distribution as Measured by SEC-ICP From the Thermal Treatment of the 454°C to 677°C Distillation Cut From California AR No. 1. (Reproduced with permission from Reference 25. Copyright 1986, Marcel Dekker, Inc.)

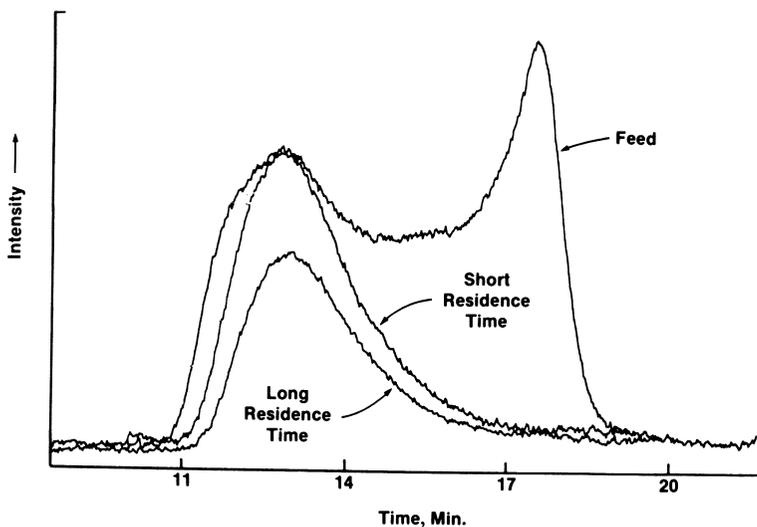


Figure 5. Changes in the Vanadium Distribution as Measured by SEC-ICP From Fixed-Bed Treatment of California AR No. 1 at Different Reaction Times. (Reproduced with permission from Reference 25. Copyright 1986, Marcel Dekker, Inc.)

From the figure, the following conclusions can be made: The catalytic processing (1) removes metals in the size range of the catalyst pore most efficiently and (2) requires longer residence times to remove the metal-containing compounds larger than the pore size of the catalyst.

#### Behavior of Metallopetroporphyrins During Fixed-Bed Processing

Examination of the profiles in Figure 5 shows the metallopetroporphyrins are rapidly and completely processed out. This may be a consequence of their small size, by fitting in the pores of the catalyst, or their intrinsic demetalation rate may be very fast. Because they were processed completely, we had to resort to less severe fixed-bed processing to examine their reaction sequence. To do this, we selected a larger-pore, less active, commercially available hydroprocessing catalyst and a completely deactivated catalyst.

California AR No. 3 was processed over a low activity fixed-bed catalyst. Figure 6 shows the V SEC-ICP profile of the feed and a low severity product. The feed profile has a typical bimodal distribution, where the maximum at small molecular size has been assigned to petroporphyrins. The product profile corresponds to 40% total V removal.

The product profile indicates this catalyst is removing metals from all size ranges, with some preference for the smaller molecular size metals. This preference could be explained by a higher density of small pores in the catalyst.

In contrast to the high activity catalyst, this catalyst has a much broader pore size distribution, and this is reflected in the metals removal behavior. At approximately the same removal activity, it is clear when comparing Figure 5 and 6, the low activity catalyst removes a much broader size range of metals than the small pore, high activity catalyst. The low activity catalyst is not as effective in removing the metals in the small molecular size range (including the V petroporphyrins). This allows for possible detection to the intermediates formed during the demetalation of the V petroporphyrins. (See below.)

Figure 7 is the V SEC-ICP profile for California AR No. 3 and product obtained by processing the feed over a totally deactivated catalyst. The process product corresponds to ~6% V removal. Three features are evident in this profile: (1) some larger size V compounds have disappeared, (2) there is a shift to smaller size compounds, and (3) a substantial amount of small molecular size material is being formed, which is not present in the feed. This behavior of the metals is similar to that of the thermal processing described above. Because the catalyst was virtually dead, the temperature of operation was near the thermal reaction threshold.

The metallopetroporphyrin fraction of this profile was examined by UV-vis spectroscopy and revealed ~45% V petroporphyrin removal. The fate of these metallopetroporphyrins is discussed below.

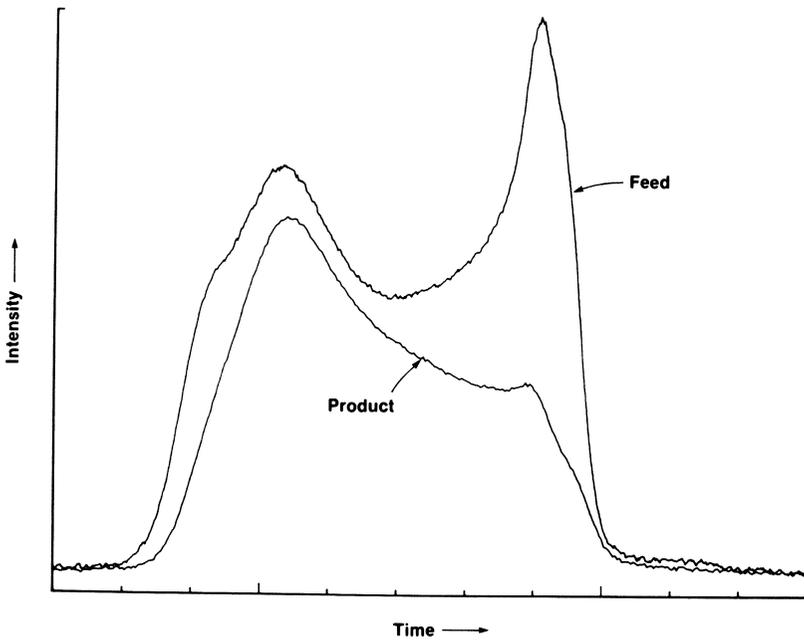


Figure 6. Changes in the Vanadium Distribution as Measured by SEC-ICP From Lower Severity Fixed-Bed Treatment of California AR No. 3.

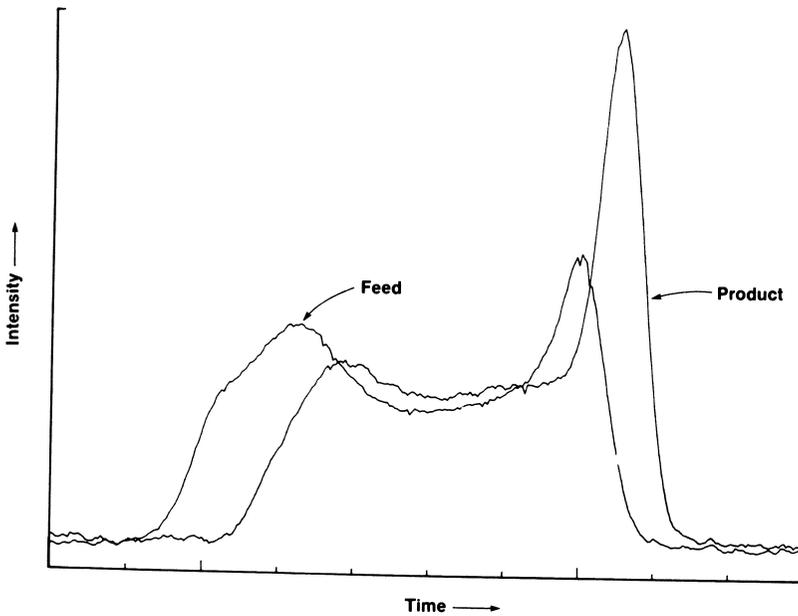


Figure 7. Changes in the Vanadium Distribution as Measured by SEC-ICP From Deactivated Fixed-Bed Treatment of California AR No. 3.

Possible Reaction Pathway for the Metallopetroporphyrins

Detailed UV-vis spectroscopic studies were made on all products where the metallopetroporphyrins were still evident--the low thermal severity products, the deactivated catalyst products, and the low activity catalyst products. In all these cases, spectral evidence suggested the presence of reduction products of the V petroporphyrins. Figure 8 shows the second derivative UV-vis spectrum for the low severity thermal product in the 500 to 650 nm range. The typical 408 nm Soret band was observed, but because of general interference by organic chromophores, it was not used for quantitation of the metallopetroporphyrins.

In addition to the minimum at 572 nm which is assigned as vanadyl etio porphyrin (VOetio) (27), a minimum is also seen at 628 to 630 nm, which have been assigned as vanadyl etio chlorin (VOetio2H) (28). This compound also has a band at 574 nm with an extinction coefficient of approximately 25% of the etio complex. Because of this spectral overlap, care must be taken not to introduce errors in porphyrin determinations of processed products by UV-vis spectroscopy. These compounds are represented in Figure 9 as generalized vanadyl porphyrin-type Structures 1 and 2, respectively.

The minimum at 594 nm has not been assigned, but could be further reduction intermediates, 3 and/or 4, or demetalated metallopetroporphyrins (or demetalated reduced metallopetroporphyrins) 5-7. A spectral blue shift has been observed in the reduction sequence of vanadyl tetraphenyl porphyrin (VOTPP) (29). We are not assigning this band to VOetio2H because its intensity varies independently of the 628 nm band.

Table I. Distribution of V Petroporphyrins and Reduced Petroporphyrin Species by UV-Vis Spectroscopy

Sample	572 nm	628 nm	594 nm
California AR No. 3, %	15.0	0.0	0.0
Low Activity Product, %	6.0	1.0	0.5
Inactive Product, %	9.0	3.0	1.0

Table I summarizes the concentrations of the V petroporphyrins and the related reduction compounds from the low activity and the inactive catalyst products. Substantial concentrations of these species are evident, especially for the inactive catalyst product. These reduced species are consistent with literature results (see below) and suggest the demetalation sequence shown in Figure 9. The vanadyl petroporphyrins are reduced to the chlorins in Step I. Because the other intermediates observed in our products have not been unequivocally identified, the speculation of further reduction before demetalation is possible, with the metal finally coming out due to ring strain.

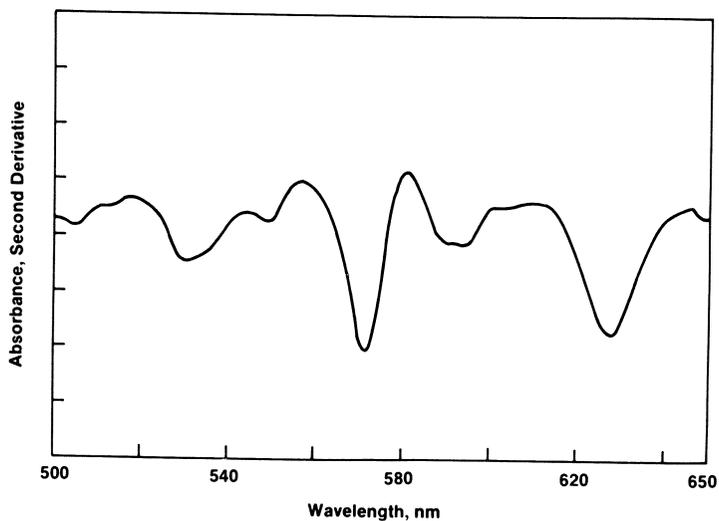


Figure 8. Second Derivative UV-Vis Spectrum from the Low Thermal Severity Treatment of California AR No. 1.

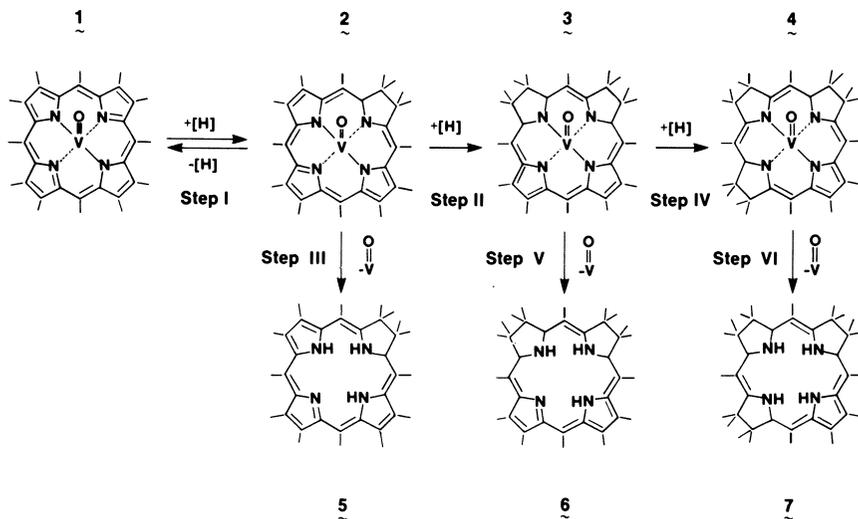


Figure 9. Reaction Sequences and Possible Reaction Sequences for Demetalation of Vanadyl Petroporphyrins in Heavy Residua.

The reduction of vanadyl porphyrins to vanadyl chlorins, Step I, has been well documented for model compounds (14,15,29). Evidence for this has also been seen in reduction of metallopetroporphyrins which have been extracted from Arabian Light vacuum residuum (22). Our results give additional evidence for this step.

The further reduction of vanadyl chlorins to other hydrogenated vanadyl porphyrin forms is a matter of debate. Reduction studies over Co-Mo/Alumina hydroprocessing catalyst of VOetio dissolved in white oil at temperatures from 280 to 350°C and hydrogen pressures of 4.14 to 9.65 MPa show only one intermediate, 2 (15). In contrast, autoclave reactions of VOTPP dissolved in Tetralin at 420°C and 40-50 kg/cm<sup>2</sup> show definite evidence of higher reduction products, with demetalation occurring after the formation of VOTPP6H (29).

The differences in these results can be rationalized. The Co-Mo/Alumina experiments are done in white oil, which is a mixture of saturated hydrocarbons with little hydrogen transfer capacity. The kinetics suggest hydrogen addition, Step I, then demetalation, Step II. When white oil is used as the solvent, hydrogen transfer is poor, and either the tetrahydro species (VOetio4H) is not formed and Step II dominates, or VOetio4H is formed, Step III, and demetalation is observed before further reduction, as in Step IV. (VOetio4H was not observed in the VOetio model compound studies.)

When Tetralin is used as the solvent, hydrogen transfer is good (30), and further reduced species are formed, Step III, then Step V, before demetalation, Step VI. (VOTPP6H was observed in the VOTPP studies.) VOTPP hydrogenation reactions in 1-methylnaphthalene, although not quantitated, also showed the presence of species other than the VOTPP2H intermediate (16).

Residua have many indigenous hydrogen transfer compounds (31) in addition to hydrogen sulfide produced during processing (32). These species contribute to a very rich hydrogen transfer environment during processing of actual feeds. The intermediates which we are observing may be a result of the medium in which the experiments are conducted. We are doing further reactions to verify these observations and separating the reaction products for unequivocal identification.

It must be mentioned, however, the demetalation mechanism is different for different model compounds. Ni meso tetraphenyl porphyrins demetalate in a pathway which resembles the VOTPP pathway, where further reduction intermediates are detected, than the VOetio. Therefore, the VOTPP results could be just a consequence of the choice of model compounds. This still does not account for the minimum at 594 nm. The alternate assignment of this species as a demetalated petroporphyrin would solve the ambiguity. But it has been shown demetalated porphyrin rapidly go to pyrroles (16) in this processing environment and would be very short lived.

### Conclusions

We analyzed the metallopetroporphyrins and the metallo-nonporphyrins during thermal and catalytic upgrading of heavy

residua. By size exclusion chromatography with element specific detection (SEC-ICP), we found thermal treatment reduces the size of the remaining metal-containing compounds, while with certain catalysts, fixed-bed treatment preferentially removes the metal-containing molecules in the size range of the catalyst pore.

For the metallopetroporphyrins, the severity of the thermal or catalytic treatment determines the extent of removal. Moderate thermal treatment appears to completely remove the metallopetroporphyrins, while less severe treatment allows for spectral observation of potential intermediates. Lessening the severity of the fixed-bed catalytic treatment also has a similar effect.

By applying column chromatography and UV-Vis spectroscopy, we have been able to detect and quantify some possible intermediates of the demetalation sequence for vanadyl petroporphyrins under commercial processing conditions with actual feeds. These results are consistent with the demetalation pathway being the reduction of the metallopetroporphyrins to chlorins and other reduced species. These results are in close agreement with metalloporphyrin model compound work reported in the literature.

#### Acknowledgments

We thank Thomas F. Finger for his fine technical assistance, and Chevron Research for supporting this research.

#### Literature Cited

1. Schuetze, B.; Hofmann, H. Hydrocarbon Proc. February 1984, 75-82.
2. Biggs, W. R.; Fetzer, J. C.; Brown, R. J.; Reynolds, J. G. Liq. Fuels Tech. 1985, 3 (4), 397-421.
3. Treibs, A. Ang. Chem. 1936, 49, 682-686.
4. Fish, R. H.; Komlenic, J. J. Anal. Chem. 1984, 56, 510-517.
5. Fish, R. H.; Komlenic, J. J.; Wines, B. K. Anal. Chem. 1984, 56, 2452-2460.
6. Reynolds, J. G. Liq. Fuels Tech. 1985, 3 (1), 75-105.
7. Reynolds, J. G.; Biggs, W. R.; Fetzer, J. C. Liq. Fuels Tech. 1985, 3 (4), 423-448.
8. Reynolds, J. G.; Gallegos, E. J.; Fish, R. H.; Komlenic, J. J. Submitted Energy and Fuels 1986.
9. Reynolds, J. G. Submitted Energy and Fuels 1986.
10. McCormick, B. J. Inorg. Chem. 1968, 7 (10), 1965-1970.
11. Shiro, M.; Fernando, Q. Chem Comm. 1971, 63-64.
12. Stoklosa, H. J.; Wasson, J. R.; McCormick, B. J. Inorg. Chem. 1974, 13 (3), 592-597.
13. Vigeo, G.; Selbin, J. J. Inorg. Nucl. Chem. 1969, 31, 3187-3194.
14. Hung, C. W.; Wei, J. Ind. Eng. Chem. Process Des. Dev. 1980, 19 (2), 257-283.
15. Agrawal, R.; Wei, J. Ind. Eng. Chem. Process Des. Dev. 1984, 23, 505-514.
16. Rankel, L. ACS Div. of Petrol. Chem., Preprints 1981, 26 (3), 689-698.

17. Ware, R. A.; Wei, J. ACS Div. of Petrol. Chem., Preprints 1985, 30 (1), 62-69.
18. Webster, I. A.; Wei, J. ACS Div. of Petrol Chem., Preprints 1985, 30 (1), 37-49.
19. Ware, R. A.; Wei, J. J. of Catal. 1985, 93, 100-121.
20. Ware, R. A.; Wei, J. J. of Catal. 1985, 93, 122-134.
21. Hung, C. W.; Wei, J. J. Ind. Eng. Chem. Process Des. Dev. 1980, 19 (2), 250-257.
22. Rankel, L.; Rollmann, L. D. Fuel 1983, 62, 44-46.
23. Gould, K. A. Fuel 1980, 59, 733-736.
24. Sugihara, J. M.; Branthaver, J. F.; Willcox, K. W. ACS Div. of Petrol. Chem., Preprints 1973, 18, 645-647.
25. Reynolds, J. G.; Biggs, W. R. Fuel Sci. Tech., Int.'1 1986, 4 (5), 593-619.
26. Boduszynski, M. M. ACS Div. of Petrol. Chem., Preprints 1985, 30 (4), 626-630.
27. Sundararaman, P. Anal. Chem. 1985, 57, 2204-2206.
28. Bonnett, R.; Brewer, P.; Noro, K.; Noro, T. Tetrahedron 1978, 34, 379-385.
29. Kameyama, H.; Yamada, M.; Amano, A. J. Japan Petrol. Inst. 1981, 24 (5), 317-321.
30. Pratt, K. C.; Christoverson, V. Fuel 1982, 61, 460-462.
31. Payzant, J. D.; Hogg, A. M.; Montgomery, D. S.; Strausz, O. P. AOSTRA J. of Res. 1985, 1 (3), 175-182.
32. Lambert, Jr., J. M. Fuel 1982, 61, 777-778.

RECEIVED October 30, 1986

## Chapter 14

# Upgrading Studies with Californian, Mexican, and Middle Eastern Heavy Oils

Geoffrey E. Dolbear, Alice Tang, and Eric L. Moorehead<sup>1</sup>

Unocal Science and Technology Division, Fred L. Hartley Research Center,  
376 South Valencia, Brea, CA 92621

Conversions of the ever-increasing amounts of heavy crudes into transportation fuels is a challenge facing all refiners. Hydroprocessing is one route to meet this challenge, and new technology permits the upgrading of heavy oils from a variety of sources.

One parameter rarely discussed in studies of heavy oil upgrading is the differences in chemical nature of the various oils. It is usually assumed, incorrectly, that it is more difficult to treat oils with higher levels of contaminants and lower API Gravities. This paper reports detailed comparisons of the measured chemical compositions of oils from California, Mexico, and the Middle East, along with their reactivities in Unocal's Unicracking HDS process. Reactivity for removing nickel and vanadium was found to be a function of the distribution of metals between asphaltenes and resins, while sulfur reactivity was independent of these patterns.

Refiners are all facing the challenge of converting increasing amounts of heavy crude oils into transportation fuels. Many processes have been developed to meet this challenge. The process schemes fall into two categories, those that remove carbon and those that add hydrogen. Unocal's Unicracking/HDS process is an example of the latter.

One factor that is often overlooked in these upgrading schemes is the difference in chemical reactivities of heavy oils. Because the chemical makeup of heavy oils is complex, finding out what controls reactivity is not simple. In the past several years we have studied the reactivity of over thirty crude oils. This paper presents some of our results for oils from California, Mexico, and the Middle East. We found that gross properties such as gravity and

---

<sup>1</sup>Current address: Engelhard Corporation, Specialty Chemicals Division, Menlo Park, P.O. Box 2900, Edison, NJ 08818-2900

sulfur content are not good predictors of hydroprocessing behavior. We will discuss some of the properties that do relate to reactivities.

### Heavy Oils - What Are They?

Heavy Oil is a non-specific term that applies to crude oils with API gravity less than 20 (1). Within this definition there is a wide range of compositions and physical properties. Heavy oils typically have high levels of sulfur, nitrogen, nickel and vanadium, and are rich in the condensed polyaromatic compounds which react readily to form coke. Many of the processes used in refineries rely on catalysts which are poisoned or destroyed by these components and refiners see them as impurities to be eliminated. Refineries are designed to eliminate these components from the liquids to protect the catalysts as well as to produce environmentally acceptable products.

By convention, the fraction of a crude oil which boils above 650°F (343°C) is called atmospheric resid. Refineries typically make their initial distillation cut at this temperature; a second cut is made at about 1050°F (565°C), the 1050°F-plus products called vacuum resid (or vacuum tower bottoms, VTB) and the intermediate boiling range liquids (650-1050°F) called vacuum gas oil (VGO). Refinery conversion units are specifically designed to handle these boiling range liquids.

Atmospheric resid can be separated into three components on the basis of polarity or solubility. These components, in roughly increasing polarity and molecular weight, are called oils, resins, and asphaltenes. The combination of oils and resins is also referred to as maltenes. It is generally accepted that the resin portion contains asphaltene-like molecules which serve as a solvent for the asphaltenes in the less polar oil portion. Koots and Speight (2) demonstrated this by separating the three fractions and recombining them. The asphaltene was only soluble in the presence of the resin fraction.

Number average molecular weights of resins are generally lower than those of asphaltenes and their sulfur, nitrogen, and metals levels are generally lower. Typically resins range from 600-5000 in molecular weight and contain 10-20% of the metals, 50-70% of the sulfur and contain 50-70% of the nitrogen. Up to 50% of the 1050°F-plus (565°C-plus) fraction will be asphaltenes.

Asphaltenes have molecular weights ranging from 5000-10000 and contain 80-90% of the metals, 2-20% of the sulfur and nitrogen. Yen (3) has proposed a structural model of asphaltenes which describes them as stacks of sheets or plates, rather than long chains like conventional polymers (Figure 1). More recent work (4,5,6) implies that, under proper solvent and temperature conditions, the sheets can separate from the stacks and move about the solution individually. This behavior further complicates asphaltene chemistry.

### Unicracking/HDS Technology

Unocal's Unicracking/HDS process is a proprietary fixed bed, catalytic hydrotreater designed for upgrading heavy oils. It was

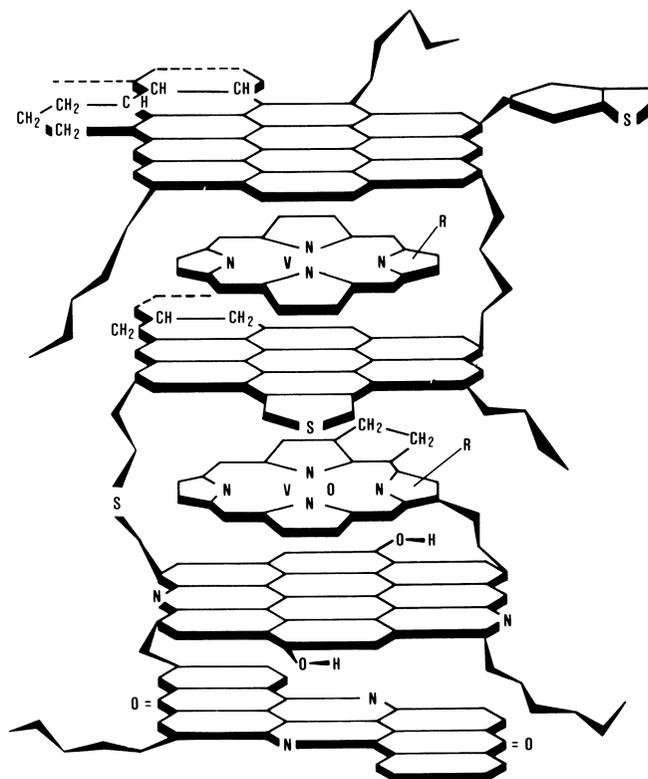


Figure 1. Hypothetical Asphaltene Partial Molecule.

originally developed for producing low sulfur fuel oil from low metals-containing oils, but UK/HDS has evolved into a flexible process capable of upgrading high metals feedstocks. Depending on the individual refiner's needs, the process can operate in either a high or low conversion mode. Conversion refers to the extent of 1050°F-plus (565°C) converted into distillates. In either mode the product oil has substantially reduced levels of sulfur and metals.

### Experimental

In this study a pilot plant unit using an experimental demetallization catalyst was used. The operation was carried out under moderate pressure but at relatively low temperatures. Each test feed was alternated with our reference oil, and reactivity was calculated relative to it. We chose Heavy Arabian as our reference because it is widely available. This method accounts for changes in catalyst activity caused by metals, sulfur, or carbon depositing on the catalyst. We verified this by testing a blend of California and Alaska oils at the beginning of our feed study and again later in the run. We found that the reactivity remained constant relative to Heavy Arabian.

The study tested more than thirty oils. We will discuss the results for five of these oils:

Heavy Arabian,

California-Alaska blend, consisting of 50% North Slope, 35% Santa Maria, and 15% LA Basin oils,

Hondo, a large California offshore field north of Santa Barbara,

Maya, a Mexican heavy crude processed by a number of U.S. refiners, and

Gach Saran, a heavy Iranian crude processed almost as widely as Heavy Arabian.

The discussion will center on these oils because, except for the Blend, they are generally available. The conclusions are supported by the results from the other crudes in the study.

All measurements and reactions were done with 650°F-plus (343°C-plus) fractions (Table I) except for Hondo, where high viscosity forced us to use 400°F-plus (204°C-plus) liquids. Wherever appropriate, ASTM methods were used in measuring compositions. Asphaltenes were isolated by pentane precipitation, resins by absorption on a column of attapulgas clay and elution with dichloromethane.

Reactivity is defined as the rate constant under constant conditions for sulfur or metals removal. The values we report are relative to our reference Heavy Arabian, defined as 100 in each case.

Table I. Properties of Heavy Oils

	Hvy. Arab.	Hondo	Maya	Gach Saran	Blend
Gravity, °API	12.6	13.4	9.4	15.6	11.3
Total Ni + V, wppm	115	372	496	144	222
Ni, wppm	28	92	83	36	67
V, wppm	87	280	413	108	155
Total Sulfur, wt%	4.23	5.10	4.42	2.60	2.77
Total Nitrogen, wt%	0.26	0.70	0.52	0.41	0.67
1050°F-plus, wt%	51	46	59	50	50
Conradson Carbon, wt%	12.6	10.8	15.3	8.8	11.0
Asphaltenes (C-5), wt%	12.6	13.9	25.2	6.8	11.4

### Properties and Reactivities

The key to the experiment was a thorough and detailed set of characterization data for each feed and treated product.

**Properties.** There is a great variation in the bulk chemical and physical properties. If we look at these oils closely, we can see differences in the relative amounts of oils, resins, and asphaltenes (Table II and Figure 2). The biggest differences between the samples is in the relative amounts of oils, and asphaltenes.

Table II. Oils, Resins and Asphaltenes in Heavy Oils

	Hvy. Arab.	Hondo	Maya	Gach Saran	Blend
Oil Fraction, wt %	59.9	43.9	48.9	64.7	52.6
Resin Fraction, wt%	27.5	40.2	25.9	28.5	36.0
Asphaltenes (C-5), wt%	12.6	13.9	25.2	6.8	11.4

We can go farther and examine the distribution of sulfur and metals (nickel plus vanadium) among the oils, resins and asphaltene fractions. The data (Table III and Figures 3 and 4) show that the 5

Table III. Distribution of Nickel, Vanadium and Sulfur in Heavy Oils

	Hvy. Arab.	Hondo	Maya	Gach Saran	Blend
<b>Oil Fraction</b>					
Sulfur, wt%	2.76	2.97	2.59	1.74	1.86
Ni + V, wppm	0	2.4	1	0	0
Ni, wppm	0	2.4	1	0	0
V, wppm	0	0	0	0	0
<b>Resin Fraction</b>					
Sulfur, wt%	5.92	6.70	5.39	4.19	3.51
Ni + V, wppm	83	238	233	241	200
Ni, wppm	25	83	45	64	70
V, wppm	58	155	188	177	130
<b>Asphaltene Fraction</b>					
Sulfur, wt%	6.53	7.73	6.44	5.11	3.76
Ni + V, wppm	656	1547	1887	1466	1235
Ni, wppm	158	417	317	366	345
V, wppm	498	1130	1570	1100	890

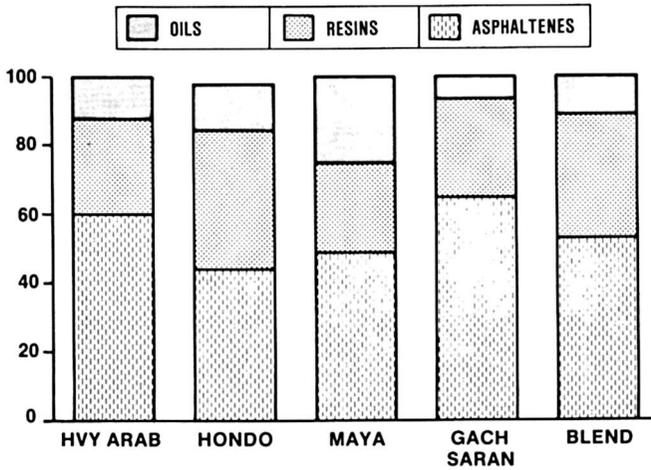


Figure 2. Oils, Resins, and Asphaltenes.

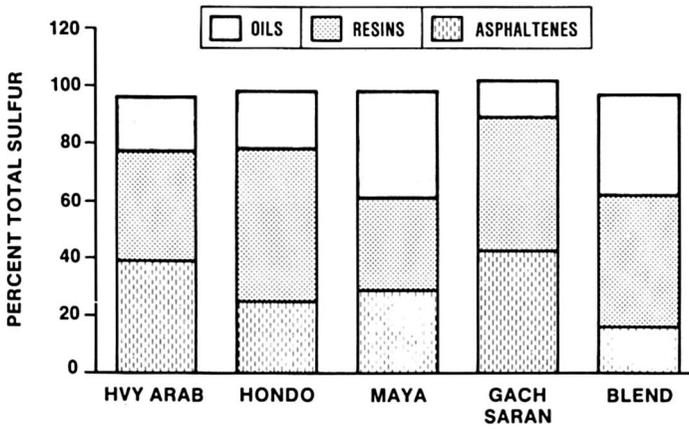


Figure 3. Sulfur Distributions in Oils, Resins, and Asphaltenes.

oils have significantly different bulk properties, and the distributions of the contaminants among the oils, resins, and asphaltenes are also different.

Reactivities. With this wide range of properties, it is not surprising that reactivities vary widely. Sulfur relative reactivities vary by more than a factor of two (Table IV, Figure 5). Gach Saran, the Blend, and Hondo are about twice as reactive as Heavy Arabian, and Maya is slightly more reactive. Both Maya and Hondo have more sulfur than Heavy Arabian.

One may suppose that metals reactivities are similar to sulfur reactivities. But that is not true (Table IV and Figure 6). Hondo and Gach Saran are still much more reactive than Heavy Arabian, the

Table IV. Reactivities of Heavy Oils

	Hvy. Arab.	Hondo	Maya	Gach Saran	Blend
HDS	100	179	116	206	188
HDM	100	157	45	168	85

Blend is about the same, and Maya is considerably less. Not only do sulfur and metals reactivities not correlate (Figure 7), but the metals and sulfur content cannot predict reactivities.

When we tested for reactivity effects in the distribution of metals, we found that demetallization reactivities increase with increasing fraction of metals in the resins fractions (Figure 8). However, we found no correlations with the distribution of sulfur among the oils, resins, and asphaltenes fractions.

We also measured reductions of asphaltenes and Conradson Carbon. The results are presented as percent conversion. In general (Table V, Figure 9) the feeds behave similarly, probably because these conversions are very sensitive to temperature, which was the same for all five oils.

Table V. Conversion of Asphaltenes and Carbon Residue

	Hvy. Arab.	Hondo	Maya	Gach Saran	Blend
Asphaltene Conv. %	57	63	52	54	55
CCR Conv. %	41	52	32	47	32

While conversions of the asphaltenes and associated carbon residue are similar, conversions of 1050°F-plus material to distillates (Table VI) shows a much wider variation. When the

Table VI. VGO and Vacuum Resid in Feed and Product Oils

	Hvy. Arab.	Hondo	Maya	Gach Saran	Blend
1050°F-plus, wt%					
Feed	51	46	59	50	50
Product	46	34	58	34	47
Conv. %	10	27	0	31	5
650-1050°F, wt%					
Feed	44	36	37	44	47
Product	48	40	33	54	45

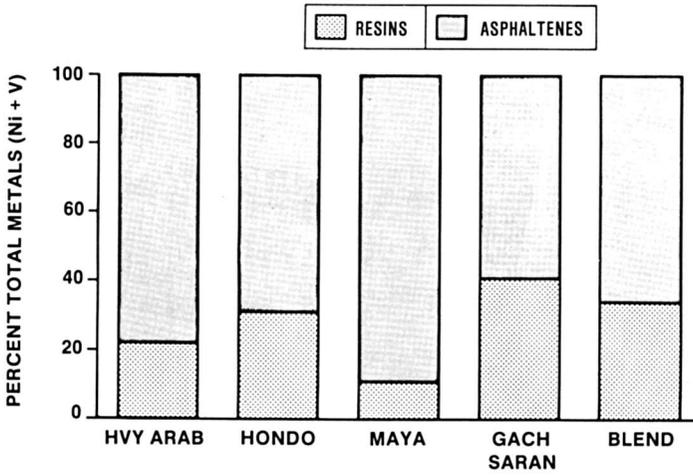


Figure 4. Metals Distributions in Oils, Resins, and Asphaltenes.

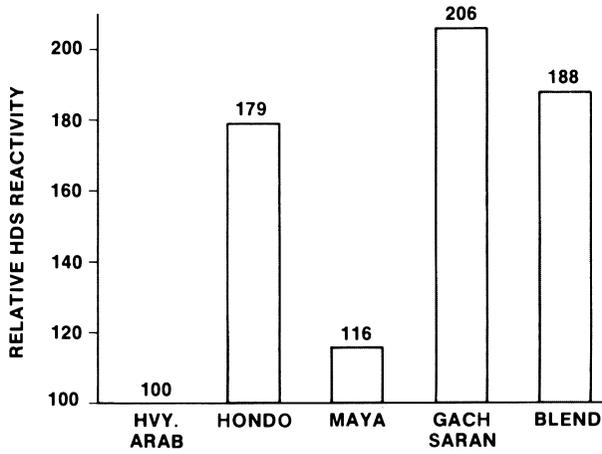


Figure 5. Relative Sulfur Reactivities.

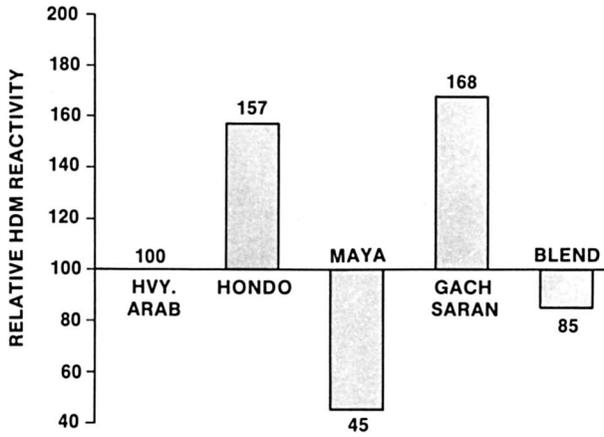


Figure 6. Relative Metals Reactivities.

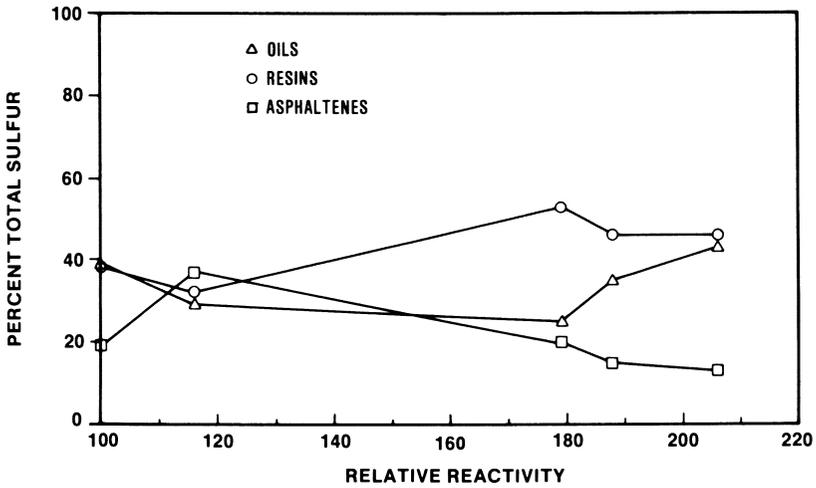


Figure 7. Sulfur Reactivity and Sulfur Distribution.

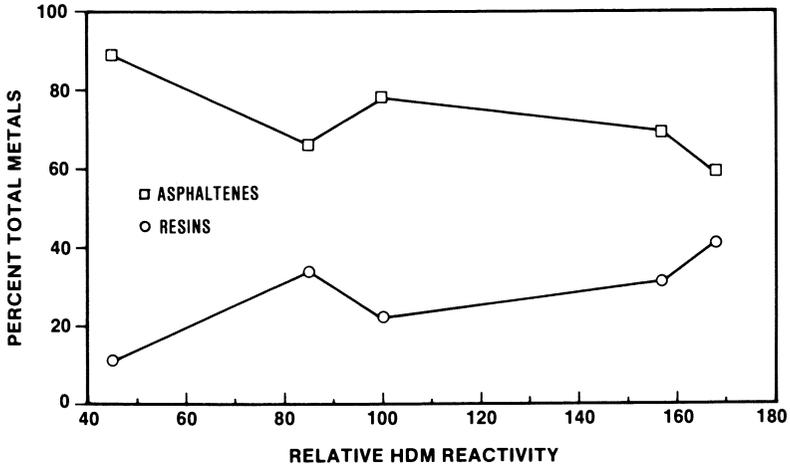


Figure 8. Metals Reactivity and Metals Distribution.

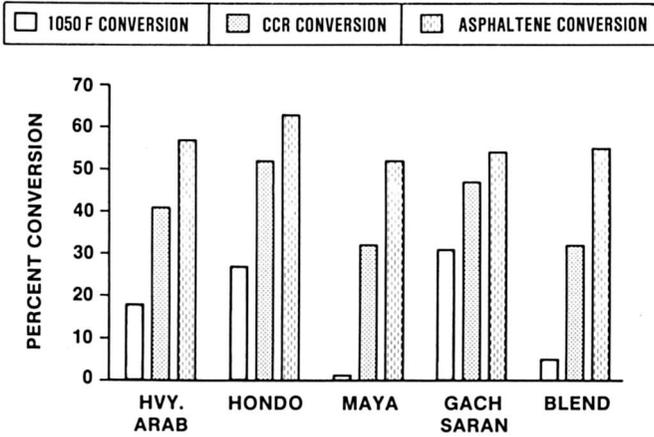


Figure 9. Conversions of 1050°F-Plus, Conradson Carbon, and Asphaltenes.

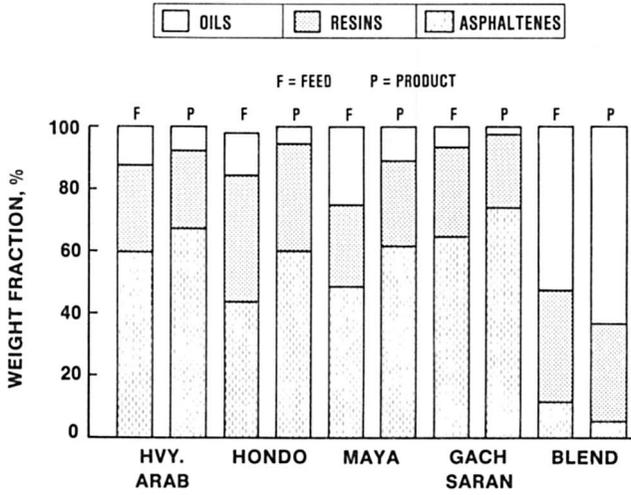


Figure 10. Oils, Resins, and Asphaltenes in Feeds and Products.

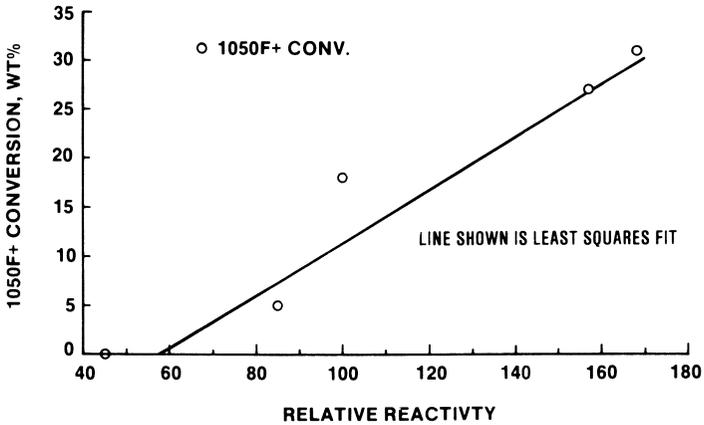


Figure 11. Metals Reactivity Predicts 1050°F-Plus Conversions.

material boiling above 1050°F is converted to lighter materials, it does not necessarily result in an increase in VG0, the cut boiling between 650-1050°F (Table VI). The simplest explanation for this behavior is that VG0 is being converted to distillates boiling below 650°F as rapidly as it is being formed.

This interpretation is supported by results with the Blend: it had 6% 1050°F-plus conversion but the 650-1050°F conversion was higher, resulting in a net decrease in the VG0 fraction. Maya showed this behavior to a greater extent, with no 1050°F-plus conversion and 4% of the 650-1050°F fraction converted into lighter materials. The other feeds showed an increase in the 650-1050°F fraction.

Maya presents us with unique behavior. Both Conradson Carbon and asphaltenes decrease, but there is no measurable 1050°F-plus conversion. When the asphaltenes in Maya react, they may be converted into the lower molecular weight, less polar resins and oils (7), just as the other feeds (Figure 10). But with Maya, these resins and oils are so large that they still boil above 1050°F.

These results also show that, for both the Blend and Maya, the 1050°F-plus fraction is very refractory. These two feeds were also the least reactive for metals removal. When we plot 1050°F-plus conversion versus metals reactivity (Figure 11) we find a definite relationship. This is not too surprising because all the metals are in the 1050°F-plus fraction. It implies that demetallization and cracking are related processes. And a refractory 1050°F-plus material like Maya will also be difficult to demetallize.

Takeuchi and coworkers (8) compared reactivities for several resids in Chiyoda's asphaltene cracking process. They found that metals removal reactivities for five vacuum resids were roughly proportional to total metals levels. This relationship did not hold for asphaltene removals or, apparently, for sulfur.

Based on the bulk physical and chemical properties we could not have predicted our observations. A more detailed chemical analysis of the molecular species present in these oils is needed before we can explain all our reactivity data.

### Conclusions

We have shown that five heavy oils behave differently under hydro-processing and their reactivities cannot be predicted from the levels of contaminants. The factors that control the reactivities are complex and not completely understood. For nickel and vanadium, we have shown a relationship between reactivity and the weight fraction of these metals in the feed resins. We also find that 1050°F-plus conversion is related to metals reactivity.

### Literature Cited

1. Byramjee, R. J. Oil and Gas J., 4 July 1983, 78.
2. Koots, J. A.; Speight, J. G. Fuel 1975 54, 179.
3. Dickie, J. P.; Yen, T. F. Anal Chem 1967 39, 1847.
4. Richardson, R. L.; Alley, S. K. ACS Symposium Series 20, 1975.

5. Moschopedis, S. E.; Fryer, J. F.; Speight, J. G. Fuel 1976, 55, 227.
6. Speight, J. G.; Moschopedis, S. E. In Chemistry of Asphaltenes; Bunger, J. W.; Li, N. C., Eds.; Advances in Chemistry Series No 195; American Chemical Society: Washington, DC, 1981; p 1.
7. R. B. Long, In Chemistry of Asphaltenes; Bunger, J. W.; Li, N. C., Eds.; Advances in Chemistry Series No 195; American Chemical Society: Washington, DC, 1981; 17.
8. Takeuchi, C.; Fukui, Y.; Nakamura, M.; Shiroto, Y. Ind. Eng. Chem. Process Des. Dev. 1983, 22, 236; Asakoa, S.; Nakata, S.; Shiroto, Y.; Takeuchi, C. ibid, 1983, 22, 242.

RECEIVED November 24, 1986

## Chapter 15

# Modes of Operation in Hydrodemetallization

Frits M. Dautzenberg and Jacques C. De Deken

Catalytica, 430 Ferguson Drive, Building 3, Mountain View, CA 94043

Some important chemical and engineering principles are examined in this paper to provide a basis for comparing various bottom-of-the-barrel process alternatives. The extent of how successfully the various hydroconversion approaches can cope with asphaltene conversion and metal removal is examined. Typical representative hydrogen-addition technologies are compared, including fixed-bed (FBR), back-mixed (BMR), and liquid-phase reactor approaches. The emphasis on catalysis for these approaches varies widely. Noncatalytic thermal (hydro-) demetallization appears to be the most attractive approach from an economic standpoint for stand-alone, grass-roots situations. BMR technology comes in second place, and FBR technology is third. Taking into account the sequence of historical developments and the apparent relation between economic attractiveness and the use of catalysis, the fundamental reasons for the observed trends are discussed.

Some important chemical and engineering principles are examined in this paper to provide a basis for comparing various process alternatives for the conversion of the "bottom-of-the-barrel." Key economic issues are highlighted to facilitate the discussion.

Coking is presently the most widely used primary upgrading process. In coking, a significant fraction of the feed, however, is converted to gas and coke. Hydroconversion offers the potential of complete or nearly complete recovery of the feed, including the asphaltene coke precursors. Hydroconversion using extended conventional technology has not become competitive with coking, however, mainly because of the presence of vanadium and nickel in the asphaltenes. In thermal hydroconversion, the removal of metals also plays an important role. The extent of how

successfully the various hydroconversion approaches can cope with asphaltene conversion and metal removal is discussed in this paper. For catalytic approaches, a sound knowledge of kinetic behavior as a function of the reactor system is important in selecting the best catalyst-reactor system combination.

#### Historic and Economic Perspective

At equivalent liquid product demand, a lower crude intake is required for hydroconversion than for carbon-rejection technologies. Within hydrogen-addition processes, a wide range of approaches is possible. Various representative hydrogen-addition technologies are compared in Table I. The Shell-Hydrodemetallization/Hydroconversion (HDM/HCON) process (1) was selected as representative of the fixed-bed reactor (FBR) residue hydroprocessing approaches. In this case, trickle-flow reactors are used throughout. Back-mixed reactors (BMR) are used by H-Oil and LC-Fining (2,3). The ebullating-bed technologies are catalytic with respect to desulfurization and demetallization, but are thermal with respect to conversion. As indicated in Table I, the emphasis on catalysis ranges from zero catalyst holdup for the Veba-Combi-Cracking process to a maximum for the Shell-HDM/HCON process. Noncatalytic thermal hydrocracking is applied by the Veba-Combi-Cracking process (4) using liquid-phase reactors. In the three slurry-phase processes (5-7), the metals from the feedstocks are removed by adsorption on finely divided catalysts or additives, ending up in a concentrated form in the reactor bottom product.

It is interesting to note that the Veba process--with a noncatalytic approach--probably has the longest developmental history, followed by Shell, which is 100% catalytic. Subsequent to these two technologies, the ebullating-bed reactors and, more recently, the slurry-phase processes, were developed, all of which represent a shift away from catalysis and a lowering of catalyst holdup in the reactor. The most recently proposed technology, the Gulf-Donor-Refined Bitumen (DRB) process (8), is a liquid-phase technology like the Veba Combi-Cracking process. Thus the historical development path has followed a complete cycle.

The question arises whether it is justified to conclude that for heavy oil upgrading and the associated demetallization, the noncatalytic thermal hydrocracking route is indeed the most appropriate one, as suggested by history. To provide an answer to this question, a qualitative economic assessment was prepared to compare the three advanced hydrogen-addition technologies listed in Table I. Flexicoking was included for the sake of completeness, since it is the most advanced carbon-rejection technology. A 150,000-bbl/day synthetic crude plant was assumed, which uses Canadian tar sands bitumen as feedstock. Each upgrading complex contains a primary unit, followed by complementary secondary hydrotreating to yield a synthetic crude of about equal composition and quality, comparable to the synthetic crude presently manufactured at commercial scale in Canada (9). Natural gas is used for hydrogen manufacturing and

for supplementary fuel if required. A 20-year project life, a 50% tax rate, and a 10% declining balance for depreciation were assumed.

The relative positions of the four technologies are indicated in Figure 1 using relative scales from 0 to 100 for capital investment, total manufacturing costs, gross profit (before tax), and return on investment (after tax). All hydrogen-addition processes are less capital intensive and higher in operating costs than Flexicoking. High operating costs, however, are largely compensated by the higher yields of the hydrogen-addition processes. Relevant to this discussion is the fact that the noncatalytic thermal hydrocracking route (Veba-Combi-Cracking) is most attractive, followed by the BMR technologies (ebullating-bed, H-Oil), and then the extended conventional FBR technology (Shell-HDM/HCON). An equal ranking is obtained if catalyst holdup is used as a measure.

Taking into account the sequence of historical developments and the apparent relation between economic attractiveness and the use of catalysis, a study was started to investigate whether there are fundamental reasons for the observed trends. Will noncatalytic hydrothermal processes always be superior, or are there applications where catalytic hydroprocessing/demetallization is preferable? These questions are addressed in subsequent sections of this paper. It is noteworthy that development of the emerging technologies mentioned in Table I (M-Coke, CANMET, and Aurabon) is warranted and consistent with the observed trends. Similar to Veba-Combi-Cracking, thermal hydrocracking is applied as the basic conversion principle; these emerging technologies all have low catalyst holdups and the metals are finally removed from the system as a small "drag-stream" in one way or another. This is not a coincidental observation, but is based on sound chemistry principles as explained in the next section.

#### Asphaltene Conversion and Demetallization

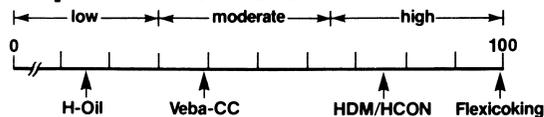
The exact nature of asphaltenes in residual oil fractions is not clear. The asphaltene content is defined as the material that precipitates when the oil is mixed with a light straight-chain aliphatic solution, usually pentane (10). Molecular weight determinations have indicated a broad range of sizes of asphaltenes ranging from 600-140,000 g/mole (11). Hall and Herron (12) reported that the average size of asphaltene is approximately 60-90 Å. Their data further confirm that the majority of the heteroatoms is concentrated in the asphaltenes. Asphaltenes seem to form micellar structures in the oil; these structures can decompose to an extent dependant on the solvent environment and the temperature (13). Asphaltenes as such are dark brown solids and insoluble in the oil fractions. Due to the presence of resins, they remain dispersed in the oil medium. The degree of aromaticity and the proportion of heteroatoms in the resins appear to determine the solubilizing power of the resins. A hypothetical asphaltene structure is shown in Figure 2 (14). The stacking of aromatic plates to form the micellar agglomerates is shown in Figure 3.

Table I. Comparison of Various Hydrogen-Addition Approaches

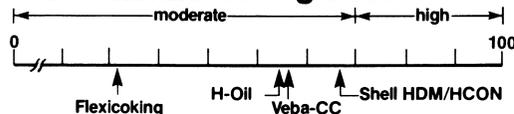
Reactor Technology:	Liquid-Phase	Slurry-Phase	Ebullating-Bed	Trickle-Bed
Well-developed Technologies:*	Veba-Combi-Cracking		H-Oil LC-Fining	Shell-HDM/ HCON
Developing Technologies:*	Gulf-DRB	CANMET Aurabon M-Coke		
Conversion:	← Thermal hydrocracking →			Catalytic
Desulfurization:	← Catalytic →			
Metal Removal:	Concentrated in reactor bottoms	"Adsorbed" on catalyst/additive in reactor bottoms	Catalytic	Catalytic
Catalyst Holdup:	Zero	Low	Medium	Maximum

\*See the Appendix for brief process characterizations.

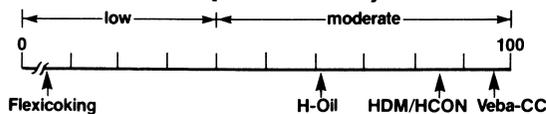
### 1. Capital Investment



### 2. Total Manufacturing Cost



### 3. Gross Profit (before tax)



### 4. Return on Investment (after tax)

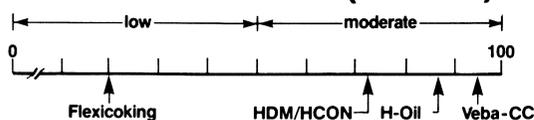


Figure 1. Relative Economics for Various Upgrading Processes.

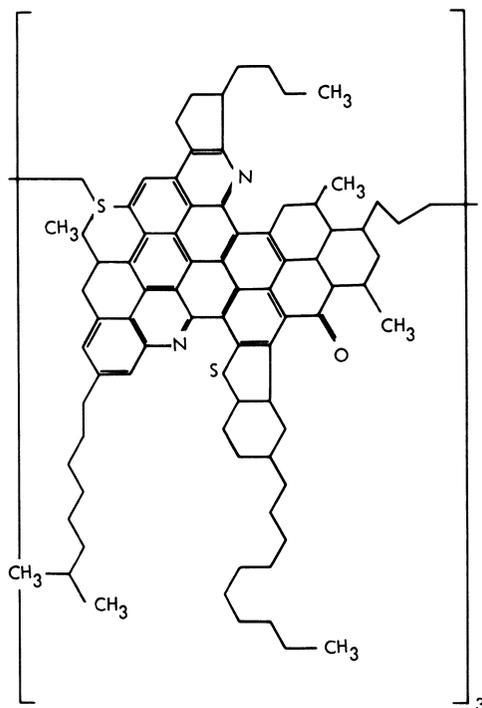


Figure 2. A Hypothetical Asphaltene Structure from Venezuelan Crude Oil. (Reproduced with permission from Ref. 14. Copyright 1980 Marcel Dekker, Inc.)

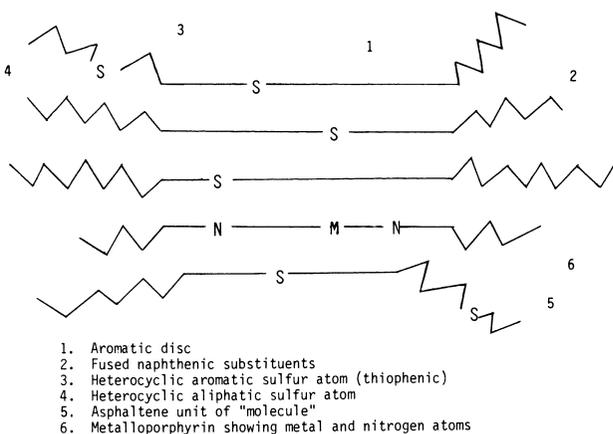
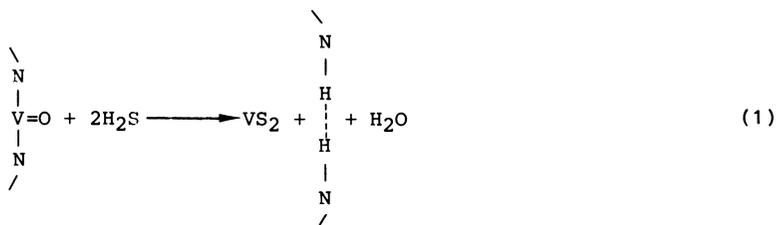
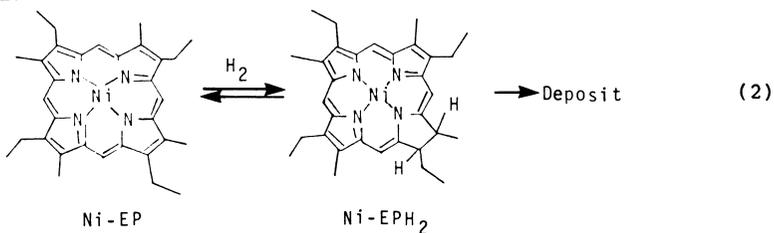


Figure 3. Hypothetical Structure for an Asphaltene "Particle". (Reproduced with permission from Ref. 13. Copyright 1972 ACS.)

Metalloporphyrins have been identified as the major metal-containing species in residues (15). Usually the vanadium and nickel complexes are square pyramids with four donor (N) atoms situated coplanar in the basal planes. The tetrapyrrolic aromatic structures in porphyrins are similar to the aromatic sheets in the asphaltenes. For this reason porphyrins can be incorporated readily into the asphaltene micelles (Figure 3). It is well known that sulfur can be coordinated strongly as a donor atom to vanadium as well as to nickel. Consequently, it is reasonable to expect that the covalent metal-nitrogen bonds are weakened in the presence of  $H_2/H_2S$ . This can lead to demetallization of the porphyrins according to Equation 1:



Wei and co-workers (16-18) have shown that coordination with sulfur is not a requirement. They showed in their model experiments that metalloporphyrin demetallization occurs via a sequential mechanism involving initial hydrogenation of peripheral double bonds to activate the porphyrin, followed by a thermal hydrogenolysis step which fragments the molecule and removes the metal:



These two reactions can be accelerated by absorbing the porphyrins on the surface of a catalyst or by providing sufficient thermal energy. With actual residue feedstocks, a high hydrogen partial pressure will be required to suppress coke formation.

Demetallization and S, N, and O removal are therefore proposed to be the main reactions related to asphaltene conversion (19). A model of asphaltene cracking is shown in Figure 4. Reaction "a" represents the destruction of the asphaltene micelles and the removal of the metal component (demetallization). Subsequently, further molecular weight reduction occurs (reaction "b") by the removal of heteroatoms such as sulfur. Following this model, deep demetallization and desulfurization followed by hydrocracking of the products are required to achieve substantial asphaltene conversion. The proposed mechanism suggests that without demetallization of the asphaltenes, deep conversion of the bottom-of-the-barrel fraction becomes impossible.

Basic Process Selection Considerations

In catalytic hydroprocessing studies, Takeuchi (20) showed that the average molecular weight of the aromatic sheets in the liquid product was hardly influenced. Consistent with the above model, this means that cracking takes place without attacking the individual aromatic sheets. It is further observed that the nitrogen left in the resulting product molecules is very refractory, another indication that the aromatic sheets and demetallized porphyrins have not been attacked. Another problem with a catalytic approach is asphaltene flocculation. This occurs because during catalytic processing at 380-400°C, resins crack faster than asphaltenes, which disturbs the solubility equilibrium between them. The latter problem has been observed in many catalytic experiments at moderate overall conversions.

Under thermal hydroprocessing conditions at temperatures above 430°C (4-7), noncatalytic demetallization takes place as a result of sulfur-metal coordination and the attack of the nitrogen-metal bonds by activated hydrogen. At these elevated temperatures, asphaltene and resin conversion takes place in parallel and no asphaltene flocculation occurs. Moreover, the aromatic sheets as well as the base porphyrins are cracked, which means that the nitrogen compounds left in the product are considerably less refractory. Overall, much higher conversions can be achieved than during catalytic hydroprocessing. Consequently, noncatalytic thermal hydrocracking is the most suitable way to achieve high conversions and metal removal.

In situations where demetallization and desulfurization are prime requirements (as opposed to conversion), catalytic processing, however, may still be a preferable option. The following discussion is presented to illustrate this point. Using the total investment for the Flexicoking case (see Historic and Economic Perspective section) as a reference base, the distribution of the capital investments for the installed equipment in the various parts of the upgrading complex has been plotted in Figure 5. Off-site costs are about the same for each hydrogen-addition technology.

However, the distribution between primary and secondary upgrading facilities varies significantly. This different investment distribution becomes significant if one of these schemes is integrated into an existing refinery processing scheme. In such a case, part of the secondary facilities might already be in place or could be accommodated by retrofitting or debottlenecking existing facilities. In such situations, the Veba process may not be the preferred one. Indeed, the H-Oil process may be more attractive, assuming, for example, that all secondary units exist. The Shell-HDM/HCON and Flexicoking processes will be about equally attractive. Clearly, a general conclusion cannot be reached as can be done for the stand-alone, grass-roots bitumen-upgrading complex considered previously. Each refinery retrofit must be studied in detail to determine which process can be tailored to best match existing facilities. Parameters to be considered in selecting the best catalyst-reactor combination will be developed and presented in the subsequent section.

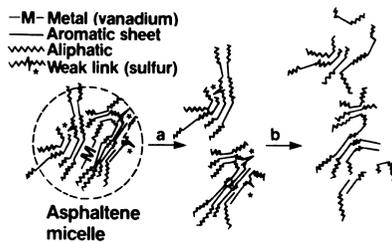


Figure 4. Model of Asphaltene Cracking. (Reproduced with permission from Ref. 19. Copyright 1983 ACS.)

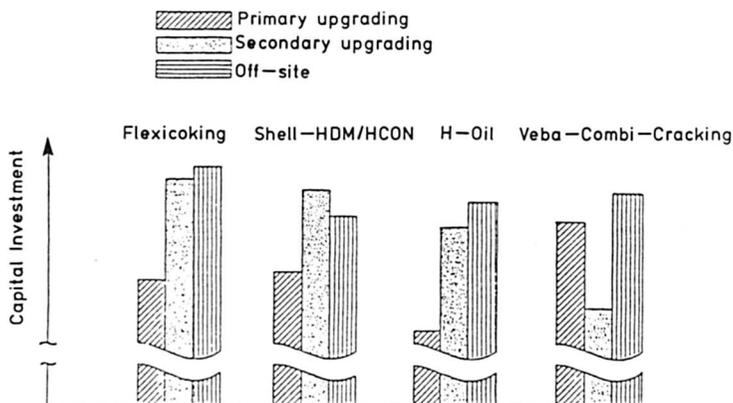


Figure 5. Capital Investment Distributions for a Stand-Alone, Grass-Roots Upgrading Complex Using Various Technologies.

Apparent Kinetics of Contaminant Removal

In order to assess the merits of the conventional reactor technologies for metal and sulfur removal, the apparent kinetics of hydrometallization and hydrodesulfurization in the different reactor systems involved must be understood. In view of the great variety of metal- and sulfur-containing compounds in heavy crudes, it is reasonable to state that their hydrometallization and hydrodesulfurization take place through complex networks of both parallel and consecutive irreversible reactions (21,22). Even when pseudohomogeneous first-order kinetics are believed to apply individually to each contaminant-containing compound, the differences in reactivity between the different metal-containing (16,23,24) and sulfur-containing (25,26) compounds no longer justify the use of simplified first-order kinetics to describe the global contaminant (S- and metal-containing compounds) removal from the feedstock (22). The early depletion of the more reactive compounds and the slower disappearance of the more refractive compounds in the reactor artificially result in global reaction orders greater than one (22,27,28), provided a power law rate model still applies. Theoretical substantiation of such observations have been presented by several authors (29-33).

The applicability of a constant-order, power law rate model to the overall removal of contaminant over a sufficiently wide range of operating conditions presupposes, however, the validity of some underlying assumptions. For a plug flow behavior, for instance, it can be shown that its applicability strictly requires that all contaminant-containing compounds individually react according to irreversible first-order kinetics and that the distribution of their reactivities closely obeys a gamma distribution. If  $x(t,k)$  denotes the fraction of material with rate-constant in the interval  $(k, k + dk)$  at time  $t$ , the continuity equation for irreversible first-order reaction of this fraction can be written as (see List of Symbols):

$$\frac{\partial}{\partial t}x(t,k) = -kx(t,k) \quad (3)$$

or, in integrated form, as:

$$x(t,k) = x(o,k)e^{-kt} \quad (4)$$

The total fraction of the original amount of contaminant remaining at time  $t$ ,  $X(t)$ , can then be expressed as (33):

$$X(t) = \int_0^{\infty} x(t,k)dk \quad (5)$$

or, through relation 4, as:

$$X(t) = \int_0^{\infty} x(o,k)e^{-kt}dk \quad (6)$$

with

$$X(o) = \int_0^{\infty} x(o,k)dk = 1 \quad (7)$$

The applicability of a power law rate model to  $X(t)$ :

$$\frac{d}{dt} X(t) = -\bar{k}X^n(t) \quad (8)$$

or

$$X(t) = [1 + k(n-1)t]^{-\frac{1}{n-1}} \quad (9)$$

then indeed requires the identity of relations 6 and 9. Taking the inverse Laplace transforms of the right-hand sides of these equations, one can easily verify that their identity only holds if:

$$X(o,k) = \frac{\frac{k}{e^{(n-1)k}} \frac{2-n}{k^{n-1}}}{\left(\frac{2-n}{n-1}\right)! (n\bar{k} - \bar{k})^{\frac{1}{n-1}}} \quad (10)$$

Or, in other words, if the reactivities of the different contaminant-containing fractions of the feed obey a gamma distribution, the mean of which being the average reactivity:

$$\bar{k} = \frac{\int_0^{\infty} kx(o,k) dk}{\int_0^{\infty} x(o,k) dk} \stackrel{(7)}{=} \int_0^{\infty} kx(o,k) dk \quad (11)$$

Because the above derivation only holds for plug-flow behavior of the heavy crude, owing to the nature of the continuity equations used, one can anticipate that different kinetic orders will apply to different reaction systems. Theoretical evidence for this expectation has actually been given by van Zijll Langhout and co-workers (22), who showed that, on the basis of a gamma distribution of the contaminant reactivities, the following relationship approximately holds between the kinetic orders in a plug-flow ( $n_{pFR}$ ) and back-mixed flow ( $n_{BMR}$ ) reactor:

$$n_{BMR} = 1 + 0.5 (n_{pFR} - 1) \quad (12)$$

Experimental evidence for this result in the case of hydrodesulfurization of heavy crudes is presented in Table II, which summarizes the various kinetic orders obtained for both hydrodesulfurization and hydrodemetallization systems over a wide range of operating conditions in different reactor systems.

Table II. Kinetic Orders for Hydrodesulfurization and Hydrodemetallization in Plug-Flow and Back-mixed Flow Reactor Systems

	HDS	HDM
$n_{\text{PFR}}$	2.0 (21,34-36)	1.5 (22,27)
$n_{\text{BMR}}$	1.5 (22,37)	1.0 (22,27,37)

Deviation from relation 12 in the case of hydrodemetallization is not well understood, but could be due to a deviation from first-order kinetics for the individual metal-containing species. Fractional kinetic orders have indeed been reported for several vanadyl- and nickel-containing compounds (16).

#### Catalyst Selectivity and Reactor Volume Requirements

The concept of an averaged reactivity for contaminant removal appears useful in that a single parameter suffices to describe the selectivity of a given catalyst toward hydrodemetallization or hydrodesulfurization. Taking the nominal orders of Table II for a plug-flow, e.g., trickle-bed (38), reactor into account, continuity equation 6 can also be stated as:

$$V_{\text{PFR}} = \frac{F}{k_s} \left( \frac{X_s}{1 - X_s} \right) \quad (13)$$

or:

$$V_{\text{PFR}} = \frac{2F}{k_m} \left[ \frac{1}{(1 - X_m)^{0.5}} - 1 \right] \quad (14)$$

if demetallization and desulfurization are considered to occur independently. Elimination of the reactor volume from the above equations then yields the following unique relation between the demetallization and desulfurization conversions:

$$X_m = 1 - \left[ \frac{1}{1 + \frac{\bar{k}_m}{2\bar{k}_s} \left( \frac{X_s}{1 - X_s} \right)} \right]^2 \quad (15)$$

in which the single parameter  $\bar{k}_m/\bar{k}_s$  constitutes a convenient measure for the selectivity of the catalyst considered. The selectivity behavior shown in Figure 6 for different values of  $\bar{k}_m/\bar{k}_s$  is indeed typical for the industrial catalysts reported in reference 8. It has been argued elsewhere (39,40) that the catalyst selectivity can be altered by varying the pore size to

particle diameter ratio and by adding Co (Ni)/Mo sulfides instead of Ni/V subsulfides as active catalyst components.

The above equations can also be used to estimate the tolerable amount of metals in a feedstock that would give, at a required degree of desulfurization, a minimum desired catalyst lifetime. The minimum catalyst volume required for a specified lifetime is given by:

$$V_{\min} = \dot{m}L_o / (\rho_{\text{cat}} C^*) \quad (16)$$

where  $C^*$  represents the overall metal load on the catalyst, averaged over the length of the reactor, which would render the catalyst inactive for the desired degree of desulfurization,  $X_s$ . The metal deposition rate,  $\dot{m}$ , on the other hand, follows from:

$$\dot{m} = C_m X_m F \quad (17)$$

where  $C_m$  represents the metal content of the feedstock. Equation of relations 13 and 16 and substitution of  $X_m$  and  $\dot{m}$  by the right-hand sides of equations 15 and 17, respectively, finally yields:

$$C_m \text{ (for a required life } L_o) = \frac{C^* \rho_{\text{cat}} \left( \frac{X_s}{1 - X_s} \right)}{L_o \bar{k}_s \left\{ 1 - \left[ \frac{1}{1 + \frac{\bar{k}_m}{2\bar{k}_s} \left( \frac{X_s}{1 - X_s} \right)} \right]^2 \right\}} \quad (18)$$

The results of equation 18 are shown in Figure 7 for a specified catalyst life of 6 months and assuming metal-uptake capacities ranging from 10 to 25% w/w, realizing that higher metal-uptake capacities can be achieved with modern catalysts. This figure illustrates that for a specific Ni + V content, a mean catalyst life of 6 months can be attained for a reasonable range of conversions (for 30-90% desulfurization) assuming a catalyst or catalyst combination with a sufficiently high metal uptake capacity is used. For equivalent desulfurization and run-length requirements with higher metal content, a catalyst with a higher metal-uptake capacity is required.

The graph further shows that there is a higher tolerable metal content in the feed for a higher desired degree of desulfurization. This is not a contradiction; it is caused by the nonlinearity of  $X_s$  and  $X_m$  versus  $V_{\text{PFR}}$  in relations 13 and 14 combined with the proportionality between  $X_m$  and the amount of metal deposited over a given catalyst life (equation 17). For example, to increase the degree of desulfurization from 40 to 80%, a six-fold increase in catalyst volume is needed. Consequently, the total metal that can be accommodated also increases by a factor of 6. The degree of demetallization, however, only increases from approximately 10 to 43%. The corresponding

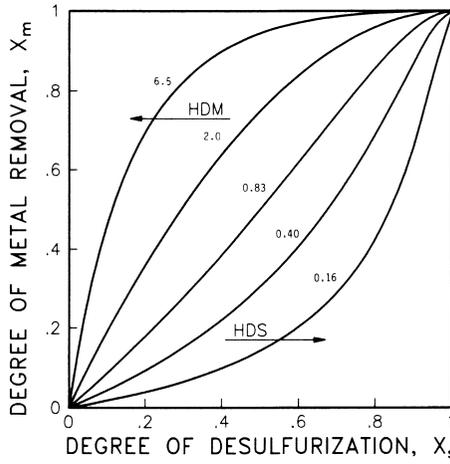


Figure 6. Catalyst Selectivity for Metal and Sulfur Removal at Different  $k_m/k_s$  Ratios.

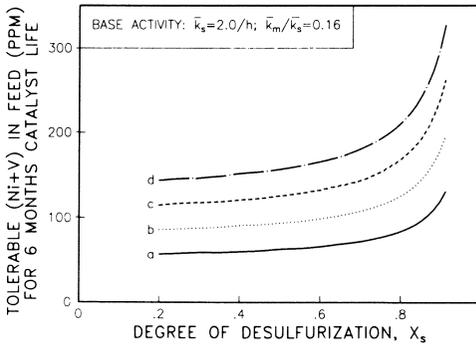


Figure 7. Tolerable Amount of Metal in the Feed as a Function of the Desulfurization Conversion for Catalysts with Different Metal Uptake Capacity. Curve a:  $C^* = 10$  wt%; curve b:  $C^* = 15$  wt%; curve c:  $C^* = 20$  wt%; curve d:  $C^* = 25$  wt%.

increase in metal deposited therefore only increases by a factor of 4.3, lower than the amount that can be accommodated to achieve the higher degree of desulfurization. Consequently, either  $L_0$  can be prolonged at the same  $C_m$ , or  $C_m$  can be increased at the same  $L_0$ .

#### Comparison of Reactor Technologies

Similar considerations apply to back-mixed flow--e.g., ebullating-bed--reactors (38). To obtain high conversions, two or three ebullating-bed reactors, in series, are usually used. The total volume of a battery of  $N$  (equal-volume) back-mixed flow reactors in series required to achieve a given degree of demetallization can be calculated through the appropriate continuity equation, assuming first-order power law kinetics (Table II) and allowing for catalyst bed expansion, as (see List of Symbols):

$$V_{BMR} = \frac{NF}{\bar{k}_{m,BMR} (1 - \xi_b)} \left[ \frac{1 - (1 - X_m)^{1/N}}{(1 - X_m)^{1/N}} \right] \quad (19)$$

A comparison with the reactor volume required in plug-flow operation:

$$V_{PFR} = \frac{2F}{\bar{k}_{m,PFR}} \left[ \frac{1}{(1 - X_m)^{0.5}} - 1 \right] \quad (14')$$

has been made in Figure 8 at two activity ratios,  $\bar{k}_{m,BMR}/\bar{k}_{m,PFR}$ , and assuming three back-mixed reactors in series. The apparent activity difference is believed to be realistic in view of the higher operating temperatures usually encountered in ebullating-bed hydrotreating. The results show that, purely in terms of reactor volume requirements, ebullating-bed operation in more than one reactor ( $N > 1$ ) is to be preferred at sufficiently high activity ratios. Additionally, the metal uptake potential of catalyst installed in an ebullating-bed reactor can be used to a greater extent than in fixed-bed operation because of the absence of any metal deposition profile, which is characteristic of the latter technology. Even the higher volumetric catalyst hold-up in fixed-bed reactors, which is compensated for by the smaller particles used in ebullating-bed operation, cannot offset this advantage of back-mixed flow technology. A moving-bed technology, e.g. Shell's "bunker" reactor design (1), could reduce the associated inherent disadvantage of fixed-bed technology in terms of limited metal uptake potential.

Whatever technology is used, it is clear that catalysts with high activity, high metal uptake capacity, and longevity are required. None of the present catalysts successfully combines all of these requirements. A conceptual hydrodemetallization catalyst design that could achieve this is presented in Figure 9. Small,

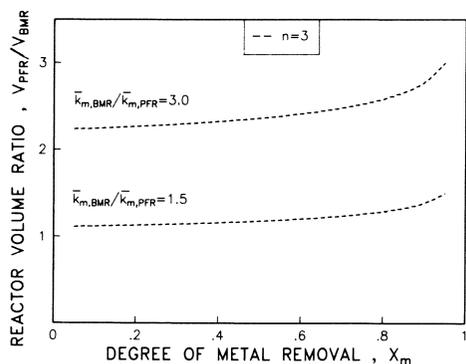


Figure 8. Ratio of the plug flow and backmixed flow reactor volumes at two activity ratios as a function of the demetallization conversion, assuming kinetic orders of 1.5 and 1.0 for plug flow and backmixed flow, respectively ( $N$  = the number of backmixed reactors in series).



Figure 9. Conceptual high-performance hydrodemetallization catalyst design.

highly porous catalyst particles are contained in a macroporous basket made of a strong attrition-resistant material. Hydrodynamically, the catalyst will give low pressure drop and can avoid bed-plugging if applied in a fixed-bed reactor. From a kinetic point of view, such a catalyst behaves like an extremely small catalyst particle: high demetallization activity combined with high metal storage capacity can be provided. It remains to be investigated whether the exterior basket can be made strong enough to withstand the various catalyst handling operations in practice.

#### A New Process Combination: Back-mixed Reactor Hydrodemetallization Followed by Delayed Coking

It was pointed out previously that in existing refineries with installed high conversion capability, the introduction of catalytic upgrading may well be a suitable method to dig deeper into the "bottom-of-the-barrel." Such a situation exists in many U.S. refineries with delayed cokers.

Delayed coking is a well-established residue conversion route based on carbon rejection and molecular-weight reduction. The rejected carbon is petroleum coke. The metals in the feedstock will almost quantitatively concentrate in the coke. The sulfur content of the coke is generally 1.2 to 1.5 times the sulfur content of the feedstock. Of the 65 delayed cokers in the United States, about 30 of them produce fuel-grade coke--the sulfur and/or metals content of the coke is too high to allow the coke to be used in the production of anodes for aluminum manufacturing. Demetallization of the feed could, therefore, result in coke being sold as anode grade rather than fuel grade. For a "typical" coker producing 600 M tons/year, an increase in revenue (and profit) of \$12 MM per year could be achieved, assuming the upgraded coke would sell for, e.g., \$30/ton instead of \$15/ton. This higher revenue can be realized by installation of a hydrodemetallization reactor system upstream of the delayed coker.

Figure 10 shows the proposed process configuration. In terms of conversion, the delayed coker remains the most important unit. As with all coker schemes, the coker gas oil needs further hydrotreating before it can be used as feedstock for FCC conversion. The above scheme appears to be viable if the sulfur content of the feed is not the overriding constraint and the metals can be reduced to less than 50 ppm in the delayed coke. Furthermore, high metal loadings on the catalyst need to be achieved. Especially for this reason back-mixed reactor operation seems to be most attractive. In order to cut catalyst consumption costs, regeneration is highly desirable. For hydrodemetallization the hydrogen consumption cost is relatively low. It is, therefore, assumed that the additional hydrogen requirements can be supplied from existing sources.

A very similar scheme has been put into operation by Chevron at their Pascagoula refinery (41). Instead of back-mixed demetallization reactors, fixed-bed resid upgraders are applied. These require a substantial dedicated hydrogen supply. The Pascagoula scheme provides an existing base to which the proposed BMR/delayed coking option can be compared.

Appendix

Noncatalytic Hydrothermal Cracking. The Veba-Combi-Cracking process (4) combines noncatalytic liquid-phase conversion and metal removal with gas-phase desulfurization in a fixed-bed reactor. This technology originates from the old Bergius process used in World War II to convert coal to gasoline. Veba plans a 30,000-bbl/day commercial unit for their refinery at Gelsenkirchen, West Germany, to be in operation by 1987 (Figure 11).

In the Veba process, the liquid-phase hydrogenation is achieved in simple upflow, cold-wall reactors with internal refractory. The linking with the gas-phase hydrogenation process provides great flexibility in handling a wide variety of feedstocks at conversions of up to 99%. The integration of liquid-phase and gas-phase reactors, however, makes the process rather complex, requiring highly trained personnel and/or computer-assisted steady-state operation.

Fixed-Bed Reactor Operation. Shells' HDM/HCON (1) trickle-bed technology resulted primarily from the understanding that high metal tolerance and high desulfurization activity are incompatible properties in today's hydrotreating catalysts. Moreover, it was found that tailor-made catalysts specific to each of these properties could be prepared by adjusting pore size. By adjusting the catalyst configuration and the operating conditions, Shell's process can accommodate any product specification (Figure 12).

For large-scale operations (>100,00 bbl/day), the total number of reactors and auxiliaries (vessels, pumps, compressors, etc.) required in the Shell-HDM/HCON process may become very large. The catalyst handling system adds to this complexity. The hydrometallization and hydroconversion catalysts are commercially available, and improvements continue to be made. Shell has also developed a regeneration process that uses a series of physical and chemical treatments, including an acid-leaching step, to optionally recover the metals from the spent catalyst. The technology will be fully commercial after the test runs in the Cardon, Venezuela, demonstration plant. A large-scale commercial unit is planned for operation by 1987, probably at Shell's Pernis refinery in Holland.

Ebullating-Bed Operation. Both the H-Oil and LC-Fining processes (Figure 13) (2,3) use ebullating-bed reactors and are based on the same pattern of technology originally utilized by Cities Service Research and Development Company. Since the 1970 Bayway, New Jersey, explosion resulting from temperature runaway, considerable reactor engineering improvements have been implemented, including the use of external recirculation pumps and the application of an internal refractory lining to reduce exposure of the reactor wall to excessively high temperature. The key risk in this process is its ability to operate at high conversions without asphaltene precipitation, internal or external to the reactor. Hydrocarbon Research, Inc. (HRI), suggests that vacuum bottom recycling can solve this problem, although it has not yet been proved on a commercial scale. The high conceptual flexibility of the H-Oil and LC-Fining processes has justified their integration in various

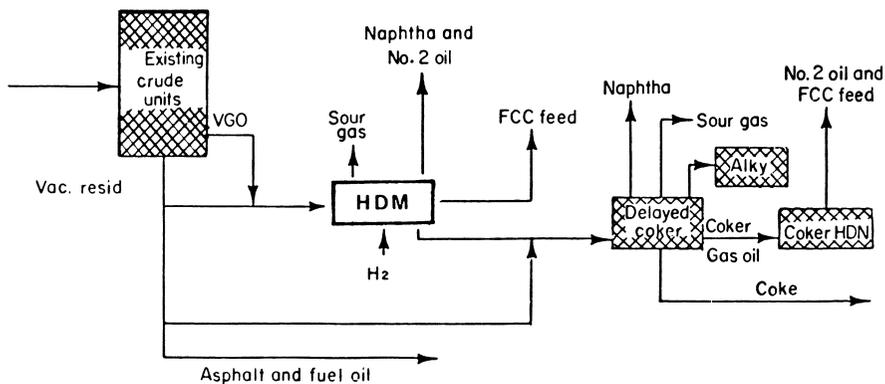


Figure 10. Back-mixed Reactor Hydrodemetallization Followed by Delayed Coking.

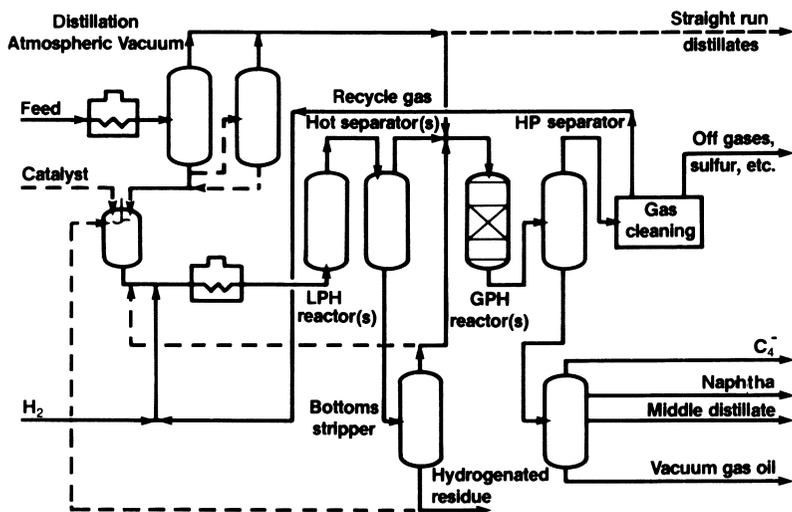


Figure 11. The Veba-Combi-Cracking Process.

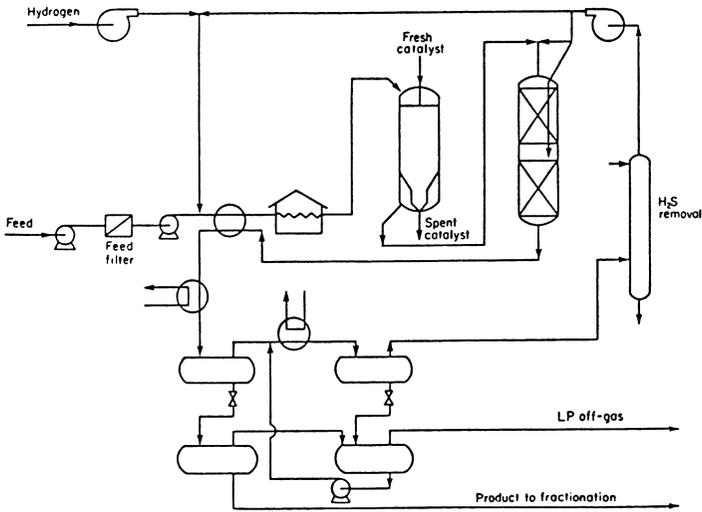


Figure 12. Flowsheet for the Shell-HDM/HCON Process.

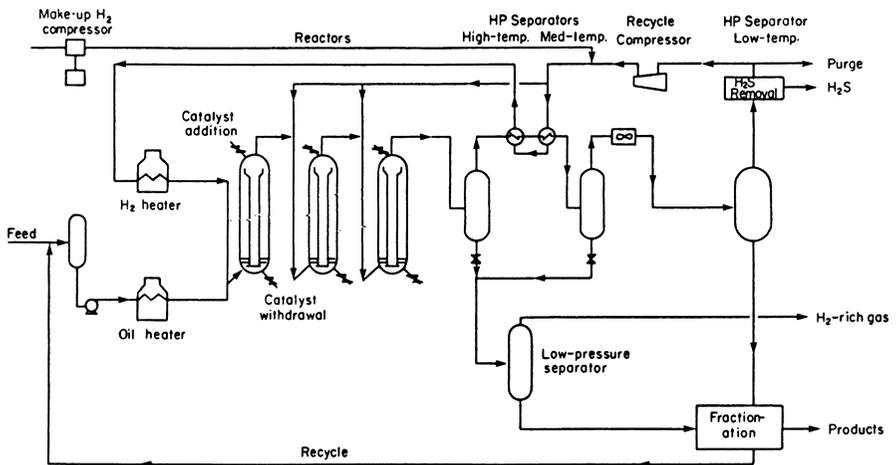


Figure 13. Typical Flowsheet for a BMR Process (LC-Fining).

refinery schemes. On-stream addition and withdrawal of inexpensive, disposable catalysts has been practiced commercially since 1984.

Slurry-Phase Operation. The CANMET, Aurabon, and M-Coke processes (5-7) all use slurry-phase operation. Although different micron-sized catalysts are used, the conceptual approach to hydroconversion is basically the same for all three processes. Contrary to the conventional approach, the hydroconversion mechanism is conceived as a primarily thermally induced, free-radical cracking reaction, with rapid subsequent hydrogenation of the unstable radicals to oil in the presence of hydrogen and catalyst. Essential to this concept is that the catalyst be highly dispersed in the oil feed to engage the free radical intermediates as quickly as possible at any point in the reactor, preventing undesirable side reactions such as coke formation. High conversions are achieved with minimal amounts of catalyst at operating temperatures slightly higher than in conventional hydrotreating. The slurry-phase processes are still in an early stage of development; a major problem is the lack of reliable scale-up and design rules for slurry-phase reactors. Commercialization is not expected before the 1990s (Figure 14).

Full Liquid Operation with H-Donor Solvent. The Gulf-Canada donor upgrading process (8), Gulf-DRB, differs from slurry-phase operation only in that the hydrogenation of thermally formed radicals is achieved through the use of an adequate hydrogen-donor solvent, which is recycled after regeneration. The need for a catalyst is eliminated, and no hydrogen overpressure seems to be required to achieve high conversions without coke formation. Appropriate options for residuum disposal must be developed for this process (Figure 15).

#### List of Symbols and Abbreviations

BMR	Back-mixed flow reactor
C*	Averaged metal-uptake capacity (kg/kg)
CC	Combi-cracking
C <sub>m</sub>	Metal content of feedstock (kg/m <sup>3</sup> )
DRB	Donor-refined bitumen
F	Feed rate of heavy crude (m <sup>3</sup> /h)
HCON	Hydroconversion
HDM	Hydrodemetallization
HDS	Hydrodesulfurization
k	First-order rate constant for contaminant removal (h <sup>-1</sup> )
$\bar{k}$	Averaged rate constant for contaminant removal (h <sup>-1</sup> )
$\bar{k}_m$	Averaged demetallization rate constant (h <sup>-1</sup> )
$\bar{k}_s$	Averaged desulfurization rate constant (h <sup>-1</sup> )
L <sub>O</sub>	Required run length (h)
m	Metal deposition rate (kg/h)
n	Kinetic order in power law rate model
N	Number of back-mixed flow reactors in series
PFR	Plug-flow reactor
t	Run time (h)

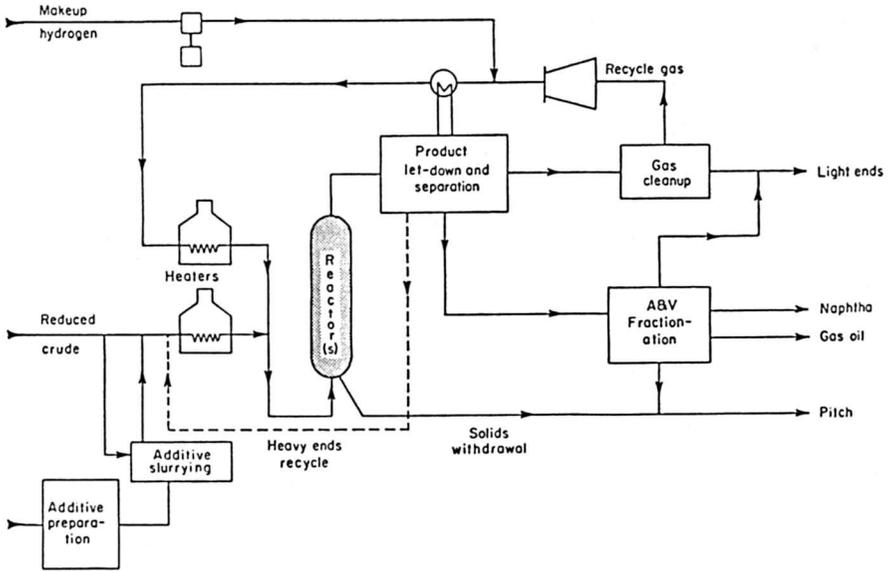


Figure 14. The CANMET Hydrocracking Process.

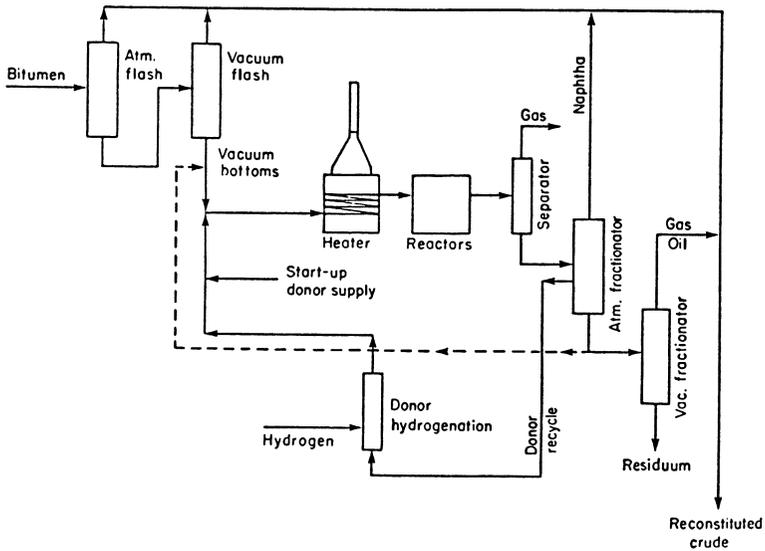


Figure 15. The Gulf-DRB Process.

$V_{BMR}$	Total volume of a battery of N back-mixed flow reactors in series ( $m^3$ )
$V_{min}$	Required volume of a plug-flow reactor for metal storage ( $m^3$ )
$V_{PFR}$	Volume of a plug-flow reactor ( $m^3$ )
x	Fraction of contaminant-containing compound
X	Total fraction of original amount of contaminant remaining
$X_m$	Degree of metal removal
$X_s$	Degree of desulfurization
$\rho_{cat}$	Bulk density of catalyst ( $kg/m^3$ )
$\xi_b$	Catalyst bed expansion ( $m^3/m^3$ )

### Literature Cited

1. Ouwerkerk, C.; Kwant, P.B.; Tjan, P.W.H.L.; Dautzenberg, F.M.; 1982; "Shell's Residue HDM/HCON Process;" paper presented at 32nd Conf. Canadian Soc. for Chem. Eng.; Vancouver; October 3-6.
2. Eccles, R.M.; 1981; The Future of Heavy Crude Oils and Tar Sands, First Intern. Conf.; Meyer, R.F., and Steele, C.T., Eds.; McGraw Hill; New York; 625.
3. Van Driesen, R.P.; Caspers, J.; Campbell, A.R.; Lumin, G.; 1979; Proc. of the Am. Pet. Inst. Ref. Dept.; 58; 33.
4. Graeser, U.; Niemann, K.; 1982; Oil Gas J.; 80; (12); 121.
5. Menzies, M.A.; Silva, A.E.; Denis, J.M.; 1981; Chem. Eng.; 88; (4); 46.
6. Adams, F.H.; Gatsis, J.G.; Sikonia, J.G.; 1981; The Future of Heavy Crude Oils and Tar Sands, First Intern. Conf.; Meyer, R.F., and Steele, C.T., Eds.; McGraw Hill; New York; 632.
7. Bearden, R.; Aldridge, C.L.; 1981; Energy Prog.; 1; (1-4); 44.
8. Deutscher, R.R.; Fisher, I.P.; Souhrada, F.; Woods, H.J.; 1982; Energy Processing Canada; 74; (7); 35.
9. Yeung, C.; Dautzenberg, F.M.; 1983; "Adaptation of Canadian Refineries to the Use of Synthetic Crudes;" 11th World Petroleum Congress; London; Aug. 28-Sept. 2.
10. Long, R.B.; 1981; "The Concept of Asphaltenes;" in Chemistry of Asphaltenes; Bunger, J.W., and Li, N.C., Eds.; Adv. Chem. Ser.; 195; 17.
11. Speight, J.G.; Moschopedis, S.E.; 1981; "On the Molecular Nature of Petroleum Asphaltenes;" in Chemistry of Asphaltenes; Bunger, J.W., and Li, N.C., Eds.; Adv. Chem. Ser.; 195; 1.
12. Hall, G.; Herron, S.P.; 1981; "Size Characterization of Petroleum Asphaltenes;" in Chemistry of Asphaltenes; Bunger, J.W., and Li, N. C., Eds.; Adv. Chem. Ser.; 195; 137.
13. Drushel, H.V.; 1972; Preprint Div. Pet. Chem. ACS; 17; (4); F92.
14. Speight, J.G.; 1980; The Chemistry and Technology of Petroleum; Marcel Dekker, Inc.; New York; 200.
15. Elliott, J.J.; Melchior, M.T.; 1982; Kirk-Othmer Encyclopedia of Chem. Tech.; 3rd Ed; Vol. 17; John Wiley & Sons; New York; 119.
16. Hung, C.W.; Wei, J.; 1980; Ind. Eng. Chem. Proc. Des. Dev.; 19; (2); 250, 257.

17. Ware, R.A.; Wei, J.; 1982; Paper No. 61a; presented at Annual AIChE Mtg.; Los Angeles; Nov. 14-19.
18. Webster, I.A.; 1984; Catalytic Hydrometallization of Nickel Porphyrins: Reactivity and Catalyst Surface Studies; Thesis; Massachusetts Institute of Technology; Feb.
19. Asaoka, S.; Nakata, S.; Shioto, Y.; Takeuchi, C.; 1983; Ind. Eng. Chem. Proc. Des. Dev.; (22); 242.
20. Takeuchi, C.; Fukui, Y.; Shioto, Y.; Nakamura, M.; 1983; RTD4(1); 11th World Petroleum Congress; London.
21. Beuther, H.; Schmid, B.K.; 1963; "Reaction Mechanisms and Rates in Residue Hydrodesulfurization;" Proceedings of the Sixth World Petroleum Congress, Processing and Refining of Oil and Gas; Section III; Paper 20; PD7; Frankfurt/Main; June 19-26.
22. van Zijll Langhout, W.E.; Ouwkerk, C.; Pronk, K.M.A.; 1980; "Development of and Experience with the Shell Residue Hydroprocesses;" paper presented at the 88th National Meeting of the American Institute of Chemical Engineers; Philadelphia; June 8-12.
23. Tamm, P.W.; Harnsberger, H.F.; Bridge, A.G.; 1981; Ind. Eng. Chem. Proc. Des. Dev.; 20; (2); 262.
24. Sato, M.; Takayama, N.; Kurita, S; Kwan, T.; 1971; Nippon Kagaku Sarski; 92; (10); 834.
25. Schuman, S.C.; Shalit, H.; 1970; Catal. Rev. Sci. Eng.; 4; (2); 245.
26. Houalla, M.; Broderick, D.H.; Sapre, A.V.; Nag, N.K.; de Beer, V.H.J.; Gates, B.C.; Kwart, H.; 1980; J. Catal.; 61; 523.
27. Dautzenberg, F.M.; George, S.E.; Ouwkerk, C.; Sie, S.T.; 1982; "Advances in the Catalytic Upgrading of Heavy Oils and Residues;" paper presented at the Symposium on the Advances in Catalytic Chemistry II; Salt Lake City; May 18-21.
28. Gates, B.C.; Katzer, J.R.; Schuit, G.C.A.; 1979; Chemistry of Catalytic Processes; McGraw-Hill; New York.
29. Kemp, R.R.D; Wojciechowski, B.W.; 1974; Ind. Eng. Chem. Fundam.; 13; (4); 332.
30. Hutchinson, P.; Luss, D.; 1970; Chem. Eng. J.; 1; 123.
31. Luss, D.; Hutchinson, P.; 1971; Chem. Eng. J.; 2; 172.
32. Aris, R.; Gavalas, G.R.; 1966; "Theory of Reaction in Continuous Mixtures;" Phil. Transactions of the Royal Society of London; A260; 351.
33. Aris, R.; 1968; Arch. Rational Mech. Anal.; 27; (5); 356.
34. van Deemter, J.J.; 1984; Proceedings of the 3rd European Symposium on Chemical Reaction Engineering; Amsterdam; 215.
35. Massagutov, R.M.; Berg, G.A.; Kulinich, G.M.; Kirilov, T.S.; 1967; Proceedings of the 7th World Petroleum Congress; 4; Mexico; 177.
36. de Brujin, A.; 1976; Proceedings of the 6th International Congress on Catalysis; Paper B 34; London.
37. Dautzenberg, F.M.; van Klinken, J.; Pronk, K.M.A.; Sie, S.T.; Wijffels, J.-B.; 1978; "Catalyst Deactivation through Pore Mouth Plugging during Residue Desulfurization;" paper presented at the 5th International Symposium on Chemical Reaction Engineering; Houston; March 13-15.

38. Dautzenberg, F.M.; De Deken, J.C.; 1984; Catal. Rev. Sci. Eng.; 26; (3&4); 421.
39. Douwes, C.T.; van Klinken, J.; Wijffels, J.-B.; van Zijll Langhout, W.C.; 1979; "Development in Hydroconversion Processes for Residues," 10th World Petroleum Congress; Panel Discussion 10; Bucharest.
40. Wolk, R.H.; Robesti, W.C.; 1973; "Demetallization of Heavy Residual Oils;" Phase I; U.S. EPA; U.S. Dept. Comm. Natl. Tech. Info. Serv.; PB277568; December.
41. Teichman, D.P.; Bridge, A.G.; Reed, E.M.; 1982; "Chevron Residuum Hydrotreating to Increase Refinery Flexibility;" paper presented at National Petroleum Refiners Association Annual Meeting; San Antonio; March 21-23.

RECEIVED February 12, 1987

## Chapter 16

# Degradation of Metalloporphyrins in Heavy Oils Before and During Processing

## Effects of Heat, Air, Hydrogen, and Hydrogen Sulfide on Pteroporphyrin Species

Lillian A. Rankel

Central Research Laboratory, Mobil Research and Development Corporation,  
P.O. Box 1025, Princeton, NJ 08540

Thermal and gaseous conditions during recovery, storage, distillation, desalting and visbreaking can cause compositional changes in heavy oils. This prior history can effect downstream processing of the modified heavy oil. Therefore, model compound porphyrins and metalloporphyrins have been exposed to "preprocess conditions" of heat, air, hydrogen or hydrogen sulfide. Types of changes undergone by these model compounds were determined. This was followed by treating Arabian Heavy crude and Arabian Heavy resid under similar conditions and extracting their petroporphyrins. The petroporphyrins have limited thermal stability. Heating in atmospheres containing air, hydrogen, or hydrogen sulfide gases further accelerates petroporphyrin decomposition. Mechanisms for these decomposition processes are discussed. Downstream processing of compositionally modified oils is considered.

During recovery, storage, desalting, distillation, and visbreaking, heavy oils are exposed to various thermal and gaseous conditions. These "preprocess" conditions consisting of heat, air, hydrogen and hydrogen sulfide can cause changes in heavy oil components. For instance, metalloporphyrins and petroporphyrins undergo degradation to polypyrroles (e.g., bilin, tripyrrin, and dipyrromethane derivatives) in the presence of hydrogen sulfide (1). This has been observed in my laboratory with model metalloporphyrins under such mild conditions as 464°F and one atmosphere of hydrogen sulfide. Using an Arabian Heavy vacuum resid, it was further shown that thermal treatment (850°F, 500 psig hydrogen + 20% hydrogen sulfide) reduced the petroporphyrin content of the asphaltene fraction by more than 50%.

A study of the reactivity of metalloporphyrins and petroporphyrins has now been extended to thermal exposure with air, hydrogen and heat. Atmospheric pressure air oxidation of model compound metalloporphyrins and porphyrins were studied. Also, the air oxidation of Arabian Heavy crude and visible spectroscopy of the

methanesulfonic acid extracted petroporphyrins were examined. Some work with thermal treatment in the presence of helium or hydrogen was done as well.

### Experimental

The model compounds used for this study were H<sub>2</sub>(TPP) (where TPP = tetraphenylporphyrin), VO(TPP), Ni(TPP) and Ni(OEP) (where OEP = octaethylporphyrin). The air oxidations were carried out in refluxing 1-methylnaphthalene (464°F) using 10 cc/min of air flow with 50 cc of a saturated model compound solution. Samples were withdrawn periodically and visible spectra measured.

Arabian Heavy crude was air oxidized in a tubular reactor packed with either Vycor or 10% V2O<sub>5</sub> on alumina. Temperatures ranged from 392 to 464°F at 200 to 500 psig air. Arabian Heavy crude was also thermally treated at 750°F in helium at 500 psig. Petroporphyrins from the Arabian Heavy crude were extracted with methanesulfonic acid (1-3) and visible spectra measured. In this way, the micrograms of petroporphyrin per gram of oil were determined.

Arabian Heavy 1075°F<sup>+</sup> vacuum resid was thermally treated at 500 psig of hydrogen. Some of the thermally treated residua were pentane deasphalted (15 to 1 pentane-to-oil) and are referred to as C<sub>5</sub>-solubles and C<sub>5</sub>-insolubles. Again, petroporphyrins were extracted with methanesulfonic acid. Calculations for micrograms petroporphyrin per gram of oil were based on  $\epsilon = 17 \times 10^3$  and an average M.W. of ~455 for the petroporphyrin. The  $\mu\text{g}$  porphyrin/g oil were then calculated from the absorption of the cationic petroporphyrin at 545 nm. Chemical analyses of the crude and resid are shown in Table I.

Table I. Analysis of Feeds

	Arabian Heavy Crude	Arabian Heavy Resid
% C	83.3	85.1
% H	11.8	10.2
% N	0.16	0.43
% O	<0.1	0.46
% S	2.89	5.24
Ni, ppm	19	60
V, ppm	57	160
% C <sub>5</sub> -insolubles	7.3	24.2
<u>B.P. Distribution</u>		
IBP-420°F	16.8	
420-650	18.8	
650-850	16.6	
850°F <sup>+</sup>	47.8	100

Results and Discussion

Model Compound Air Oxidation. Air oxidation of the model compounds H<sub>2</sub>(TPP), VO(TPP), Ni(TPP), and Ni(OEP) causes loss of  $\pi$ -conjugation in the aromatic porphyrin ring. Reaction of the porphyrin ring manifests itself as a decrease in the absorptions at ~400 nm (Soret band) and ~550 nm. As these bands decrease, a band at ~330 nm grows. This 330 nm absorption results from the production of linear polypyrrolic degradation products from porphyrins (1).

Figure 1 shows visible spectra for Ni(TPP) after 24 hours of air oxidation at 464°F. About 75% of the Ni(TPP) has been degraded. Ni(OEP) model compound is more labile to oxidation than Ni(TPP) (Figure 2). Here complete destruction of the porphyrin ring occurs in 24 hours from air oxidation.

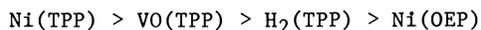
Degradation of porphyrins can be measured by using an absorption ratio. As the porphyrin concentration approaches zero,

$$\frac{A(330 \text{ nm})}{A(330 \text{ nm}) + A(400 \text{ nm})} \text{ approaches unity}$$

This relationship is used in Figure 3 to show the stability of various model compounds to air oxidation.

The oxidation catalyst V<sub>2</sub>O<sub>5</sub> accelerates the decomposition of petroporphyrins in air at 464°F as shown in Figure 3. As one would expect, more catalyst accelerates decomposition. One run used 50 cc of solution and 0.5 g V<sub>2</sub>O<sub>5</sub> where >75% of the Ni(TPP) was destroyed in 2 hours. Another run had 0.1 g V<sub>2</sub>O<sub>5</sub> in VO(TPP) solution and a slight increase in the oxidation rate occurred compared to uncatalyzed oxidation.

Using Figure 3, model compound stability to initial oxidation follows the order:



Previous work showed the same reactivity order for the tetraphenylporphyrin compounds when exposed to hydrogen sulfide (1). However, Ni(OEP) was as stable to attack by hydrogen sulfide as Ni(TPP). The lack of oxidative stability of Ni(OEP) may be due to the ease of oxidation of the ethyl groups.

Arabian Heavy Crude Air Oxidation. The degree of air oxidation undergone by Arabian Heavy crude oil depends upon pressure, temperature, liquid hourly space velocity (LHSV), and oxidation catalyst (Table II). For instance, air oxidation at 500 psig, 392°F and 2 LHSV (Run 1) increases the oxygen content of the processed oil to 1.55% oxygen (Table II), while lower pressure (Run 3 at 200 psig) and higher temperature (464°F) give 1.28% oxygen in the oil. At the same temperature of 464°F, 2 LHSV (Run 2) incorporates 1.77% oxygen while 4 LHSV (Run 4) has 1.34% oxygen. V<sub>2</sub>O<sub>5</sub> catalyst also improved oxidation (see Runs 2 and 3). Air versus He gas during thermal treatment gives marked differences in oxygen content (compare Runs 3 and 5).

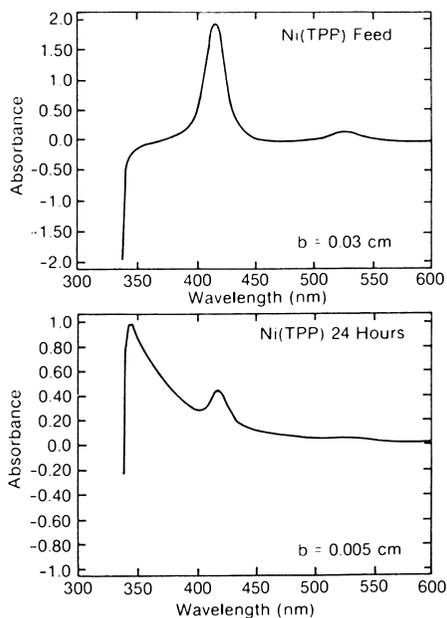


Figure 1. Air oxidation of Ni(TPP) at 464°F in refluxing 1-methylnaphthalene.

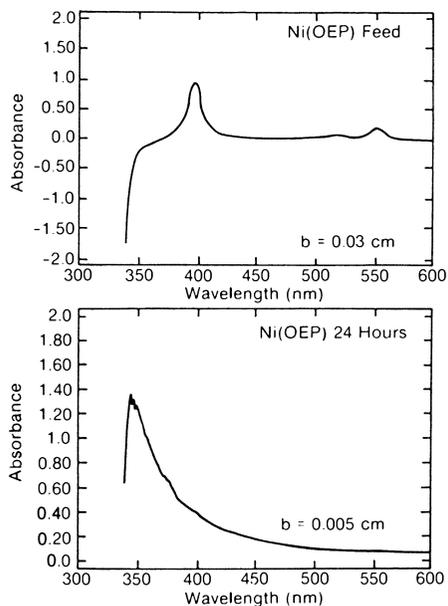


Figure 2. Air oxidation of Ni(OEP) at 464°F in refluxing 1-methylnaphthalene.

Table II. Air Oxidation or Thermal Treatment of Arabian Heavy Crude

Run in 5/8 in tubular reactor (15 cc/vol);  
 Reactor Packing: (1) V<sub>2</sub>O<sub>5</sub> = V<sub>2</sub>O<sub>5</sub>/alumina 10% V<sub>2</sub>O<sub>5</sub> (12/20 mesh),  
 (2) Vycor 12/20 mesh sized; Flow: 100 cc/min

Run Number	Feed	1	2	3	4	5
Reaction temp., °F		392	464	464	464	752
LHSV (hrs. <sup>-1</sup> )		2	2	2	4	2
Reactor packing		Vycor	V <sub>2</sub> O <sub>5</sub>	Vycor	V <sub>2</sub> O <sub>5</sub>	Vycor
Gas used		Air	Air	Air	Air	He
Pressure, psig		500	200	200	200	500
µg P/g oil	400	28.4	21.3	-	30.5	44.4
% Oxygen in oil	>0.1	1.55	1.77	1.28	1.34	0.84

As the degree of crude oxidation increases, more petroporphyrins are degraded. A half hour exposure of Arabian Heavy crude oil to air at 392°F, 500 psig air reduces the petroporphyrin content from 400 µg porphyrin/gram of oil to 28.4 µg porphyrin/g oil (Run 1). Catalytic oxidation reduces the petroporphyrin content even more (Run 2).

Vanadyl porphyrins are known to promote asphalt oxidation, particularly as measured by increases in ketone content (4). Oxygenation can also cause polymerization reactions and molecular weight increases. As more higher metals crudes and resids become refinery feeds, oxidation during handling could present more difficulties for refiners.

Thermal Treatment of Arabian Heavy Crude and Resid. A 752°F thermal treatment of Arabian Heavy crude for a half hour reduces the petroporphyrin content by 90% (Table II, Run 5). Additional heating at this temperature would degrade more petroporphyrins. During a vacuum distillation to produce resid, the heavy fraction of oil is exposed to temperatures around 800°F for about 15 minutes. This thermal exposure can degrade as much as 90% of the petroporphyrins. Arabian Heavy resid (Table III) contains 36.4 µg porphyrin/g oil while its parent Arabian Heavy crude has 400 µg/g oil (Table II). Thus, the thermal history of crudes and resids can markedly change the amount of petroporphyrins present. In addition, thermal treatment can remove Ni and V and cause size reduction in the metal containing compounds (5).

Effects of Hydrogen and Hydrogen + Hydrogen Sulfide on Resid. Comparisons between thermal treatment with hydrogen and hydrogen + hydrogen sulfide showed that hydrogen sulfide accelerates petroporphyrin degradation (Table III). This enhanced degradation by hydrogen sulfide is more pronounced at low space velocities and 750°F (Table III, LHSV = 0.3). At 750°F thermal reactions are slower than at 850°F and the effects of hydrogen sulfide can be seen. Hydrogen sulfide at atmospheric pressure also causes decomposition of model compound porphyrins and metalloporphyrins under mild conditions (464°F, refluxing 1-methylnaphthalene) (1).

Table III. Micrograms Porphyrin Per Gram Of Oil

		Assumed M.W.	µg Porphyrin/ g oil
	Arabian Heavy 1075°F <sup>+</sup> Resid	455	36.4
	C <sub>5</sub> -soluble	432	13.8
	C <sub>5</sub> -insoluble	520	73.0
<u>LHSV</u>	<u>Processed Oil:</u>		
5.5	H <sub>2</sub> , 850°F	455	29.0
	C <sub>5</sub> -soluble		00.0
	C <sub>5</sub> -insoluble		35.6
5.5	H <sub>2</sub> + H <sub>2</sub> S (20%), 850°F	455	27.0
	C <sub>5</sub> -soluble		00.0
	C <sub>5</sub> -insoluble	520	35.6
1.0	H <sub>2</sub> , 850°F	455	21.0
1.0	H <sub>2</sub> + H <sub>2</sub> S, 850°F	455	20.0
0.3	H <sub>2</sub> , 750°F	455	35.1
0.3	H <sub>2</sub> + H <sub>2</sub> S, 750°F	455	24.7

Demetallation of metalloporphyrins occurs through sequential hydrogenation of the peripheral double bonds followed by final fragmentation of the ring and metal removal (1,6-8). Hydrogen sulfide can also add to double bonds and therefore aid in ring saturation (9) (Figure 4). Acid cracking of the ring and metal sulfide formation can occur as well (1).

Processing Oils Exposed to Air, H<sub>2</sub>S, H<sub>2</sub> or Heat. Metal containing petroporphyrins degraded to polypyrroles by air, hydrogen sulfide, hydrogen, or thermal exposure would probably be easier to hydrodemetallate with a catalyst (1,6-8). Depending upon the percentage of metal coordinated by the petroporphyrins, this could be significant for hydrodemetallation processing. Estimates for petroporphyrin coordinated metal range from 10 to 60% (10).

Oil molecules that have undergone air oxidation, hydrogen and/or hydrogen sulfide addition, or thermal cracking may be easier to crack but oxygen or sulfur added to the resids by the above treatments will cause processing problems.

### Summary

The model compound porphyrins Ni(TPP), VO(TPP), Ni(OEP), and H<sub>2</sub>(TPP) are many times more stable to air oxidation, hydrogen sulfide, hydrogen or heat than petroporphyrins. Air oxidation at 464°F converts the model compounds into polypyrrolics within 24 hours while >90% of Arabian Heavy crude petroporphyrins degrade in one half hour with air oxidation or are >95% degraded on V<sub>2</sub>O<sub>5</sub>. At 464°F, model compound porphyrins are stable for many hours while Arabian Heavy resid

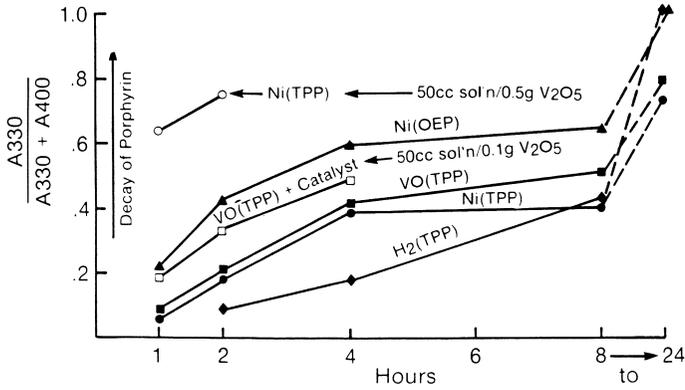


Figure 3. Air oxidation of model compound porphyrins.

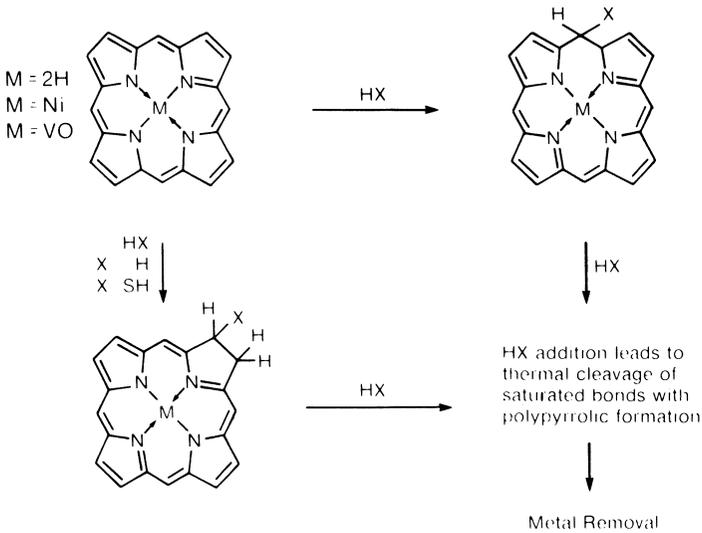


Figure 4. Routes for porphyrin ring degradation by H<sub>2</sub> or H<sub>2</sub>S.

petroporphyrins are significantly decomposed in one-half hour. When Arabian Heavy resid is exposed to a mixture of H<sub>2</sub> and H<sub>2</sub>S, accelerated decomposition of the petroporphyrins in the resid takes place. Thus petroporphyrins in resids can be markedly decomposed by thermal treatment and exposure to reactive gases.

Air, hydrogen sulfide, hydrogen or heat degraded petroporphyrins would probably be easier to catalytically demetallate because the aromatic porphyrin ring has been disrupted. However, oxygen or sulfur introduced into the oil during processing might cause molecular weight increases and other problems in refining these treated resids.

#### Literature Cited

1. Rankel, L. A. Preprints, Div. Petrol. Chem., ACS 1981, 26, 689.
2. Baker, E. W.; Yen T. F.; et al J. Amer. Chem. Soc. 1967, 89, 3631.
3. Erdman, J. G. U.S. Patent 3 190 829, 1965.
4. Branthaver, J. F.; Nazir, M.; et al Liq. Fuels Tech. 1984, 2, 67.
5. Reynolds, J. G.; Biggs, W. R. Preprints, Div. Petrol. Chem., ACS 1985, 30, 679.
6. Ware, R. A.; Wei, J. J. Catalysis 1985, 93, 100.
7. Ware, R. A.; Wei, J. J. Catalysis 1985, 93, 122.
8. Ware, R. A.; Wei, J. J. Catalysis 1985, 93, 135.
9. Khimmi, U. Russ. Chem. Rev. 1963, 32, 399.
10. Filby, R. H. "The Role of Trace Metals in Petroleum"; Yen, T. F., Ed.; Ann Arbor Science, Ann Arbor, MI, 1975; Chap. 2.

RECEIVED October 16, 1986

## Chapter 17

# Hydrodemetallization with Phosphorus Compounds over Aluminas in a Trickle-Bed Reactor

S. G. Kukes, A. W. Aldag, and S. L. Parrott

Phillips Petroleum Company, Bartlesville, OK 74004

Oil soluble phosphorous compounds were found to be active and selective for vanadium removal in hydro-processing resids over either high or low surface area aluminas. The phosphorus compounds preferentially reacted with the low molecular weight species in the resin fraction of the oil resulting in the interstitial deposition of a vanadium - phosphorus material. No effect was observed on the rate of nickel removal and the HDS activity was actually inhibited by phosphorus.

Earlier we reported extensive studies in the area of chemical demetallization of heavy oils and resids (1, 2). A variety of chemical reagents, such as strong inorganic acids, chlorinating compounds, chelating agents, strong oxidants, etc., exhibited some activity for metals and heteroatom removal. Most of these reagents were oil soluble chemicals which were heated with oil in a batch reactor without catalyst present. Unfortunately, the most active of these chemicals also produced side reactions including element incorporation, cracking, polymerization, etc., and in fact resulted in a degraded oil. Phosphorous compounds were unique in showing high activity for vanadium removal with relatively low level of side reactions (3, 4). It was found that both organic and some inorganic phosphorous compounds were effective for vanadium removal from heavy oils and resids at temperatures in excess of 370 C (Table I). Vanadium removal can occur at lower temperatures at lower asphaltene concentration (Table II) as typically seen in heavy oil extracts.

0097-6156/87/0344-0265\$06.00/0  
© 1987 American Chemical Society

Table I

Effect of Phosphorous Compounds on Metal Removal  
From Monagas Pipe Line Oil (Batch Reactor)

<u>Run</u>	<u>Additive and Concentration</u>	<u>Temp C</u>	<u>% V Removed</u>	<u>% Ni Removed</u>
1	None	417	71	64
2	3.0% P <sub>4</sub> S <sub>3</sub>	417	99	90
3	3.0% P <sub>2</sub> S <sub>5</sub>	417	99	80
4	3.0 Red P	417	97	59
5	3.0% (PhO) <sub>2</sub> P(O)H	417	99	71
6	1.0% (CH <sub>3</sub> O) <sub>3</sub> P	417	99	58
7	None	400	15	10
8	1.0% (CH <sub>3</sub> O) <sub>3</sub> P	400	84	12
9	0.7% (PhO) <sub>2</sub> P(O)H	400	69	20
10	3.0% P <sub>4</sub> S <sub>3</sub>	400	90	18
11	1.0% (PhO) <sub>2</sub> P(O)H	388	65	8

Residence Time: 1 hour

Table II

Effect of Phosphorous Compounds on Vanadium Removal  
From Heavy Oil Extract (Batch Reactor)

<u>Additive</u>	<u>Temp C</u>	<u>Residence Time (min)</u>	<u>% Removal</u>	
			<u>V</u>	<u>Ni</u>
None	360	60	0	0
10% (CH <sub>3</sub> O) <sub>3</sub> PO	360	60	83	0
2% (CH <sub>3</sub> O) <sub>3</sub> PO	360	60	50	2
2% (CH <sub>3</sub> O) <sub>3</sub> PO	360	20	32	0
11% (CH <sub>3</sub> O) <sub>3</sub> PO	317	60	54	0
11% (CH <sub>3</sub> O) <sub>3</sub> PO	317	20	45	0
2% (CH <sub>3</sub> O) <sub>3</sub> PO	317	20	21	0
10% (CH <sub>3</sub> O) <sub>3</sub> P	317	60	82	0
10% (CH <sub>3</sub> O) <sub>3</sub> P	317	20	79	0
2% (CH <sub>3</sub> O) <sub>3</sub> P	317	20	61	0

The solubility of the phosphorous compounds and particularly the steric effects of groups attached to the phosphorous are very important parameters. The effectiveness of the additives declined in the following order:



where R - alkyl and Ar - phenyl.

Initial studies also indicated that phosphorous compounds were effective in a trickle bed reactor packed with alundum (low surface area alumina  $<1.0\text{m}^2/\text{g}$ ) (Table III).

Table III

Effect of Phosphorous Additives in a Flow Reactor

Feed	Additive	Temp C	% V Removal
Arabian Light	None	420	13
Arabian Light	1.5% Diphenyl Phosphite	420	82
Maya	None	400	8
Maya	0.5% Triethyl Phosphate	400	78

Hydrogen pressure = 2250 psig

Residence time = 50 min

The effects of temperature, residence time, hydrogen flow, and concentration of phosphorous compounds on vanadium removal from Monagas pipeline oil were investigated with alundum as a packing material (1, 2). Almost no effects were observed on nickel or sulfur removal. The lengths of the runs were relatively short (3-80 hours) because significant interstitial deposition of solid materials was observed. These deposits might be attributed to vanadium and phosphorous species since their rate of removal was very high (Figure 1).

The aim of this work was to investigate the effects of the presence of a porous alumina on vanadium removal with phosphorous compounds.

### Experimental

Triethylphosphate (Aldrich) was blended with Maya 400 F+ feed (3.9 % S, 59 ppm Ni, 304 ppm V) or with a blend of Maya, North Slope, and West Texas Sour (2.2 % S, 34 ppm Ni, 151 ppm V) and pumped through an induction tube into a trickle bed reactor, 28.5 inches long and 0.75 inches in diameter. The oil pump used was a Whitey model LP-10 (a reciprocating pump with a diaphragm-sealed head; marketed by Whitey Corp., Highland Heights, Ohio). The oil induction tube extended to the catalyst bed (located about 3.5 inches below the reactor top) comprising a top layer of about 40 cc of 14 mesh alundum (Norton Chemical Process Products, Akron, Ohio), a middle layer of 50 cc of high surface area alumina ( $159\text{m}^2/\text{gram}$ , average pore diameter 290 angstroms, and pore volume  $1.09\text{cc}/\text{gram}$ ) mixed with 70 cc of the same 14 mesh alundum, and finally a bottom layer of about 20 cc of 1/8 inch alundum. The hydrogen was introduced into the reactor through a tube concentrically surrounding the oil induction tube, but extending only as far as the top of the reactor. The reactor was heated with a Thermcraft (Winston-Salem, N.C.) Model 211 3-zone furnace. The reactor temperature was

measured in the catalyst bed at three different locations by three separate thermocouples embedded in an axial thermocouple well (0.25 inch O.D.). Samples of liquid oil product were collected once a day for analysis and the gaseous products were vented. Nickel, vanadium, sulfur and phosphorus contents were determined by plasma emission analysis. Used catalysts and reactor plugs were analyzed with an electron microprobe giving both quantitative elemental analysis and determination of concentration profiles through the catalyst pellets. The molecular weight distributions of phosphorous and vanadium compounds remaining in the treated oils were analyzed using size exclusion chromatography with an inductively coupled plasma detector (LC - ICP) (5).

### Results and Discussion

The effects of low (20 ppm) and high (750 ppm) concentrations of phosphorus in the feed on demetallization and desulfurization activities of high surface area alumina are shown on Figures 2-4. Neither concentration affected the rate of nickel removal (Figure 2). The rate of sulfur removal, however was lower in the presence of phosphorus (Figure 3). Since metal phosphides are less active for hydrogenation and desulfurization than corresponding metal sulfides, the observed effect on the rate of sulfur removal can be attributed to metal-phosphorus interaction. The rate of vanadium removal was not increased at low phosphorus concentration; however, 750 ppm phosphorus in the feed resulted in a considerable improvement in vanadium removal (Figure 4).

Vanadium removal occurs by two parallel and independent mechanisms: a homogeneous reaction with phosphorus in the feed and a heterogeneous reaction on the alumina surface. The heterogeneous rate increases as nickel and vanadium accumulate on the alumina. The initial demetallization activity of pure alumina is extremely low and the high activity for vanadium removal at zero time in the presence of phosphorus can be attributed to the homogeneous reaction. Extrapolation to zero time shows no vanadium removal with 0 or 20 ppm phosphorus in the feed and 30%, or 90 ppm, vanadium removal with 750 ppm phosphorus. LC-ICP analysis of the product showed that phosphorus selectively removed the vanadium associated with the low molecular weight species (less than 1000 by polystyrene calibration). Analysis of the SARA (saturate - aromatic - resin - asphaltene) fractions of the product in the beginning of the run indicated that the vanadium was removed almost exclusively from the resin fraction. Similar results were observed earlier (2) in a batch reactor without alumina or hydrogen present, and also when alumina was replaced with alundum in a trickle bed reactor (Figures 5 - 7). The data for the trickle bed is summarized in Table IV.

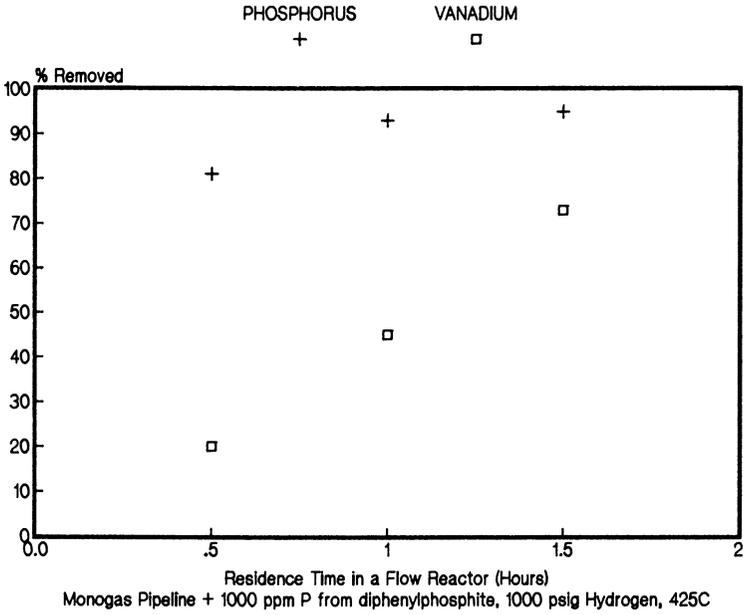


Figure 1. Effect of Residence Time (Alundum Packing)

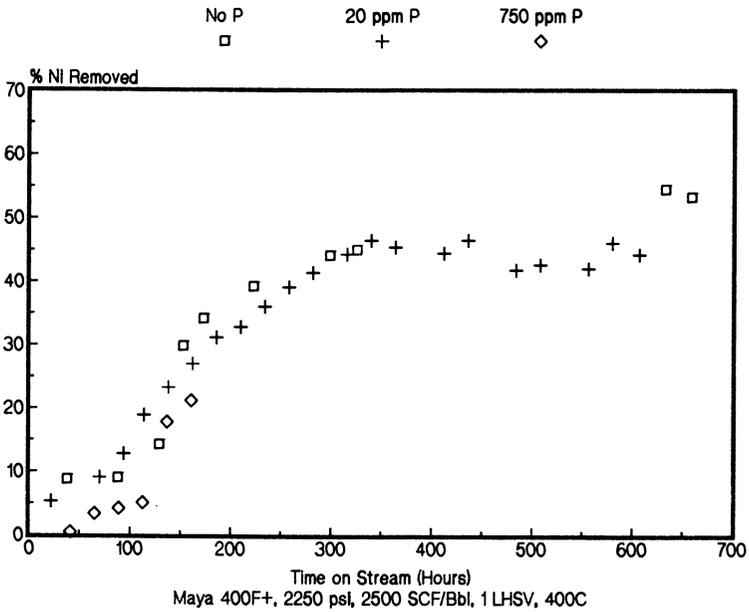


Figure 2. Effect of P on Nickel Removal (Alumina Packing)

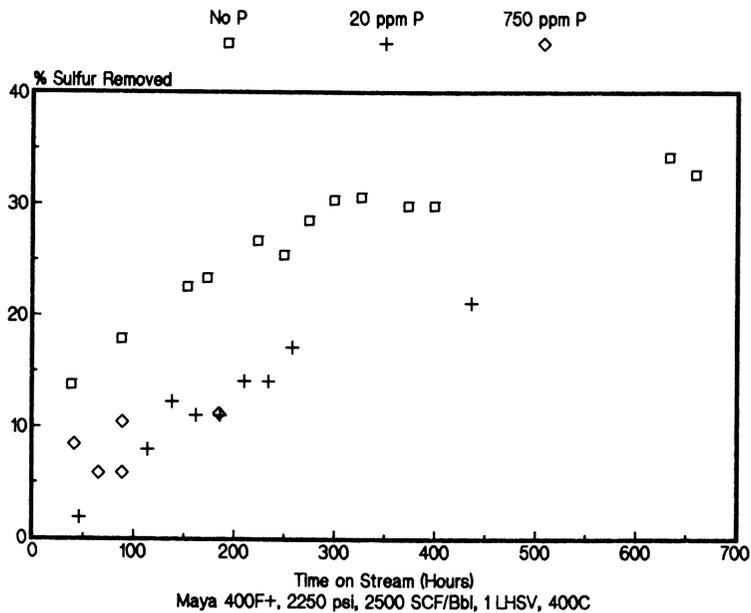


Figure 3. Effect of P on Sulfur Removal (Alumina Packing)

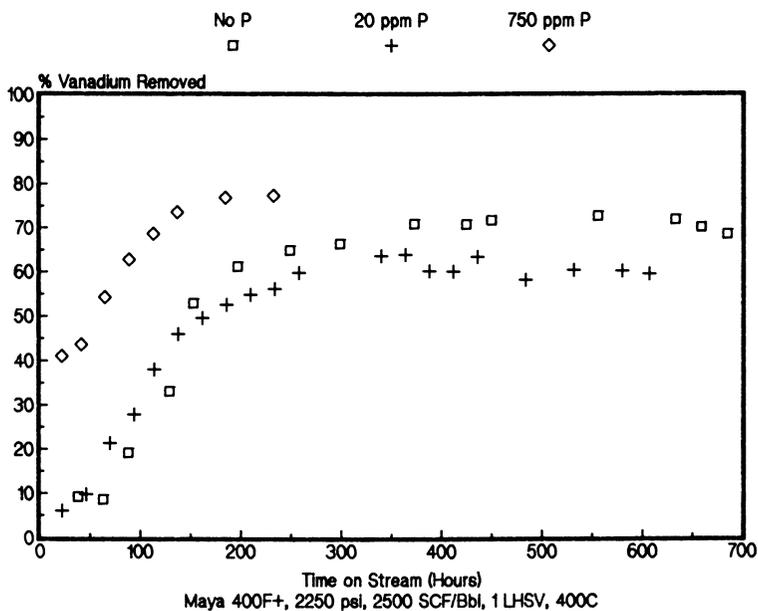


Figure 4. Effect of P on Vanadium Removal (Alumina Packing)

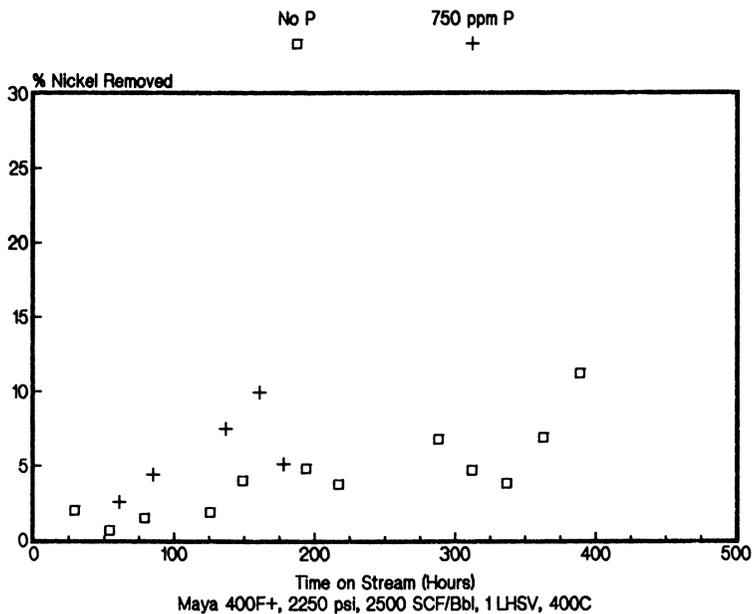


Figure 5. Effect of P on Nickel Removal (Alundum Packing)

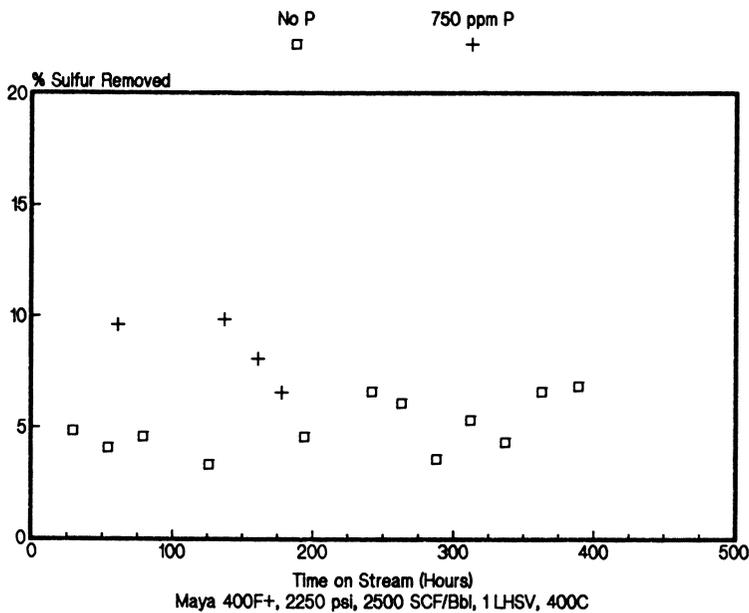


Figure 6. Effect of P on Sulfur Removal (Alundum Packing)

Table IV

	% Vanadium Removed					
	Alundum			Alumina		
Hours on stream	0	30	150	0	30	150
0 ppm phosphorus	0	8	10	0	11	50
750 ppm phosphorus	30	42	80	30	42	80

As these data show, the hydrodemetallization (HDM) activity of the high surface area alumina increases with time much faster than that of alundum in the absence of phosphorus. However, the HDM activity for both systems is remarkably similar and increases with time in the presence of large phosphorus concentrations. This is apparently due to the development of heterogeneous activity on vanadium species which have deposited interstitially. In both cases severe plugging problems occurred after 200 - 300 hundred hours on stream. Electron microprobe data confirmed that only a small fraction of the vanadium deposited in the alumina pellets. Analysis of the interstitial deposits revealed the presence of high concentrations of phosphorus, vanadium, and carbon.

Low levels of phosphorus in the feed (20 ppm) did not affect the HDM activities of alumina or alundum even after 600 hours on stream and no pressure drop was observed at the end of the run.

The effect of phosphorus concentration on the HDM activity of the high surface area alumina after the heterogeneous rate became relatively constant (600 hours on stream, 10 wt.% metals accumulated) was investigated (Figure 8). Neither 135 nor 275 ppm phosphorus showed any effect on the rate of vanadium removal; however, after 500 hours of continuous phosphorus addition, the reactor plugged. These results support the proposed mechanism of a homogeneous reaction of the phosphorous compounds with the low molecular weight vanadium species. These vanadium species are more reactive than the corresponding high molecular weight vanadium species even under heterogeneous reaction conditions (6). When the rate of the heterogeneous reaction is high and most of the low molecular weight vanadium compounds are removed, phosphorus addition does not affect the rate of vanadium removal. However, the phosphorylation of asphaltenes was still observed at these conditions which resulted in asphaltene precipitation, and an excessive reactor pressure drop. LC-ICP analyses of precipitate showed presence of phosphorous in a high molecular weight species (more than 5000 by polystyrene calibration).

### Conclusions

Phosphorus promotes the rate of vanadium removal during hydro-processing over high and low surface area aluminas. This reaction occurs homogeneously and results in the interstitial deposition of

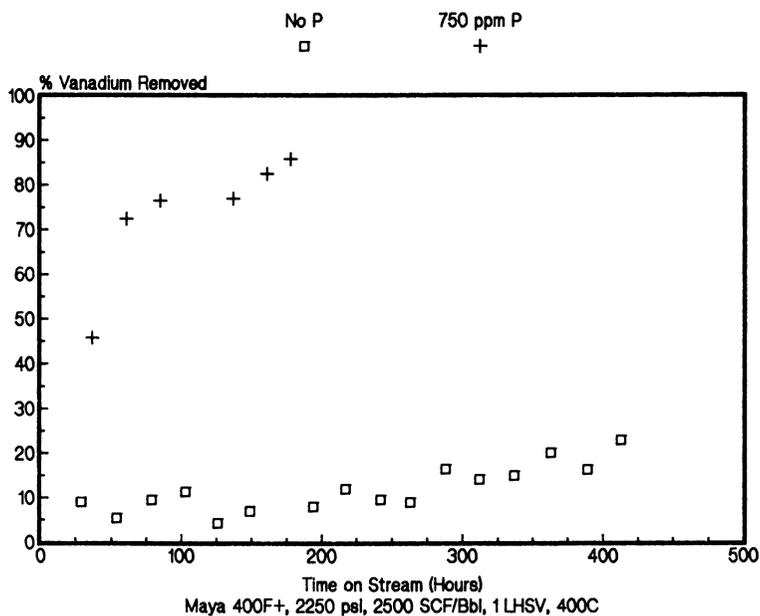


Figure 7. Effect of P on Vanadium Removal (Alundum Packing)

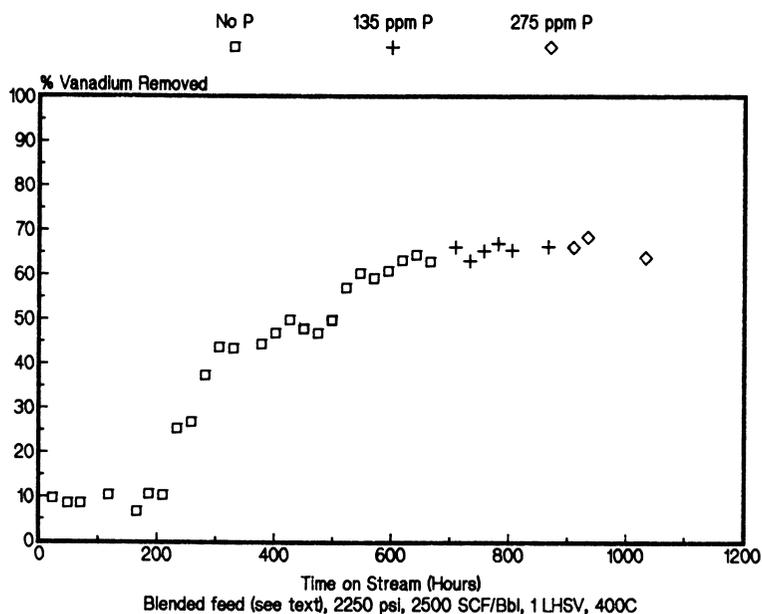


Figure 8. Effect of P on Vanadium Removal (Alumina Packing)

a vanadium - phosphorous species which results in heterogeneous activity. Phosphorus preferentially removes low molecular weight vanadium species in the resin fraction. Phosphorus was found to have no effect on the rate of nickel removal and actually inhibits the HDS activity.

#### Acknowledgments

The authors would like to acknowledge the assistance of M. D. Phillips for electron microprobe analysis.

#### Literature Cited

- (1) Kukes, S. G. 34th Can. Chem. Eng. Conf., Quebec, 1984, p. 146.
- (2) Kukes, S. G.; Aldag, A. W. Preprints, Div. of Petrol. Chem., ACS, 1985, 30 (1), 119.
- (3) Kukes, S. G. U. S. patent 4,529,503, 1985.
- (4) Kukes, S. G. et al. U. S. Patents Nos. 4,419,225, 1983; 4,421,638, 1983; 4,522,702, 1985.
- (5) Hausler, D. W.; Carlson, R. S. Preprints, Div. of Petrol. Chem., ACS, 1985, 30 (1), 28.
- (6) Bridge, A. G.; Green, D. C. "Diffusional Considerations in Residium Hydrodemetalization", Chem Tech '80, Symposium 5.

RECEIVED October 30, 1986

## Chapter 18

# Characteristics of Vanadium Complexes in Petroleum Before and After Hydrotreating

S. Asaoka, S. Nakata, Y. Shiroto, and C. Takeuchi

Chiyoda Chemical Engineering and Construction Company, R&D Center,  
3-13 Moriya-cho, Kanagawa-Ku, Yokohama, 221 Japan

Vanadium removal from asphaltenes plays an important role in hydrotreating of heavy oils. Vanadium is mainly concentrated in asphaltenes as vanadyl porphyrins involved in associations with other large hydrocarbon molecules to form asphaltene micelles, which cause difficulties in hydrodemetallization. Dissociation of asphaltene micelles enhances metal removal. Vanadyl porphyrins in the non-asphaltene portion of heavy oils are less associated and are readily removed. Vanadium removed during hydro-treatment of heavy oils is deposited on catalysts initially as four-sulfur coordinated vanadyl compounds, which react further to form vanadium sulfide. Remaining vanadium complexes in treated oils are involved in smaller associations than the asphaltene micelles of the feed.

During the hydrotreating of heavy oils, hydrodemetallization depends significantly on catalyst pore structure, which changes with hours-on-stream and depends on the molecular sizes of the reacting materials. The preferable catalyst pore structure for hydrotreating reactions is determined by the nature of metal deposition on catalysts. It also has been shown that vanadium sulfide deposited on a catalyst during hydrotreating not only causes catalyst pore structure changes, but has autocatalytic activity. A hydrodemetallization mechanism on catalysts is proposed which considers this autocatalytic activity derived from the deposited vanadium sulfide.

As is generally known, it is not easy to hydrocatalytically upgrade heavy petroleum residues. This is because they contain large quantities of metals, mainly vanadium, which are complexed with porphyrins and possibly with other large molecules containing condensed polyaromatic rings. Much fundamental research on the characteristics of metal complexes in heavy oils has been carried

out to study hydrotreating behavior. Petroleum residues are mixtures of asphaltene micelles containing resin components colloiddally dispersed in maltenes (non-asphaltenes) as the dispersing medium (1). Asphaltenes are rich in heteroatom compounds, and vanadium compounds also are concentrated in asphaltenes. Vanadium compounds play a significant role in hydrotreating (2), and this role may be clarified by examination of the nature of hydrodemetallized vanadium deposited on catalysts and the changes observed in non-demetallized vanadium complexes. In this paper, extensive studies done during the development of hydrotreating catalysts and processes for heavy oil upgrading are described.

### Experimental

A main feedstock used for the hydrotreating tests is Boscan crude produced in Venezuela. Other feedstocks used are Bachaquero atmospheric residue, Khafji vacuum residue, Gach Saran vacuum residue, Basrah Heavy vacuum residue, Athabasca tar sand bitumen, etc.

The hydrotreating tests were carried out by a high-temperature, high-pressure, flow-type unit. The feed oil and hydrogen passed by the once-through upflow mode through a fixed-bed reactor, and the catalyst bed was maintained isothermally. The reactions were carried out under the following conditions: pressure, 90 to 180 kg/cm<sup>2</sup>; temperature, 360 to 430°C; LHSV, 0.2 to 1.5 h<sup>-1</sup>; and hydrogen to liquid ratio in volume, 600 to 1000 NL/L. The thermal treatments were done without catalyst in a similar way.

The catalysts, especially prepared for the tests, were all of the cobalt-molybdenum type, supported on a carrier of an oxide. The sizes and shapes of these catalysts were the same, cylinders 0.8mm in diameter and about 3mm in length.

Analytical gel permeation chromatograms (GPC) were obtained by means of a Japan Anal. Ind. LC-08 chromatograph, equipped with four columns of 600mm length and 20mm diameter in series, filled with Shodex A-802 x 1, A-803 x 2 and A-804 x 1, respectively. Molecular weight distributions were calibrated by the use of polystyrene. After fractionation by GPC, each fraction was subjected to elemental analysis by radiation method so that the distributions of heteroatom compounds were obtained.

ESR spectra were obtained using a JEOL EF-1 spectrometer operating at X-band frequency (9.2 GHz) with 100 kHz field modulation. The microwave cavity for measurements at high temperature was equipped with a hot-air blower. The ESR spectra were obtained at temperatures between 20 and 270°C. The ESR techniques and analytical procedures used in this study were according to Tynan et al. (4)

The analytical methods used for characterization of deposited vanadium were common ones characteristic of each analytical instrument: Spark Source Mass Spectrometer (JEOL, 01BM, ED-01), X-ray Diffractometer (Rigaku Denki), X-Ray Fluorescence Spectrometer (Philips, PW-1400), Fourier Transform Infrared Spectrometer (JEOL, JIR-100), Transmission Electron Microscope (JEOL), Scanning Electron Microscope (Hitachi, S-650), Energy Dispersive X-Ray Spectrometer (Philips, EDAX), Electron Probe Micro Analyzer (Shimadzu, EMX-SM&7), X-Ray Photoelectron Spectrometer (Shimadzu, ESCA-750).

### Molecular Weight Distribution of Vanadium Containing Compounds

When a heavy oil such as Boscan crude is analyzed by gel permeation chromatography (GPC), vanadium is concentrated in the heavy fractions, as illustrated in Figure 1a. Asphaltenes, which are demetallized with difficulty, are of greater molecular weight than most of the sulfur and some of the vanadium compounds in the non-asphaltene portion of Boscan crude. In a previous report (3) it has been indicated that cracking of asphaltenes is very important in the hydroprocessing of heavy oils. Both hydrodemetallization and hydrodesulfurization are closely related to asphaltene cracking. It is observed that the number-average molecular weights of asphaltenes and of sulfur- and vanadium-containing components change as a result of hydrotreating. However, the changes of the number-average molecular weights of the sulfur and vanadium compounds, which decrease from 1200 to 1100 and 1700 to 1500 respectively, is small compared to the change observed for the asphaltenes, which are reduced from 4600 to 2200 (Figure 1). In addition, the molecular weight distributions of the asphaltenes and the sulfur and vanadium complexes become narrower. These facts illustrate that under the hydrotreating conditions we employed, the larger molecules are more easily cracked as the molecular weights of vanadium compounds are reduced.

### ESR Spectra of Vanadyl Ion in Asphaltenes and Maltenes

Vanadium compounds in asphaltenes mainly exist as vanadyl porphyrins, which interact with other molecules to form large associations. Electron Spin Resonance (ESR) has been used to study the environment of vanadyl in petroporphyrins and other complexes (4). The behavior of vanadyl compounds in asphaltene cracking reactions and in hydrodemetallization has been described (3). The characteristic changes in vanadyl porphyrins during hydrotreating and thermal treating have been further studied using ESR. In general, vanadyl groups in petroleum exhibit two types of ESR signals. One is a 16-line anisotropic spectrum due to "bound" vanadyl groups. The other is an 8-line isotropic spectrum due to "free" vanadyl groups.

Asphaltenes dissolved in a solvent have anisotropic ESR spectra similar to asphaltenes in the solid state (Figure 2). Therefore vanadium compounds in asphaltenes are considered to be involved in very large molecular associations. When asphaltenes obtained from hydrotreated Boscan crude are examined by ESR, isotropic spectral lines are observed in addition to the anisotropic spectrum. The isotropic peaks are quite small. Maltenes of the parent crude dissolved in a solvent exhibit anisotropic and isotropic spectra of equal magnitude. Maltenes of hydrotreated Boscan crude have ESR spectra in which the isotropic peaks are larger than anisotropic peaks. Therefore, the relative sizes of the molecular associations involving vanadium are:

free asphaltenes > product asphaltenes >>  
feed maltenes > product maltenes

The degree of association of vanadium in the hydrotreated product is not greatly changed from that of the parent crude, although the number-average molecular weight of the asphaltenes of the product is greatly changed. There also is little change in association of vanadium remaining in maltenes after hydrotreating. This suggests

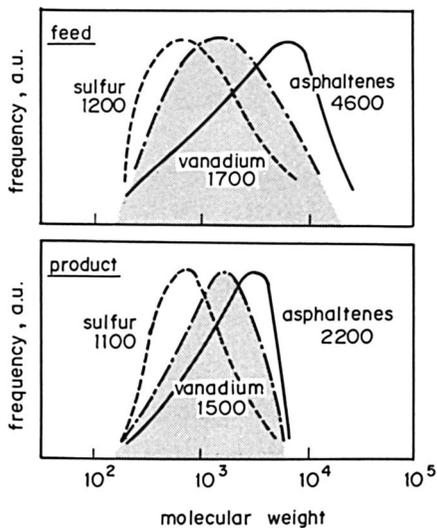


Figure 1. Molecular Weight Distributions of S-, V-compound and Asphaltenes (a) before and (b) after Hydrotreating (Boscan Crude).

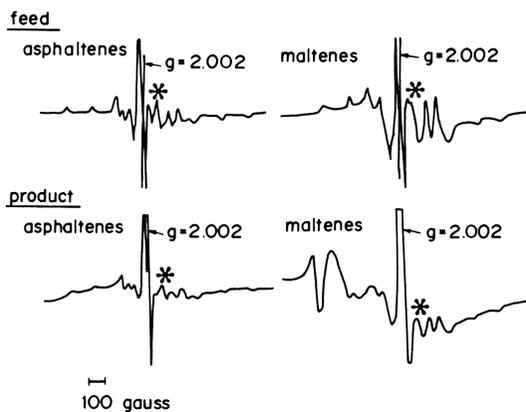


Figure 2. ESR Spectra of Asphaltenes and Maltenes (Boscan Crude).

that maltene and asphaltene associations containing vanadium are not cracked without demetallization. Indeed, it should be noted that those molecules that are cracked are almost free of vanadium. A model of this behavior is shown in Figure 3.

#### Characteristic Changes of Vanadyls in Asphaltenes During Hydro-treating

As shown in Figure 2, the vanadium in asphaltenes from both the feed and product oils give the same anisotropic ESR spectra. This is a 16-line spectrum and is characteristic of vanadyl ion in petroleum asphaltenes at low temperatures. At higher temperatures, an 8-line isotropic spectrum is observed. This isotropic spectrum has been quantitatively studied over a range of temperatures in order to understand the effects of hydrotreating on vanadyl coordination. This analysis has been described in detail previously (3). The analysis centers on the ratio of the magnitude of the No. 5 line in the isotropic spectrum to that of the No. 6 line in the anisotropic spectrum. This ratio is temperature dependent, and dissociation energies of ligands axially coordinated to vanadyl groups may be calculated from the ratio by means of Arrhenius plots. The relative amounts of "bound" and "free" vanadyl species present at a given temperature can be calculated from the ratio.

Dissociation energies of vanadyl complexes in asphaltenes from various feeds are calculated to be about 15 to 18 kcal/mol using the above method, whereas the vanadyl complexes in the asphaltenes of the hydrotreated crudes have dissociation energies of 8 to 10 kcal/mol (Figure 4). If dissociation energies and the amount of vanadyl in the "bound" state reflect strengths and quantities of binding respectively, it may be inferred that vanadyls in feed oil asphaltenes are associated with heteroatom-containing species. In the product oil asphaltenes, many heteroatoms have been removed, and vanadyl axial coordination if believed to be involved with aromatic sheets.

This analysis is supported by results reported by Tynan, et al. (4). These investigators report the energy of dimerization of formic acid to be 14 kcal/mol, and the energy of association of ethanol tetramer to be 23 kcal/mol. The energy of association between aromatic layers in asphaltenes is about 1 kcal/mol, while the energy of hydrogen bonding between aromatic sheets is 2 to 8 kcal/mol. It may be inferred that some asphaltene micelles are broken up during hydrotreating and that some vanadium in them is removed. The remaining vanadium compounds form new asphaltene associations by interaction with stacked aromatic sheets. Asphaltenes are not readily demetallized thermally, but undergo hydrodemetallization in catalyst pores as a result of overall reduction in molecular weight of asphaltenes in catalytic hydrotreating.

#### Thermal Treatment (Visbreaking and Hydrovisbreaking), Hydrotreating, and Their Combination

Many processes are known to accomplish heavy oil upgrading. Among these are visbreaking and hydrovisbreaking. Visbreaking is a simple thermal treatment, whereas hydrovisbreaking is a thermal treatment under hydrogen pressure. A combination of the thermal treatment and a hydrotreatment has been proposed (5).

The characteristic changes in vanadyl coordination were examined

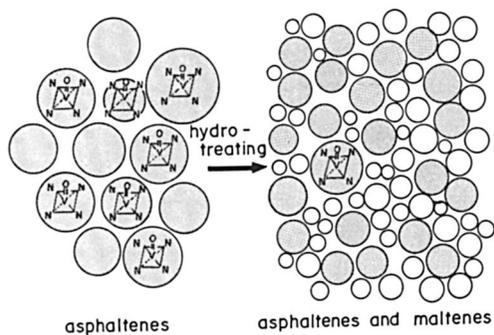


Figure 3. Model of Hydrotreating (Asphaltene Cracking) from ESR Analysis for Boscan Crude.

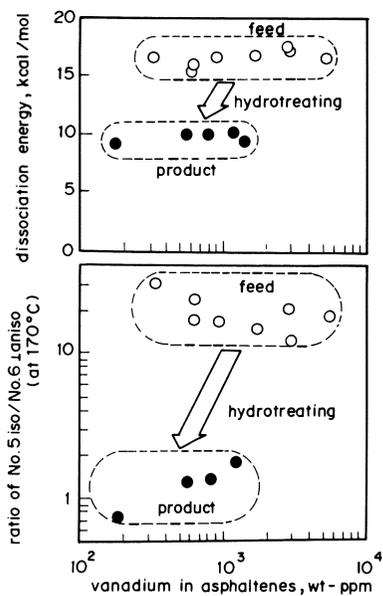


Figure 4. Change of Characteristics for Vanadyls during Hydrotreating.

for an oil subjected to these processes. As shown in Figure 5, there is only a small change in vanadyl coordination in products from the two thermal processes compared with the feed, and little vanadium is lost. Hydrotreating causes loss of vanadium, and that vanadium which survives is in a more "bound" state and has a lower dissociation energy. When hydrotreating follows a thermal process, the surviving vanadium is converted almost entirely into a "bound" state with a dissociation energy intermediate between the vanadium in the feed and when the feed is hydrotreated without a prior thermal treatment. Obviously, the effect of a combination of processes on vanadium is not additive (5).

#### Vanadium in Catalyst Pores

The bonding of vanadyl compounds to the inner surface of catalyst pores also was studied by ESR. Large- and small-pore catalysts with sharp pore distributions were prepared. These pore diameters were completely different from each other. Each catalyst was contacted with solutions of asphaltenes from a feedstock and asphaltenes from a hydrotreated feedstock at room temperature. Vanadyl compounds from these solutions diffused into the catalyst pores. ESR spectra of these vanadyl complexes were taken at 100°C.

As shown in Figure 6, the vanadyl complexes from the feed asphaltenes which diffuse into the small-pore catalyst are "free" when compared with the vanadyl complexes that diffused into the large-pore catalyst. The pore size in the large-pore catalyst is believed to approximate the size of asphaltene micelles. These micelles are dissociated when heated to 100°C, and some smaller vanadyl complexes become strongly adsorbed on the catalyst surface. These adsorbed vanadyl complexes are not reintegrated into micelle structures on cooling. A second increase in temperature results in vanadyl complexes having the same degree of freedom for feed asphaltenes in both the small- and large-pore catalyst. Asphaltenes from the hydrotreated product do not have micellar aggregations. The vanadyl complexes in these asphaltenes are strongly bound to the surface of the catalyst and would be expected to be reactive in any subsequent catalytic demetallization. Therefore in catalytic hydrodemetallization, it is important to consider molecular sizes of feed vanadyl complexes. It must be remembered in the design of hydrotreating catalysts for heavy oil upgrading that the molecules to be treated can exist in large associations.

#### Dependence of Catalytic Activities on Pore Structure and Changes Due to Metal Deposition

It is well known that pore structure (volume, diameter, surface area, etc.) is one of the most important properties of hydrotreating catalysts for heavy oils (6). For example, reactivities of catalysts with similar pore volumes depend on pore diameters. As illustrated in Figure 7, hydrodemetallization (HDM) activity depends on pore diameter. The pore diameter giving maximum activity is about 25 nm for a fresh catalyst. As metals deposit, reactivity becomes maximized at larger pore diameters. Hydrodeasphalting (HDA) activity shows a similar tendency to HDM activity. On the other hand, hydrodesulfurization (HDS) shows a maximum activity at pore diameters of about 10 nm. This means that the HDS activity is distinctly different from HDM or HDA activity. HDA is also affected by metal deposition.

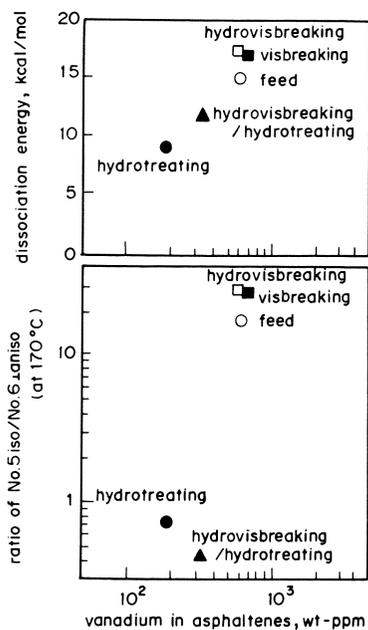


Figure 5. Vanadyls in hydrotreating, Thermal-treating and Combination of Those.

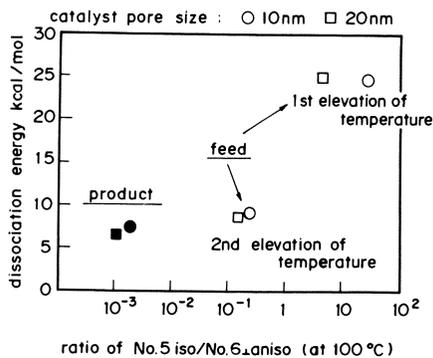


Figure 6. Vanadyls in Catalyst Pores.

Changes in pore structure due to metal deposition are determined by the amount of metal deposited and its distribution in the catalyst particle. Theoretical studies of metal deposition and distribution have been reported (7). The characterization of deposited vanadium is important to the understanding of catalyst activity, especially HDM activity.

#### Characterization of Vanadium Deposited on Catalysts

Vanadium deposits onto catalysts with a specific distribution. As shown in Figure 8, this distribution occurs along the reactor axial length and along the radius of individual catalyst particles. These particles were examined by X-ray microanalysis (XMA). Vanadium deposits were found to be concentrated near the reactor inlet and near the outer surfaces of catalyst particles. Metal deposits decrease along the reactor axis and toward the center of catalyst particles. At the reactor inlet itself, vanadium is less concentrated. There is also less vanadium in a very thin layer at the outside of catalyst particles. This phenomenon indicates that the HDM process requires hydrogen sulfide. As shown in the broken lines in Figure 8, the phenomenon disappears if HDM is performed with added hydrogen sulfide.

Deposited metals exist as sulfides and show X-ray diffraction (XRD) patterns attributable to a crystalline  $V_3S_4$  phase (8), as shown in Figure 9. In this  $V_3S_4$  phase, vanadium may be substituted by other transition metals such as nickel.  $V_3S_4$  is a non-stoichiometric compound in which the atomic ratio of sulfur to vanadium can vary from 1.2 to 1.5.

When vanadium sulfide deposits over catalyst outer surfaces, the polycrystalline state can be observed by scanning electron microscopy (SEM), as shown in Figure 10a. In catalyst pores, vanadium sulfide forms rod-shaped deposits several tens of nanometers thick and hundreds of nanometers in length, as determined by transmission electron microscopy (TEM) on an ultra-thin sample (Figure 10b). Electron diffraction (ED) studies also were performed (Figure 10c).

Since the deposited vanadium has been identified as  $V_3S_4$ , information about the surface of the vanadium sulfide has been obtained by X-ray photoelectron spectroscopy (XPS) and ESR. The XPS spectra are shown in Figure 11. The vanadium in the  $V_3S_4$  exists partly as  $V^{+4}$ , and on the outer surface of catalyst particles partly as  $V^0$ . Catalytic activities of the surface thus will vary with the makeup of the  $V_3S_4$  metal cluster compound. ESR spectra (Figure 12) show that some vanadium dispersed on catalyst surfaces exists as vanadyl ( $V=O$ )<sup>+</sup> ion.

#### The Change of Vanadyl Coordination

As reported previously (3), the nature of the ligands involved in chelation with vanadium may be determined by ESR spectra. This is done by examining the isotropic parameters  $g$  and  $A_0$  (the hyperfine constant). Ligand systems of vanadyl ion remaining in treated crudes are of the four-nitrogen donor type ( $VON_4$ ) (Figure 13). Vanadyl ion deposited on catalysts is complexed with sulfur ( $VOS_4$ ).

#### Catalytic Activity of Vanadium Sulfide

It has been shown that vanadium sulfide deposits grow in a directionally selective manner as the  $V_3S_4$  phase builds up. This growing

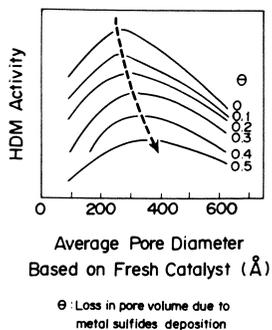


Figure 7. Hydrodemetallization Activity with Average Pore Diameter.

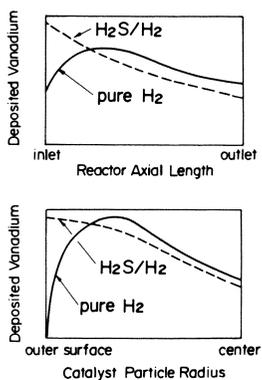


Figure 8. Distribution of Deposited Vanadium.

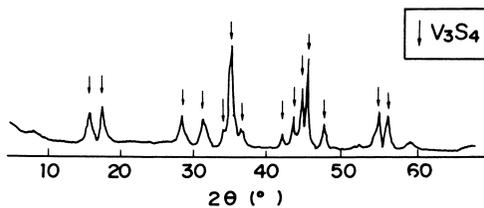


Figure 9. X-ray Diffraction Pattern.

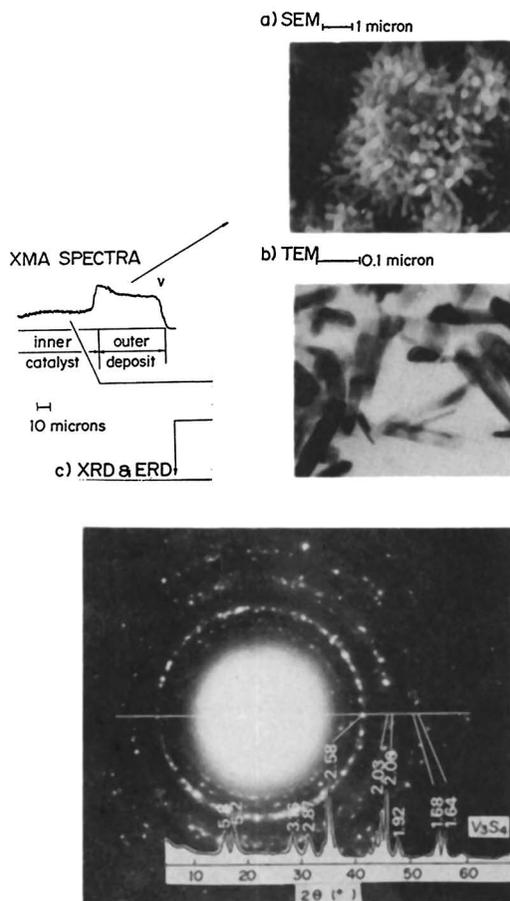


Figure 10. Observation of Deposited Vanadium Sulfide with SEM and TEM.

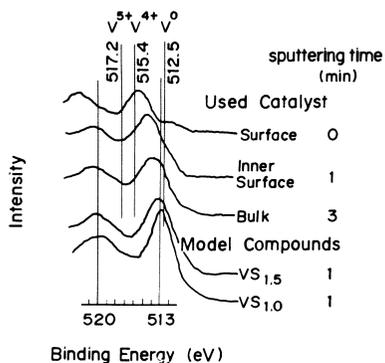


Figure 11. Oxidation State of Vanadium.

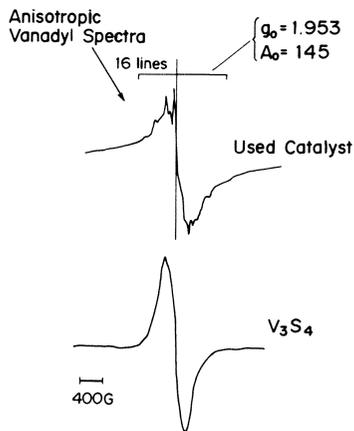


Figure 12. ESR Spectra of Vanadiums.

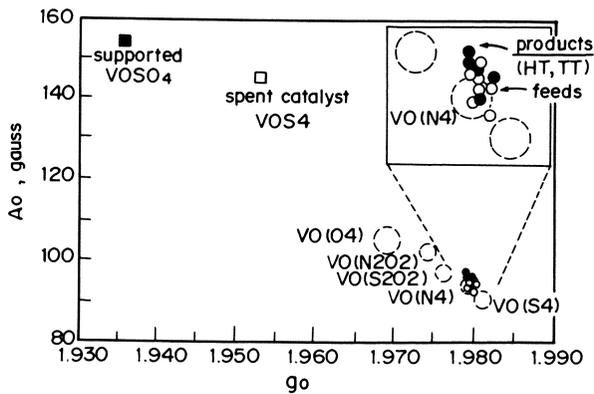


Figure 13. Characterization for Coordination of Vanadyls by ESR Parameters.

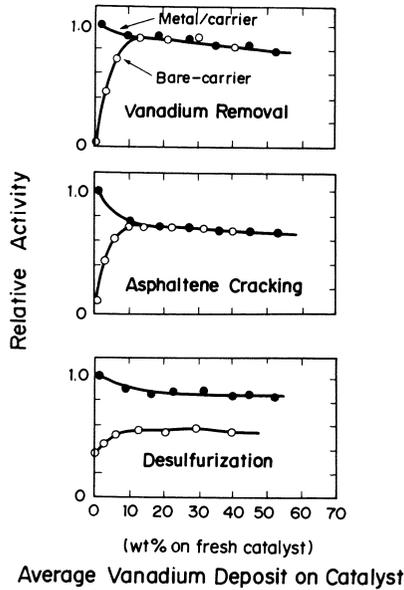


Figure 14. Catalytic Activities of Deposited Vanadium.

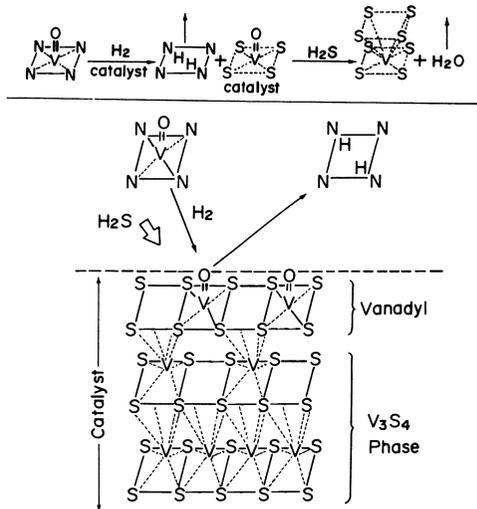


Figure 15. Model of HDM on Vanadium Sulfide.

surface has interesting characteristics and shows autocatalytic activity in HDM. A study was made of vanadium sulfide deposited on bare supports. Figure 14 shows the HDM and HDA activities of heavy oil on a bare support compared with activities on a supported catalyst. The Activities of both reactions changed in each case as vanadium deposition progressed. HDM and HDA activities catalyzed by vanadium sulfide are low at early stages compared with catalysts containing nickel, cobalt, and molybdenum. When the bare support becomes coated with a 10%  $V_2S_3$  phase, the HDM and HDA of the catalysts are observed to be similar. At this level of vanadium sulfide deposition, the activity of the supported catalyst also may be attributed to vanadium sulfide deposits. HDS activities of the two materials always show a distinct difference.

#### Proposed Reaction Mechanism of HDM with Vanadium Sulfide

From the above results, a mechanism for the HDM of heavy oil is proposed in Figure 15. Vanadyl porphyrins react with sulfur of deposited vanadium sulfide and further with hydrogen sulfide. Thus vanadium from the heavy crude becomes incorporated into the vanadium sulfide deposit on the catalyst. This substance also is effective for HDA.

#### Conclusions

Vanadium removal from asphaltenes plays an important role in hydro-treatment of heavy oils. The behavior of vanadyl compounds in heavy oils before and after treatment has been studied by various instrumental techniques, from which the following facts have emerged.

In the asphaltene cracking reaction, asphaltene micelles are destroyed along with the removal of vanadium. Vanadium compounds remaining in a treated heavy oil do not become involved in micelle formation, but are involved in smaller associations. These remaining vanadium compounds are reactive toward subsequent catalytic hydro-treating. Studies also were made on thermal treatments followed by hydrotreating of a heavy crude.

In the hydrotreating of heavy crudes, HDM and HDA depend greatly on catalyst pore structure, which changes with hours-on-stream and depends on the molecular size of the reactants. The pore structure for these reactions therefore should be determined by consideration of metals deposition.

Vanadium compounds in feed oils appear to have four-nitrogen coordination and are porphyrins or similar compounds. The vanadium deposited on catalyst surfaces is bonded to sulfur.

Vanadium sulfide deposited on a catalyst during HDM not only causes changes in catalyst pore structure, but also has autocatalytic activities for HDM and HDA. A HDM mechanism on catalyst surfaces has been proposed which considers the HDM activity derived from the deposited vanadium sulfide.

#### Literature Cited

1. Dickie, J.P.; Yen, T.F., Anal. Chem., 1967, 39, 1847.
2. Takeuchi, C.; Fukui, Y.; Nakamura, M.; Shiroto, Y., Ind. Eng. Chem. Process Des. Dev., 1983, 22, 236.
3. Asaoka, S.; Nakata, S.; Shiroto, Y.; Takeuchi, C., Ind. Eng. Chem. Process Des. Dev., 1983, 22, 242.

4. Tynan, E.C.; Yen, T.F., Fuel (London), 1969, 43, 191.
5. Komatsu, S.; Kasiwara, H.; Shimizu, S.; Suzuki, H., The Third International Conference on Heavy Crude and Tar Sands (UNITAR), California, 1985.
6. U.S. Patent 4, 422, 960.
7. Shimura, M.; Shiroto, Y.; Takeuchi, C., Div. Colloid and Surf. Chem., ACS, Las Vegas Meeting, April 1982.
8. Kawada, I.; Nakano-Onoda, M.; Ishii, M.; Saeki, M.; Nakahira, M., J. Solid State Chem., 15, 246 (1975).

RECEIVED December 10, 1986

## Chapter 19

# Characterization of Humic Matter Associated with Heavy Minerals from Oil Sand

Abdul Majid and John A. Ripmeester

Division of Chemistry, National Research Council of Canada, Ottawa,  
Ontario K1A 0R9, Canada

Humic matter associated with heavy metal minerals present in Athabasca oil sands, was isolated using sodium hydroxide extraction and by dissolving the mineral matter in acids. These fractions were analyzed by elemental analysis and infrared, proton and  $^{13}\text{C}$  NMR spectroscopy. Comparison of this data with the corresponding data for humic acids from sub-bituminous coal and peat and asphaltenes from bituminous feed stock, suggest the similarity of this humic material with humic matter from sub-bituminous coal. It appears to have very little potential for hydrocarbons production because of its position in the Van Krevelen diagram. Origin of this organic matter could be different from that of the greater part of the bitumen of the Athabasca oil sands.

Athabasca oil sand is a complex, variable mixture of bitumen, sand, water and clays (1). The total reserves of oil sand deposits are estimated to contain close to  $2.15 \times 10^{11} \text{ m}^3$  of bitumen in place (2-5). The Athabasca deposit is currently under commercial exploitation, by Suncor and Syncrude using the hot water extraction process developed in the 1920's by K.A. Clark (6). This process results in very large volumes of tailings, consisting mainly of sand and a dispersion of various clays containing residual organic matter (1,7-9). The sand settles rapidly from the tailings and is used to build containment dikes for aqueous sludges that show little tendency to dewater, even when subjected to mechanical dewatering procedures (10). It is the buildup of these partially settled clay sludges which presents not only an environmental problem but also a significant repository for non-recycleable water.

The reason for the intractability of the clay slimes has been a subject of considerable study (1,7,9,11-13). Considerable quantities of insoluble organic material are known to be associated with these clay slimes (8,14-15). Most of this organic material is strongly associated with the mineral fines and is insoluble in organic solvents under mild conditions (16).

0097-6156/87/0344-0290\$06.00/0  
Published 1987 American Chemical Society

Based on the results of published work it is generally believed that the interaction of organics with the clay minerals is important in determining the nature of the oil sand slimes (8,14-15). The interaction is thought to provide a hydrophobic character to the clay particle surfaces allowing bridging through residual bitumen to set up a weak gel structure.

Relatively little information is currently available concerning the nature of the unextractable organic matter. In a recent publication Ignasiak et al. have reported that this organic matter consists of humic and non-humic components containing numerous oxygen functions (17). In our previous work we have attempted to isolate and then concentrate this organic matter using oil phase agglomeration and acid dissolution techniques followed by the removal of soluble organic material by a Soxhlet extraction method using benzene/methanol (8,18-19). These organic materials were then studied using elemental analyses and spectroscopic techniques. The data was discussed in terms of the chemical structure and the nature of bonding between the mineral phase and the organic phase of oil sands.

In this investigation we have attempted to isolate this strongly bound organic matter from heavy metal mineral fractions by successive extractions with aqueous sodium hydroxide over a prolonged period of time. Elemental analyses and spectroscopic techniques were used for the characterization of organic material from oil phase solids (OPS). Comparisons have been made among peat and coal humic acids, asphaltenes from oil sand bitumen and the organic matter adhering to the mineral fines in oil sands in an attempt to understand the formation of oil sand deposits. It is also hoped that study might provide insight into beneficiation and enrichment of the organic matter in low grade oil sands that are known to contain significant quantities of unextractable organic matter (16).

### Experimental Methods

Sample Description. Aqueous tailings in 5-gallon to barrel-size lots were obtained from the Suncor plant sludge pond, and contained 5-12% solids by weight, although in some lots the solids content ranged as high as 30%.

Oil Phase Solids. Oil phase solids (OPS), the heavy metal minerals fraction containing unextractable organic matter were isolated from Suncor sludge using oil phase agglomeration techniques reported elsewhere (19).

Humic Acid Extraction. Figure 1 is a flow-sheet for the extraction of humic and fulvic acids from oil phase solids (OPS). A 20g sample of oil phase solids (OPS) was digested with 200 ml 2% aqueous NaOH at 70°C under N<sub>2</sub> for a period of one month. The digestion was repeated six times with successive fresh portions of aqueous NaOH solution, decanting the spent NaOH each time. The alkaline solution was subsequently separated from the sand by centrifugation, and acidified to pH 2 with 5N HCl. After 24 hours,

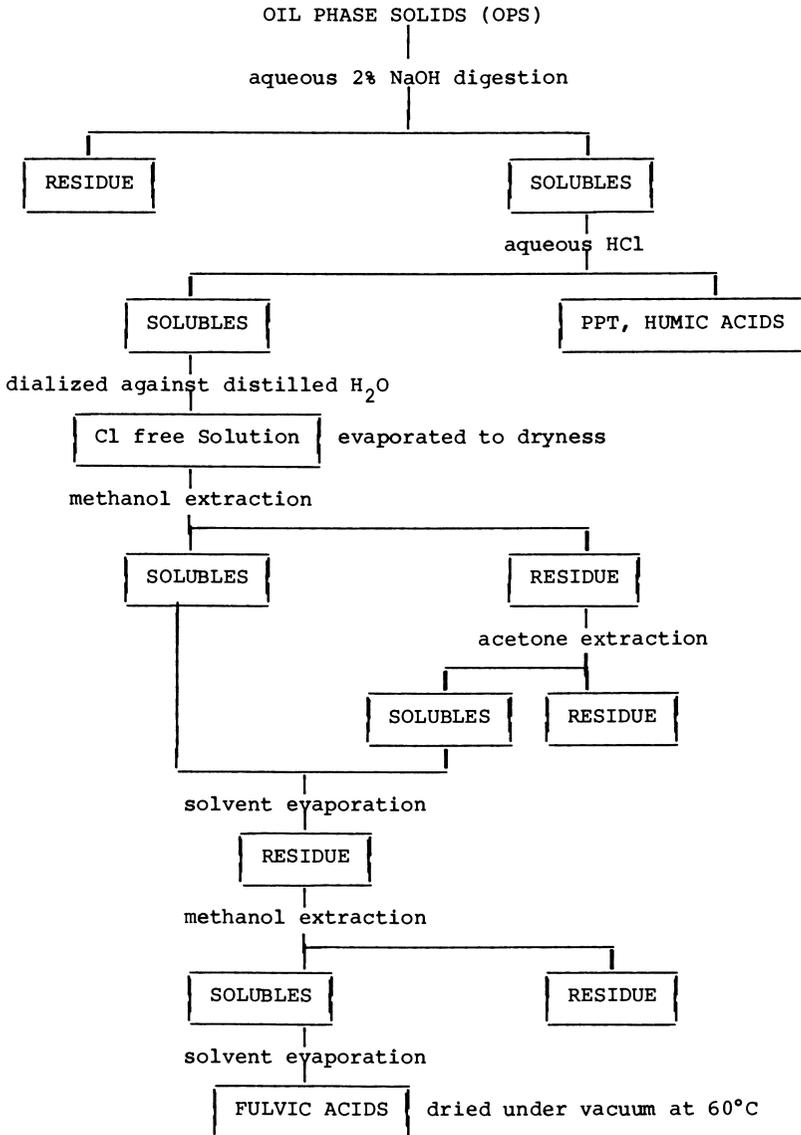


Figure 1 Flow sheet for the extraction of Humic and Fulvic Acids.

the precipitated humic acids were recovered from the solution by filtration. The precipitate was washed several times with 1% HCl. The total amount of humic acids extracted after six extractions corresponded to 12.0% of the weight of the OPS. Although more humic acids could be extracted from OPS, complete recovery of humic matter from OPS was an extremely time consuming procedure and hence stopped after six extractions.

Fulvic Acid Extraction. The solution obtained after removal of humic acids was dialyzed against distilled water until free of Cl, and then concentrated by evaporation of water at 50°C. The residue was then extracted with methanol, followed by acetone. The two extracts were combined, the solvents distilled, and the residue was repeatedly redissolved in methanol until no residue was observed. Finally, the solvent was removed from the clear methanol solution, yielding the fulvic acids. The humic and fulvic acids were dried in a vacuum oven at 60°C to constant weight.

Bitumen. Analytical data reported for bitumen from bituminous feed stock sand was taken from a round robin study (20). The sample used in this study was a coker feed bitumen from Suncor, obtained in February, 1981.

Asphaltenes. Asphaltenes were precipitated from benzene solution of the above mentioned bitumen by the addition of a fifty fold excess of n-pentane over a period of 4-6 hours while stirring under N<sub>2</sub>. The precipitated asphaltenes were filtered through a Whatman filter paper #42, washed several times with n-pentane until the filtrate became almost colorless and finally dried in a vacuum oven at 60°C.

Humic Acid from Oil Sand. Analytical data reported for humic acid extracted from oil sands was taken from D.S. Montgomery (21).

Organic Matter from Low Grade Oil Sands. A low grade oil sand sample (bitumen content ≈5%) obtained from Alberta Research Council sample bank was used for isolating the toluene insoluble organic matter associated with the mineral fraction of oil sands. The sample was first extracted with toluene in a Soxhlet apparatus for 48 hours. Residue was dried at 100°C overnight and then treated with 6 N HCl to decompose carbonates, followed by digestion with concentrated HCl to dryness. The residue was repeatedly washed with warm water until free from chloride. It was then digested with 35% HF to dryness and washed repeatedly with warm water until the washings became neutral. The organic matter concentrate so obtained was then dried under vacuum at 50°C.

Elemental Analysis. C, H and N analyses were performed using a Perkin-Elmer model 240 CHN analyser. Mineral carbon was measured titrimetrically after acid digestion. Organic carbon was then determined by subtracting carbonate carbon from total carbon. Sulfur was analysed as total sulfur using X-ray fluorescence spectroscopy. Oxygen was determined directly (20). For mineral samples containing adsorbed organic matter, the ultimate analysis was done at the Energy, Mines and Resources laboratory using ASTM procedure D271.

Ash Content. Ash content of oil phase solids and their solid fractions was determined by heating at 380 ± 10°C to constant weight. After cooling to room temperature, the samples were soaked in water for 4 hours and finally dried at 110°C to constant weight. The difference between the initial and the final weights was taken as "loss-on-ignition" (21).

Instrumental Analysis. Infrared spectra were recorded using a Perkin-Elmer model 683 IR spectrometer. Samples were run as KBr pellets.

Proton NMR measurements were performed on a Bruker MSL 300 NMR spectrometer (300 MHz). The spectra were recorded in solution in NaOD and deuterated DMSO.

All solid state C-13 NMR spectra were obtained at 22.6 MHz on a Bruker CXP180/90 NMR spectrometer using the cross polarization (CP) technique with magic angle spinning (MAS). A contact time of 1 ms and a repetition time of 2s were selected. The magic angle spinning speeds were 3.0-3.4 KHz. Chemical shifts were determined by position relative to tetramethylsilane (TMS). Each spectrum was the Fourier transform of 3000-10000 free-induction decay curves.

C-13 solution spectra of  $\approx 5\%$  humic acid in NaOD were run at 75.47 MHz on Bruker MSL 300 NMR spectrometer, employing inverse gated decoupling and 30,000-40,000  $45^\circ$  pulses at intervals of 3 seconds.

### Results and Discussion

A typical analysis of the heavy metal mineral fraction containing unextractable organic matter (oil phase solids, OPS, loss on ignition at  $380^\circ\text{C}$ , 32.5%) is given in Table I.

Table I  
Analytical Data for a Typical Oil Phase Solid Sample

	wt. %
Carbon	19.3
Hydrogen	1.4
Nitrogen	0.3
Sulfur	3.5
SiO <sub>2</sub>	13.0
Al <sub>2</sub> O <sub>3</sub>	5.0
Ti	18.0
Zr	2.0
Fe	8.6
Cu	0.05
Ni	0.03
Mn	0.21
Zn	0.04

The fact that a major portion of this organic matter associated with heavy metal minerals can be extracted with aqueous NaOH, strongly suggests the humic nature of this organic matter. One of the most important characteristic of humic substances is their ability to interact with metal ions, metal oxides and metal hydroxides to form associations of widely differing chemical and biological stabilities (22, 23). It is believed that ion exchange, surface adsorption, chelation, coagulation and peptization processes are involved in such interactions (24-26). Also, the

humic substances are known to form both chelated and ionic complexes with Al, Ba, Co, Cr, Cu, Fe, Mn, Ni, Ti and V(27-30). It is therefore, very likely that most of the metals occurring in OPS are associated with the humic matter in the form of humic matter-metal or metal oxide complexes.

The elemental compositions of bitumen, asphaltenes, organic matter from a sample of toluene extracted low grade oil sand, humic acid extracted from oil sands, OPS and humic and fulvic acids extracted from OPS are given in Table II. Examination of the data leads to the following conclusions:

Table II  
Elemental Analyses (in Percentage of dry, ash free basis)

Sample	wt. %					Atomic Ratios	
	C	H	N	S	O	H:C	O:C
Humic Acid extracted from OPS	67.37	4.40	1.00	3.0	24.23	0.78	0.237
Fulvic Acid extracted from OPS	39.23	5.05	1.12	10.24	44.36	1.54	0.848
Organic Matter associated with OPS	61.24	5.22	2.82	4.15	26.57	1.02	0.33
A Typical Oil Sand Bitumen Sample	83.01	10.48	0.44	4.74	0.91	1.51	0.008
Asphaltenes from Oil Sand Bitumen	80.87	8.32	1.02	7.61	2.29	1.23	0.021
Humic Acid from Oil Sands	67.41	4.34	1.42	2.66	24.17	0.77	0.27
Organic Matter from Low Grade Oil Sands	57.0	4.8	-	15.5	22.67	1.01	0.30

1. The elemental composition of the humic acid extracted from OPS is remarkably similar to that of the one extracted from oil sands. Both of these substances have considerably higher carbon content and lower nitrogen and oxygen contents compared with the soil or aquatic humic acids (28). The composition of the humic acids extracted from OPS and oil sands resembles that of coal humic acid more so than aquatic or peat humic acids (28).

2. Oxygen is the most abundant heteroatom in OPS, humic and fulvic acids, and toluene extracted low grade oil sands organic matter.

3. The carbon content of these fractions is considerably lower compared to those of the corresponding asphaltene and bitumen of the bituminous sand feedstock.
4. The sulfur content of the fulvic acid and toluene extracted oil sands is considerably higher than those of other fractions presumably due to the presence of inorganic sulfur (19).
5. The nitrogen content of OPS is about twice that of humic and fulvic acids extracted from it.

Comparable elemental compositions of the humic acids extracted from oil sands and OPS suggest that no appreciable alteration of the humic matter occurs either during hot water extraction of bitumen from oil sands or during storage in the tailings ponds.

Higher oxygen content of these fractions is typical of humic materials as these materials are known to contain considerable quantities of oxygen containing functional groups such as carboxyls, phenolics, alcoholic hydroxyls, carbonyls and methoxyls (28).

Lower nitrogen content of humic and fulvic acid fractions compared with the feed stock could be due to the loss of some nitrogen by hydrolysis of some nitrogen compounds during extraction (31). Also one of the reviewers has suggested that NaOH may have left N-containing material unextracted on the OPS.

The Van Krevelen diagram, which is a graph of atomic H/C versus O/C ratios provides a useful approach for the characterization of coals, kerogens and humic matter (32-33). These materials can be classified into one of the three types based on the Van Krevelen diagram.

Humic and unextractable organic matter from oil sands were plotted on the Van Krevelen diagram as shown in Figure 2. All of these fractions appear to be similar to type 3 kerogens. These types of kerogens are known to be comprised of an important proportion of polyaromatic nuclei and heteroatomic ketone and carboxylic acid groups (33). Aliphatic groups are subordinate constituents in varying proportions of this organic matter. They consist of a few long chains originating from higher plant waxes, some chains of medium length from vegetable fats, methyl groups and other short chains. This type of organic matter is derived essentially from terrestrial plants, and is incorporated in sediment either directly or through its alteration products in the form of soil humic acids. Humic coals have been classified under this category (34). This type of organic matter is least favourable for oil generation (33).

Infrared Spectra. The infrared spectra provide some indication of the chemical nature of the material. It enables one to detect the presence of chemical groups, preclude or limit the existence of proposed structures, and demonstrate similarities and differences in chemical structure of the organic materials studied. Infrared

spectra of humic acid, fulvic acid, OPS and a sample of asphaltenes are shown in Figure 3. The assignment of the various bands is based on the published work for coal, asphaltenes and humic materials (35-45). The main zones of interest are as follows:

1. A broad absorption band around  $3200-3400\text{ cm}^{-1}$ , related to H-bonded OH groups (phenolic, alcoholic, carboxylic OH), small contributions from N-H groups being also possible;
2. Weak to strong absorptions in the  $\approx 2900\text{ cm}^{-1}$  region are attributed to  $\text{CH}_2$  and  $\text{CH}_3$  aliphatic groups;
3. A broad band centered at  $1720\text{ cm}^{-1}$ , related to various C=O groups (ketones, acids, esters);
4. A medium intensity broad band centered at  $1600\text{ cm}^{-1}$ , attributed partly to conjugated C=C bonds and partly to carbonyl of ketones and/or quinones;
5. Varying intensity bands at  $1450$  and  $1380\text{ cm}^{-1}$  are due to bending frequencies of asymmetric C- $\text{CH}_3$  bond and/or methylene and symmetric C- $\text{CH}_3$  bond respectively.
6. A group of bands located around  $1100$ ,  $1030$  and  $900\text{ cm}^{-1}$  are assigned to C-O stretch in aromatic oxygenated compounds, such as aromatic ethers, sulfoxides and polysaccharides.
7. Strong bands in the infrared spectrum of fulvic acid at  $800$ ,  $650$  and  $550\text{ cm}^{-1}$  are considered aromatic out of the plane frequencies and are important with regard to the nature of the structure of aromatic clusters.

Fulvic acid shows a strong absorption at  $3200\text{ cm}^{-1}$  compared with humic acid and OPS. This indicates much higher OH groups contents in fulvic acid compared with other fractions suggesting greater hydrogen bonding.

Humic acid has a stronger absorption in the  $2900\text{ cm}^{-1}$  region compared with weak absorption for fulvic acid. This indicates the presence of greater numbers of  $\text{CH}_2$  and  $\text{CH}_3$  groups in humic acid compared with the fulvic acid. Two bands at  $2420$  and  $2340\text{ cm}^{-1}$  in the infrared spectrum of fulvic acids appear to be due to the presence of an impurity. Phosphates are known to absorb in this region (46). Fulvic acid has an extremely large and broad absorption at  $1450\text{ cm}^{-1}$  compared with well resolved weak absorptions at  $1450$  and  $1380\text{ cm}^{-1}$  for humic acid, asphaltenes and OPS. The much higher intensity of this band compared with the CH stretching vibrations around  $2900\text{ cm}^{-1}$  preclude the assignment for this band due to deformation vibrations of  $\text{CH}_3$  and  $\text{CH}_2$  groups. Ignasiak et al. have recently reported a similar pattern in a polar fraction extracted from oil sands (17). They assigned this absorption to strongly polarizable carbonyl groups such as diketones and/or  $\alpha$ ,  $\beta$ -unsaturated ketones complexed to  $\text{FeCl}_3$ . The presence of considerable quantities of iron in the ash from fulvic

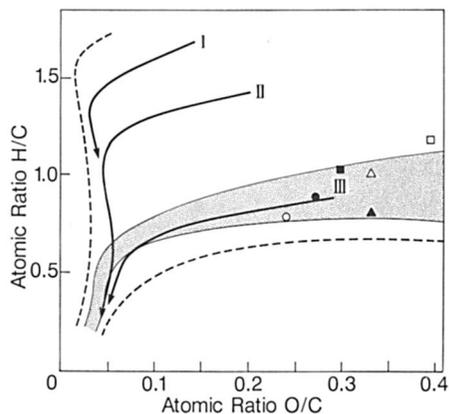


Figure 2. Van Krevelen diagram showing the principal types and evolution paths of kerogens. OPS,  $\Delta$ ; Humic acid from OPS,  $\circ$ ; Peat,  $\square$ ; Coal humic acid,  $\blacktriangle$ ; Lignites,  $\bullet$ ; Organic matter from low grade oil sand,  $\blacksquare$ .

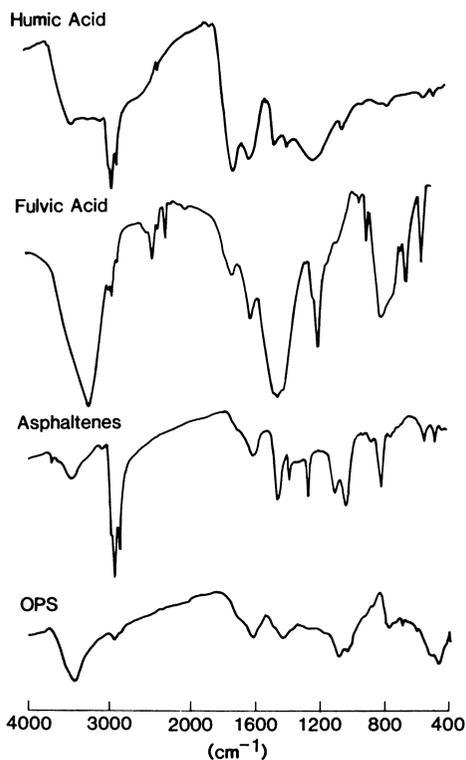


Figure 3. Infrared spectra of OPS, humic and fulvic acids and asphaltenes.

acid supports the possibility of such an assignment in the present case.

The absorption due to C-O stretching and OH deformation of COOH group and aryl ethers, is stronger and sharper for fulvic acid compared with humic acid.

Bands for the aromatic out of plane frequencies around 800-500  $\text{cm}^{-1}$  are also much stronger for fulvic acid compared with humic acid.

The essential features of the humic and fulvic acid spectra are the same as of OPS and asphaltenes. The major difference in the spectrum of fulvic acid from those of other fractions is the relative intensities of the various bands.

Proton NMR Spectra. Figure 4 shows the proton NMR spectra for humic and fulvic acids. General features of the two spectra are similar. However, the humic acid spectrum shows a relatively sharper and stronger signals compared with the fulvic acid spectrum. Both spectra show a resonance around 0.7 ppm due to  $-\text{CH}_3$  protons. Humic acid shows two signals due to  $-\text{CH}_2$  protons at 1.0 and 1.1 ppm. Corresponding signals in the fulvic acid spectrum are located at 1.0 and 1.3 ppm. Weak signals around  $\approx 2.0$  ppm in the fulvic acid spectrum could be due to the hydrogen on carbon atoms  $\alpha$  to ring.

Aromatic protons appear as a broad signal between 7-9 ppm in the humic acid spectrum. Fulvic acid has a barely detectable broad signal partly overlapped by the residual protons from heavy water.

$^{13}\text{C}$  NMR Spectra. The CP/MAS- $^{13}\text{C}$  nmr spectra of the strongly bound organic matter associated with heavy metal minerals and fines from oil sands and three humic acid samples extracted from OPS, sub-bituminous coal, and a sample of peat are shown in Figure 5. Interpretation of the  $^{13}\text{C}$  nmr spectra has been based on the published data on humic substances and coal related materials (47-57). The spectra are poorly resolved and show only bands rather than sharp peaks.

The presence of a broad range of aliphatic compounds in all the spectra is indicated by the resonance in the 10-50 ppm range. The large peak at 30 ppm is due to the presence of a number of repeating polymethylene units in humic macromolecules. The presence of two small peaks at  $\approx 14$  and 20 ppm in the spectrum of OPS humic acid sample indicates the presence of long-chain-terminating methyl groups. A small signal at 38 ppm in the spectrum of humic acid from OPS could be due to the bridgehead or other CH naphthenic carbons.

As the nitrogen content is low compared to the oxygen content for these samples, carbohydrates, ether and methoxy groups are expected to be the major contributors to the resonance in the 50-100 ppm region. Distinct bands in this region are displayed by the Peat humic acid and OPS humic acid. It is most likely that

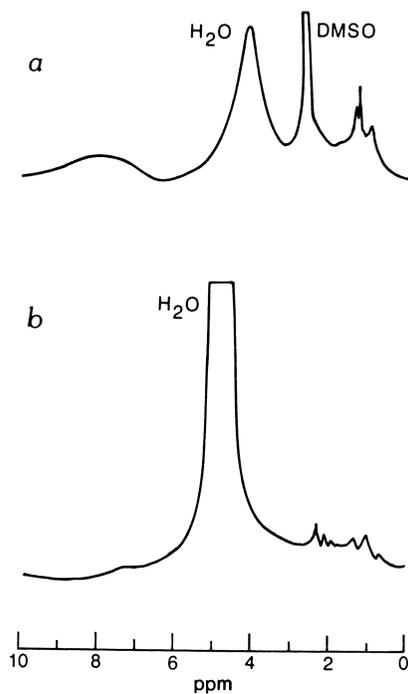


Figure 4. Proton NMR spectra of a) Humic acid from OPS, b) Fulvic acid from OPS.

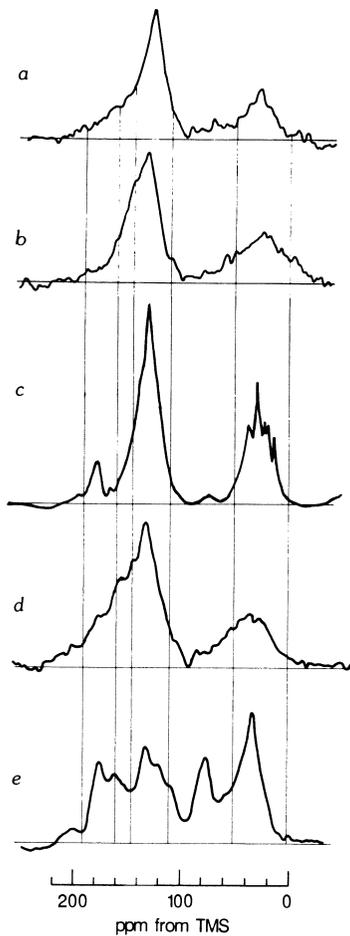


Figure 5. CP/MAS  $^{13}\text{C}$  NMR spectra of a) Toluene extracted low grade oil sand, acid leached b) OPS, d) humic acid from sub-bituminous coal and e) peat humic acid, and c)  $^{13}\text{C}$  NMR spectrum of humic acid from OPS in NaOD.

this band is derived from carbohydrates considering the fact that carbohydrates have been identified as major components of some sedimentary humic acids (58). However, the relative contribution of polysaccharides in humic matter from oil sand and sub-bituminous coal is small compared with the Peat humic acid.

The aromatic region extends from 110-160 ppm. Aromatic ether and phenolic carbons appear between 150-160 ppm, aromatic bridgehead and substituted aromatic carbons between 130 and 150 ppm. The phenolic carbons in the humic matter from oil sands are not resolvable as distinct peaks.

A distinct broad peak is observed at  $\approx 180$  ppm in the  $^{13}\text{C}$  spectra of humic acids from OPS and Peat. This peak represents carboxyl, amide and ester carbons, all of which have been identified as important functionalities of humic acids (58). Additional resonances are observed downfield of the carboxyl resonance in the region of approximately 200-220 ppm. These resonances are characteristic of aldehyde and ketone carbons. Although no distinct resolved peaks are observed, their presence is obvious in the spectra of all three humic acids as a broad band, with contributions of about 0.5-5% of the total signal.

The integration of each spectrum was carried out by division into regions and subsequent determination of their individual areas. The position of regional boundaries in spectra is a matter of definition, as no representative model compounds for these substances are available. The limits were chosen according to Ibarra et al. and Verheyen et al. (55,56). The spectra were divided into four regions as listed in Table III, below.

Aliphatic ethers and alcohols are usually considered to make only a minor contribution to the structure of humic acids (55).

Table III  
Assignment of  $^{13}\text{C}$  Chemical Shift Ranges

Region	Chemical Shift Range	Carbon Type
A <sub>1</sub>	0-50	Aliphatic
A <sub>2</sub>	50-110	Aliphatic C-OH, C-OR, Carbohydrate
B	110-145	Aromatic C-H Aromatic C-C Alkyl substituted aromatic carbon
C	145-160	Aromatic C-OH, C-OR
D <sub>1</sub>	160-190	Acid, ester, COOH, COOR
D <sub>2</sub>	190-230	Aldehyde, ketone

Aliphatic carbon ( $\text{C}_{\text{al}}$ ) is given in the spectrum by region A<sub>1</sub> and A<sub>2</sub> and Aromatic carbon ( $\text{C}_{\text{ar}}$ ) by region B and C. The quantitative  $^{13}\text{C}$  nmr measurements are given in Table IV.

Table IV  
Quantitative  $^{13}\text{C}$  NMR of Humic Acids and Related Materials

Sample	Area of Total Spectrum			(% Atomic		$\Delta$	$F_a$	
	$A_1+A_2$	B	C	$D_1$	$D_2$ O/C			
OPS	39.1	38.8	12.4	9.2	0.5	0.31	-0.02	56
Humic acid from OPS	43.1	38.7	5.7	9.0	3.5	0.24	0.0	51
Organic matter from low grade oil sands	32.6	46.2	9.3	9.6	2.3	0.31	+0.01	63
Humic acid from sub-bituminous coal	34.0	35.6	12.0	13.8	4.6	0.44	?	59
Peat humic acid	55.4	21.7	7.7	13.4	1.8	0.36	?	35

The contribution of oxygen bound to aliphatic carbons can be estimated, according to Verheyen et al. (56), by comparing the O/C ratios calculated from elemental analysis and by  $^{13}\text{C}$  nmr measurements ( $C+2D_1+D_2/100$ ). If all the oxygen is present in carbonyl, carboxylic and phenolic structures, the ratios calculated by both methods should be comparable. Table IV shows the difference ( $\Delta$ ) between the O/C ratios calculated by the two methods. The results indicate that aliphatic oxygen functions are not significant compared with the proportion of carbonyl, carboxylic and phenolic groups in the humic matter from oil sands.

Table IV also lists the aromaticities calculated by integrating peak areas assigned to aromatic carbons (100-160 ppm) and normalizing to total area less the area of carboxyl carbons (54). It is evident from the table that at least one half of the total carbons in the humic matter from oil sands and sub-bituminous coal are in aromatic locations. The aromaticities of unextractable organic matter from oil sands and heavy metal minerals present in oil sands (OPS) and of humic acids extracted from OPS are comparable to the corresponding value for humic acid from sub-bituminous coal, and much higher compared with the value for peat humic acids. This suggests that the unextractable organic matter from oil sands could be humic matter comparable in maturity to that of sub-bituminous coal.

### Conclusions

Significant portion of the organic matter adhering to the heavy metal minerals from oil sands appears to be humic because of its solubility in NaOH. Also, the elemental analysis, infrared and NMR spectroscopic results indicate a remarkable similarity of this organic matter to the humic acid extracted from oil sands. Infrared and NMR spectroscopic results indicate the presence of such species as hydrogen bonded phenols, alcohols, ethers, polysaccharides, amides, polyaromatics with long paraffinic chains, carboxylic acids, quinones and ketones. This is again consistent with the material being humic. Most of the above mentioned functionalities are capable of forming chemical bonds with metals, and metal oxides. Chemical bonding between phenols, ethers, amides,

carboxylic acids, quinones and ketones and metals appears more probable.

Humic matter from oil sands has H/C and O/C distributions comparable to the gross composition of peat, lignite and subbituminous coal. It falls in the region of kerogen (III) on the Van Krevelen diagram. This type of organic matter is usually derived from plants of terrestrial origin and is rich in polyaromatic nuclei and heteroatomic ketone and carboxylic acid groups (33). Type III kerogen is not considered to have potential for hydrocarbon generation and usually matures to give coal (33). It appears to be of comparable maturity to that of humic acids from lignite or sub-bituminous coals and is relatively immature when considered in light of its oil generation potential.

These observations are consistent with two possibilities. One is that the entire oil sand deposit is immature, and that bitumen and the type III Humic material simply represent independent development of distinct source materials. Asphaltenes could then be thought of at least as being related to type I Kerogen (33).

The second possibility is that bitumen was formed elsewhere, perhaps in an older formation, and migrated to its current location. In establishing relationships between the different types of organic matter, the role of degradation and the presence of metallic minerals is still largely unknown.

#### Acknowledgments

The elemental analyses were performed by V. Clancy and J.R.H. Seguin for which we are grateful. We are also indebted to G.T. Gardner for infrared spectra and Mrs. M.R. Miedema for heavy metal analyses. The assistance from the Energy lab of Energy Mines and Resources in the analysis of some samples using ASTM procedure D271 is also gratefully acknowledged.

#### Literature Cited

1. Camp, F.W. "The Tar Sands of Alberta, Canada"; Cameron Engineers Inc.: Denver, 1969.
2. Outtrim, C.P.; Evans, R.G. In "The Oil Sands of Canada - Venezuela"; Redford, D.A.; Winestock, A.G., Ed.; Can. Inst. Min. Metallurgy: Montreal, 1977; vol. 1, p. 36.
3. Mossop, G.D. In "Facts and Principles of World Petroleum Occurrence"; Miall, A.D., Ed.: Can. Soc. Petrol. Geol. Memoir: 1980; vol. 6, p. 609.
4. Mossop, G.D. *Science* 1980, 207, 145-152.
5. Towson, D.E. *J. Can. Pet. Technol.* 1979, 18, 10-12.
6. Clark, K.A.; Pasternack, D.S. *Ind. Eng. Chem.* 1932, 24, 1410-1416.
7. Kessick, M.A. *Proc. Surf. Phenom. Enhanced Oil Recovery*, 1981, p. 559.
8. Ripmeester, J.A.; Sirianni, A.F. *J. Can. Pet. Technol.* 1981, p. 131.
9. Young, R.N.; Sethi, A.J. *J. Can. Pet. Technol.* 1978, 76, 76.

10. Camp, F.W. Can. J. Chem. Engin. 1977, 55, 581.
11. Kessick, M.A. CIM Bulletin 1978, 71, 80.
12. Kessick, M.A. International J. Min. Process 1980, 6, 277.
13. Hall, H.S.; Tollefson, E.L. Can. J. Chem. Engin. 1982, 60, 812.
14. Majid, A.; Ripmeester, J.A. J. Separ. Proc. Technol. 1983, 4, 20-22.
15. Kessick, M.A. J. Can. Pet. Technol. 1979, 77, 49.
16. Majid, A.; Sirianni, A.F.; Ripmeester, J.A. Fuel 1982, 61, 477.
17. Ignasiak, T.M.; Zhang, Q.; Kratochvil, B.; Maitra, C.; Montgomery, D.S.; Strausz, O.P. AOSTRA J. Res. 1985, 2, 21.
18. Majid, A.; Ripmeester, J.A.; Davidson, D.W. "Organic Matter Adsorbed to Heavy Metal Minerals in Oil Sands"; NRC, Chem. Div. Rep. #C1095-82S, 1982.
19. Majid, A.; Ripmeester, J.A. Fuel 1986 (in press).
20. Culmo, R. Mikrochimica Acta 1968, 811.
21. Majid, A.; Sparks, B.D. Fuel 1983, 62, 772.
22. Ruggiero, P.; Sciacovelli, O.; Testini, C.; Interesse, F.S. Geochimica et. Cosmochimica Acta 1978, 42, 411.
23. Senesi, N.; Griffith, S.M.; Schnitzer, M. and Townsend, M.G. Geochimica et. Cosmochimica Acta 1977, 41, 969.
24. Alhksandrova, L.N. Soviet Soil Sci 1967, 7, 903.
25. Broadent, F.E. and Ott, J.B. Soil Sci 1957, 83, 419.
26. Kononova, M.M. "Soil Organic Matter", Pergamon Press, New York, 1966.
27. Cheshire, M.V.; Berrow, M.L. Goodman, B.A.; Mundie, C.M. Geochim Cosmochim Acta 1974, 41, 1131.
28. Schnitzer M. and Khan, S.U. "Humic substances in the Environment"; Marcell Dekker, New York, 1972.
29. Adhikari, M.; Chakrabarti, K.K., and Chakrabarti, G. J. Indian Chem. Soc. 1978, 35, 439.
30. Adhikari, M.; Chakrabarti, G. J. Indian Chem. Soc. 1977, 54, 573.
31. Debyser, Y.; Gadel, F. "Geochemimie Organique des Sediments Marines Profonds"; Orgon I, Mer de Norvege; 1977, 247.
32. Krevelen, van, D.W. "Coal"; Elsevier: Amsterdam, 1961.
33. Tissot, B.P.; Welte, W.H. "Petroleum Formation and Occurrence"; Springer-Verlag: Berlin, 1984.
34. Durand, B.; Monin, J.C. In "Insoluble Organic Matter from Sedimentary Rocks", Durand, B. Ed. Editions Technip; Paris, 1980.
35. Friedel, R.A.; Queiser, J.A. Anal. Chem. 1956, 28, 22.
36. Friedel, R.A.; Retcofsky, H.L. In "Spectrometry of Fuels"; Friedel, R.A. Ed.; Plenum: New York, 1970, 46.
37. Taylor, S.R.; Galya, L.G.; Brown, B.J.; Li, L.C. Spectroscopy Letters 1976, 9, 733.
38. Smith, A.L. "Applied Infrared Spectroscopy"; John Wiley and Sons Inc.: New York, 1979.
39. Wiberly, S.E.; Gonzalez, R.D. Appl. Spec. 1961, 15, 174.
40. Bellamy, L.J. "The Infrared Spectra of Complex Organic Molecules"; John Wiley and Sons Inc.: New York, 1966.
41. Moschopedis, S.E.; Speight, J.G. Fuel; 1976, 55, 334.

42. Jennings, P.W.; Pribanic, J.A.S.; Dawson, K.R.; Bricca, C.E. Preprints Div. of Petroleum Chemistry; American Chemical Society: Washington, D.C., 1981, p. 915.
43. Wen, C.S.; Chilingarian; Yen, T.F. "Developments in Petroleum Science"; American Chemical Society: Washington, D.C., 1978, 7, 155.
44. Stevensen, F.J.; Goh, K.M. Geochimica et Cosmochimica Acta 1971, 35, 471.
45. Gerasimowicz, W.V.; Byler, D.M. Soil Science 1985, 139, 270.
46. Szymanski, H.A.; Erickson, R.E. "Infrared Band Handbook";IFI/Plenum: New York, 1970.
47. Bartle, K.D.; Ladner, W.R.; Snape, C.E.; Martin, T.G.; Williams, D.F. Fuel 1979, 58, 413.
48. Snape, C.E.; Ladner, W.R.; Bartle, K.D. Anal. Chem. 1979, 51, 2189.
49. Suzuki, T.; Itoh, M.; Takegami, Y.; Watanabe, Y. Fuel 1982, 61, 402.
50. Yoshida, T.; Nakata, Y.; Yoshida, R.; Ueda, S.; Kanda, N.; Maekawa, Y. Fuel 1982, 61, 824.
51. Barron, R.F.; Wilson, M.A. Nature 1981, 289, 275.
52. Dereppe, J.M.; Moreaux, C.; Debyser, Y. Org. Geochem. 1980, 2, 117.
53. Hatcher, P.G.; Vanderhart, D.L.; Earl, W. Org. Geochem. 1980, 2, 87.
54. Hatcher, P.G.; Schnitzer, M.; Dennis, L.W.; Maciel, G.E. Soil Sci. Soc. Amer. J. 1981, 45, 1089.
55. Ibarra, J.V.; Juan, R. Fuel 1985, 64, 650.
56. Verheyen, T.V.; Johns, R.B.; Blackburn, D.T. Geochim. Cosmochim Acta 1982, 46, 269.
57. Hatcher, P.G.; Breger, I.A.; Szeverenyi, N.; Maciel, G.E. Org. Geochem. 1982, 4, 9.
58. Christman, R.F.; Gjessing, E.T. "Aquatic and Terrestrial Humic Materials"; Ann Arbor Sci. Pub: Ann Arbor, 1983.

RECEIVED November 13, 1986

## Chapter 20

# Techniques for Isolation and Characterization of the Geoporphyrins and Chlorins

J. M. E. Quirke

Department of Chemistry, Florida International University, Tamiami Trail,  
Miami, FL 33199

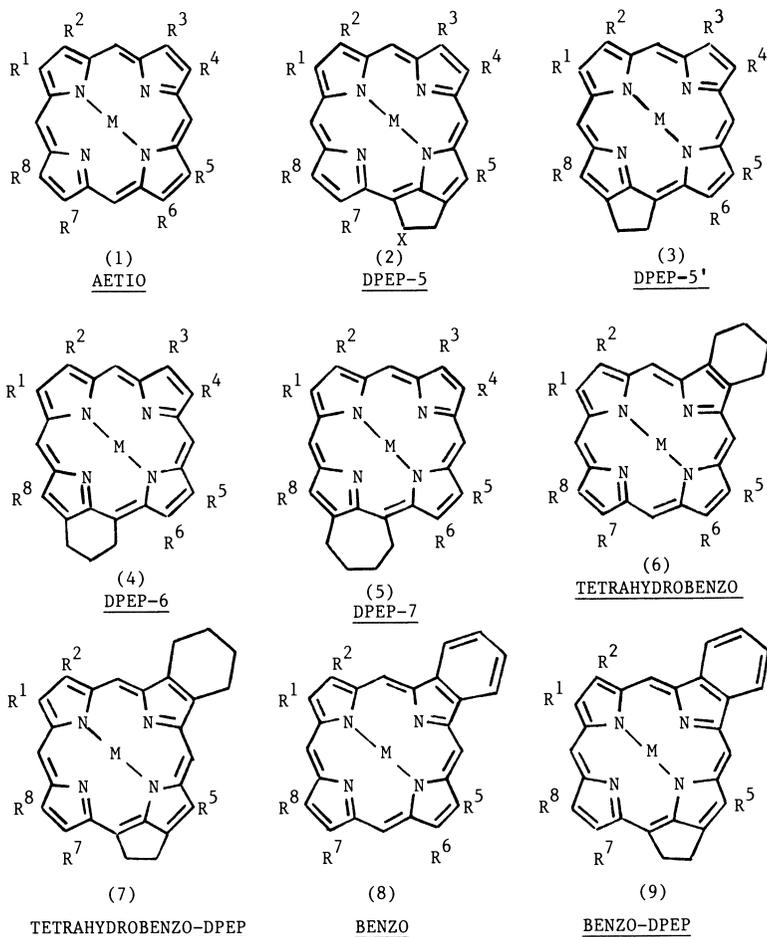
The methodologies for the isolation of porphyrins, metalloporphyrins and chlorins from sediments, oils, oil shales, bitumens, coals and kerogens are reviewed. The techniques for the analysis and characterization of intact geoporphyrin mixtures are described. The methods for the isolation, and elucidation of the individual geoporphyrins are discussed.

The task of reviewing the methods of isolation of the geoporphyrins is a particularly onerous one, in view of the many different isolation and purification schemes which have been employed, and the differences in the aims of the research. Emphasis has been placed on outlining methods which have general application to the analysis of geoporphyrin mixtures. Clearly it will be essential for the reader to modify all the isolation techniques to take into account both the nature of the sample, and the objective of the study in hand. The significance of the geoporphyrins and their role in industrial processes are reviewed elsewhere.<sup>(1,2)</sup> The structures of the different skeletal types of geoporphyrins, and their abbreviated names are shown in Figure 1.

The strategies used for the isolation of geoporphyrins depend both on the nature of the sample containing the porphyrins, and on the type of studies to be undertaken on the extract. If the study of total porphyrin mixtures is the objective, emphasis must be placed on optimising the recovery of the porphyrins. Conversely, if characterization of individual components is the goal, the emphasis lies in obtaining samples of the highest possible purity.

The initial extraction procedures are largely independent of the subsequent studies undertaken. The purification of total porphyrin mixtures, and the purification techniques for the study of individual porphyrins are discussed in turn.

0097-6156/87/0344-0308\$07.00/0  
© 1987 American Chemical Society



- 1(a)  $R^1, R^3, R^5, R^8 = \text{CH}_3$ ;  $R^2, R^4, R^6, R^7 = \text{C}_2\text{H}_5$   
 1(b)  $R^1, R^3, R^5, R^8 = \text{CH}_3$ ;  $R^2, R^4, R^7 = \text{C}_2\text{H}_5$ ;  $R^6 = \text{H}$   
 2(a)  $R^1, R^3, R^5, R^8 = \text{CH}_3$ ;  $R^2, R^4, R^7 = \text{C}_2\text{H}_5$ ;  $X = \text{OH}$   
 2(b)  $R^1, R^3, R^5, R^8 = \text{CH}_3$ ;  $R^2, R^4, R^7 = \text{C}_2\text{H}_5$ ;  $X = \text{H}$   
 2(c)  $R^1, R^3, R^5, R^8 = \text{CH}_3$ ;  $R^2, R^4 = \text{C}_2\text{H}_5$ ;  $R^7 = \text{CH}_2\text{CH}_2\text{CO}_2\text{H}$ ;  $X = \text{H}$

Figure 1. Structures of alkyl geoporphyrin skeletal types and their abbreviated names.

The Isolation of Nickel and Vanadyl Alkyl Geoporphyrins from Sediments, Bitumens and Petroleums.

The Extraction of Porphyrins from Sediments. The samples must be pulverized for efficient extraction. The porphyrin concentrate is usually isolated either by soxhlet extraction, or by sonication, or by means of a ball mill, which has been used extensively by Baker and co-workers. The technique of ball milling with an appropriate solvent is probably the best method as it avoids the risks of thermal alteration, and bond cleavage encountered in soxhlet extraction and sonication respectively.(5,7 and references therein)

There have been many different solvent systems employed for the extraction of geoporphyrins from sedimentary rocks. Toluene-methanol or benzene-methanol (1:1, vol:vol) (3) chloroform (4), and acetone-methanol (9:1, vol:vol) (5) are among the most common. Owing to the variety of sediments, it is advisable to experiment with solvent systems to optimize recovery. Nevertheless, an initial extraction with acetone-methanol followed by extractions either with benzene or with benzene-acetone (1:1, vol:vol) is generally a very sound choice, provided that the sole objective is the isolation of the geoporphyrins- other geolipids may be modified by the acetone.(5) Toluene can be used instead of benzene in this scheme. Chloroform-pyridine (9:1, vol:vol) is also a very effective system provided that a rotary evaporator with a very efficient vacuum system is available.(6)

Extraction of Bitumens and Crude Oils. There are significantly different problems in working with bitumens and crude oils compared to working with sediments. As these substances are almost exclusively organic, and usually viscous, the extraction techniques described above are generally inappropriate.

The porphyrins may be isolated by demetallation, using methanesulfonic acid (MSA). The demetallated geoporphyrins may be rapidly purified as described subsequently. The disadvantages are that the data on the metalloporphyrin distributions is lost, and that artifacts may be generated. Additionally, there may be preferential degradation of some of the porphyrin components under the vigorous demetallation conditions.(7,8)

The porphyrins may be isolated by column chromatography of the entire crude oil. This method has the advantage that the dangers of generation of artifacts is avoided.(9) There are problems with the aberrant chromatographic behavior of the asphaltenes, which can precipitate on the column. The nickel porphyrins may be separated from the vanadyl on the alumina (grade I, Brockmann) or the silica gel (100-200 mesh) column by gradient elution using dichloromethane in hexane.

The porphyrins may be isolated by solvent extraction. In this approach, the oil or bitumen is dispersed on a solid surface e.g. cellulose (10), alumina (Brockmann Grade I-II) (7), or even sand (11), and extracted initially with either toluene-methanol (1:2, vol:vol) or acetone-methanol (9:1, vol:vol). A second extraction using benzene-acetone (1:1 vol:vol) is advisable when working with complex geoporphyrin mixtures.

Purification of nickel and vanadyl alkyl geoporphyrin mixtures.

Purification of total porphyrin mixtures. It is usually essential to carry out extensive chromatography using as wide a range of columns as possible. The chromatographic conditions should be optimized for each sample studied. The solvent conditions described in the following paragraphs are a good starting point. All chromatographic procedures should be carried out on columns which are protected from sunlight to prevent photodecomposition- a particularly important precaution when working with porphyrins bearing functional groups. When studying small quantities of porphyrins, it may be necessary to reduce the number of chromatographic steps to improve sample recovery.

Probably the best initial purification step is gel permeation chromatography (GPC) either using sephadex LH-20 (5,7,12) or Bio beads S-X2 (13). The chromatograms are developed in tetrahydrofuran. High molecular weight compounds (ca. >4000 daltons), are removed. Low molecular weight components, and any salts present are retarded. The advantage of GPC as a preliminary step is that it reduces aberrant chromatographic behavior in later separations owing to the presence of asphaltenes. An alternative approach is to remove the asphaltenes by precipitation with hexane, and study these substances separately.

Column chromatography using either alumina or silica gel is by far the most common purification technique.(7) Generally it is advisable to purify on both alumina and silica columns. It is not clear whether there is any advantage to be gained using silica as the initial column followed by alumina or vice versa.

A wide range of solvent gradients have been used in silica gel chromatography. (e.g.4,5,7,13-17) A gradient elution of a silica gel column (100-200 mesh, packed in hexane) from hexane to chloroform is usually a very effective system. Most of the nickel porphyrins should elute in ca. 10-20%  $\text{CHCl}_3$ . The vanadyl porphyrins should elute in ca. 30-50%  $\text{CHCl}_3$ . There is sufficient variation between samples, and in the activity of the silica gel and humidity that careful monitoring of the eluant by visible spectroscopy is essential. The vanadyl or nickel geoporphyrin mixtures themselves may be partially resolved on the silica gel columns, but the fractions may be recombined if necessary. It is important to carry out the separations fairly rapidly as there is the possibility of generating artifacts. DPEP porphyrins can undergo hydroxylation at the isocyclic ring during chromatography on silica gel.(18) Usually this is not a major process, but it should be considered if polar geoporphyrins are isolated.

Ekstrom and co-workers have purified vanadyl porphyrins using Kieselgel 60 (Merck) eluting with a gradient of chloroform and carbon tetrachloride.(4) Barwise and co-workers have chromatographed vanadyl porphyrins over "functionalized" silica.(19) The sulphonic acid groups attached to the silica help to remove interfering nitrogenous bases. Using such columns, it is possible to obtain very clean samples; however, both nickel and metal-free porphyrins are lost on the column. In addition, it is possible that artifacts are generated, therefore residence times on the column should be minimised. There were substantial alterations in the daughter

spectra of molecular ions of high carbon number ( $> C_{33}$ ) vanadyl porphyrins purified on functionalized silica compared with those of the untreated vanadyl porphyrin fraction. In both cases the background on the mass spectra was low.(20)

Alumina columns (grade II, Brockmann) are developed by gradient elution using a variety of solvent mixtures, and are monitored by visible spectroscopy.(e.g. 5,8,13-15,21,22) A gradient elution from hexane to dichloromethane via toluene is an effective system. The nickel geoporphyryns are likely to elute in 30-50% toluene in hexane and the vanadyl porphyrins in 30-60% dichloromethane in toluene. There is a possibility of partial decomposition of the geoporphyryns, particularly the nickel complexes, on alumina columns thus it is advisable to effect the chromatography as rapidly as possible.

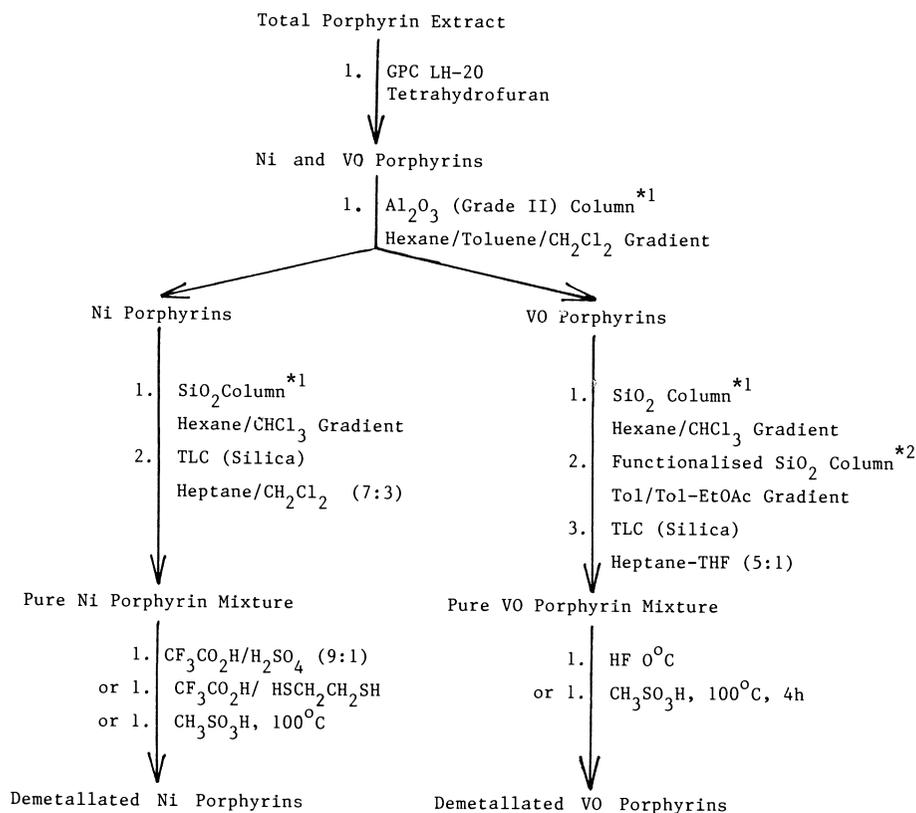
There have been recent developments in the role of low and medium pressure liquid chromatography (LPLC and MPLC). Thus Baker and co-workers purify nickel geoporphyryn mixtures on alumina columns, eluting with acetone-petroleum ether mixtures. The porphyrins elute in 3.5-5.0% acetone-petroleum ether.(5) Barwise and Roberts used MPLC on silica in their study of the porphyrins of El Lajun shale; however, the eluting solvents were not divulged.(23)

Thin layer chromatography (TLC) is also very useful in the final stages of purification of total mixtures. Nickel geoporphyryns have been purified on silica gel plates either carbon tetrachloride (24) or heptane-dichloromethane (7:3, vol:vol) as eluant. Similarly, vanadyl porphyrins may be purified using heptane-tetrahydrofuran (5:1, vol:vol).(25)

The separated geoporphyryn mixtures are often demetallated prior to further analysis.(e.g. 7,8,19,23,26,27) Typically the geoporphyryn mixtures are demetallated by the Erdman procedure using methanesulfonic acid at 100°C (4 hours).(28) The harsh conditions are required to demetallate the vanadyl components, but nickel porphyrins are demetallated in less than an hour. Yields vary, and there is the possibility of preferential decomposition of geoporphyryn species.

Demetallation of nickel porphyrins using either trifluoroacetic acid (TFA) and 1,2 ethanedithiol (29) or 10% sulphuric acid-TFA at ambient temperature may replace the Erdman demetallation process.(30) Vanadyl porphyrins are demetallated by anhydrous hydrofluoric acid at 0°C.(31) Extensive chromatography of the demetallated porphyrins should be avoided if the objective of the analysis is the study of the intact porphyrin mixtures. A good purification process for isolating the metal-free porphyrins is described subsequently. A summary of a reasonably efficient purification procedure for the isolation of intact nickel and/or vanadyl geoporphyryn mixtures is shown in figure 2.

Purification of Individual Geoporphyryn Components. The initial chromatographic stages of isolation are essentially the same as those described previously. The purified metalloporphyryn fractions are efficiently separated on TLC. The nickel complexes may be separated using hexane-toluene (3:2, vol:vol), and the vanadyl porphyrins using hexane-tetrahydrofuran (5:1, vol:vol).(25) The resolution may be improved by multiple elutions or by the continuous



Tol = Toluene; EtOAc = Ethyl Acetate; THF = Tetrahydrofuran

\* 1. Conventional Columns may be replaced by MPLC.

\* 2. Chromatograph rapidly to prevent unnecessary generation of artifacts.

Figure 2. Purification scheme for the study of total nickel and vanadyl alkyl geoporphyrin mixtures.

elution method.(14) Nickel geoporphyrins may be partially fractionated on calcium carbonate columns developing the chromatogram in benzene-petroleum ether (4:1, vol:vol). (32)

Usually it is necessary to demetallate the mixtures to effect the isolation of individual porphyrin components. The range of polarities of the metal-free geoporphyrins is greater than those of the metalloporphyrins. It is often possible to isolate individual metal free porphyrins from metalloporphyrin fractions by preparative TLC on silica gel. (e.g. 6, 9, 14, 17, 33, 34) Toluene-dichloromethane (1:1, vol:vol) is an effective solvent system. The mode of separation seems to be as follows:(14, 35)

- 1) Porphyrins bearing isocyclic rings are more polar than etio porphyrins similar carbon number.
- 2) The polarity of each skeletal class of porphyrin is inversely proportional to the carbon number.
- 3) An unsubstituted  $\beta$ -position causes a reduction in polarity equivalent to an additional 2-3 methylene units. Thus a C<sub>29</sub> etio porphyrin with 1 unsubstituted  $\beta$ -position is intermediate in polarity between fully  $\beta$ -alkylated C<sub>31</sub> and C<sub>32</sub> etio porphyrins.

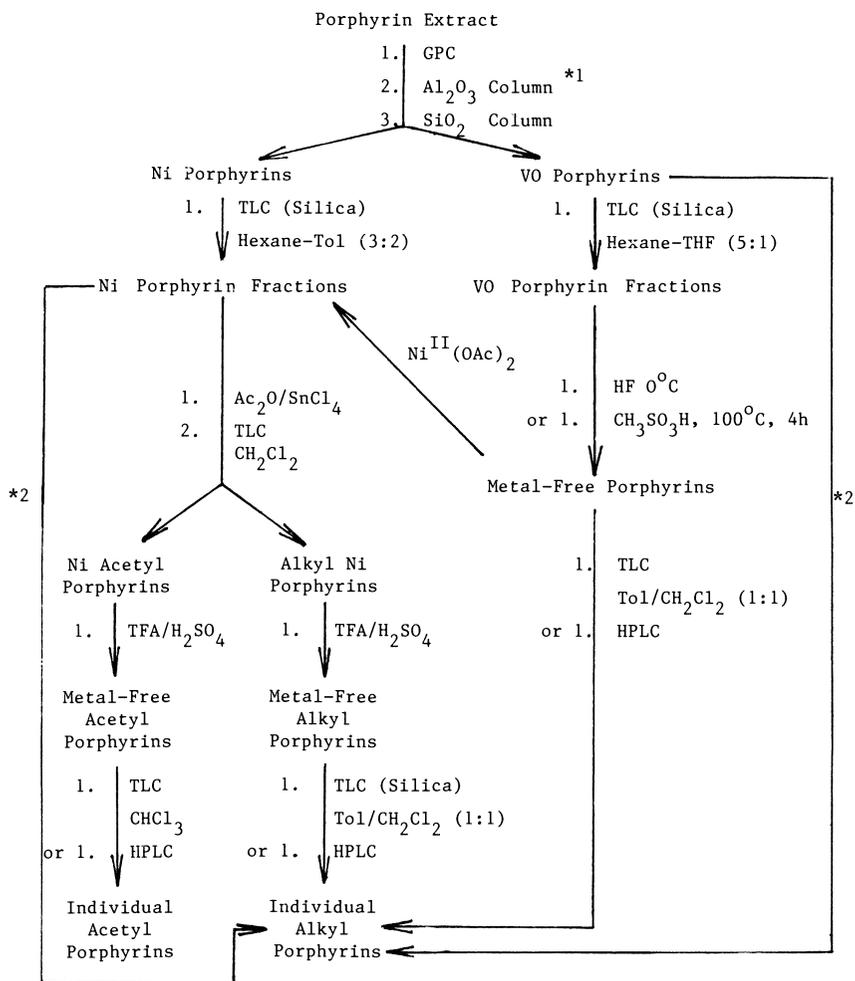
The separation is greatly facilitated by carrying out Friedel-Crafts acetylations on the geoporphyrin mixtures. The reaction specifically converts unsubstituted  $\beta$ -positions on the porphyrin macrocycle into acetyl moieties. The reaction may be carried out on the nickel geoporphyrin mixtures themselves. Vanadyl porphyrin must be demetallated, and converted to the nickel, copper or iron porphyrins before acetylation. The metalloporphyrin in dichloromethane is treated at 0°C with anhydrous tin(IV) chloride and acetic anhydride. After standing for a short time, the solution is neutralized, and the porphyrins are extracted. The acetylated porphyrins are readily separated by TLC from the fully  $\beta$ -alkylated geoporphyrins. The individual acetylated porphyrins may then be isolated, and characterized by nuclear magnetic resonance spectroscopy.(36) The method has yet to be employed in the study of geoporphyrins bearing > 2 unsubstituted  $\beta$ -positions. Isolation of individual porphyrins by High Performance Liquid Chromatography (HPLC) - the best final purification technique- is discussed below. A summary of useful isolation procedures is shown in Figure 3.

#### The Isolation and Purification of Geoporphyrins from Other Geological Sources.

There have been few studies on the geoporphyrins in coals and kerogens. The isolation methods employed in these cases are very different from those described in the previous sections because of the different nature of the samples and the geoporphyrins themselves.

The isolation of Porphyrins from Coals. The principal recent work done in this area is that of the Bonnett group, and that of Palmer and co-workers. Neither group use the method of Treibs, who carried out an initial extraction of the coal with pyridine.(37, 38)

The approach of Palmer involved extraction of ground coal particles (20-mesh) with MSA (100°C, 3 h). The porphyrins were then



Tol = Toluene; TFA = Trifluoroacetic Acid; THF = Tetrahydrofuran;  
Ac<sub>2</sub>O = Acetic Anhydride.

\* 1. See Figure 2.

\* 2. Demetallate and separate on HPLC

Figure 3. Procedures for the isolation of individual porphyrins from nickel and vanadyl alkyl geoporphyrin mixtures.

purified using GPC on Sephadex LH-20, before mass spectrometric analyses. (39)

The Bonnett approach of an initial treatment of the finely ground coal with 7%  $H_2SO_4-CH_3OH$  for 12 hours at room temperature yields the metalloporphyrins intact. The porphyrins were extracted with chloroform, and neutralized. Using these methods, gallium (III), iron (III), and manganese (II) porphyrins were detected in coals.

Gallium porphyrins were isolated and purified by column chromatography on silica gel using gradient elution of benzene-methanol, in the presence of 0.02-0.03 molar anhydrous ammonia. The porphyrin extracts are further purified on silica gel TLC plates, eluting with benzene-methanol (4:1) in the presence of ca. 0.1 molar anhydrous ammonia and then rechromatographed in 4.15 molar methanolic ammonia. The gallium porphyrins may be analysed on reverse phase HPLC using a Waters Bondapak column  $C_{18}$ /Porasil eluting with methanol:water (17:3). (40,41) Gallium porphyrin methyl esters may be analysed on Techsil 5C 18 columns eluting with methanol-water (4:1). (42)

Iron porphyrins are isolated somewhat differently. After the initial extraction with 7% sulphuric acid-methanol, the porphyrins are chromatographed on silica gel TLC plates eluting with 15% 1 molar ammoniacal methanol-toluene. (43) Any porphyrin acids should be converted into their methyl esters. The porphyrins may then be demetallated, and analysed by HPLC using Apex ODS columns and eluting with 3% methanol-acetonitrile. (42)

The Isolation of Porphyrins from Kerogens. There is very little information on the generation of porphyrins from kerogens even though there have been many hypotheses on the nature of the porphyrins within the kerogen matrix. Van Berkel and Filby have made a detailed study on the subject, and their approach to the problem is summarized here. (44)

The bitumen is removed from the finely ground shale. The kerogen concentrate is prepared by a method similar to that of Durand. (45) The concentrate is sonicated to remove organic solubles associated with the minerals which associate with the kerogen after treatment with hydrofluoric acid. Then the kerogen is pyrolysed in toluene at the selected temperature under an atmosphere of nitrogen. The pyrolysed kerogen is isolated by centrifugation, and then sonicated with toluene or toluene-methanol, and the organic extract is combined with the filtrate from the pyrolysis. The porphyrins may be isolated using the methodologies described earlier. The kerogen may then be pyrolysed again at a higher temperature. Typically, the pyrolyses temperatures are selected in the range 100-450°C.

Using this method it is possible to distinguish the bituminous porphyrins from those porphyrins associated with inorganic minerals- but not intimately bound into the kerogen matrix- and from the porphyrins associated with the kerogen. It is also possible to obtain information on the order in which the geoporphyrins are liberated from the kerogen. The studies indicate that the majority of the porphyrins are liberated at 300°C.

### The isolation of Unusual Cyclic Tetrapyrroles.

With the exception of coals, nickel and vanadyl alkyl porphyrins are the dominant porphyrin species in sedimentary rocks and petroleum. Nevertheless, other porphyrin species have also been isolated. The methodology for the isolation of these components will be discussed.

Copper Geoporphyrins. Copper Porphyrins have very similar chromatographic and chemical properties to nickel porphyrins. Thus they are isolated in the same manner as described previously. They may be demetallated in the same way as the nickel porphyrins. In all isolation procedures, it is particularly important to rigorously exclude copper salts, because metal free porphyrins chelate with copper (II) ions very readily.(46)

Metal-Free Geoporphyrins. Metal-free porphyrins occur rarely in geological samples; however, they are perhaps the easiest species to isolate. The simplest isolation procedure is to treat the total organic extract in ethereal solution with fresh dilute (<6M) hydrochloric acid.(5,6,47) This process protonates the metal free porphyrins to form the dications, but should not demetallate any nickel or vanadyl porphyrins present (thus these compounds remain in the ether layer). The extraction is complete once the acid layer ceases to fluoresce red in UV light. Then the porphyrins are isolated by back extraction into an organic solvent after neutralisation of the acid layer with sodium bicarbonate. Individual porphyrins may be isolated as described earlier

Isolation of Porphyrins Bearing Functional Groups. There are very little data on such compounds. To date, the only functionalized geoporphyrins bearing functional groups to be isolated are porphyrin carboxylic acids. It is probable that the DPEP porphyrins bearing a hydroxyl moiety on the isocyclic ring (2a) are artifacts formed during silica gel chromatography.(48,18) The nickel methylated carboxyl porphyrins are isolated using a strategy similar to that described above.(49-51)

Isolation and Purification of Chlorins Baker and co-workers carried out extensive studies on these compounds.(5 and references therein) In contrast to the geoporphyrins, the geochlorins bear a variety of functional groups, and are rather labile.

The isolation procedures are the same as those of the geoporphyrins. The purification process is very different. The chlorins usually elute faster than the nickel and vanadyl porphyrins on GPC using Sephadex LH-20. Column chromatography is carried out on microcrystalline cellulose, a milder support than either alumina or silica. A gradient elution of from hexane to acetone is used. The non-polar chlorins e.g. the pheophytins, decarboxylated and phytolated phorbides elute in ca. 5% acetone-hexane. Mono-carboxylic tetrapyrroles e.g. pheophorbide a elute in 5-25% acetone hexane, and the polar chlorins, bearing two or three carboxyl moieties, elute in

50-100% acetone-hexane. It is essential to esterify the carboxylic acids using diazomethane before further purification. (5,7,12,52)

### Characterisation of Total Porphyrin Mixtures.

Spectrophotometric Methods. Visible spectroscopy is invaluable for the analysis of geoporphyrin mixtures, and has been reviewed in detail by Baker and Palmer.(7) In addition to a major peak at ca. 400 nm, most metalloporphyrins are characterized by a two-banded visible spectrum (Table I) while the metal-free species have four bands (Table II). Using this method it is possible to distinguish nickel porphyrins from vanadyl porphyrins. Similarly the etio porphyrins are readily distinguished from porphyrins bearing isocyclic rings, and benzoporphyrins (Fig. 1). The method also provides an approximate quantitative method for estimating the porphyrin content in either the total organic extracts, or chromatographic fractions. Usually, quantitation is based on extinction coefficient(s) selected as being representative of the nickel and/or the vanadyl geoporphyrins.

Mass Spectrometry. Mass spectrometry is indispensable for both the analyses of the total geoporphyrin homologous series and in structural determination studies. The electron impact mass spectra (EIMS) of the alkyl porphyrins are characterized by a large molecular ion,  $M^+$ , (usually the base peak), and a significant doubly charged ion. Fragmentation in both free base porphyrins and metalloporphyrins occurs primarily by beta cleavage of the alkyl substituents, e.g. an (M-15) fragment ion will be observed if an ethyl group undergoes fragmentation.(56) Usually the nickel and vanadyl porphyrin suites of homologues will be separated prior to the MS analysis. It is possible to use the solids probe as a microdistillation device, and remove the volatile non-porphyrinic components by holding the probe at a low initial temperature so that the contaminants are removed, and then heating rapidly to volatilize the porphyrins in a short burst. The temperatures for this operation vary with the instrument, and the porphyrins studied. The molecular ions of the geoporphyrin series are listed in Table III.

EIMS at the standard ionising voltage, 70eV, can be used to obtain a qualitative measure of the carbon number range of the geoporphyrin mixture. The data for low carbon number porphyrins are unreliable because of the coincidence of high carbon number fragments ions with the molecular ions of the lower pseudohomologues.

For quantitation of geoporphyrin components by EIMS, there are three problems which need to be addressed.

- (1) The problem of differential volatilisation geoporphyrins is readily solved by averaging the spectra over the range of volatility of the sample, a facile process with current MS data systems.
- (2) The problem of differential fragmentation of the porphyrins. This is a more serious problem. It is possible to partially solve the problem by reducing the ionizing voltage from 70eV to ca. 14 eV. This will reduce fragmentation, but also leads to a drop in sensitivity.(7)

Table I. Visible Spectral Data for Metalloporphyrins

Compound	Solvent	$\lambda_{\max}$ nm ( $\epsilon$ mM)
VOOEP	CH <sub>2</sub> Cl <sub>2</sub>	407 (331); 533 (16.2); 572 (31.6)
NIOEP	Dioxan	391 (219); 516 (11.0); 551 (33.1)
CuOEP	CHCl <sub>3</sub> /MeOH	399 (305); 522 (13.0); 560 (24.5)
Ga(OEP)	Benzene	404 (288); 537 (16.2); 574 (21.9)
Fe(OEP)OMe	CH <sub>2</sub> Cl <sub>2</sub> /MeOH	356 (55); 396 (105); 477 (11.8); 592 (19.9)
Mn(OEP)BrPy	Benzene	355 (49); 437(42); 462(20.4); 557 (8.9)

Me = CH<sub>3</sub>; OEP = Octaethylporphyrin; Py = Pyridine.

SOURCE: Data are from reference 53.

Table II. Typical Visible Spectroscopic Data for Metal Free Geoporphyrins

Compound Class <sup>a</sup>	Solvent	Band					Band Ratios	Ref.
		Soret	IV	III	II	I		
Etio	CH <sub>2</sub> Cl <sub>2</sub>	399	499	532	566	619	IV>III>II>I <sup>b</sup>	(14)
DPEP-5	CH <sub>2</sub> Cl <sub>2</sub>	399	500	534	565	619	IV>II,I>III <sup>c</sup>	(14)
DPEP-6	CH <sub>2</sub> Cl <sub>2</sub>	400	498	533	568	622	IV>II>III>I	(54)
BenzoD	CH <sub>2</sub> Cl <sub>2</sub>	407	505	542	574	628	III>IV>II>I	(55)

<sup>a</sup> See Figure I. UV data for pure metal free benzo etio, and DPEP-7 (5) porphyrins are unavailable.

<sup>b</sup> The intensity of band III is diminished in the  $\beta$ -unsubstituted etio porphyrins compared to the fully substituted components.

<sup>c</sup> The isomeric DPEP-5 (3) is similar.

Table III. Molecular Ions of Geoporphyrins

C No.	Porphyrin Molecular ions <sup>a</sup>														
	Etio			Isocyclic			Benzo			Benzo D.			TetraBD		
	Ni	VO	FB	Ni	VO	FB	Ni	VO	FB	Ni	VO	FB	Ni	VO	FB
20	366	375	310	-	-	-	-	-	-	-	-	-	-	-	-
21	380	389	324	-	-	-	-	-	-	-	-	-	-	-	-
22	394	403	338	392	401	336	-	-	-	-	-	-	-	-	-
23	408	417	352	406	415	350	-	-	-	-	-	-	-	-	-
24	422	431	366	420	429	364	416	425	360	414	423	358	-	-	-
25	436	445	380	434	443	378	430	439	374	428	437	372	-	-	-
26	450	459	394	448	457	392	444	453	388	442	451	386	446	455	390
27	464	473	408	462	471	406	458	467	402	456	465	400	460	469	404
28	478	487	422	476	485	420	472	481	416	470	479	414	474	483	418
29	492	501	436	490	499	434	486	495	430	484	493	428	488	497	432
30	506	515	450	504	513	448	500	509	444	498	507	442	502	511	446
31	520	529	464	518	527	462	514	523	458	512	521	456	516	525	460
32	534	543	478	532	541	476	528	537	472	526	535	470	530	539	474
33	548	557	492	546	555	490	542	551	486	540	549	484	544	553	488
34	562	571	506	560	569	504	556	565	500	554	563	498	558	567	502
35	576	585	520	574	583	518	570	579	514	568	577	512	572	581	516
36	590	599	534	588	597	532	584	593	528	582	591	526	586	595	530
37	604	613	548	602	611	546	598	607	542	596	605	540	600	609	544
38	618	627	562	616	625	560	612	621	556	610	619	554	614	623	558
39	632	641	576	630	639	574	626	635	570	624	633	568	628	637	572
40	646	655	590	644	653	588	640	649	584	638	647	582	642	651	586

<sup>a</sup> The molecular ions are based on <sup>12</sup>C, <sup>14</sup>N, <sup>58</sup>Ni. Higher carbon number porphyrins (>C<sub>44</sub>) may be observed at 1 dalton above the calculated value owing to rounding up the partial mass to the next integer.

Isocyclic = Molecular ions for all porphyrins bearing an isocyclic ring, and tetrahydrobenzo porphyrins (2-6, Figure 1.)

Benzo = Benzo porphyrins (8, Figure 1.)

Benzo D. = Benzo DPEP porphyrins (9, Figure 1.)

TetraBD = Tetrahydrobenzo DPEP porphyrins (7, Figure 1.)

FB = Free Base; Ni = Nickel; VO = vanadyl porphyrin.

(3) It is essential to correct for isotopic contributions from  $^{13}\text{C}$ ,  $^{15}\text{N}$  and  $^{60}\text{Ni}$  (where appropriate) in quantitation to distinguish between molecular ions and coincident isotope peaks from other components. Such correction procedures have been described.<sup>(7)</sup>

Chemical Ionisation Mass Spectrometry (CIMS) may provide a better solution to the quantitation problem once the problem of reproducibility is overcome. In CIMS using hydrogen or methane as reagent gases, porphyrins may either fragment to form their individual pyrrole rings or yield the desired molecular ion without any major fragments.<sup>(57,58)</sup> The mode of fragmentation appears to be dependent on the temperature of the source.

Analysis of geoporphyrins mixtures using Fast Atom Bombardment (FAB) methods may prove valuable, although the technique may not be sufficiently sensitive for quantitative work.

The techniques of GC-MS and HPLC-MS are both methods of great potential. The developments in GLC using silylated silicon porphyrin derivatives by Eglinton and co-workers are particularly exciting. McFadden *et al.*, have carried out HPLC-MS analysis on geoporphyrin mixtures. The data confirm the potential of the method. The only impediment lies in the efficient interfacing of the HPLC and the MS.<sup>(59)</sup>

Mass spectrometric analyses of total mixtures gives only limited structural data. Analyses of metastable ions gives information on the nature of the substituents on the porphyrin macrocycle. In this way, Titov and co-workers were able to confirm the presence of geoporphyrins with extended alkyl substituents ( $\text{C}_{12}$ ).<sup>(60)</sup>

Tandem mass spectrometric (MS/MS) is another valuable analytical tool.<sup>(61,62)</sup> Using this technique in the EI mode it is possible to obtain daughter ions and neutral losses from the molecular ions of the porphyrin components without prior separation of the mixture. These data provide information on the type of the substituents on all the porphyrins of single carbon number. The predominant mode of cleavage of the molecular ions is  $\beta$ -cleavage of the substituents. The data indicate that high carbon number ( $>\text{C}_{33}$ ) geoporphyrins have more than one site of extended alkylation, and there may be several isomeric porphyrinic species present.<sup>(63-65)</sup> The daughter spectra of the molecular ions may prove to be valuable "fingerprints" in correlation studies. The technique of CIMS/MS has great potential for the analysis of geoporphyrin mixtures also, but there are problems of reproducibility at present.<sup>(20)</sup>

Chromatographic Methods. HPLC is the most valuable analytical technique. The porphyrins eluting from the various columns are monitored by visible spectrophotometry. The choice of detecting wavelength is dependent on the nature of porphyrin species being studied. (Tables I,II). Demetallated porphyrin mixtures are usually analysed using normal phase silica columns. Maxwell, Barwise and co-workers have achieved the best separations of such mixtures to date.<sup>(e.g 23)</sup> Finally, after over four years since the original publications, the chromatographic conditions are to be published in "Journal of Chromatography".

Sundaraman and co-workers have succeeded in the efficient separation of vanadyl porphyrin mixtures; unfortunately the precise

conditions employed have not been divulged.(66) Nickel porphyrins are not usually analysed in the metallated state; however, Fookes reported the separation of the nickel porphyrins of Julia Creek oil shale into 30 fractions on a C-18 column eluting with methanol.(24)

Eglinton and co-workers have made notable advances in the GLC and GC-MS analyses of porphyrins.(e.g. 67-70) Although it is possible to chromatograph several metalloporphyrin species including gallium, aluminium and rhodium (III) complexes, analysis of the silicon(IV) derivatives is the preferred method.(68) The procedure is summarized below.

The demetallated porphyrins in dry toluene are converted into their silicon derivatives by treatment with hexachlorodisilane, for 2 hours at ambient temperature. The porphyrins are purified on alumina TLC, eluting with dichloromethane, and the hydroxy ligands are silylated using BSTFA-pyridine. The chromatography is carried out on either OV-1 or CPSil 5 capillary columns, using helium as the carrier gas (50-120 cm sec<sup>-1</sup> flow rate). The initial oven temperature is 60°C, and the temperature is increased linearly to ca. 300°C.

The advantages of GC-MS analysis of geoporphyrins for fingerprinting of crude oils and correlation studies are obvious. Clearly, GC-MS-MS would be a yet more powerful analytical tool.

In addition to its role as a purification technique, GPC has been used in the study of the molecular weight distributions of geoporphyrin mixtures. Blumer and co-workers studied the porphyrins of the Serpiano shale, and obtained evidence for very high molecular weight porphyrin species, and even dimeric porphyrins.(71,72)

More recently, Fish and co-workers have used size exclusion HPLC to investigate the nature of the nickel and vanadium compounds in petroleum. The eluates from the 50-100 μ Sphergel column were analysed by graphite furnace atomic absorption. Using this technique it is possible to deduce the molecular weight range of such species.(73)

Degradative Methods. The degradation of porphyrin mixtures to maleimides (2,5-pyrrolediones) using chromic acid gives valuable information on the substituent patterns of the geoporphyrins.(9,74,75) Each pyrrolic subunit is converted to a maleimide bearing the original pair of substituents. The isocyclic ring-bearing pyrroles are converted to maleimide carboxylic acids.(76) The method complements chromatographic and mass spectrometric analyses of such geoporphyrin mixtures. An efficient procedure is outlined below.(9)

Treatment of the demetallated porphyrin mixture in trifluoroacetic acid with chromium trioxide in sulphuric acid at 0°C for 2 hours yields the maleimides. These compounds may be analysed by GLC or GC-MS using OV-1 or Carbowax capillary columns programmed from 60°C to 260°C at 4°C min<sup>-1</sup>. The maleimides usually show molecular ions, and a characteristic fragment ion, m/z 125. To obtain better peak shapes, the maleimides may be silylated prior to analysis.

There are three other degradative techniques, which may be used for the analysis of geoporphyrin mixtures. Oxidation of porphyrins using lead (IV) dioxide (4h, ambient temperature) to the corresponding 5,10,15,20-tetraoxoporphyrinogens is a potentially

valuable method. These compounds fragment in EIMS to give the individual pyrrolic species, together with di- and tri-pyrrolic fragments from the tetrapyrrolic macrocycle.(77) Treatment of the porphyrins with hydriodic acid gives the individual pyrroles, which may then be analysed by GC-MS. The method has been superceded by the developments in CIMS.(78) The oxidative degradation of porphyrins by potassium permanganate to form 2,5-pyrrole dicarboxylic acids could be used for geoporphyrin analyses, but it too has been superceded by CIMS.(79)

#### Characterisation of Individual Porphyrin Components.

This is the area of geoporphyrin chemistry in which the greatest advances have been made. The developments in NMR in particular have resulted in a clarification of the Treibs' hypothesis on the origin of the geoporphyrins, and confirmed that these compounds are derived from naturally-occurring chlorophylls. In addition, it is possible to determine in some cases the precise precursor of specific geoporphyrins.(51,80)

Spectrophotometric Methods. UV/Visible spectrophotometry provide information on the skeletal type of porphyrin present. Otherwise it is of little value in structural elucidation. The most important role for this technique is in the characterisation of the geochlorins.(12)

Mass Spectrometric Methods. High resolution EIMS yields the molecular formula of a porphyrin. The primary mode of fragmentation of the porphyrins in the EIMS is cleavage  $\beta$  to the porphyrin ring. Thus determination of the daughter ions of the molecular ion provides limited structural information.(56,63,64)

The CIMS analysis of porphyrins using hydrogen as reagent gas and a source temperature of 200°C reveals pyrrole, dipyrrole and tripyrrole fragments, which can be used to sequence the pyrrole units within the porphyrin macrocycle, and requires very little sample (ca. 1  $\mu$ g).(58,81) More reproducible results are obtained by using ammonia as reagent gas.(82) This is usually the best analytical technique when working such small quantities of porphyrin that NMR is infeasible. The method will probably be further improved by using CIMS-MS with ammonia as the reagent gas.

Nuclear Magnetic Resonance Methods. The use of NMR has revolutionized the study of the geoporphyrins. In fact it is by far the most important method currently employed for the analysis of individual geoporphyrins. The technique is ideal for such studies as it can be effected on fairly small samples (<1 mg), and the sample need not be absolutely pure- usually good data are readily obtained on samples of ca. 90% purity. The method has allowed the partial or complete characterisation, of over 30 porphyrins including four new skeletal types.(51,80).

At present, the small amounts of sample available exclude the study of nuclei other than  $^1\text{H}$ . The basic spectrum is of limited value, giving only the number and type of substituents on the porphyrin macrocycle. Nevertheless porphyrins with either seven or

eight identical substituents are unambiguously assigned by this method.(14)

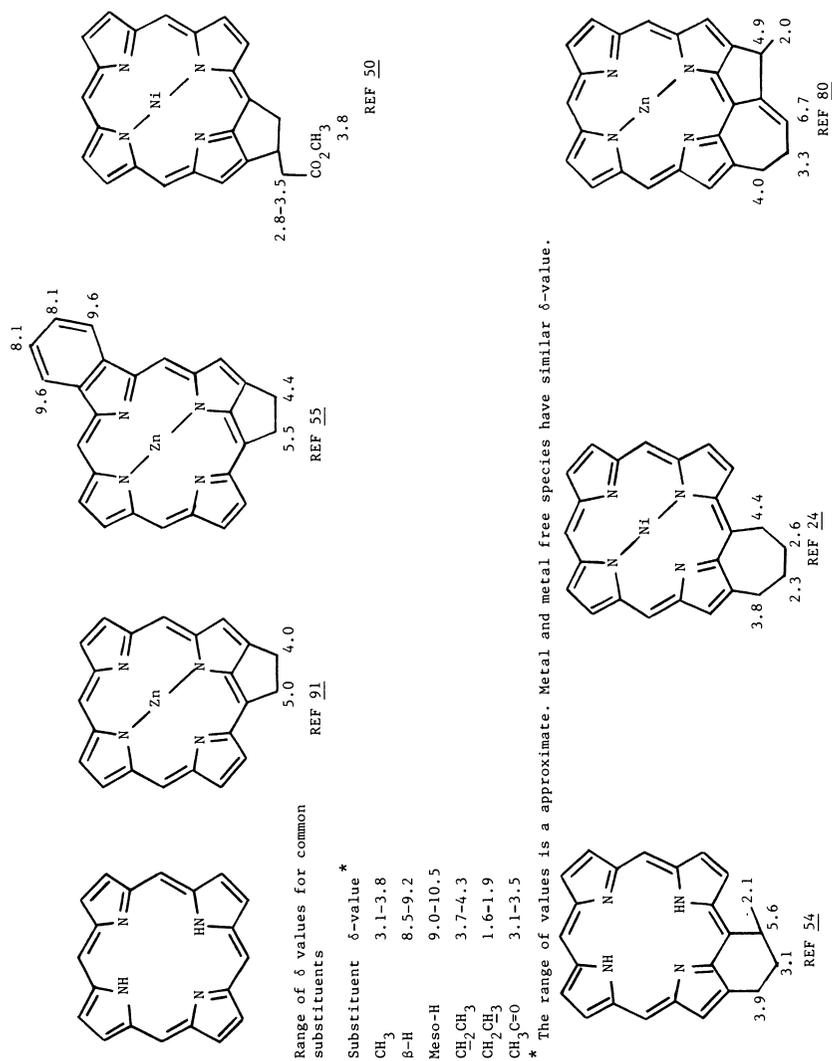
Analysis of porphyrins by nuclear Overhauser difference (nOe) techniques has been the method of choice provided that all the meso (bridge) protons are fully resolved.(21,22,24,55,80,83-91) In such cases, it is possible to assign the structure of the porphyrins by irradiating each signal in turn, and determining which of the other signals are enhanced by difference spectroscopy. The sequence of the substituents is readily ascertained because nOe enhancements are observed only for groups close to that which was irradiated. Ideally the experiments should be effected on the porphyrin zinc or nickel complexes, in the presence of pyridine or pyrrolidine, to eliminate the possibility of aggregation effects. There are three impurity peaks which are often observed in the spectra at  $0.88\delta$ ,  $1.25\delta$  (alkane-like impurities) and at  $1.5\delta$  (water). These peaks do not coincide with most of the signals from the geoporphyrins; however, they may prove a problem in studies on porphyrins bearing extended ( $>C_2$ ) substituents. The chemical shift of the water peak may be varied by altering the pyridine concentration.

Porphyrins bearing isocyclic rings are ideally suited for nOe analysis. Geochlorins will also be readily analysed by the nOe technique because these compounds bear a reduced pyrrolic ring which ensures that the meso protons are well resolved. In addition the substituents on the reduced pyrrolic ring are very readily assigned which will greatly facilitate such studies. Porphyrins bearing an unsubstituted  $\beta$ -position may be analysed directly by the nOe method, but better results are obtained if the porphyrins are initially acetylated by the Friedel-Crafts acylation reaction.(86,87) Usually the technique is of little value for the characterisation of fully  $\beta$ -alkylated etio porphyrins as the meso protons coincide.

There have been two other approaches to the analysis of porphyrins by NMR. A  $C_{32}$  etio porphyrin in Gilsonite was identified as etioporphyrin-III (Ia) by converting the porphyrin into its "mercury sandwich" complex in which two porphyrin macrocycles are interspersed between three mercury ions. The mercury sandwich complex of each of the four porphyrin type isomers has a different  $^1H$  NMR spectrum. These metal-free type isomers have virtually identical NMR spectra.(17) The method is limited because it is essential to obtain spectra of all the possible isomers for comparison. Also the complex readily decomposes to the 1:1 complex; hence, the  $CDCl_3$  solvent should be passed through alumina to remove traces of acid. Krane and co-workers used aggregation studies to assign the structure of the  $C_{32}$  etioporphyrin in Marl slate as etioporphyrin-III.(91) This approach is likely to be the method of choice for the analysis of porphyrins which are not amenable to nOe analysis.

The chemical shifts of some important geoporphyrinic substituents are shown in Fig. 4.

Degradative Techniques. The maleimide degradation may be used to confirm the NMR data.(14,17,82) Otherwise, the method is of little value for precise structure determination.

Figure 4.  $^1\text{H}$  NMR chemical shift data for common geoporphyrin substituents and exocyclic rings.

Synthetic and Chromatographic Methods. The method of structure elucidation by comparison of the isolated compound with all the possible structural isomers is impractical except for research groups specialising in porphyrin synthesis. (91-96) A typical total synthesis will take over twenty steps from readily available starting materials, and involves a moderate yield cyclisation step. (91-96) The method was successfully used to determine the structure of the desethyl C<sub>30</sub> etio porphyrin (1 b). (97) Four isomers of the compounds were synthesized, and separated by HPLC on 10  $\mu$  ODS-HC-Sil-XI eluting with acetonitrile, and the structure of the geoporphyrin was assigned by co-injection. The only occasion when it is essential to employ this strategy is if the structure determination of porphyrins cannot be readily determined by other techniques.

Crystallographic Methods. The major difficulty in using the technique is that it is very difficult to grow crystals of sufficient quality, when working with small amounts (< 1 mg) of sample. Nevertheless the nickel complexes of deoxophylloerythroetioporphyrin and deoxophylloerythrin (2a, 2b) have been characterized by X-ray crystallography. (4,98)

#### Characterisation of Bound Porphyrins.

There have been very few studies on the nature of the porphyrins within the organic substances or inorganic mineral matrix. The techniques available for such studies have been mainly applied to model compounds.

Bergaya and van Damme have studied the stability of metalloporphyrins adsorbed onto a clay surface. (99) The porphyrin species were investigated by using UV-visible diffuse reflectance and diffuse transmission spectra. The diffuse transmittance spectra were identical with conventional transmission spectra. Provided that the sample is a highly dispersed suspension, it is also possible to obtain quantitative data. The diffuse reflectance spectra are not as easily compared; however a direct comparison gives enough information for distinguishing the nature of the porphyrin species present. For rigorous work the two parameters are correlated through the Kubelka-Munk function:

$$(1-R_{\infty})^2/2R_{\infty} = k/s$$

$R_{\infty}$  = the reflectance of a layer sufficiently thick that further concentration does not change the reflectance.

$k$  = absorption coefficient (molar extinction times concentration)

$s$  = scattering coefficient.

Cady and Pinnavaia used a similar approach; however the visible spectroscopic data were obtained by dispersing the mica-silicate bearing the porphyrin in a nujol mull. Infra red studies were effected by running the spectra of the solid material as thin films supported between KBr plates. (100)

Electron spin resonance spectroscopy (ESR) is a powerful technique for the study of bound vanadyl porphyrins. Typically, the spectra show eight weak parallel lines (three may be hidden) and

eight perpendicular lines, which are readily recognized. The basic methodology, and interpretation of the data has been reviewed recently by Lin.(101) Using the method, evidence has been obtained for the presence of non-porphyrinic vanadyl compounds in petroleum and tar sands.(102,103)

Goulon *et al.* have reported x-ray absorption spectroscopic analysis on asphaltenes which indicated that the vanadium was associated with porphyrins, and that the porphyrin content may be greater than indicated by visible spectroscopy.(104,105)

### Summary

There is still no one scheme which is ideal for the isolation of porphyrins from all types of geological samples. This is not surprising because of the substantial variations in the sedimentary environment. The development of HPLC, and the advances in mass spectrometry have been major assets in the characterisation of total geoporphyrin mixtures. In the future, GC, GC-MS, HPLC-MS will yield even more information. The advent of <sup>1</sup>H NMR has provided the geochemist with by far the most important tool for the structural elucidation of individual geoporphyrins. No doubt, <sup>13</sup>C NMR studies will become feasible as the sensitivity of the instruments is improved. MS-MS will also be a valuable technique for the study of individual components within intact geoporphyrin mixtures. The major area of the field which is yet to be thoroughly investigated is the study of the bound geoporphyrins. It is essential that there are more studies in this area if the chemistry of the geoporphyrins is to be fully understood.

### Acknowledgments

I am grateful to Dr. J.F. Branthaver (Western Research Institute, Laramie), Dr. R.H. Filby and Mr. G.J. van Berkel (Washington State University, Pullman), Dr. K.M. Smith and his students (University of California, Davis) for useful discussions in the preparation of this manuscript.

### References

1. Filby, R.H.; Van Berkel, G.J., this volume.
2. Branthaver, J.F., this volume.
3. Thomas, D.W.; Blumer, M., Geochim. Cosmochim. Acta 1964, 28, 1147-1154.
4. Ekstrom, A.; Fookes, C.J.R.; Hambley, T.; Loeh, H.J.; Miller, S.A.; Taylor, J.C. Nature 1983, 306, 173-174.
5. Louda, J.W.; Baker, E.W. In "Initial Reports of the Deep Sea Drilling Project"; Yeats, R.S.; Haq, B.U. *et al.*, Eds.; U.S. Government Printing Office: Washington, 1981; Vol.LXIII, pp.785-818.
6. Quirke, J.M.E.; Dale, T.; Britton, E.D.; Yost, R.A.; Trichet, J.; Belayoumi, H. Org. Geochem. submitted.
7. Baker, E.W.; Palmer, S.E. In "The Porphyrins"; Dolphin, D., Ed.; Academic: New York, 1978; Vol.I, pp. 485-622.
8. Baker, E.W. J. Am. Chem. Soc. 1966, 88, 2311-2315.

9. Quirke, J.M.E.; Shaw, G.J.; Soper, P.D.; Maxwell, J.R. Tetrahedron 1980, 36, 3261-3267.
10. HajIbrahim, S.K.; Tibbetts, P.J.C.; Watts, C.D.; Maxwell, J.R.; Eglinton, G.; Colin, H.; Guichon, G. Anal. Chem. 1978, 50, 549-553.
11. Quirke, J.M.E.; Abedi, V., unpublished data.
12. Baker, E.W. and Louda, J.W. In "Advances in Organic Geochemistry" Bjorøy, M. et al., Eds.; Wiley: Chichester, 1983, pp. 401-421, and references therein.
13. Kowanko, N.; Branthaver, J.F.; Sugihara, J.M. Fuel 1978, 57, 769-775.
14. Quirke, J.M.E.; Eglinton, G.; Maxwell, J.R. J. Am. Chem. Soc. 1978, 101, 7693-7697.
15. Dunning, H.N.; Rabon, N.A. Ind. Eng. Chem. 1956, 48, 951-955.
16. Baker, E.W.; Louda, J.W., Org. Geochem. 1984, 6, 183-192.
17. Quirke, J.M.E.; Maxwell, J.R. Tetrahedron 1980, 36, 3453-3458.
18. Ponomarev, G.V.; Shul'ga, A.M. Khim. Gretertsikl. Soedin. 1984, 19, 485-489.
19. Barwise, A.J.G.; Whitehead, E.V. In "Advances in Organic Geochemistry 1979" Douglas, A.J.; Maxwell, J.R., Eds.; Pergamon: Oxford, 1980, pp. 181-192.
20. Britton, E.D., M.Sc. Thesis, University of Florida, Gainesville, 1985.
21. Branthaver, J.F.; Trudell, L.G.; Heppner, R.A. Org. Geochem. 1982, 4, 1-7.
22. Branthaver, J.F.; Storm, C.B.; Baker, E.W. Org. Geochem. 1983, 4, 121-134.
23. Barwise, A.J.G.; Roberts, I. Organic Geochemistry In "Advances in Organic Geochemistry, 1983" Schenck, P.A. and De Leeuw, J.W. Eds.; Pergamon Oxford
24. Fookes, C.J.R. J. Chem. Soc., Chem. Comm. 1983, 1472-1473.
25. Van Berkel, G.J.; Filby, R.H.; Quirke, J.M.E., unpublished data.
26. Baker, E.W.; Yen, T.F.; Dickie, J.P.; Rhodes, R.E.; Clark, L.F. J. Am. Chem. Soc. 1967, 89, 3631-3639.
27. Aizenshtat, Z.; Dinur, D.; Nissenbaum, A. Chem. Geol. 1979, 24, 161-174.
28. Erdman, G.J. U.S. Patent 3 190 829, 1965.
29. Battersby, A.R.; Jones, K., Snow, R.J. Angew. Chem., Int. Ed. 1983, 22, 734-736.
30. K. Snow, personal communication.
31. Branthaver, J.F. Ph.D. Thesis, North Dakota State University, Fargo, 1976.
32. Sugihara, J.M. and McGee, L.R. J. Org. Chem. 1957, 22, 795-798.
33. Blumer, M. An. Acad. Brasil. Cienc. 1974, 46, 77-81.
34. Alturki, Y.I.A.; Eglinton, G. and Pillinger, C.T. In "Advances in Organic Geochemistry 1971" von Gaertner, H.R.; Wehner, H., Eds.; Pergamon: Oxford, 1972, pp.135-150.
35. HajIbrahim, S.K.; Quirke, J.M.E.; Eglinton, G. Chem. Geol. 1982, 35, 69-85.
36. Quirke, J.M.E. In "Advances in Organic Geochemistry, 1981" Bjorøy et al., Eds.; Wiley: Chichester, 1983, pp.733-737.
37. Treibs, A. Ann. Chem. 1935, 517, 172-196.
38. Treibs, A. Ann. Chem. 1935, 520, 144-151.

- 39 Palmer, S.E.; Baker, E.W.; Charney, L.S.; Louda, J.W. Geochim. Cosmochim. Acta 1982, 46, 1233-1241.
40. Bonnett, R.; Czechowski, F. J. Chem. Soc., Perkin Trans I 1984, 125-131.
41. Bonnett, R.; Czechowski, F. Phil. Trans. Roy. Soc. London Ser. A 1981, 300, 51-63.
42. Bonnett, R.; Burke, P.J.; Czechowski, F., this volume.
43. Bonnett, R.; Burke, P.J., Geochim. Cosmochim. Acta 1985, 1487-1489.
44. Van Berkel, G.J.; Filby, R.H., this volume.
45. Durand, B.; Nicaise, G. In "Kerogen: Insoluble Organic Matter from Sedimentary Rocks" Durand, B., Ed.; Edition Technips: Paris, 1980, pp.36-53.
46. Palmer, S.E.; Baker, E.W. Science, 1978, 201, 49-51.
47. Baker, E.W. and Louda, J.W. In "advances in Organic Geochemistry 1985", Julich in press.
48. Krane, J.; Skjetne, T.; Telnaes, N.; Bjoroy, M.; Schou, L.; Solli, H. Org. Geochem. 1984, 6, 193-201.
49. Ocampo, R.; Callot, H.J.; Albrecht, P.; Kintzinger, J.P. Tetrahedron Lett. 1984, 25, 2589-2592.
50. Ocampo, R.; Callot, H.J.; Albrecht, P. J. Chem. Soc., Chem. Comm. 1985, 200-201.
51. Ocampo, R.; Callot, H.J.; Albrecht, P., this volume.
52. Baker, E.W.; Louda, J.W. In "Initial Reports of the Deep Sea Drilling Project" Curray, J.R.; Moore, D.G. et al.; U.S. Government Printing Office: Washington; Vol. LXIV, Part 2; 1982, pp. 789-814.
53. Smith, K.M. "Porphyrins and Metalloporphyrins" Elsevier: Amsterdam, 1975, p.884.
54. Chicarelli, M.I.; Wolff, G.A.; Murray, M.; Maxwell, J.R. Tetrahedron 1984, 40, 4033-4039.
55. Kaur, S. Chicarelli, M.I., Maxwell, J.R. J. Am. Chem. Soc. 1986, 108, 1347-1348.
56. Budzikiewicz, H. In "The Porphyrins" Dolphin, D., Ed.; Academic Press: New York, 1978; Vol. III, pp. 395-461.
57. Shaw, G.; Quirke, J.M.E.; Eglinton, G; J. Chem. Soc., Perkin Trans. I 1979, 1655-1659.
58. Shaw, G.; Eglinton, G.; Quirke, J.M.E. Anal. Chem. 1981, 53, 2014-2020.
59. McFadden, W.H.; Bradford, D.C.; HajIbrahim, S.K.; Nicolaidis, N. J. Chrom. Sci 1979, 17, 518-522.
60. Suboch, V.P.; Antipenko, V.R.; Titov, V.I.; Gurinovich, G.P. Zh. Prikl. Spektrosk. 1976, 24, 637-642.
61. McLafferty, F.W. (Ed.) "Tandem Mass Spectrometry" Wiley: New York; 1983.
62. Yost, R.A.; Enke, C.G. Anal. Chem. 1979, 51, 1251A-1264A
63. Johnson, J.V.; Britton, E.D.; Yost, R.A.; Quirke, J.M.E.; Cuesta, L.L. Anal. Chem. 1986, 58, 1325-1329.
64. Quirke, J.M.E.; Cuesta, L.L.; Britton, E.D., Johnson, J.V.; Yost, R.A. Org. Geochem. in press.
65. Quirke, J.M.E ; Perez, M.; Britton E.D.; Yost, R.A. Org. Geochem. submitted.
66. Sundaraman, P. Anal. Chem. 1985, 57, 2204-2206.

67. Alexander, R.; Eglinton, G.; Gill, J.P.; Volkman, J.K. J. High Resol. Chromat. Chromat. Comm. 1980, 3, 521-522.
68. Marriott, P.J.; Gill, J.P.; Eglinton, G.; J. Chromatogr. 1982, 249, 291-310.
69. Marriott, P.J.; Gill, J.P.; Eglinton, G.; J. Chromatogr. 1984, 107-128.
70. Eglinton, G.; Marriott, P.J.; Evershed, R.P.; Gill, J.P. Org. Geochem. 1984, 6, 157-165.
71. Blumer, M.; Rudrum, M. J. Inst. Pet. 1970, 56, 99-106.
72. Blumer, M.; Snyder, W.D. Chem. Geol. 1967, 2, 35-45.
73. Fish, R.H.; Komlenic, J.J. Anal. Chem. 1984, 56, 510-517.
74. Didyk, B.; Alturki, Y.I.A.; Pillingier, C.T.; Eglinton, G. Chem. Geol. 1975, 15, 193-208.
75. Hodgson G.W.; Strosher, M.; Casagrande, D.J. (1972) In "Advances in Organic Geochemistry, 1971"; von Gaertner, H.R. Wehner, H., Eds.; Pergamon:Oxford, 1972, pp.151-161
76. Brockmann, H.; Tacke-Karimdadian, R. Ann. Chem. 1979, 419-430.
77. Boylan, D.B. Org. Mass Spectrom. 1970, 3, 339-351.
78. Chapman, R.A.; Roomi, M.W.; Morton, T.C.; Krajcarski, D.T.; MacDonald, S.F. Canad. J. Chem. 1971, 49, 3544-3564.
79. Nicolaus, R.A.; Mangoni; L. Caglioti, L. Ann. Chim. (Rome) 1956, 46, 793-805
80. Chicarelli, M.I.; Kaur, S.; Maxwell, J.R., this volume.
81. Wolff, G.A.; Chicarelli, M.I.; Shaw, G.J.; Evershed, R.P.; Quirke, J.M.E.; Maxwell, J.R. Tetrahedron 1984, 40, 3777-3786.
82. Tolf, B.-R.; Jiang, X.-Y.; Wegmann-Szente, A.; Kehres, L.A.; Bunnembergh, E.; Djerassi, C. J. Am. Chem. Soc. 1986, 108, 1363-1374.
83. Quirke, J.M.E.; Maxwell, J.R.; Eglinton, G.; Sanders, J.K.M. Tetrahedron Lett. 1980, 21, 2987-2990.
84. Fookes, C.J.R. J. Chem. Soc., Chem. Comm. 1983, 1474-1476.
85. Fookes, C.J.R. J. Chem. Soc., Chem. Comm. 1985, 706-708.
86. Chicarelli, M.I.; J.R. Maxwell Tetrahedron Lett. 1984, 25, 4701-4704.
87. Chicarelli, M.I.; Wolff, G.A.; Maxwell, J.R. J. Chem. Soc., Chem. Comm. 1985, 723-724.
88. Wolff, G.A.; Murray, M.; Maxwell, J.R.; Hunter, B.; Sanders, J.K.M. J. Chem. Soc., Chem. Commun. 1983, 922-924.
89. Ocampo, R.; Callot, H.J.; Albrecht, P. J. Chem Soc., Chem. Comm. 1985, 198-200.
90. Storm, C.B.; Krane, J.; Skjetne, T.; Telnaes, N.; Branthaver, J.F.; Baker, E.W. Science 1984, 223, 1075-1076.
91. Krane, J.; Skjetne, T.; Telnaes, N.; Bjoroy, M. Solli, H. Tetrahedron 1983, 39, 4109-4119.
92. Baker, E.W.; Corwin, E.W.; Klesper, E.; Wei, P.E.; J. Org. Chem. 1968, 33, 3144-3148.
93. Flaugh, M.E.; Rapoport, H. J. Am. Chem. Soc. 1968, 90, 6877-6879.
94. Smith, K.M.; Langry, K.C.; Minnetian, O.M. J. Org. Chem. 1984, 49, 4602-4609.
95. Clezy, P.S.; Mizra, A.H. Aust. J. Chem. 1982, 35, 197-209.
96. Morgan, A.R.; Pangka, V.S.; Dolphin, D. J. Chem. Soc., Chem. Comm. 1984, 1047-1048.

97. Clewlow, P.J.; Jackson, A.H.; Roberts, I. J. Chem. Soc., Chem. Comm. 1985, 724-726.
98. Habermehl, G.G.; Springer, G.; Frank, M.H. Naturwissenschaften 1984, 71, 261-263.
99. Bergaya, F.; van Damme, H. Geochim. Cosmochim. Acta 1982, 46, 349-360.
100. Cady, S.S.; Pinnavaia, T.J. Inorg. Chem. 1978, 17, 1501-1507.
101. Lin, W.C. In "The Porphyrins"; Dolphin, D., Ed.; Academic: New York, 1978; Vol IV, pp.355-377.
102. Malhotra, V.M.; Buckmaster, H.A.; Fuel 1985, 64,335-341.
103. Reynolds, J.G.; Biggs, W.R.; Fetzer, J.C. Liq. Fuels Technol. 1985, 3, 423-448.
104. Goulon, J.; Esselin, C.; Friant, P.; Berthe, C.; Muller, J.F.; Poncet, J.L.; Guilard, R.; Escalier, J.C.; Neff, B. Collect. Colloq. Semin. (Inst. Fr. Pet.) 1984, 40, 158-163.
105. Goulon, J.; Retournard, P.F.; Goulon-Ginet, C.; Berthe, C.; Muller, J.F.; Poncet, J.C., Guilard, R., Escalier, J.C.; Neff, B. J. Chem. Soc., Dalton Trans. 1984, 1095-1103.

RECEIVED March 11, 1987

## Chapter 21

# Molecular Characterization of Nickel and Vanadium Nonporphyrin Compounds Found in Heavy Crude Petroleums and Bitumens

Richard H. Fish<sup>1</sup>, John G. Reynolds<sup>2</sup>, and Emilio J. Gallegos<sup>2</sup>

<sup>1</sup>Lawrence Berkeley Laboratory, University of California—Berkeley,  
Berkeley, CA 94720

<sup>2</sup>Chevron Research Company, Richmond, CA 94802

Pyridine/water extracts of selected crude petroleums were separated by polarity on a high performance liquid chromatography (HPLC) octadecylsilane column (ODS) into three fractions; low, moderate, and high polar. The moderate and low polar fractions were examined by electron impact mass spectroscopy (EIMS) to elucidate structural and behavioral characteristics of vanadyl petroporphyrin and metallo-nonporphyrin compounds. The EIMS results indicated vanadyl petroporphyrins in Cerro Negro and Wilmington moderate polar fractions and possibly in the Wilmington low polar fraction. These EIMS results showed the presence of petroporphyrins in the above-mentioned fractions, but no discrete information about the metallo-nonporphyrins.

A highly polar nickel fraction from a Wilmington crude petroleum pyridine/water extract, separated on the ODS column, was further purified on a cyano normal phase column. This fraction had a nickel concentration of approximately 15,000 wppm, and was examined by EIMS mass spectroscopy. The spectral results indicated several homologous series structures possible for the binding sites of nickel. Further examination of the same fraction by positive ion fast atom bombardment (FAB+) mass spectroscopy, using a metal ion exchange technique, showed a substantially simplified spectrum and indicated the possibility of the nickel binding sites being small molecular weight naphthenic (carboxylic) acid salts.

Gilsonite, a bitumen, was analyzed by reversed-phase HPLC with graphite furnace atomic absorption (RP-HPLC-GFAA) element specific detection, which indicated that the nickel is predominantly bound as metallopetroporphyrin, while a small portion eluted as a highly polar metallo-nonporphyrin fraction.

These results are important in the identification of nonporphyrin metal-containing compounds in heavy crude petroleums and residua and could be beneficial for future petroleum exploration as metallo-biomarkers.

We have extensively examined various crude petroleums and separated fractions to determine the characteristics of the metal-containing compounds, particularly the metallo-nonporphyrins. Recently, we reported the molecular weights (MW) of the vanadium and nickel compounds found in selected heavy crude petroleums -- Boscan, Cerro Negro,

Wilmington, and Prudhoe Bay -- and their extracts (1,2) by size exclusion chromatography in conjunction with graphite furnace atomic absorption selective metal detection (SEC-HPLC-GFAA). The metals distribution was found to be unique for each petroleum, while the histogrammic metals profiles may have utility for fingerprinting the heavy crude petroleum. In the case of vanadium, the majority of the metal-containing compounds falls into the 2,000 to 9,000 dalton MW range, while 3 to 7% was found in the MW range > 9,000 daltons. The low MW range was calibrated by vanadyl and nickel model compounds, with 23 to 30% having a MW range of <400 daltons. Although these molecular weights may be exaggerated in the high MW range (3,4), we feel this low MW range result provides strong evidence for the metallo-nonporphyrin coordination sphere.

Pyridine/water extractions have been applied to the same heavy crude petroleum for further identification of these metal-containing molecules (2). The extraction procedure removes metal-containing compounds from all molecular weight ranges, placing the compounds in the size range of vanadyl and nickel model compounds. As well, 40 to 80% of the vanadium comes from the MW range >2,000 daltons. The extract consists predominantly of very small MW compounds with an average MW of approximately 350 daltons. By comparison with nickel and vanadyl model compounds of similar MW, we also feel this further substantiates metallo-nonporphyrin coordination spheres.

These pyridine/water extracts were separated by RP-HPLC into three fractions based on polarity, and the fractions were monitored by element specific detection (GFAA) and UV-vis spectroscopy (2). Most of the nickel-containing compounds eluted in the most polar fractions. Comparison with model compound retention times indicated these compounds are nonporphyrin bound. Most of the vanadium-containing compounds were found in the moderate polar fractions. Rapid scan (RS) UV-vis data showed a prominent Soret band in this fraction for Boscan and Cerro Negro indicating at least some of the vanadium is bound as petroporphyrin. This was not the case for Wilmington and Prudhoe Bay moderate polar fractions where the RS-UV-vis exhibited little or no Soret. At this time, we have no adequate model compounds that co-elute in this fraction. The least polar fraction also contained vanadium (up to 30% of total in crude). Model compound retention times showed the model porphyrins eluted in this fraction, but the absence of a prominent Soret in this fraction for most of the crudes suggests nonporphyrins.

The moderate and low polar RP-HPLC fractions from Boscan, Cerro Negro, Wilmington, and Prudhoe Bay crude petroleum, were examined by electron paramagnetic resonance (EPR) spectroscopy to further elucidate the structure of the average coordination sphere around the vanadium-containing molecules (5). Several nonporphyrin coordination spheres for the vanadyl ion were observed: 1) Boscan moderate polar and Prudhoe Bay moderate and low polar fractions exhibited  $N_2S_2$  coordination. 2) Cerro Negro and Wilmington moderate polar fractions showed  $S_4$  coordination. 3) Boscan low polar fraction showed  $N_4$  coordination. 4) Cerro Negro had distinctively different parameters showing a  $NOS_2$  coordination.

We have also examined the RP-HPLC fractions by EIMS to further identify the metallo-nonporphyrin components. Unfortunately, the EIMS spectral studies only revealed the presence of metallopetroporphyrins in certain fractions. The metallo-nonporphyrins remained undifferentiated in the organic matrix.

We have attempted to elucidate the structure of nickel-containing molecules in the high polar RP-HPLC fractions by using C-18 ODS reversed-phase and cyano normal phase chromatography techniques to purify the pyridine/water extract of Wilmington crude petroleum. We have examined the resulting purified fractions with EIMS, FAB+, and metal replacement FAB+ mass spectroscopies. We have also attempted to verify the existence of these highly polar nickel components in other carbonaceous materials. For example, we examined Gilsonite by RP-HPLC-GFAA and found this highly polar nickel complexes may also be present in this petroleum precursor.

### *Results and Discussion*

*Spectral Analyses of the Moderate and Low Polar RP-HPLC Fractions.* In efforts to identify the elusive nonporphyrin metal-containing species, the moderate and low polar fractions,

obtained by the RP-HPLC separation of the pyridine/water extracts of Boscan, Cerro Negro, Prudhoe Bay and Wilmington crude petroleums, were examined by EPR, EIMS, and RS-UV-vis spectroscopies. The EPR techniques employed utilize vanadyl square pyramidal model compounds to elucidate the average first coordination sphere of the vanadium-containing compounds in the sample studied (6-10). The EPR (5) and RS-UV-vis (1,2) results have been reported elsewhere.

The EIMS of the RP-HPLC fractions, in general, identified the existence of vanadyl petroporphyrins when present. Figure 1 shows the EIMS for Cerro Negro moderate polar fraction for  $m/z$  of 200 to 800. Although some individual peaks stand out, the vanadyl etio homologous series is evident from  $m/z$  of 473 to 557. The vanadyl deoxophylloerythroetio (DPEP) homologous series, although less prominent, is evident from  $m/z$  of 499 to 575.

The same spectral characteristics were observed in the Wilmington moderate polar fraction indicating vanadyl petroporphyrins. RS-UV-vis examination of these moderate polar fractions also indicated the presence of vanadyl petroporphyrins by the appearance of the distinctive 408 nm Soret band (1,2).

The vanadyl porphyrin model compounds elute in the low polar fraction. We do not have model compounds with a Soret at 408 nm which co-elute in the moderate polar fraction. These could represent metallopetroporphyrins with a carboxylic acid functionality, (11,12) dimers of petroporphyrins (13,14), or petroporphyrins of much higher molecular weight (15).

These EIMS results do not necessarily conflict with the EPR data for these fractions which showed  $N_2S_2$  average first coordination sphere around the vanadyl ion (5). The EPR techniques are average parameter techniques and would not necessarily be able to resolve a minor percentage of the  $N_4$  coordination sphere. The EIMS method also only detects the petroporphyrins, but does not quantitate them.

The EIMS spectrum of Prudhoe Bay low polar fraction, Figure 2, shows no metallopetroporphyrin homologous series. This spectrum is very typical of those fractions which contained no discernible petroporphyrins. As can be seen by Figure 2, any individual homologous series are overwhelmed by the organic matrix. The same spectral characteristics were observed for Boscan and Cerro Negro low polar fractions indicating very low levels or no petroporphyrins. This is corroborated by only a weak 408 nm Soret found by RS-UV-vis.

The EPR of these fractions indicated  $N_4$  coordination for the Boscan and Prudhoe Bay low polar fractions and  $NOS_2$  coordination for the Cerro Negro low polar fraction. The  $N_4$  nonporphyrin coordination sphere has been seen before in the EPR studies and suggests a variety of nonporphyrin ligand structures (5,16,17).

*Purification of the Highly Polar Nickel Compounds Found in Wilmington Heavy Crude Petroleum.* RP-HPLC-GFAA examination of the pyridine/water extracts of several heavy crude petroleums indicated the majority of the nickel-containing compounds eluted in the high polar fraction. The lack of EIMS spectral identification of these fractions suggested the need for further purification.

Wilmington crude petroleum was extracted with pyridine/water and the extract was separated on the ODS column into a highly polar fraction (methanol eluted) and a less polar fraction (methylene chloride eluted). The highly polar fraction was re-chromatographed on the ODS column, and was found to increase its nickel concentration from 8000 to 11000 wppm. Table I shows the concentrations of these fractions.

Further purification was performed on a cyano column using a methylene chloride to methanol solvent gradient. The use of bonded phase HPLC separations, either reversed-phase or cyano columns, offer several unique advantages over the more conventional silica columns (18). Because polar solvents can be used, bonded packings are capable of separating highly polar metal-containing complexes. These highly polar complexes would be irreversibly bonded to silica, because silica packings rapidly degrade in polar solvents. Reversed-phase packings allow for partition separations where the more polar components elute first. Cyano columns can be operated in normal or reversed-phase modes providing increased flexibility over silica columns

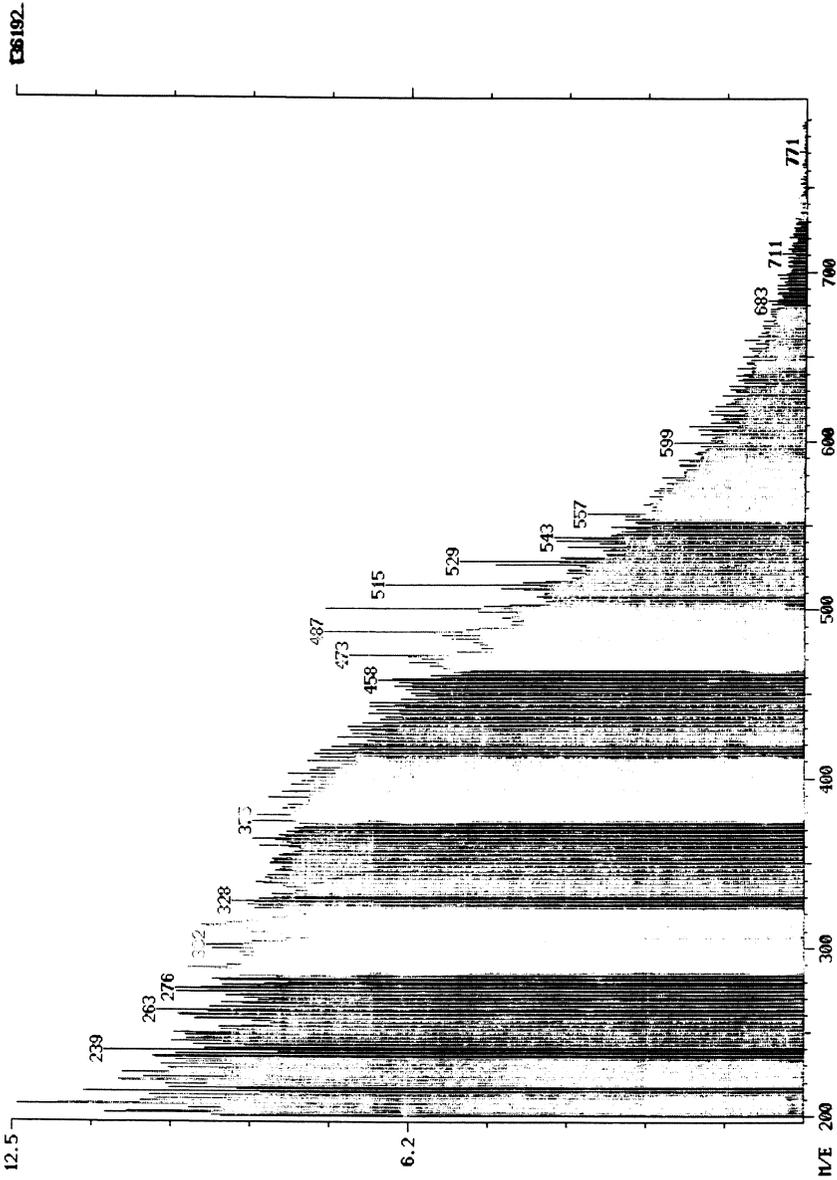


Figure 1. Electron Impact Mass Spectrum for Cerro Negro Moderate Polar Fraction.

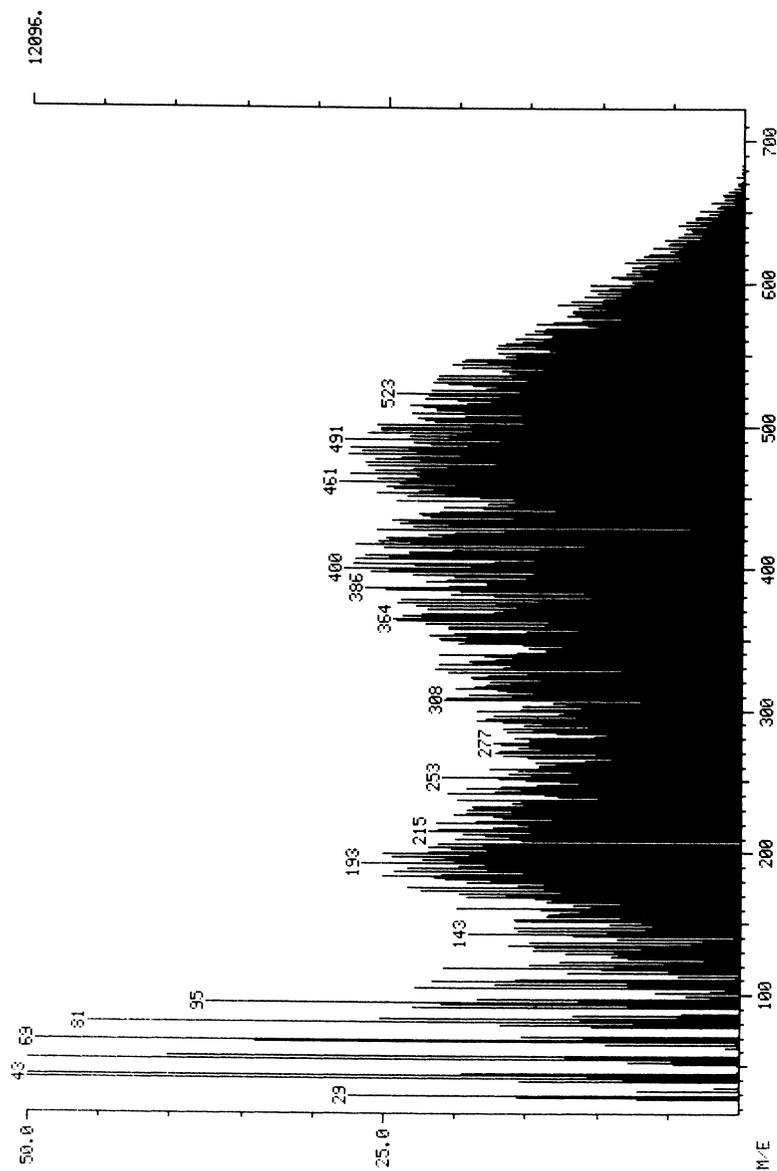


Figure 2. Electron Impact Mass Spectrum for Prudhoe Bay Low Polar Fraction.

**Table I: Nickel Concentrations of  
Preparatively Collected Fractions from the  
Wilmington Petroleum Extract<sup>1</sup>**

	ODS I	ODS II <sup>2</sup>	Cyano Peak I <sup>3</sup>
Ni, (ppm)	8,040	11,000	14,250
Wt. of Collected fraction, (mg)	60	25.2	4.0
Nickel Complexes, (wt %) <sup>4</sup>	4.1	5.7	7.4

<sup>1</sup>Concentrations Determined Using Aqua Regia Conditions and Standards Plots

<sup>2</sup>Rechromatography of ODS I Using ODS Column

<sup>3</sup>Rechromatography of ODS II Using Cyano Column

<sup>4</sup>Assumed Molecular Weight of Complexes 300 - Daltons

Figure 3 shows the elution profile for this separation with the effluent monitored for both UV-vis wavelength of 254 nm, and GFAA wavelength of 232 nm. Organic impurities eluted quickly at approximately 3 minutes. Two fractions of nickel complexes eluted; the first in the 50% methylene chloride solvent mixture. This corresponded to several sharp maxima in the UV-vis monitor. A second fraction eluted shortly after the solvent system was changed to 100% methanol. This fraction corresponded to a broader maximum in the UV-vis monitor. These nickel compounds are more polar than the nickel nonporphyrin model complexes which eluted at approximately 10 percent methanol. In contrast, nickel (II) chloride eluted at approximately 28 minutes, which is substantially longer than the second nickel fraction in Figure 3 and precludes the possibility of inorganic nickel.

Table I shows the further concentration of the nickel fraction by chromatography on a cyano column and this corresponds to 7.4 wt % nickel complex in the sample (assuming an average molecular weight of 300 daltons based on model compound elution times from SEC-HPLC-GFAA studies).

*Mass Spectral Analyses of the Cyano Column Separated Nickel Fraction.* In order to interpret the mass spectral results of the fraction derived from the cyano column separation, we examined in detail, the mass spectral (19) behavior of several nickel and vanadium model compounds by EIMS, FAB, field ionization and field desorption (FI/FD), and chemical ionization (CI) in positive or negative ionization modes.

Figure 4 shows nickel (II) bis(diethylthiocarbamate), nickel (II) tetramethyl-dibenzotetraaza-[14]-annulene (TADA), and nickel (II) bis(dipivaloylmethane) (DPM) by EIMS. All three parent ions are observable at  $m/z$  354, 400, and 424 respectively. Even though the parent ion is the dominant ion, for the dithiocarbamate complex, the spectrum is complicated by substantial fragmentation. This extensive fragmentation is not evident for the other model compounds, but the Ni(DPM)<sub>2</sub> spectrum shows a fragment ion to be the dominant peak. While these spectra give identifiable patterns, they do not exhibit any systematic behavior. Interpretation of unknown species can be substantially complicated by the lack of systematic behavior, and we do not necessarily expect to identify the metallo-nonporphyrin compounds by this method.

Thin layer and RP-HPLC chromatography indicated that nickel carboxylate model compounds have a very similar polarity behavior, when compared to these concentrated nickel fractions. Because this is the case, nickel carboxylates were selected as model com-

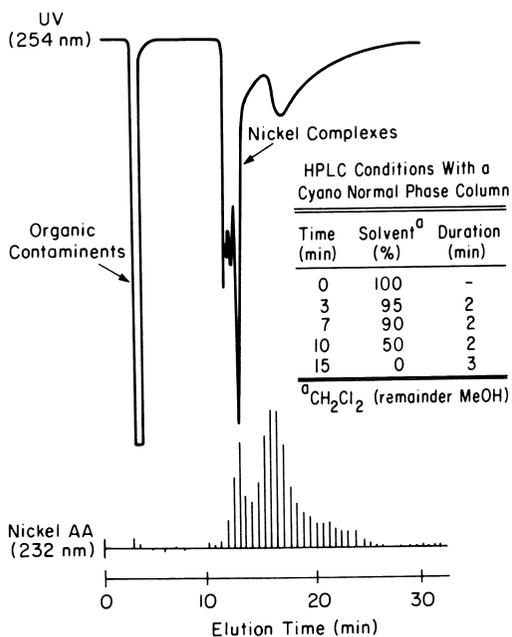


Figure 3. HPLC-GFAA Profile for the Nickel Complexes from the Cyano Column Separation of the High Polar Reversed-Phase Fraction of Wilmington Crude Petroleum Extract.

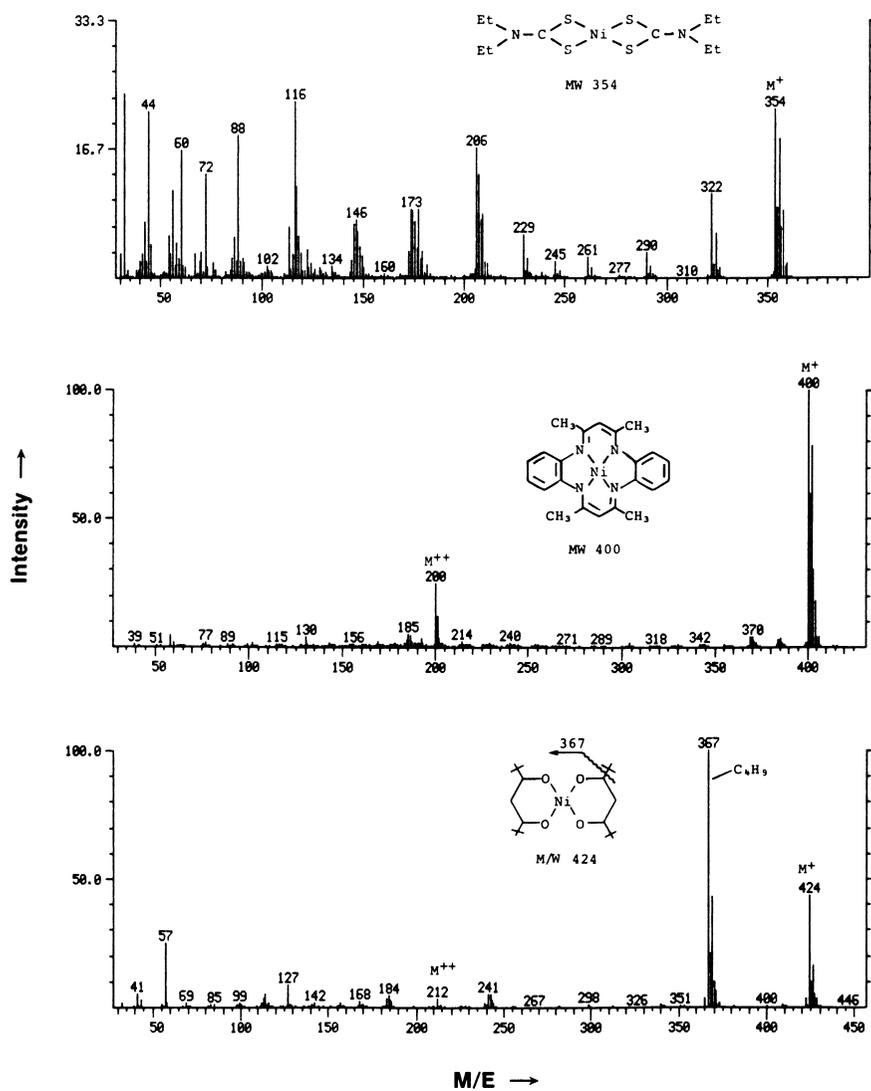


Figure 4. Electron Impact Mass Spectra of Selected Nickel Model Compounds.

pounds. Carboxylic acids are appropriate choices because they have been detected and characterized in carbonaceous materials and can constitute up to 3 wt % of the crude petroleum (20).

We also examined nickel acetate, nickel bis(2-ethylhexanoate), and a naphthenic acid extract from crude petroleum in which the nickel was synthetically placed. Figure 5 shows the EIMS of the nickel naphthenates. Clearly, the parent ion homologous series is evident in the spectrum. The naphthenates show even mass molecular ions extending from about  $m/z$  426 to 582. Note, though, the intensity of the molecular ions is substantially less than that of the major fragments. The presence of impurities would easily overwhelm the parent ions, causing substantial interpretation problem in mixtures.

The cyano column purified nickel fractions of the Wilmington crude petroleum extract were combined and examined by EIMS and compared to the spectra of the nickel model compounds. The spectrum of the purified nickel fraction is shown in Figure 6. Unfortunately, as expected from the complicated spectrum of the nickel naphthenates, no clearly defined metallo-nonporphyrin species are identifiable. Several homologous series are discernible, but their association with nickel is tenuous.

The cyano column purified nickel fraction was also examined by EIMS for metalloporphyrins at  $m/z$  values where porphyrins should be detected (not shown). At the concentration of nickel in this sample, the petroporphyrins would be overwhelmingly evident; however, no porphyrins were detected. Thus, it is evident that these compounds are not metalloporphyrins.

*Positive Ion Fast Atom Bombardment (FAB+) Mass Spectroscopic Analyses of the Cyano Column HPLC Fractions.* FAB+ is a particularly efficient method for examining polar components in hydrocarbon mixtures. The technique allows the observation of the polar portion of a sample without the complication of the neutral organic components (these are not observed by the FAB+ technique), and greatly simplifies analyses of the spectra. In addition, only certain ionic species are observable, i.e., vanadium and nickel complexes do not show ligand-metal ions, while calcium, magnesium, silver, and iron do show these ions. In addition, only certain metal complexes are also seen, e.g., porphyrins and acetylacetonates are not necessarily observed, while carboxylic acid complexes are observed.

Several carboxylic acid model compounds were examined by FAB+. Nickel (II) bis(2-ethylhexanoate) was examined using triethanolamine (TEA) as the hydrogen source. Although some fragments of the acid are apparent in the spectrum (not shown), the parent ions necessary for identification of the model compound are not present in high enough concentration to be evident. Fragments of Ni + TEA are also evident. In the FAB+ spectrum, the metal ion fragments from the complex are detected, but the ligands are not apparent. Figure 7 shows the FAB+ spectrum of nickel naphthenates and TEA, which also gave reasonable EIMS spectra (Figure 5). The metal-ligand parent ions are not obvious; however, Ni + TEA ions are evident. Although the technique is not viable for ligand identification, it may have utility for metal ion identification.

Recent developments (21) have shown, using calcium compounds with a FAB+ ion source, well resolved spectra of naphthenic (carboxylic) acids. This technique exchanges the metal ion of the complex with calcium and gives a calcium naphthenate ion spectrum. Figure 8 shows the FAB+ spectrum of the nickel naphthenate mixture with TEA and calcium acetate. Several homologous series of carboxylic acids + Ca + TEA are apparent in the spectrum. (FAB- shows the naphthenic acid series with a maximum at  $m/z$  of 251.) These match identically to FAB+ spectra of calcium naphthenates synthetically prepared from the same naphthenic acid source. The FAB+ results of several carboxylic acid model compounds of different metals also responded similarly with calcium compounds and TEA. The results of these experiments and the development of the technique will be published elsewhere (21).

The cyano column purified nickel fraction from the Wilmington crude petroleum extract was examined by the FAB+ metal exchange technique. The FAB+ spectrum of the fraction with just TEA shows no apparent parent ions, just the Ni(TEA)<sub>2</sub> ion. This feature was also common to model compound spectra. Figure 9 shows the corresponding FAB+

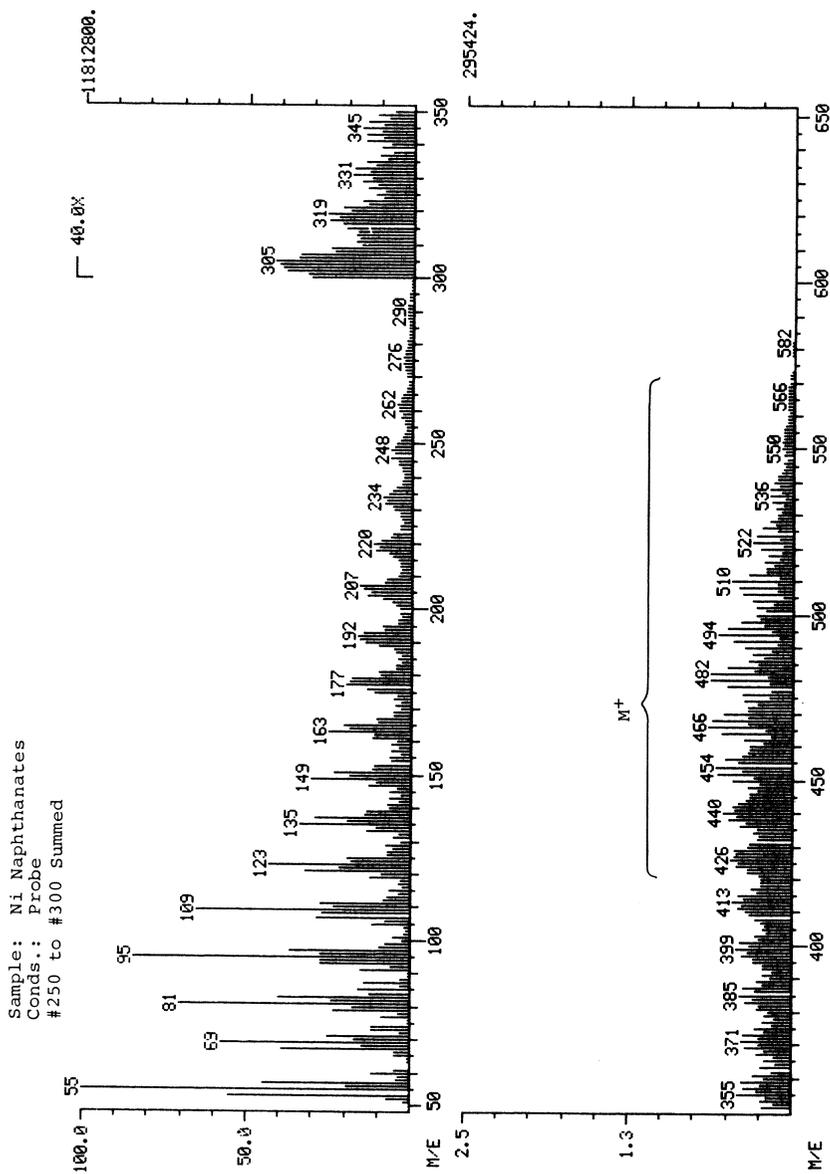


Figure 5. Electron Impact Mass Spectrum of Synthesized Nickel Naphthenates.

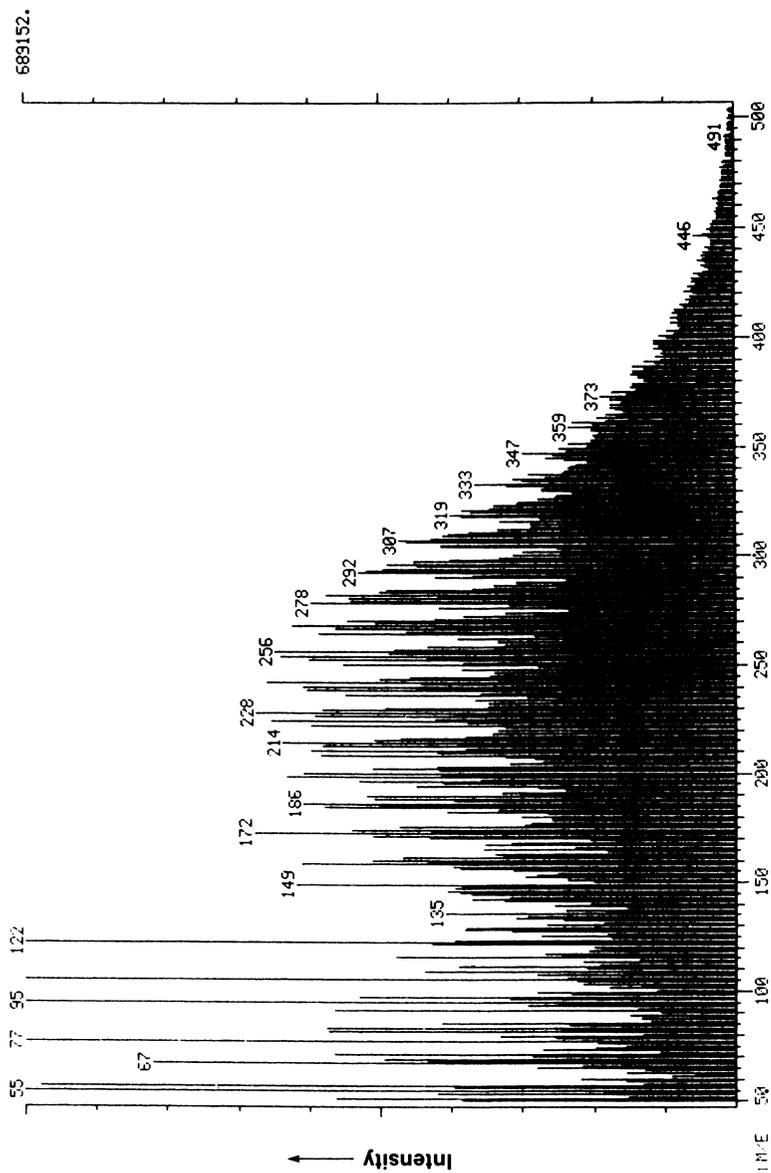


Figure 6. Electron Impact Mass Spectrum of the Cyano HPLC Column Purified Nickel Fraction from Wilmington Crude Petroleum Extract.

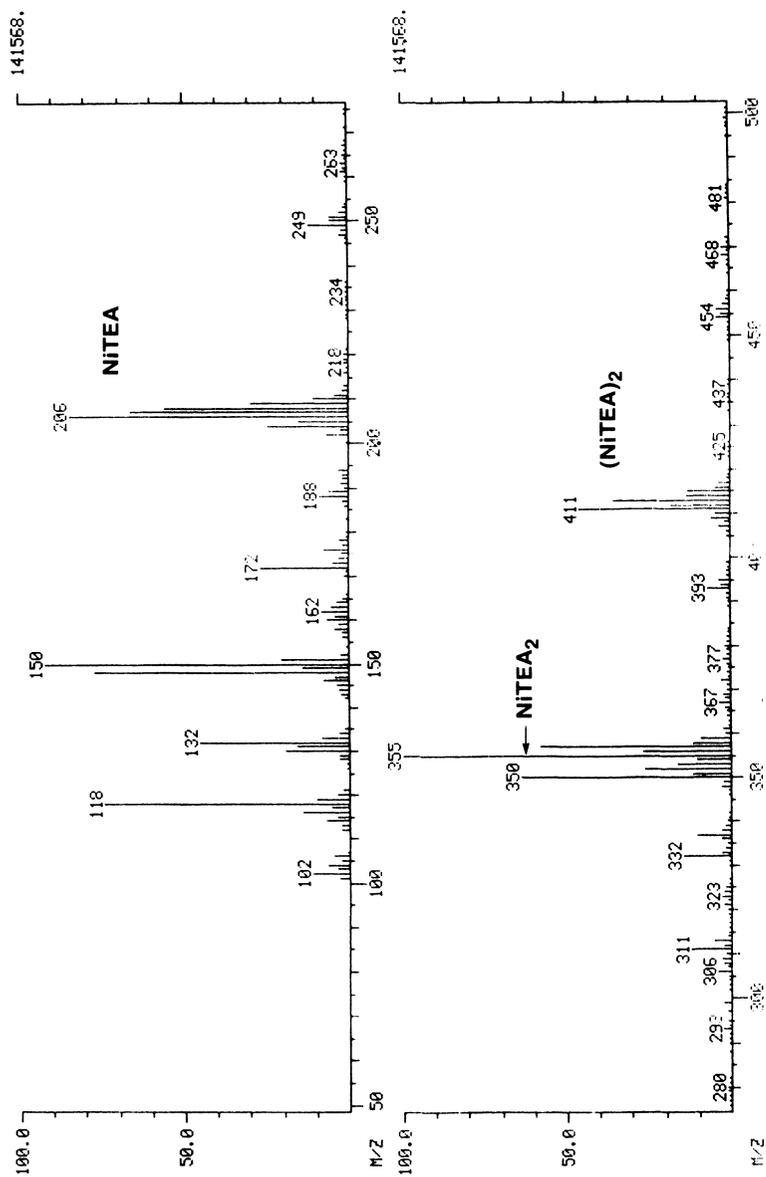


Figure 7. Positive Ion Fast Atom Bombardment Spectrum of Synthesized Nickel Naphthenates.

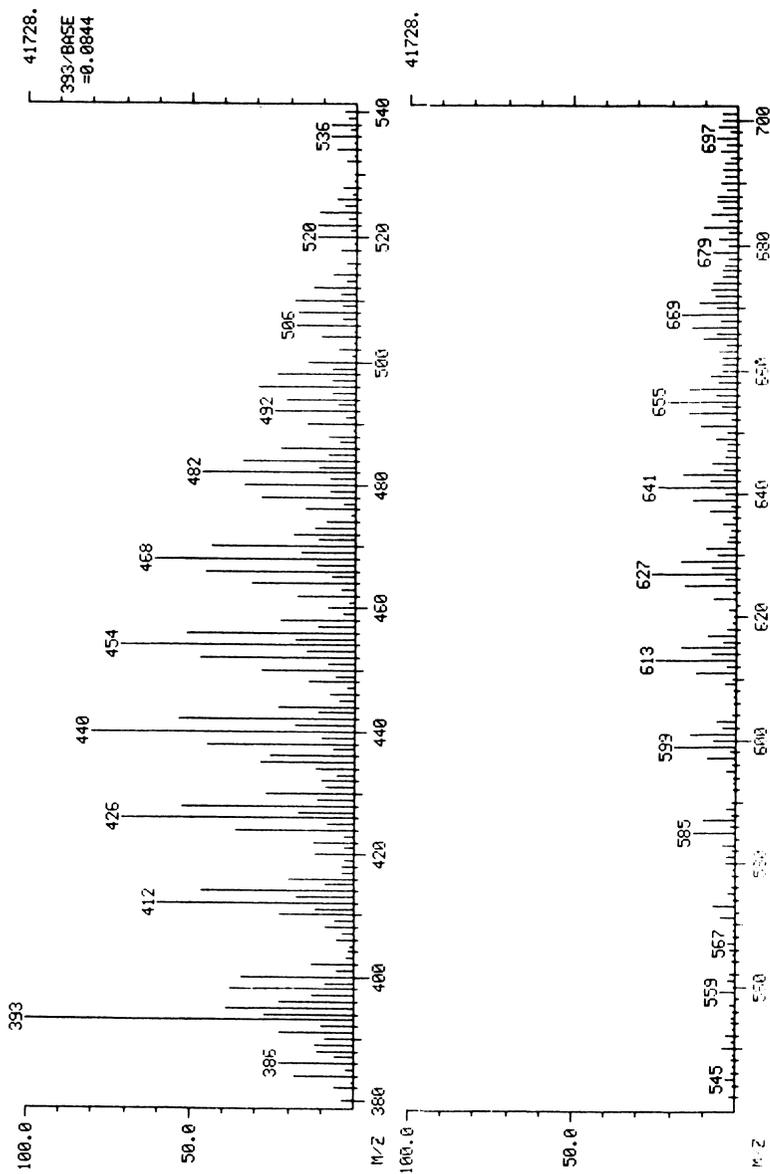


Figure 8. Positive Ion Fast Atom Bombardment Spectrum of Synthesized Nickel Naphthenates with TEA and Calcium Acetate.

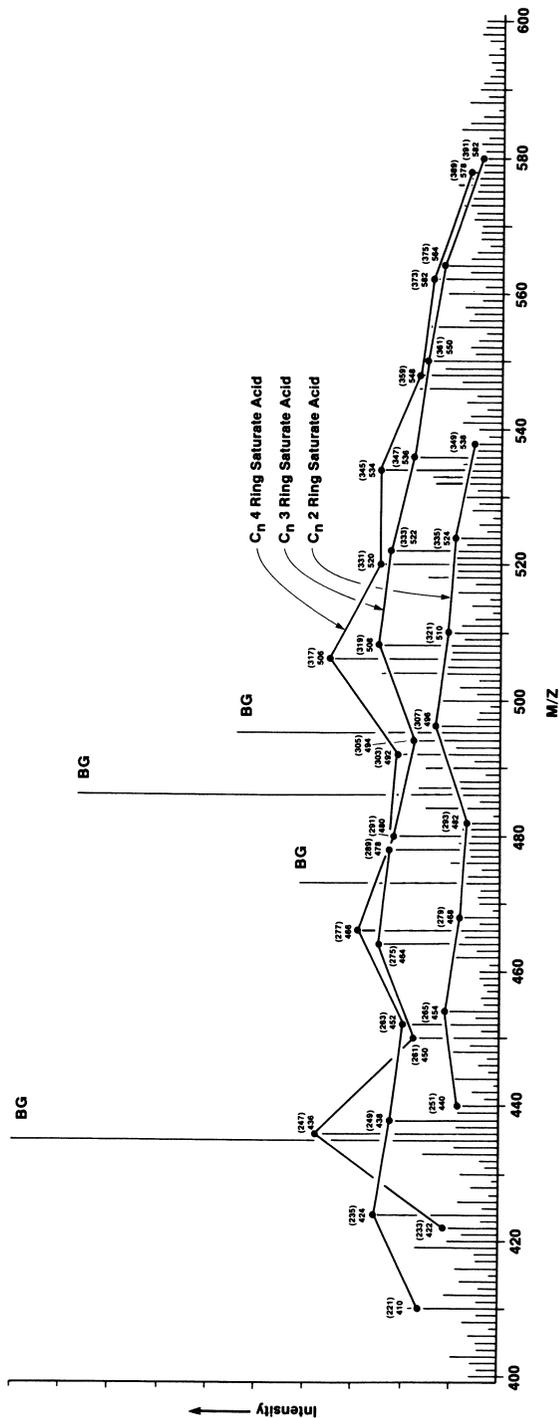
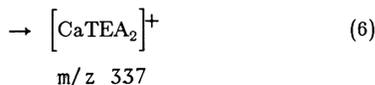
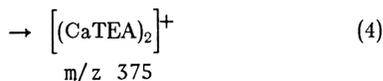
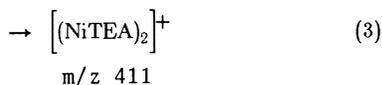
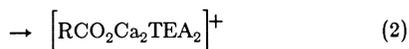
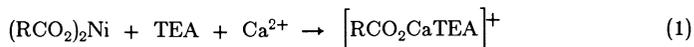


Figure 9. Positive Ion Fast Atom Bombardment Spectrum of Cyano HPLC Column Purified Nickel Fraction from Wilmington Crude Petroleum Extract with TEA and Calcium Acetate.

spectrum with Ca and TEA. Apparently, there are several homologous series of nickel compounds that are thought to be carboxylic acids complexes. In addition, detailed examination of the spectrum further shows that carboxylic acids are possible binding sites for the nickel, when compared to the EIMS spectrum of the same material (Figure 6).

Reactions 1 through 8 are presumed to take place as the calcium and TEA doped with the nickel fraction is bombarded with krypton neutral atoms in the fast atom bombardment process. These reactions explain most of the ions observed in the metal atom exchange technique. The mechanism of this exchange has not been elucidated, but the nickel appears to be removed, and the calcium complex is formed with only one carboxylic acid ligand. The other coordination site on the calcium is taken with a TEA fragment (this adds  $m/z$  of 189 to the free acid parent fragment).



The acid molecular weight can be ascertained from the EIMS of the sample. In the EIMS, the intensity of the metal-containing molecular ion is about 1/200 of the fragments. As a result, when comparing the FAB+ spectrum to the EIMS spectrum of the same material, one must look for the acid anion in the EIMS spectrum, not the nickel complex.

In Figure 9, three homologous series are clearly indicated with the possibility of several more. The corresponding carboxylic acid fragment, as observed in the EIMS spectrum (Figure 6) of the sample, are indicated in parentheses above the corresponding metal-ligand peak. The homologous series in the FAB+ spectrum starting at  $m/z$  422 could correspond to the EIMS series starting at  $m/z$  233. This series is apparent in the EIMS figure on the lower right side of the massive peak ( $m/z$  373 and 359). This could be attributed to four ring saturated naphthenic acids. Likewise, the homologous series starting at  $m/z$  410 in the

FAB+ spectrum possibly correlates with three ring saturated naphthenic acids, and the series starting at  $m/z$  440 corresponds to two ring saturated naphthenic acids.

The two most intense peaks in Figure 9 correspond to the C20 four ring saturated acid at  $m/z$  506 and the C15 four ring saturated acid at  $m/z$  436 and can be related by an isoprene unit (C5). This suggests the two, three, four, and five ring components are due to bicyclic sesquiterpanoic, tricyclic diterpanoic, and four and five ring triterpanoic (steranoic and hopanoic) acids. Figure 10 shows generalized structures of these acid ligands. Model compound data, by the metal replacement technique, also indicates replacement reactions as shown in reaction 2. This reaction adds another 187 mass units to the molecule. Although, peaks corresponding to the homologous series formed by reaction 2 can be located in the FAB+ spectrum (not shown), the noise inhibits any clear identification of these species.

*RP-HPLC-GFAA Studies on Gilsonite.* Gilsonite, a bitumen (Eocene, Uinta Basin, Utah), has a high concentration of nickel (100 wppm), but a low concentration of vanadium. We chose Gilsonite as another possible source of the highly polar nickel compounds, because it already had been examined for petroporphyrins (22). In addition, Gilsonite is associated with the Green River Formation and has petroporphyrins which should have experienced mild thermal alterations. Thus, we wanted to ascertain whether the presumed nickel carboxylates in Wilmington crude petroleum were present in Gilsonite.

Gilsonite was dissolved in THF and separated on the C-18 ODS column and the effluent monitored by GFAA. Figure 11 shows the nickel RP-HPLC-GFAA profile of the column effluent, which was also monitored at 320 and 408 nm. Three different component classes containing nickel were separated: compounds eluting at 1) the solvent front, 2) 24 minutes (80% THF), and 3) 36 minutes (100% THF). The most polar nickel components eluted at the solvent front, but are in minor amounts compared to other bands. The middle fraction eluted at the same time as nickel etioporphyrin. The 408 nm response also indicates that at least some of these compounds are porphyrins. We did not have standards which elute at the same time as the third fraction (36 min). The prominent Soret indicates these are petroporphyrin components. Unfortunately, we have not been able to obtain the needed concentrations of this highly polar nickel compound fraction to verify the metal-containing components by FAB+ as nickel carboxylates. However, we speculate that these are small amounts of nickel carboxylates in Gilsonite, which are potential conduits for nickelation of porphyrin ligands during fossilization.

### Conclusion

We have separated pyridine/water extracts of selected crude petroleums by reversed-phase chromatography, and examined the vanadium-containing compounds in the moderate and low polar fractions by mass spectroscopy. The EIMS results indicated vanadyl petroporphyrins in Cerro Negro and Wilmington moderate polar fraction and possibly in the Wilmington low polar fraction. The EIMS results provided no additional information on the metallo-nonporphyrins.

By further purification of the highly polar fraction from the ODS separation of the Wilmington crude petroleum extract, we have seen evidence of bonding for at least one type of nickel-containing nonporphyrin compound. EIMS and FAB+ with metal exchange indicates this nickel is bound as carboxylates (naphthenates).

We are continuing our molecular characterization studies in order to further determine the highly polar nickel compounds as carboxylic salts and as well in our attempts to identify the vanadyl nonporphyrin compounds found in heavy crude petroleums and their precursors.

### Experimental

The reversed-phase separations were performed by methods and on equipment described previously (1,2). EIMS were obtained on equipment described previously (23). The vanadyl etio and DPEP petroporphyrins were observed, when present, around  $m/z$  of 500. In addition, a plethora of peaks is also evident. This overwhelming continuum was characteristic of all fractions studied, and prevented us from using EIMS for any metal characterization other than vanadium petroporphyrin detection in the RP-HPLC fractions.

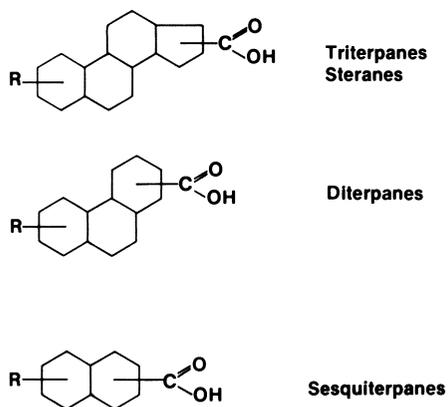


Figure 10. Possible Carboxylic Acid Ligands for Nickel Complexes in the Cyano HPLC Column Purified Nickel Fraction from Wilmington Crude Petroleum.

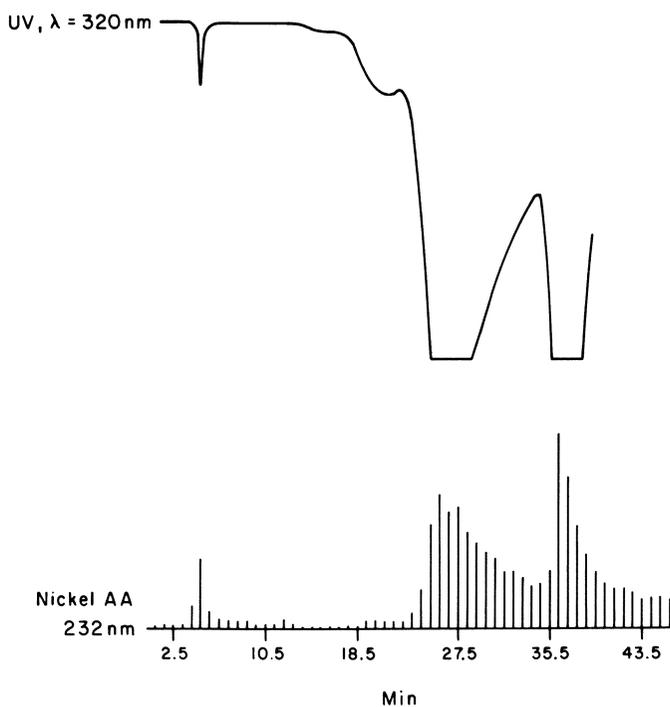


Figure 11. RP-HPLC-GFAA Nickel Profile for a Gilsonite Sample Dissolved in THF.

The separation procedures for the nickel carboxylate fraction isolated from Wilmington crude petroleum utilized both reversed-phase (ODS) and cyano normal phase HPLC techniques and details will be published elsewhere (24). The FAB+ mass spectral methods will also be discussed elsewhere (21). Model compounds for the studies were either purchased from Alfa Chemical Company, or synthesized by literature methods. The Gilsonite sample was separated by RP-HPLC-GFAA techniques and details will be reported elsewhere (24).

#### *Acknowledgments*

We thank John J. Komlenic and Alejandro Izquierdo for experimental assistance, Dr. Geoffrey Eglinton of the University of Bristol for helpful suggestions, and Dr. Robert M. Carlson of Chevron Oil Field Research for the Gilsonite sample. The Lawrence Berkeley Laboratory studies were supported by the Assistant Secretary of Fossil Energy, Division of Oil, Gas, and Shale technology, and the Bartlesville Project Office of the U.S. Department of Energy under contract DE-AC03-765F00098.

#### *Literature Cited*

- (1) Fish, R.H.; Komlenic, J.J. *Anal. Chem.* 1984, 56, 510.
- (2) Fish, R.H.; Komlenic, J.J.; Wines, B.K. *Anal. Chem.* 1984, 56, 2452.
- (3) Boduszynski, M.M.; McKay, J.F.; Latham, D.R. *Assoc. of Asphalt Paving Tech.* 1980, 49, 123.
- (4) Boduszynski, M.M. In "Chemistry of Asphaltenes." J.W. Bunger (ed.), *Adv. in Chem. Ser.* 1981, 195, 119.
- (5) Reynolds, J.G.; Gallegos, E.J.; Fish, R.H.; Komlenic, J.J. Submitted to *Energy and Fuels* 1986.
- (6) Dickson, F.E.; Kunesh, C.J.; McGinnis, E.L.; Petrakis, L. *Anal. Chem.* 1972, 44, 978.
- (7) Dickson, F.E.; Petrakis, L. *Anal. Chem.* 1974, 44, 1129.
- (8) Yen, T.F.; Boucher, L.J.; Dickie, J.P.; Tynan, E.C.; Vaughan, G.B. *J. Inst. Petrol.* 1969, 55, 87.
- (9) Yen, T.F. In "The Role of Trace Metals in Petroleum." T.F. Yen (ed.), *Ann Arbor Sci.*, 1975, Ann Arbor, MI. Chap. 1, 1.
- (10) McCormick, B.J.; Bellott, E.M. *Inorg. Chem.* 1970, 9, 1779.
- (11) More, K.M.; Eaton, S.S.; Eaton, G.R. *J. Amer. Chem. Soc.* 1981, 103, 1087.
- (12) Ocampo, R.; Callot, H.J.; Albrecht, P. *J. Chem. Soc., Chem. Comm.* 1985, 198.
- (13) Blumer, M.; Synder, W.D. *Chem. Geol.* 1967, 2, 35.
- (14) Blumer, M.; Rudrum, R. *J. Inst. of Petrol.* 1970, 56(548), 99.
- (15) Johnson, J.V.; Britton, E.D.; Yost, R.A.; Quirke, J.M.E.; Cuesta, L.L. *Anal. Chem.* 1986, 58, 1325.
- (16) Reynolds, J.G. *Liq. Fuels Tech.* 1985, 3(1), 73.
- (17) Reynolds, J.G.; Biggs, W.R.; Fetzer, J.C. *Liq. Fuels Tech.* 1985, 3(4), 423.
- (18) O'Laughlin, J.W. *J. of Liq. Chrom.* 1984, 7, 127.
- (19) Reynolds, J.G.; Gallegos, E.J.; Fish, R.H. Manuscript in preparation, 1986.
- (20) Seifert, W.K. *Progress in Chem. Org. Nat. Products* 1975, 32, 1.
- (21) Gallegos, E.J.; Reynolds, J.G.; Fish, R.H. 33rd Annual Conference on Mass Spectrometry and Allied Topics, San Diego, 1985.
- (22) Quirke, J.M.E.; Eglinton, G.; Maxwell, J.R. *J. Amer. Chem. Soc.* 1979, 101, 7693.
- (23) Sundaraman, P.; Gallegos, E.J.; Baker, E.W.; Slayback, J.R.B.; Johnston, M.R. *Anal. Chem.* 1984, 56, 2552.
- (24) Fish, R.H.; Reynolds, J.G.; Gallegos, E.J. Manuscript in preparation, 1986.

RECEIVED November 13, 1986

## Chapter 22

# Gel Permeation Chromatographic Behavior of Metalloporphyrins from a Rock Extract

G. Šebor

Department of Petroleum Technology and Petrochemistry,  
Institute of Chemical Technology, 166 28 Prague 6, Czechoslovakia

The number of carbon atoms present in the porphine substituents and mainly the different geometry of nickel and vanadyl ions in the molecule of metalloporphyrins were found to be the main factors influencing the GPC separation of these etio and deoxophylloerythroetio type complexes. This chromatographic technique provided an effective separation of nickel from vanadyl porphyrins present in a rock extract from the vicinity of petroleum deposit in the Persian Gulf area. Both metalloporphyrins were isolated by the combination of adsorption chromatography on silica gel and GPC on styrene-divinylbenzene copolymer. In order to study the GPC behavior of these complexes, GPC fractions were collected and analyzed by mass spectrometry.

For many years already, considerable attention has been paid to the character of nickel and vanadyl petroporphyrins found in fossil fuels and both ancient and recent sediments. The knowledge of the type of petroporphyrins found in fossil fuels is significant both for geochemical correlations and for the study of the behavior of both types of the relevant metalloporphyrins during fossil fuels processing.

An effective separation of petroporphyrins from the sample is a necessary prerequisite for their detailed characterization. The methods used for the separation of petroporphyrins may be divided into two basic groups, viz. extraction methods and chromatographic methods. An appropriate combination of both types of methods is also applied very frequently. Numerous organic solvents and both organic and mineral acids have been used as extraction reagents (1). It is especially the extraction

0097-6156/87/0344-0350\$06.00/0

© 1987 American Chemical Society

of petroporphyrins with an acid, which starts as a demetalation of the metalloporphyrins present, and is frequently used as the first step in the isolation of the relevant compounds (2). There is a disadvantage however, in that changes in the original structure of the compounds may occur during demetalation and the subsequent extraction of free porphyrins (3-6). The basic assumption made is that every compound decomposes to the same extent, e.g. the relative amounts of the various compounds present are unchanged after demetalation (2).

In the field of chromatographic methods, high-performance liquid chromatography has recently been considered an extremely promising technique (7-12). This chromatographic technique enables separation of homologous series and types of metalloporphyrins as well as structural isomers (12). With the exception of ion-exchange chromatography, other liquid chromatography techniques have been employed for petroporphyrins separations, viz. adsorption column chromatography, thin layer chromatography, paper chromatography, and gel permeation chromatography (2). The last method has been used by some authors for separation of nickel and vanadyl porphyrins (13,14). To date however the mechanism of GPC separation of these compounds has not been discussed in a detailed manner.

In the present paper, the characteristics of nickel and vanadyl porphyrins, found in the rock extract obtained in the vicinity of crude oil deposits, are presented. The relevant metalloporphyrins have been separated by a combination of adsorption chromatography on silica gel and GPC on a styrene-divinylbenzene copolymer. Gel permeation chromatographic behavior of nickel and vanadyl metalloporphyrins has been studied in a detailed manner.

### Experimental

Sample Preparation. Drillings were made to a depth of 6 m in the vicinity of crude oil deposits in the Persian Gulf area. The rock extracts obtained from the bore hole were crushed; 450 g were extracted with benzene in a Soxhlet extractor and the extracts were weighed. The yields of extractable mass were within the range of 0.1-15 wt%, usually about 0.15 wt%. Extract samples marked KB6a, KB7a, and KB9b were supplied by Professor W. D. Gill. The original extracts were characterized by means of their content of nickel, vanadium, and metalloporphyrins; the results have been published previously (15). For the present study, the KB6a sample has been chosen.

Adsorption Chromatography. Adsorption chromatography of the extract was carried out on a glass column (60 cm x 8 mm i.d.) packed with silica gel (Woelm Eschwege)

deactivated by addition of 3 wt% water. Saturated hydrocarbons and aromatics were eluted with 50% ether in pentane. The metalloporphyrins were eluted with ether. The eluent was delivered with a MC 300<sub>1</sub> micropump (Microtechna, Prague) at a flow rate of 1 mL min<sup>-1</sup> and monitored with a UV-VIS detector (KNAUER) for quantitative isolation of metalloporphyrins. The detector was set at 400 nm.

Gel Permeation Chromatography. Gel permeation chromatography of the metalloporphyrins concentrate was performed on a glass column (150 cm x 14 mm i.d.) packed with a styrene-divinylbenzene copolymer containing 3 wt% of divinylbenzene (the gel was prepared at the Institute of Macromolecular Chemistry, Czechoslovak Academy of Sciences, Prague). The gel was characterized by particle size of 40-120 μm and an exclusion limit of about 2000. It was swelled in a methanol-benzene mixture containing 10% methanol. The column was closed at both ends with brass stoppers equipped with Teflon seals, and the gel was fixed on both ends by a glass wool layer. The methanol-benzene mobile phase was delivered by means of a device working on Mariotti's principle; a constant flow rate of 1.5 mL min<sup>-1</sup> was maintained. A six way stop cock with a sampling loop was used for the injection of the metalloporphyrins concentrate prepared by adsorption chromatography. The eluent was constantly monitored with a UV-VIS detector (KNAUER) set at 550 and 572 nm, respectively.

Mass Spectrometry. Mass spectra were recorded on an A.E.I. MS 902 spectrometer at an ionization energy of 70 eV. The samples were introduced by means of a direct insertion probe. The mass scale was calibrated with the use of perfluorotributylamine. Spectra were measured with a resolution of 3000 on a 10% valley.

### Results and Discussion

By means of adsorption chromatography of the rock extract, about 100 mg of a concentrate of nickel and vanadyl porphyrins was obtained. The course of GPC analysis of the concentrate is shown in Figure 1. It is evident that gel chromatography resulted in an effective separation of nickel and vanadyl porphyrins present in the above mentioned concentrate.

The fact that vanadyl porphyrins are eluted from the column earlier than nickel porphyrins means that the separation of both metalloporphyrins is probably controlled by the steric factor to a considerable degree. The coordination sphere geometry of nickel porphyrins is planar, the nickel atom being located in the plane formed by the nitrogen atoms of the four pyrrole rings that form the basic porphyrin skeleton. Vanadyl porphyrins are complex compounds with tetragonal pyramidal geometry,

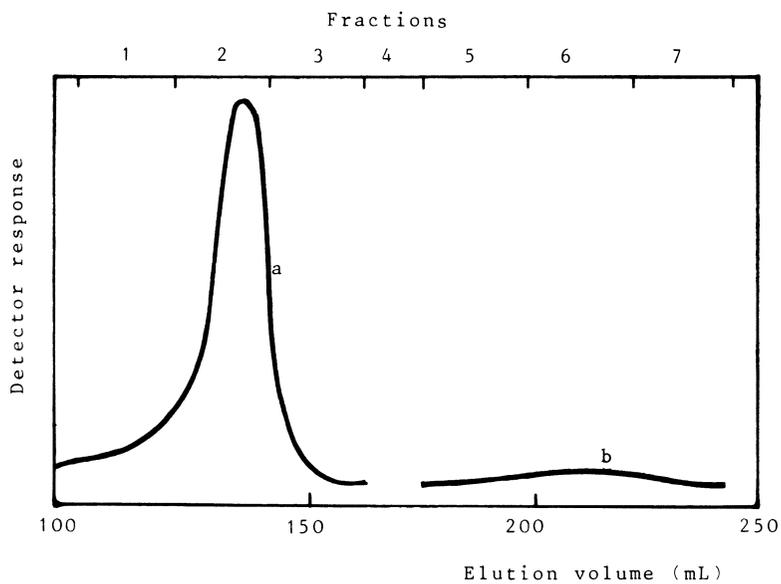


Figure 1. Chromatogram of metalloporphyrins isolated from a rock sample on styrene-divinylbenzene copolymer (a-the elution curve of vanadyl porphyrins, b-the elution curve of nickel porphyrins)

with the oxygen atom occupying the apex of the pyramid and the vanadyl group lying outside the plane formed by the four nitrogen atoms. Also, it may be derived from the course of elution of both metalloporphyrins observed that the analyzed concentrate of metalloporphyrins is a complex mixture of the relevant compounds.

In order to study the GPC behavior of both types of metalloporphyrins on the styrene-divinylbenzene copolymer, seven fractions were collected (see Figure 1) and analyzed by mass spectrometry. Tables I and II present a summary of the mass spectrometric data obtained.

In fractions 1, 2, and 3, the following ions have been identified (see Table I): ions of the homologous series of vanadyl porphyrins of the etio type ( $M=375+14n$ , where  $n$  is an integer), and ions of the homologous series of vanadyl porphyrins of the deoxophylloerythroetio type (the mass of which is  $M=373+14m$ , where  $m$  is an integer  $\geq 2$ ). With respect to the identified members of homologous series of both types of vanadyl porphyrins in GPC fractions (Table I), it may be demonstrated that GPC behavior of these compounds is affected by the molecular sieve effect, i.e., their separation correlates roughly with the number of carbon atoms in their porphine substituents. In fraction no. 4, two series of ions have been identified:  $M_1=371+14n$ ,  $M_2=379+14n$ ; for both series,  $n$  lies in the range of 7-11. From the theoretical point of view, any of the following structures may be ascribed (16) to the  $M_1$  series of mass lines: porphine derivatives with two isocyclic rings in their molecules ( $I_2$ ), chlorins with one benzosubstituent on pyrrole in  $\beta, \beta'$  position ( $H_1B_1$ ), chlorins with three isocyclic rings ( $H_1I_3$ ), or porphyrins with three benzosubstituents on pyrrole rings in  $\beta, \beta'$  positions ( $B_3$ ). In case of the  $M_2$  series of mass lines, the following structures may be considered (16): chlorins in which the  $\beta, \beta'$  double bond on another pyrrole is also hydrogenated, i.e. tetrahydroporphyrins ( $H_2$ ), hexahydroporphyrins with one isocyclic ring ( $H_3I_1$ ), porphyrins with two isocyclic rings and one benzo-substituent ( $B_1I_2$ ), or tetrabenzoporphyrins ( $B_4$ ). Exact mass measurements have not been carried out. A detailed analysis of fraction 4 was beyond the scope of the present study.

Fractions 5, 6, and 7 contained nickel porphyrins. As in the case of vanadyl porphyrin analysis, members of the homologous series of DPEP and etio porphyrins have been identified in these fractions (see Table II). In this case, the evaluation of mass spectra obtained is somewhat more complicated due to the fact that nickel has several natural isotopes ( $^{58}\text{Ni}$ , 67.88%;  $^{60}\text{Ni}$ , 26.23%;  $^{61}\text{Ni}$ , 1.19%;  $^{62}\text{Ni}$ , 3.66%; and  $^{64}\text{Ni}$ , 1.08%). The evaluated intensities may be used for determination of  $I_{\text{DPEP}}^{60}\text{Ni}$  intensities as follows:

$$I_{\text{DPEP}}^{60}\text{Ni} = I_{\text{DPEP}}^{58}\text{Ni} \cdot \frac{26.23}{67.88}$$

Table I. Mass Spectrometric Data for Vanadyl Porphyrins Fractions Trapped from GPC

Fractions <sup>a</sup>	Etio range <sup>b</sup> Molecular ions	nC	Maximum Molecular ion	nC	DPEP range Molecular ions	nC	Maximum Molecular ion	nC
1	641-543	19-12	543	12	639-541	19-12	541	12
2	599-487	16-8	515	10	597-485	16-8	513	10
3	557-459	13-6	487	8	555-457	13-6	485	8
4	n.d. <sup>c</sup>				n.d.			

<sup>a</sup> see Figure 1

<sup>b</sup> number of carbon atoms substituted on porphine

<sup>c</sup> not detected

Table II. Mass Spectrometric Data for Nickel Porphyrins Fractions Trapped from GPC

Fractions <sup>a</sup>	Etio range <sup>b</sup> Molecular ions	nC	Maximum Molecular ion	nC	DPEP range Molecular ions	nC	Maximum Molecular ion	nC
5	576-506	15-10	520	11	574-504	15-10	518	11
6	548-478	13-8	492	9	546-476	13-8	490	9
7	520-436	11-5	464	7	518-434	11-5	462	4

<sup>a</sup> see Figure 1

<sup>b</sup> number of carbon atoms substituted on porphine

It is also possible to identify in the spectra a series of ions for which  $M=366+14m$ . Their intensities may be expressed as

$$I = I_{DPEP}^{60Ni} + I_{etio}^{58Ni}$$

Consequently,  $I_{etio}$  may be obtained via subtraction from  $I$ . As seen from the mass spectrometric data shown in Table II, the GPC behavior of nickel porphyrins is also affected by the molecular sieve effect.

On the basis of the course of elution observed for nickel and vanadyl porphyrins (Figure 1) and mass spectrometric data (Tables I and II), the following conclusions are derived: The primary factor affecting GPC behavior of both metalloporphyrins is the geometry of the nickel ion or the vanadyl ion in the metalloporphyrin molecule. To a lesser extent, this behavior also depends upon the number of carbon atoms in porphine substituents. These conclusions are confirmed by the fact that, in fraction no. 3 for example (elution volume 141-164 mL), vanadyl porphyrins with the following values of molecular mass have been identified: 457, 459, 471, 473, 485, and 487. On the other hand, in fraction 6, with a higher elution volume (175-200 mL), nickel porphyrins of molecular mass between 504 and 576 have been identified.

Gel permeation chromatography enables effective separations of nickel and vanadyl porphyrins. Its application is advantageous particularly as the first step in quantitative isolation of metalloporphyrins found in asphaltenes from various types of fossil fuels. In contrast to the commonly applied extraction of metalloporphyrins with an acid, GPC separation of the relevant compounds is non-destructive and enables to obtain a representative concentrate of metalloporphyrins present in an analyzed sample.

#### Acknowledgments

I would like to thank Professor W. D. Gill, Imperial College, London for providing the rock extract studied and Dr. V. Kubelka, Department of Mass Spectrometry, Institute of Chemical Technology, Prague for measuring the mass spectra.

#### Literature Cited

1. Baker, E. W. in "Organic Geochemistry"; Eglinton, G.; Murphy, M. T. J., Eds.; Springer-Verlag: Berlin-Heidelberg-New York, 1969; p. 464.
2. Šebor, G.; Weisser, O.; Novák, M. Chem. listy 1979, 73, 23.
3. Howe, W. W.; Blumer, M. Anal. Chem. 1961, 33, 1288.
4. Millson, M. F.; Montgomery, D. S.; Brown, S. R. Geochim. Cosmochim. Acta 1966, 30, 207.

5. Sugihara, J. M.; Branthaver, J. F.; Wu, G. Y.; Weatherbee, C. Div. of Petrol. Chem., ACS 1970, 15, C5.
6. Chang, Y.; Clezy, P. S.; Morell, D. B. Australian J. Chem. 1967, 20, 959.
7. Hajibrahim, S. K.; Tibbetts, P. J. C.; Watts, C. D.; Maxwell, J. R.; Eglinton, G.; Colin, H.; Guiochon, G. Anal. Chem. 1978, 50, 549.
8. Ekstrom, A.; Loeh, H.; Dale, L. Div. of Petrol. Chem., ACS 1983, 28, 166.
9. Fish, R. H.; Komlenic, J. J. Anal. Chem. 1984, 56, 510.
10. Fish, R. H.; Komlenic, J. J.; Wines, B. K. Anal. Chem. 1984, 56, 2452.
11. Vásquez, Y.; Ceballo, C.; Sánchez, V.; Carbognani, L.; Sucre, L.; Lubkowitz, J. Proc. Int. Symposium on "Characterization of Heavy Crude Oils and Petroleum Residues": Lyon, 1984; p. 62.
12. Sundararaman, P. Anal. Chem. 1985, 57, 2204.
13. Rosscup, R. J.; Pohlmann, H. P. Div. of Petrol. Chem., ACS 1967, 12, A103.
14. Šebor, G.; Weisser, O.; Šešulka, V. Riv. Combust. 1975, 29, 380.
15. Popl, M.; Dolanský, V.; Šebor, G.; Stejskal, M. Fuel 1978, 57, 565.
16. Yen, T. F.; Boucher, L. J.; Dickie, J. P.; Tynam, E. C.; Vaughan, G. B. J. Inst. Petrol. 1969, 55, 87.

RECEIVED November 10, 1986

## Chapter 23

# **Analysis of Metal Species in Petroleum and Tar Sands Using the Electron Paramagnetic Resonance and Fourier Transform Infrared Techniques**

W. R. M. Graham

Department of Physics, Texas Christian University, Fort Worth, TX 76129

The results are reviewed from studies carried out to demonstrate the versatility of the electron paramagnetic resonance (EPR) technique supplemented by Fourier transform infrared (FTIR) spectroscopy in characterizing the metals in crude oils and tar sands. Application of the highly sensitive, but nondestructive, EPR technique can provide detailed information on the occurrence of metals in metalloporphyrins, in other organic complexes, or in associated mineral matter. The vanadyl ion has been identified bound to a porphyrin and associated with clay in tar sand samples. Examples of manganese in bitumen and in carbonate minerals, and the origin of ferric iron are also discussed.

The identification of metal species in crude oils, source rocks, tar sands, and oil shales is of fundamental interest in understanding the geochemical origin of petroleum, and has important implications for the extraction, processing, and upgrading of petroleum and synfuels. Just as significant as the identification of the metal elements present, which can be done by standard analytical techniques, is the determination of the site of the metal species. Whether they occur in metalloporphyrins, in other organic complexes in the bitumen, or are associated with minerals or clays, has important consequences for their behavior and influence in processing.

Electron paramagnetic resonance (EPR) has several unique advantages over more commonly used analytical techniques. It is extremely sensitive, with the capability of detecting concentrations of metal ions as low as a few ppm. At the same time it is nondestructive, which means that EPR analysis can be carried out without altering the original environment, site, or complex containing the metal species. This is an important advantage since the magnetic constants derived from standard EPR measurements, particularly the  $g$ -value and hyperfine splitting constants, are extremely sensitive to the chemical bonding to the paramagnetic ion and the structure in which it is located, and thus they provide an extremely useful probe for the characterization of metals in organic complexes and minerals.

0097-6156/87/0344-0358\$06.00/0  
© 1987 American Chemical Society

The purpose of this paper is to demonstrate the kind of information about metal species in petroleum and synfuels which can be drawn from the application of EPR, supplemented to some extent by Fourier transform infrared (FTIR) spectroscopy. Examples are discussed from the results of work carried out in this laboratory (1-6), principally on tar sands, but also on coal and petroleum. The principles involved are generally applicable to petroleum and synfuels. An intrinsic limitation of the technique which should be acknowledged, is that the metal species investigated must be either paramagnetic, ferromagnetic, or ferrimagnetic in order to be detectable using an EPR spectrometer; however, a large percentage of the metals of interest such as iron, vanadium, and manganese fall into these categories. Before a discussion of some examples of the application of the EPR technique to metals in petroleum and tar sands, a brief outline of the principles of EPR spectroscopy is presented in the next section. Detailed treatments of EPR theory at both the introductory (7) and advanced (8) levels are available elsewhere. Hall (9,10) has reviewed the application of EPR to studies of clay minerals.

### Principles of EPR Spectroscopy

The EPR phenomenon depends on the property that any atomic or molecular system with one or more unpaired electrons possesses a magnetic moment which interacts with an applied magnetic field,  $H$ . Of principal interest in the case of fossil fuels are the transition metal ions, such as  $V^{4+}$ ,  $Mn^{2+}$ , or  $Fe^{3+}$ , and free radicals, which are fragments of organic molecules. In the simplest case of one unpaired electron (total spin  $S = 1/2$ ) the magnetic moment is aligned either parallel or antiparallel to the external magnetic field, corresponding to the two spin states  $M = -1/2$  and  $+1/2$ . The difference in energy between these two spin states is zero in the absence of the magnetic field, but equal to  $g\beta H$  (the Zeeman splitting) in its presence, where  $\beta$  is the Bohr magneton and  $g$  is the  $g$  factor. Thus, as shown in Figure 1, the energy difference increases with  $H$ . A transition can be induced between the two states by radiation of frequency  $\nu$ , providing the resonance condition

$$h\nu = g\beta H \quad (1)$$

is fulfilled. For an x-band EPR spectrometer the required microwave energy is of frequency  $\nu = 9.2$  GHz, and is fixed. The EPR spectrum is then obtained by varying the magnetic field until the resonance condition given by Equation 1 is met. For a free electron  $g = 2.0023$  and the transition occurs at  $\approx 330$  mT (center field). The transition is recorded as the first derivative of the absorption curve.

Complexity is introduced to the spectrum when the paramagnetic ion possesses a nonzero nuclear spin  $I$ , which interacts with the electron spin  $S$ . This interaction causes hyperfine splitting of the spin levels and, therefore, of the EPR lines into  $2I + 1$  components. Thus for an ion with  $I = 1/2$  the original EPR line is split into a doublet as shown in Figure 1. The magnitude of the hyperfine splitting,  $A$ , reflects the character of the metal ligand bonds.

In the more general case of more than one unpaired electron, the external magnetic field produces  $2S + 1$  spin levels, and transitions

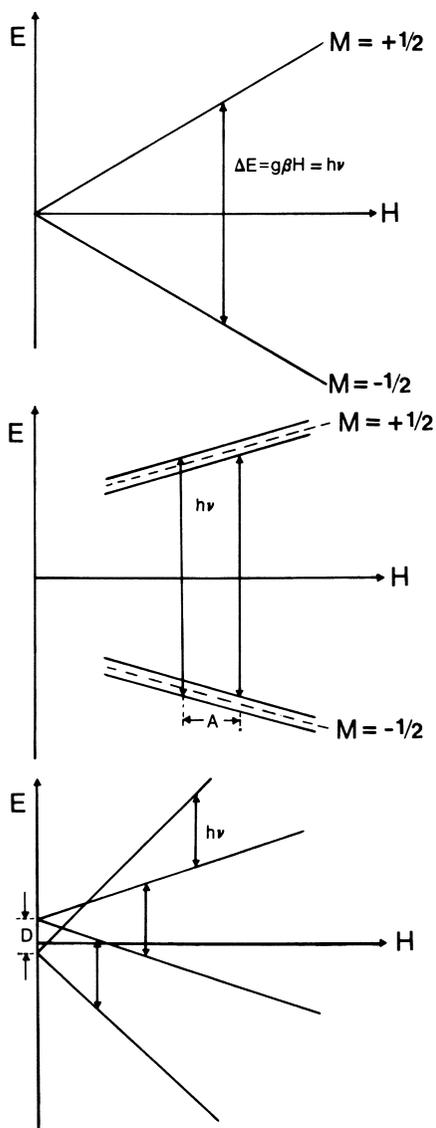


Figure 1. Energy levels and allowed EPR transitions for a system with: (top) a single unpaired electron,  $S = 1/2$ ; (middle) nuclear spin  $I = 1/2$  and  $S = 1/2$ , showing the hyperfine splitting,  $A$ ; and (bottom)  $S = 3/2$ , showing the zero-field splitting,  $D$ .

are induced between adjacent levels according to the selection rule  $\Delta M = \pm 1$ . When the paramagnetic ion occurs in a crystal (for example, in a mineral) the crystalline field may be sufficient to split the spin levels (zero-field splitting), even in the absence of an external field, as shown in Figure 1 for  $S = 3/2$ . Since the crystalline field is determined by the electric charge on neighboring atoms, the zero-field splitting parameter,  $D$ , measured from the EPR spectrum reflects the environment of the paramagnetic ion.

In general, the relevant magnetic parameters are obtained by solving the appropriate spin Hamiltonian  $H$ , for the required symmetry:

$$H = \beta \underline{H} \cdot \underline{g} \cdot \underline{S} + \underline{S} \cdot \underline{A} \cdot \underline{I} + \underline{S} \cdot \underline{D} \cdot \underline{S} \quad (2)$$

In Equation 2,  $A$  is the hyperfine splitting constant, and  $D$ , the zero-field splitting constant. It is the evaluation of  $g$ ,  $A$ , and  $D$  which can lead unambiguously to the identification of both the metal ion, and the mineral crystal or organic molecular structure in which it occurs.

### Procedure

The EPR measurements in this work were all made using a Varian V-4500 spectrometer operating at 9.2 GHz with 100 kHz magnetic field modulation. Samples were placed in 3 mm O.D. quartz tubes, and the temperature was continuously monitored with a chromel-constantan thermocouple. A Varian V-4557 variable temperature accessory was used in recording spectra at temperatures down to 80 K.

The supplementary infrared spectra were recorded on a Nicolet 5DXE FTIR spectrometer. Samples were usually made following procedures discussed elsewhere (5) in the form of pressed pellets of mixtures of mineral in KBr in a 1:100 ratio by weight.

In the case of the tar sand samples discussed here, various fractions were obtained using extraction techniques which have been previously reported in detail (3,11).

### Results and Discussion

Vanadium. Vanadium in divalent and tetravalent oxidation states with configurations  $3d^3$  and  $3d^1$ , respectively, is readily observable by EPR (7,8). In contrast to  $V^{2+}$  and  $V^{4+}$ ,  $V^{3+}$  would only be observable under special circumstances (7) at low temperatures, and is less likely to be important in fossil fuels. In petroleum or tar sands  $V^{4+}$  is expected to occur most commonly in the form of the vanadyl cation,  $VO^{2+}$ . Its EPR spectrum is characterized by an 8-line pattern arising from the splitting into  $2I + 1$  components which is produced by the hyperfine interaction between the  $S = 1/2$  spin of the unpaired electron and the  $I = 7/2$  spin of the vanadium nucleus according to the second term in the spin Hamiltonian given above (Equation 2).

Figure 2 is the central portion of the EPR spectrum recorded for the asphaltene fraction of Circle Cliffs tar sand (4). Two sets of features each show the 8-line pattern characteristic of vanadium. The EPR spectrum of axially symmetric paramagnetic systems which are randomly oriented in a powder exhibits two characteristic line components corresponding to the orientation of the symmetry axis paral-

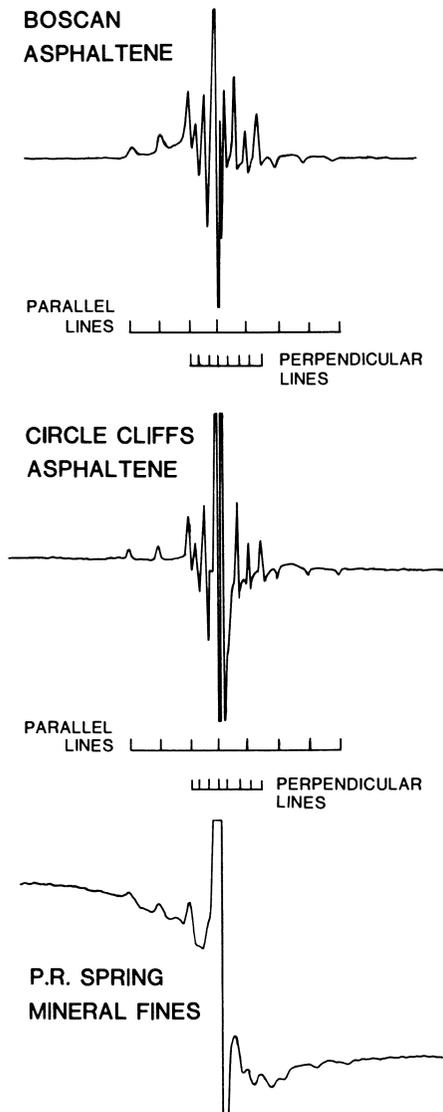


Figure 2. EPR spectra of  $\text{VO}^{2+}$  observed for Boscan asphaltene, Circle Cliffs tar sand asphaltene, and mineral fines extracted from P.R. Spring bitumen.

TABLE I. Comparison of EPR Parameters for VO<sup>2+</sup>

Sample	$g_{\perp}$	$g_{\parallel}$	$A_{\perp}$ (mT)	$A_{\parallel}$ (mT)	Ref.
Circle Cliffs asphaltene	1.986	1.962	6.08	17.20	4
Boscan asphaltene	1.9861	1.9598	5.93	17.30	3
Vanadyl etioporphyrin	1.9862	1.9629	6.01	17.13	12
Vanadyl tetrabenzo- porphyrin	1.985	1.962	5.0	15.0	13
P.R. Spring mineral fines	1.9928	1.9432	7.26	18.51	3
Mg <sup>2+</sup> -hectorite (5% VO <sup>2+</sup> )			7.1	19.4	14
$\gamma$ -Al <sub>2</sub> O <sub>3</sub> (2% VO <sup>2+</sup> )	1.989	1.916	7.08	18.12	15
SiO <sub>2</sub> (2% VO <sup>2+</sup> )	1.982	1.922	7.72	19.51	15

lel and perpendicular to the magnetic field. The typical, parallel and perpendicular line shapes observed in Figure 2 indicate that V<sup>4+</sup> occurs at an axially symmetric site. A very similar spectrum is observed for Boscan petroleum asphaltenes. In Table I, an examination of the perpendicular and parallel components of the magnetic constants  $g$  and  $A$  ( $1\text{mT} = 10$  gauss), for the Circle Cliffs and Boscan asphaltenes readily confirms that the vanadium present in both samples is in the form of vanadyl etioporphyrin.

Table I also gives the magnetic constants measured for a vanadyl spectrum which was observed for mineral fines which remained in P.R. Spring tar sand bitumen after conventional Soxhlet extraction techniques had been applied (3). Subsequent extraction (11) of these fines from the bitumen was accomplished by centrifuging the mixture, which had been redissolved in benzene, at  $8000\text{ rev min}^{-1}$  for 35 min at  $4^{\circ}\text{C}$ , decanting the liquid, and then repeatedly washing the remaining clay particles with benzene until the solvent was colorless. Even though the clay particles were exhaustively treated to remove all organic material, the possibility exists, of course, that the vanadyl in this case originates from porphyrin in bitumen which had been adsorbed onto the surfaces of the mineral fines. Table II shows the results of an FTIR analysis of the bulk of the P.R. Spring tar sand mineral matter obtained by the spectral subtraction method and discussed in detail elsewhere (5). As can be seen, the bulk mineral matter, which was obtained by the conventional Soxhlet extraction method to remove the bitumen, contains <1% by weight of clays; however, the mineral fines which required drastic solvent treatment to remove them from the bitumen were found by FTIR analysis to consist of smectite and illite clays. Comparison of the magnetic constants shown in Table I, for the mineral fines confirms that in this case, the vanadyl originates with clays or minerals, with the closest match being provided by hectorite.

TABLE II. FTIR Analysis of Circle Cliffs and P.R. Spring Tar Sand Bulk Mineral Matter

Source	Mineral Component	Weight %
Circle Cliffs	Illite	42
	Dolomite	19
	Quartz	15
	Kaolinite	13
	Anhydrite	11
P.R. Spring	Microcline	77
	Quartz	23
	Clays	<1

In general,  $g_{\perp}$  and  $g_{\parallel}$  values for porphyrin-bound vanadium are  $\sim 1.96$  and  $\sim 1.986$ , respectively, compared to  $\sim 1.98$  and  $\sim 1.93$  for  $\text{VO}^{2+}$  adsorbed on clays and minerals. The  $A_{\perp}$  and  $A_{\parallel}$  values are typically  $\sim 6$  and  $\sim 17$  mT, respectively, for porphyrins compared with 7-8 and 18-19 mT, respectively, for minerals. It can thus be seen that although spectra of vanadyl compounds may be quite similar in superficial appearance, a distinction between vanadium in porphyrins and in minerals can be made on the basis of the magnetic constants  $g$  and  $A$ . In the case of good spectra, the identity of the specific porphyrin is possible (4).

**Manganese.** This ion occurs in a variety of fossil fuels and source rocks.  $\text{Mn}^{2+}$  is a paramagnetic ion with  $S = 1/2$  and  $I = 5/2$ . The  $M = 1/2 \rightarrow -1/2$  transition at center field is split, therefore, into  $2I + 1$  components, and consequently, the spectrum exhibits a characteristic 6-line pattern. Evidence of manganese was observed in the EPR spectrum of Circle Cliffs tar sand; Soxhlet extraction revealed that it was associated with the bulk mineral matter separated from the bitumen. Figure 3a shows the spectrum observed at center field and the characteristic grouping into patterns of 6 features (4). A spectrum due to manganese was also observed in Pittsburgh No. 8 coal; however, it was relatively simpler in appearance. Comparison of its derived magnetic constants given in Table III shows that coal-bearing manganese is present in the mineral calcite (1). The FTIR analysis (see Table II) of Circle Cliffs tar sand indicates the presence of dolomite rather than calcite. Because of the complexity of the spectrum which has numerous overlapping features, it was necessary to perform a computer simulation in order to positively identify dolomite as the carrier of  $\text{Mn}^{2+}$ . Comparison of this simulation shown in Figure 3b with the observed spectrum, and the measured magnetic constants with those for dolomite in Table III, shows excellent agreement for both  $\text{Mn}^{2+}$  sites (designated I and II) in the dolomite crystal lattice, and proves conclusively that dolomite is, in fact, the source of the manganese spectrum in Circle Cliffs tar sand.

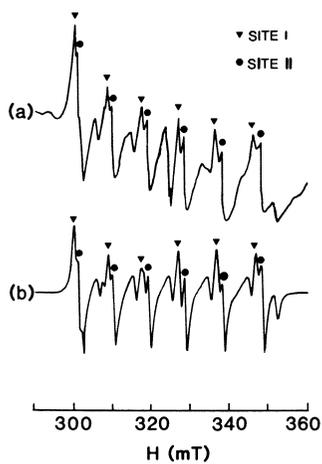


Figure 3. (a) EPR spectrum of  $\text{Mn}^{2+}$  observed for Circle Cliffs bulk mineral matter and (b) a computer simulation of the observed  $\text{Mn}^{2+}$  spectrum using the magnetic constants for  $\text{Mn}^{2+}$  in dolomite ( $\nu = 9.177$  GHz).

TABLE III. Comparison of EPR Parameters for  $Mn^{2+}$ 

Sample	g	D(mT)	A(mT)	Ref.
Pittsburgh No. 8 coal	2.002	7.7	-9.6	1
Calcite	2.0018	8.00	-9.40	16
Circle Cliffs tar sand I	2.003	-9.26	14.60	4
II	2.003	-9.48	-----	
Dolomite I	2.0028	-9.25	14.60	16
II	2.0020	-9.48	-----	

TABLE IV. Comparison of EPR Parameters for  $Fe^{3+}$ 

Sample	g	E/D	Ref.
Circle Cliffs tar sand extracted mineral	4.2		5
P.R. Spring tar sand fines (acid treated)	4.32 9.65	0.33	3
Smectite	4.33 9.6	0.33	17
Kaolinite	4.2		18
Illite	4.4		19

Iron. This metal frequently occurs in fossil fuels as  $Fe^{2+}$ , which is not generally observable using EPR; as  $Fe^{3+}$ , which is paramagnetic; and in ferro- and ferrimagnetic minerals. It would be of considerable interest if any of the iron were organically bound. EPR spectra of the bulk mineral matter extracted from Circle Cliffs sands and of the mineral fines, from P.R. Spring tar sands both exhibit a broad line at  $g \approx 4$  characteristic of  $Fe^{3+}$  substituted at sites of orthorhombic symmetry in clays. The measured g values are shown in Table IV together with the corresponding data for smectite, kaolinite, and illite clays. The D and E parameters are the axial and non-axial components of the zero-field splitting. Comparison readily shows that in the Circle Cliffs mineral matter  $Fe^{3+}$  occurs in kaolinite clay. In the case of the P.R. Spring mineral fines, the carrier is

smectite. Thus any iron detected in the P.R. Spring bitumen or asphaltene is due to  $\text{Fe}^{3+}$  in fine clay particles, rather than organically bound iron.

Iron can also be detected as a component in ferro- and ferrimagnetic minerals using the same EPR spectrometer. This technique has recently been employed successfully in identifying magnetite in coal (6). The general principles of the FMR technique in characterization studies of fossil fuels have been discussed in a previous paper (2).

### Conclusion

EPR can be a useful tool in identifying paramagnetic metal ions and in discriminating between bonding with organic structures or the mineral crystal lattice. Its abilities to detect a few ppm of a metal and to give the specific site of the metal make it potentially valuable in the study of metals in petroleum, tar sands, and other syn-fuels.

### Acknowledgments

The samples of Boscan asphaltene, and Circle Cliffs and P.R. Spring tar sands were obtained through the generosity of Dr. Jan F. Brant-haver of the Western Research Institute, Laramie, WY. Support of this research by the TCU Research Fund and partial support by The Welch Foundation are gratefully acknowledged.

### Literature Cited

1. Malhotra, V.M.; Graham, W.R.M. Fuel 1985, 64, 270.
2. Malhotra, V.M.; Graham, W.R.M. Fuel 1985, 64, 579.
3. Malhotra, V.M.; Graham, W.R.M. Preprints Div. Fuel Chem., ACS 1984, 29, 261.
4. Shepherd, R.A.; Graham, W.R.M. Bull. Am. Phys. Soc. 1983, 28, 202; Fuel (in press).
5. Shepherd, R.A.; Kiefer, W.S.; Graham, W.R.M. Fuel 1986, 65, 1286.
6. Malhotra, V.M.; Graham, W.R.M. J. Appl. Phys. 1985, 57, 1270.
7. Wertz, J.E.; Bolton, J.R. "Electron Spin Resonance - Elementary Theory and Applications"; McGraw-Hill: New York, 1972.
8. Abragam, A.; Bleaney, B. "Electron Paramagnetic Resonance of Transition Ions"; Oxford Press, 1970.
9. Hall, P. Clay Minerals 1980, 15, 321.
10. Hall, P. Clay Minerals 1980, 15, 337.
11. Malhotra, V.M.; Graham, W.R.M. Fuel 1983, 62, 1255.
12. Tynan, E.C.; Yen, T.F. J. Magn. Res. 1970, 3, 327.
13. Lau, P.W.; Lin W.C. J. Inorg. Nucl. Chem. 1975, 37, 2389.
14. McBride, M.B. Clays Clay Miner. 1979, 27, 91.
15. Van Reijen, L.L.; Cossee, P. Disc. Faraday Soc. 1966, 41, 277.
16. Shepherd, R.A.; Graham, W.R.M. J. Chem. Phys. 1984, 81, 6080.
17. Goodman, B.A. Clay Minerals 1978, 13, 35.
18. Angell, B.R.; Hall, P.L. Proc. Int. Clay. Conf. Madrid 1973, p. 47.
19. Matyash, I.V.; Polshin, E.V.; Kalinchenko, A.M. Geokhimiya 1969, 7, 840.

RECEIVED April 28, 1987

## Chapter 24

# Axial Coordination in Nickel and Vanadium Porphyrins: Transient and Difference Raman Spectroscopy

J. A. Shelnutt<sup>1</sup>, E. W. Findsen<sup>2</sup>, M. R. Ondrias<sup>2</sup>, and K. Alston<sup>3</sup>

<sup>1</sup>Process Research Division 6254, Sandia National Laboratories, Albuquerque, NM 87185

<sup>2</sup>Department of Chemistry, University of New Mexico, Albuquerque, NM 87131

<sup>3</sup>Department of Natural Sciences, Benedict College, Columbia, SC 29204

Nickel- and vanadium-porphyrin complexes and Ni(II)-reconstituted hemoglobin (N<sup>+</sup>Hb) and myoglobin (N<sup>+</sup>Mb) have been investigated using cw and transient resonance Raman spectroscopy. The state of axial coordination at the metal in these materials can be determined using the characteristic frequencies of the Raman marker lines arising from the porphyrin moiety. The state of axial ligation is highly sensitive to the molecular environment of these geoporphyrin analogs. Whether vanadium porphyrins are 5- or 6-coordinate depends on solvent and  $\pi$ - $\pi$  aggregation and complexation. Similarly, nickel porphyrins exhibit 4-, 5-, or 6-coordination depending on the molecular environment. Nickel-reconstituted proteins provide well characterized models of hydrophobic cavities such as might exist in a heterogeneous petroleum environment. In the protein cavity a novel 5-coordinate Ni-porphyrin complex is observed. The existence of only one axial ligand is supported by identification of the axial ligand-Ni stretching vibration by isotopic substitution. The frequency of the Ni-ligand mode is consistent with histidine as the fifth ligand. The effects of the T $\rightarrow$ R change in quaternary structure of the protein environment of the Ni porphyrin are also observed in the Raman spectrum. The photoinitiated ligand-release and ligand-uptake processes in excited states of the Ni porphyrins and Ni-reconstituted proteins were also investigated. Laser excitation ( $\sim$ 10-ns duration) of the complexes formed in coordinating solvents induces the release of axial ligands, but does not induce release of the histidine ligand of Ni-reconstituted hemoglobin and myoglobin. The results indicate that the protein matrix controls ligation dynamics by promoting rapid geminate recombination of the ligand.

0097-6156/87/0344-0368\$06.00/0  
© 1987 American Chemical Society

Both nickel(II)- and vanadium(IV)-porphyrins commonly occur in petroleum and shale deposits (1,2). Axial ligation at the metal in metallogeoporphyrins may play a role in catalyst inactivation and in the diagenesis of these important molecular fossils found in petroleum and source rocks. These metalloporphyrins display complex axial ligation behavior. Spectral shifts occur upon addition of axially coordinated ligands in both the resonance Raman spectrum (3-5) and in the uv-visible absorption spectrum (1,3-5). The spectral shifts may prove to be useful in separation and identification methods based on these techniques.

The utility of resonance Raman spectroscopy as a means of studying the axial ligation behavior of the metallogeoporphyrins in a variety of well characterized molecular environments has been investigated. The environments examined include solution studies in non-coordinating and coordinating solvents (3-5), aqueous surfactant micelles (4,7), self-aggregates (3,8,9),  $\pi$ - $\pi$  complexes (10-12), adsorbed onto surfaces (13), and incorporated into well-characterized asymmetric sites in proteins (4,5,7). Each of the environments mentioned affect the ligation properties of the metal in the central core of the porphyrin and, in some cases, the dynamical aspects of ligand binding. It is anticipated that the results of these model studies may find counterparts in the present day porphyrin environment in source rocks and petroleum, in the early natural environment during diagenesis of the deposits, and in commercial processing environments.

In this work we stress the generality of the influence of the molecular environments on axial ligation, as well as some of the novel ligation processes that are a consequence of special metalloporphyrin sites. Although the model metalloporphyrin sites (e. g. the protein binding sites) at first may seem unrelated to petroleum environments, when considered more generally (e. g. as a hydrophobic cavity containing a possible metal ligand) they actually mimic certain aspects of the petroleum environment quite well. Examples of some of the unusual properties specific to the model environments investigated are: (1) A novel nickel-porphyrin complex with only a single axial ligand is observed in the protein matrix (4). (2) An novel  $V(OH)_2$  porphyrin occurs in certain aqueous environments rather than the usual vanadyl ( $VO^{2+}$ ) porphyrin (3). (3) Photoinduced ligand loss or uptake processes are observed in nickel porphyrins in solution and different dynamic behavior is observed for the same Ni porphyrins in the protein environment (7).

### Materials and Methods

Vanadyl uroporphyrin ( $VO(UroP)$ ),  $VO$  octaethylporphyrin ( $VO(OEP)$ ), nickel protoporphyrin IX ( $Ni(ProtoP)$ ),  $Ni$  uroporphyrin ( $Ni(UroP)$ ), and  $Ni$  octaethylporphyrin ( $Ni(OEP)$ ) were obtained from Porphyrin Products and used without further purification.  $^{61}Ni$ Hb and  $^{64}Ni$ -reconstituted Hb were prepared according to reported methods (14).  $^{61}Ni$ Mb was made by the method of Alston and Storm (15). Solutions of the proteins in 0.05 M phosphate buffer at pH 7.5 were used for obtaining spectra. The  $Ni$  globins are stable in air and do not photodecompose. All solvents were of highest purity obtainable from commercial sources. All materials showed the literature uv-visible

absorption spectra. Absorption spectra were obtained on a Perkin-Elmer Model 330 spectrophotometer.

Raman spectra were obtained on selected pairs of samples using a Raman difference spectrometer described previously (10). The 90° scattering geometry was employed. Spectral resolution was 4 cm<sup>-1</sup>. All spectra were obtained at room temperature. Samples were excited with a krypton ion laser (Coherent 3000K) using the 413.1-nm laser line. Visible excitation was accomplished with an argon ion laser (CR-20) using the 528.7-nm line. To avoid heating, the samples were irradiated in a rotating (100 Hz) cell with two compartments. The laser power at the sample was less than 300 mW in a partially defocused beam. The Ni porphyrins are very stable to visible light and even higher powers could be used. No sample decomposition was observed as determined by the lack of changes in successive scans of the Raman spectrum during signal averaging and in the absorption spectrum taken before and after the Raman spectrum.

Nanosecond resonance Raman spectra were obtained using a nitrogen pumped dye laser (Molelectron) and a spectrometer system described elsewhere (16). The ~180° backscattering geometry was used. "Low power" laser pulses (~0.3 mJ/pulse) slightly focused with a cylindrical lens (f.l.= 250 mm) gave an energy density of ~5 mJ/cm<sup>2</sup>. For "high power" spectra, the beam was tightly focused with a spherical lens (f.l.= 100 mm); the photon density is ~100 times greater than for the low power spectra. The pulse repetition rate was 10 Hz. Static cuvettes held the sample and the temperature was 20-25 C.

## Results and Discussion

### Axial Ligation in Vanadium Porphyrins

Non-Coordinating and Coordinating Solvents. Vanadium in geoporphyrins exists exclusively in the V(IV) valence state as the vanadyl ion (VO<sup>2+</sup>) with the oxo atom bound axially. The vanadium atom is displaced 0.5 Å out of the mean porphyrin plane toward the doubly bound oxygen (17,18). The porphyrin core size (center-to-nitrogen distance) is 2.03-2.07 Å (17,18). In non-coordinating solvents the VO porphyrins maintain this geometry and state of axial ligation. However, in coordinating solvents, even as mildly coordinating as water, other coordination behavior is observed. For example, Walker et al. (19) noted a large red shift (578 → 605 nm) in the  $\alpha$  band of the absorption spectrum of VO tetra-p-methylphenylporphyrin (VO(TpCH<sub>3</sub>PP)) in piperidine indicating formation of the piperidine adduct.

Similar complexes are also formed by pyrrole-substituted VO porphyrins in strong bases. These porphyrins are better models for the geoporphyrins. As an example, Figure 1 shows the absorption spectrum of VO(OEP) in the weakly coordinating solvent pyridine and the strong base pyrrolidine. The  $\alpha$  band red shifts from 572 to 582 nm and the Soret band red shifts from 407 to 425 nm upon formation of the VO(OEP)-monopyrrolidine adduct. In the non-coordinating solvent toluene the  $\alpha$  band is at 571 nm and the Soret band is at 407 nm -- close to the pyridine peak wavelengths. In addition, the  $\alpha/\beta$  absorbance ratio greatly decreases from about 2 for the 5-coordinate

form to much less than 1 for the pyrrolidine adduct. Complex formation is not complete in either solvent.

The Raman spectrum of VO(OEP) in pyrrolidine shows lines from both the 5-coordinate VO(OEP) and the monopyrrolidine adduct. For example, the core-size marker line (20,21)  $\nu_{10}$  is at 1628  $\text{cm}^{-1}$  for the 5-coordinate species and down at 1611  $\text{cm}^{-1}$  for the 6-coordinate pyrrolidine complex (spectrum not shown). Another core-size marker line  $\nu_{19}$  is at 1569  $\text{cm}^{-1}$  for the 5-coordinate form and decreases to 1555  $\text{cm}^{-1}$  for the 6-coordinate complex. The decrease in the marker line frequencies indicates an expansion of the central core of the porphyrin macrocycle by about 0.03 Å relative to the 5-coordinate complex.

In aqueous solution monomeric VO porphyrins convert to the dihydroxyvanadium(IV)-porphyrin complex. (See Figure 4.) Figure 2 shows the absorption spectrum of the monomeric species obtained when VO(UroP) is dissolved in 0.1 M NaOH. A red shift in the  $\alpha$  band relative to the monomeric model VO porphyrins in non-coordinating solvents (e. g. 578 nm versus 562 nm for VO(OEP) in benzene) is observed. In addition, the  $\alpha/\beta$  ratio is strongly decreased relative to that of monomeric, 5-coordinate V=O porphyrins as was previously noted for the 6-coordinate VO(OEP)-pyrrolidine complex.

The Raman spectrum of the dihydroxy species is shown in Figure 3 (dotted line) in the marker line region from 1300 to 1700  $\text{cm}^{-1}$ . The core-size marker lines  $\nu_{10}$  (1620  $\text{cm}^{-1}$ ),  $\nu_{19}$  (1561  $\text{cm}^{-1}$ ), and  $\nu_3$  (1488  $\text{cm}^{-1}$ ) are lower than for VO(OEP) 5-coordinate models. A similar decrease in the core-size marker line frequencies was observed for the VO(OEP)-monopyrrolidine complex. In basic solution, hydrolysis of the vanadium oxo complex to form a dihydroxyvanadium-porphyrin complex as illustrated in Figure 4 is likely (3). Hydrogen bonding may play a part in the reaction as suggested by species 2. Hydrogen bonding to the vanadyl oxygen is observed in the X-ray crystal structure of the 1,4-dihydroxybenzene adduct with oxovanadium(IV)etioporphyrin II (22).

#### Effects of Environment on Vanadium-Porphyrin Complexes.

**Aggregation.** Figure 2 shows the effect of salt-induced dimerization on the absorption spectrum of V(OH)<sub>2</sub>(UroP) in 0.1 M NaOH. Addition of NaCl (5.5 M) results in shielding of the eight negatively charged carboxylates at the periphery of the uroporphyrin ring. Shielding of the deprotonated acid groups allows  $\pi$ - $\pi$  dimerization of the porphyrin rings after removal of one of the  $\text{UH}^-$  axial ligands and reformation of the V=O complex. Thus, in the presence of salt the absorption spectrum in the visible region is typical of VO(OEP) in non-coordinating solvents. The Soret band of the dimer, however, displays the characteristic excitonic blue shift of the  $\pi$ - $\pi$  dimers (8).

In Figure 3 the Raman spectrum of the dimer is shown. The core-size marker line frequencies are 1635 ( $\nu_{10}$ ), 1581 ( $\nu_{19}$ ), and 1498  $\text{cm}^{-1}$  ( $\nu_3$ ). The values are much closer to V=O porphyrins in non-coordinating solvents although possibly a few wavenumbers high. The slightly high marker line frequencies may partly result from dimerization which is known to cause about 3- $\text{cm}^{-1}$  shifts to higher frequency (8).

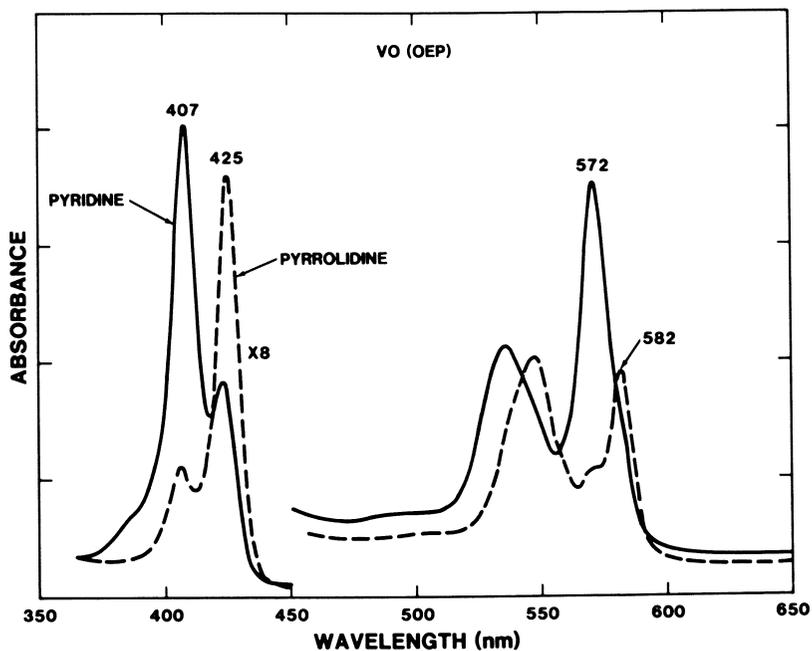


Figure 1. Absorption spectra of vanadyl octaethylporphyrin in pyridine (—) and in pyrrolidine (-----).

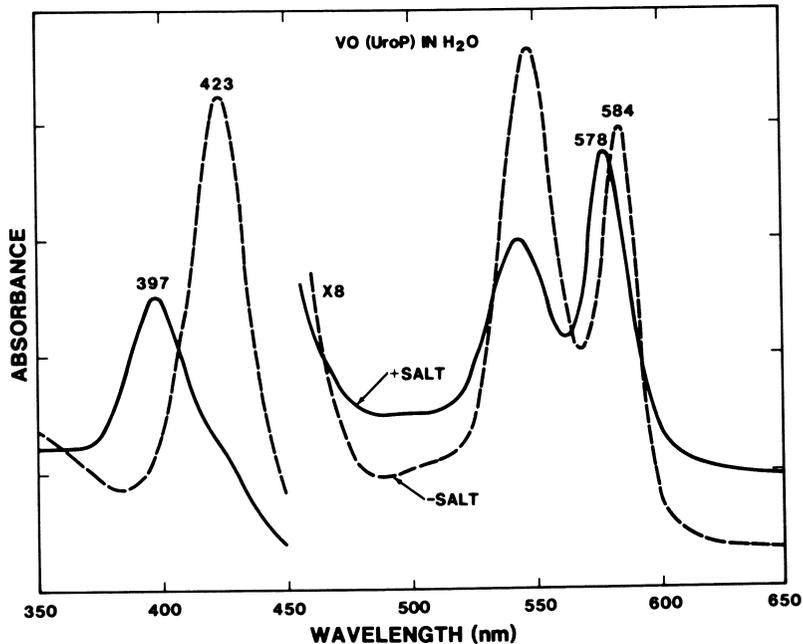


Figure 2. Absorption spectra of vanadyl uroporphyrin I in water in the presence (—) and absence (-----) of 5.5 M NaCl.

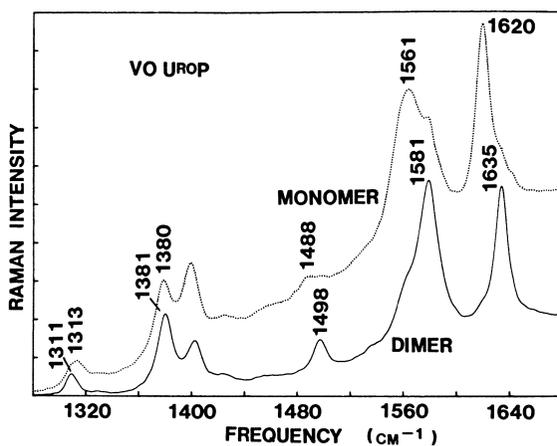


Figure 3. Raman spectrum of vanadyl uroporphyrin I in the presence (—) and absence (.....) of 5.5 M NaCl.

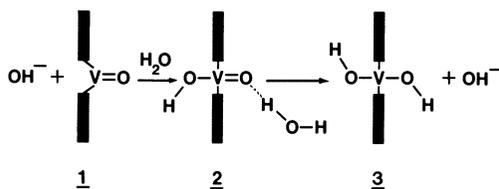


Figure 4. Scheme for formation of dihydroxyvanadium uroporphyrin I in aqueous base.

Lowering the pH causes protonation of the acid substituents of uroporphyrin and the resulting neutralization of charge allows dimerization. Changes in the absorption and Raman spectra similar to those observed upon salt dimerization occur. Therefore, blocking of the sixth coordination position by formation of a  $\pi$ - $\pi$  dimer is apparently sufficient to disrupt the 6-coordinate dihydroxy complex.

$\pi$ - $\pi$  Complexes. Large aromatic acceptor molecules like phenanthroline and methylviologen form  $\pi$ - $\pi$  complexes with metallouroporphyrins in aqueous base (10-12,23,24). The equilibrium binding constant  $K$  is 110 at 25° C for phenanthroline which forms a 1:1 complex (3). The large ring system of the aromatic molecule lies flat on the porphyrin ring where it can displace the ligand(s) and block the metal ligation sites if the ligands are only weakly bound (3,8). On the other hand, strongly bound axial ligands are known to prevent  $\pi$ - $\pi$  complex formation (25,26). Shelnutt and Dobry (3) demonstrated that shifts in the absorption spectra of V0(UroP) similar to those in Figures 1 and 2 are also observed upon complexation with phenanthroline or methyl viologen. Further, the shifts in the Raman core-size and oxidation-state marker lines when phenanthroline is added to an aqueous solution (pH 13) of V0(UroP) are almost identical to those seen in Figure 3.

The effects of aggregation and  $\pi$ - $\pi$  complex formation on axial coordination are similar. The effects in the case of both phenomena suggest 6-coordination rather than some kind of interaction between the addend and the oxo atom of vanadyl. Only one ligand ( $\text{OH}^-$ ) is removed by aggregation or  $\pi$ - $\pi$  complexation, consistent with the apparent binding of only one phenanthroline molecule to V0(UroP). Upon aggregation, V0(UroP), which cannot form units larger than dimers because of steric hindrance caused by the vanadyl oxygen, does not precipitate. In contrast, Cu(UroP) which is 4-coordinate can bind two phenanthrolines. Although the pK of 6.7 for acid dimer formation for copper uroporphyrin is the same as for V0(UroP), Cu(UroP) forms stacked polymers and precipitates. As another illustration of the blocking of  $\pi$ - $\pi$  complexes by strongly bound axial ligands, dihydroxytin(IV) uroporphyrin has both hydroxides strongly bound and, consequently, binds neither methyl viologen nor phenanthroline in a  $\pi$ - $\pi$  complex and does not dimerize (25,26). The spectroscopic results further support the 6-coordinate vanadium-porphyrin species being the dihydroxy complex because the anomalous Raman and absorption spectrum is observed only when both axial sites are unblocked; if one side of the porphyrin is blocked, then the vanadyl species is formed instead.

The shifts in the core-size marker lines suggest that the 6-coordinate form has the metal atom in plane and this further suggests that the dihydroxide is formed as illustrated in Figure 4. Movement of the vanadium atom into the porphyrin plane would most likely cause an expansion of the core. Indeed, the core expands by 0.03 Å as indicated by the shift in  $\nu_{10}$  (3). A similar shift is observed for the pyrrolidine-V0(OEP) complex, suggesting that both complexes have the metal in the porphyrin plane. This finding probably applies to the piperidine-V0(TpCH<sub>3</sub>PP) complex as well (19).

### Axial Coordination in Nickel Porphyrins

**Non-Coordinating and Coordinating Solvents.** Nickel porphyrins are in the Ni(II) valence state in geoporphyrins. They can exist without ligands or acquire either one or two depending on the molecular environment. Figure 5 shows the absorption spectrum of Ni(ProtoP) in the weakly coordinating solvent pyridine and in pyrrolidine. The spectral changes occurring upon axial ligation by two (27) pyrrolidine molecules are similar to the VO(OEP) case shown in Figure 1. A red shift of the  $\alpha$  band (560  $\rightarrow$  588 nm) and also a red shift of the Soret band (403  $\rightarrow$  431 nm) occur. However, closer inspection shows that the shifts are larger for the nickel porphyrin ( $\Delta\alpha$ , 28 nm;  $\Delta$ Soret, 28 nm) than for the vanadyl porphyrin ( $\Delta\alpha$ , 10 nm;  $\Delta$ Soret, 18 nm). The large shifts for nickel porphyrins are due in part to a d-d transition that occurs upon ligand binding. In fact, the d-d transition probably accounts for about two-thirds of the shift (vide infra) (6,7) and addition of two ligands accounts for the rest of the shift (28-30). The d-d transition of the  $d^8$  nickel ion is from  $d_{z^2} \rightarrow d_{z^2-1}, d_{x^2-y^2}$  (31). In contrast, vanadium is  $d^1$  with no d-d transition involved in ligation (19,32,33). Therefore, for vanadium porphyrins only the smaller shift resulting from addition of a ligand is expected.

The association constant for addition of ligands depends somewhat on the electron withdrawing ability of the peripheral substituents on the porphyrin ring. For example, Ni(OEP) with eight electron donating ethyl groups is almost completely 4-coordinate in pyridine, whereas Ni(ProtoP) with two electron withdrawing vinyl substituents is about 50% coordinated. Even water can be a ligand for Ni porphyrins with several electron withdrawing groups at the periphery (34). This differential affinity of porphyrins with different peripheral substituents could form the basis of a method of separation and identification of metallogeoporphyrins.

Figure 6 compares the Soret resonance Raman spectra of 4-coordinate Ni(ProtoP) in aqueous cetyltrimethylammonium bromide (CTAB) micelles and 5-coordinate Ni(ProtoP) in pyrrolidine. As in the case of the absorption spectra, the shifts for the Raman marker lines are similar for vanadyl and nickel porphyrins. Specifically, addition of ligands causes downshifts in the core-size marker line frequencies. For example,  $\nu_{10}$  (1657  $\rightarrow$  1616  $\text{cm}^{-1}$ ),  $\nu_2$  (1592  $\rightarrow$  1563  $\text{cm}^{-1}$ ), and  $\nu_3$  (1519  $\rightarrow$  1476  $\text{cm}^{-1}$ ) decrease by up to 41  $\text{cm}^{-1}$ .

The downshifts in the core-size markers are mostly a result of the d-d transition accompanying ligand binding. We have observed this d-d state directly with transient Raman scattering techniques (5-7). This low lying d-d state has a lifetime of about 250 ps (35-37). Almost complete conversion to the excited d-d state ( $d_{z^2-1}, d_{x^2-y^2}$ ) is achieved early in a high power 10-ns laser pulse and is maintained while the rest of the pulse generates the Raman spectrum from the d-d state. The frequencies of the core-size lines of the d-d state of Ni(ProtoP) in CTAB are:  $\nu_{10}$ , 1627  $\text{cm}^{-1}$ ;  $\nu_2$ , 1572  $\text{cm}^{-1}$ ;  $\nu_3$ , 1492  $\text{cm}^{-1}$  (7).

Core expansion is not unexpected because the d-d transition moves an electron into the antibonding  $d_{z^2-1}, d_{x^2-y^2}$  orbital with its lobes pointing toward the pyrrole nitrogens of the ring. Indeed, the core expands by about 0.06 Å based on the decrease in core-size marker line  $\nu_{10}$ . In addition, the core expands by an additional 0.02 Å upon binding two ligands as indicated by the further decrease in  $\nu_{10}$  (Figure 6). The total expansion of 0.08 Å agrees with the value

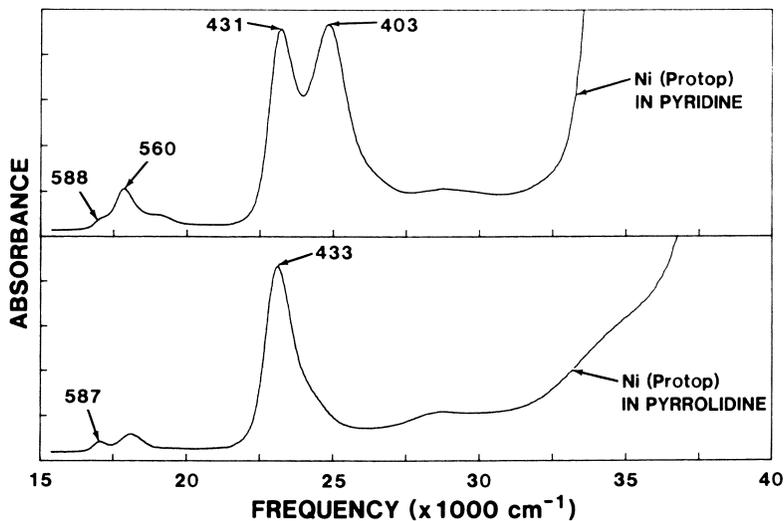


Figure 5. Absorption spectrum of nickel protoporphyrin IX in pyridine (top) and the spectrum of nickel protoporphyrin in pyrrolidine (bottom).

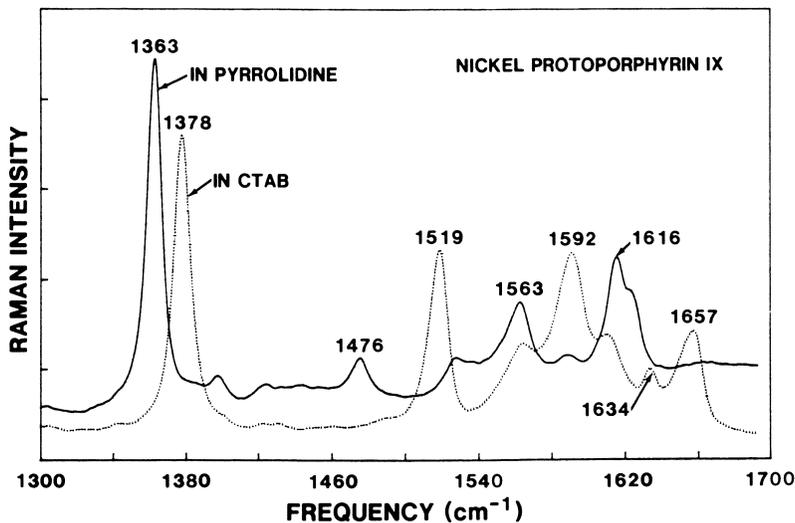


Figure 6. Raman spectra of nickel protoporphyrin IX in pyrrolidine (—) and in aqueous cetyltrimethylammonium bromide micelles (.....).

determined from the 4- and 6-coordinate Ni-porphyrin crystal structures (38,39).

### Effects of Environment on Nickel-Porphyrin Complexes

$\pi$ - $\pi$  Complexes and Aggregates. The effects of  $\pi$ - $\pi$  complex formation and aggregation on axial ligation have not been fully investigated for the Ni porphyrins. Competition between the two types of complexes is expected. When piperidine or 2-methylimidazole is added to Ni(UroP) dimers in a nearly saturated KCl solution (pH 13), the dimer absorption spectrum is replaced by the monomer Ni(UroP) spectrum. Although no 5- or 6-coordinate forms are detected, some weak interaction must take place to account for breaking up the dimers.

Protein Binding. Ni(ProtoP) bound to a site in a polypeptide matrix which provides potential endogenous axial ligands was investigated with both Raman difference spectroscopy and transient Raman techniques. The idea is to model a heterogeneous catalyst having cavities that contain a basic ligand. Toward this end a series of Ni-protoporphyrin reconstituted hemoproteins were investigated (4-7). From the native hemoproteins, hemoglobin (Hb), myoglobin (Mb), and isolated  $\alpha$  chains of hemoglobin ( $\alpha_{SH}$ ), the Fe(ProtoP) molecule was removed and replaced with Ni(ProtoP). By a number of spectroscopic and chemical techniques it was found that the protein conformation is identical to that of the native Fe globins (14,40-42). Because the X-ray crystal structures of Hb and Mb are known (43-44) and the protein conformation is not significantly affected by reconstitution, the Ni globins provide a structurally well-characterized protein cavity for the Ni porphyrin.

The effect on ligand affinity of porphyrin binding in the cavity in the globin is large. Imidazole is normally a poor ligand; even in neat liquid 1-methylimidazole almost none of the Ni porphyrin is axially coordinated. In contrast, in the protein pocket imidazole is almost entirely bound for  $NiMb$  and a little less than half-bound for  $NiHb$ . This is in spite of the fact that the actual imidazole concentration is low (i. e., the same as the protein concentration or about  $0.1-1.0 \times 10^{-4}$  M for these experiments). The degree of binding has been estimated from the relative intensities of the red and blue Soret components in the absorption spectra. Figure 7 shows the absorption spectrum of  $NiHb$ .

At first glance the spectrum of  $NiHb$  is similar to that of Ni(ProtoP) in pyridine (Figure 5). However, closer examination shows that the red-shifted Soret component at 419 nm is shifted considerably less (21 nm) from the 4-coordinate position than the 6-coordinate pyridine (28 nm) or pyrrolidine (30 nm) Soret bands. In fact, no 6-coordinate Ni(ProtoP) in solution has the Soret band near that of the coordinated Ni-globins's Soret bands (4).

The Ni-porphyrin in the protein cavity has a unique absorption spectrum. Because of the great similarity between the spectrum of the Ni globins and the 6-coordinate models, however, axial coordination is implicated. The anomalous spectrum of the Ni globins is most likely the result of axial coordination of only a single ligand provided by a protein side chain. Iron in the native protein is bound to the imidazole of the proximal histidine in the

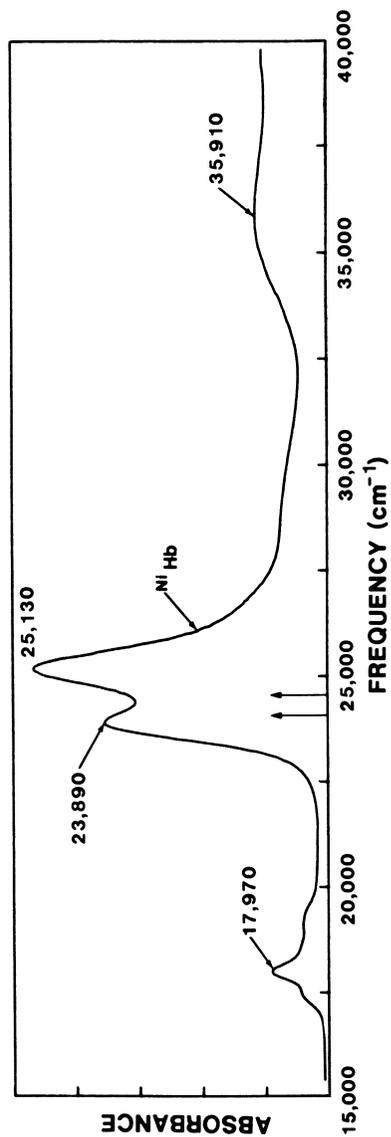


Figure 7. Absorption spectrum of nickel hemoglobin A in 0.05 M phosphate buffer pH 7.05.

heme pocket. Binding to the proximal histidine in the case of the Ni globins is confirmed by our identification of the Ni-histidine stretching mode at  $236\text{ cm}^{-1}$  in  $\text{Ni}^{\text{Hb}}$  by isotopic substitution with  $^{64}\text{Ni}$  (4). Thus, binding of the Ni porphyrin to the asymmetric cavity results in both enhanced ligand affinity and the possibility of forming a 5-coordinate complex.

Reconstitution of Ni into hemoglobin also provides us with an opportunity to examine the effect on axial ligation of a well-characterized change in the structure of the cavity in which the porphyrin resides. Hemoglobin has two quaternary conformations distinguished by their affinity for small exogenous ligands like  $\text{O}_2$  and CO. Ni hemoglobin does not bind these gases, but, nevertheless, the Ni porphyrin, like the Fe porphyrin, responds to the change in quaternary structure of the protein. Figure 8 shows a comparison of the resonance Raman spectra of  $\text{Ni}^{\text{Hb}}$  which has the T or deoxy  $\text{Fe}^{\text{Hb}}$  conformation and  $\alpha_{\text{SH}}$  chains which have the R or ligated  $\text{Fe}^{\text{Hb}}$  conformation. The most obvious difference in the two spectra is the difference in number of sites that are ligated. This is seen by noting the difference in relative intensities of the core-size markers. In the Ni  $\alpha$  chains, nickel is mostly 4-coordinate. This is apparently not a consequence of the quaternary structure, however, because Ni  $\beta$  chains and  $\text{Ni}^{\text{Mb}}$  both are also R-like protein structures and are either fully 5-coordinate ( $\text{Ni}^{\text{Mb}}$ ) or possess about the same ratio of 4- and 5-coordinate sites ( $\beta_4$  tetramer) as  $\text{Ni}^{\text{Hb}}$  which has the T conformation.

Much has been made of the specific structural change that occurs at the metal-histidine bond as a result of the T  $\rightarrow$  R conformational change in Hb. In native  $\text{Fe}^{\text{Hb}}$  the T/R difference in frequency of the Fe-histidine vibration is  $3\text{--}8\text{ cm}^{-1}$ . The increase in frequency noted for the Fe-histidine stretching mode is also observed for the metal-histidine stretch of the Ni globins. For the  $\alpha_{\text{SH}}$  chains the increase in  $\nu(\text{Ni-his})$  is  $7\text{ cm}^{-1}$ . A similar increase ( $\sim 5\text{ cm}^{-1}$ ) has been measured for the  $\text{Ni}^{\text{Hb}}/\text{Ni}^{\text{Mb}}$  T  $\rightarrow$  R comparison (4,5). The increase in the Ni-histidine force constant in the case of the  $\alpha$  chains is apparently not reflected in a higher affinity for the ligand. Affinity considerations require an assessment of the energetics of the entire Ni-globin molecule.

Closer examination of the spectra obtained with the Raman difference spectrometer shown in Figure 8 reveals many small R/T shifts in the core-size and oxidation-state marker lines. The shifts are observed for the 4-coordinate as well as 5-coordinate sites. The shifts in the core-size marker lines of the 5-coordinate sites are  $\Delta\nu_3 = 0.1\text{ cm}^{-1}$ ,  $\Delta\nu_2 = -1.7\text{ cm}^{-1}$ , and  $\Delta\nu_{10} = -1.2\text{ cm}^{-1}$ ; for the 4-coordinate sites the T/R shifts are  $\Delta\nu_3 = -0.7\text{ cm}^{-1}$ ,  $\Delta\nu_2 = -0.4\text{ cm}^{-1}$ , and  $\Delta\nu_{10} = -1.0\text{ cm}^{-1}$ . For the 5-coordinate sites the oxidation-state marker  $\nu_4$  shift is  $\Delta\nu_4 = 0.4\text{ cm}^{-1}$ . The shifts noted for the 4-coordinate sites must indicate changes in Ni-porphyrin structure that cannot be associated with the change that occurs at the metal-histidine bond since no bond exists. One possibility is a difference in the porphyrin ring's interaction with residues in van der Waals contact with it (45). Indeed, the formation of  $\pi\text{--}\pi$  complexes has been shown to result in shifts in the Raman marker lines similar to those determined from the data in Figure 8 (10,23,24).

Protein Effects on Photoinduced Ligand Ejection and Uptake. Figure 9 shows the results of transient Raman scattering measurements on  $\text{Ni}^{\text{II}}$ Hb (5,7). Unlike the 6-coordinate Ni-porphyrin complexes, pulsed laser excitation at resonance with the 5-coordinate sites of  $\text{Ni}^{\text{II}}$ Hb (Figure 9) or  $\text{Ni}^{\text{II}}$ Mb (5,7) do not show ligand release. In the 6-coordinate models ligand release is revealed by an increase in intensity of the 4-coordinate core-size marker lines relative to the 6-coordinate markers for spectra obtained at high power. No significant difference in core-size marker intensities is observed in the high and low power spectra taken with 420-nm excitation and displayed in Figure 9. Because the lowest lying excited state predicted for both the 6- and 5-coordinate species is the dissociative d-d state (31), we ascribe the difference in photodissociative behavior of the ligand in the protein to rapid cage recombination of the ligand (5,7). The lifetime of the photodissociated state must be reduced from  $>20$  ns to much less than a nanosecond. Thus, the protein has a large effect on ligand binding dynamics, in particular the on-rate. The increase in on-rate is consistent with the Ni-globin's enhanced affinity for imidazole.

Photoinduced ligand uptake is also affected by the presence of the protein matrix about the Ni porphyrin.  $\text{Ni}^{\text{II}}$ As can be seen in Figure 9, excitation of the 4-coordinate sites of  $\text{Ni}^{\text{II}}$ Hb using 406-nm excitation causes conversion to the 5-coordinate species. This is most easily seen in the change in relative intensities of the 4- and 5-coordinate lines corresponding to  $\nu_{10}$  at high laser power. At low power the spectrum is identical to the cw spectrum obtained with 406.7-nm excitation with the  $\text{Kr}^+$  laser and reflects the ground state equilibrium between the two species. At high power, however, the relative intensity of the 4-coordinate core-size markers (e. g.  $\nu_{10}$  at  $1658\text{ cm}^{-1}$ ) are decreased compared to the 5-coordinate lines (e. g.  $\nu_{10}$  at  $1619\text{ cm}^{-1}$ ).

The 5-coordinate species is formed in the protein, not the 6-coordinate form. One might have expected transient formation of the 6-coordinate form because a potential sixth ligand, the distal histidine, is nearby. The core-size lines,  $\nu_3$  in particular, show differences in frequency between the 5- and 6-coordinate forms, and  $\nu_3$ 's position ( $1485\text{ cm}^{-1}$ ) in the high power 406-nm spectrum demonstrates transient formation of the 5-, not 6-coordinate form. Apparently, the distal histidine is too far away and constrained so that it cannot move into position to bind as a sixth ligand.

The fact that a ligand binds at all within the 10-ns laser pulse indicates the close proximity of the histidine ligand and, therefore, confirms that the 4-coordinate sites in  $\text{Ni}^{\text{II}}$ Hb are the normal heme pocket. This is supported by the fact that the spectrum of the transient 5-coordinate form does not differ significantly from the cw 5-coordinate species.

### Conclusions

On the basis of these model studies of metalloporphyrins it is expected that axial ligation will be strongly affected by the particular environment in which the porphyrin is situated. In particular, various sites which naturally occur in the heterogeneous environment of petroleum processing may lead to novel coordination

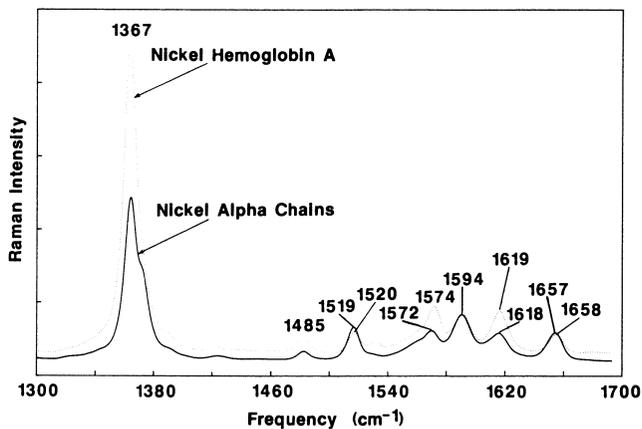


Figure 8. Resonance Raman spectra of nickel hemoglobin A (.....) and nickel-reconstituted  $\alpha$  chains (—).

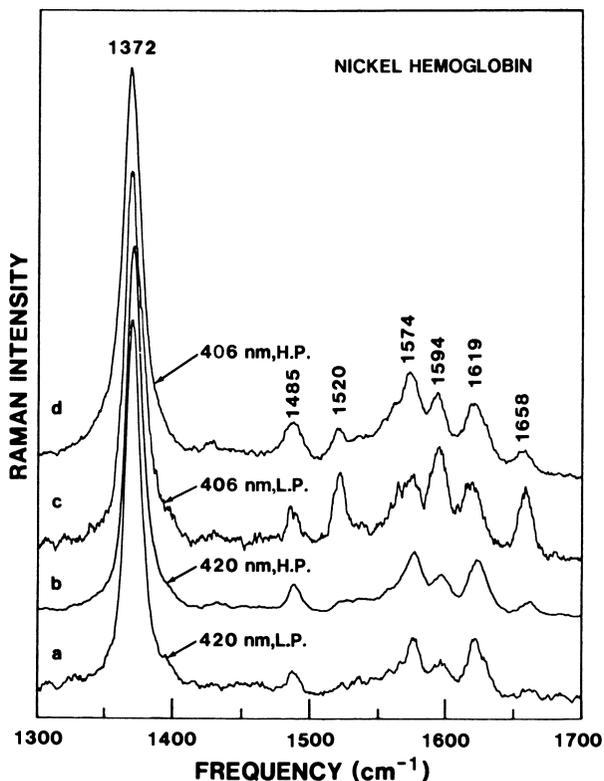


Figure 9. Transient resonance Raman spectra of nickel hemoglobin A at high (H.P.) and low (L.P.) power with excitation at Soret resonance for the 5-coordinate sites (420 nm) and the 4-coordinate sites (406 nm).

complexes similar to the complexes we have observed in proteins. We have shown that ligand binding affinities, binding dynamics, and axial ligand bond strengths may all be influenced by binding to a cavity in a catalyst. The structure of the cavity itself also further influences each of these properties.

Stacking type interactions, involved in  $\pi$ - $\pi$  complexes and aggregates, may also influence coordination at the metal under homogeneous solution conditions and at surfaces. The nature of the porphyrin's peripheral substituents will also play a role in the metals affinity for additional ligands. The novel coordination chemistries that result from various porphyrin environments may play a role in geoporphyrin reactions during petroleum processing and during diagenesis.

### Acknowledgments

This work performed at Sandia National Laboratories and supported by the United States Department of Energy Contract DE-AC04-76DP-00789 and the Gas Research Institute Contract 5082-260-0767.

### Literature Cited

1. Baker, E. W.; Palmer, S. E. In "The Porphyrins" Vol. 1, Part II; Dolphin, D., Ed.; Academic: New York, 1978, p. 486.
2. Treibs, A. Angew. Chem. 1936, 49, 682.
3. Shelnut, J. A.; Dobry, M. M. J. Phys. Chem. 1983, 87, 3012.
4. Shelnut, J. A.; Alston, K.; Ho, J-Y.; Yu, N-T.; Yamamoto, T.; Rifkind, J. M. Biochemistry 1986, 25, 620.
5. Shelnut, J. A.; Alston, K.; Finsden, E. W.; Ondrias, M. R.; Rifkind, J. M. Proc. Conf. Excited States Dynamics Porphyrins 1986, in press.
6. Finsden, E. W.; Shelnut, J. A.; Friedman, J. M.; Ondrias, M. R. Chem. Phys. Lett. 1986, 126, 465.
7. Finsden, E. W.; Shelnut, J. A.; Alston, K.; Ondrias, M. R. J. Am. Chem. Soc. 1986, 108, 4009.
8. Shelnut, J. A.; Dobry, M. M.; Satterlee, J. D. J. Phys. Chem. 1984, 88, 4980.
9. Shelnut, J. A. J. Phys. Chem. 1984, 88, 4988.
10. Shelnut, J. A. J. Phys. Chem. 1983, 87, 605.
11. Shelnut, J. A. J. Am. Chem. Soc. 1983, 105, 774.
12. Shelnut, J. A. J. Phys. Chem. 1984, 88, 6121.
13. Shelnut, J. A.; Ginley, D. S. J. Phys. Chem. 1985, 89, 5473.
14. Alston, K.; Schechter, A. N.; Arcoleo, J. P.; Greer, J.; Parr, G. R.; Friedman, F. K. Hemoglobin 1984, 8, 47.
15. Alston, K.; Storm, C. B. Biochemistry 1979, 18, 4292.
16. Finsden, E. W.; Ondrias, M. R. J. Am. Chem. Soc. 1984, 106, 5736.
17. Pettersen, R. C. Acta Cryst. 1969, B25, 2527.
18. Molinaro, F. S.; Ibers, J. A. Inorg. Chem. 1976, 15, 2278.
19. Walker, F. A.; Hui, E.; Walker, J. M. J. Am. Chem. Soc. 1975, 97, 2390.
20. Spaulding, L. D.; Chang, C. C.; Yu, N-T.; Felton, R. H. J. Am. Chem. Soc. 1975, 97, 2517.
21. Spiro, T. G. In "Iron Porphyrins"; Lever, A. B. P.; Gray, H. B., Eds.; Addison-Wesley: Reading, 1982, Part II, p. 89.

22. Drew, M. G. B.; Mitchell, P. C. H.; Scott, C. E. Inorg. Chim. Acta 1984, 82, 63.
23. Shelnut, J. A. J. Am. Chem. Soc. 1981, 103, 4275.
24. Shelnut, J. A. Inorg. Chem. 1983, 22, 2575.
25. Shelnut, J. A. J. Am. Chem. Soc. 1983, 105, 7179.
26. Shelnut, J. A. U. S. Patent No. 4,568,435, 1986.
27. LaMar, G. N.; Walker(Jensen), F. A. In "The Porphyrins" Vol. IV, Part B; Dolphin, D., Ed.; Academic Press: New York, 1979, p. 61.
28. Shelnut, J. A.; Straub, K. D.; Rentzepis, P. M.; Gouterman, M.; Davidson, E. R. Biochemistry 1984, 23, 3946.
29. Shelnut, J. A.; Ondrias, M. R. Inorg. Chem. 1984, 23, 1175.
30. Shelnut, J. A.; Ortiz, V. J. Phys. Chem. 1985, 89, 4733.
31. Ake, R. L.; Gouterman, M. Theoret. Chim. Acta 1970, 17, 408.
32. Gouterman, M. In "The Porphyrins" Vol. 3, Part A; Academic Press: New York, 1978, p. 1.
33. Gouterman, M.; Shelnut, J. A., unpublished results.
34. Pasternack, R. F.; Spiro, E. G.; Teach, M. J. Inorg. Nucl. Chem. 1974, 36, 599.
35. Kim, D.; Holten, D. Chem. Phys. 1983, 75, 305.
36. Kim, D.; Kirmaier, C.; Holten, D. Chem. Phys. Lett. 1983, 98, 584.
37. Holten, D.; Gouterman, M. Proc. Symp. Optical Properties and Structure of Tetrapyrroles 1984, Konstanz, Aug. 12-17.
38. Cullen, D. L.; Meyer, Jr., E. F. J. Am. Chem. Soc. 1974, 96, 2095.
39. Kirner, J. F.; Garofalo, Jr., J.; Scheidt, W. R. Inorg. Nucl. Chem. Lett. 1975, 11, 107.
40. Alston, K.; Dean, A.; Schechter, A. N. Mol. Immunol. 1980, 17, 1475.
41. Alston, K.; Park, C. M.; Rodgers, D. W.; Edelstein, S. T.; Nagel, R. L. Blood 1985, Vol. 64, Part II, 556.
42. Manoharan, P. T.; Alston, K.; Rifkind, J. M. Proc. Copper Coordination Conf. 1986, Albany, NY, in press.
43. Takano, T. J. Mol. Biol. 1977, 110, 569.
44. Baldwin, J.; Chothia, C. J. Mol. Biol. 1979, 129, 175.
45. Shelnut, J. A.; Rousseau, D. L.; Friedman, J. M.; Simon, S. R. Proc. Natl. Acad. Sci. USA 1979, 76, 4409.

RECEIVED January 9, 1987

## Chapter 25

# Interaction of Ni(II) Complexes with Athabasca Asphaltenes

S. N. Nguyen and Royston H. Filby

Department of Chemistry and Nuclear Radiation Center, Washington State University,  
Pullman, WA 99164-1300

The reactions of Athabasca oil-sand asphaltenes with the non-porphyrin complex Ni(II) acetylacetonate, Ni(acac)<sub>2</sub>, and the nickel porphyrins Ni(II) octaethylporphyrin (NiOEP) and Ni(II) mesoporphyrin IX dimethyl ester (NiDME) were studied in chloroform solution. The reaction of asphaltenes with Ni(acac)<sub>2</sub> occurs with the monomeric square planar complex and involves the association of Ni(acac)<sub>2</sub> molecules with the asphaltenes and a reaction of the asphaltenes with Ni<sup>2+</sup> via ligand exchange. The reaction between the asphaltenes and NiOEP and NiDME involves an association of the porphyrins with asphaltene components and is stronger with the more polar NiDME. Size exclusion chromatography showed that the distribution of <sup>63</sup>Ni from Ni(acac)<sub>2</sub> and NiDME reactions were similar to the distribution of the inherent nickel in the asphaltenes. The data are consistent with the concept of most of the nickel in the asphaltenes being non-porphyrin in nature.

The Alberta oil-sands, which are considered as biodegraded and water-washed conventional crude oils, contain relatively high nickel and vanadium contents (1). Both nickel and vanadium occur in the bitumen entirely as organic complexes (1), partly as desoxophylloerythroetioporphyrin (DPEP), etioporphyrin (etio), tetrahydrobenzoporphyrin (THBD), and benzoporphyrin (benzo) complexes (2,3) and, in higher concentrations, as unidentified "non-porphyrin" complexes associated primarily with the asphaltenes (1,4). In the case of nickel, there is evidence for the presence of non-porphyrin species in the maltenes (1,3). Although the Ni(II) and VO(II) porphyrins in Alberta oil sands and related oils have been investigated (3,5), the non-porphyrin species remain unidentified; their geochemical origin and significance and relationship to the porphyrin complexes are not known. This is due, in most part, to the virtual impossibility of separating discrete non-porphyrin complexes from the asphaltene matrix, either by solvent extraction or by chromatographic techniques. Several hypothetical structures have been described for non-porphyrin Ni(II) and VO(II) species in crude oils. Yen (6) postulated that

non-porphyrin species include modified or very complex porphyrins, or are porphyrin degradation products. Several authors (7,8) have concluded from electron spin resonance (ESR) studies that the metal ion ( $V^{4+}$ ) in non-porphyrin VO(II) complexes in heavy oil asphaltenes is complexed with mixed tetradentate ligands containing nitrogen, sulfur, and oxygen. However, Malhotra and Buckmaster (9) concluded that even high precision ESR parameters measured at 34 GeV cannot be used to determine unequivocally the ligand environment of V(IV) in asphaltenes. Fish *et al.* (10) have suggested that Ni(II) and VO(II) non-porphyrin complexes in the Boscan heavy oil contain mixed nitrogen and oxygen ligands and that these metal complexes are of lower molecular weight than the VO(II) or Ni(II) geoporphyrins. These conclusions, however, are based on molecular weights estimated from size exclusion chromatography (SEC) data and model compound studies. Jacobs (1) and Fish *et al.* (10) have also suggested that non-porphyrin Ni(II) species in Athabasca bitumen and Boscan oil, respectively, may contain naphthenic acid salts. In these studies and other studies of non-porphyrin species in crude oils, no discrete complexes of Ni(II) or VO(II) have been conclusively identified. There is evidence from X-ray photon spectroscopy (XPS) (11), laser-microprobe mass-analysis (LAMMA) spectroscopy (11), infra-red (IR) spectroscopy (11), and X-ray absorption spectroscopy (12,13) that non-porphyrin VO(II) (11,12) and Ni(II) (13) species in crude oils may in fact be porphyrinic. Tooulakou (Strong) and Filby (3,14) demonstrated that sequential solvent extraction of Athabasca asphaltenes with *n*-pentane followed by methanol-acetone (12:88 v/v) extracted more than twenty-five percent of the total vanadium in the form of VO(II) porphyrins which differ from the VO(II) porphyrins in the oil-sand bitumen only in relative abundances determined by porphyrin polarity. These data confirm those of Jacobs (1) who showed, on the basis of sequential-elution solvent chromatography (SESC), that at least part of the non-porphyrin VO(II) in Athabasca asphaltenes was present as metalloporphyrin complexes. Strong and Filby (3) also concluded, on the basis of UV-visible spectroscopic data, that the Ni(II) species extracted by methanol-acetone from the asphaltenes were predominantly non-porphyrin. This finding is consistent with the much lower fraction of total nickel present as Ni(II) porphyrins compared to the fraction of vanadium as VO(II) porphyrins in the Athabasca bitumen (1). Recent studies thus suggest that much of the vanadium content in the asphaltenes, which has been considered as "non-porphyrin," comprises VO(II) porphyrins which are either strongly associated with the asphaltenes by  $\pi$ - $\pi$  bonding, or are trapped in the micellar structure of the asphaltenes (e.g., between aromatic hydrocarbon sheets). On the other hand, a significant fraction (>50%) of the nickel content of the asphaltenes may be non-porphyrin complexes. The mode of association of Ni(II) or VO(II) porphyrins with asphaltenes has not been studied, although it has been shown that the spectroscopic properties of metalloporphyrins (e.g., molar absorptivities) are modified significantly in the presence of asphaltenes (12), presumably as a result of chemical interactions.

Lewan and Maynard (15) have shown that the vanadium and nickel in crude oils probably have been derived from metal ions in the water column during sediment deposition or during subsequent sediment compaction and diagenesis. Although this may be the source of nickel

in Ni(II) porphyrins which occur in immature sediments, it is possible that non-porphyrin Ni(II) species in crude oils form later in the geochemical evolution of the sediment. Asphaltenes may complex Ni(II) ions from mineral surfaces during formation of bitumen from maturing kerogens in source rocks, during migration of a crude oil, or during maturation and alteration of the oil in a reservoir. Alternatively, polar Ni(II) non-porphyrin complexes may dissolve, or be formed, in the bitumen at some stage during its geochemical evolution and may strongly associate with components of the asphaltene micelles. The complexation of metal cations, such as VO(II), Ni(II), Cu(II), Co(II), Zn(II), and Mg(II) from colloidal silicates by petroleum asphaltenes (16) has been demonstrated. Also, Erdman and Harju (17) showed that some crude oil asphaltenes were under-saturated with respect to metal content and that the vanadium content could be increased by reaction with VO(acac)<sub>2</sub> in benzene solution. Their data, however, do not allow a distinction to be made between complexation of VO<sup>2+</sup> by ligand groups in the asphaltenes or some form of association of the VO(acac)<sub>2</sub> complex with the asphaltenes.

In this study, the reactions of the non-porphyrin Ni(II) complex, Ni(acac)<sub>2</sub>, and the Ni(II) porphyrin complexes (NiOEP and NiDME) with Athabasca oil-sand asphaltenes were studied in chloroform solution.

### Experimental Procedures

Asphaltene Separation Procedure. Athabasca bitumen was separated into maltenes and asphaltenes by precipitation with 40:1 volume ratio of n-pentane to bitumen. The n-pentane asphaltenes were dissolved in toluene and reprecipitated with a 20:1 volume ratio of methanol to toluene. The asphaltenes were then Soxhlet-extracted with 12:88 v/v methanol-acetone until the solvent return to the solvent reservoir was colorless.

Synthesis of Labeled Compounds. The Ni(II) and Cu(II) acetylacetonates were synthesized according to the method of Charles *et al.* (18). The Ni(acac)<sub>2</sub> was synthesized either with <sup>63</sup>Ni or with <sup>14</sup>C-labeled 2,4-<sup>14</sup>C acetylacetonate (acac). The Cu(acac)<sub>2</sub> was synthesized using <sup>64</sup>Cu labeled Cu(NO<sub>3</sub>)<sub>2</sub>.

Nickel octaethylporphyrin (NiOEP) and nickel mesoporphyrin IX dimethyl ester (NiDME) were synthesized with <sup>63</sup>Ni labels using the acetate method described by Bucher (19).

Reaction of Metal Complexes with Asphaltenes. The metal complexes labeled either with radioactive metal ion or <sup>14</sup>C-acac and 50 mg of asphaltenes were reacted in 30 mL of chloroform in closed glass reaction vessels for periods of up to 1440 minutes depending on the reaction. For the acetylacetonate complexes, 30 mL of methanol was added at the end of the reaction to convert the excess unreacted Ni(acac)<sub>2</sub> (or Cu(acac)<sub>2</sub>) in the solution to its unreactive polymeric form. An additional 100 mL methanol was added to complete the precipitation of the asphaltenes and the solution was then filtered through a 0.45 μm Nucleopore PTFE filter. The solid asphaltenes were washed with 50 mL of methanol to remove excess metal complex.

To determine the adsorption of Ni(acac)<sub>2</sub> on solid asphaltenes, the asphaltenes were shaken with a methanol solution of Ni(acac)<sub>2</sub> of

different concentrations. The asphaltenes were then filtered and washed as described above.

The reactions of NiDME and NiOEP with asphaltenes were studied in chloroform solutions under experimental conditions similar to those for the acetylacetonates. The asphaltenes were precipitated with 1:1 v/v methanol-acetone mixture for these experiments because of the higher solubility of NiDME and NiOEP in methanol-acetone versus methanol.

Size Exclusion Chromatography (SEC). Asphaltenes were separated into molecular-weight fractions by SEC on Bio-Beads SX-1 (nominal molecular-weight exclusion limit, 14,000 daltons) using tetrahydrofuran at 1 mL/min as the mobile phase. Polystyrene molecular-weight standards and rubrene, C<sub>42</sub>H<sub>28</sub>, were used for column calibration.

Determination of <sup>63</sup>Ni, <sup>14</sup>C, and <sup>64</sup>Cu. Liquid scintillation counting (LSC) was used to measure <sup>63</sup>Ni and <sup>14</sup>C activities in the reacted asphaltenes. Because of the low energy of <sup>63</sup>Ni beta particles (E<sub>max</sub> = 66 keV), oxidation techniques were used to eliminate color quenching by asphaltenes in the LSC cocktail. An aliquot of the asphaltenes was wet-ashed with 2 mL H<sub>2</sub>SO<sub>4</sub> in a 20 mL LSC vial at 100°C for 6 hr. The solution was evaporated to dryness and then ashed in air in a muffle furnace at 450°C for 6 hr. The residue was dissolved in 0.2 mL 6M HCl, 1 mL double distilled water added and then 18.8 mL of AQUASOL-2 cocktail solution was added to the vial. Because color quenching was not as severe for <sup>14</sup>C as for <sup>63</sup>Ni, samples and <sup>14</sup>C standards were adjusted to contain the same amount of asphaltenes by the addition of unlabeled asphaltenes to the <sup>14</sup>C standard solutions. The <sup>14</sup>C was determined using 0.2 mg of <sup>14</sup>C-containing asphaltenes, dissolved in 1 mL chloroform, plus 19 mL Scintilene cocktail. The <sup>64</sup>Cu activities of asphaltenes were measured using the 511 keV annihilation peak with a 3" x 3" NaI(Tl) detector interfaced to a single channel analyzer (SCA).

## Results

### Reaction of Asphaltenes with Ni(II) and Cu(II) Acetylacetonates.

Ultra violet-visible spectroscopic examination of chloroform solutions of Ni(acac)<sub>2</sub> showed that both the monomeric and a trimeric species, [Ni(acac)<sub>2</sub>]<sub>3</sub>, were present. When solid Ni(acac)<sub>2</sub> was dissolved in chloroform at 25°C, equilibrium between the monomer and the trimer was established only after 8 hours, as can be seen from Figure 1. In Figure 1, the absorbance ratio (A<sub>265</sub> monomer)/(A<sub>295</sub> trimer) is shown as a function of time after solid dissolution. The monomer-trimer equilibrium was found to be very sensitive to other compounds (particularly oxygenated compounds) in solution and less than 1 percent methanol shifted the equilibrium completely to the trimeric species. However, the rate of reaction of Athabasca asphaltenes with previously equilibrated chloroform solutions of Ni(acac)<sub>2</sub> was very rapid as shown in Table I. The reaction between Ni(acac)<sub>2</sub> and asphaltenes was essentially complete in less than 5 minutes, although it is not clear whether true equilibrium was reached.

The influence of the Ni(acac)<sub>2</sub> solution-equilibration time on the Ni(acac)<sub>2</sub>-asphaltenes reaction can be seen from Figure 2, in

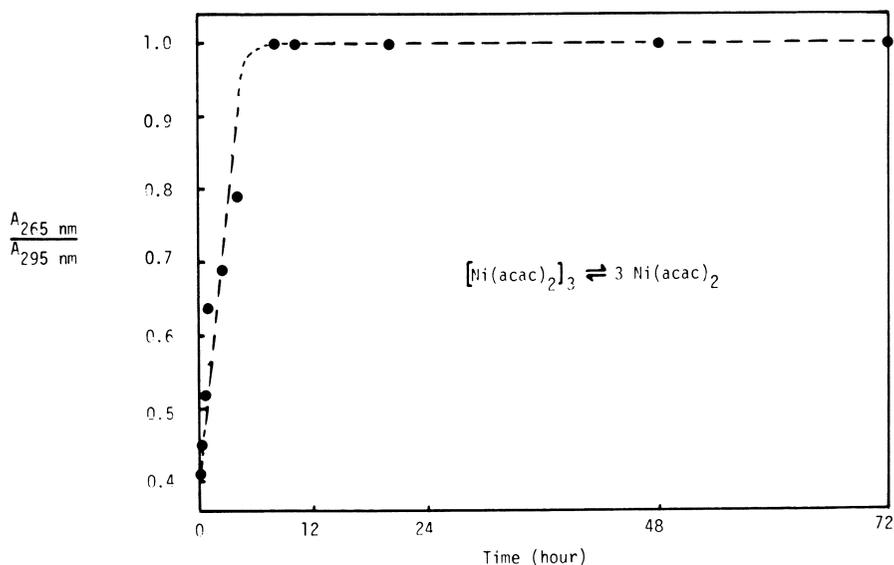


Figure 1. UV absorbance ratio for  $\text{Ni}(\text{acac})_2$  monomer ( $A_{265}$ ) to trimeric species ( $A_{295}$ ).

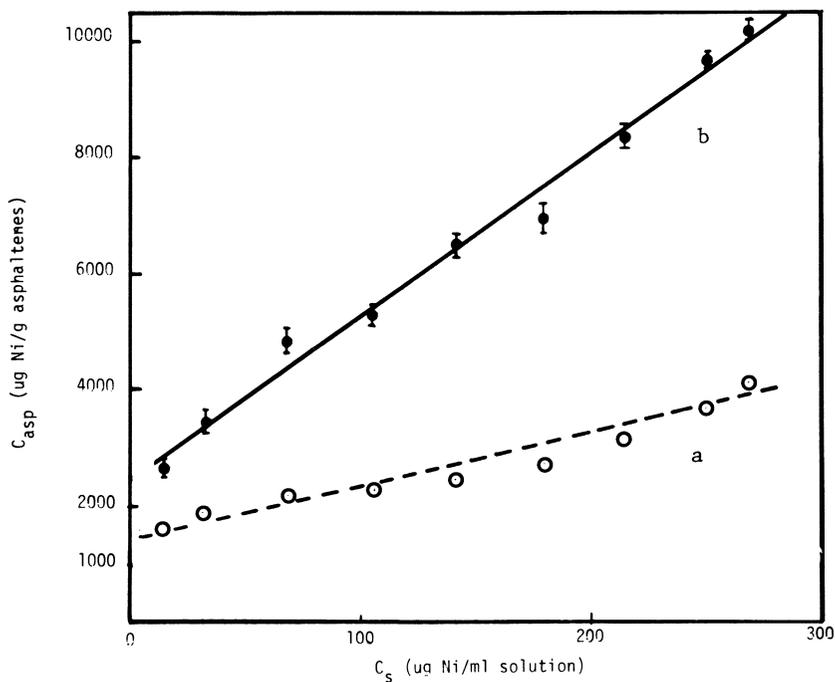


Figure 2. Variation of  $^{63}\text{Ni}$  content of asphaltenes with concentration of  $^{63}\text{Ni}(\text{acac})_2$  in solution for equilibration times of a) 1 hr (o); b) 12 hr (●).

Table I. Uptake of  $^{63}\text{Ni}$  by Asphaltenes from  $^{63}\text{Ni}(\text{acac})_2$  in Chloroform Solution as a Function of Reaction Time<sup>a</sup>

Reaction Time (min)	$^{63}\text{Ni}$ Content	
	as $\mu\text{g Ni/g}$ asphaltenes	as $\mu\text{mole Ni/g}$ asphaltenes
5	2540 $\pm$ 69 <sup>b</sup>	43.3 $\pm$ 1.2 <sup>b</sup>
15	2570 $\pm$ 85	43.8 $\pm$ 1.5
30	2400 $\pm$ 72	40.8 $\pm$ 1.2
60	2640 $\pm$ 109	45.0 $\pm$ 1.9
120	2650 $\pm$ 179	45.2 $\pm$ 3.0
240	2610 $\pm$ 95	44.5 $\pm$ 1.6
480	2640 $\pm$ 79	45.0 $\pm$ 1.3
720	2390 $\pm$ 59	40.7 $\pm$ 1.0
1440	2550 $\pm$ 214	43.5 $\pm$ 3.6

<sup>a</sup>Concentration of  $\text{Ni}(\text{acac})_2$  in initial solution = 0.32 mM; mass of asphaltenes = 50 mg; volume of solution = 30 mL.

<sup>b</sup>Error terms are  $\pm$  one standard deviation from counting statistics.

which data for 1 hr and 12 hr monomer-trimer equilibration times are presented. It is apparent that the reacting species of  $\text{Ni}(\text{acac})_2$  is the square planar monomer rather than the octahedral trimer. This is inferred from a) the lower  $\text{Ni}(\text{II})$  uptake by asphaltenes at the 1 hr equilibration time compared to 12 hr, and b) the uptake of  $\text{Ni}(\text{II})$  by asphaltenes from equilibrated solutions of  $\text{Ni}(\text{acac})_2$  does not increase with reaction time (Table I). The monomer/polymer ratio could not be measured spectroscopically in the asphaltene- $\text{Ni}(\text{acac})_2$  solutions because of the very high asphaltene absorbance in the 250-300 nm range. However, it is likely that components of the asphaltenes (e.g., phenols, acidic species, etc.) shift the  $\text{Ni}(\text{acac})_2$  species equilibrium to the trimer, as does methanol and other oxygenated compounds. Thus, the asphaltenes react rapidly with the monomeric complex and unreacted  $\text{Ni}(\text{acac})_2$  in the solution is converted to the unreactive trimeric form. The monomer is expected to be more reactive with asphaltene components because axial bond formation between the  $\text{Ni}^{2+}$  ion and heteroatom-containing ligands in asphaltenes is possible. The octahedral geometry of the  $\text{Ni}^{2+}$  ion in the trimeric species requires breaking a Ni-O bond in the complex in order for bonding of  $\text{Ni}^{2+}$  to another ligand to occur.

Figure 2 demonstrates that there is substantial uptake of nickel by asphaltenes from  $\text{Ni}(\text{acac})_2$  in chloroform solution and that a saturation concentration is not reached below 10,000  $\mu\text{g Ni/g}$  asphaltenes. However, it is not possible to distinguish between association (e.g., chemisorption) of the  $\text{Ni}(\text{acac})_2$  complex with asphaltenes or a chemical reaction involving ligand replacement on

Table II. Total  $^{63}\text{Ni}$ ,  $^{14}\text{C-Ni}(\text{acac})_2$ , and  $\text{Ni}^{2+}$  Uptake by Athabasca Asphaltenes Function of  $\text{Ni}(\text{acac})_2$  Concentration as in Chloroform<sup>a</sup>

$[\text{Ni}(\text{acac})_2]_{\text{sol}}$ (mM)	Total $^{63}\text{Ni}$ Uptake $[\text{Ni}]_{\text{asp}}$ ( $\mu\text{mole/g}$ )	$^{14}\text{C-Ni}(\text{acac})_2$ Uptake <sup>b</sup> $[\text{Ni}(\text{acac})_2]_{\text{asp}}$ ( $\mu\text{mole/g}$ )	$\text{Ni}^{2+}$ Complexed $[\text{Ni}^{2+}]_{\text{asp}}$ ( $\mu\text{mole/g}$ )
0.24	45.4 $\pm$ 3.0 <sup>c</sup>	14.6 $\pm$ 3.1 <sup>c</sup>	30.8 $\pm$ 4.3 <sup>c</sup>
0.55	59.1 $\pm$ 3.6	19.3 $\pm$ 3.1	39.8 $\pm$ 4.8
1.16	82.5 $\pm$ 3.4	20.5 $\pm$ 3.1	62.0 $\pm$ 4.6
1.80	90.5 $\pm$ 3.1	17.3 $\pm$ 3.1	73.2 $\pm$ 4.4
2.41	111 $\pm$ 3.6	16.9 $\pm$ 3.1	94.1 $\pm$ 4.8
3.04	119 $\pm$ 4.1	21.2 $\pm$ 3.1	97.8 $\pm$ 5.1
3.65	142 $\pm$ 3.2	22.7 $\pm$ 3.1	119 $\pm$ 4.5
4.27	165 $\pm$ 2.4	20.8 $\pm$ 3.1	144 $\pm$ 3.9
4.58	174 $\pm$ 3.5	18.0 $\pm$ 3.1	156 $\pm$ 4.7

<sup>a</sup>Reaction conditions: mass of asphaltenes = 50 mg; solution volume = 30 mL; reaction time = 4 hr.

<sup>b</sup> $^{14}\text{C-Ni}(\text{acac})_2$  content corrected for  $^{14}\text{C-acac}$  uptake by asphaltenes.

<sup>c</sup>Error terms are  $\pm$  one standard deviation from counting statistics.

the metal complex. To distinguish between the reaction mechanisms,  $\text{Ni}(\text{acac})_2$  was synthesized and reacted with asphaltenes under conditions identical to those used for  $^{63}\text{Ni-Ni}(\text{acac})_2$ . Retention of  $^{14}\text{C}$  by asphaltenes after reaction could result from the uptake of discrete  $\text{Ni}(\text{acac})_2$  molecules or from association of  $^{14}\text{C-acac}$  liberated by ligand exchange with the asphaltenes. Hence, the reaction of  $^{14}\text{C-acac}$  with asphaltenes was studied under experimental conditions similar to those of the metal complex-asphaltene system. Table II lists uptake data for the asphaltenes- $\text{Ni}(\text{acac})_2$  reaction as a function of initial  $\text{Ni}(\text{acac})_2$  solution concentration. The nickel uptake (measured by  $^{63}\text{Ni}$  activity) is expressed as  $\mu\text{mole Ni(II)/g}$  asphaltenes and the  $^{14}\text{C}$  content of the asphaltenes is expressed as  $[(\mu\text{moles acac})_2]/\text{g}$  asphaltenes. Both concentrations are thus equivalent to  $\mu\text{moles Ni}(\text{acac})_2/\text{g}$  asphaltenes. Column 3 of Table II lists the  $^{14}\text{C}$  uptake data corrected for  $^{14}\text{C-acac}$  incorporation in the asphaltenes, i.e., the concentration of  $\text{Ni}(\text{acac})_2$  molecules in the asphaltenes. The difference between the total  $\text{Ni(II)}$  content (from the  $^{63}\text{Ni}$  data) and the  $\text{Ni}(\text{acac})_2$  content (from the  $^{14}\text{C}$  data) is the amount of nickel incorporated into the asphaltenes by ligand replacement,  $[\text{Ni}^{2+}]_{\text{asp}}$  (Column 4). The variation of total nickel taken up by the asphaltenes,  $[\text{Ni}]_{\text{asp}}$ , and that of the molecular complex,  $[\text{Ni}(\text{acac})_2]_{\text{asp}}$ , with solution concentration of  $\text{Ni}(\text{acac})_2$  at equilibrium,  $[\text{Ni}(\text{acac})_2]_{\text{sol}}$ , is shown in Figure 3. This figure shows

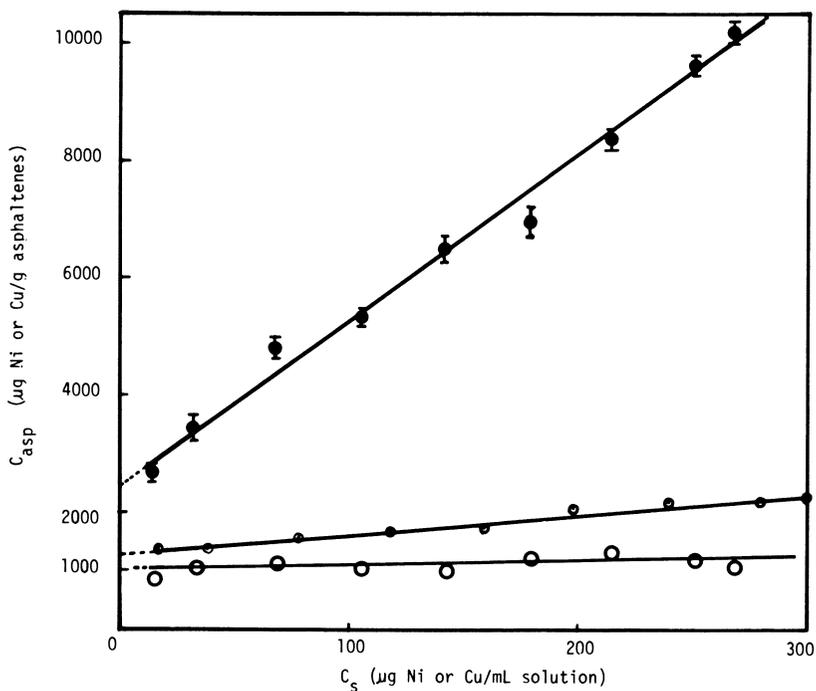


Figure 3. Variation of total Ni ( $\bullet$ ),  $\text{Ni}(\text{acac})_2$  ( $\circ$ ), and total Cu ( $\circ$ ) concentrations in asphaltenes,  $C_{\text{asp}}$ , as a function of concentration of  $\text{Ni}(\text{acac})_2$  or  $\text{Cu}(\text{acac})_2$  in chloroform solution,  $C_s$ .

Table III. Elemental Composition (wt%) of Athabasca Asphaltenes

Element:	C	H	O	N	S <sup>a</sup>	Ni <sup>b</sup>
	80.31	7.80	1.18	2.47	8.24	0.0317

<sup>a</sup>Sulfur obtained by difference from 100%.

<sup>b</sup>Ni determined by neutron activation analysis (4).

that at least two reaction mechanisms are involved in the reaction of Ni(acac)<sub>2</sub> with asphaltenes: a) a chemical reaction between Ni(acac)<sub>2</sub> and asphaltenes leading to ligand (acac) replacement, which is a function of the concentration of Ni(acac)<sub>2</sub> in solution, and b) an association of molecular Ni(acac)<sub>2</sub> with asphaltenes (19.1 + 2.5 μmole/g) that is independent of solution concentration within experimental error at the 95% confidence limits.

The concentration independent uptake of Ni(acac)<sub>2</sub> implies an association with concentration limiting specific sites in the asphaltenes. A distribution of Ni(acac)<sub>2</sub> between asphaltenes and the chloroform solution, or partition of the complex between solid asphaltenes and the methanol-chloroform solution during precipitation would lead, in both cases, to a concentration-dependent behavior.

The variation of nickel incorporated into the asphaltenes by ligand replacement, [Ni<sup>2+</sup>]<sub>asp</sub>, with [Ni(acac)<sub>2</sub>]<sub>sol</sub> is of the form:

$$[\text{Ni}^{2+}]_{\text{asp}} = K_{\text{Ni}} [\text{Ni}(\text{acac})_2]_{\text{sol}} + b$$

where  $b = 23.0 \mu\text{mole Ni/g asphaltenes (1350 } \mu\text{g Ni/g)}$

$$K_{\text{Ni}} = 26.1 \text{ mL/g; } r = 0.99$$

The intercept of 23.0 μmole Ni/g shows that the reaction between Ni(acac)<sub>2</sub> and asphaltenes may involve more than one ligand exchange mechanism. A possible explanation of the extrapolated zero solution concentration of 23.0 μmole Ni/g is that there is a specific functional group (or groups) in the asphaltenes that is present at a concentration equivalent to 23.0 μmole Ni/g and which has a very high affinity for Ni<sup>2+</sup> ion.

The nature of the functional groups, or molecular species, in the asphaltene structure that react with Ni(acac)<sub>2</sub>, has not been determined but undoubtedly involves functional groups containing nitrogen, oxygen, and possibly sulfur. The elemental composition of the asphaltenes used in this study is shown in Table III. Although oxygen is the least abundant heteroatom, it may be most important in terms of reactive functional groups that complex Ni<sup>2+</sup> ion. Ketone, phenol, quinone, and ester groups have been identified in asphaltenes, but phenolic groups have been shown (20) to account for more than 60 percent of the oxygen in Athabasca asphaltenes. Specific functional groupings such as diphenols, α-hydroxy N-heterocyclics, etc. may also be important in complexing Ni(II) since such compounds (e.g., hydroxyquinolines, polyphenols) form strong complexes with Ni(II).

The possibility that the retention of nickel by the asphaltenes involves the surface adsorption of Ni(acac)<sub>2</sub> on asphaltenes during

Table IV. Concentration of Ni (as  $^{63}\text{Ni}$ ) in Asphaltenes after Reaction of  $\text{Ni}(\text{acac})_2$  in Methanol (Heterogeneous System)<sup>a</sup>

[Ni(acac) <sub>2</sub> ] <sub>sol</sub> <sup>b</sup> (mM)	Total Ni Uptake [Ni] <sub>asp</sub>	
	μg Ni/g	μmole Ni/g
1.3	2.12 ± 0.20	36.1 ± 3.4
2.6	1.79 ± 0.20	30.5 ± 3.4
3.9	1.99 ± 0.17	33.9 ± 2.9
5.2	2.45 ± 0.21	41.7 ± 3.6
6.5	2.67 ± 0.20	45.5 ± 3.4
7.8	2.13 ± 0.20	36.3 ± 3.4
9.1	2.30 ± 0.20	39.2 ± 3.4
10.4	1.89 ± 0.18	32.2 ± 3.1
13.0	2.07 ± 0.20	35.3 ± 3.4

<sup>a</sup>Mass of asphaltenes = 50 mg; volume of reaction medium = 30 mL; reaction time = 4 hr.

<sup>b</sup>Concentration of  $\text{Ni}(\text{acac})_2$  in initial solution.

<sup>c</sup>Error terms are ± one standard deviation from counting statistics.

precipitation by methanol was studied by measuring the adsorption of  $^{63}\text{Ni}(\text{acac})_2$  on solid asphaltenes in methanol medium. The data, shown in Table IV, indicate that adsorption or surface complexation of  $\text{Ni}^{2+}$  or adsorption of  $\text{Ni}(\text{acac})_2$  is extremely small (30.5–45.5 nmole Ni/g) and is independent of concentration. If this minor adsorption results from adsorption of trimeric  $\text{Ni}(\text{acac})_2$  (form of the complex in methanol) or a reaction involving ligand exchange on the surface, the number of active sites must be very small and concentration limiting.

The factors which determine the occurrence of Ni(II) and VO(II) porphyrins to the exclusion of other metalloporphyrins in crude oils and oil-sand bitumens have been discussed by several authors (21,22). Nickel and vanadium are normally the most abundant metals in petroleum asphaltenes (1,4,6) and this may be the result of incorporation of the metalloporphyrins. However, the enrichment of asphaltenes in Ni(II) and VO(II) non-porphyrin complexes due to a preferential reaction of Ni(II) and VO(II) complexes with specific binding sites in the asphaltenes should also be considered. Thus the reaction of other metal complexes, e.g.,  $\text{Cu}(\text{acac})_2$  with asphaltenes should be less significant. The reaction between asphaltenes and  $^{64}\text{Cu}(\text{acac})_2$  was therefore studied in chloroform solution under the same conditions used for  $\text{Ni}(\text{acac})_2$ -asphaltene reaction. Copper was chosen because stable Cu(II) porphyrins are found in immature sediments, although not in crude oils. Thus, non-porphyrin complexes of Cu(II) may be formed in these sediments and they eventually associate with asphaltenes in the source-rock bitumen. The  $^{64}\text{Cu}$

content was determined by gamma-ray spectrometry and the uptake data are compared with the Ni(acac)<sub>2</sub> data in Figure 3. Figure 3 shows that Cu(II) was taken up by the asphaltenes to a much smaller extent than Ni(II), although a linear relationship was also observed. The reaction of Cu(acac)<sub>2</sub> with asphaltenes in chloroform follows the equation:

$$[\text{Cu}]_{\text{asp}} = K_{\text{Cu}} [\text{Cu}(\text{acac})_2]_{\text{sol}} + b$$

where  $K_{\text{Cu}} = 3.47 \text{ mL/g}$   
 $b = 20.1 \text{ } \mu\text{mole/g}$   
 $r = 0.98$

The intercept value of 20.1  $\mu\text{mole/g}$  indicates that either Cu(acac)<sub>2</sub> associates (e.g., adsorbs) with the asphaltenes to a similar degree as Ni(acac)<sub>2</sub> (19.1  $\mu\text{mole/g}$ ) or that a similar mechanism operates for the reaction of Cu<sup>2+</sup> via ligand replacement as for the concentration independent reaction of Ni<sup>2+</sup> with the asphaltenes (23.0  $\mu\text{mole/g}$ ). The value of 3.47 for  $K_{\text{Cu}}$  indicates that the asphaltenes react to a much smaller extent with Cu<sup>2+</sup> than with Ni<sup>2+</sup> ( $K_{\text{Ni}} = 26.1$ ).

Reaction of Asphaltenes with the Nickel Porphyrins, NiOEP and NiDME.  
 The reactions of asphaltenes with NiOEP and NiDME were studied to determine the relative affinity of Ni(II) porphyrins for asphaltenes and to compare the degree of association with the incorporation of non-porphyrin Ni(II) species in the asphaltenes. For both porphyrins, a ligand-exchange reaction is improbable because of the difficulty of demetallation of Ni porphyrins under the conditions used in this experiment; hence chemical reaction is unlikely. The uptake of NiOEP and NiDME by asphaltenes is shown in Table V. For both porphyrins there is a linear dependence of concentration in the asphaltenes,  $[\text{NiP}]_{\text{asp}}$ , with equilibrium solution concentration,  $[\text{NiP}]_{\text{sol}}$ . The equations expressing the Ni(II) porphyrin uptake are:

$$\text{NiOEP: } [\text{NiP}]_{\text{asp}} = K_{\text{OEP}} [\text{NiP}]_{\text{sol}} - 0.036 \quad (r = 0.97)$$

$$\text{NiDME: } [\text{NiP}]_{\text{asp}} = K_{\text{DME}} [\text{NiP}]_{\text{sol}} - 0.48 \quad (r = 0.99)$$

where  $K_{\text{OEP}} = 1.65 \text{ mL/g}$   
 $K_{\text{DME}} = 42.7 \text{ mL/g}$

For both porphyrins, the data can be approximated by:

$$\frac{[\text{NiP}]_{\text{asp}}}{[\text{NiP}]_{\text{sol}}} = K$$

The possibility that NiOEP and NiDME either coprecipitated with the asphaltenes during precipitation or distributed between the solid asphaltene phase and the solution after precipitation was considered. A series of reactions of NiOEP with asphaltenes in chloroform were performed in which the precipitating solvent was changed from methanol-acetone to *n*-pentane. Figure 4 shows the relationship of  $\log [\text{NiOEP}]_{\text{asp}}$  vs  $\log [\text{NiOEP}]_{\text{sol}}$  for both methanol-acetone and *n*-pentane deasphalting solvents. Changing the deasphalting solvent has only a small effect on the NiOEP uptake by the asphaltenes. Thus it appears that the reaction between NiOEP and asphaltenes occurs in the chloroform solution and is not dependent on the asphal-

Table V.  $^{63}\text{Ni}$  Contents of Asphaltenes after Reaction with NiOEP and NiDME in Chloroform<sup>a</sup>

$[\text{NiOEP}]_{\text{sol}}$ <sup>b</sup> moles/mL	$[^{63}\text{NiOEP}]_{\text{asp}}$ mole/g	$[\text{NiDME}]_{\text{sol}}$ <sup>b</sup> mole/mL	$[\text{NiDME}]_{\text{asp}}$ mole/g
0.00563	0.0043 $\pm$ 0.0028	0.00473	0.22 $\pm$ 0.02
0.0112	0.0124 $\pm$ 0.0021	0.00943	0.48 $\pm$ 0.03
0.0224	0.0639 $\pm$ 0.0082	0.0189	0.90 $\pm$ 0.03
0.0449	0.0686 $\pm$ 0.011	0.0380	1.81 $\pm$ 0.02
0.0562	0.0712 $\pm$ 0.012	0.0473	2.24 $\pm$ 0.02
0.0845	0.118 $\pm$ 0.0087	0.0707	3.56 $\pm$ 0.02
0.112	0.140 $\pm$ 0.014	0.0950	4.38 $\pm$ 0.02
0.225	0.267 $\pm$ 0.0092	0.190	8.73 $\pm$ 0.01
0.393	0.425 $\pm$ 0.0065	0.329	16.5 $\pm$ 0.01
0.562	0.759 $\pm$ 0.007	0.471	23.7 $\pm$ 0.01
0.844	1.530 $\pm$ 0.0051	0.712	33.0 $\pm$ 0.01
		0.956	40.5 $\pm$ 0.02

<sup>a</sup>Mass of asphaltenes used in each reaction = 50 mg, volume of the reaction medium = 30 mL, reaction time = 4 hr, deasphalting/wash solvent = methanol-acetone (1:1 v/v).

<sup>b</sup>Solution concentrations at equilibrium ( $\mu\text{M}$ ).

<sup>c</sup>Error terms are  $\pm$  one standard deviation from counting statistics.

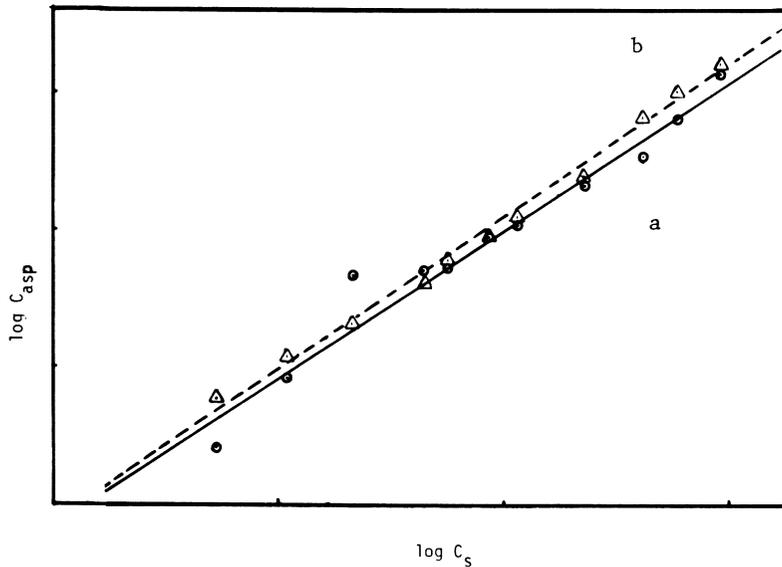


Figure 4. Effect of precipitating solvent on NiOEP uptake by asphaltenes: a) methanol-acetone (o); b) n-pentane ( $\Delta$ ).

tene precipitation conditions. The mechanism of association of the porphyrins with the asphaltenes may be  $\pi$ - $\pi$  bonding between asphaltene polycondensed-sheet structures and the porphyrin macrocycle, similar to that between planar aromatic structures in an asphaltene micelle. However, axial bonding of nitrogen-containing asphaltene constituents to the  $\text{Ni}^{2+}$  ion is also possible. The stronger association exhibited by NiDME with asphaltenes compared to that of NiOEP undoubtedly results from hydrogen-bonding from asphaltene components to the oxygen functionality of the ester groups on the DME ligand.

The distribution of nickel in the asphaltenes as a function of molecular weight before and after reaction with  $\text{Ni}(\text{acac})_2$  and NiDME, respectively, was measured by size exclusion chromatography (SEC). The nickel (as  $^{63}\text{Ni}$ ) contents in the four nominal molecular-weight ranges, >9000, 9000-3600, 3600-2350, and <2350 daltons were determined. The asphaltene mass distributions and nickel concentrations of the molecular-weight ranges are shown in Figures 5 and 6. Figure 5 indicates that the reaction of asphaltenes with  $\text{Ni}(\text{acac})_2$  and NiDME, respectively, did not significantly change the mass distribution of asphaltene components among the molecular weight fractions. Figure 6 shows that the distributions of the inherent nickel in the asphaltenes, the  $^{63}\text{Ni}$  in the asphaltenes from the reaction with  $\text{Ni}(\text{acac})_2$ , and the  $^{63}\text{Ni}$  from the reaction with NiDME are very similar. The NiDME concentration in the lowest molecular weight fraction is higher than for the intermediate fractions due probably to the separation of a small amount of free NiDME which coprecipitated with the asphaltenes. Ignasiak *et al.* (23) have shown that different molecular-weight fractions of Athabasca asphaltenes have similar chemical compositions (atomic ratios) and probably differ only in the degree of association of smaller units. Previous studies have shown, however, that the highest nickel and vanadium concentrations are found in the highest molecular-weight fractions (24,25) which may imply that these fractions have a higher proportion of functional groups. The distribution of nickel ( $^{63}\text{Ni}$ ) in the asphaltenes resulting from reaction with  $\text{Ni}(\text{acac})_2$  also indicates that the higher molecular-weight fractions contain proportionally more reactive functional groups that complex  $\text{Ni}^{2+}$  than do the lower molecular-weight fractions. The distribution of NiDME among the fractions indicates that the NiDME associates strongly with asphaltene species in all molecular-weight ranges. As for the other nickel species, the greatest concentration of NiDME is observed in the highest molecular-weight fraction. Whether this is a result of a larger number of functional groups or a higher proportion of polycondensed aromatic species in the highest molecular-weight fraction is not clear.

### Discussion

Nickel and vanadium are distributed among all molecular-weight ranges of crude oil asphaltenes with the highest concentrations found in the highest molecular-weight fractions (24,25). This observation, among others, has been interpreted as evidence for non-porphyrin species of the metals (1,10) or as evidence for complex or high molecular-weight porphyrins in the asphaltenes (26). The

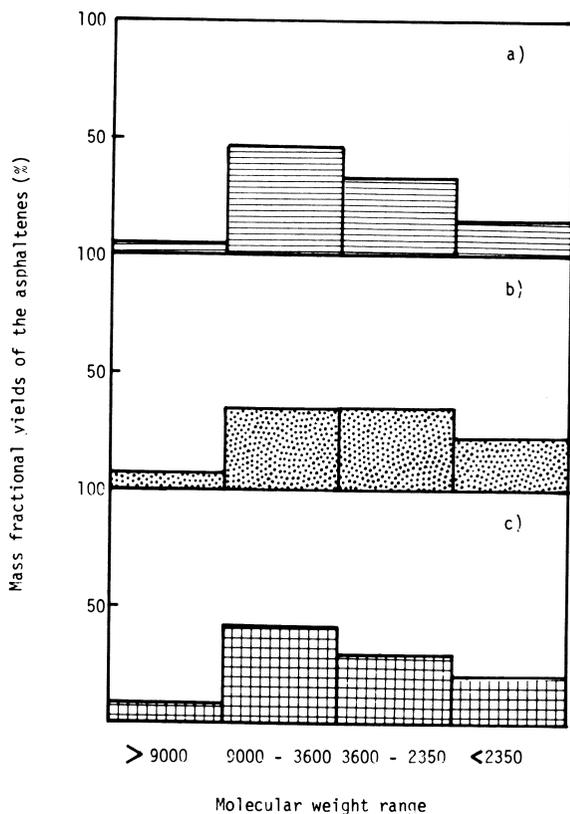


Figure 5. Mass distribution of asphaltenes as a function of molecular weight range for a) original asphaltenes, b) after reaction with  $\text{Ni}(\text{acac})_2$ , and c) after reaction with  $\text{NiDME}$ .

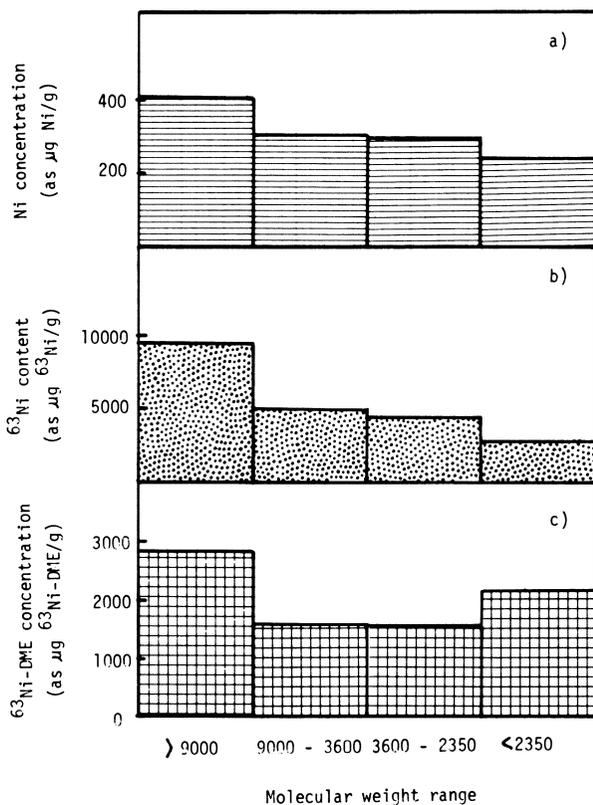


Figure 6. Distribution of Ni species in asphaltenes as a function of molecular weight range for a) original asphaltenes, b) after reaction with  $\text{Ni}(\text{acac})_2$ , and c) after reaction with  $\text{NiDME}$ .

reaction of Athabasca asphaltenes with  $\text{Ni}(\text{acac})_2$  and with  $\text{Ni}(\text{II})$  porphyrins demonstrates that metals may be incorporated into asphaltenes by more than one mechanism. Polar non-porphyrin  $\text{Ni}(\text{acac})_2$  may associate with the asphaltenes and  $\text{Ni}^{2+}$  may be incorporated by ligand exchange. At high  $\text{Ni}(\text{acac})_2$  concentrations, the reaction of asphaltene functional groups with  $\text{Ni}^{2+}$  is the dominant mechanism. These data provide evidence that incorporation of non-porphyrin nickel species into asphaltenes may occur in the geological environment. The extrapolated zero concentration value for nickel uptake from  $\text{Ni}(\text{acac})_2$  solutions is  $42.1 \mu\text{mol/g}$  ( $2470 \mu\text{g Ni/g}$ ). This value is much greater than the inherent nickel content of the asphaltenes ( $317 \mu\text{g/g}$ ) and demonstrates that the Athabasca asphaltenes are undersaturated with respect to nickel. Thus, during the formation of asphaltenes from kerogen in a source rock, the nickel content of the kerogen or the mineral-pore water-bitumen system is probably the controlling factor in determining the non-porphyrin nickel content of the asphaltenes. The distribution of non-porphyrin  $^{63}\text{Ni}$  among the molecular-weight fractions is essentially the same as that of the inherent nickel content. However, because of the similarity among the nickel non-porphyrin and porphyrin distributions, it cannot be concluded that the inherent nickel content is non-porphyrin.

The reaction of  $\text{NiOEP}$  and  $\text{NiDME}$  with asphaltenes demonstrates that an asphaltene-metalloporphyrin association occurs in the chloroform solution. This association mechanism is found for all molecular-weight fractions and is related to the polarity of the porphyrin species. Assuming that the relatively weak association of the fully alkylated  $\text{NiOEP}$  with asphaltenes in chloroform is similar in magnitude to that of the nickel geoporphyryns in the oil sand bitumen, the porphyrin content of the asphaltene can be estimated. Assuming a "free"  $\text{Ni}(\text{II})$  porphyrin content equivalent to  $3 \mu\text{g Ni/g}$  bitumen (1) for the Athabasca bitumen, the calculated value of the "associated"  $\text{Ni}(\text{II})$  porphyrin content of the asphaltene is approximately  $5 \mu\text{g Ni/g}$  asphaltenes. The inherent asphaltene  $\text{Ni}$  content of  $317 \mu\text{g Ni/g}$  thus appears to be almost entirely non-porphyrin unless the  $\text{Ni}(\text{II})$  porphyrins associated with the asphaltenes are much more polar than  $\text{NiOEP}$ . This may be the case if more polar  $\text{Ni}(\text{II})$  benzo or tetrahydrobenzoDPEP porphyrins are preferentially associated with the asphaltenes, as has been shown for vanadyl porphyrins (3).

#### Literature Cited

1. Jacobs, F.S., Ph.D. Thesis, Washington State University, Pullman, Washington, U.S.A. (1982).
2. Baker, E.W. *J. Amer. Chem. Soc.* 1966, 88, 2311-15.
3. Strong, D., and Filby, R.H., this volume.
4. Jacobs, F.S., and Filby, R.H. *Anal. Chem.* 1983, 55, 74-7.
5. Baker, E.W., Yen, T.F., Dickie, J.P., Rhodes, R.E., and Clarke, L.F. *J. Amer. Chem. Soc.* 1967, 89, 3631-39.
6. Yen, T.F., in "The Role of Trace Metals in Petroleum," T.F. Yen, Ed. Ann Arbor Science Publishers: Ann Arbor, 1975, 1-30.
7. Boucher, L.J., Tynan, E.C., and Yen, T.F., in "Electron Spin Resonance of Metal Complexes," T.F. Yen, Ed. Plenum, NY, 1969, 111-30.

8. Yen, T.F., Erdman, J.G., and Saraceno, A.J., Anal. Chem. 1962, 34, 694.
9. Malhotra, V.M. and Buckmaster, H.A., Fuel 1985, 64, 335-41.
10. Fish, R.H., Komlenic, J.J., and Wines, B.K., Anal. Chem. 1984, 56, 2452-60.
11. Berthe, C., Muller, J.F., Cagniant, D., Grimblot, J., and Bonnelle, J.P., in "Characterization of Heavy Crude Oils and Petroleum Residues," Editions Technip: Paris, 1984, 164-8.
12. Goulon, J., Retournard, A., Friant, P., Goulon-Giret, C., Berthe, C., Muller, J.F., Poncet, J.L., Guillard, R., Escalier, J.C., and Neff, B., J. Chem. Soc. Dalton Trans. 1984, 1095-1103.
13. Antonio, M.R., Hodges, M.G., Joyner, R.W., Meehan, P., Robert, I., and Scammelles, D.V., Preprints. ACS Div. Petrol. Chem. 1986, 31, 635.
14. Tooulakou (Strong), D., and Filby, R.H., in "Geochemical Biomarkers," T.F. Yen and J.M. Moldowan, Eds. (in press).
15. Lewan, M.D. and Maynard, J.B., Geochim. Cosmochim. Acta 1982, 46, 2547-60.
16. Bergaya, F., Perruchot, A., and Van Damme, H., Geochim. Cosmochim. Acta 1983, 47, 915-24.
17. Erdman, J.G. and Harju, P.H., Preprints. ACS Div. Petrol. Chem. 1962, 7, 43-56.
18. Charles, R.G., and Pawlikowski, M.A., J. Phys. Chem. 1958, 62, 440.
19. Bucher, J.W., in "Porphyrins and Metalloporphyrins," Smith, K.S., Ed., Elsevier, 1975, 157-231.
20. Ignasiak, T., Strauss, O.P., and Montgomery, D.S., Fuel 1977, 56, 359.
21. Quirke, J.M.E., this volume.
22. Lewan, M.D. Geochim. Cosmochim. Acta 1984, 48, 2231-38.
23. Ignasiak, T.M., Kotlyar, L., Samman, N., Montgomery, D.S., and Strausz, O.P. Fuel 1983, 62, 363.
24. Furimsky, E. and Champagne, F.J. Fuel Processing Technology 1982, 6, 269.
25. Jacobs, F.S., Bachelor, F.W., and Filby, R.H. Proc. 5th International Conf. Nuclear Methods in Environmental and Energy Research, J.R. Vogt, Ed., U.S. DOE CONF-840408, 1984, 438-49.
26. Blumer, M. and Rudrum, M., J. Inst. Petrol. 1970, 56, 99-106.

RECEIVED March 30, 1987

## Chapter 26

# Group Isolation of Nickel and Vanadyl Porphyrins from Crude Oil Using Macroporous Silica Gel

David H. Freeman<sup>1</sup>, Rosalie M. Angeles<sup>1</sup>, Katherine H. Freeman<sup>2,3</sup>, Thomas C. Hoering<sup>2</sup>, Joseph S. Flynn<sup>1,4</sup>, Tracie A. Lango<sup>1</sup>, and C. T. Homonay-Preyer<sup>1</sup>

<sup>1</sup>Department of Chemistry and Biochemistry, University of Maryland, College Park, MD 20742

<sup>2</sup>Geophysical Laboratory, Carnegie Institution of Washington, 2801 Upton Street, Washington, DC 20008

<sup>3</sup>Department of Geology, Wellesley College, Wellesley, MA 02181

<sup>4</sup>U.S. Naval Academy, Annapolis, MD 21412

An efficient, ten-fold concentration of combined nickel and vanadyl porphyrins in crude oil is obtained by liquid column chromatography with disposable, macroporous silica gel. The concentrate contains the biomarker metalloporphyrins based on chromatographic and spectral comparisons with etioporphyrin-I standard compounds. The concentrate is free of asphaltene materials that would otherwise cause major chromatographic interference.

The procedure, in brief, begins with one gram of crude oil sorbed on top of a column containing 5 grams of 500Å pore size silica gel. The initial elution is with petroleum ether:methylene chloride (97v:3v) to remove saturated and aromatic hydrocarbons. The metalloporphyrins are eluted next with methyl acetate while the remaining asphaltene components are immobilized. In a second step, 100Å silica gel is used to further separate the metalloporphyrins.

The method is rapid, simple and reproducible. It is applicable to processing large numbers of samples and it is economical in its use of solvent and adsorbent. Details on the considerable effort expended on this method development are given.

Multi-step separation and purification procedures are needed to isolate metalloporphyrin pigments from geological samples. The many reported procedures vary from minimal methodology preceding mass spectrometry (1) to lengthy isolations of individual compounds for X-ray crystallography (2), combined mass spectrometric and NMR analysis (3) and high resolution HPLC and mass spectrometry (4).

The goal of the present study is to develop a rugged and robust method for group separation of traces of metalloporphyrins. This includes reliability and minimal modification when applied to a wide range of samples. Isolation from a geological matrix involves dealing with uncertain numbers of porphyrin homologues and isomers, and unbounded numbers of other compounds that are also present. Trace enrichment with high recovery and minimal interference is needed to assure qualitative and quantitative accuracy (5-7).

Optimization of a multi-step separations scheme requires an experimental approach, but not exclusively. A proper choice of liquid chromatographic variables is essential, at least in a practical sense (8). Many single step optimization criteria are available (9), although mixtures containing unbounded numbers of compounds are the most difficult. Solvent and adsorptive routes to chemical selectivity have become more accessible and faster (10). In dealing with highly complex mixtures, the first step may be the most difficult to work out, and the most important.

Extensive experimentation was needed to achieve the present goal, details of which are given below. First, it was demonstrated that a multimodal liquid chromatographic procedure, using silica gel, Sephadex LH-20 and C-18 bonded phase as substrates could make the desired separation. Thin layer chromatography proved to be a valid method for rapid metalloporphyrin scouting. Many solvent systems were tried before a basis for improved eluent composition was found. Column testing showed that crude oil fractionation on narrow pore silica gel is not appropriate in the first step.

An optimum eluent sequence was found on the basis of two dimensional TLC scouting experiments. The breakthrough came when it was observed that conventional silica gel did not provide the needed retentive capacity for the dark asphaltene fraction that seriously interferes with chromatographic separation and analysis. A critical testing of silica gel porosity lead to the use of macroporous silica gel. A dual optimization of solvent and adsorbent was thus obtained and the separation goal was reached.

## Experimental

Test of Multi-Modal LPLC. The use of non-redundant sorptive modes is known to be theoretically well-suited

for isolating compounds from extremely complex mixtures (10) such as crude oils. A feasibility study was made using low pressure liquid chromatography (LPLC) to concentrate the metalloporphyrins, specifically the predominant nickel porphyrin (NiP) group in the Messel Shale of Germany (11). Freshly pulverized samples of the shale were extracted with benzene and methanol (1:1 volume/volume) solution. One gram of the organic extract remained after rotary evaporation. The extract was (A) eluted successively with hexane and benzene from a 60cm by 5 cm preparative chromatographic column of silica gel (Grade 62, Davison Chemical Co., Baltimore, MD). Collection of the red porphyrin band in the benzene eluate was estimated visually. Then, (B) similar preparative chromatography with Sephadex LH-20 gel in 1:1 benzene and methanol solution was carried out on the concentrate from step (A). These two steps are based on procedures described by Baker (12).

HPLC apparatus was then used with (C) C-18 bonded phase, Sep-Pak cartridges used as short, disposable chromatographic columns (Waters Associates, Framingham, MA). A linear gradient was used from 1:1 acetonitrile (MeCN) and water to pure MeCN. The metalloporphyrin concentrate was chromatographed in a similar way (D) on Sep-Pak silica gel using a linear gradient of hexane to benzene. The cartridges used in C and D were confined to a tight-fitting metal holder and the insertion of machined end fittings reduced the dead volume. Independent tests showed at 1 ml/min flow rate that column efficiencies of ca. 40 theoretical plates could be achieved. The Sep-Pak columns burst occasionally, perhaps due to migrated particles that plugged the end frit.

Enrichment of the NiP group was monitored by visible absorption spectrophotometry after each step and is demonstrated in Figure 1 wherein the Soret B-band at 408 nm emerges from the UV absorbing background. Definitive, single peak isolation of the metalloporphyrins, shown in Figure 2, were obtained by monitoring the effluent at 550nm in a flow spectrophotometer.

It is concluded that the use of short disposable column chromatography in steps C and D (See Figures 1 and 2) is indeed applicable to the problem, given that the bulk of the sample matrix, the non-analyte group, has been previously removed by steps A and B. The A and B steps were costly in terms of time, sorbent and carrier liquid. This experiment defined the overall goal: to streamline the initial clean-up procedure and produce a metalloporphyrin concentrate that is suitable for high resolution chromatographic separation.

Preliminary Test of LP-LSC. Silica gel is a versatile and inexpensive adsorbent that is attractive for potential use in the clean-up procedure sought in this

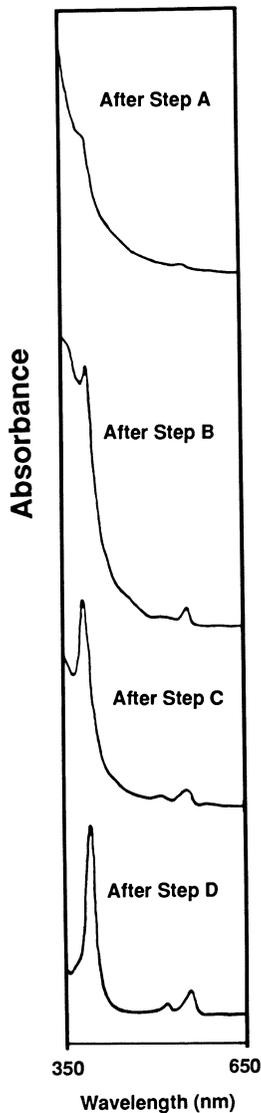


Figure 1. Nickel petroporphyrins (NiP) extracted from the Messel shale are monitored by spectrophotometry as they are concentrated in four-step preparative column chromatography: elution with (A) benzene on silica, and (B) benzene-methanol on LH-20, (C) water-MeCN gradient on Sep-Pak C-18, and (D) hexane-benzene gradient on Sep-Pak silica.

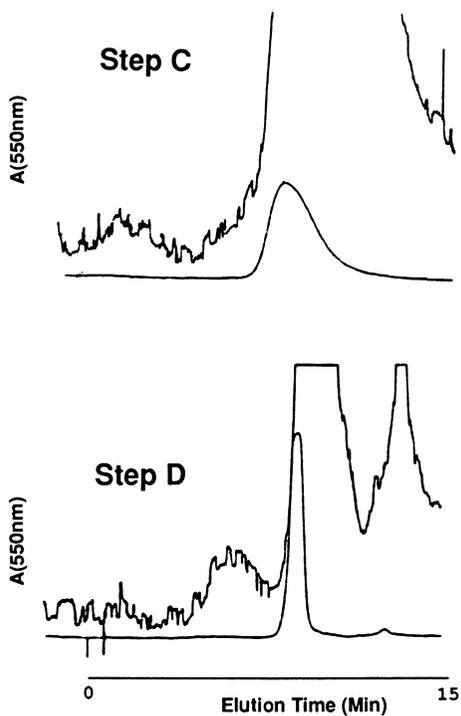


Figure 2. The C-18 Sep-Pak column, step C of Figure 1, is shown with a linear gradient at 1ml/min from 1:1 MeCN-water to pure MeCN (10 min) with NiP elution at 20 min. Similarly, in step D a silica Sep-Pak column, elution gradient from pure hexane to 1:2 hexane:benzene (9 min), is shown. The NiP peak elutes at 13 min. The feasibility of short column clean-up procedures is demonstrated.

work. Preliminary column tests were performed with silica gel in an attempt to define proper chromatographic conditions. An glass column with an adjustable bed of the Michel-Miller design (Ace Glass Co., Vineland, N.J.) was packed with 100g of Woelm silica gel, 32-63 $\mu$ m particle size. A carrier gradient was run from cyclohexane to dichloromethane wherein the solvent strength was varied by 0.04 per column volume (13). Ni and vanadyl porphyrin complexes, NiP and VOP, of etioporphyrin-I (Mid-Century Chemicals, Posen, IL) were used to monitor the separations. Resolution of the NiP and VOP standards by themselves was demonstrated as shown in the upper chromatogram of Figure 3. A similar test with a 1% load of North Belridge crude oil (Union Oil Company, Brea, CA), that had been spiked with equivalent amount of standards, gave much worse results as shown in the lower chromatogram of Figure 3. Here, the NiP and VOP separations were incomplete and irreproducible. The highly polar and darkly pigmented asphaltene materials, sorbed initially at the head of the column, bled off and coated the adsorbent, thus changing column conditions as the separation proceeded.

An additional complication was anticipated because vanadyl metalloporphyrins form strong complexes with Lewis bases (14) that are possible components of crude oil. Such complex formation will change their chromatographic behavior (15). Therefore, the present work is not confined to the isolation of a definite class of metalloporphyrins, but to a class that may change its composition during the analysis.

A preliminary strategy was formulated from these experiments. An inexpensive sorbent with practical mass loading for adsorbed asphaltene is needed. A more detailed knowledge of solvent selectivity effects is needed. An unnecessary complication would be avoided by finding conditions that minimize separation behavior of the NiP and VOP components.

Effect of Silica Gel Porosity. It is known that macroporosity tends to boost the macromolecular sample load capacity of silica gel and its bonded phase derivatives. The preparative separation of proteins and other macromolecules can be improved on this basis. Because asphaltene contains macromolecular components, the effect of silica gel pore size was studied using a series of Matrex silica gel samples provided by the Amicon Corporation (Danvers, MA). A test solution was prepared consisting of 1.00g of Boscan oil (Phillips Petroleum Company, Bartlesville, OK) dissolved in 40ml of petroleum ether and methylene chloride solution (50:1). The latter was added to retard deasphalting. The chromatographic columns used in this work were glass Flex-Columns (Kontes, Vineland, NJ).

The test solution turned the silica gel black at the inlet end of the column as the pigmented components

were adsorbed. The black zone was found to be correlated in size with the mass of oil sample. The sample load capacity, mass of oil per unit mass of silica gel bed that had become dark, was thereby ascertained. Preliminary experiments were carried out with silica gel samples of 20-45 $\mu$ m and 35-70 $\mu$ m particle sizes, with 60, 100, 250, 500 and 1000 $\text{\AA}$  average pore sizes. The load capacity was highest for the 500 $\text{\AA}$  pore size and 20-45 $\mu$ m particle size range, and ten-fold higher than that obtained with 60 $\text{\AA}$  and 35-70 $\mu$ m. With specific regard to the retention of the asphaltene-like group, the experiments showed that column length can be shortened by proportion to load capacity for this simple group separation. While the present results are specific for the Boscan reference oil, the high sample load capacity of the 250 $\text{\AA}$  and 500 $\text{\AA}$  materials for the asphaltene component have been verified in the initial adsorption step with several dozen crude oil samples. A more detailed investigation of the effect of pore size is being made (16).

Thin layer chromatography. 5 $\mu$ g samples of NiP and/or VOP standards were spotted on aluminum backed silica gel sheet (Eastman Kodak), 5cmX5cm squares, and developed in the presence of solvent vapor. 700 $\mu$ g of spiked crude oil (dissolved in methylene chloride) was spotted over 5 $\mu$ g spots of each of the standards.

Photodegradation was observed after NiP and VOP spots were exposed for 16 hours to a 60 watt incandescent or 16 watt fluorescent light (6 inch distance from light to sample). After the exposure, TLC development showed a new, more deeply colored and more highly retained band. NiP and VOP standards, following TLC development, were also found to darken on silica after two weeks of storage at room temperature in the dark. The results showed certain limitations but TLC appears to be valid for metalloporphyrin scouting under restricted exposure to light, air and contact with the TLC adsorbent (17,18).

The TLC elution window for metalloporphyrins has a wide solvent activity range (19). Over one hundred TLC scouting tests were carried out on the spiked crude oil. Single and binary solvent solutions were used for development in the solvent activity range shown in Figure 4. The quality of the results was unsatisfactory and multiple problems were apparent. Practically all of the individual solvents appeared to be inappropriate. In toluene, for example, NiP and VOP migration was satisfactory but the dark asphaltenes showed marked forward streaking, or fronting. Metalloporphyrin tailing occurred in acetonitrile (MeCN), lighter alcohols and methyl acetate (MeOAc). In polar solvents such as, MeCN, some of the initial sample spot occasionally failed to dissolve and remained at the origin. In halogenated hydrocarbon solvent, such as

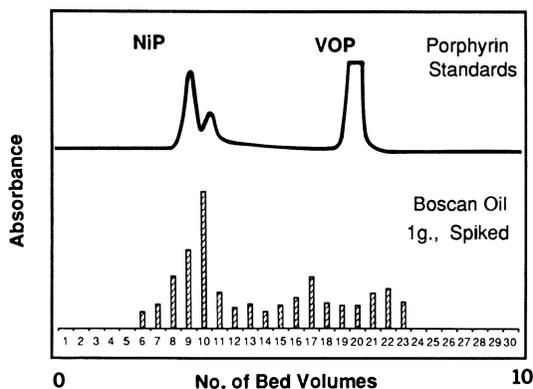


Figure 3. Liquid chromatography of NiP and VOP standards, alone and in crude oil is shown for a 60Å silica gel column; solvent gradient from cyclohexane to methylene chloride. Chromatography of 10µg of injected standards, monitored at 405nm, gave satisfactory NiP/VOP separation. This selectivity is lost in the lower chromatogram where 1.0g of Boscan crude oil, containing 0.1% of each of NiP and VOP standards, was injected.

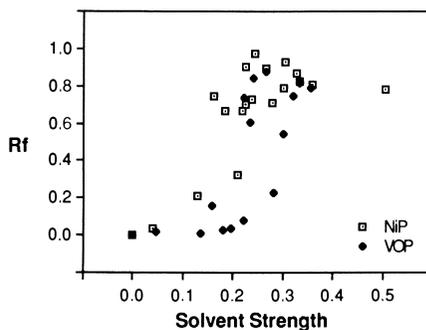


Figure 4. Over one hundred different individual and binary solvent compositions were mapped in TLC experiments. Typical Rf values are shown in the above (see ref 18, p. 230). The presence of crude oil (not shown) consistently interfered with the quality of the results.

methylene chloride, the darkly colored asphaltene-like components migrated along with the metalloporphyrins.

Solvent blending was tried. Improved band sharpness was observed in the presence of the more volatile solvents, especially methylene chloride, MC, and petroleum ether, PE, (Baker Chemical Co., 35-60°C).

Two dimensional TLC scouting. This approach gives a closer parallel to the desired sequence in which saturated and at least some aromatic hydrocarbons are eluted before desorbing the metalloporphyrin group with a stronger solvent. The initial TLC development was done with 3:97 MC:PE. A one-minute pause was made for solvent evaporation. The TLC plate was then rotated for perpendicular development. The solvents are listed in Table I.

Silica Gel TLC Scouting for Optimum Eluent Composition.

The retention and selectivity of the two metalloporphyrins standards, NiP and VOP, were apt to vary markedly with solvent composition. This is illustrated by the TLC xerographs shown in Figure 5. The capacity factors,  $k'$  (NiP) and  $k'$  (VOP), and corresponding VOP/NiP selectivities were calculated from the  $R_f$  values obtained in the TLC experiments using the well-known relationship,  $k' = (1 - R_f)/R_f$ . The selectivity,  $\alpha$ , is defined as the ratio of two designated  $k'$  values--larger over smaller. The observed selectivity maxima for two binary solvent systems are shown in Figure 6. Selectivity variations present two options, species separation under conditions of high selectivity and group separations under conditions of low selectivity. In the first stage of a multi-step separation, group separation is normally preferred.

The characteristics of the NiP and VOP standards were studied alone and as spikes added to a sample of a Boscan crude oil (Phillips Petroleum Co.), an asphaltene-rich and metalloporphyrin-rich oil used for reference purposes. The effects of solvent composition on the metalloporphyrin and the asphaltene-like groups were studied.

Three of the more highly differentiated TLC results are illustrated in Figure 7(a-c). In Figure 7(a) with toluene-cyclohexane (1:1) intermediate retention occurs but the NiP band is badly tailed. The strongly retained, darkly colored, asphaltene-like matrix shows pronounced forward streaking, or fronting. In Figure 7(b) with THF-cyclohexane (7:3) the metalloporphyrin standards and the dark matrix components appear to exhibit fractionation of the asphaltene-like group which is not strongly retained and which brackets the metalloporphyrins. This may be due to excessive strength of the THF component. In Figure 7(c) with MeCN-methylene chloride solvents (1:1) the asphaltene-like band was retained without predominant fronting.

Table I. Results of 1D and 2D Scouting Tests by TLC

<u>SOLVENT</u>	$\epsilon_0$	<u>STDS.</u>	<u>1D</u>	<u>2D</u>
Pet. Ether (PE)	0.0		R	R
Toluene	0.29	N	N	N
Methylene Chloride	0.42	GN	GN	GN
Ethylene Chloride	0.49	GN	G	GN
MeCN-MC-PE (Fig. 7f)	0.5			
1:1:4 (0)		GN	GN	GN
1:2:3 (3)		G	G	GN
1:3:2 (6)		GN	GN	GNR
1:4:1 (3)		GN	GN	GN
2:3:1 (6)		G	G	GNR
2:1:0 (6)		G	GR	GNR
Methyl Acetate (MeOAc)	0.60	G	GR	GNR
Dimethylsulfoxide *	0.62		R	GR
Morpholine *	0.63		GNR	GNR
Nitromethane	0.64	G	GR	GR
Acetonitrile (MeCN)	0.65	G	GR	GR
Methanol	0.95		R	R
Acetic Anhydride *	1		R	R
Dimethylformamide *	1	GN	GNR	GNR

The solvent strength parameter values,  $\epsilon_0$ , are mainly from Snyder (19). Above, 1D and 2D, refer to TLC of Boscan crude oil spiked with NiP and VOP standards. Other notes:

- G = NiP and VOP Group Isolation ( $R_f > 0.7$ ).
- N = Non-tailing of metalloporphyrins
- R = Asphaltene strongly retained ( $R_f < 0.2$ ).
- \* = Slow TLC development.

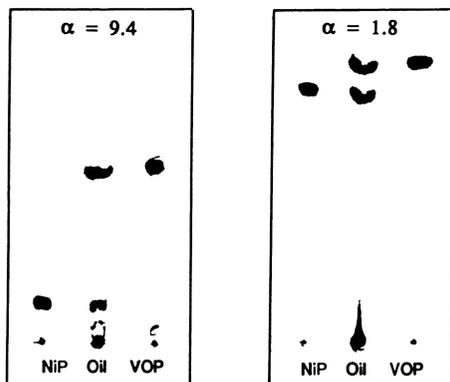


Figure 5. Silica TLC xerography shows how the adsorption selectivity for NiP and VOP standards varies five-fold as the cyclohexane to methylene chloride (MC) system is changed from 1:1 (left) to pure MC (right).

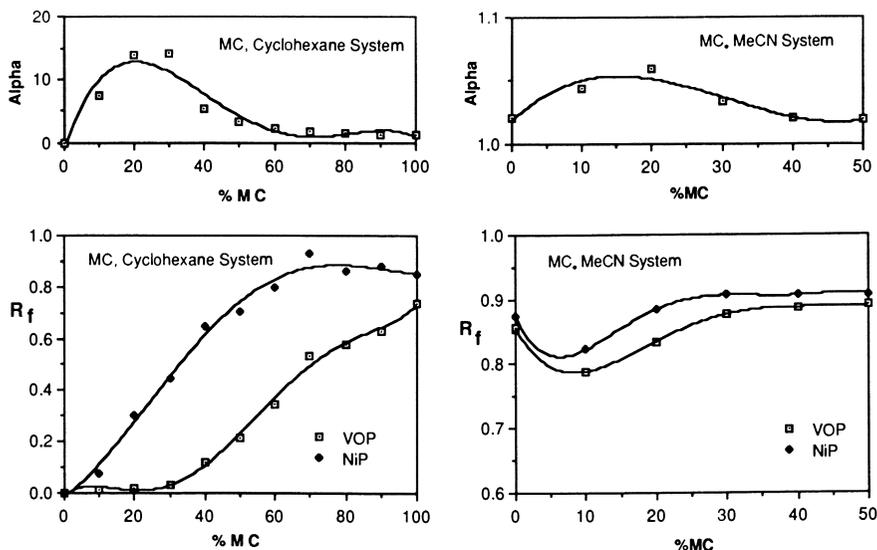


Figure 6. NiP and VOP standards on silica gel TLC give varied  $R_f$  and selectivity ( $\alpha$ ) values. While high metal speciation is obtainable, the minimal metal species selectivity needed for porphyrin group separation is obtained at low  $\alpha$ , preferably on the MC-rich side with cyclohexane.

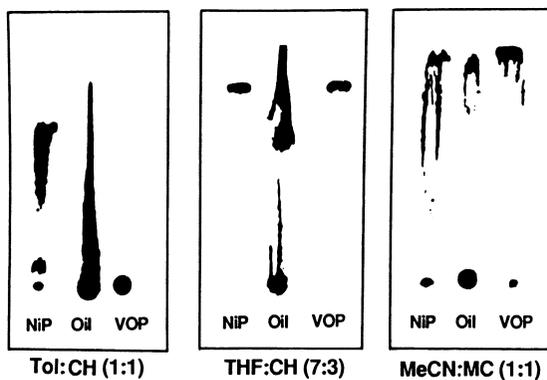


Figure 7. Xerographed silica TLC scouting results are shown for NiP and VOP spiked Boscan oil at the center of each TLC. At left: asphaltene components migrate with marked forward streaking which is typical of aromatic solvent systems. Middle: metalloporphyrins migrate together with asphaltenes. Right: this was the first indication of asphaltenes being retained while metalloporphyrins migrate.

Metalloporphyrin migration was obtained at the same time. The potential for separating the metalloporphyrins from the asphaltene-like group was indicated for the first time by this result.

The collected TLC results provided a key evidence for the use of silica gel to separate metalloporphyrins from the asphaltene group interferences. Further, in Figure 7(c) it is seen that NiP and VOP approach co-elution due to their high  $R_f$  values. Other problems were apparent including metalloporphyrin tailing and less than complete retention of the asphaltene-like components. Yellow pigmented components were observed with diverse affinities for silica gel although this is not apparent in the xerographic records.

Optimization of TLC Solvent Triad. Binary solvent solutions showed qualified advantages, notably MeCN or methylene chloride combined with a saturated alkane diluent such as cyclohexane (CH) or petroleum ether (PE). A ternary mixture offered the potential that the different advantages of binary blends might be combined. An optimization study is usually based on the resolution of a limited number of compounds (20). We adapted this type of approach to study the TLC of the highly complex mixture of NiP and VOP spiked crude oil with the MeCN-MC-PE solvent triad. This extends the data in Figure 6 beyond the two sets of binary mixtures which are part of this triad.

These TLC experiments generated over one hundred qualitative observations. The results were informative, in general terms fair to good overall, but no one solvent blend seemed to be excellent.

A quantitative description of the results was made in order to obtain a more precise composite description of each TLC result. The observation set was refined by assigning numerical values to previously qualitative criteria. The following evaluation criteria were defined: (a) miscibility of solvent blends, (b) non-tailing of the metalloporphyrin spikes, (c) similar high  $R_f$  values for the metalloporphyrin spikes--since that converges toward suppressed VOP/NiP selectivity, (d) non-fronting of the NSO-asphaltene band, and (e) lack of yellow substances that were apt to co-elute with the metalloporphyrins. These performance criteria designated p(a) through p(e), were measured on two scales, 0-1 for the first, solvent miscibility, and 0-3 for the others. The scales are both positive; zero is bad and high values are good. To illustrate, if the porphyrin exhibited pronounced tailing then that result was graded zero, p(c) = 0 for that particular solvent composition. Or, strong asphaltene retention with no discernable fronting would score three, p(d) = 3. The scales have worst case zero values, so zero level performance in any criterion at any composition forces a corresponding zero value in the composite product value.

The numerical scores for each of the criteria are shown in Figure 8(a-e) for each performance criterion and composition coordinates as designated within the triangular plots. A composite performance index,  $P$ , was obtained by multiplying the individual performance values together at each solvent composition.

$$P = p(a)p(b)p(c)p(d)p(e)$$

The composite performance indices reached to 36 out of 81 as a possible maximum. Conveniently, the results gave single digit integer values after division by 6. The results are shown in Figure 8(f). Figure 8(f) shows the numerically highest composite indices ( $P = 6$ ) that denote the optimal carrier compositions based upon these one dimensional TLC experiments.

These scouting experiments were carried further by testing several intermediate liquid compositions adjacent to a line connecting the TLC performance maxima at  $P = 6$ . No improvement was observed.

Bidimensional TLC as a Solvent Screen. It was recognized that the one dimensional 1D TLC experiments were not strictly analogous to the planned two-step isolation of the metalloporphyrin group. A TLC scouting study was carried out so as to be more analogous to an initial development to remove the saturates group. A second dimension, obtained by perpendicular development, was done with various solvents believed capable of properly desorbing the sought metalloporphyrins. An essential goal was that the asphaltene-like group remain adsorbed.

The 2D TLC results summarized in Table I confirm the 1D TLC findings given in Figure 8. The three optimal solvent blends noted in the MeCN-MC-PE system, as well as three new systems, gave good group separation of the combined NiP and VOP spikes from crude oil. The 2D TLC experiments gave results that differed significantly from the 1D TLC. In four instances, as shown in Table I, the preliminary removal of the saturates group improved the quality of the second TLC development. This is apparent from the improvement trend implied by the overall results in Table I. An important example of this occurs with MeOAc (methyl acetate) which gave gross tailing during 1D-TLC of the metalloporphyrin standards, alone and in the spiked Boscan. In 2D-TLC this tailing effect disappeared and MeOAc joined the solvents designated with superior performance. Among the solvents tested, the low boiling point and low viscosity of MeOAc are marked advantages. It is concluded that the presence of the saturated and aromatic hydrocarbons, soon to be called the A1 fraction, is able to interfere with the subsequent removal of the metalloporphyrins.

As the solvent strength (21) was increased further,

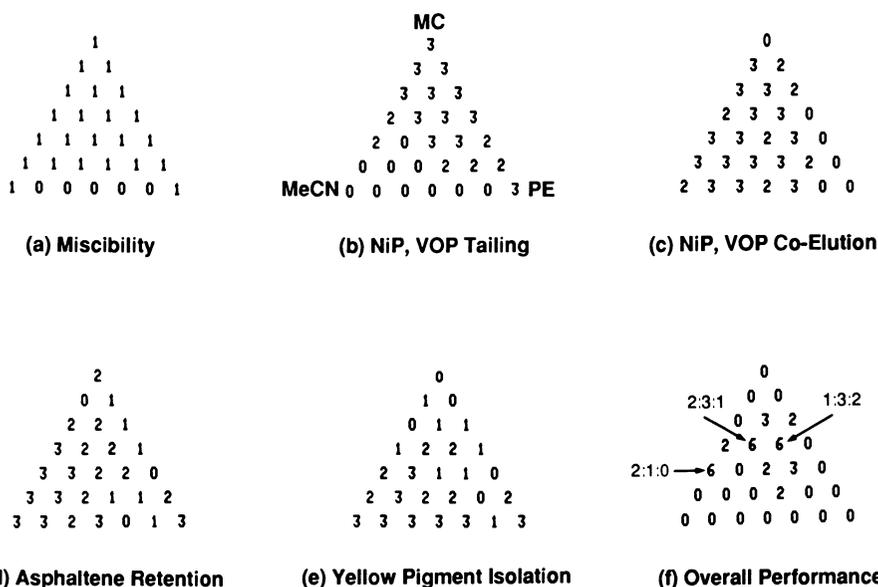


Figure 8. A 28-point TLC optimization is calculated from estimated quality of separation broken down by category. 0 is bad, 1 is minimal and 3 is maximal, as described in the text. In (a) MC prevents MeCN/PE immiscibility while in (b) MC counters metalloporphyrin tailing. In (c) MeCN boosts NiP and VOP co-elution while in (d) it promotes asphaltene retention. In (e) high levels of yellow pigmented contamination, appearing immediately following the metalloporphyrin spikes, is seen at  $p = 0$  or  $1$  in only three liquid compositions. The "best" overall performance compositions are shown in (f); see also table I.

the 2D TLC performance improved and then deteriorated. One high polarity solvent, dimethylformamide, qualified as a superior metalloporphyrin desorbant. (Less beneficial: it exhibited slow TLC development and it has a high boiling point.) Its distinctive role in vanadyl porphyrin extraction was reported in the work of Spencer et al (22). It is likely that other attractive solvent systems can be found to satisfy the performance criteria named so far.

The 2D TLC results for the best solvents in Table I show that the isolation of the NiP and VOP biomarker group was evaluated with regard to three key properties: it was weakly retained, R<sub>f</sub> values of 0.7 or higher (class "G" in Table I), without apparent tailing (class "N" in Table I) and with strong retention of the asphaltene-like group (class "R"). Based on TLC, column elution of the metalloporphyrin group by the best solvents are designated by the trio of satisfactory criteria, "GNR" in Table I. The G alone means that the combined biomarkers are expected to be completely eluted within one column volume after the front of the metalloporphyrin band. With four solvent systems, designated with an asterisk in Table I, the TLC migration was conspicuously slower. These systems were not considered acceptable for column application based upon poor dynamic behavior.

Desorption of Metalloporphyrins. Tests were made of the desorption of adsorbed metalloporphyrins from a macroporous silica gel column using the unspiked Boscan reference oil. Initially the oil was adsorbed from cyclohexane with 3% MC as described in the experimental section. Then, 1:3:2 MeCN:MC:PE was added as the second solvent to desorb the metalloporphyrins. This solvent blend ranked among the best based on the TLC triad optimization (see Figure 8) and it had the least amount of the higher boiling MeCN solvent. However, the collected fractions showed tailing that spanned over eight column volumes. This was measured at 20% sample load (Boscan reference oil) as shown in Figure 9. This desorption characteristic was consistently poor even at substantially smaller sample loads. This failure in retrospect should not be considered too surprising because the TLC tests did not actually test for desorption.

Comparison was made, again at 20% sample load, with MeOAc solvent for metalloporphyrin desorption. These results are also shown in Figure 9. The metalloporphyrin desorption was 95% complete within two column volumes. Although 20% sample mass loading may seem unusually high, we have so far only rarely observed evidence for overload during the initial adsorption step. Thus, the initial metalloporphyrin group isolation is achieved: strong retention of the asphaltene-like group while the saturates fraction is

removed, and high recovery of the desorbed metalloporphyrins while the remainder of the asphaltene-like group is not desorbed.

### Final Results and Conclusions

Petroporphyrins in Boscan Crude Oil. As the result of the experiments on macroporous silica gel, and two dimensional TLC as given above, a group separation of porphyrin classes was devised. The final scheme that was adopted is presented in Figure 10. Three major porphyrin fractions in the Boscan crude oil and in other petroleum subsequently studied are defined by their relative behavior in this scheme: B-1 the low polarity NiP and VOP biomarker molecules; B-2 the polar porphyrins and A-3, asphaltene-bound material. Details of the experimental method comprising this scheme are as follows.

A five gram bed of Matrex silica gel (500Å pores, 20-45µm particle size) was packed in a 2.5cm i.d. by 10 cm Flex column (Kontes, Vineland, NJ) with a resulting bed height of about 3.5 cm. The silica gel had been dried overnight at 105°C. The bed was equilibrated with methylene chloride and then washed with five column volumes of a hydrocarbon solvent; hexane or petroleum ether gave similar results. A one gram sample of Boscan crude oil was applied in 40ml of cyclohexane with 3% added methylene chloride. The methylene chloride retards asphaltene precipitation and promotes elution of yellow non-porphyrins that interfere with spectrophotometry. The column was then eluted with 50ml of hexane and methylene chloride (97:3). Metalloporphyrins are significantly more soluble in cyclohexane than in petroleum ether and, depending on the condition of the silica and the asphaltene content, some NiP may be eluted with this solvent. It is important to test the initial hydrocarbon-rich eluant for losses of porphyrins.

The solvent was changed to methyl acetate to desorb the metalloporphyrins. A sharply defined asphaltene band remained strongly retained while the deeply colored metalloporphyrin groups moved together down the white column. Ethyl acetate was subsequently found to behave about the same.

Retention of the Asphaltene-like Group. The chromatographic retention of the asphaltene-like interferences is the key to the separation scheme. The adsorption/desorption steps are at least in part controlled by solubility related processes. The A1/A2/A3 solvent step gradient (Figure 10) exerts control to a significant extent by providing low solubility of the asphaltene-like group in the two initial solvents where the predominant alkane and then methyl acetate have the common characteristic that

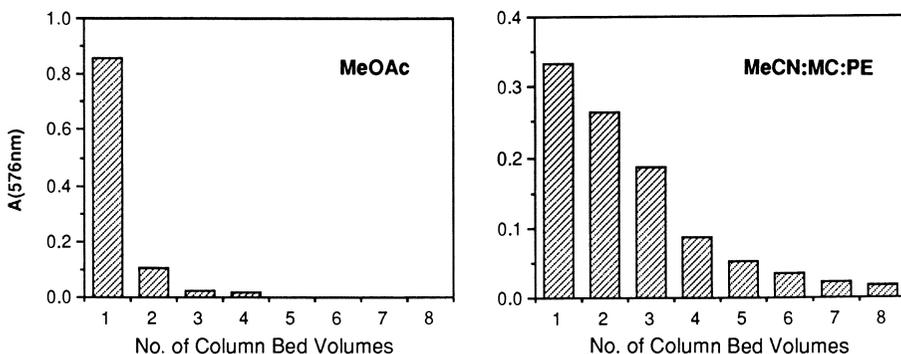


Figure 9. The biomarker fraction from the Boscan is separated from the retained asphaltene fraction at high sample load lg oil/5g silica gel. The metalloporphyrin elution in MeCN-MC-PE is badly tailed. However, 95% of the biomarker metalloporphyrins eluted in methyl acetate solvent within two column volumes. (At last!)

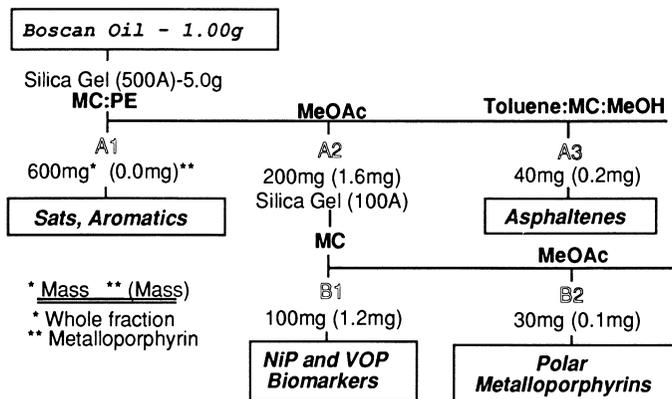


Figure 10. Short column chromatography with macroporous silica provides three initial fractions of specified mass, with the designated metalloporphyrin mass ( ) based on Soret band spectrophotometry. Various second stage options are available. In the above, silica gel separates the biomarker metalloporphyrins concentrated ten-fold followed by a more polar metalloporphyrin fraction.

asphaltene group is strongly retained and but sparingly soluble. The asphaltene-like group is retained during the initial desorption conditions: (1) the elution of the saturated hydrocarbons with some aromatic compounds in fraction A1, and (2) during the desorption of the metalloporphyrin A2 fraction. Note that the A2 fraction contains metalloporphyrins concentrated five-fold, but A2 is still over 99% non-porphyrinic as stated in Figure 10. The final desorption of the A3 asphaltene group depends upon asphaltene solubility in the MeOH:Toluene:MC blend.

The "asphaltene-like" group A3 is defined operationally by the present chromatographic procedure. This appears to overlap the original Boussingault definition made in 1837 (23) in which asphaltene solubility in turpentine and insolubility in methanol are both specified. This is discussed in greater detail by Bockrath and Schweighardt (24). The asphaltene-like material, as defined by the present chromatographic procedure, appears to be unlike the simpler operational definition based on insolubility in a specified lower alkane solvent (25). Alkane precipitated asphaltenes normally contain metalloporphyrins while the "asphaltene-like" components defined here do not, except possibly to a minor extent. It is quite possible that the latter metalloporphyrins are chemically distinct from those obtained by elution with MeOAc. The effect of this optimized separation is a much faster chromatographic basis for sub-dividing the crude oil into a fraction that contains the metalloporphyrin groups which elute easily, and the asphaltene interferences that are strongly adsorbed.

The measured 10-fold range in the sorption capacity of silica gel, depending upon pore size and particle size, shows itself in the finding that column heights of only a few (3.5) centimeters were needed to carry out the present group separations. The optimized asphaltene group sorption capacity provided by macroporous silica gel means that correspondingly less silica gel is required. Correspondingly smaller quantities of elution solvent and of elution time are the result.

It is noted in Figure 10 that the retained column load is 200 mg of A2 and 40mg for A3 fractions. This suggests that the effective load should be restricted to the adsorbed components: this corresponds to 5% based on adsorbed mass of the Boscan sample per mass of the macroporous silica. This view is less inflated than the 20% of column load, stated earlier. The latter includes components that do not adsorb and, perhaps, should not be counted.

The Boscan B1 metalloporphyrin fraction is concentrated approximately ten-fold as indicated in Figure 10. In the testing done so far, minor amounts of the more polar B2 metalloporphyrins have been observed in other crude oil samples. In sum, the scheme

generates the A2 fraction and the B1 and B2 sub-fractions which appear to be methodologically robust. The B1 and B2 classifications are easily modified to separate the NiP and VOP components by varying the eluant ratio of methylene chloride and alkane diluent. The key to this flexibility is the prior removal of the major interferences in the initial step. This enables more definitive subsequent isolations in succeeding steps. These facile group separations are obtained because of the interferences that have been removed.

The method development concludes with the finding that it is the first separation step that is of primary importance. In the present case, metalloporphyrin isolation is simplified by the initial removal of the major interference. It is because of this that the defined NiP and VOP biomarkers can be separated from either the A2 or B1 groups.

### Acknowledgments

This research was funded in part by a grant from the U.S. Department of Energy. Clifford Walters and Patrick L. Grizzle with the Sun Exploration and Production Co. provided helpful guidance and support.

Technical discussions and silica gel samples were helpfully provided by the Chromatography Marketing Department of Amicon Corporation.

### Literature Cited

1. Baker, E.W.; Palmer, S.E.; and Huang, W.Y., "Init. Rep. Deep Sea Drilling Proj.", National Science Foundation, Suppl. 1978a, 38-41, pp. 639-647.
2. S.A. Miller, T.W. Hambley and J.C. Taylor, Aust. J. Chem. 1983, 37, 761-66.
3. J.M.E. Quirke, J.K. Maxwell, G. Eglington, J.K.M Sanders, Tetrahedron Lett., 1980, 21, 2987-2990.
4. P. Sundararaman, Anal. Chem. 1985, 57, 2204-2206.
5. F. Amore, Nat. Bur. of Standards Spl. Pub. 244, Vol. 2, 1976, pp. 661-8.
6. ACS Subcommittee on Environmental Analytical Chemistry, Anal. Chem. 1980, 52, 2242-2240.
7. G. Wernimont in "Validation of the Measurement Process," J.R. DeVoe, Ed., ACS SYMPOSIUM SERIES No. 63, American Chemical Society: Washington, D.C., 1977, 1-29.
8. V.R. Meyer, J. Chromatogr. 334, 197-209 (1985).
9. H.J.G. Debets, J. Liquid Chromatogr. 8, 2725-2780 (1985).
10. D.H. Freeman In "Ultra-high Resolution Chromatography"; ACS SYMPOSIUM SERIES No. 250, American Chemical Society: Washington, D.C., 1984, pp.77-90.
11. K.H. Freeman, Honors Thesis in Geology, Wellesley College, Wellesley, MA 1984.

12. E.W. Baker In "Organic Geochemistry", G. Eglinton and M.T.J. Murphy, Eds., Springer-Verlag, 1969, Chap. 19.
13. L.R. Snyder and D.L. Saunders, J. Chromatogr. Sci. 1969, 7, 195-207.
14. J. S. Flynn and D. H. Freeman, J. Chromatogr., 1987, 386 111-121.
15. E.W. Baker, M.S. Brookhart and A.H. Corwin, J. Am. Chem. Soc. 1964, 86, 4587-90
16. To be published.
17. J.-H. Furhop and K.M. Smith in "Porphyrins and Metalloporphyrins," K.M. Smith, Ed., Elsevier, New York, 1975, p.841.
18. S.R. Abbott, LC:GC 1986, 4, 522.
19. L. R. Snyder and D.L. Saunders in "Chromatography in Petroleum Analysis," Chromatographic Science Series, K.H. Altgelt and T.H. Gouw, M. Dekker, 1979, pp. 215-272.
20. J.L. Glajch and J.J. Kirkland, Anal. Chem. 1982, 55, 319A-336A.
21. L.R. Snyder, "Principles of Adsorption Chromatography", M. Dekker, New York, 1968, pp.194-5.
22. W.A. Spencer, J.F. Galobardes, M.A. Curtis and L.B. Rogers, Separation Sci. and Tech. 1982, 17, 797-819.
23. J.B. Boussingault, Ann. Chim. Phys. 64, 141 (1837).
24. B.C. Bockrath and F.K. Schweighardt In "Chemistry of Asphaltenes", ADVANCES IN CHEMISTRY SERIES No. 195, American Chemical Society, Washington, D.C., 1981, pp.29-39.
25. R.B. Long, *ibid.* pp. 17-27.

RECEIVED January 2, 1987

## Author Index

- Albrecht, P., 68  
Aldag, A. W., 265  
Alston, K., 368  
Angeles, Rosalie M., 402  
Asaoka, S., 275  
Barwise, A. J. G., 100  
Bezman, Susan A., 205  
Biggs, Wilton R., 205  
Bonnett, Raymond, 173  
Branthaver, Jan F., 84,188  
Burke, Philip J., 173  
Callot, H. J., 68  
Chicarelli, M. Inês, 40  
Curiale, Joseph A., 135  
Czechowski, Franciszek, 173  
Dautzenberg, Frits M., 233  
De Deken, Jacques C., 233  
Dolbear, Geoffrey E., 220  
Filby, Royston H., 2,84,110,154,384  
Findsen, E. W., 368  
Fish, Richard H., 332  
Flynn, Joseph S., 402  
Freeman, David H., 402  
Freeman, Katherine H., 402  
Gallegos, Emilio J., 332  
Graham, W. R. M., 358  
Hirner, Alfred V., 146  
Hoering, Thomas C., 402  
Homony-Preyer, C. T., 402  
Kaur, Surinder, 40  
Kukes, S. G., 265  
Lango, Tracie A., 402  
Majid, Abdul, 290  
Maxwell, James R., 40  
Moorehead, Eric L., 220  
Nakata, S., 275  
Nguyen, S. N., 384  
Ocampo, R., 68  
Ondrias, M. R., 368  
Parrott, S. L., 265  
Quirke, J. M. E., 74,308  
Rankel, Lillian A., 257  
Reynolds, John G., 205,332  
Ripmeester, John A., 290  
Šebor, G., 350  
Shelnutt, J. A., 368  
Shiroto, Y., 275  
Strong, Despina, 154  
Takeuchi, C., 275  
Tang, Alice, 220  
Van Berkel, Gary J., 2,110

## Affiliation Index

- Benedict College, 368  
BP Research Centre, 100  
Carnegie Institution of Washington, 402  
Catalytica, 233  
Chevron Research Company, 205,332  
Chiyoda Chemical Engineering and Construction Company, 275  
Florida International University, 74,308  
Institute of Chemical Technology, 350  
Mineralogisch–Petrographisches Institut der Universität, 146  
Mobil Research and Development Corporation, 257  
National Research Council of Canada, 290  
Phillips Petroleum Company, 265  
Queen Mary College, 173  
Sandia National Laboratories, 368  
Texas Christian University, 358  
U.S. Naval Academy, 402  
Université Louis Pasteur, 68  
University of Bristol, 40  
University of California—Berkeley, 332  
University of Maryland, 402  
University of New Mexico, 368  
Unocal Research, 135  
Unocal Science and Technology Division, 220  
Washington State University, 2,84,110,154,384  
Wellesley College, 402  
Western Research Institute, 84,188

## Subject Index

### A

- Absorption ratio, measure of porphyrin degradation, 259
- Adsorption chromatography, rock extract, 351-352
- Actioporphyrin III, chlorophyll origin, 45
- Aggregation, vanadium porphyrin complexes, 371-374
- Air oxidation
- Arabian heavy crude, 259-261
  - metalloporphyrins, 259
  - nickel octaethylporphyrin, 260f
  - nickel tetraphenylporphyrin, 260f
  - porphyrins, 263f
- Alberta oil sands, content, 384
- Alkyl geoporphyryns
- purification scheme, 313f
  - skeletal types, 309f
- Alkylation, porphyrins, 20-21
- Alumina columns, gradient elution, 312
- Aluminas, hydrometallization with phosphorus compounds, 265-274
- Analytical techniques, trace element suites, 94
- Anoxic sediments, copper geoporphyrin occurrence, 81
- Anthracites, porphyrins, 30
- Arabian heavy crude, air oxidation, 259-261
- Arsenic acids, geochemical interest, 32
- Ash content, oil-phase solids, 293
- Asphaltenes
- aggregate formation from kerogen, 91f
  - amount in feed and products, 230f
  - biomarkers, 23-24,95
  - catalytic decomposition, 197
  - chromatographic retention, 418-421
  - complexation of metal cations, 386
  - content, 276
  - conversion and demetallization, 235-238
  - cracking, 231,277,288
  - Cu(II) uptake, 394
  - definition, 221,235
  - degree of extraction, 166
  - description, 189,221
  - distribution
    - as function of molecular weight, 398f
    - of nickel and vanadium, 397
- Asphaltenes—*Continued*
- ESR spectra of vanadyl ion, 277-279
  - evidence of nonporphyrin species, 397-400
  - infrared spectra, 298f
  - mechanism of Ni(II) acetylacetonate reactions, 392
  - metal complexes, 128,189,386
  - metal distributions, 227f
  - metalloporphyrin fraction, 420
  - metalloporphyrin separation, 414
  - micelles, porphyrin incorporation, 238
  - Molasse Basin, metal contents, 146-152
  - nickel concentration after Ni(II) acetylacetonate reaction, 393t
  - nickel incorporation by ligand replacement, 392
  - nickel uptake, 390t
  - nonporphyrin complex enrichment, 393
  - nonporphyrin metal complexes, 90,385
  - nonporphyrins, 385
  - partial molecule, 222f
  - particle, 237f
  - phosphorylation, 272
  - polarity, 166
  - porphyrin content, 400
  - porphyrin-type complexes, 21
  - reactions
    - with Cu(II) acetylacetonate, 393-394
    - with metal complexes, 386-387
    - with Ni(II) and Cu(II) acetylacetonates, 387-394
    - with nickel porphyrins, 394-397
  - reduction, 226-231
  - related to type-I kerogen, 304
  - S and V compounds, 278f
  - separation procedure, 386
  - stability of biomarkers, 95
  - structure, Venezuelan crude oil, 237f
  - sulfur distributions, 225f
  - trace element binding, 147
  - uptake of Ni, 389t
  - vanadium, 279,288
  - X-ray absorption, 327
- See also* Athabasca asphaltenes
- Athabasca asphaltenes
- elemental composition, 392t,397
  - interaction of Ni(II) complexes, 384-400
  - oxygen, 392
- See also* Asphaltenes

- Athabasca bitumen, nonporphyrin Ni(II) species, 385
- Athabasca oil sand, composition, 290
- Axial coordination  
 effects of aggregation and complex formation, 374  
 nickel porphyrins, 368-382  
 vanadium porphyrins, 368-382
- Axial ligation, vanadium porphyrins, 370-371
- B**
- Back-mixed flow reactors  
 demetallization, 246  
 flowsheet, 251f  
 hydrodemetallization followed by delayed coking, 248  
 kinetics for hydrodemetallization, 243t
- Bacteriochlorophylls, 10,71
- Bidimensional thin layer chromatography  
 use as a solvent screen, 415-417  
*See also* Thin layer chromatography
- Biodegradation  
 effect on porphyrins, 29-30,95-96  
 effect on vanadyl porphyrin distribution, 156,169
- Biological markers, assignment of structures, 40-41
- Biological precursors, geoporphyryns, 6-10
- Biomarker fraction, Boscan crude oil, 419f
- Biomarkers  
 asphaltenes, 23-24,95  
 future research needs, 96  
 generation from kerogen, 110  
 types, 154
- Bitumen components  
 porphyrin ratios, 167f  
 separation scheme, 157f
- Bitumen-I, porphyrin compositions, 126
- Bitumens  
 distribution of organic constituents in micellar structure, 165  
 formation dependence, 15-17  
 migration, 304  
 nickel and vanadium nonporphyrins, 332-349  
 porphyrin changes with maturity, 130  
 porphyrin extraction, 310  
 relationship to crude oils, 94
- Bonnett approach, porphyrin isolation, 31
- Boscan crude oil  
 biomarker fraction, 419f  
 high molecular weight  
 benzoporphyryns, 52-55  
 isolation of rhodoporphyryns, 47  
 metalloporphyrin desorption from silica gel, 417-418  
 metalloporphyrin separation by TLC, 418  
 porphyrin content, 26
- Boscan crude oil—*Continued*  
 spectral data for a demetallated chromatographic fraction, 55f
- C**
- Calcite  
 metalloporphyryns, 173-184  
*See also* Pink calcite
- Canonical variables, North Alaskan oil study, 138t
- Carbohydrates, contained in humic acids, 302
- Carbon number  
 effect on oil-sand distribution, 165  
 vanadyl porphyrins, 159
- Carbon rejection, 199-200
- Carbon residue, reduction, 226-231
- Carboxylic acid ligands, nickel complexes in heavy crude petroleum, 348f
- Carboxylic acid model compounds, examined by FAB+, 340
- Carboxylic acids, role in porphyrin formation, 72
- Catagenesis  
 description, 6  
 kerogen generation of porphyrins, 110-133  
 porphyrin changes, 17-22  
 ratio of porphyrin types, 15
- Catalyst  
 cracking process, 191-192  
 effect on demetallation, 213  
 lifetime, 244  
 petroporphyrin decomposition, 259  
 reduction of vanadyl chlorins, 217  
 vanadium deposition, 283
- Catalyst matrix  
 optimization of properties, 193  
 trapping areas, 193
- Catalyst poisons, unmetallated porphyrins, 197
- Catalyst pores, bonding of vanadyl compounds, 281
- Catalyst selectivity  
 metal and sulfur removal, 245f  
 reactor volume requirements, 243-246
- Catalytic activities, dependence on pore structure, 281-283
- Catalytic cracking  
 catalyst matrix optimization, 193  
 description, 191  
 effect of metal complexes in petroleum, 191-194
- Catalytic hydrodemetallization, mechanism, 195
- Catalytic hydroprocessing, effect on cracking mechanism, 239

- Characterization  
 bound porphyrins, 326  
 individual porphyrin components, 323-332  
 porphyrin mixtures, 318-323
- Chelation  
 influencing factors, 76  
 selectivity of geoporphyrins, 76
- Chemical ionization mass spectrometry,  
 porphyrin mixtures, 321
- Chemical reagents, activity for metals and  
 heteroatom removal, 265-266
- Chemicals, ability to demetallize heavy  
 oils, 200
- Chlorins  
 isolation and characterization, 308-327  
 similarity to sedimentary porphyrin, 56  
 structures, 190f
- Chlorobium* chlorophyll, evidence as  
 porphyrin precursors, 7
- Chloroform solution,  
 asphaltene-metalloporphyrin  
 association, 400
- Chlorophyll a, 68,85
- Chlorophyll c, 71
- Chlorophylls  
 degradation in coal, 30  
 early diagenesis, 10-12  
 geoporphyrin source, 10  
 transformation into geoporphyrins, 3,68
- Chromatography, purification of porphyrin  
 mixtures, 311
- Chromium porphyrins, stability, 74,77
- Clay slimes, intractability in extraction  
 process, 290
- Clays  
 porphyrin stability, 81  
 role in porphyrin formation in  
 sediments, 15  
 Soxhlet extraction of bitumen, 363
- Cluster analysis, utility, 141
- Coal rank, effect on porphyrin  
 distribution, 174
- Coals  
 etioporphyrin precursors, 9  
 etioporphyrin predominance, 17  
 formation, 6  
 geochemistry of metal complexes, 2-34  
 metalloporphyrins, 30-32,173-184  
 porphyrin developments, 174  
 porphyrin isolation, 314-316  
*See also* Colorado coal
- Coking  
 "bottom of the barrel" conversion, 233  
*See also* Delayed coking
- Colorado coal  
 characteristics, 176t  
 iron porphyrins, 176-179  
*See also* Coals
- Column chromatography, porphyrin isolation  
 method, 310
- Column heights, TLC of  
 metalloporphyrins, 420
- Composite performance index, solvents used  
 for TLC of metalloporphyrins, 415
- Contamination index, catalytic cracking, 192
- Coordination complexes, petroleum, 380-382
- Copper, distribution in  
 asphaltenes, 388f,391f,399f
- Copper porphyrins, isolation, 317
- Correlation studies, metals to crude  
 oils, 149
- Cracking, asphaltenes, 277
- Cretaceous crude oils, vanadium-nickel  
 ratios, 93
- Crude oil  
 analysis of trace metals, 144  
 categories of Ni and V, 206  
 demetallization, 194  
 DPEP-etio ratio, 28  
 effect of migration on vanadyl  
 porphyrins, 169  
 maturation indicators, 90-92  
 maturity ranking, 107  
 metalloporphyrins, 24-27  
 porphyrin content, 25t  
 porphyrin correlation with reservoir  
 age, 27  
 porphyrin extraction, 310  
 porphyrin isolation using silica  
 gel, 402-421  
 predominance of Ni(II) and VO(II)  
 porphyrins, 393-394  
 relationship between gravity and  
 transition-metal content, 138  
 relationship of Ni and Co contents, 152  
 relationship to solid bitumens, 94  
 relationship to vanadyl and nickel  
 porphyrins, 13-14  
 residual fractions, 193  
 source of vanadium and nickel, 385-386  
 trace element content, 32,147-148  
 vanadyl porphyrins, 207f  
*See also* Heavy crude oil
- Crystallography, porphyrin  
 characterization, 326
- Cu(II) acetylacetonates, reactions with  
 asphaltenes, 387-394
- Cyclic tetrapyrroles, isolation, 317-318
- Cytochromes, precursors to Fe(III)  
 porphyrins in coals, 30

## D

- Dealkylation, porphyrins, 20-21
- Deep Sea Drilling Project, study, 10

- Degradation  
 DPEP and etioporphyrins, 129  
 metalloporphyrins in heavy oils, 257-264
- Dehydroporphyrin, transition to porphyrin, 11
- Delayed coking  
 description, 248  
*See also* Coking
- Demetallation  
 HPLC distributions, 58  
 mechanism, 217  
 metalloporphyrins, 206,262,312  
 nickel porphyrins, 312  
 porphyrins on clay materials, 19  
 use of methanesulfonic acid, 310
- Demetallization  
 back-mixed flow reactors, 246  
 crude oil, 194  
 effect of phosphorus, 268  
 nickel etioporphyrin I, 196  
 plug-flow reactors, 246  
 porphyrins, 238
- Demineralization, shale, 126-128
- Deoxophylloerythroetioporphyrins (DPEP)  
 conversion to etioporphyrins, 155  
 degradation, 129  
 distribution in bitumen fractions, 165  
 geochemical evolution, 33,44  
 hydroxylation, 311  
 sediment levels, 108f
- Deoxophylloerythroetioporphyrin–etioporphyrin ratio (DPEP–etio ratio)  
 crude oil, 28t  
 effect of pyrolysis temperature, 129  
 formation mechanisms, 155  
 mechanisms of alteration, 100-109  
 thermal stress effect, 107  
 use, 155
- Desorption, metalloporphyrins, 417-418
- Desulfurization  
 catalyst effect, 244  
 effect of phosphorus, 268
- Diagenesis  
 chlorophylls, 10-12  
 description, 6  
 etioporphyrin formation, 107  
 late, description, 12
- Dihydroxyvanadium uroporphyrin I, formation in aqueous base, 373f
- Dihydroxyvanadium(IV) porphyrin complex, Raman spectrum, 371
- Dimethylformamide, metalloporphyrin desorbent, 417
- Dissociation energies, vanadyl complexes in asphaltenes, 279
- Ditume, mobilization, 23-24
- E
- Ebullating-bed operation, 246,249-251
- Economic effects, metal chelates in fossil fuels, 200-201
- Electron impact mass spectra  
 alkyl porphyrins, 318  
 geoporphyrin components, 318-321  
 nickel compounds, 339f  
 nickel fraction of heavy crude petroleum, 337,342f  
 polar fraction of heavy crude petroleum, 334,335f,336f  
 synthesized nickel naphthenates, 340,341f
- Electron paramagnetic resonance (EPR)  
 advantages, 358  
 asphaltene fraction of tar sand, 361-363  
 manganese, 364-365  
 metal species in petroleum and tar sands, 358-367  
 principle, 359-361  
 spectra  
   manganese ion, 366f  
   vanadyl cation, 362f  
 spectrometer, microwave energy, 359  
 transitions, 360  
 used in metal species study, 361  
 vanadyl cation, 363t
- Electron spin resonance (ESR)  
 spectra  
   vanadyl ion in asphaltenes and maltenes, 277-279  
 spectroscopy  
   bound vanadyl porphyrins, 326-327  
   vanadium nonporphyrin coordination spheres, 333
- Elements, abundance in seawater and shale, 78t
- Etioporphyrin–benzoporphyrin ratio, oil-sand bitumens, 169-170
- Etioporphyrin–deoxophylloerythroetioporphyrin ratio (Etio–DPEP ratio)  
 different oil-sand fractions, 165  
 research needs, 96
- Etioporphyrin–tetrahydrobenzo-DPEP ratio, oil-sand bitumens, 169-170
- Etioporphyrins  
 derived from low-temperature diagenetic processes, 105  
 formation via DPEP conversion, 87  
 generation from kerogen, 18-20  
 mesosubstituted amounts, 102  
 origin, 9,70,87  
 spectrophotometric methods, 318
- Evolution, DPEP and etioporphyrins, 26-27
- Exocyclic alkanone ring, abundance of compounds, 58
- Exocyclic ring moiety, sedimentary porphyrin, 50
- Expulsion, effect on the DPEP–etio ratio, 107

Expulsion rate  
 metals in bitumen, 130  
 nickel and vanadium in kerogen, 122t  
 Expulsion yields, kerogen pyrolysates, 121  
 Extraction  
 fulvic acid, 293  
 geoporphyrins, 308  
 humic acid, 291-292  
 porphyrins from sediments, 310

## F

Fast atom bombardment (FAB+), methods, 321  
 Fe(II) porphyrin, crude oil  
 identification, 24  
 Feeds, analysis in heavy oil degradation  
 study, 258t  
 Feedstocks, hydrodesulfurization  
 treatments, 194-195  
 Fixed-bed processing, 210-214  
 Fixed-bed reactor (FBR)  
 operation, 249  
 residue hydroprocessing approach, 234  
 Fixed-bed resid upgraders, 248  
 Flexicoking, economics, 234-235  
 Flowsheet, extraction of humic and fulvic  
 acids, 292f  
 Fossil fuel operations, environmental  
 concerns, 200-201  
 Fossil fuels  
 commercial metal recovery, 201  
 influence of metal complexes on industrial  
 operations, 188-201  
 metal chelate concentrations, 188  
 organometallic compounds, 32  
 Fourier transform infrared (FTIR)  
 spectroscopy, metal species in petroleum and  
 tar sands, 358  
 Friedel-Crafts acylation,  
 porphyrins, 314,324  
 Full liquid operation, H-donor solvent, 252  
 Fulvic acid  
 C-O stretching, 299  
 extraction, 293  
 IR absorption, 297  
 NMR spectra, 299-303  
 oil-phase solid 298f

## G

Ga(III) porphyrins, stability, 32  
 Gallium mesoporphyrin IX dimethyl ester,  
 HPLC, 183f  
 Gallium porphyrins  
 bituminous coals, 173  
 isolation and purification, 316

Gallium porphyrins—*Continued*  
 prevalence, 81  
 relationship to vitrinite content, 180  
 Gel permeation chromatography (GPC)  
 factor affecting metalloporphyrin  
 elution, 356  
 metalloporphyrins from a rock  
 extract, 350-356  
 purification of porphyrin mixtures, 311  
 Genetic relationship, porphyrin and  
 nonporphyrin species, 87  
 Geochemical cycling, role of organic  
 substances, 146  
 Geochemistry, metal complexes, 2-34  
 Geoporphyrin mixtures  
 characterization, 327  
 purification, 311-314  
 Geoporphyrin substituents, NMR chemical  
 shift data, 325f  
 Geoporphyrins  
 biological precursors, 6-10  
 chemistry, 3-32  
 diagenetic pathways, 5f,31f  
 environment and metal speciation, 34  
 isolation and characterization, 308-327  
 metal-free  
 isolation, 317  
 spectroscopy, 319t  
 molecular ions, 320t  
 polarities, 314  
 precursors, 8f  
 purification of individual  
 components, 312-314  
 separation techniques, 154  
 strategies used for isolation, 308  
 unstable elements, 80  
 Gilsonite  
 distribution of demetallated  
 porphyrins, 103f  
 etioporphyrin types, 102  
 nickel profile, 348f  
 source of polar nickel compounds, 347  
 Gilsonite bitumen  
 free bases, 50-52  
 porphyrin distribution, 58  
 Gold(III) porphyrins, stability basis, 77  
 Gulf of Suez, crude oil data, 109t

## H

Heavy crude oil  
 conversion into fuels, 220  
 hydrotreating, 288  
 processing strategies, 199-200  
 refining, 191  
*See also* Crude oil, Heavy oils

- Heavy crude petroleum  
 hydrocatalytic upgrade, 275-276  
 nickel and vanadium nonporphyrins, 332-349  
 nickel compounds, 334-337, 338f  
 pyridine-water extractions, 333  
 reversed-phase HPLC fractions, 333-334  
 vanadium-containing compounds, 333
- Heavy oils  
 asphaltenes, 224t  
 description, 221  
 formation before light oils, 92  
 hydrodemetallation processing, 262  
 metal chelates, importance, 201  
 metalloporphyrin degradation, 257-264  
 oils, 224t  
 preprocess conditions, 257  
 properties, 224-226  
 reactivities, 226  
 resins, 224t  
 upgrading studies, 220  
*See also* Crude oil, Heavy crude oil
- Heavy residua  
 hydrogen-transfer compounds, 217  
 vanadyl porphyrins, 207f
- Heavy residuum upgrading, metalloporphyrin  
 reaction sequence, 205-218
- Hemoglobin, reconstitution of nickel, 379
- High-performance liquid chromatography  
 (HPLC)  
 isolation of sediment porphyrins, 41  
 methods used in kerogen study, 114  
 porphyrin mixtures, 321  
 separation of metalloporphyrins, 351
- Hot water extraction process,  
 description, 290
- Humic acids  
 chemical shift ranges, 302t  
 extraction, 291-292  
 infrared spectra, 296-299  
 proton NMR spectra, 299-303
- Humic substances  
 ability to interact with metal ions, 294  
 characterization in oil sand, 290-304  
 complexes, 294-295  
 metal ion complexation, 32
- Hydroconversion, "bottom of the barrel"  
 conversion, 233
- Hydrocracking process, 235f
- Hydrodemetallization  
 activity  
 alumina, 272  
 effect of pore size, 284f  
 back-mixed reactor and delayed  
 coking, 250f  
 catalyst  
 design, 246-248  
 metals deposition, 196  
 comparison of reactor  
 technologies, 246-248
- Hydrodemetallization—*Continued*  
 dependence on pore size, 281-283  
 heavy oil, mechanism, 288  
 historic and economic perspective, 234  
 kinetic orders in plug-flow and back-mixed  
 flow reactor systems, 243t  
 modes of operation, 233  
 phosphorus compounds over  
 aluminas, 265-274  
 selectivity of a catalyst, 243-246
- Hydrodesulfurization  
 effect of metal complexes in  
 petroleum, 194-199  
 thiophene, 197  
*See also* Sulfur
- Hydrogen, effect on residual crude  
 oil, 261-262
- Hydrogen addition, 199-200
- Hydrogen fluoride, removal of metals from  
 crude oil, 195
- Hydrogen sulfide  
 effect on petroporphyrins, 257-264  
 effect on residual crude oil, 261-262
- Hydroprocessing  
 vanadium removal, 272-274  
*See also* Hydrotreating
- Hydrotreating  
 combined with thermal treatment, 279-281  
 model, 280f  
 vanadium complexes, 275-288  
*See also* Hydroprocessing
- Hydrovisbreaking, definition, 279
- I
- Industrial operations, effect of metal  
 complexes in fossil fuels, 188
- Infrared spectra, humic acids, 296-299
- Ion carrier, importance to metal  
 chelation, 77-79
- Iraq, crude oil origin, 93
- Iron  
 EPR analysis, 365-367  
 EPR parameters, 365t  
 oil identification use, 143
- Iron porphyrins  
 Colorado coal, 176-179  
 isolation and purification, 316  
 location in maceral components of  
 coal, 180  
 occurrence in coal, 81, 180
- Isocyclic ring, oxidative cleavage, 17, 105
- Isolation, nickel alkyl geoporphyrins, 310
- J
- Janina coal  
 chemical and petrographic analyses, 179  
 mass spectra of metalloporphyrins, 181f

Janina coal—*Continued*

metalloporphyrin contents, 180

## K

## Kerogen

catagenesis, 90,130

composition, 114-115

decomposition, initial stages, 92

effect on Ni and V concentration, 131f

elemental composition, 118t,119f

etioporphyrin generation, 18-20,105

generation of nickel and vanadyl

porphyrins, 110-133

geochemistry of Ni and V complexes, 130

mechanism of porphyrin association, 21

modes of porphyrin association, 128

Molasse Basin, 149-151

nickel and titanium relationship, 151f

nickel and vanadium

concentration, 19,115,120t

organically associated Ni, 149

porphyrin chemisorption, 20

porphyrin isolation, 316

pyrolysis, 112,113t,115-118

relationship to asphaltene, 304

role in catagenesis, 34

role in porphyrin evolution, 15-23

selective binding of vanadyl

porphyrins, 128

titanium content, 149

trace element binding, 147

type 3, 296

Kerogen-porphyrin association,

mechanisms, 22f

## Kinetics

contaminant removal in

hydrodemetallization, 241-243

plug-flow and back-mixed flow reactor, 242

## L

Ligand-exchange reaction, nickel porphyrins

and asphaltenes, 394

Lignite, metalloporphyrins, 173-184

Liquid chromatography

low and medium pressure, 312

nickel and vanadyl porphyrin

standards, 409f

Low-grade oil sands, organic matter, 293

Low-pressure liquid chromatography,

metalloporphyrin concentration, 404

## M

Magnetic moment, transition-metal ions in

fossil fuels, 359

Magnetic parameters, EPR spectrum of metalloporphyrins, 361

Mahalanobis distances, use, 141-143

Maltenes

definition, 189,221

ESR spectra of vanadyl ion, 277-279

metal enrichment, 149

Manganese

EPR spectrum, 364-365

paramagnetic ion, 364

Manganese ion, EPR, 365t,366f

Manganese(III) porphyrins, occurrence in coal, 81

Mass spectral analyses, nickel fraction of heavy crude petroleum, 337-340

Mass spectrometry

porphyrin mixtures, 318-321,323

rock extract, 352

Maturation, kerogen, 130

Messel oil shale

high molecular weight petroporphyrins, 72

immaturity, 69

petroporphyrins, 70

porphyrin precursors, 71

Metal

behavior during thermal

processing, 208-210

chelation ease, 77-79

fixed-bed processing, 210-213

incorporation of asphaltenes, 400

origin in crude oils, 136

percentage as metalloporphyrin, 26

reactivities, 228f-230f

tolerable amount in feed, 245f

Metal atom exchange technique, reaction

mechanism, 346

Metal chelation, occurrence in

diagenesis, 11

Metal complexes

characterization in heavy oils, 275-276

effects of crude oil migration, 95-96

influence in fossil fuels on industrial

operations, 188-201

petroleum, 189-190

use in petroleum exploration, 84-96

Metal deposition, effect on catalytic

activity in hydrotreatment, 281-283

Metal distributions, exploration

studies, 90-95

Metal-histidine bond, hemoglobin, 379

Metal insertion

first stage, 77

porphyrin complexes, 74

Metal ion, origin in coal porphyrins, 30-32

Metal ion transport, sedimentation, 32

Metal-nitrogen bond, stability role in

geoporphyrins, 79

Metal passivation, 192-193,200

- Metal species, petroleum and tar sands, 358-367
- Metallation  
 porphyrins, conditions necessary, 13  
 source of iron porphyrins, 180
- Metallononporphyrins  
 structure, 206  
 vanadium compounds, 206
- Metalloporphyrins  
 abundance in lignite, coal, and calcite, 173-184  
 axial ligation at the metal, 369  
 behavior during thermal processing, 210  
 bidimensional TLC as a solvent screen, 415  
 catalytic treatment, 218  
 chromatogram, 353f  
 coals, 30-32  
 content  
   in asphaltenes, 238  
   in crude oil components, 27-29  
 crude oil, 24-27  
 degradation in heavy oils, 257-264  
 demetallation, 206  
 desorption, 417-418  
 distribution  
   during fractionation process, 27  
   role of minerals, 81  
   use in depositional environment reconstruction, 86  
 effect of petroleum migration, 23-24  
 effect on metalloporphyrin distribution, 155-156  
 fixed-bed processing, 213-214  
 formation  
   role of the mineral matrix, 14-15  
   sedimentary environment, 12-15  
 found in pyrolyzed kerogens, 121-126  
 geochemical evolution, 3-6  
 GPC, 350-356  
 heavy residuum upgrading, 205-218  
 identification in asphaltenes, 26  
 isolation from Colorado coal, 177f  
 maturity and correlation studies, 85-87  
 origins, 188  
 pigments, separation and purification, 403  
 reaction pathway in heavy residuum process, 215-217  
 SEC, 208  
 separation from metallononporphyrins, 210  
 sites, relationship to petroleum environments, 369  
 stability, 79t  
 thermodynamic and kinetic stability, 14  
 TLC elution window, 408  
 visible spectra data, 319
- Metallouporphyrins, complexes, 374
- Migration  
 adsorption of metal chelates on rocks, 93
- Migration—*Continued*  
 effect on metal complex distribution, 95-96  
 effect on vanadyl porphyrins, 169
- Mineral-porphyrin reactions, 16f,34
- Molasse Basin  
 metals in fossil fuels, 146-152  
 oil families, 147
- Molecular sieve effect, vanadyl porphyrins in GPC, 354
- Molecular weights, vanadium and nickel compounds in heavy crude petroleum, 332-333
- N
- Ni(II) acetylacetonate  
 reactions with asphaltenes, 387-394  
 UV absorbance, 388f
- Ni(II) mesoporphyrin IX dimethyl ester, reaction with asphaltenes, 394-397
- Ni(II) octaethylporphyrin, reaction with asphaltenes, 394-397
- Nickel  
 chemical state in kerogen, 111  
 concentration in heavy crude petroleum, 337t  
 concentration in kerogens, 115t,120t  
 distribution  
   in asphaltenes, 388f,391f,397,399f  
   in heavy oils, 224,337t  
 effect on cracking catalysts, 192  
 enrichment in sediment bitumen, 13  
 nonporphyrin species, 32-33  
 source in crude oils, 385-386
- Nickel-63, asphaltene content, 395t
- Nickel alkyl geoporphyris, isolation, 310
- Nickel carboxylate fraction, separation from crude petroleum, 349
- Nickel complexes, interaction with Athabasca asphaltenes, 384-400
- Nickel components, Gilsonite, 347
- Nickel compounds, heavy crude petroleum, 334-337
- Nickel-containing nonporphyrins, bonding, 347
- Nickel etioporphyrin I, demetallization, 196
- Nickel hemoglobin A  
 absorption spectrum, 378f  
 Raman spectra, 381f
- Nickel naphthenates  
 EIMS, 340  
 FAB+ spectrum, 340
- Nickel nonporphyrin compounds, molecular characterization, 332-349

- Nickel octaethylporphyrin, air oxidation, 260f
- Nickel ore smelting, 200
- Nickel porphyrins  
 association constant for addition of ligands, 375  
 axial coordination, 368-382  
 coordination-sphere geometry, 352  
 core expansion, 375-377  
 demetallation, 312  
 effects of environment, 377  
 explanation for prevalence, 82  
 formation mechanism, 111  
 generation in kerogen, 110-133  
 geosphere predominance, 74-82  
 isolation from crude oil, 402-421  
 mass spectrometric data, 355t  
 preparative column chromatography, 405f  
 protein binding, 377-379  
 spectrophotometric methods, 318  
 TLC, 408
- Nickel protoporphyrin IX  
 absorption spectrum, 375,376f  
 Raman spectra, 375
- Nickel tetraphenylporphyrin, air oxidation, 260f
- Nickel-vanadyl porphyrin ratio, 18-20
- NMR methods, porphyrins, 323
- NMR spectra  
 humic acid from oil-phase solid, 300f  
 low-grade oil sand, 301f
- Noncatalytic hydrothermal cracking, 249
- Noncatalytic thermal hydrocracking, heavy oil, 234-235
- Nonporphyrin complexes  
 geochemical correlations, 87-90  
 kerogen catagenesis, 90
- Nonporphyrin metal chelates  
 existence, 198  
 petroleum, 189
- Nonporphyrin metal complexes, geochemical significance, 32-33
- Nonporphyrin species  
 origin, 87  
 proof of existence, 33
- North Alaskan oils  
 element concentrations, 138t  
 identification and type assignment, 137t  
 iron and nickel, 143  
 oil types, 136  
 transition-metal distribution, 135-144  
*See also* North Slope oils
- North Slope oils  
 concentration of nickel versus vanadium, 139f  
*See also* North Alaskan oils
- O
- Octaethylporphyrin  
 air oxidations, 258  
 deuteration of metal complexes, 80t
- Oil bitumen, trace metal content, 150f
- Oil families, Molasse Basin, 147
- Oil-oil correlation parameters, use of transition metals, 135
- Oil-phase solid  
 analytical data, 294  
 ash content, 293  
 elemental composition of humic acid, 295  
 infrared spectra, 298f  
 isolation, 291  
 nitrogen content, 296  
 oxygen abundance, 295-296
- Oil-sand bitumens, vanadyl porphyrin distribution, 154
- Oil-sand slimes, composition determination, 291
- Oil sands  
 aromaticities of unextractable organic matter, 303  
 elemental analyses, 295t  
 geochemical porphyrin data, 168t  
 humic matter characterization, 290-304  
 nonporphyrin species, 384  
 sulfur content, 296
- Oil shale, porphyrin origin, 68-72
- Oil types  
 source distinction, 143  
 statistical discrimination using metal data, 141  
 transition-metal use, 143
- Oils  
 amount in feed and products, 230f  
 metal distributions, 227f  
 sulfur distributions, 225f
- Organic matter, oil sands, composition, 303-304
- Organometallic compounds, fossil fuels, 32
- Oxygen, bound to aliphatic carbons in humic matter, 303
- P
- Paleozoic crude oils, vanadium contents, 92
- Pannonian Basin, trace element suites of oils, 94
- Petrolenes, definition, 189
- Petroleum  
 metal complexes, 2-34,189-190  
 metal species, 358-367  
 nonporphyrin metal chelate, 189
- Petroleum exploration, application of metal complexes, 84-96
- Petroleum migration, metalloporphyrin distribution, 23-24

- Petroleum residues, content, 276
- Petroporphyrins  
 categories, 71  
 complex mixtures, 69  
 effect of hydrogen sulfide, 257-264  
 Messel oil shale, 70  
 oil content, 262t  
 questions of origin, 69  
 separation from Boscan crude oil, 418  
 separation groups, 350-351  
 stability, 198  
 thermal treatment, 264
- pH, effect on nickel-vanadium porphyrin ratios, 81
- Phorbides  
 metal chelation, 11-12  
 role in porphyrin evolution, 10-11
- Phosphorus  
 effect on hydrodemetallization of alumina, 272  
 effect on nickel removal, 269f,271f  
 effect on sulfur removal, 270f,271f  
 effect on vanadium removal, 270f,273f
- Phosphorus additives, effect in a flow reactor, 267t
- Phosphorus compounds  
 hydrodemetallization, 265-271  
 removal from heavy oils, 265-267  
 steric effects of groups, 266
- Phosphorylation, asphaltenes, 272
- Photoinduced ligand uptake, protein effects, 380
- Pink calcite  
 emission spectrum, 182f  
 gallium porphyrin analysis, 180  
*See also* Calcite
- Plug-flow reactors  
 demetallization, 246  
 kinetics for hydrodemetallization, 243t
- Polypeptide matrix, binding of nickel protoporphyrin, 377-379
- Polypyrrroles, formation, 257
- Porphyrin mixtures  
 characterization, 318-323  
 chromatographic methods, 321-322  
 degradative methods, 322-323  
 mass spectrometry, 318-321  
 spectrophotometric methods, 318
- Porphyrin polarity  
 effect on distribution in oil, 29  
 effect on oil-sand bitumens, 170  
 effect on oil-sand distribution, 165
- Porphyrin ratios  
 geochemical correlation parameters, 166-170  
 pyrolyzed kerogens, 121-126
- Porphyrin suites, hydrodesulfurization, 199
- Porphyryns  
 abundances in bitumens, 159  
 air oxidation, 263f  
 alkylation and dealkylation, 20-21  
 alternate series, 21-22  
 anthracites, 30  
 bound, characterization, 326  
 changes in sediment during catagenesis, 17  
 chromatographic methods of characterization, 326  
 composition, 189  
 conversion to mercury sandwich complex, 324  
 crude oils and oil shales, 24  
 decomposition, 195  
 degradation to maleimides, 322  
 degradative techniques of characterization, 324-326  
 demetallization, 238  
 differences in hydrodemetallization behavior, 198-199  
 distribution  
 effect of biodegradation, 95-96  
 effect of maturation, 166  
 elements that form chelates, 75f  
 evolution, role of kerogen, 15-23  
 extraction  
 from sediments, 310  
 of bitumens and crude oils, 310  
 free-base  
 mass spectrometric examination, 11  
 metallation during late diagenesis, 12  
 origin, 24  
 functional groups, 317  
 gas chromatography-mass spectrometry, 322  
 geochemistry research needs, 33-34  
 HPLC, 59f  
 hydrogenation, 198,206  
 index of coalification, 32  
 indicators of sediment maturity, 85-86  
 isocyclic rings, 324  
 isolation, 3,27,314,316  
 isolation scheme, 315f  
 lower carbon numbers, 128  
 mass spectrometric methods, 323  
 nickel and vanadium predominance, 74-82  
 NMR methods, 323-324  
 oil-oil correlations, 88-89t  
 oil-source rock correlation, 86  
 origin in oil shale, 68-72  
 relationship to petrographic components, 179-183  
 ring degradation, 263f  
 separation difficulty, 85  
 spectrophotometric methods, 323  
 stability, 34,262-264  
 structures, 101f,190f

- Porphyrins—*Continued*  
   thermal cracking, 20  
   thermal destruction, 105-107  
   thermal hydrogenolysis, 238  
   use as thermal maturity indices, 170  
 Positive ion fast atom bombardment (FAB+)  
   heavy crude petroleum, 340-347  
   nickel fraction of heavy crude petroleum, 345f  
   synthesized nickel naphthenates, 343f,344f  
 Postchelation factors, 79-81  
 Power law rate model, application, 241  
 Protein, effects on photoinduced ligand ejection and uptake, 380  
 Protein binding, nickel porphyrin complexes, 377-379  
 Purification  
   geoporphyrin mixtures, 311-314  
   nickel compounds in heavy crude petroleum, 334-337  
 Pyridine–water extractions, heavy crude petroleum, 333  
 Pyrolysis  
   biomarkers, 166  
   effect on kerogen composition, 117,118  
   effect on Ni and V contents in kerogen, 118-121  
   Pyrolysis temperature  
     effect on porphyrin distribution, 126  
     effect on vanadyl porphyrins, 130
- R
- Raman spectroscopy  
   axial coordination of porphyrins, 368-382  
   use in studying axial ligation, 369  
 Raman spectrum  
   dihydroxyvanadium(IV) porphyrin complex, 371  
   dimer of vanadyl uroporphyrin, 371  
   methods in axial coordination study, 370  
   vanadyl octaethylporphyrin, 371  
 Reservoir rocks, age correlations with trace metals, 92  
 Resins  
   amount in feed and products, 230f  
   metals distributions, 227f  
   sulfur distributions, 225f  
 Retention, asphaltenes on silica gel, 418-421  
 Rhodoporphyrins  
   chlorophyll origin, 45  
   isolation from Boscan crude oil, 47  
 Ring degradation, porphyrin, 263f
- S
- Scouting tests, TLC, 410,411t  
 Sediment, thermal maturity, 17  
 Sediment maturity, indicator, 155  
 Sedimentary alkyl porphyrins, use, 41  
 Sedimentary environment, metalloporphyrin formation, 12-15  
 Sedimentary porphyrins  
   categories, 41-44  
   complexity, 64  
   plausible origins, 58-64  
 Sediments  
   DPEP–etio ratio, 100-109  
   extraction of porphyrins, 310  
   organometallic species origin, 146  
 Separation  
   nonporphyrin complexes from the asphaltene matrix, 384  
   optimization, 403  
 Serpiano oil shale, origin of porphyrin, 56  
 Shale  
   bitumen yields after pyrolysis, 117  
   demineralization, 121,126-128  
 Shell process, flowsheet, 251f  
 Silica gel  
   chromatography, solvent gradients, 311  
   desorption of metalloporphyrins, 417-418  
   porosity, effect of metalloporphyrin separation, 407-408  
   porphyrin isolation from crude oil, 402-421  
   sorption capacity, 420  
   thin layer chromatography scouting, optimum eluent composition, 410-414  
 Silicon porphyrins, stability basis, 77  
 Size exclusion chromatography (SEC)  
   asphaltenes, 387  
   heavy residua, 208-214  
   metalloporphyrins, 208,213-214  
   metals during fixed-bed processing, 210-213  
 Slurry-phase operation, 252  
 Solvent extraction—*See* Extraction  
 Solvent gradients, silica gel chromatography, 311  
 Solvents  
   composition in TLC study, 409f  
   effect on axial ligation in nickel porphyrins, 375-377  
   effect on axial ligation in vanadium porphyrins, 370  
   effect on metalloporphyrin separation, 410  
   TLC of metalloporphyrins, 408-410  
 Soret peak integrated absorbance, kerogen pyrolysates, 125f

- Sorption capacity, silica gel, 420  
 Source rock, geochemistry of metal complexes, 2-34  
 Source rock maturity, percent DPEP use, 86  
 Spectrophotometric methods  
   etioporphyrins, 318  
   nickel porphyrins, 318  
   porphyrin mixtures, 318  
   vanadyl porphyrins, 318  
 Stability  
   chromium porphyrins, 74  
   effect on DPEP-*etio* ratio, 17  
   Ga(III) porphyrins, 32  
   metalloporphyrins, 14,79t,326  
   petroporphyrins, 198,259  
   porphyrins, 34,262-264  
 Stability index, 79-80  
 Structure, sediment porphyrins, 41  
 Suez sediments  
   crude oil data, 106f  
   DPEP-*etio* ratio, 102-105  
   porphyrin index versus depth of burial, 104f  
 Sulfur  
   distribution in heavy oils, 224  
   reactivities, 227f-228f  
   removal from heavy oil, 268  
   *See also* Hydrodesulfurization
- T
- Tandem mass spectrometry, porphyrin mixtures, 321  
 Tar sands  
   FTIR analysis, 364  
   metal species, 358-367  
 Temperature, effect on pyrolysates of kerogen, 117-118  
 Tetraphenylporphyrin, air oxidations, 258  
 Tetrapyrroles  
   discovery in coals, 174t  
   grafted onto cellular macromolecules, 20  
   major group, 174  
   research areas, 184  
 Thermal cracking, porphyrins, 20  
 Thermal destruction, porphyrins, 105-107  
 Thermal hydroconversion, "bottom of the barrel" conversion, 233  
 Thermal hydrocracking, description, 200  
 Thermal hydrogenolysis, porphyrins, 238  
 Thermal stress, effect on DPEP-*etio* ratio, 100  
 Thermal treatment  
   Arabian heavy crude, 261  
   combined with hydrotreating, 279-281  
   metalloporphyrins, 218  
   porphyrin decomposition, 198  
   Thin layer chromatography (TLC)  
   isolation of metal-free porphyrins, 314  
   nickel and vanadium porphyrins, 408-410  
   optimization, 416f  
   purification of porphyrin mixtures, 312  
   *See also* Bidimensional thin layer chromatography  
   Thin layer chromatography scouting  
   Boscan oil, 413f  
   two-dimensional, 410,411t  
   Thin layer chromatography solvent triad, optimization, 414-415  
   Thin layer chromatography xerographs, nickel and vanadyl porphyrins, 410,412f  
   Thiophene, hydrodesulfurization, 197  
   Trace element analysis, kerogen samples, 112  
   Trace element concentrations, Southern Germany, 148f  
   Trace elements  
   analytical techniques, 94  
   concentrations in Molasse Basin oils, 147-148  
   Trace metal, correlation with reservoir rock, 92  
   Transition elements  
   oil family determinants, 136-137  
   presence in crude oil, 136  
   Transition metals  
   concentration in North Alaskan oils, 137-141  
   distribution in North Alaskan oils, 135-144  
   Trapping areas, catalyst matrix, 193  
   Treibs-Corwin scheme, chlorophyll to metalloporphyrins, 4f  
   Treibs scheme, 6-7,68  
   Trickle-bed reactor,  
   hydrodemetallization, 265-274  
   Trivalent metal ions, coal porphyrins, 30
- U
- Ultraviolet-visible (UV-vis) spectra  
 Athabasca porphyrin aggregate, 158f  
 weight percent of Ni and V after pyrolysis, 123f  
 Ultraviolet-visible (UV-vis) spectroscopy  
 distribution of V petroporphyrins, 215t  
 heavy residuum processing, 215-217  
 Ultraviolet-visible (UV-vis) spectrum,  
 thermally treated heavy residua, 216f  
 Unicracking-hydrodesulfurization technology, 221-223  
 Upgrading facilities, distribution between primary and secondary, 239  
 Upgrading processes, economics, 236f  
 Upgrading studies, heavy oils, 220

## V

- Vacuum gas oil  
 amount in feed and product oils, 226t  
 conversion to distillates, 226-231  
 Van Krevelen diagram, 296,298f,304
- Vanadium  
 catalytic activities, 287f  
 chemical state in kerogen, 111  
 concentrations, kerogens and pyrolyzed kerogens, 120t  
 content in kerogen, 115t  
 deposition catalysts in  
 hydrotreatment, 283  
 distribution  
 effect of thermal treatment of heavy residue, 211f,212f,214f  
 in catalyst pores, 281  
 in oils, 92,224  
 effect on cracking catalysts, 192  
 enrichment in sediment bitumen, 13  
 EPR results, 361  
 ESR spectra, 286f  
 heterogeneous activity, 272  
 magnetic constants, 364  
 nonporphyrin species, 32-33  
 oxidation state, 285f  
 removal from oil, 268  
 source in crude oils, 93,385-386
- Vanadium complexes, characteristics in petroleum, 275-278
- Vanadium compounds, molecular weight distribution, 277
- Vanadium nonporphyrin compounds, molecular characterization, 332-349
- Vanadium porphyrins  
 axial coordination, 368-382  
 axial ligation, 370-371  
 effects of environment, 371-374  
 geosphere predominance, 74-82  
 metal location, 374
- Vanadium sulfide  
 catalytic activity, 283-288  
 role in hydrodemetallization, 287f,288
- Vanadyl cation  
 EPR parameters, 363t  
 EPR spectra, 362f  
 origin, 363-364
- Vanadyl chlorins, reduction, 217
- Vanadyl compounds, change in asphaltenes during hydrotreatment, 279
- Vanadyl coordination, 283
- Vanadyl etioporphyrin I, demetallation, 196
- Vanadyl extraction, dimethylformamide, 417
- Vanadyl octaethylporphyrin, absorption spectra, 372f
- Vanadyl petroporphyrins, demetallation, 216f
- Vanadyl porphyrins  
 abundance in bitumen, 127t  
 carbon numbers, 159  
 chromatographic separations, 158f  
 coordination-sphere geometry, 352  
 crude oils, 207f  
 distribution  
 in bitumen, 159-166  
 in oil sands, 154-170  
 explanation for prevalence, 82  
 generation in kerogen, 110-133  
 GPC elution, 352  
 heavy residua, 207f  
 isolation from crude oil, 402-421  
 mass spectra, 159,355t  
 molecular ion histograms, 160-163f  
 promotion of asphalt oxidation, 261  
 purification, 156  
 reduction to vanadyl chlorins, 217  
 separation  
 from bitumens, 156  
 from nickel porphyrins, 356  
 spectrophotometric methods, 318  
 TLC, 408
- Vanadyl tetraphenyl porphyrin, UV-vis spectroscopy, 215
- Vanadyl uroporphyrin, dimerization, 374
- Vanadyl uroporphyrin I, absorption spectra, 372f
- Vanadyls  
 catalyst pores, 282f  
 characteristics during  
 hydrotreatment, 280f,282f  
 characterization for coordination, 287f  
 Veba process, 234,250f  
 Visbreaking, definition, 279
- VO(II) porphyrins, kerogen-enhanced bonding, 19-20

## X

- X-ray absorption, asphaltenes, 327
- X-ray photon spectroscopy, nonporphyrin VO(II) and Ni(II) species, 385

## Z

- Zelite catalysts, effect of vanadium, 192